Morphology and taxonomy of *Quetzalcoatlus* Lawson 1975 (Pterodactyloidea: Azhdarchoidea)

Brian Andres & Wann Langston Jr.

Published online: 07 Dec 2021.

Submit your article to this journal ⬈

View related articles ⬈

View Crossmark data ⬈

MEMOIR ARTICLE

MORPHOLOGY AND TAXONOMY OF *QUETZALCOATLUS* LAWSON 1975 (PTERODACTYLOIDEA: AZHDARCHOIDEA)

BRIAN ANDRES, [1*] and WANN LANGSTON JR.[2†]

[1]Department of Animal & Plant Sciences, Alfred Denny Building, University of Sheffield, Sheffield, S10 2TN U.K.,
brian.andres@aya.yale.edu;
[2]University of Texas at Austin R7600, Vertebrate Paleontology Laboratory PRC 6, 10100 Burnet Road, Austin, Texas 78758, U.S.A.

ABSTRACT—*Quetzalcoatlus* is the largest flying organism ever known and one of the most familiar pterosaurs to the public. Despite a half century of interest, it remains very incompletely described. This shortfall is addressed here through a full morphological description of *Quetzalcoatlus* and the other pterosaur material of Big Bend National Park, Texas. The first reported material was described and named *Quetzalcoatlus northropi* by Douglas Lawson in 1975, but in two separate publications. A ruling by the International Commission of Zoological Nomenclature was required for the name to be made available. Review of the pterosaur fauna of the Park recovers three valid species of azhdarchid pterosaurs in the latest Cretaceous Period Javelina and Black Peaks formations. The size and occurrence of these species are correlated with depositional environment. The holotype of the giant *Quetzalcoatlus northropi* and six other giant specimens referred to it occur in stream-channel deposits, including the youngest reported pterosaur. The vast majority of specimens (200+) are from large pterosaurs found in the abandoned channel-lake deposits at Pterodactyl Ridge; they form a diagnosable natural group erected as the new species *Quetzalcoatlus lawsoni*. A moderate-sized partial skull and cervical series also found in the abandoned channel-lake deposits at Pterodactyl Ridge, but lower in the section, is distinct from both species and is erected as *Wellnhopterus brevirostris*, gen. et sp. nov. Overbank flood-plain facies preserve another eleven specimens of extreme size variation, including small azhdarchids. The Big Bend pterosaur fauna provides the greatest known sample of azhdarchid pterosaurs and three-dimensional pterosaur morphology.

INTRODUCTION

There are extinct organisms that defy the imagination and push the boundaries of what we knew life was capable of. We name them accordingly, with etymologies taken from mythology and history. In 1975, Douglas A. Lawson reported the discovery of the largest known flying animal and named it after the Aztec feathered serpent god Quetzalcoatl (Lawson, 1975a, 1975b). *Quetzalcoatlus* enthralled scientists and the public in a way that few other discoveries have. Reported throughout the world on television and radio, it was greeted by excitement comparable to the discovery of dinosaur eggs on the Central Asiatic Expeditions (Langston, 1978). *Quetzalcoatlus* has become one of the most discussed pterosaurs. Over 500 scientific publications refer to it, *Quetzalcoatlus northropi* Lawson, 1975b, is the most cited pterosaur species, and *Quetzalcoatlus* is the fourth most cited pterosaur genus after *Pterodactylus*, *Rhamphorhynchus*, and *Pteranodon*, all of which were named a century or more earlier and have had dozens of species referred to them. However, despite almost a half century of interest, little is generally known about the *Quetzalcoatlus* material because little has been studied scientifically. This memoir addresses that shortfall, and the present contribution provides the primary morphological description and taxonomic revision to understand the largest known flying animal.

The popularity of *Quetzalcoatlus* is tied in part to its discovery in the great state of Texas, and it is compatible with the perception of that state as a large and impressive land (Andres and Myers, 2013). Specifically, it was found in the Big Bend region of Texas within the eponymous Big Bend National Park, itself one of the largest parks in the United States. The region and Park take their names from a large southern deflection of the Rio Grande River that bends through the Trans-Pecos region of Texas and encompasses the Chisos Mountain Range as well as a large stretch of the Chihuahuan Desert (Wauer and Fleming, 2002). The geology of the Park spans a half billion years, including one of the few places in the world that records the Cretaceous-Paleogene (K-Pg) boundary (Lehman, 2021). The holotype of *Q. northropi* was found about 1.5 meters below that boundary, and a referred specimen lies within centimeters of it (Lehman, 2021). *Quetzalcoatlus* is the largest known pterosaur, and it is also the geochronologically youngest.

Quetzalcoatlus has made important contributions to our understanding of pterosaurs, even though it has not been extensively described until now. At the time of its discovery, nearly all

pterosaurs were known from marine sediments, to the point that they were suggested to be an almost exclusively marine group (e.g., Wellnhofer, 1978; McGowan, 1991). *Quetzalcoatlus*, however, was found more than 400 km inland from the nearest ancient shoreline (Lawson, 1975a). At the time, almost all Cretaceous pterosaur species known were pteranodontoids. *Quetzalcoatlus* was one of the first species discovered that would comprise the group Azhdarchoidea, and it is presented here as one of the most complete and abundant members of that group. It established the Azhdarchoidea as a clade of earth-circling giants that forms one of the great radiations in the Pterosauria.

Several kinds of paleobiological problems that hold great interest for scientists and the public alike depend on accurate description of the available material and a reasoned assessment of its taxonomic status. These problems include: (1) size (notably wingspan and mass); (2) diversity of *Quetzalcoatlus* species; and (3) functional morphology and ecology.

The great size of *Quetzalcoatlus* has stimulated many estimates of its wingspan and mass, but these have been hampered by the incompleteness of the material. Over 50 wingspan estimates of *Q. northropi* have been put forward, ranging from 5.2 to 25.8 meters (17.2–84.6 feet) (Brower and Veinus, 1981). These began as quite large and wide-ranging estimates that have decreased and coalesced over time: 15.5 m (Lawson, 1972, 1975a; Langston, 1978; Wellnhofer, 1978; de Buisonje, 1981), 21 m (Lawson, 1975a), 11 m (Lawson, 1975a; McMasters, 1976; Padian, 1984c; Paul, 1987, 1991, 2002; Unwin, 2006; Pêgas et al., 2017), 5.25 m (Greenewalt, 1975), 16 m (Lawson, 1975b), 5.239–25.81 m (settled on 11.43 m) (Brower and Veinus, 1981), 11.6–12.2 m (Padian, 1984a), 11–12 m (Langston, 1986; Busbey and Lehman, 1989; Murry et al., 1991; Wellnhofer, 1991b), 10.4 m (Marden, 1994), 12 m (Shipman, 1998), 10.39 m (Chatterjee and Templin, 2004), 10–11 m (Witton, 2007), and 9.64 m (Witton, 2008). A similar set of discrepancies developed for the mass estimates of *Q. northropi*, ranging from an anorexic 30 kg (Greenewalt, 1975) to an obese 544 kg (Henderson, 2010), but with the trend converging on larger masses over time: 30–440 kg (Greenewalt, 1975), 75 kg (Brower and Veinus, 1981), 86 kg (Langston, 1981; Wellnhofer, 1991b), 65 kg (Padian, 1984c), 64 kg (MacCready, 1985), 113 kg (Paul, 1987), 200 kg (Paul, 1991), 250 kg (Marden, 1994; Paul, 2002), 127 kg (Shipman, 1998), 63–77 kg (Atanassov and Strauss, 2002), 70 kg (Chatterjee and Templin, 2004), 50 kg (Unwin, 2006), 70–85 kg (Witton, 2007), 259 kg (Witton, 2008), 276 kg (Sato et al., 2009), 200–250 kg (Witton and Habib, 2010), 544 kg (Henderson, 2010), at least 350 kg (Henderson et al., 2018), and 150 kg (Padian et al., 2021).

As opposed to scaling up other pterosaur species or even birds, phylogenetic analysis can use the evolutionary relationships of *Quetzalcoatlus* to reconstruct the missing elements needed to determine its wingspan directly. Ancestral state reconstruction of the relative lengths of the missing or incomplete wing bones of *Q. northropi* using the phylogenetic analysis provided in this memoir (e.g., Andres, 2021), in combination with the wingspan measurement method of Bennett (2001b), produces a wingspan of almost exactly 10 meters for *Q. northropi* (Fig. 1). Individuals of a second species of *Quetzalcoatlus* erected in this treatise, *Quetzalcoatlus lawsoni*, sp. nov., have been regarded as about half the size of *Q. northropi* (Brower and Veinus, 1981; Langston, 1981; Padian, 1984a, 1984c; Kellner and Langston, 1996) and are reconstructed here as approximately 4.5 meters in wingspan. The third pterosaur species identified in Big Bend and named here *Wellnhopterus brevirostris*, gen. et sp. nov., is reconstructed with about a 3 meter wingspan. There is some small azhdarchid material in the Park, but it lacks the complete elements necessary to reconstruct its wingspan. However, the widths of its preserved limb bones are about half that of *Q. lawsoni*, and so these specimens would likely have been somewhere in the 2 meter wingspan range. We follow Witton and Habib (2010) in considering

pterosaurs with greater than 7 meter wingspans such as *Q. northropi* as 'giant' pterosaurs, and pterosaurs with greater than 4 meter wingspans such as *Q. lawsoni* as 'large' pterosaurs. Martin-Silverstone et al. (2016) added 2.5–3 meter wingspan pterosaurs as 'medium-sized' and less than two meter wingspan pterosaurs as 'small'. We opt for the term 'moderate-sized' for the slightly larger *W. brevirostris* but retain the term 'small' for the smallest azhdarchid material in the Park. The wingspan estimate for *Q. northropi* exceeds the size estimate of all other pterosaur species calculated in the same manner and agrees with the estimate of Padian et al. (2021). *Quetzalcoatlus northropi* remains the largest known flying organism.

The ecology of *Quetzalcoatlus* has had similarly wide-ranging hypotheses, including: carrion-feeding (Lawson, 1975a), flightlessness (Langston, 1978; Sato et al., 2009; Henderson, 2010; but see Witton and Habib, 2010), probing for mollusks or arthropods (Langston, 1981; Wellnhofer, 1991b; Lehman and Langston, 1996), skimming (Nesov, 1984, 1991; Martill et al., 1998; Prieto, 1998; Averianov, 2013)—although 'dip-feeding' (Witton, 2007; Witton and Naish, 2008) or 'water-trawling' (Witton and Naish, 2015) may be a more appropriate term, heron or stork-like plucking of prey from shorelines or marshes and fields (Padian, 1988; Bennett, 2001b; Witton, 2007; Padian et al., 2021), waders or surface swimmers (Chatterjee and Templin, 2004), terrestrial foraging with a carnivorous diet (Witton, 2007; Witton and Naish, 2008; Witton, 2013; Witton and Naish, 2015; Naish and Witton, 2017; Zhou et al., 2017), and opportunistic generalism (Longrich et al., 2018). Two recent reviews have found that azhdarchids as a whole have had more kinds of diets attributed to them (insectivory, piscivory, carnivory, durophagy, frugivory, omnivory, scavenging, etc.) than any other pterosaur group (Zhou et al., 2017; Bestwick et al., 2018). In addition, it has been suggested that the giant holotype of *Q. northropi* and the smaller pterosaur specimens found some distance away, referred to as *Quetzalcoatlus* sp. in the literature (*Quetzalcoatlus lawsoni*, sp. nov.), coexisted with one another and were partitioned into distinct ecological resource and adaptive zones (Naish et al., 2013a; Vremir et al., 2013a, 2013b). Padian et al. (2021) provide evidence that skimming and carrion-feeding were unlikely for *Quetzalcoatlus* and support a terrestrial and shallow-water feeding environment, much like storks and herons exploit today in searching for small vertebrates and insects, respectively. Lehman (2021) advocates a solitary lifestyle preferring riparian habitats for *Q. northropi* and a gregarious wading bird-like lifestyle feeding on invertebrates for *Q. lawsoni*. These ecologies are congruent with the morphology described here.

Much of the confusion around the taxonomy and functional ecology of *Quetzalcoatlus* stems from the possibility that there were two species of different size. Lawson (1972) mentioned only a giant specimen. However, Lawson (1975a) later suggested that two smaller partial skeletons found 40 km away could be referred to the same species as the larger specimen. Lawson (1975b) put forward the original giant specimen for the holotype of *Q. northropi* and stated that there was a nearly complete smaller specimen. Whether the two pterosaur discoveries belong to the same species has been called into question ever since (Unwin, 2006). Langston (1981) restricted *Q. northropi* to the holotype and classified the smaller individuals as *Quetzalcoatlus* sp., an undetermined species; this taxonomy remains in effect to this day. Later, Kellner and Langston (1996) inferred that the smaller individuals most likely represent a different taxon and that a characterization of a new species of *Quetzalcoatlus* was in preparation, but this was never published. Long bones were histologically sampled from both *Q. northropi* and *Q.* sp. by de Ricqlès et al. (2000), but fungal destruction obscured the tissues of the former, and the latter were still actively growing; so the small available sample could not confirm whether the smaller individuals could be juveniles of the larger (de Ricqlès et al., 2000).
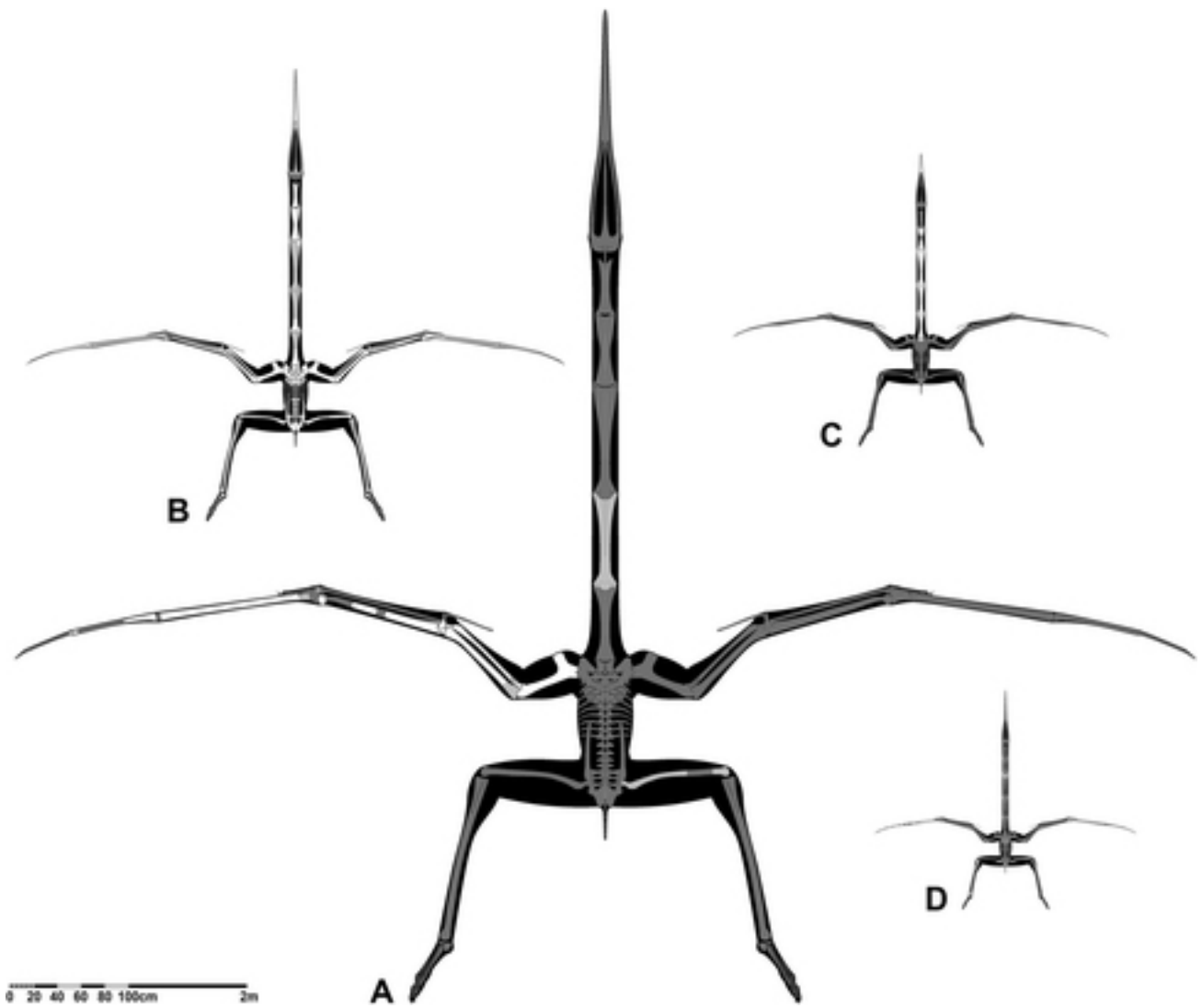
FIGURE 1. Skeletal drawings depicting elements preserved in **A**, *Quetzalcoatlus northropi* and specimens referred to cf. *northropi*; **B**, *Quetzalcoatlus lawsoni*, sp. nov.; **C**, *Wellnhopterus brevirostris*, gen. et sp. nov.; and **D**, small specimens identified as Azhdarchidae indet. White bones indicate elements preserved in the holotype and/or most complete specimen, light gray bones indicate elements preserved in referred specimens, and dark gray bones indicate unknown elements. Outlines and scale bar courtesy of J. Conway (johnconway.art). Scale bar equals 2 meters.

At stake is whether it is valid to use the smaller individuals to reconstruct the giant. The holotype of *Q. northropi* consists only of a giant partial left wing, whereas the smaller *Q.* sp. (*Q. lawsoni*, sp. nov.) comprises over 200 specimens and over 300 elements, preserving most of the bones from nearly every region of the body (Table 1). To make inferences about the giant, it would be easiest to refer the smaller individuals to *Q. northropi* and use their greater completeness to fill in the missing portions of the larger species. However, this would violate the original (i.e., Lawson, 1972) and current (i.e., Langston, 1981) taxonomy of *Quetzalcoatlus*. Even without considering historical usage, the referral of both larger and smaller morphs to the same species is not the most defensible explanation of the data. They are separated by over 40 km in distance (Lawson, 1975a; Langston, 1981), differ in size by a factor of two (Langston, 1981), are found in different paleoenvironments (Lehman, 2021), are preserved in different lithologies (Lehman, 2021), occur at different stratigraphic levels (Lehman, 2021), and include both osteological adults and subadults. The present contribution adds a greater sample of pterosaurs found

throughout Big Bend National Park, smaller and less mature specimens of *Q. northropi*, and diagnostic apomorphies to distinguish *Q. northropi* and *Q. lawsoni* as separate species. In the end, the validity of using the smaller individuals to reconstruct *Q. northropi* depends on the proportional comparability of the elements of both, and the projected allometric differences that would be expected as shape changes with size. These considerations are beyond the scope of the present contribution.

Despite the large amount of attention, few actual anatomical features of *Quetzalcoatlus* have been described, and the material has largely been under study for the past 50 years. The *Quetzalcoatlus* material is described and its taxonomy revised here in order to provide a basis for colleagues to formulate and test hypotheses about the paleobiology of the largest known flying organism. It is unfortunate that the work of W.L. on *Quetzalcoatlus* ended with his passing in 2013. His files contained copious notes, handwritten descriptions, a few pages of typescript, but no manuscripts. The authors of this memoir convened to publish a special volume for the Society of Vertebrate

TABLE 1. *Quetzalcoatlus* and other pterosaur specimens collected from Big Bend National Park. Holotype specimens in italics.

Specimen	Material
Quetzalcoatlus northropi	
TMM 41450	
TMM 41450-3	Holotype: Partial left wing
TMM 41450-3.1	Left humerus
TMM 41450-3.2	Left radius
TMM 41450-3.3	Left ulna in two pieces
TMM 41450-3.4	Left proximal syncarpal
TMM 41450-3.5	Left distal syncarpal
TMM 41450-3.6	Left first phalanx manual digit III proximal end and distal articulation
TMM 41450-3.7	Left first phalanx manual digit I proximal end
TMM 41450-3.8	Left metacarpal III distal end
TMM 41450-3.9	Left wing metacarpal proximal end, shaft fragment, distal dorsal condyle
TMM 41450-3.10	Left first wing phalanx proximal and distal portions in four pieces
TMM 41450-3.11	Left second wing phalanx proximal and distal ends
TMM 41450-3.12	Left first phalanx manual digit II proximal end
TMM 41450-3.13	Left third phalanx manual digit II ungual proximal end
TMM 41450-3.14	Left third wing phalanx proximal and distal ends
TMM 41450-3.15	Left second phalanx manual digit III shaft fragment
TMM 41450-3.16	Left fourth phalanx manual digit III ungual midsection
TMM 41450-3.17	Five probable manual fragments
TMM 41450-4	Approximately a thousand bone fragments
TMM 44036	
TMM 44036-1	Left ulna proximal end and shaft fragment
Quetzalcoatlus cf. *northropi*	
TMM 41047	
TMM 41047-1	Right femur proximal majority, two distal shaft fragments, and distal end medial half
TMM 41398	
TMM 41398-3	Left femur proximal end missing head and greater trochanter
TMM 41398-4	Right first wing phalanx proximal end missing articulation in two pieces
TMM 42889	
TMM 42889-1	Cervical vertebra VI missing prezygapophyses
Quetzalcoatlus lawsoni, sp. nov.	
TMM 41544	
TMM 41544-1	Twenty limb bone fragments
TMM 41544-2	Right femur
TMM 41544-3	Right first wing phalanx
TMM 41544-4	Cervical V prezygapophyses and posterior condyle, cervical VI anterior end in two pieces, and a cervical shaft fragment
TMM 41544-5	Right second phalanx manual digit I ungual
TMM 41544-6	Right fourth phalanx manual digit III ungual fragment
TMM 41544-7	Left second phalanx manual digit III
TMM 41544-8	Cervical IV
TMM 41544-9	Left humerus proximal end
TMM 41544-10	Right humerus distal end
TMM 41544-11	Right ulna in three pieces and a plaster cast of a portion removed for sectioning
TMM 41544-12	Cervical VI posterior end fragment
TMM 41544-14	Shaft fragment
TMM 41544-15	Cervical V
TMM 41544-16	Cervical III
TMM 41544-17	Right femur shaft
TMM 41544-19	Right distal syncarpal
TMM 41544-20	Left second wing phalanx missing distal end
TMM 41544-21	Left second wing phalanx distal end and third wing phalanx proximal end
TMM 41544-22	Mandible
TMM 41544-23	Left second wing phalanx distal end and ten shaft fragments
TMM 41544-24	Left ulna in two pieces missing proximal end
TMM 41544-25	Right scapulocoracoid
TMM 41544-26	Left scapulocoracoid missing proximal ends
TMM 41544-27	Right femur missing proximal end
TMM 41544-28	Right radius distal half
TMM 41544-29	Right first wing phalanx in two pieces missing proximal extremity
TMM 41544-30	Left metatarsal IV missing distal end but mold present
TMM 41544-31	Left first phalanx manual digit III
TMM 41544-32	Two limb bone shaft fragments and 62 small fragments
TMM 41544-34	Right distal tarsals in articulation
TMM 41544-34.1	Right lateral distal tarsal
TMM 41544-34.2	Right medial distal tarsal
TMM 41545	
TMM 41545-1	Right proximal syncarpal
TMM 41546	
TMM 41546-1	Left cervical V postzygapophysis and eight boxes of fragments
TMM 41546-2	Cervical III
TMM 41546-3	Left wing metacarpal distal end and first wing phalanx proximal end
TMM 41546-3.1	Left wing metacarpal distal end

TABLE 1. Continued.

Specimen	Material
TMM 41546-3.2	Left first wing phalanx proximal end
TMM 41546-4	Bone fragment
TMM 41546-5	Four fragments of a humerus
TMM 41546-6	Left humerus in 12 pieces
TMM 41546-7	Cervical III right prezygapophysis
TMM 41546-8	Cervical VI posterior condyle
TMM 41547	
TMM 41547-1	Right second wing phalanx missing distal end
TMM 41547-2	Right second wing phalanx shaft and distal end as well as three limb bone fragments sectioned into five pieces
TMM 41954	
TMM 41954-1	Forty-three bone fragments in concretions
TMM 41954-2	Right wing metacarpal shaft fragment and nine fragments in concretions
TMM 41954-3	Limb bone in three pieces in a concretion
TMM 41954-4	Left ulna proximal end
TMM 41954-5	Skull including mandible and long bone in two pieces in concretions
TMM 41954-5.1	Fragmentary rostrum
TMM 41954-5.2	Mandible in four pieces
TMM 41954-5.3	Long bone in two pieces
TMM 41954-6	Right first wing phalanx
TMM 41954-7	Cervical V with left tibiotarsus distal end (TMM 41954-79) attached
TMM 41954-8	Right metacarpus and left pes
TMM 41954-8.1	Left metatarsal I
TMM 41954-8.2	Left metatarsal II
TMM 41954-8.3	Left metatarsal III proximal half
TMM 41954-8.4	Left metatarsal IV in two pieces
TMM 41954-8.5	Left lateral distal tarsal
TMM 41954-8.6	Right metacarpal I
TMM 41954-8.7	Right metacarpal II in three pieces
TMM 41954-8.8	Right metacarpal III
TMM 41954-9	Right wing metacarpal shaft
TMM 41954-10	Cervical VI posterior end
TMM 41954-11	Left second wing phalanx missing distal end
TMM 41954-12	Right wing metacarpal distal shaft fragment
TMM 41954-13	Left fifth phalanx pedal digit IV ungual
TMM 41954-14	Left first wing phalanx missing proximal end
TMM 41954-20	Left radius proximal end
TMM 41954-21	Left pteroid
TMM 41954-22	Right pteroid
TMM 41954-23	Twenty-seven bone fragments
TMM 41954-25	Left first phalanx manual digit III
TMM 41954-26	Right humerus proximal half
TMM 41954-27	Left humerus proximal half
TMM 41954-28	Left lateral distal tarsal
TMM 41954-29	Left coracoid
TMM 41954-30	Cervical VI anterior end
TMM 41954-31	Cervical V right prezygapophysis
TMM 41954-32	Right first phalanx pedal digit II
TMM 41954-33	Left radius distal half
TMM 41954-34	Left proximal syncarpal
TMM 41954-35	Limb bone fragment
TMM 41954-36	Left ulna proximal end
TMM 41954-37	Right metatarsal V
TMM 41954-39	Atlantoaxis
TMM 41954-40	Cervical IX
TMM 41954-41	Cervical VII in two pieces
TMM 41954-42	Cervical VIII
TMM 41954-43	Right distal syncarpal
TMM 41954-48	Right proximal syncarpal
TMM 41954-49	Left first phalanx manual digit III
TMM 41954-50	Right partial metacarpus
TMM 41954-50.1	Right metacarpal II
TMM 41954-50.2	Right metacarpal III
TMM 41954-51	Right second phalanx manual digit I ungual
TMM 41954-52	Right radius in two pieces
TMM 41954-53	Bone fragments in plaster jacket
TMM 41954-54	Right second wing phalanx
TMM 41954-55	Right ulna in distal end
TMM 41954-56	Right metacarpal III
TMM 41954-57	Left pelvis and synsacral vertebrae
TMM 41954-58	Left prepubis
TMM 41954-59	Left carpal sesamoid and right femur distal end
TMM 41954-59.1	Left carpal sesamoid
TMM 41954-59.2	Right femur distal end
TMM 41954-60	Notarium and ribs

(Continued)

TABLE 1. Continued.

Specimen	Material
TMM 41954-60.1	Notarium of four vertebrae
TMM 41954-60.2	Left second notarial rib
TMM 41954-60.3	Right first notarial rib
TMM 41954-61	Right medial carpal
TMM 41954-62	Skull missing posterior end
TMM 41954-63	Right humerus proximal half and about a dozen fragments
TMM 41954-64	Left partial pes
TMM 41954-64.1	Left metatarsal I missing distal end
TMM 41954-64.2	Left metatarsal II missing part of shaft
TMM 41954-64.3	Left lateral distal tarsal
TMM 41954-64.4	Left medial distal tarsal
TMM 41954-64.5	Probable partial left metatarsal V
TMM 41954-65	Cervical VI
TMM 41954-66	Right wing metacarpal shaft in five pieces
TMM 41954-67	Right ulna in two shaft fragments and a distal end fragment
TMM 41954-68	Right fourth pedal phalanx digit III ungual
TMM 41954-69	Right pteroid
TMM 41954-70	Right third and fourth wing phalanges
TMM 41954-70.1	Right third wing phalanx
TMM 41954-70.2	Right fourth wing phalanx proximal end
TMM 41954-71	Right wing metacarpal
TMM 41954-72	Right first phalanx manual digit III missing distal end
TMM 41954-73	Dorsal vertebra I
TMM 41954-74	Right proximal syncarpal
TMM 41954-76	Left notarium rib II
TMM 41954-78	Left second pedal phalanx digit I ungual
TMM 41954-79	Left tibiotarsus distal end attached to a cervical V (TMM 41954-7)
TMM 41954-80	Right distal syncarpal fragment
TMM 41954-81	Right humeral head
TMM 41954-82	Wing metacarpal shaft fragments
TMM 41954-83	Right femur shaft
TMM 41954-84	Left first wing phalanx shaft fragment
TMM 41954-85	Right radius distal half
TMM 41954-86	Left third wing phalanx with damaged distal end
TMM 41954-87	Right second pedal phalanx digit II
TMM 41954-88	Cervical VII posterior end
TMM 41954-89	Right lateral distal tarsal
TMM 41954-90	Limb bone fragment in concretion
TMM 41954-91	Limb bone fragment in concretion
TMM 41961	
TMM 41961-1	Holotype partial skeleton
TMM 41961-1.1	Cranium missing anterior and posterior ends
TMM 41961-1.2	Mandible missing anterior end
TMM 41961-1.3	Left wing metacarpal
TMM 41961-1.4	Left first wing phalanx
TMM 41961-1.5	Left second wing phalanx
TMM 41961-1.6	Left third wing phalanx
TMM 41961-1.7	Left fourth wing phalanx proximal end
TMM 41961-1.8	Left ulna distal end
TMM 41961-1.9	Right proximal syncarpal
TMM 41961-1.10	Right distal syncarpal
TMM 41961-1.11	Right pteroid attached to cervical VI (TMM 41961-1.29)
TMM 41961-1.12	Left pteroid in three pieces
TMM 41961-1.13	Right wing metacarpal proximal half
TMM 41961-1.14	Right medial carpal
TMM 41961-1.15	Right first wing phalanx missing proximal end
TMM 41961-1.16	Right second wing phalanx
TMM 41961-1.17	Right third wing phalanx
TMM 41961-1.18	Right second phalanx manual digit III
TMM 41961-1.19	Right third phalanx manual digit III
TMM 41961-1.20	Right fourth phalanx manual digit III ungual
TMM 41961-1.21	Right third phalanx manual digit II ungual
TMM 41961-1.22	Left femur missing proximal end
TMM 41961-1.23	Left tibiotarsus
TMM 41961-1.24	Right femur shaft fragment
TMM 41961-1.25	Right tibiotarsus in two pieces attached to right manual digit III
TMM 41961-1.26	Right metatarsal II shaft and associated distal end
TMM 41961-1.27	Left metatarsal I shaft fragment
TMM 41961-1.28	Cervical V missing right prezygapophysis
TMM 41961-1.29	Cervical VI in two pieces attached to right pteroid (TMM 41961-1.11) and cervical VII (TMM 41961-1.30)
TMM 41961-1.30	Cervical VII anterior half attached to cervical VI (TMM 41961-1.29)
TMM 41961-1.31	Left first pedal phalanx digit I distal end
TMM 41961-2	Right wing phalanx fragments in three pieces plus cortical fragments
TMM 41961-4	Long bone shaft fragment in concretion

(Continued)

TABLE 1.   Continued.

Specimen	Material
TMM 42138	
TMM 42138-1	Right pectoral girdle and wing
TMM 42138-1.1	Right scapulocoracoid
TMM 42138-1.2	Right humerus
TMM 42138-1.3	Right ulna in two pieces
TMM 42138-1.4	Right radius proximal end
TMM 42138-1.5	Sternum anterior fragment
TMM 42138-1.6	Right metacarpal IV
TMM 42138-1.7	Right first wing phalanx proximal half and 11 shaft fragments
TMM 42138-1.8	Right second wing phalanx missing distal end
TMM 42138-1.9	Left third manual phalanx digit II ungual
TMM 42138-1.10	Right fourth wing phalanx proximal end
TMM 42138-2	Left tibiotarsus and pes as well as right distal tarsals
TMM 42138-2.1	Left tibiotarsus in two pieces
TMM 42138-2.2	Left metatarsal V
TMM 42138-2.3	Right lateral distal tarsal
TMM 42138-2.4	Right medial distal tarsal
TMM 42138-2.5	Left second pedal phalanx digit II
TMM 42138-2.6	Left fourth pedal phalanx digit IV
TMM 42138-2.7	Left third pedal phalanx digit III
TMM 42138-2.8	Left fourth pedal phalanx digit III ungual
TMM 42138-2.9	Left third pedal phalanx digit II ungual
TMM 42138-3	Right second phalanx manual digit II
TMM 42138-4	Left first phalanx manual digit III
TMM 42157	
TMM 42157-2	Right distal syncarpal
TMM 42161	
TMM 42161-1	Cranium and middle-series cervicals
TMM 42161-1.1	Cranium missing anterior and posterior portions
TMM 42161-1.3	Cervical III
TMM 42161-1.4	Cervical V
TMM 42161-1.5	Cervical VII
TMM 42161-2	Mandible
TMM 42161-3	Cervical VI missing posterior end
TMM 42180	
TMM 42180-1	Cervical III
TMM 42180-2	Cervical V in three pieces
TMM 42180-3	Cervical VI anterior end
TMM 42180-4	Left first wing phalanx proximal end
TMM 42180-5	Atlantoaxis
TMM 42180-6	Left distal syncarpal
TMM 42180-7	Forty-five fragments of limb bones
TMM 42180-8	Right proximal syncarpal
TMM 42180-9	Right scapulocoracoid distal end including glenoid
TMM 42180-10	Left scapulocoracoid in eight fragments
TMM 42180-11	Right humerus proximal portion including deltopectoral crest
TMM 42180-12	Sternum anterior end
TMM 42180-13	Nine limb bone fragments
TMM 42180-14	Partial skeleton
TMM 42180-14.1	Left humerus missing deltopectoral crest
TMM 42180-14.2	Left radius in two pieces
TMM 42180-14.3	Left ulna
TMM 42180-14.4	Left medial carpal
TMM 42180-14.5	Left wing metacarpal missing proximal end
TMM 42180-14.6	Right wing metacarpal missing distal end
TMM 42180-14.7	Left lateral distal tarsal
TMM 42180-14.8	Left metatarsal IV proximal end
TMM 42180-14.9	Left metatarsal V
TMM 42180-14.10	Cervical VI
TMM 42180-14.11	Cervical VII
TMM 42180-14.12	Left proximal syncarpal
TMM 42180-14.13	Left distal syncarpal
TMM 42180-15	Right wing metacarpal distal end
TMM 42180-16	Long bone fragment
TMM 42180-17	Right wing metacarpal distal portion
TMM 42180-18	Left metatarsal III
TMM 42180-19	Cervical VI
TMM 42180-20	Left tibiotarsus missing distal end in two pieces
TMM 42180-21	Right distal second wing phalanx and proximal third wing phalanx
TMM 42180-21.1	Right second wing phalanx distal end
TMM 42180-21.2	Right third wing phalanx proximal end
TMM 42180-22	Bone fragment in two pieces in concretion
TMM 42180-23	Limb bone fragment
TMM 42180-24	Premaxillonasal bar in 16 fragments

(Continued)

TABLE 1. Continued.

Specimen	Material
TMM 42180-25	Eight limb bone fragments
TMM 42246	
TMM 42246-1	Right distal syncarpal
TMM 42246-2	Right proximal syncarpal
TMM 42246-3	Notarium
TMM 42246-4	Right first wing phalanx in four pieces
TMM 42259	
TMM 42259-1	Cervical VI and VII
TMM 42259-1.1	Cervical VI anterior end
TMM 42259-1.2	Cervical VII
TMM 42272	
TMM 42272-1	Left femur proximal end missing head in three pieces
TMM 42272-2	Left tibiotarsus shaft in two pieces
TMM 42272-3	Seventeen long bone fragments
TMM 42272-4	Left first wing phalanx shaft fragment in two pieces
TMM 42297	
TMM 42297-1	Right femur shaft in two fragments
TMM 42422	
TMM 42422-1	Left radius
TMM 42422-2	Left first wing phalanx in two pieces
TMM 42422-3	Left distal syncarpal
TMM 42422-4	Left proximal syncarpal
TMM 42422-5	Left second wing phalanx
TMM 42422-6	Left third and fourth wing phalanges
TMM 42422-6.1	Left third wing phalanx
TMM 42422-6.2	Left fourth wing phalanx
TMM 42422-7	Cervical IX
TMM 42422-8	Cervical VIII
TMM 42422-9	Right tibiotarsus
TMM 42422-10	Left tibiotarsus with impression of distal end
TMM 42422-11	Right tibiotarsus
TMM 42422-12	Right scapulocoracoid
TMM 42422-13	Left ulna
TMM 42422-14	Right third manual phalanx digit II ungual missing distal end
TMM 42422-15	Left first and second manual digit I phalanges
TMM 42422-15.1	Left first phalanx manual digit I
TMM 42422-15.2	Left second phalanx manual digit I ungual missing tip
TMM 42422-16	Right metatarsal V missing distal end
TMM 42422-17	Left first wing phalanx shaft in two pieces with plaster cast of portion removed for sectioning
TMM 42422-18	Right humerus
TMM 42422-19	Right first phalanx manual digit II
TMM 42422-20	Cervical VI
TMM 42422-21	Left first phalanx manual digit III
TMM 42422-22	Cervical V
TMM 42422-23	Left humerus missing deltopectoral crest
TMM 42422-24	Cervical III
TMM 42422-25	Left scapulocoracoid missing ventral end
TMM 42422-26	Left ulna distal end and eight fragments
TMM 42422-27	Right femur proximal end
TMM 42422-28	Right femur missing head and much of distal end in two pieces
TMM 42422-29	Sternum anterior half
TMM 42422-30	Skull fragments
TMM 42422-31	Cervical VII
TMM 42422-32	Cervical V
TMM 42422-37	Carpal sesamoid
TMM 42422-38	Three bone fragments
TMM 42422-39	Premaxillonasal bar fragment
TMM 42462	
TMM 42462-1	Cervical IV posterior end fragment
TMM 42521	
TMM 42521-1	Fifteen rib fragments
TMM 44037	
TMM 44037-1	Limb bone shaft fragment
TMM 44037-2	Limb bone shaft fragment
TMM 44048	
TMM 44048-1	Articulated left medial carpal and carpal sesamoid
TMM 44048-1.1	Left medial carpal
TMM 44048-1.2	Left carpal sesamoid
TMM 45977	
TMM 45977-1	Limb bone shaft fragment
TMM 45977-2	Limb bone shaft fragment
TMM 45997	
TMM 45997-1	Right partial forelimb
TMM 45997-1.1	Right wing metacarpal

TABLE 1.   Continued.

Specimen	Material
TMM 45997-1.2	Right first wing phalanx proximal end in two pieces
TMM 45997-1.3	Right distal syncarpal
TMM 45997-1.4	Right radius distal end
TMM 45997-1.5	Right ulna in distal end
TMM 45997-1.6	Right proximal syncarpal
TMM 45997-2	Right third wing phalanx proximal end
TMM 45997-3	Left first manual phalanx digit II distal end
TMM 45997-4	Nine cervical VII fragments
***Wellnhopterus brevirostris*, gen. et sp. nov.**	
TMM 42489-2	Cranium and mandible anterior ends with cervicals IV–VIII
TMM 42489-2.1	Cranium anterior end and right jugal fragment
TMM 42489-2.2	Mandible anterior end
TMM 42489-2.3	Cervical IV posterior half
TMM 42489-2.4	Cervical V
TMM 42489-2.5	Cervical VI
TMM 42489-2.6	Cervical VII
TMM 42489-2.7	Cervical VIII
TMM 42489-2.8	Cervical IV anterior end and 17 concretions containing long bones
TMM 42489-2.9	Long bone fragment and 11 concretions containing long bones
Javelina Formation indeterminate pterosaurs	
TMM 41839	
TMM 41839-2	Right wing metacarpal distal end and first wing phalanx proximal end in articulation
TMM 41839-2.1	Right wing metacarpal distal end
TMM 41839-2.2	Right first wing phalanx proximal end in three pieces
TMM 41839-3	Limb bone fragments
TMM 41839-3.1	Left femur proximal end
TMM 41839-3.2	Right femur in two pieces missing head and distal end
TMM 41839-3.3	Left tibiotarsus proximal and distal ends
TMM 41839-3.4	Left first wing phalanx shaft fragments in five pieces
TMM 41839-3.5	Limb shaft fragment
TMM 41839-3.6	Left third wing phalanx shaft fragment
TMM 41839-3.7	Three left second wing phalanx fragments
TMM 41839-7	Right first wing phalanx in two pieces missing ends
TMM 41839-8	Left first wing phalanx shaft fragment
TMM 41839-10	Left metatarsal II missing distal end
TMM 41839-11	Left metatarsal III shaft and proximal articulation ventral end
TMM 41839-12	Left metatarsal I shaft fragment
TMM 42538	
TMM 42538-1	Mid-cervical vertebra midsection anterior fragment
TMM 45616	
TMM 45616-2	Sixty-six bone shaft fragments in nodules
TMM 45616-3	Forty-two bone shaft fragments in nodules
TMM 45888	
TMM 45888-2	Twenty-four bone fragments in nodules
TMM 45888-2.1	Mid-cervical vertebra anterior end missing right prezygapophysis
TMM 45888-2.2	Left distal syncarpal
TMM 45888-2.3	Six fragments in nodules
TMM 45888-2.4	Three fragments in nodules
TMM 45888-2.5	Thirteen fragments in nodules
Aguja Formation non-pterosaurs	
TMM 42335	
TMM 42335-7	Coelurosaur femur fragment
TMM 42335-48	Twenty-six bone fragments
TMM 42335-77	Fourteen bone fragments
TMM 43057	
TMM 43057-13	Nine bone fragments including a chelonian neural osteoderm
TMM 43057-151	Crocodilian right jaw ramus

Paleontology on *Quetzalcoatlus*, of which this detailed description is part. Wann Langston is included as an author on this paper based on the fundamental and essential work he did to bring the animal to light, and on the many conversations and notes he left to inform and stimulate our work.

MATERIALS AND METHODS

All *Quetzalcoatlus* and other pterosaur material from Big Bend National Park was collected under permit from the United States National Park Service and is housed at The Texas Vertebrate Paleontology Collections (TMM) at The University of Texas at Austin (UT). This material has been curated at UT under the institutional prefix 'TMM', described by a five-digit locality number, followed by a catalog number (Brown et al., 2021). Specimen numbers and element identifications are listed in Table 1.

Specimens were prepared mechanically, with the exception of the posterior segment of the skull belonging to an associated skeleton (TMM 41961-1.1), which was partially prepared with acid (Kellner and Langston, 1996). Measurements were taken with a pair of 200-mm digital Mitutoyo calipers (accurate to 0.02 mm). Measurements greater than 200 mm come from measuring lengths using the digital calipers taken along a 151-cm tailor's tape measure; although not as accurate as the shorter measurements, the resolution is sub-millimetric. Angular and curvature dimensions were measured from photographs using the Fiji computer program (Schindelin et al.,

2012): angular measurements were directly made with the Angle Tool, and curvature measurements were calculated by inputting the chord length (measured using the Straight Line tool) and the arc length (measured using the Freehand Line tool to trace the curve) of the curve into an online calculator (i.e., http://www.handymath.com) to facilitate the iterative estimation required to calculate degrees of curvature from these dimensions.

Digital photography was captured with a 12-megapixel Canon EOS 40D single-lens reflex camera using a Sigma EX 50 mm 1:2.8 DG macro lens with a SUNPAK 55 mm ultraviolet filter for smaller specimens, a Canon EF 28-80 mm 1:3.5–5.6 zoom lens for larger specimens, and Sigma EX 10–20 mm 1:4–5.6 DC HSM zoom lens for the largest specimens. No flash was used. Photographs were taken in shutter priority mode (Tv: Time Value) at 1/30 frames per second and full manual mode (M). An International Organization for Standardization (ISO) of 160 and automatic exposure bracketing of 2/3 or single full-stops were used. The resolution of the Canon 40D is 14-bit 3888 × 2592 pixels. All photographs were saved in Canon RAW version 2 (.CR2) format. The physical setup for the digital photography consisted of the camera mounted on a Manfrotto Variable Friction Magic Arm and four external lights mounted on Manfrotto Heavy-Duty Flex Arms to allow adjustable positions, all attached to a table surface using Manfrotto Super Clamps. The lighting used was four Bescor 180-watt battery-operated LED lights, although electrical cords would often be used to power and/or charge them. Photographs were taken with all lights turned on as well as various combinations of individual lights turned on and off to capture both maximum depth of focus and surface texture of specimens, respectively. A 150-mm Society of Vertebrate Paleontology scale bar was used for scale and a white velvet cloth was used for background. This photography setup provides a large amount of low-heat light to capture the three-dimensionality of specimens, but this light does not have neutral color balance. To correct the color balance, the custom white balance setting of the camera was used with the white cloth background as reference, as well as post-processing in Adobe Photoshop CC 2019 using an Auto Contrast and a Brightness Adjustment Layer in 8-bit depth. The posterior view of TMM 41961-1.1 as well as the proximal and distal views of TMM 42422-5 were kindly provided by M. Brown using a Sony NEX-5R E camera with an 18–55 mm F3.5-5.6 OSS lens without a flash. Finally, image sizes and resolution were altered to journal specifications. Original photographs including metadata are available in the Texas Vertebrate Paleontology Archives.

The positional terminology adopted by Bennett (2001a) for *Pteranodon* was used for the morphological description, which he notes is similar to that of Wellnhofer (1985, 1991a). In this manner, the body lies in the horizontal plane with the wings outstretched laterally as in flight, and the hind limb is vertical as in standing pose. Thus, the leading edge of the wing is anterior, the upper surface is dorsal, the trailing edge is posterior, and the underside is ventral regardless of the orientation of the wing in various life activities (see also Baumel and Witmer, 1993). The terms medial and lateral are therefore not significantly used in the description with the exception of the medial carpal, which is a homology statement instead of a positional statement. The complimentary torsion of the humerus and forearm shafts (Padian, 1983a) gives the elbow about a 45° rotation, but this rotation is not marked by a change in positional terms here. For simplicity, the borders of bones are termed margins, and the borders of fenestrae, foramina, and other openings are termed edges.

The wingspan estimate of 10 meters for *Quetzalcoatlus northropi* was calculated in part using the method of Bennett (2001b), in which the lengths of the humeri, ulnae, wing metacarpals, and wing phalanges are summed to calculate the wingspan.

The omission of the carpus, pectoral girdle, and torso are meant to offset the use of straight linear measurements without consideration of the flexures of the wing (Bennett, 2001b). The lengths of the missing or incomplete wing elements were reconstructed using the phylogenetic analysis provided in this memoir (e.g., Andres, 2021). The continuous characters of this analysis code the ratios of the lengths of all these wing bones with respect to one another. Missing ratios and their concomitant bone lengths can be estimated using ancestral state reconstruction, specifically optimizing values using square-changed parsimony with the MAP command of TNT (Goloboff and Catalano, 2016). The input of the length of one of these complete bones (e.g., humerus) into these ratios can be used to successively calculate the length of all others in succession and summed for both wings to provide the wingspan estimate. Often a range of values is reconstructed for a missing ratio, and so the wingspan estimate reported here is the average of the wingspan calculated from the minimum values and the wingspan calculated from the maximum values.

The International Code of Zoological Nomenclature (ICZN, 1999) is used here for species (alpha) taxonomy, and the Phylo-Code (Cantino and de Queiroz, 2020) is used here for clade (beta) taxonomy, but every endeavor was made to integrate the two. Phylogenetic definitions for the clade names discussed follow PhyloCode format, and they can be found in the phylogenetic companion piece to this treatise (e.g., Andres, 2021). Under this phylogenetic taxonomy, the Azhdarchidae includes the following species: *Quetzalcoatlus northropi* Lawson, 1975b, *Quetzalcoatlus lawsoni*, sp. nov., *Arambourgiania philadelphiae* (Arambourg, 1959), *Hatzegopteryx thambema* Buffetaut et al., 2002, *Wellnhopterus brevirostris*, gen. et sp. nov., *Cryodrakon boreas* Hone et al., 2019, *Zhejiangopterus linhaiensis* Cai and Wei, 1994, *Eurazhdarcho langendorfensis* Vremir et al., 2013, *Phosphatodraco mauritanicus* Pereda-Suberbiola et al., 2003, *Aralazhdarcho bostobensis* Averianov, 2007, *Aerotitan sudamericanus* Novas et al., 2012, *Mistralazhdarcho maggii* Vullo et al., 2018, *Albadraco tharmisensis* Solomon et al., 2020, and *Azhdarcho lancicollis* Nesov, 1984. *Montanazhdarcho minor* Padian et al., 1995, and *Radiodactylus langstoni* Andres and Myers, 2013, are successive sister groups to the Azhdarchidae, that is, non-azhdarchid azhdarchiforms (sensu Andres, 2021).

Abbreviations

AMNH, American Museum of Natural History, New York, New York; **BMR**, Burpee Museum of Natural History, Rockford, Illinois; **BSPG**, Bayerische Staatssammlung für Paläontologie und Geologie, München, Germany; **CCMGE**, Chernyshev's Central Museum of Geological Exploration, Saint Petersburg, Russia; **CMN**, Canadian Museum of Nature, Ottawa, Canada; **DFMMh/FV**, Dinosaurier-Freilichtmuseum Münchehagen/Verein zur Förderung der Niedersächsischen Paläontologie e.V., Rehburg, OT Münchehagen, Germany; **DGM**, Museum de Ciencia da Terra/Departmento Nacional Producao Mineral, Rio de Janeiro, Brasil; **EME**, Transylvanian Museum Society, Cluj-Napoca, Romania; **FSAC**, Faculté des Sciences Aïn Chock, Casablanca, Morocco; **KCM**, Kumamoto City Museum, Kumamoto, Japan; **LINHM**, Long Island Natural History Museum, New York; **LPB**, Laboratory of Fossil Vertebrates, Faculty of Geology and Geophysics, University of Bucharest, Bucharest, Romania; **MC**, Musée de Cruzy, Cruzy, France; **MCNA**, Museo de Ciencias Naturales de Álava, Vitoria, Spain; **MDM**, Mifune Dinosaur Museum, Mifune, Japan; **ME**, Museé des Dinosaures, Espéraza, France; **MFSN**, Museo Friulano di Storia Naturale, Udine, Italy; **MGUV**, Museo del Departamento de Geología, Universidad de Valencia, Valencia, Spain; **MN**, Paleovertebrate Sector, Department of Geology and Paleontology, Museu Nacional/Universidade Federal do Rio de Janeiro,

Rio de Janeiro, Brasil; **MPC**, Institute of Paleontology and Geology, Mongolian Academy of Sciences, Ulaanbaatar, Mongolia; **MPPM**, Memphis Pink Palace Museum, Memphis, Tennessee; **MPV**, Museo Paleontológico Municipal de Valencia, Valencia, Spain; **MTM**, Magyar Természettudományi Múzeum, Budapest, Hungary; **MV**, Department of Historical Geology and Paleontology of the University Museum, The University of Tokyo, Tokyo, Japan; **NHMUK**, Natural History Museum, London, United Kingdom; **NJSM**, New Jersey State Museum, New Jersey; **NSM**, National Science Museum, Tokyo, Japan; **NZGS**, New Zealand Geological Survey, Lower Hutt, New Zealand; **OMNH**, Sam Noble Oklahoma Museum of Natural History, Norman, Oklahoma; **QM**, Queensland Museum, Brisbane, Australia; **RBCM**: Royal British Columbia Museum, Victoria, Canada; **SGU**, Saratov State University, Saratov, Russia; **SMNK**, Staatliches Museum für Naturkunde, Karlsruhe, Karlsruhe, Germany; **SMP**, State Museum of Pennsylvania, Harrisburg, Pennsylvania; **TMM**, Texas Vertebrate Paleontology Collections, The University of Texas at Austin, Austin, Texas; **TMP**, Royal Tyrrell Museum of Paleontology, Drumheller, Canada; **UBB**, Muzeul de Paleontologie-Stratigrafie Universitatea Babeș-Bolyai, Cluj-Napoca, Romania; **UCMP**, University of California Museum of Paleontology, Berkeley, California; **UJA**, University of Jordan, Department of Geology, Amman, Jordan; **UNCUYO**, Universidad Nacional de Cuyo, Mendoza, Argentina; **UT**, University of Texas at Austin, Austin, Texas; **UWPI**, Paläontologisches Institut der Universität Wien, Vienna, Austria; **WAM**, Western Australian Museum, Perth, Australia; **WDC**, Wyoming Dinosaur Center, Thermopolis, Wyoming; **YPM**, Yale Peabody Museum, New Haven, Connecticut; **VGI**, Volzhsk Humanitarian Institute, Volzhsk, Russia; and **ZIN PH**, Paleoherpetological Collection, Zoological Institute of the Russian Academy of Sciences, Saint Petersburg, Russia.

SYSTEMATIC PALEONTOLOGY

PTEROSAURIA Owen, 1842 [Andres and Padian, 2020a]
PTERODACTYLOIDEA Plieninger, 1901 [Andres and Padian, 2020b]
ORNITHOCHEIROIDEA Seeley, 1891, sensu Kellner, 2003
AZHDARCHOIDEA Unwin, 1995, sensu Kellner, 2003, and Unwin, 2003
NEOAZHDARCHIA Unwin, 2003
AZHDARCHIDAE Padian, 1986, sensu Unwin, 2003
QUETZALCOATLINAE Andres, Clark, and Xu, 2014
QUETZALCOATLUS Lawson, 1975b

Phylogenetic Definition—The least inclusive clade containing *Quetzalcoatlus northropi* Lawson, 1975b and *Quetzalcoatlus lawsoni*, sp. nov. (Andres, 2021).

Type Species—*Quetzalcoatlus northropi* Lawson, 1975b.

Localities and Horizons—Specimens were collected from the basal lag deposits of the stream-channel facies and abandoned channel-lake facies of the localities TMM 41450, TMM 41047, TMM 41398, TMM 44036, and Pterodactyl Ridge in the north and west regions of Big Bend National Park, Brewster County, Texas, U.S.A. These specimens were located in unit 12, unit 15, and the uppermost of the Javelina Formation as well as lower Black Peaks Formation, late Maastrichtian Age, latest Cretaceous Period (Lehman, 2021).

Diagnosis—Large to giant azhdarchid pterosaurs (wingspan 4.5–10 meters) characterized by the following autapomorphies: humerus middle constriction less than 71% proximal width and less than 55% distal width, humerus distal end more than 129% proximal width and more than 157% times proximal

height, humerus proximal articulation surface depth greater than 58% its width, humerus ulnar crest terminally bulbous and height greater than 65% humerus mid-width, humerus ulnar crest curves posteroventrally, humerus deltopectoral crest height more than 163% deltopectoral crest mid-width, humerus supracondylar process greatly enlarged, humerus ectepicondyle terminates anteriorly in proximally curving hook, ulna proximal surface with posterior fossa, ulna proximal end with intercotylar ridge, ulna distal tuberculum positioned posteriorly, radius proximal half with ventral crest, radius distal end with ventral articular surface that reaches posterior surface, proximal syncarpal dorsal surface with large sulcus, proximal syncarpal anterior process with tubercle on anterior margin, proximal syncarpal dorsal surface with foramen between large sulcus and dorsal intersyncarpal articular facet, and manual digit I first phalanx with ridge on posterior surface.

Remarks—In the last and only review of *Quetzalcoatlus* taxonomy, Langston (1981) restricted *Quetzalcoatlus northropi* to the giant holotype and classified the smaller individuals as *Quetzalcoatlus* sp. (*Quetzalcoatlus lawsoni*, sp. nov.) pending new discoveries (with 4.5 meter wingspans, these are still considered large pterosaurs). New discoveries and the survey of Big Bend pterosaur material presented here indicate that size does have a bearing on the distribution of this material. There is a correlation between size and depositional environment: the giant individuals (TMM 41450-3, 44036-1, 41047-1, 41398-3 and 4, and 42889-1) are found in stream-channel deposits, the moderate- to large-sized individuals in abandoned channel-lake deposits (*W. brevirostris*, as well as *Q. lawsoni*, TMM, 45616-2 and 3, and 45888-2, respectively), and the smallest individuals in overbank flood-plain deposits (TMM 41839-2 to 8 and 42538-1). Whereas stream-channel deposits contain only giant individuals and channel-lake deposits contain only moderate- to large-sized individuals, the overbank flood-plain deposits are much more variable, including small individuals (TMM 41839-2 to 8 and 42538-1) as well as metatarsals from giant individuals (TMM 41839-10 to 12).

There is also a relationship between stratigraphic distribution and size. The large-sized individuals are roughly in the middle of the stratigraphic levels where pterosaurs are found in the Park. Both the biggest and smallest individuals are highest in the section (TMM 41450-3 and 44036-1 as well as TMM 41839-2 to 8, respectively). However, three of the more diminutive of the giant individuals from two localities (TMM 42889-1 as well as 41398-3 and 4) are found in the stream-channel deposits between the levels of the moderate-sized *W. brevirostris* and large *Q. lawsoni*. The small TMM 42538-1 is the lowest pterosaur specimen in the Park. A similar distinction is evident in the geographic distribution and size: the moderate-sized *W. brevirostris* and large *Q. lawsoni* are known only from Pterodactyl Ridge, whereas the giant individuals are found at five localities, and the small individuals are found at two localities (including TMM 42538-1). Three large-sized pterosaur specimens from two localities (TMM 45888-2 as well as 45616-2 and 3) are the only pterosaur specimens found in putative abandoned channel-lake deposits outside Pterodactyl Ridge (Brown et al., 2021).

It seems possible to likely that these correlated distributions of size, paleoenvironment, stratigraphy, and geography reflect taxonomy, but whether taxonomy should be based on these distributions is an important question. The large *Quetzalcoatlus* sp. individuals are known from a single area (Pterodactyl Ridge localities) and horizon (stratigraphic unit 15), with the overwhelming majority known from the main quarry level at the Amaral Site. These specimens are a diagnosable natural group of similar-sized individuals living at the same place and time that is erected here as the new species *Quetzalcoatlus lawsoni*. TMM 42489-2 is a moderate-sized individual also found at

Pterodactyl Ridge, but about 45 meters lower in the section and significantly smaller and diagnostically distinct from *Quetzalcoatlus*; it is erected as a new species *Wellnhopterus brevirostris*, gen. et sp. nov. The small individuals (TMM 41839-2 to 8 and 42538-1), found in the overbank flood-plain deposits, are very incomplete and poorly preserved; they can be identified as azhdarchid pterosaurs but nothing further about their taxonomy can be determined. The TMM 45888-2, 45616-2, and 45616-3 specimens are too poorly preserved to be classified, but they appear to be similar in size to *Q. lawsoni*. The most important question that remains is the relationship of the holotype of *Q. northropi* to the other giant pterosaur material of the Park.

The giant material comprises six specimens from five localities found in stream-channel deposits, but unfortunately only a few specimens include overlapping elements. The holotype of *Q. northropi* (TMM 41450-3) and the Black Peaks Formation specimen (TMM 44036-1) are two of the youngest pterosaurs known. Both include the proximal end of the ulna and can be referred to the same species based on their autapomorphies. TMM 44036-1 is roughly three-quarters the size of TMM 41450-3, and so there is at least some variation in the size of known *Q. northropi* individuals. TMM 41047-1 and TMM 41398-3 both include parts of the proximal end of the femur. Although TMM 41398-3 is poorly preserved, both it and TMM 41047-1 share a fossa on the proximal end of the anterior surface and can be referred to the same taxon. The complete length of neither can be determined, but the width of TMM 41047-1 is over twice the size of the *Q. lawsoni* femora, the same putative difference in size between *Q. northropi* and *Q. lawsoni* individuals (Langston, 1981). TMM 41398-3 lies roughly in between the size of those femora. TMM 41398-4, from the same locality, is a first wing phalanx proximal shaft that is also between the sizes of the *Q. northropi* holotype and *Q. lawsoni*; it would be the appropriate size for a *Q. northropi* holotype second wing phalanx, but there is no sign of a 'T-shaped' cross-section that would confirm that identification. TMM 41047-1 is stratigraphically just higher than the *Q. lawsoni* material, but TMM 41398-3 and 4 are about 30 m below it (Lehman, 2021). TMM 41398-3 and 4 also happen to be the first pterosaur material discovered by Lawson and the first pterosaur material discovered in Big Bend, predating the *Q. northropi* holotype. The last giant specimen, TMM 42889-1, is the third oldest from the Park. Originally identified as a fifth cervical vertebra by someone with a red pencil (presumably by W.L. and presumably based on its great length), it is relatively larger than any other pterosaur vertebra in the Park and is morphologically distinct from that material. TMM 42889-1 closely approximates a very large sixth cervical in morphology. It does not reach twice the size, but it is significantly larger than the sixth and all the cervicals of *Q. lawsoni*.

TMM 44036-1 is referred to *Q. northropi* based on overlapping elements and autapomorphies, despite their difference in size. TMM 41047-1 is the appropriate size for the holotype of *Q. northropi* and also shares overlapping elements and an apomorphy with a significantly smaller specimen lower in the section, TMM 41398-3. These two specimens are referable to the same species, whether or not it is *Q. northropi*. TMM 41398-3 and 4 belong to comparably sized individuals. TMM 42889-1 also comes from roughly the same stratigraphic level as TMM 41398-3 and 4, and if all were referred to *Q. northropi* would indicate that the *Q. northropi* and *Q. lawsoni* lineages had diverged by at least 69 Ma and overlapped in time, coexisting but living in different environments.

The taxonomy of TMM 42889-1 is a non-trivial issue; it is some of the only material referable to *Q. northropi* that overlaps in preservation with *A. philadelphiae*, and therefore can resolve

the relationships between these giant pterosaur species. In traditional and current taxonomic paleontology practices, all of the Big Bend stream-channel pterosaur material would be referred to *Q. northropi*. This would make intuitive sense: this material is found in the same depositional environment; it is distinct from the *Q. lawsoni* lineage; and it would not require two giant azhdarchid species to live in the same general time, area, and environment. However, one of the specimens (TMM 44036-1) can be referred to *Q. northropi* with greater certainty than the other material using autapomorphies. To address this issue, TMM 44036-1 is directly referred to *Q. northropi* whereas TMM 41047-1, 41398-3 and 4, and 42889-1 are referred to as *Quetzalcoatlus* cf. *northropi*. It is up to individual researchers to determine whether referral of the four latter specimens is warranted for their studies, but it would seem more appropriate for macroevolutionary studies on the clade level such as phylogenetic analysis and less appropriate for microevolutionary studies on the population or subpopulation level. To determine what effect this taxonomy has on our understanding of pterosaur evolution, the phylogenetic analysis in the accompanying chapter (Andres, 2021) was run with and without the referred cf. *northropi* material. It differed only in the resolution of *A. philadelphiae* with respect to *Quetzalcoatlus*, a single node in the analysis.

QUETZALCOATLUS NORTHROPI Lawson, 1975b
(Figs. 1–10)
"*Pteranodon gigas*" (Lawson, 1972:118, pl. VII, fig. 4) (original unpublished description).
Pterosaur from the Latest Cretaceous of West Texas (Lawson, 1975a:947, fig. 1) (original description).
Quetzalcoatlus northropi Lawson 1975b:678 (original name).

Holotype—TMM 41450-3, partial left wing: humerus (TMM 41450-3.1); radius (TMM 41450-3.2); ulna (TMM 41450-3.3); proximal syncarpal (TMM 41450-3.4); distal syncarpal (TMM 41450-3.5); metacarpal III digit end (TMM 41450-3.8); wing metacarpal proximal end, shaft fragment, and distal dorsal condyle (TMM 41450-3.9); first phalanx manual digit I proximal end (TMM 41450-3.7); first phalanx manual digit II proximal end (TMM 41450-3.12); third phalanx manual digit II proximal end (TMM 41450-3.13); first phalanx manual digit III proximal end and distal articulation (TMM 41450-3.6); second phalanx manual digit III shaft (TMM 41450-3.15); fourth phalanx manual digit III ungual proximal end (TMM 41450-3.16); five other unidentified manual phalanx fragments (TMM 41450-3.17); first wing phalanx shaft (TMM 41450-3.10); second wing phalanx proximal and distal ends (TMM 41450-3.11); third wing phalanx proximal and distal end (TMM 41450-3.14); and approximately a thousand unidentified bone fragments (TMM 41450-4).

Localities and Horizons—Specimens were collected from the stream-channel deposits of localities TMM 41450, TMM 41047, TMM 41398, TMM 44036, and TMM 42889 in the north and west regions of Big Bend National Park, Brewster County, Texas, USA, including all referred specimens. These specimens were located in the uppermost and unit 12 of the Javelina Formation as well as the lower Black Peaks Formation, late Maastrichtian Age, latest Cretaceous Period, including all referred specimens (Lehman, 2021).

Diagnosis—Giant azhdarchid pterosaur (wingspan 10 meters) that can be distinguished from *Quetzalcoatlus lawsoni* and other pterosaurs by the following autapomorphies: humerus hourglass-shaped with middle constriction less than 50% proximal width and less than 33% distal width, humerus distal end more than 150% proximal width and more than 175% the proximal height, humerus proximal articulation surface depth
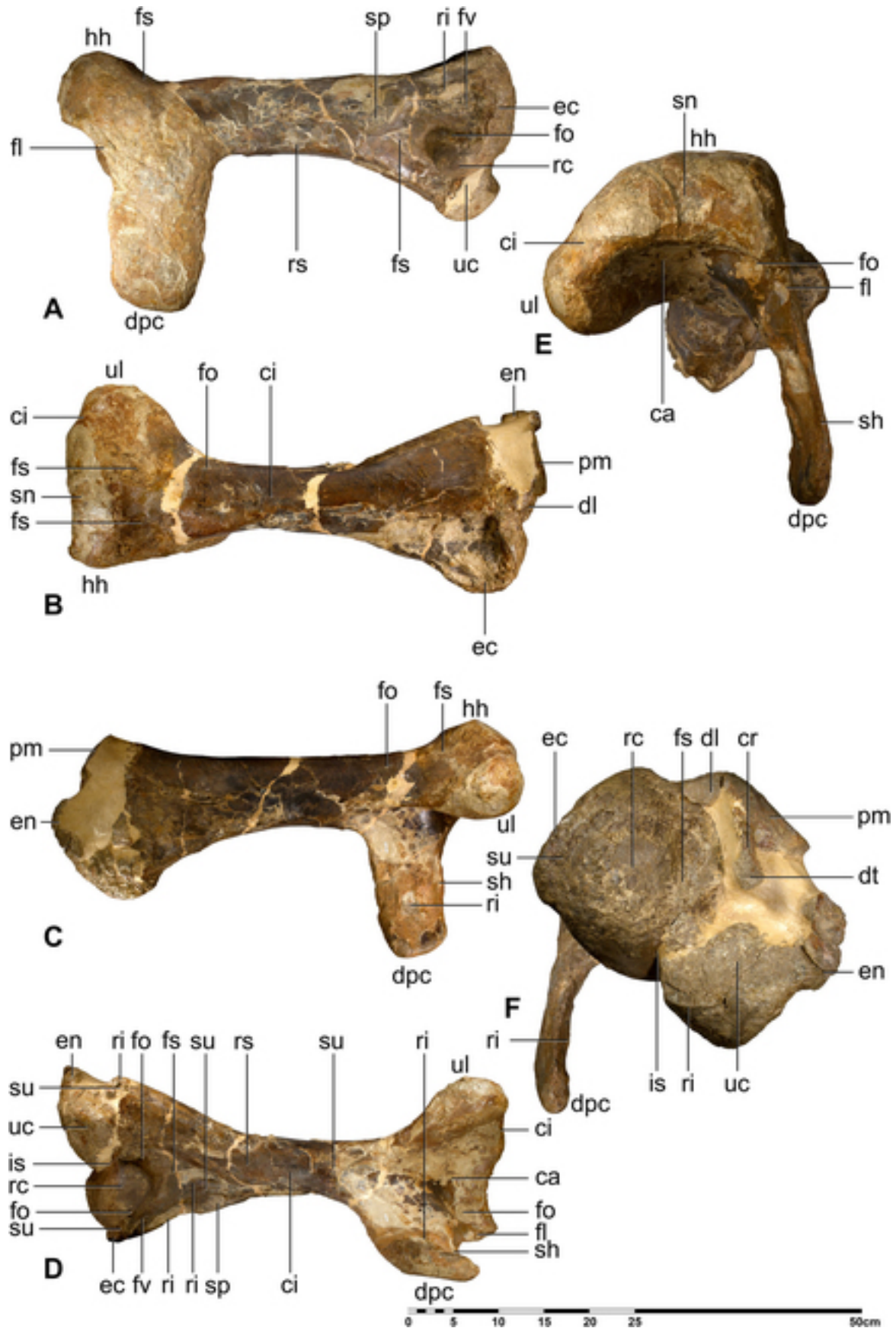
FIGURE 2. *Quetzalcoatlus northropi* left humerus (TMM 41450-3.1) photographs in **A**, anterior; **B**, dorsal; **C**, posterior; **D**, ventral; **E**, proximal; and **F**, distal views. **Abbreviations: ca**, concavity; **ci**, constriction; **cr**, crest; **dpc**, deltopectoral crest; **dl**, dorsal lip; **dt**, distal tubercle; **ec**, ectepicondyle; **en**, entepicondyle; **fl**, flange; **fo**, foramen; **fs**, fossa; **fv**, fovea; **hh**, humeral head; **is**, intercondylar sulcus; **pm**, prominence; **rc**, radial condyle; **ri**, ridge; **rs**, rise; **sh**, shelf; **sn**, scapulocoracoid articulation; **sp**, supracondylar process; **su**, sulcus; **uc**, ulnar condyle; and **ul**, ulnar crest. Scale bar equals 50 cm.
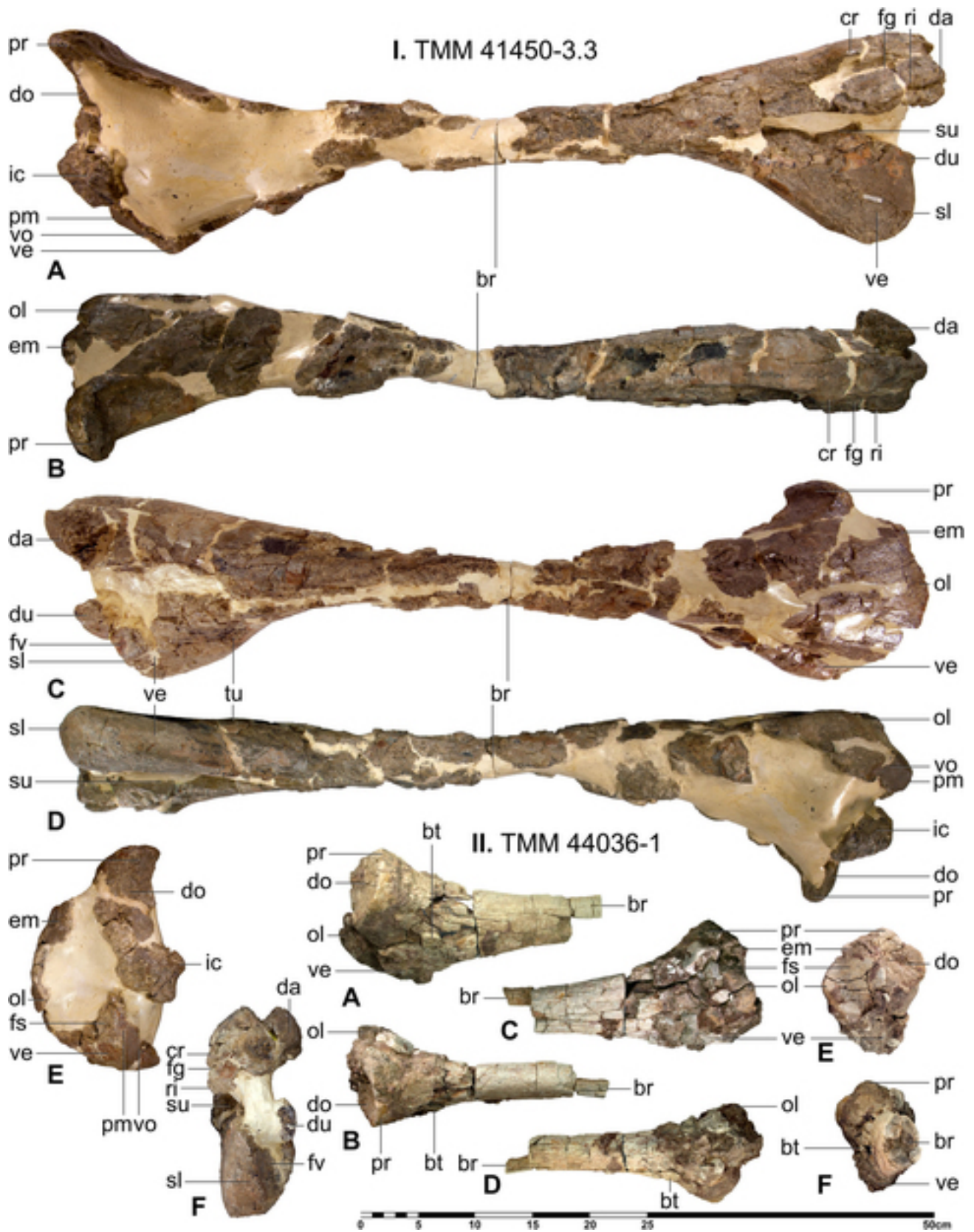
FIGURE 3. *Quetzalcoatlus northropi* left ulna photographs of **I.** holotype (TMM 41450-3.3) and **II.** referred specimen (TMM 44036-1) in **A**, anterior; **B**, dorsal; **C**, posterior; **D**, ventral; **E**, proximal; and **F**, distal views. **Abbreviations: br**, break; **bt**, biceps tubercle; **cr**, crest; **da**, dorsal articular surface; **do**, dorsal cotyle; **du**, distal tuberculum; **em**, eminence; **fg**, flexor tendon groove; **fs**, fossa; **fv**, fovea; **ic**, intercotylar crest; **ol**, olecranon; **pm**, prominence; **pr**, process; **ri**, ridge; **sl**, styloid prominence; **su**, sulcus; **tu**, tubercle; **ve**, ventral expansion; and **vo**, ventral cotyle. Scale bar equals 50 cm.
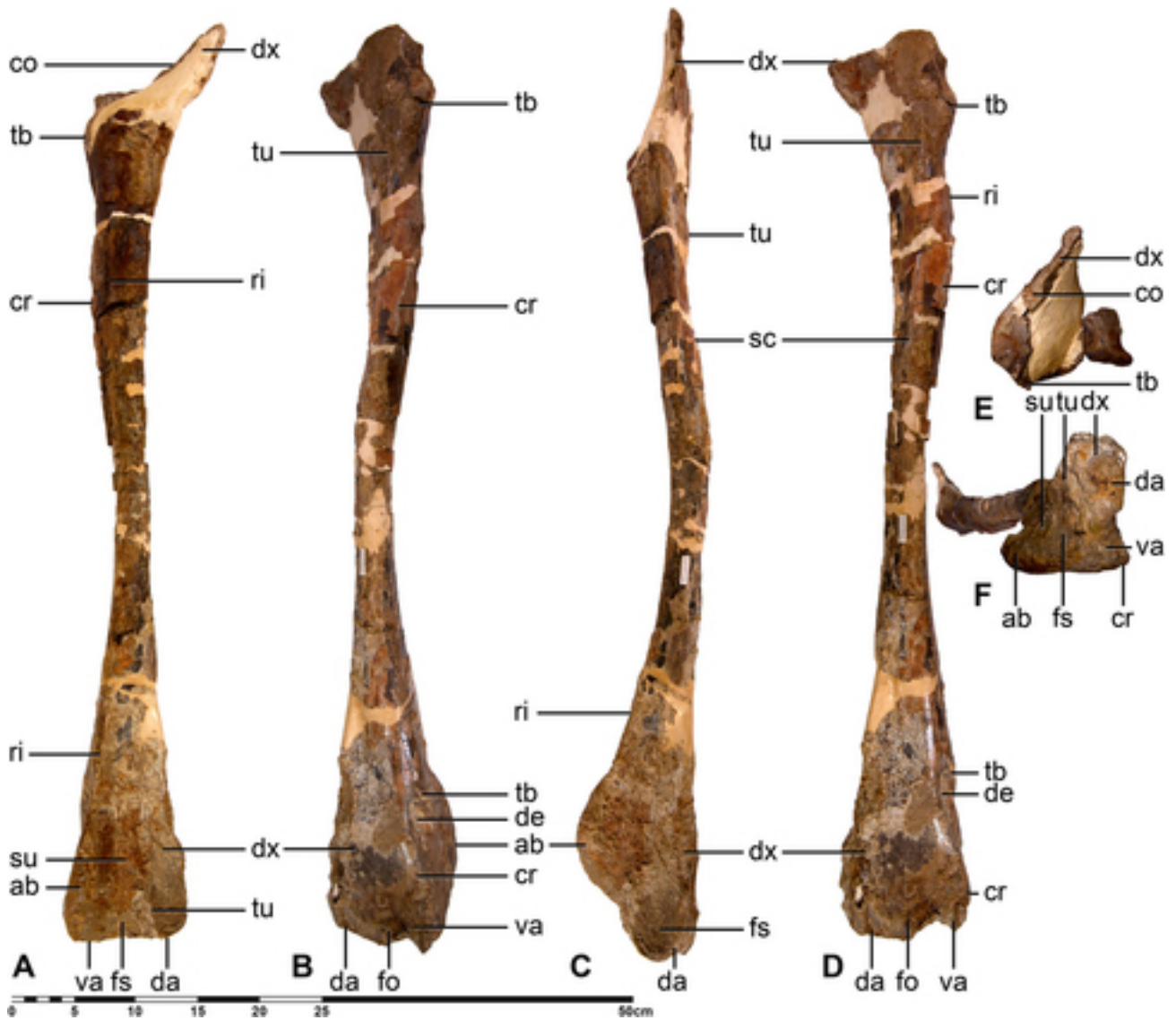
FIGURE 4. *Quetzalcoatlus northropi* left radius of holotype (TMM 41450-3.2) photographs in **A**, anterior; **B**, ventral; **C**, dorsal; **D**, posterior; **E**, proximal; and **F**, distal views. **Abbreviations: ab**, anterior tuberosity; **co**, cotyle; **cr**, crest; **da**, dorsal articular surface; **de**, depression; **dx**, dorsal expansion; **fo**, foramen; **fs**, fossa; **ri**, ridge; **sc**, scar; **su**, sulcus; **tb**, tuberosity; **tu**, tubercle; and **va**, ventral articular surface. Scale bar equals 50 cm.

greater than 63% its width, humerus deltopectoral crest with shelf on proximal margin, humerus ulnar crest massive and greater than mid-width, humerus deltopectoral crest height more than 163% deltopectoral crest mid-width, humerus proximal end concavity extends distal to deltopectoral crest distal margin, humerus supracondylar process massive, humerus with ridge between supracondylar process and ectepicondyle, humerus distal tuberculum connected to posterior surface by crest, radius shaft substantially posteriorly curved, radius proximal end with trifurcate ridges on ventral surface, radius distal end with massive anterior tuberosity, proximal syncarpal blocky with length less than 60% width, proximal syncarpal with triangular concave surface and without foramen ventral to radial dorsal articular facet, proximal syncarpal dorsal intersyncarpal facet much smaller than ventral intersyncarpal facet, distal syncarpal ventral surface with posteroventral process on distal margin, wing metacarpal proximal end inverted piriform in cross-section, wing metacarpal with massive proximal tuberculum, wing metacarpal proximal end with bulbous anterior tumescence, wing metacarpal proximal end with groove dorsal to anterior tumescence, wing metacarpal ventral expansion without anteriorly directed flange and flexor tendon groove on proximal end, wing metacarpal shaft with flat-topped cylinder shape, and wing metacarpal anteroposterior mid-width greater than dorsoventral mid-depth. Including all referred specimens: cervical vertebra VI elongated with length over 20 times mid-depth, cervical vertebra VI neural canal anterior end with deeply incised V-shaped dorsal margin, cervical vertebra VI neural canal posterior end rectangular in outline and pneumatic foramina lateral to neural canal triangular in outline, cervical vertebra VI body dorsoventrally depressed with elliptical cross-section and lacking lateral constriction, femur head attaches to neck on lateral half, femur proximal end anterior surface with distinct fossa, and femur shaft mediolaterally wider than anteroposteriorly broad.
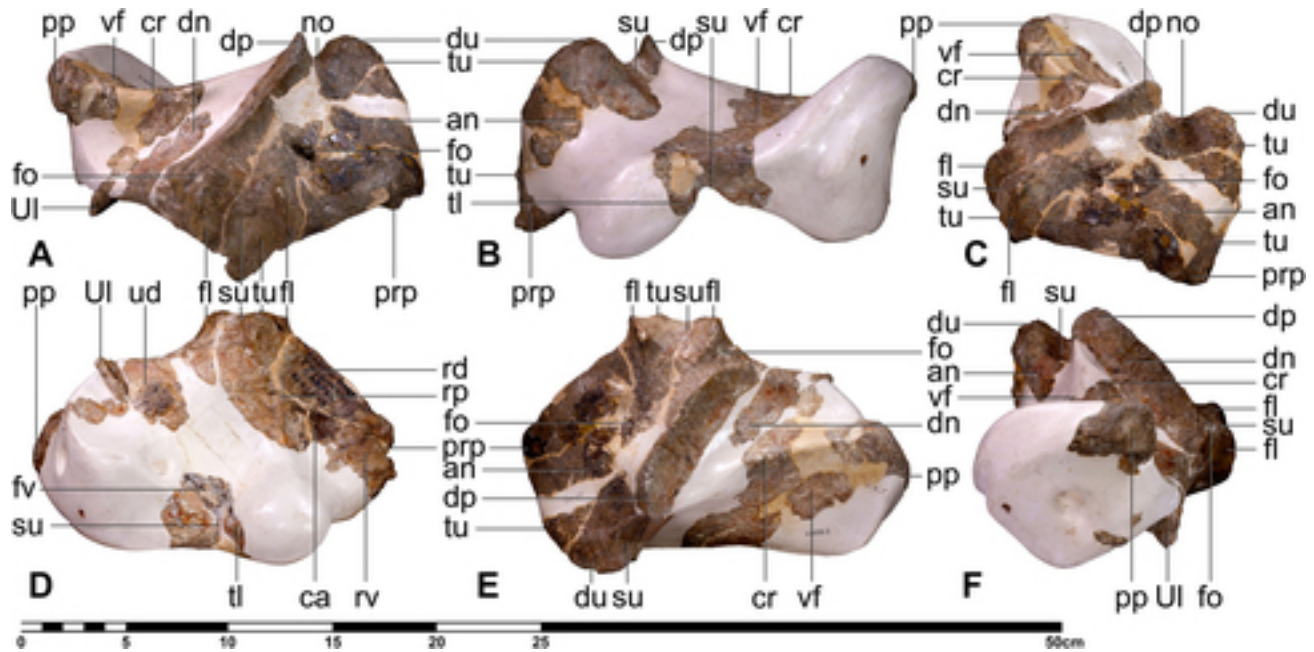
FIGURE 5. *Quetzalcoatlus northropi* left proximal syncarpal of holotype (TMM 41450-3.4) photographs in **A**, dorsal; **B**, ventral; **C**, anterior; **D**, proximal; **E**, distal; and **F**, posterior views. **Abbreviations: an**, anterior process; **ca**, concavity; **cr**, crest; **dn**, dorsal intersyncarpal articular facet; **dp**, distal process; **du**, distal tuberculum; **fl**, flange; **fo**, foramen; **fv**, fovea; **no**, notch; **pp**, posterior process; **prp**, proximal process; **rd**, radial dorsal articular facet; **rp**, raised prominence; **rv**, radial ventral articular facet; **su**, sulcus; **tl**, tuberculum; **tu**, tubercle; **ud**, ulnar dorsal articular surface; **Ul**, ulna; and **vf**, ventral intersyncarpal articular facet. Scale bar equals 50 cm.

Referred Specimen—Left proximal ulna and shaft fragments (TMM 44036-1) from the Black Peaks Formation at locality TMM 44036, Big Bend National Park, Brewster County, Texas, U.S.A.

Remarks—The taxonomic history of *Quetzalcoatlus* is quite complex, or "very confused" in the words of Averianov (2014:10). The holotype of *Quetzalcoatlus northropi* was discovered in 1971 as part of Douglas Lawson's Master's research at UT into the paleoecology of the Tornillo Group in Big Bend National Park (Lawson, 1972). This material was reported to include a giant left radius and ulna, proximal and distal syncarpals, as well as the proximal end of a wing metacarpal (metacarpal IV) (Lawson, 1972). Originally given the specimen number TMM 41501, it was corrected to 41450-3 four years later (TMM catalog). Lawson described and termed this material "*Pteranodon gigas*" in his thesis, providing the single sentence diagnosis that it was "nearly twice as large as any previously described species of *Pteranodon*" (Lawson, 1972:118). This species name is not available according to the International Code of Zoological Nomenclature (ICZN, 1999) because his thesis is not considered 'published' in the meaning of ICZN's articles (ICZN Articles 8.1, 9.7, and 11.1): It was not issued for the purpose of providing a public and permanent scientific record, not obtainable free of charge or by purchase when first issued, and not produced in an edition containing simultaneously obtainable copies (ICZN Article 8.1). In addition, this species name has not been used as a valid name, and three years later Lawson (1975b) made this specimen the holotype of *Quetzalcoatlus northropi*, which has been used as a presumed valid name in at least 25 works by more than ten authors within the past 50 years over a span of more than ten years (ICZN Article 23.9.1). Even if available, "*Pteranodon gigas*" (Lawson, 1972)

would be a nomen oblitum with respect to *Quetzalcoatlus northropi* Lawson, 1975b, which would in turn be a nomen protectum (ICZN Article 23.9.2). In other words, *Quetzalcoatlus northropi* is the valid name and would be given precedence over the unused "*Pteranodon gigas*" name in accordance with Article 23.9.2 of the ICZN if "*Pteranodon gigas*" were available, which it is not.

Field crews from UT led by W.L. returned to Big Bend National Park to collect more pterosaur material, discovering a large number of smaller individuals in an area 40 km from the original specimen (Lawson, 1975a). However, only the original giant material with the addition of a humerus and the first two wing phalanges, plus the remains of two new smaller individuals, were reported in the first scientific publication, Lawson (1975a). Review of this paper and the collection data suggests that the two smaller individuals were probably TMM 41544 and 41546 specimens from Pterodactyl Ridge (Table 1). Lawson (1975a) figured the left humeri of TMM 41450-3 and 41544-9 as well as the cervical V of TMM 41544-15, and he mentioned other elements that would minimally correspond to TMM 41450-3 and 41544 specimens as well as 41545-1. Despite the distance and difference in size among the specimens, he stated that "all can be referred to a single species because of the similarity of their humeri, proximal carpals, and second wing phalanges" (Lawson, 1975a:947). This is not surprising considering that this was the most complete azhdarchoid material known and only the sixth azhdarchoid species discovered at the time. Lawson (1975a) stated that a detailed description was in preparation at which time the specimens would be diagnosed, but no further description or diagnosis was ever published.

Two months later in a paper enigmatically titled "Could Pterosaurs Fly?" Lawson (1975b) named *Quetzalcoatlus northropi*, stating that:
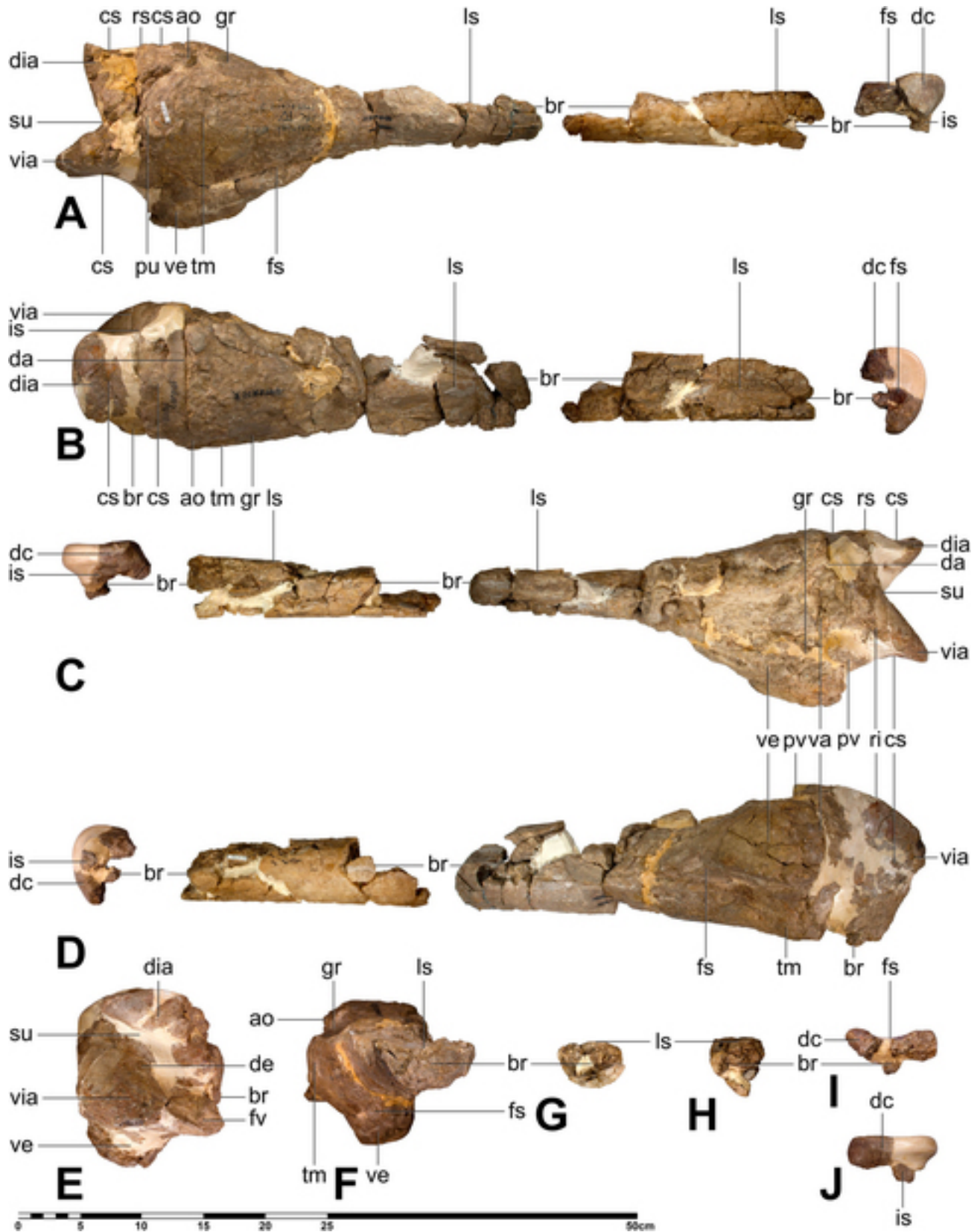
FIGURE 6. *Quetzalcoatlus northropi* left distal syncarpal (TMM 41450-3.5) as well as left wing metacarpal (IV) proximal end, shaft, and distal condyle fragments (TMM 41450-3.9) photographs of holotype in **A**, anterior; **B**, dorsal; **C**, posterior; **D**, ventral; **E**, proximal; and **F**, distal end of proximal fragment; **G**, proximal end of shaft fragment; **H**, distal end of shaft fragment; **I**, proximal end of dorsal condyle; and **J**, distal end of dorsal condyle views. **Abbreviations: ao**, anterodorsal process; **br**, break; **cs**, concave surface; **da**, dorsal articular surface; **dc**, dorsal condyle; **de**, depression; **dia**, dorsal intersyncarpal articular surface; **fs**, fossa; **fv**, fovea; **gr**, groove; **is**, intercondylar sulcus; **ls**, flat surface; **pu**, proximal tuberculum; **pv**, posteroventral process; **ri**, ridge; **rs**, rise; **su**, sulcus; **tm**, tumescence; **va**, ventral articular surface; **ve**, ventral expansion; and **via**, ventral intersyncarpal articular surface. Scale bar equals 50 cm.
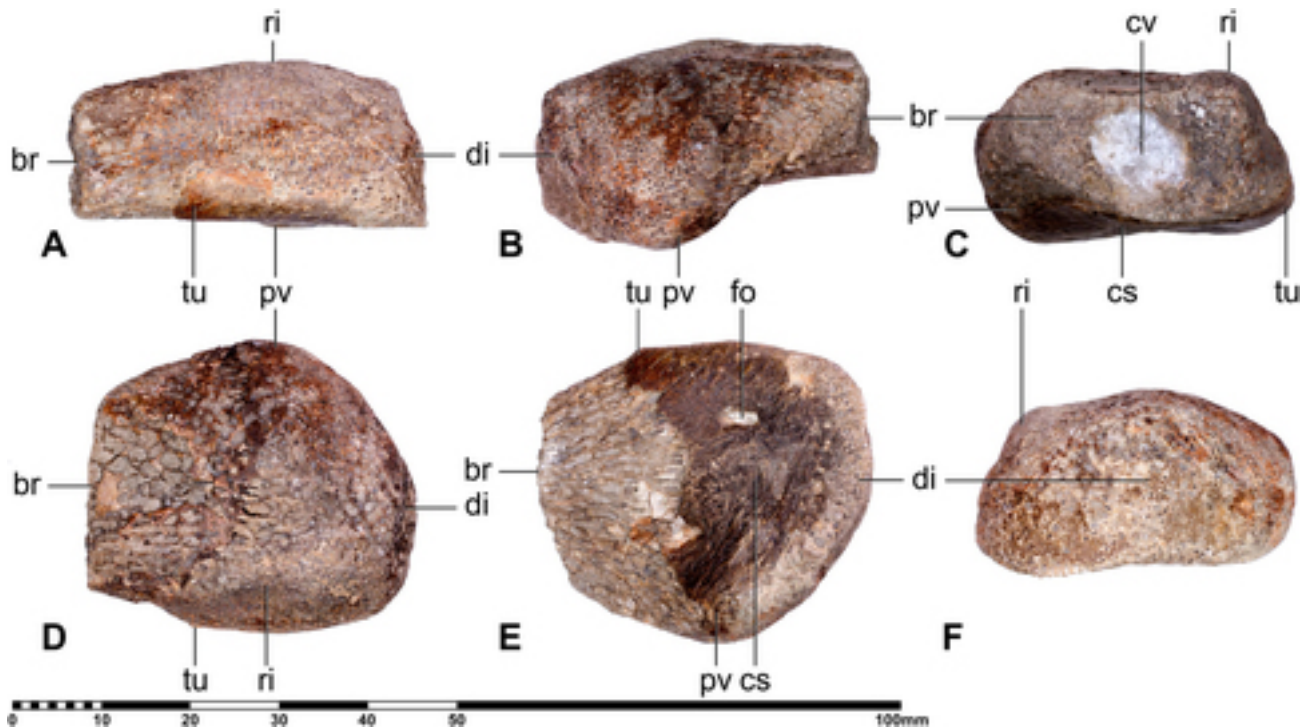
FIGURE 7. *Quetzalcoatlus northropi* left metacarpal III distal end of holotype (TMM 41450-3.8) photographs in **A**, anterior; **B**, posterior; **C**, proximal; **D**, dorsal; **E**, ventral; and **F**, distal views. **Abbreviations: br**, break; **cs**, concave surface; **cv**, cavity; **di**, distal condyle; **fo**, foramen; **pv**, posteroventral process; **ri**, ridge; and **tu**, tubercle. Scale bar equals 100 mm.

"The Texas pterosaur, hereafter to be referred to as *Quetzalcoatlus northropi*, is represented by the type Texas Memorial Museum No. 41450-3, which consists of a left humerus and partial radius, ulna, proximal and distal carpals, metacarpal, and first and second phalanges of the fourth digit. An approximate regression equation for the relation of its wingspan to its humerus length

$$W = 29.70H^{1.0116}$$

can be based on a more nearly complete, smaller specimen of the same species on the regression coefficient of *Pteranodon*. The solution of this equation for a humerus of 52 cm gives a wingspan of approximately 1600 cm." (Lawson, 1975b:678)

No mention was made of *Quetzalcoatlus* or any other Big Bend material outside these three sentences. Etymologies for the names were not provided, but they have been attributed to the Mesoamerican deity Quetzalcoatl (Anonymous, 1975; Langston, 1978; Park, 1981) and John Northrop, designer of the YB-49 'flying wing' experimental aircraft (Lawson, pers. comm.). Lawson never published on the material again.

Because this name was published after 1930, in order to be available it must be accompanied by a description or definition that states the characters that differentiate the taxon to which it refers (ICZN Article 13.1.1), or be accompanied by a bibliographic reference to such a published statement (ICZN Article 13.1.2). Lawson (1975b) named *Q. northropi*, but did not diagnose it or reference such a diagnosis. Lawson (1975a) did describe the material as well as compare and contrast it with other pterosaurs, but Lawson (1975b) made no reference to this differential description. This exchange was presumably what led Sullivan and Fowler (2011) to suggest that

Q. northropi had not been diagnosed and arguably could be considered a nomen nudum. Averianov (2014) disagreed, stating that Lawson (1975b) obviously referenced Lawson (1975a) (switched in his text) and fulfilled the requirements of ICZN Article 13.1.2. Both Lawson (1975a) and Lawson (1975b) do refer to the species as the "Texas pterosaur" (Lawson, 1975a: figs. 1 and 2; 1975b:678) and list similar elements. However, ICZN Article 13.1.2 requires a bibliographic reference, and Lawson (1975a) was not one of the four bibliographic references listed in Lawson (1975b). Nesov (1991) did later publish a diagnosis for the genus *Quetzalcoatlus*, but this did not make it or its type species available because it was based on an unavailable species name (ICZN Article 67.2.1) and unavailable material (ICZN Recommendations 16C, 72F.3, and 73B), the mere citation of which does not make it available (ICZN Article 11.5.2). Adding to the confusion, Nesov (1991) did not actually cite the original article naming *Q. northropi* but mistakenly cited the article preceding it in the journal instead, Greenewalt (1975), which might have been considered if the species had otherwise been eligible (ICZN Article 67.7).

As a result, no author has expressly proposed a new or replacement name for *Quetzalcoatlus northropi*, and so it has been a nomen nudum. It was unavailable as a name, and because it had no potentially valid synonym to replace it, a substitute name needed to be established in its place (ICZN Article 23.3.5). However, an unavailable name can be made available later for the same taxon (ICZN, 1999:111). The diagnosis, description, and treatment provided here could have made *Q. northropi* available, but it would have also required the authorship (ICZN Article 50.1) and date (ICZN Article 21) for this species to be taken from this current act of establishment. Although this scenario does not violate the Principle of Priority (ICZN Article 23.1), it runs contrary to its purpose (ICZN
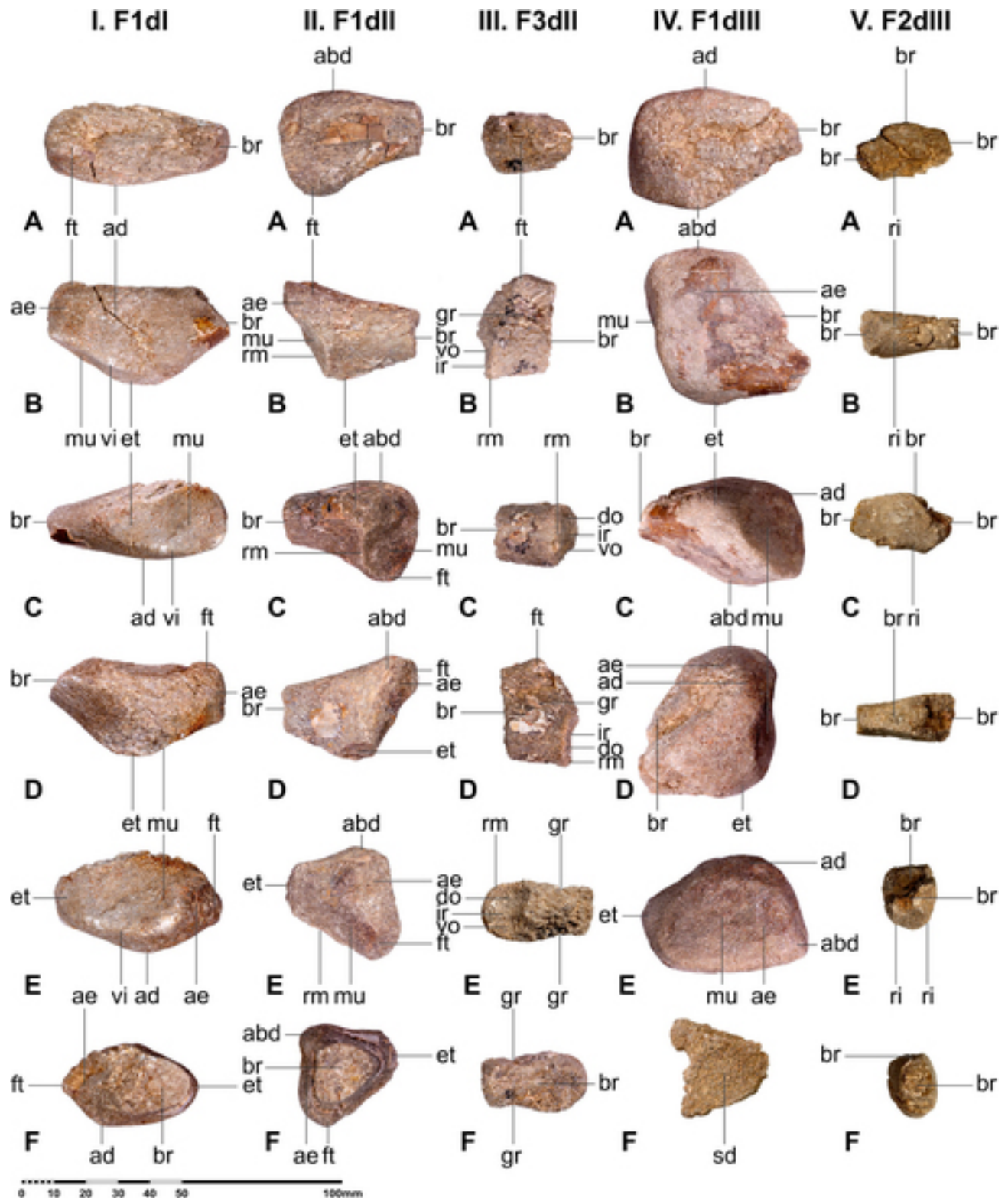
FIGURE 8. *Quetzalcoatlus northropi* left manual element photographs of **I**, first phalanx manual digit I proximal end (TMM 41450-3.7); **II**, first phalanx manual digit II proximal end (TMM 41450-3.12); **III**, third phalanx manual digit II proximal end (TMM 41450-3.13); **IV**, first phalanx manual digit III proximal end and distal articulation (shown only in F) (TMM 41450-3.6); and **V**, second phalanx manual digit III shaft (TMM 41450-3.15) of holotype in **A**, anterior; **B**, ventral; **C**, posterior; **D**, dorsal; **E**, proximal; and **F**, distal views. **Abbreviations: abd**, abductor tubercle; **ad**, adductor tubercle; **ae**, anterior expansion; **br**, break; **do**, dorsal cotyle; **et,** extensor tubercle; **ft**, flexor tubercle; **FXdY**, manual phalanx X of digit Y; **gr**, groove; **ir**, intercotylar ridge; **mu**, metacarpal articulation; **ri**, ridge; **rm**, rim; **vi**, ventral rim; and **vo**, ventral cotyle. Scale bar equals 100 mm.
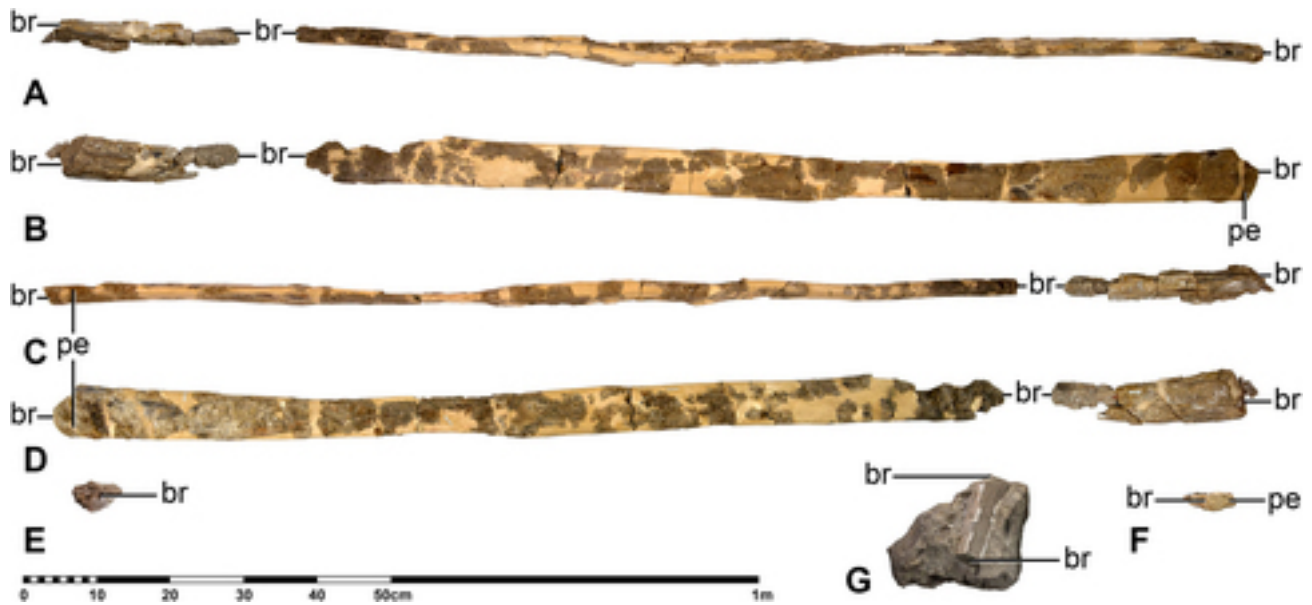
FIGURE 9. *Quetzalcoatlus northropi* left first wing phalanx proximal end and shaft of holotype (TMM 41450-3.10) photographs in **A**, anterior; **B**, ventral; **C**, posterior; **D**, dorsal; **E**, proximal; and **F**, distal views; as well as **G**, *Quetzalcoatlus* cf. *northropi* right first wing phalanx proximal end (TMM 41398-4) in ventrodistal view. **Abbreviations: br**, break; and **pe**, posterior expansion. Scale bar equals one meter.

Article 23.2) and over 45 years of use of this species name in the literature. To promote stability and universality, and avoid confusion in the literature, an application was submitted to the International Commission on Zoological Nomenclature (Case 3728: Andres et al., 2017) to use its plenary power to attribute authorship of *Quetzalcoatlus northropi* to Lawson (1975b) (ICZN Article 81.1). Specifically, they were petitioned to deem *Quetzalcoatlus* and *northropi* as available names even though they do not satisfy the criteria of ICZN Article 13.1. The generic name *Quetzalcoatlus* was established for the single species *northropi*, and so by making Lawson (1975b) available, *northropi* would become its type species by monotypy (ICZN Article 68.3). In Opinion 2440, the International Commission on Zoological Nomenclature approved Case 3728, conserving the binomen *Quetzalcoatlus northropi* by ruling that *Quetzalcoatlus* and *northropi* are available names and take authorship from Lawson (1975b) from now on (ICZN, 2019).

DESCRIPTION

Forelimb

The wing of pterosaurs consists of a robust humerus, a forearm of an elongated radius and ulna (higher aspect ratio), a carpus of fused proximal and distal syncarpals with a medial carpal and pteroid, a metacarpus of an enlarged metacarpal IV (wing metacarpal) and reduced metacarpals I–III (manual metacarpals), manual digits I–III (clawed digits), and the four phalanges of manual digit IV (wing digit). The holotype of *Quetzalcoatlus northropi* (TMM 41450-3) includes elements from all of these regions in the left wing but is missing the medial carpal, pteroid, metacarpals I–II, most of the manual phalanges, and fourth wing phalanx. Lawson (1972) reported an ulna and a radius in the original description, but he only described the ulna and labeled what appears to be the radius as the ulna in his plate VII, fig. 4. An isolated left ulna proximal end (TMM 44036-1) is referred to *Q. northropi*, and a right first wing phalanx proximal end (TMM 41398-4) is identified as cf.

northropi. There are no traces of ossified tendons in the forelimb of *Quetzalcoatlus*, as reported in nyctosauromorphs (Williston, 1903:152; Bennett, 2003:63; Frey et al., 2006:21, fig. 5; Andres and Myers, 2013:11, fig. 4) sensu Andres (2021). Much of the cortical bone in this material is damaged or missing, and so the decision was made to use photographs instead of stippled line drawings for illustrating this species.

Humerus—The humerus is the stoutest bone of the pterosaur wing, with expanded proximal and distal ends. Humeri are preserved in the azhdarchiform species *R. langstoni* (Andres and Myers, 2013) and *M. minor* (Padian et al., 1995); the azhdarchid species *Q. lawsoni* (Lawson, 1975a), *H. thambema* (Buffetaut et al., 2002), *Z. linhaiensis* (Cai and Wei, 1994), *A. bostobensis* (Averianov, 2007), *C. boreas* (Hone et al., 2019), *M. maggii* (Vullo et al., 2018), and *A. lancicollis* (Nesov, 1984); the putative azhdarchid specimens Mechin collection n°715 (Buffetaut et al., 2006), MOR 553 (Carroll et al., 2013), RBCM.EH.2009.019. 0001A (Martin-Silverstone et al., 2016), TMP 1980.16.651, TMP 1982.16.303, TMP 1997.12.163, TMP 1991.36.374 (Godfrey and Currie, 2005), UNCUYO-LD 350 (David et al., 2018), UWPI 2349/102 (Buffetaut et al., 2011), VGI 231/4 (Averianov, 2014), YPM VPPU 002246 (Padian, 1984a), as well as undescribed specimens from Petreşti-Arini, Romania (Vremir et al., 2011) and Tran, Bulgaria (Nikolov et al., 2020).

Both *Quetzalcoatlus northropi* and *Q. lawsoni* share a tapered mid-shaft with the Pteranodontoidea, but this is taken to an extreme in *Q. northropi* (TMM 41450-3.1) where the bone is the shape of a twisted hourglass (Fig. 2). The humerus is constricted at its midpoint with a width (anteroposterior) half that of the proximal end and one-third that of the distal end (Table 2). This is exacerbated by a greatly expanded distal end (Lawson, 1975a:948) that is also about 1.5 times the width and twice the height (dorsoventral) of the proximal end. This distal expansion surpasses the previous record holder, *Tethydraco regalis* Longrich et al., 2018, which has a mid-width half that of the distal end (Longrich et al., 2018:8). The humerus is the best-preserved element in *Q. northropi*, with damage only on the posterior part of the distal end.
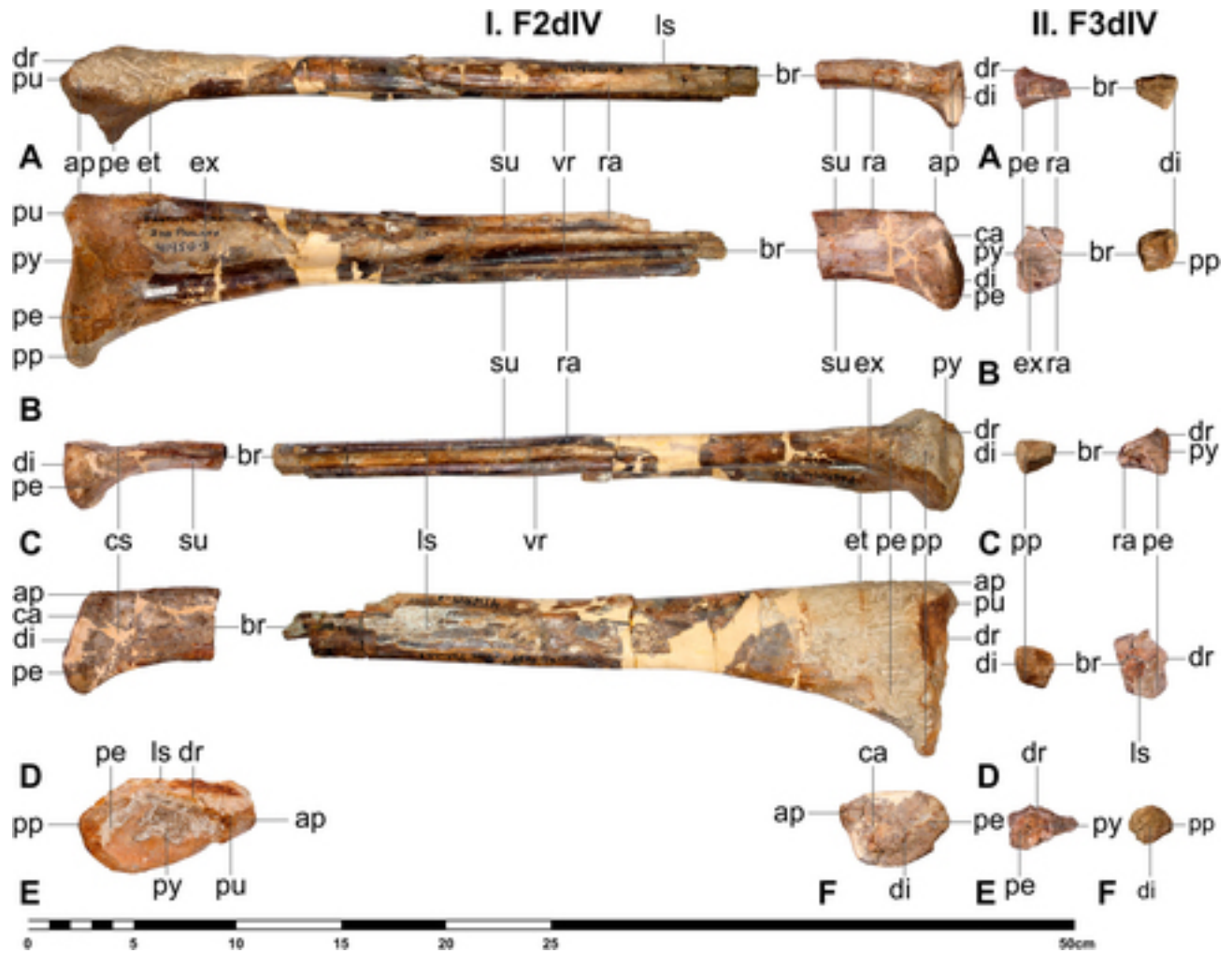
FIGURE 10. *Quetzalcoatlus northropi* wing phalanx photographs of **I.** left second wing phalanx proximal and distal ends (TMM 41450-3.11) and **II.** third wing phalanx proximal and distal ends (TMM 41450-3.14) in **A**, anterior; **B**, ventral; **C**, posterior; **D**, dorsal; **E**, proximal; and **F**, distal views. **Abbreviations: ap**, anterior point; **br**, break; **ca**, concavity; **cs**, concave surface; **di**, distal condyle; **dr**, dorsal rim; **et**, extensor tubercle; **ex**, excavation; **FXdIV**, wing phalanx X (manual phalanx X of digit IV); **ls**, flat surface; **pe**, posterior expansion; **pp**, posterior process; **pu**, proximal tubercle; **py**, proximal cotyle; **ra**, raised margin; **su**, sulcus; and **vr**, ventral ridge. Scale bar equals 50 cm.

The proximal end of the humerus is dominated by the articulation surface for the scapulocoracoid (lip of Padian, 1983a). This surface is perched on the humeral head (caput humeri of Kellner and Tomida, 2000, articular head of Sangster, 2003, or caput of Eck et al., 2011) as in all pterosaurs, but it is much larger and wraps around the head in the Azhdarchidae plus *M. minor* (Andres, 2021), described as a swollen lip in *C. boreas* (Godfrey and Currie, 2005:301), and absent in MOR 553 (Carroll et al., 2013:40). The articular surface is semicircular in proximal view, as found in other pterodactyloids but unlike the crescentic shape of more basal pterosaurs (Andres et al., 2014); the crescentic articular surface reported in *M. maggii* (Vullo et al., 2018:7) appears to be preservational. *Quetzalcoatlus northropi* shares a dorsoventrally deep articular surface with *Q. lawsoni* and *H. thambema* (Buffetaut et al., 2002:182), reaching almost two-thirds the width in *Q. northropi*. This surface is deeper anteriorly, as reported in *A. lancicollis* (Averianov, 2010:295). The articular surface can still be described as saddle-shaped (concave anteroposteriorly, convex dorsoventrally) as in all pterosaurs

(Romer, 1956; Padian, 1984b; Sereno, 1991; Bennett, 1996; Kellner, 1996). This proximal articular surface lacks the dorsal depression reported in *Pteranodon* and other pteranodontoids (Bennett, 2001a:72 and 75, fig. 73); however, this has been put forward as an ontogenetic feature (Bennett, 2001a). Absent also are a pair of dorsal and ventral depressions with a concomitant middle constriction found in *Sericipterus wucaiwanensis* Andres et al., 2010, and other rhamphorhynchid specimens. A humerus proximal end, which has been referred to *A. bostobensis* (ZIN PH 57/43) based on its location, is described as being convex in the transverse plane and flat in the horizontal plane and therefore is not saddle-shaped (Averianov et al., 2015:68). A partial humeral head (VGI 231/4) was identified as 'Ornithocheiridae gen. et sp. indet.' based on being convex in both transverse and horizontal planes (Averianov and Yarkov, 2004), but it has since been referred to the Azhdarchidae based on similarity to ZIN PH 57/43 (Averianov, 2014).

The humeral head is positioned on the long axis of the humerus, and the dorsal bowing of the head creates a large

TABLE 2. Measurements of *Quetzalcoatlus northropi* material. Values in millimeters. >, preserved value; <, maximum possible value; ~, approximate value; a-p, anteroposterior dimension; d-v, dorsoventral dimension; lat, lateral dimension; max, maximum dimension perpendicular to long axis of bone; min, minimum dimension perpendicular to long axis of bone; and p-d, proximodistal dimension. Holotype specimen in italics.

Dimension: Element: Specimen Number:	Length (p-d)	Mid-width (a-p)	Mid-depth (d-v)	Proximal articulation width (a-p)	Proximal articulation depth (d-v)	Deltopectoral crest base length (p-d)	Deltopectoral crest height (max)
Left humerus							
TMM 41450-3.1	524	71.13	88.32	145.14	91.94	158.88	164.12

	Ulnar crest base length (p-d)	Ulnar crest height (max)	Distal end width (max)	Distal end breadth (min)	Entepicondyle breadth (max)	Ectepicondyle breadth (max)
TMM 41450-3.1	122.00	71.69	225	172.58	17.91	30.45

	Length (p-d)		Mid-width (d-v)		Mid-breadth (a-p)	
Left ulna						
TMM 41450-3.3	716		42.38		45.97	
TMM 44036-1	>297		44.20		31.37	
Left radius	Length (p-d)		Mid-width (d-v)		Mid-breadth (a-p)	
TMM 41450-3.2	702		~37.34		~38.45	
Proximal syncarpal	Length (p-d)		Width (a-p)		Depth (d-v)	
TMM 41450-3.4	118.29		203		138.35	
Distal syncarpal	Length (p-d)		Width (a-p)		Depth (d-v)	
TMM 41450-3.5	129.26		188.43		145.89	
Metacarpal III	Length (p-d)		Mid-width (a-p)		Mid-depth (d-v)	
TMM 41450-3.8	>43.41		<27.18		<14.76	

Metacarpal IV	Length (p-d)	Proximal width (d-v)	Mid-width (d-v)	Mid-breadth (a-p)
TMM 41450-3.9	>604	149.63	41.61	78.85

	Length (p-d)	Mid-width (a-p)	Mid-depth (d-v)
First phalanx digit I			
TMM 41450-3.7	>52.85	21.34	16.37
First phalanx digit II	Length (p-d)	Mid-width (a-p)	Mid-depth (d-v)
TMM 41450-3.12	>55.12	16.79	15.31
Third phalanx digit II (ungual)	Length (p-d)	Base-width (a-p)	Base-breadth (d-v)
TMM 41450-3.13	>18.14	30.77	16.61
First phalanx digit III	Length (p-d)	Mid-width (a-p)	Mid-depth (d-v)
TMM 41450-3.6	>55.12	20.79	19.48
Second phalanx digit III	Length (p-d)	Mid-width (a-p)	Mid-depth (d-v)
TMM 41450-3.15	>25.24	>18.24	>19.57
Fourth phalanx digit III (ungual)	Length (p-d)	Base-width (a-p)	Base-breadth (d-v)
TMM 41450-3.16	>20.64	>18.30	>13.96
First wing phalanx	Length (p-d)	Mid-width (a-p)	Mid-depth (d-v)
TMM 41450-3.10	>1574	63.45	23.01
Second wing phalanx	Length (p-d)	Mid-width (a-p)	Mid-depth (d-v)
TMM 41450-3.11	>384.50	32.02	17.94
Third wing phalanx	Length (p-d)	Mid-width (a-p)	Mid-depth (d-v)
TMM 41450-3.14	>52.36	20.57	17.87

Quetzalcoatlus cf. *northropi*

	Total length (a-p)	Mid-width (lat)	Mid-depth (d-v)
Cervical VI			
TMM 42889-1	~440	46.32	20.29
First wing phalanx	Length (p-d)	Mid-width (a-p)	Mid-depth (d-v)
TMM 41398-4	>160.57	34.77	<26.41
Femur	Total length (a-p)	Mid-width (lat)	Mid-breadth (a-p)
TMM 41047-1	>495	47.13	26.98
TMM 41398-3	>102.01	30.79	20.14

ventral concavity beneath it (deep channel of Padian, 1983a, concave ventral area of Veldmeijer, 2003, well-marked step-like sulcus of Buffetaut et al., 2011, or intertubercular sulcus of Frey et al., 2011) as in other pterosaurs (Andres et al., 2010). This ventral concavity extends past the distal margin of the deltopectoral crest. A pair of shallow anterior and posterior fossae is on the humeral head distal to the articular surface. A small posterior fossa is reported in *Dimorphodon macronyx* (Buckland, 1829) by Sangster (2003), and a pair of shallow troughs are reported in TMP 1980.16.651 that are identified for the insertion of the M. latissimus dorsi (Godfrey and Currie, 2005:301, fig. 16.6), but these are positioned more distally. The anterior margin of the proximal articular surface terminates at a vertical flange (strong ridge of Hooley, 1913, medial lip of Padian, 1983a, acuminate point of Godfrey and Currie, 2005, moderately thin proximal flange of Bennett, 2001a, small prominence of McGowen et al., 2002, anteroventrally curving ridge or carina-like flange of Godfrey and Currie, 2005, dorsal tubercular ridge of Frey et al., 2011, or boss of Hone et al., 2019) that contacts the base of the deltopectoral crest as in other pterosaurs, except for *Elanodactylus prolatus* Andres and Ji, 2008, in which this flange is interrupted by a tubercle (Andres and Ji, 2008:455). Posterior to the vertical flange in the area between the proximal articular surface and deltopectoral crest on the ventral surface of the humeral head is a large fossa (excavation of Murry et al., 1991) containing pneumatic foramen that is

almost as large as the fossa, as in other azhdarchiforms and some other pterosaur taxa (Andres, 2021). *Quetzalcoatlus lawsoni* has a foramen in this position, but it is quite small and not positioned in a fossa. The posterior end of the proximal articular surface extends to the base of the ulnar crest. A small presumably nutrient foramen pierces the posterior surface of the humerus at the distal margin of the ulnar crest, as reported in *Jidapterus edentus* Dong et al., 2003 (Wu et al., 2017:14) and the Pteranodontia (Bennett, 2001a:73, fig. 69; Unwin, 2003; Myers, 2010:1072, figs. 2 and 3; Andres and Myers, 2013:12, fig. 4A). This is distinct from the larger pneumatic foramen found more proximally in other pterosaurs (Andres, 2021). The deep longitudinal groove identified for the insertion of the MM. deltoideus and/or teres major in *Anurognathus ammoni* Döderlein, 1923 (Bennett, 2007a:385) is not present in *Q. northropi*.

The ulnar crest (cresta medialis of Young, 1964, lateral or greater tuberosity of Padian, 1983a, medial process of Padian and Smith, 1992, posterior tuberosity of Bennett, 2001a, external tuberosity of Sangster, 2003, proximal tuberosity of the ventral tubercular ridge of Frey et al., 2011, or medial crest of Hone et al., 2019) is well developed like the rest of the Ornithocheiroidea (Andres, 2021), but it is massive and bulbous as in *Q. lawsoni*, YPM VPPU 002246 (Padian and Smith, 1992:89), and the Tran specimen (Nikolov et al., 2020:fig. 1f), surpassing the humeral shaft in width and rivaling the proximal articular surface in size in *Q. northropi*. The ulnar crest is oblong in horizontal outline and oriented ventrally as in the rest of the Azhdarchoidea (Andres, 2021), but its base is more subhorizontal so that the process curves ventrally, as in *Q. lawsoni*. This crest reaches the humerus proximal margin but is distinct from the humeral head, separated from it by a constriction (notch of Padian, 1983a, or ventro-dorsal constriction of David et al., 2018). The ulnar crest does not extend proximally as a distinct process, which has been reported in *C. boreas* (Hone et al., 2019:9).

The long, massive, and rectangular deltopectoral crest (deltoid crest of Hooley, 1913, or deltoid process of Young, 1964) of *Q. northropi* is longer than in other pterosaurs (Lawson, 1975a:948). This crest is present farther down the shaft on the anterior margin of the humerus (Averianov, 2010), a position shared with other azhdarchids as well as some *Darwinopterus* and nyctosauromorph species (Andres, 2021). This is a long, almost parallel-sided process that is longer than its base (proximodistal) length and oriented perpendicular to the humeral long axis as in other azhdarchoids (Andres, 2021). It lacks the middle constriction found in nyctosaurids and rhamphorhynchids (Andres, 2021). The apex of the deltopectoral crest is slightly thicker, as in MOR 553 and YPM VPPU 002246 (Carroll et al., 2013:40), but not as bulbous as in *D. macronyx*, *Dorygnathus banthensis* (Theodori, 1830), and *Rhamphorhynchus muensteri* Goldfuß, 1831 (Padian and Wild, 1992) or broadly expanded/thickened as in pteranodontoids (Longrich et al., 2018); although it is described as more greatly expanded than in *C. boreas* (Hone et al., 2019:8). The base of the deltopectoral crest extends for about 30% of the total humerus length. The entire crest is oriented nearly straight ventroanteriorly (i.e., on the ventral side of anteroventrally), with a flat anterior margin and a concave posterior margin, as in *H. thambema* (Witton and Habib, 2010:fig. 1B) but unlike the posteroventrally curved crests of *Q. lawsoni*, *Z. linhaiensis* (Cai and Wei, 1994:186), *A. lancicollis* (Averianov, 2010:295), and most pterosaurs. *Quetzalcoatlus northropi* lacks the warped deltopectoral crest of the pteranodontoids (Andres, 2021). The only twisting present is along the distal margin of the crest so that it has a slight clockwise torsion looking down the process, giving it a 'torted' aspect as described in YPM VPPU 0022446 (Padian and Smith, 1992:87) and *C. boreas* (Hone et al., 2019:8). A shelf on the anterior end of the proximal surface of the

deltopectoral crest extends down the crest, which appears to be present in YPM VPPU 002246 (Padian and Smith, 1992:fig. 1). A midline ridge is present on the posterior surface of the deltopectoral crest as in *M. minor* (McGowen et al., 2002:5) and may be analogous to the ventral pillar described by Longrich et al. (2018).

The shaft of the humerus of *Q. northropi* is straight as in the rest of the Eupterodactyloidea (Andres, 2021). It is constricted in a horizontal plane just distal to the deltopectoral crest as in the pteranodontoids, with a circular cross-section as in *Pteranodon* (Bennett, 2001a), as opposed to D-shaped as in *H. thambema* (Buffetaut et al., 2003:97) and *Q. lawsoni*, or triangular as in *A. lancicollis* (Averianov, 2010:295). A low but wide rise of bone extends from the deltopectoral crest to the ulnar condyle (ulnar condyle and trochlea ulnaris of Padian, 1983a, trochlea of Bennett, 2001a, ulnar trochlea of Sangster, 2003, ventral condyle of Eck et al., 2011, or medial condyle of Murry et al., 1991) that is likely homologous to a ridge between the deltopectoral crest and the supracondylar process reported in *D. macronyx* (Padian, 1983a:14) and *A. lancicollis* (Averianov, 2010:295). This rise forms the posterior margin of a distinct triangular fossa (fovea supratrochlearis ventralis of Padian, 1983a, fossa proximal to distal condyles of Murry et al., 1991, or deep fossa of Andres and Myers, 2013) proximal to the distal condyles of the humerus. This fossa is not divided into pits proximal to the distal condyles as in *Istiodactylus latidens* (Seeley, 1901) (Hooley, 1913:386). The anterior margin of the triangular fossa is formed by a massive supracondylar process (Averianov, 2010) (epiphysis overlapping the shaft of Hooley, 1913, lateral supracondyloid process and processus supracondyloideus lateralis of Padian, 1983a, b, tuberculum supracondyleum laterale of Wellnhofer, 1985, or lateral supracondylar process of Sangster, 2003) that is triangular in anterior view and continues distally as a ridge to the ectepicondyle (lateral epicondyle and epicondylus lateralis of Padian, 1983a). Supracondylar processes are reported in other pterosaurs and identified as the origin for the supinator muscle (Bennett, 2001a), but it is quite prominent in azhdarchids (Andres and Myers, 2013) and nyctosaurids (Longrich et al., 2018). *Simurghia robusta* Longrich et al., 2018, has a large and triangular supracondylar process (Longrich et al., 2018:14, fig. 10), but this is smaller than in *Q. northropi* even considering its size. Another longitudinal ridge extends parallel and posterior to this process, identified as a muscle scar in *Anhanguera spielbergi* Veldmeijer, 2003 (Veldmeijer, 2003:81, fig. 15), delineating a small sulcus between the two. A similar but shallower sulcus and ridge extends longitudinally posterior to the rise between deltopectoral crest and ulnar condyle, as reported in *M. minor* (McGowen et al., 2002:5), *I. latidens* (Hooley, 1913:386), and *D. macronyx* (Padian, 1983a:14).

The triangular fossa extends around the radial condyle (trochlea for the radius of Young, 1964; trochlear joint of Hooley, 1913; radial condyle and trochlea radialis of Padian, 1983a; lateral condyle, radial condyle, or radial trochlea of Padian, 1983b; capitulum of Bennett, 2001a; capitellum of Sangster, 2003; capitulum radialis of Dalla Vecchia, 2009; or dorsal condyle of Eck et al., 2011) on the anterior surface. Pneumatic foramina are present on the dorsal and ventral margins of the radial condyle in this fossa. The dorsal foramen is the larger of the two and pierces the dorsoproximal (i.e., on the dorsal side of proximodorsal) surface of the condyle as in *Q. lawsoni*, *M. minor* (McGowen et al., 2002:6, fig. 2C), *I. latidens* (Hooley, 1913:386), CMN 50814 (Rodrigues et al., 2011:155, fig. 7A), and an undescribed tapejarid MN 6505-V (Rodrigues et al., 2011:156). Pneumatic foramina positioned proximal to the radial condyle have been reported in *Barbaridactylus grandis* Longrich et al., 2018 (Longrich et al., 2018:19) and USNM 11925, which was previously named "*Bennettazhia oregonensis*"

(Bennett, 2018a). The more ventral foramen appears deeper and lies at the proximal end of the intercondylar sulcus as found in *Q. lawsoni*, *B. grandis* (Longrich et al., 2018:19), USNM 11925, CMN 50814 (Rodrigues et al., 2011:155, fig. 7A), and MN 6505-V (Rodrigues et al., 2011:156), but not directly between condyles as found in the pteranodontids *Pteranodon* (Bennett, 2001a:75, fig. 69) and *T. regalis* (Longrich et al., 2018:8, fig. 2A). A deep longitudinal groove on the posterior surface of the distal end (sulcus anconaeus medialis of Wellnhofer, 1985, or shallow trough for the passage of M. triceps brachii of Longrich et al., 2018) reported in *Anhanguera* (Wellnhofer, 1985:fig. 8f; Bennett, 2001b:fig. 121) is not preserved in *Q. northropi*, but the distal end of the posterior surface is damaged. The prominence in the middle of the posterior surface of the distal end (large bulbous swelling of McGowen et al., 2002, or much inflated median area of Hooley, 1913) is flat topped, as opposed to a bulbous swelling in *M. minor* (McGowen et al., 2002:7) or a distinct apex in the ornithocheiromorphs (Hooley, 1913:386, pl. 39 fig. 3; Wellnhofer, 1985:fig. 7f; Kellner and Tomida, 2000:fig. 32d; Veldmeijer, 2003:fig. 15F; Elgin, 2014:fig. 2.10).

The radial condyle is larger and is positioned more proximally on the anterior surface as part of the deflection of the humerus distal end in pterosaurs. It is a broad oval in outline and lacks the crescentic or semicircular outline of *A. lancicollis* but has a dorsal fovea as in *A. lancicollis* (Averianov, 2010:296, fig. 24A) and *M. minor* (McGowen et al., 2002:6, fig. 2C), mistakenly identified as the fovea supratrochlearis ventralis (triangular fossa in the present contribution) in these taxa. This fovea connects to the foramen on the dorsal surface of the radial condyle in *M. minor* (McGowen et al., 2002:6, fig. 2C), but these are separated in *Q. northropi*. The radial condyle distal surface is flat for articulation with the ulna dorsal cotyle as in other pterosaurs (Hooley, 1913; Bennett, 2001a). The smaller ulnar condyle is more present on the distal surface and extends more distally as the other part of the distal end deflection. It lacks the prominent groove found in *A. lancicollis* (Averianov, 2010:296, fig. 24A), but there is a thin ridge in this region in *Q. northropi*. The ventral supracondylar tubercle (medial supracondyloid tubercle and tuberculum supracondyloideum mediale of Padian, 1983b, tuberculum supracondyloideum mediale of McGowen et al., 2002, medial supracondylar tuberculum of Sangster, 2003, or the tuberculum supracondyloideum ventralis of Averianov, 2010) ventral to the ulnar condyle reported in *A. lancicollis* (Averianov, 2010:297, fig. 24A), *M. minor* (McGowen et al., 2002:6, fig. 2C), and *D. macronyx* (Padian, 1983a:14, fig. 10C) is not preserved in *Q. northropi*, but the region where it would occur is damaged and filled with plaster. The distal condyles have their long axes perpendicular to one another such that the radial condyle is oriented proximoventrally and the ulnar condyle is oriented dorsoproximally, unlike the parallel distal condyles of *Pteranodon* (Bennett, 2001a:73–74) and *Q. lawsoni*. These distal condyles are large, constituting most of the distal end, unlike the smaller or more centrally located condyles of *A. lancicollis* (Averianov, 2010:296, fig. 24A).

The present work follows Andres and Myers (2013) in considering the associated prominences and raised ridges (ridges for muscular attachment of Padian, 1983b) of the distal end as the epicondyles. These epicondyles lack the flares (Andres et al., 2010:176) or projections (Longrich et al., 2018:9) found in non-azhdarchoid pterosaur humeri. The entepicondyle (medial epicondyle and epicondylus medialis of Padian, 1983b, or ventral epicondyle of Frey et al., 2011) is damaged but appears to be similar to the smaller bump-like prominence at the posteroventral corner of the humerus distal end in *Q. lawsoni*, *A. lancicollis* (Averianov, 2010:297, fig. 24C), as well as CMN 50814 and MN 6505-V (Rodrigues et al., 2011:fig. 8). *Radiodactylus langstoni* also has a smaller bump-like

entepicondyle but it is positioned in the middle of the ventral surface (Andres and Myers, 2013:fig. 3F). The entepicondyle in *Q. northropi* differs from those of *Q. lawsoni* and most pterosaurs in being dorsoventrally wider than the ectepicondyle (Andres, 2021). The ectepicondyle is a low protuberance mainly confined to a large ectepicondylar ridge, which is appressed to the radial condyle with a sulcus (groove for passage of extensor tendons of Padian, 1983b, extensor tendon groove of Murry et al., 1991, or deep groove of Sangster, 2003) extending between the two as in other azhdarchiforms (Averianov, 2010:296–297; Andres and Myers, 2013:390). The ectepicondyle constitutes most of the dorsal surface of the humerus distal end and terminates in a proximally curving hook at its anterior end as in *Q. lawsoni*. The epicondyles are not sufficiently preserved to ascertain if there were pits (small round depressions of Averianov, 2010, or divots of Andres and Myers, 2013) on their outer surfaces as reported on the ectepicondyle of YPM VPPU 022446 (Padian, 1983b:518).

The distal end of the humerus is rectangular in outline as in other azhdarchoids (Andres, 2021) largely due to the shape of these epicondyles. The long axis of the distal end is rotated with respect to the long axis of the humeral head as in all pterosaurs (Padian, 1991), about 45° in *Q. northropi*. The ventral margin of the distal end extends more distally than the dorsal margin, creating the distal deflection of the humerus as in other pterosaurs. The intercondylar sulcus (valley for the ulnar ridge of Young, 1964, intertrochlear valley of Padian, 1983a, vallis intertrochlearis of Padian, 1983b, intertrochlear incision of Sangster, 2003, or intertrochlear sulcus of Averianov, 2010) reaches onto the distal surface. The distal surface consists of the distal condyles anteriorly and a distal fossa (valley on the distal end of the humerus and valley for the ulna ridge of Hooley, 1913, crescentic pit and humeral pit of McGowen et al., 2002, deeply cutting incision of Sangster, 2003, crescentic depression of Averianov, 2010, depressed middle part of Rodrigues et al., 2011, or olecranon fossa of Longrich et al., 2018) that is present in all but the most basal pterosaurs. This distal fossa has been mostly filled in with plaster, but part of the fossa is visible posterior to the radial condyle. It is not known if there are pneumatic foramina present in the area filled by plaster. A large distal tubercle (tubercle of the ulnar condyle of the humerus of Hooley, 1913, subconical tubercle of Bennett, 2001a, small point of McGowen et al., 2002, articular process of humerus of Godfrey and Currie, 2005, or ulnar tubercle of Averianov, 2010) is present at the end of a anteroventrally oriented crest (prominence of McGowen et al., 2002, short ridge of Averianov, 2010, or bony ridge of Rodrigues et al, 2011). Distal tubercles have been reported in azhdarchids (Godfrey and Currie, 2005:fig. 16.6G; Averianov, 2010:296, fig. 24C) plus *M. minor* (McGowen et al., 2002:6) and pteranodontids (Bennett, 2001a:73, figs. 69 and 74; Longrich et al., 2018:9, fig. 2D). The crest contacts a short dorsal lip (upper ridge of Hooley, 1913, or ridge encircling the radial side of the crescentic pit of McGowen et al., 2002) that then circles around to contact the radial condyle. This encircled area is filled with plaster in the holotype of *Q. northropi* and so the presence of a crescentic pit, foramen, or transverse groove (groove of McGowen et al., 2002, or vertical groove of Andres and Myers, 2013) is unknown. The humerus distal epiphyses appear to be fused in the holotype of *Q. northropi*.

Ulna—The forearm of pterosaurs is much longer and slimmer than the humerus but is still one of the more robust regions of the wing. The ulna dominates this region with expanded proximal and distal ends encompassing both the distal condyles of the humerus and three proximal articulation surfaces on the proximal syncarpal, respectively. Ulnae from two specimens of *Q. northropi* have been collected and can be referred to the same species based on the same autapomorphies. TMM 41450-3.3 is a

complete left ulna from the holotype (Fig. 3I), although it is missing cortical bone from its proximal end, and TMM 44036-1 is a proximal end and part of the shaft of a left ulna from a smaller individual but still a giant pterosaur from the TMM 44036 locality (Fig. 3II). TMM 41450-3.3 was collected as surface fragments in the talus and reassembled in the laboratory. As restored, the specimen consists of two almost equal longitudinal segments joined by a narrow midsection. This midsection is currently filled in with plaster except a portion of the ventral end. This gap represents a thin-section of the bone taken in this region. The thin-section demonstrates that this cross-section was originally complete bone, and so the mid-width (dorsoventral) and breadth (anteroposterior) dimensions were measured on this slide (Table 2). In pterosaurs, the ulna is slightly longer than the radius, and in TMM 41450-3 the restored ulna is 14 mm longer than the complete radius. The measured length of 716 mm for TMM 41450-3.3 is therefore put forward as accurate. Fortunately, TMM 44036-1 preserves most of the missing bone of the TMM 41450-3.3 proximal end, and vice-versa, confirming the great constriction of the shaft.

Ulnae are reported in the azhdarchiform species *M. minor* (Padian et al., 1995); the azhdarchid species *Q. lawsoni* (Padian, 1984a), *A. philadelphiae* (NHMUK PV R 9228) (Bennett, 2001a), ?*Arambourgiania* (FSAC-OB 203) (Longrich et al., 2018), *Z. linhaiensis* (Unwin and Lü, 1997), *C. boreas* (Hone et al., 2019), possibly *M. maggii* (Vullo et al., 2018), and *A. lancicollis* (Nesov, 1984); as well as the putative azhdarchid specimens CCMGE 1/12671 (Averianov, 2014), NZGS CD 467 (Wiffen and Molnar, 1988), SMP VP-1853 (Sullivan and Fowler, 2011), WAM 60.57 (Bennett and Long, 1991), ZIN 56/43 (Averianov et al., 2015), and ZIN 58/43 (Averianov, 2014). Antebrachial material is reported in MOR 553, but it is not specified whether this includes ulnae or radii (Carroll et al., 2013).

The ulna in pterosaurs varies in length from just over the length of the humerus to almost twice its length (Andres, 2021). At 1.36 times the length of the humerus, the ulna of *Q. northropi* is relatively shorter than the 1.42 average of pterosaurs and the 1.52 of *Q. lawsoni* and other azhdarchiforms (Andres, 2021). The middle constriction and expansion of the terminal ends of the ulna exceeds that of the humerus and all other pterosaur ulnae, contrasting with the almost constant width of FSAC-OB 203 (Longrich et al., 2018:fig. 15). The shaft is a third of the width and breadth of the ends, approaching one-fifth of the width in TMM 41450-3, much less than the 60% width constriction reported in *A. lancicollis* (Averianov, 2010:298) and surpassing the previously suggested record of 50% in cf. *T. regalis* (FSAC-OB 199) (Longrich et al., 2018:9) or *Aurorazhdarcho primordius* Frey et al., 2011 (Frey et al., 2011:S45). The ulna differs from the humerus in maintaining the constriction along much of the length of the shaft, about half the length of the entire bone, unlike the more gradual expansion of the ulna distal end in *Q. lawsoni*. The proximal end is expanded both dorsoventrally and anteroposteriorly, but predominantly the former, whereas the distal end is expanded almost exclusively dorsoventrally. In *A. lancicollis* (Averianov, 2010:298, fig. 25), *Pteranodon* (Bennett, 2001a:76–77, fig. 75), and other pterosaurs, both ends of the ulna have ventral expansions. However, these expansions are not symmetrical in *Q. northropi*. The proximal end is more dorsally expanded, whereas the distal end is more ventrally expanded, opposite to the condition reported in *J. edentus* (Wu et al., 2017:14). The shaft has a slight posterior bend in the horizontal plane as in other pterosaurs, previously described as a posterodorsal curvature (Bennett and Long, 1991:442; Bennett, 2001a:79). The asymmetrical expansions result in a significant dorsal deflection of the shaft towards the distal end so that the shape of the entire bone is slightly sinusoidal in the transverse plane, possibly similar to the slightly curved shaft of SMP VP-1853 (Sullivan and Fowler, 2011:395, fig. 6).

The proximal end is substantially convex posteriorly such that the ulna has a semicircular proximal outline as in *Q. lawsoni*, the ?azhdarchid specimen WAM 60.57 (Bennett, 1991:437), and *Tapejara wellnhoferi* Kellner, 1989 (Eck et al., 2011:287) as opposed to the more triangular outline of *Pteranodon* (Bennett, 2001a:76), *I. latidens* (Hooley, 1913:387), and *M. minor* (McGowen et al., 2002:6). The posterior half of the proximal surface is taken up by a large oblong fossa (shallow concavity of Hooley, 1913, circular pit of Hooley, 1914, caudal depression of Kellner and Tomida, 2000, or ovoid depression and deep proximal cavity of Godfrey and Currie, 2005) visible in TMM 44036-1 and visible at its ventral end in TMM 41450-3.3. The fossa contacts a blunt and rounded olecranon (tuberosity for the insertion of M. triceps brachii of Bennett and Long, 1991, crest for insertion of M. triceps brachii of Bennett, 2001a, large humped ridge and olecranon process of McGowen et al., 2002, prominent ventral process and olecranon process of Sangster, 2003, olecranon-like process of Dalla Vecchia, 2009, or anconeal process of Frey et al., 2011) in the center of the posterior margin that gives the proximal end of the ulna its semicircular outline. More dorsally positioned olecranons are found in *Pteranodon* (Bennett, 2001a:fig. 74) and *S. wucaiwanensis* (Andres et al., 2010:176, fig. 6C), but there is an eminence dorsal to the olecranon identified here that could possibly be or be part of the olecranon. The epiphysis at the proximal articulation of the ulna reported in *Anhanguera piscator* Kellner and Tomida, 2000 (Kellner and Tomida, 2000:55, figs. 33–34) and in BSPG 1980 I 122 (Wellnhofer, 1985:fig. 18c and e), cannot be seen as a separate element in either specimen of *Q. northropi*, and was presumably fused if present. However, it remains a remote possibility that the damaged and plaster-filled proximal fossa of the holotype represents a missing epiphysis.

The proximal cotyles of the ulna (trochlear notch of Frey et al., 2011) for articulation with the distal condyles of the humerus are massive, rounded, projected above the shaft, and oriented proximoanteriorly, as reported in *Dsungaripterus weii* Young, 1964 (Bennett, 2001a:77). As a result, these cotyles have prominent lips at their anterodistal margins (expanded portion of the proximal shaft of Padian and Wild, 1992), different from the coronoid ridge divided into dorsal and ventral tubercles (dorsal and ventral glenoidal tuberosities of Frey et al., 2011) by a shallow sulcus reported in *A. primordius* (Frey et al., 2011:S44). The dorsal expansion of the proximal end is due in part to a very large and ovoid dorsal cotyle (lateral condyle of Bennett, 1991, capitular cotyle of Bennett, 2001a, radial facet of McGowen et al., 2002, or lateral cotyle of Frey et al., 2011) for articulation with the radial condyle of the humerus. This cotyle is half complete in TMM 41450-3.3, but the shape is confirmed by a more complete example in TMM 44036-1. It extends dorsally as a process (flat/flattened tubercle of McGowen et al., 2002) as in other azhdarchids (Bennett and Long, 1991:fig. 3; McGowen et al., 2002:7, fig. 2E; Godfrey and Currie, 2005:fig. 16.7; Averianov, 2010:fig. 25) and is projected anteriorly above the shaft by about half its breadth. Its articular surface is oriented more proximally and has a very distinct rim in *Q. northropi*. The dorsal and ventral cotyles do not overlap vertically, unlike in *Q. lawsoni*. The ventral cotyle (medial condyle of Bennett, 1991, ulnar facet of Padian and Wild, 1992, trochlear cotyle of Bennett, 2001a, or ulna facet and fossa of McGowen et al., 2002) appears to be smaller than the dorsal cotyle and is seated entirely on the ventral expansion (rugose expansion ventral to the trochlear cotyle for collateral ligaments or expansion for collateral ligaments of Bennett, 2001a; crest for insertion of collateral ligaments of Averianov, 2010; 'oval area in relief on the ventro-proximal part of the ulna' of Dalla Vecchia, 2014; or ventral process, ventral crest, and long low flange of Longrich

et al., 2018). The ventral cotyle is incomplete in both *Q. northropi* specimens but appears to be more elongate proximodistally and terminates in a prominence (V-shaped ridge and transverse ridge of Hooley, 1913, knob of Padian and Wild, 1992, ulnar facet prominence of McGowen et al., 2002, or narrow ridge of Godfrey and Currie, 2005) like other azhdarchids (McGowen et al., 2002:7, fig. 2E; Averianov, 2010:fig. 25). McGowen et al. (2002:6–7) reported a small tubercle proximal to the ventral cotyle in *M. minor* and *Q. lawsoni* and suggested that it is a bony stop for hyperextension, but this appears to be what they later referred to as the ventral cotyle prominence (McGowen et al., 2002:7). The ventral cotyle is inclined distally such that its articular surface is oriented anteroproximally (e.g., on the anterior side of proximoanteriorly). These cotyles are concave, unlike the saddle-shaped dorsal cotyle in *A. lancicollis* (Averianov, 2010:298) and *C. boreas* (Godfrey and Currie, 2005:302), or the convex ventral cotyle articular surface of *A. lancicollis* (Averianov, 2010:298). The ulnar (ventral) condyle of the humerus in *A. lancicollis* has a prominent groove (Averianov, 2010:296), and so the reported convexity of its ventral cotyle is more likely a ridge that articulates with this groove, and also likely corresponds to the slight diagonal ridge reported in WAM 60.57 (Bennett and Long, 1991:437, fig. 3) and a weak ridge running along the cotyle reported in an undescribed proximal ulna (NHMUK PV R 9228) suggested to belong to *Arambourgiania* (Bennett and Long, 1991:441; Bennett, 2001a:78–79). *Quetzalcoatlus northropi* does not have a ridge preserved on its ventral cotyle, but the ventral cotyles of both specimens are not complete. A strong intercotylar crest (ulnar ridge of Young, 1964, triangle tuberosity of Godfrey and Currie, 2005, or ridge of Veldmeijer, 2003) is present on the proximal end of the anterior surface, becoming a knob-like protuberance on the proximal surface.

There are no traces of foramina, ridges, grooves, or rugosities on the proximal end of the ulnae anterior surfaces, but the area in which they would occur is missing or covered by plaster and so may or may not have been originally present. The biceps tubercle for the insertion of M. biceps brachii (Bennett, 2001a:76) is visible on TMM 44036-1 distal to the cotyles at the level of the intercotylar crest. It is damaged on its proximal and distal margins and so it is not possible to ascertain its length, but it is a robust prominence that is longer than wide. This tubercle does not appear to be divided by a groove as in *Pteranodon* (Bennett, 2001a:76, fig. 74) and *A. lancicollis* (Averianov, 2010:298) or by a pneumatic foramen as in *A. piscator* (Kellner and Tomida, 2000:57). The ulnar shaft is straight and parallel-sided up to the abrupt expansion at the distal end, similar to SMP VP-1853 (Sullivan and Fowler, 2011:395, fig. 6) and differing from the gradual distal expansion in pteranodontids (Longrich et al., 2018) and *Q. lawsoni*. The shaft cross-section is circular as in BSPG 1982 I 89 and 90 (Veldmeijer, 2003:83 and 88) and *D. macronyx* (Sangster, 2003:66), unlike the oval/suboval cross-section of many if not most pterosaurs including most *Q. lawsoni* specimens. Attachments for an interosseous membrane reported in *Pteranodon* (Bennett, 2001a:76), *A. spielbergi* (Veldmeijer, 2003:83), and *A. lancicollis* (Averianov, 2010:298) or the flexors and extensors of the carpus and manus reported in *Pteranodon* (Bennett, 2001a:76) cannot be seen in *Q. northropi*, but this region is poorly preserved in both specimens.

The distal end of the ulna consists of a large ventral expansion comprising half of its vertical width (prominent but short ventral ridge and projecting ridge of Wiffen and Molnar, 1988, thin crest of Padian and Wild, 1992, ventral crest of Kellner and Tomida, 2000, ventral surface expanded and rugose for the attachment of ulnar collateral ligaments of Bennett, 2001a, ventral ridge of Kellner et al., 2003, prominent

ridge of Sullivan and Fowler, 2011, ventral collateral tubercle of Eck et al., 2011, or flange of Dalla Vecchia, 2019). It is confined to the distal quarter of the ulna instead of the distal half in *Q. lawsoni*. This expansion has a flat anterior surface for articulation with the radius and a convex posterior surface giving the distal surface a crescentic outline similar to SMP VP-1853 (Sullivan and Fowler, 2011:395), but unlike the semicircular outline of *S. wucaiwanensis* (Andres et al., 2010:176) and basal pterosaurs, the parallelogram outline of DGM 529-R and BSPG 1980 I 122, the triangular outline of NZGS CD 467 (Wiffen and Molnar, 1988:55), or the L-shaped outline of *D. weii*, *I. latidens*, as well as BSPG 1982 I 89 and 1980 I 121 (Wiffen and Molnar, 1988:55). Although partially filled in with plaster, there is a massive sulcus in the middle of the anterior surface of the distal end. Where this sulcus reaches the distal surface, there is a notch in the distal outline in anterior/posterior view between the distal tuberculum and dorsal articular surface, like the notch reported in FSAC-OB 203 (Longrich et al., 2018:23), but this area is damaged and filled with plaster, and so it is not possible to say whether the notch was original. However, a distal sulcus and notch appear to be present in *M. minor* (McGowen et al., 2002:fig. 2E) and is likely responsible for it being described as divided into anterior and posterior tubercles distally (McGowen et al., 2002:7), although this could be the result of damage to the distal end as well (Averianov, 2010). Eck et al. (2011:fig. 7 pl. 2) figures *T. wellnhoferi* with dorsal and ventral condyles separated by a carpal trochlea and a pneumatic foramen, but the distal surface is only described as poorly preserved in the text (Eck et al., 2011:287). In *Q. northropi*, there also appears to be a plaster-filled posterior sulcus, creating a constriction in the distal outline, which is reported in NZGS CD 467, BSPG 1980 I 121, and *D. weii* (Wiffen and Molnar, 1988:55, fig. 2). The dorsal portion of the anterior surface has a longitudinal flexor tendon groove (elongated concavity of Hooley, 1913, shallower groove of Padian and Wild, 1992, groove for flexor tendon of Bennett, 2001a, deep U-shaped groove of Sangster, 2003, or 'groove' of Dalla Vecchia, 2014) flanked by a pair of ridges. Dorsally, there is a ventrally curving crest (sharp crest of Wiffen and Molnar, 1988, rugose crest that may have anchored a retinaculum of the flexor tendon of Bennett, 2001a, crest of Dalla Vecchia, 2009, or distinct ridge of Averianov, 2010) and ventrally there is a rugose ridge (rugose crest that may be the origin of the M. pronator quadratus of Bennett, 2001a, longitudinal ridge of Averianov, 2010, 'wing-shaped crest' of Dalla Vecchia et al., 2014, or broad flattened and wing-like crest of Dalla Vecchia, 2019). The posterior surface is damaged and filled with plaster so it is not possible to identify if posterior pneumatic foramina were present on the distal end. A low tubercle can be seen on the proximoventral end of the ventral expansion posterior surface. This tubercle appears to be present and larger in *A. lancicollis* (Averianov, 2010:fig. 25) and is described as a narrow patch and a muscle scar in SMP VP-1853 by Sullivan and Fowler (2011), although they label it as present on the anterior surface in their Figure 6. The rest of the anterior aspect of the ventral expansion is a convex rounded surface (convex bulbous prominence of McGowen et al., 2002), unlike the concave surface of *A. lancicollis* (Averianov, 2010:300), the broad groove of *D. banthensis* to receive the radius (Padian and Wild, 1992:72), or the longitudinal ridge reported in *I. latidens* (Hooley, 1913:388, pl. XXXIX, fig. 6). The three nutrient foramina reported on the dorsal surface of the distal end in *M. minor* (McGowen et al., 2002:7) could not be located in *Q. northropi*.

All three distal articular surfaces with the proximal syncarpal found in pterosaurs are preserved: the dorsal articular surface (articular surface on the shaft of the ulna of Hooley, 1913,

short tubercle of Padian and Wild, 1992, or trochanter on external face of Padian, 2008a), distal tuberculum (tubercle and oval convex condyle of Hooley, 1913, hemispherically convex tuberculum of Wiffen and Molnar, 1988, smaller tubercle of Padian and Wild, 1992, small prominence on posterior side of posterior tubercle of McGowen et al., 2002, small tubercle of Dalla Vecchia, 2009, or distinct tubercle of Andres et al., 2010), and ventral fovea (circular pit and deep circular basin-shaped pit of Hooley, 1913, or fovea carpalis of Wiffen and Molnar, 1988). A piece of the dorsal articular surface from the ulna remains adhered to the proximal syncarpal (TMM 42450-3.4, Fig. 5). This dorsal articular surface curves from the anterior surface over the distal end and onto the posterior surface of the ulna, as in *Pteranodon* (Bennett, 2001a:77, fig. 76) and *A. lancicollis* (Averianov, 2010:298, fig. 25). This articular surface projects greatly above the shaft in *Q. northropi*, the Dsungaripteridae (Bennett, 2001a:78), and *I. latidens* (Hooley, 1913:pl. XXXIX, fig. 7C). It is crescentic in distal outline, unlike the circular facet described in *I. latidens* (Hooley, 1913:388 and 390, pl. XXXIX, fig. 6). Only the posterior portion of the distal tuberculum is preserved at the posterior margin of the distal end, ventral to the midline of the ulna as in other azhdarchoids (Andres, 2021). This tuberculum is dorsoventrally broad as in other azhdarchids (Godfrey and Currie, 2005:fig. 16.7; Averianov, 2010: fig. 25; Longrich et al., 2018:23). The ventral fovea is a large vertical oval positioned posteriorly on the distal end. The distal end of the ventral expansion terminates in a convex rounded surface termed here the styloid prominence (distoventral styloid process of Frey et al., 2011, and possibly the posterior tubercle of McGowen et al., 2002).

TMM 44036-1 is a proximal end and part of the shaft of a left ulna (Fig. 3II). It is the only specimen besides the holotype that can be directly referred to *Q. northropi* because it shares overlapping elements with the holotype and autapomorphies. TMM 41450-3 and 44036-1 share an ulna with a greatly constricted midsection less than 38% the proximal dorsoventral width and less than 34% the proximal anteroposterior breadth, a greater dorsal expansion of the proximal end, a convex posterior margin and posterior expansion of the proximal end, a circular dorsal cotyle that projects greatly above the shaft anteriorly, dorsal and ventral cotyles that do not overlap vertically, a distally inclined ventral cotyle, a strong intercotylar crest on anterior surface of ulna, and a small blunt olecranon. TMM 44036-1 is from an individual about three-quarters the size of the holotype, making it also a giant pterosaur. This difference in size is attributed to ontogeny because the smaller individual has articular surfaces with a pitted and rough texture and a shaft with many short pores and a rough bone grain indicative of osteologically immature individuals (Bennett, 1993).

Radius—The radius articulates with the radial condyle of the humerus proximally and two articular facets on the anterior half of the proximal syncarpal distally. It is a thinner bone with dorsal expansions to complement a larger ulna with ventral expansions. Radii are known in the azhdarchiform species *M. minor* (Padian et al., 1995), the azhdarchid species *Q. lawsoni*, *A. philadelphiae* (BSPG 1966 XXV 507) (Martill and Moser, 2017), *Z. linhaiensis* (Unwin and Lü, 1997), *M. maggii* (Vullo et al., 2018), and *A. lancicollis* (Nesov, 1984), as well as in the putative azhdarchid specimens SGU 35/104a (Averianov et al., 2005), YPM VPPU 022446 (Padian, 1984a), and ZIN PH 38/43 (Averianov, 2007).

In *Q. northropi* (TMM 41450-3.2), the radius is nearly complete, lacking only the anterior part of the proximal end (Fig. 4). The tip of the distal end dorsal expansion remains adhered to the proximal syncarpal (TMM 41450-3.4, Fig. 5). Cortical bone is missing from much of the shaft but a remaining piece

attached to the midshaft allows determination of the original diameter (Table 2). The radius of *Q. northropi* is a narrow bone with gradual expansions of the ends from the midpoint of the bone. The midsection of the radius is constricted, about a third of the dorsoventral width of either end and 60% the anteroposterior breadth of either end, compared with the 50% width of the distal end reported in *A. lancicollis* (Averianov, 2010:300). It is smaller than the ulna, but their midsections are comparable in size: the radius is about 81% the diameter of the ulna, significantly more than the 75% average of the azhdarchids and the pterosaurs in general and significantly more than the 64% of *Q. lawsoni*. The radius is posteriorly bowed with a slight ventral flexure in its middle.

The missing portions of the proximal end of TMM 41450-3.2 preclude determining its proximal shape; only part of the proximal cotyle for articulation with the radial condyle of the humerus (oval cotyle for articulation with the capitulum of the humerus of Bennett, 2001a) and the dorsal expansion of the proximal end (angular ridge of Hooley, 1913, biceps tubercle of Veldmeijer, 2003, dorsal process of Andres et al., 2010, tubercle that is a dorsal projection of the proximal end of Averianov, 2010, ridge building the dorsal part of the radial head of Frey et al., 2011, large tubercle process and bicipital tubercle of Eck et al., 2011, 'crest' of Dalla Vecchia, 2014, or salient tubercle of Vullo et al., 2018) can be resolved. However, it can be seen to be proximally expanded, unlike the broad spatulate proximal radius of *D. banthensis* (Padian, 2008b:55) or the unexpanded proximal radius of *Eudimorphodon rosenfeldi*, Dalla Vecchia, 1995 (Dalla Vecchia, 2009:167). The preserved portion of the proximal cotyle is gently concave, rising gradually anteriorly, and reaches the posterior margin of the proximal end. A thickening of the bone on the end of the dorsal expansion may be part of the rugose tubercle of Bennett (2001a). The dorsal expansion continues distally as a thin ridge, as reported in *A. lancicollis* for the insertion of the M. biceps (Averianov, 2010:300), and present in *Q. lawsoni*.

A large rounded tuberosity is present on the ventral margin of the bone just distal to the proximal cotyle that is also found in *A. lancicollis* (Averianov, 2010:fig. 26E–G) and more proximally in *Q. lawsoni*. A smaller tubercle is located just distal and posterior to the rounded tuberosity. A rugose ridge extends distally along the ventral margin from the rounded tuberosity, but missing cortical bone makes it impossible to ascertain if they were connected. This rugose ridge trifurcates distally: the first branch curves onto the posterior surface and extends at least to the midpoint of the bone as a corrugated scar, the second branch extends along the ventral margin as a posteriorly curving crest, and the last branch extends along the ventral part of the anterior surface as a rugose ridge. These rugose ridges likely correspond to the U-shaped scar reported in *Pteranodon* suggested to be the origin for various carpus and manus flexors and extensors (Bennett, 2001a:79). The ventral crest is almost certainly homologous with the elongate tuberculum on the ventral margin of the proximal shaft found in *Q. lawsoni* and *A. lancicollis* (Averianov, 2010:fig. 26A–B). The shaft of the radius has about 45° of counterclockwise torsion, complementing the condition of the humerus and ulna. The shaft is subcircular in cross-section, as in *I. latidens* (Hooley, 1913:387) and BSPG 1980 1980 I 122 (Veldmeijer, 2003:88), and unlike the oval cross-sections of *Q. lawsoni*, *A. lancicollis* (Averianov, 2010:300), *T. wellnhoferi* (Eck et al., 2011:287), and BSPG 1966 XXV 507 (Martill and Moser, 2017:166), or the strong elliptical cross-section of *A. spielbergi* (Veldmeijer, 2003:88).

The distal end of the radius is dominated by a massive, anteriorly oriented crest made of the anterior tuberosity (well-developed longitudinal ridge of Hooley, 1913, acute prominence of Padian, 1984b, radius tuberculum of Sangster, 2003, anterior

tubercle of Averianov et al., 2005, slight medial crest of Padian, 2008a, large cranial tubercle of Dalla Vecchia 2009, 'distal tubercle' of Dalla Vecchia, 2014, or prominent longitudinal ridge and distal tubercle of radius of Dalla Vecchia, 2019) combined with a proximally extending ridge on the ventral half of the anterior surface, as in the crest reported in SGU no. 104a/35 (Averianov et al., 2005:436). *Montanazhdarcho minor* also has a large anterior tuberosity (McGowen et al., 2002:7, fig. 2D), but it lacks the proximal ridge and so is not considered a crest here. The anterior crest in *Q. northropi* is semicircular in horizontal outline, turning the distal end into an L-shape in cross-section similar to the triangular cross-section of other azhdarchoids (Andres, 2021). The rest of the anterior surface of the distal end is a dorsal tubercle (second smaller acute prominence of Padian, 1984b, or second dorsally-positioned anterior tubercle of Andres et al., 2014) separated from the anterior crest by a shallow midline sulcus (deep wide sulcus of Andres et al., 2014) with what appears to be a circular fossa at its distal end, similar to a depression reported in *A. spielbergi* (Veldmeijer, 2003:fig. 18C). A dorsal tubercle and a midline sulcus were labeled on the left radius of *Seazzadactylus venieri* Dalla Vecchia, 2019 (Dalla Vecchia, 2019:fig. S6), but these were termed the distal tubercle and furrow, which were described and figured more ventrally on the right radius (Dalla Vecchia, 2019:33, fig. 19). Instead of a dorsal tubercle, *M. minor* (McGowen et al., 2002:7) has a dorsal ridge that reaches the distal surface. Eck et al. (2011:fig. 7, pl. 3) labeled a tendinous sulcus dorsal to where this tubercle/ridge would be located in *T. wellnhoferi*, but such a sulcus is not apparent in *Q. northropi*. Another smaller, posteriorly oriented crest (large tubercle of Averianov, 2010, or large ventral flange of Andres et al., 2014) is present on the ventral end of the posterior surface in *Q. northropi*, described in SGU no. 104a/35 as giving that bone a T-shaped distal cross-section (Averianov et al., 2005:436). Together, the crests form a flat ventral surface for the distal end in *Q. northropi*, similar to the condition in *Kryptodrakon progenitor* Andres et al., 2014, but lacking the two tubercles reported in *K. progenitor* (Andres et al., 2014: S14, S1E). At the posterior margin of the proximal end of this flat ventral surface, there is a depression bounded proximally by a large rugose tubercle. The radius distal end has a moderate-sized dorsal expansion. The distal end of the posterior surface is predominantly flat with distal widening of the posterior crest, forming a concave surface at its extremity, which is pierced by a foramen in its middle (McGowen et al., 2002:7), contra Bennett (2001a). A depression is reported in this region of *M. minor* (McGowen et al., 2002:7), *A. spielbergi* (Veldmeijer, 2003:fig. 18A), YPM VPPU 022446 (Padian, 1984a:518), and SGU no. 104a/35 (Averianov et al., 2005:435), whereas a longitudinal groove is reported here in *I. latidens* (Hooley, 1913:387). A pneumatic foramen has been reported in this location for *M. minor* and YPM VPPU 022446 (McGowen et al., 2002:7), but not in SGU no. 104a/35 (Averianov et al., 2005:435), *M. maggii* (Vullo et al., 2018:8, fig. 5E), or *A. lancicollis* except CCMGE 10/11915, which has a series of small foramina here (Nesov, 1984:pl. VII, fig. 8b; Averianov et al., 2005:436). A large pneumatic foramen is reported in *Pteranodon* that reaches the distal surface of the radius to divide the distal articular surfaces (Bennett, 2001a:79–80, fig. 75B).

There are two separate articular surfaces on the radius distal surface in *Q. northropi*, giving it a shoeprint-shaped outline, as described in *M. minor* (McGowen et al., 2002:7), *D. banthensis* (Padian, 2008b:55), and YPM VPPU 002246 (Padian, 1984a:518; Padian and Smith, 1992:89). The dorsal articular surface (facies articularis distalis of Averianov et al., 2005) is a right triangle in outline that expands dorsally. Much of the ventral articular surface (facies articularis ventralis of Averianov

et al., 2005, or ventral condyle of Frey et al., 2011) remains adhered to the distal syncarpal (TMM 41450-3.4, Fig. 5), but it can be seen to reach onto the posterior surface as a process (pronounced boss of Padian and Wild, 1992, tubercle of Veldmeijer, 2003, large tubercle with ventral articular surface for the proximal syncarpal of Averianov, 2010, or blunt ventral styloid process of Frey et al., 2011) to combine with the posterior crest. *Pteranodon* has a smaller subcircular ventral articular surface that does not reach onto the posterior surface, although the radius is weakly expanded in this region (Bennett, 2001a:79–80). The distal margin of the radius in *Q. northropi* is flat in the anterior/posterior view, unlike the convex outline of *Q. lawsoni*, and lacks the bony stop reported in *A. spielbergi* (Veldmeijer, 2003:88, fig. 18).

Carpus

The pterosaur carpus consists of at least five elements: a proximal syncarpal, distal syncarpal, medial carpal, carpal sesamoid (sesamoid A of Bennett, 2001a), and the neomorphic pteroid. The sesamoid B and C of Bennett (2001a) could not be located in the *Quetzalcoatlus* material. For *Q. northropi*, the proximal syncarpal (TMM 41450-3.4) and distal syncarpal (TMM 41450-3.5) are the only carpal material preserved. The proximal syncarpal is missing much of its cortical bone and has had some of its surfaces restored using the articulations of the bones that contact it. The distal syncarpal remains adhered to the wing metacarpal so its distal surfaces are obscured.

Proximal Syncarpal—The proximal syncarpal of pterosaurs (proximal carpal of Hooley, 1913) is formed from the fusion of two proximal series carpals (radiale and ulnare), and hence is termed a syncarpal (Bennett, 2001a). It has a complex geometry excavated by seven articular surfaces divided between the ulna (three) and radius (two) proximally, as well as the massive intersyncarpal articular facets (two) distally. The proximal syncarpal of *Q. northropi* (TMM 41450-3.4) was found partly in situ but broken and weathered with several pieces recovered from the talus. The contacts among fragments were limited and so the only way to retain them in natural relationship was to restore the missing parts of bone in plaster. The result is that parts of the reconstructed element appear to consist of disjunct pieces, whereas all are connected beneath plaster (Fig. 5). The proximal tuberculum, ventral rim of the dorsal articular facet for the ulna, posterior surface, and ventral rim of the ventral intersyncarpal articular facet have been reconstructed in plaster, in part based on articulation with neighboring bones, but this plaster should not be taken as reflection of original morphology. Likewise, divots sculpted into the plaster on the proximal and anterior surfaces in positions of pneumatic foramina in *Q. lawsoni* do not indicate their presence in *Q. northropi*. Small pieces of the dorsal articular surface of the distal ulna, radius dorsal expansion, and ventral articular surface of the distal radius are adhered to the proximal surface of this syncarpal and can establish the natural relationships among these bones. The flexor tendon process (hooked process of Bennett, 2001a, or triangular process of McGowen et al., 2002) is neither preserved nor reconstructed in this specimen. Proximal syncarpals are preserved in the azhdarchiform species *M. minor* (Padian et al., 1995); the azhdarchid species *Q. lawsoni* (Lawson, 1975a), cf. *H. thambema* (EME VP 316) (Averianov, 2014), *Z. linhaiensis* (Unwin and Lü, 1997), and *A. lancicollis* (Bakhurina and Unwin, 1995); as well as the putative azhdarchid specimen MOR 553 (Carroll et al., 2013).

The proximal syncarpal of *Q. northropi* is blocky by pterosaur standards; its dorsoventral height is almost that of its proximodistal length, and its greatest dimension is its anteroposterior width (Table 2). However, it is not proximodistally narrow as in basal pterosaurs such as *Eudimorphodon ranzii* Zambelli, 1973

(Wild, 1979:fig. 17) and *E. rosenfeldi* (Dalla Vecchia, 2009:fig. 5B). This syncarpal is hexagonal in (parasagittal plane) cross-section as in *A. lancicollis* (Averianov, 2010:fig. 27), reminiscent of the trapezoidal outline of BEXHM: 2015.18 (Rigal et al., 2017:228, figs. 4b and 6a), but distinct from the quadrangular outlines of pteranodontians (Bennett, 2001a:fig. 79C–D; Andres and Myers, 2013:393) or the rectangular outlines of early pterosaurs (Sangster, 2003:70; Dalla Vecchia, 2009:168).

The proximal surface of the proximal syncarpal is dominated by the articulations for the ulna (ulnar articular surface of Dalla Vecchia, 2009), encompassing the posterior two-thirds of this surface. The radial articulations (concave groove and elongate cavity for the radius of Hooley, 1913, or articular surfaces for the radius and radial cotyle of Dalla Vecchia, 2009) are positioned at the anterodorsal corner of the proximal surface. Anterior to the ulnar articulations, ventral to the radial dorsal articular facet (radial facet and articulating surface for the radius of McGowen et al., 2002, or dorsocentral part of the radial cotyle of Dalla Vecchia, 2009), and posterior to the radial ventral articular facet (cranial part of the radial cotyle of Dalla Vecchia, 2009) is a triangular concave area. This area includes a large pneumatic foramen in *Q. lawsoni*, *A. lancicollis* (Averianov, 2010:302, fig. 27), *T. wellnhoferi* (Eck et al., 2011:287), *Pteranodon* (Bennett, 2001a:81), and *I. latidens* (Hooley, 1913:pl. XXXIX, fig. 8E), which is not visible in *Q. northropi*. However, the distal radius pneumatic foramen is relatively small in *Q. northropi* and the ventral end of the triangular surface has been filled with plaster, and so a pneumatic foramen could have been present in this area. Portions of the three articular surfaces for the ulna are preserved: the dorsal articular facet, fovea, and ventral tuberculum. The dorsal articular facet (concave surface and articular surface for articulation with that on the ulna of Hooley, 1913, ulnar facet of McGowen et al., 2002, ulnar cotyle of Dalla Vecchia, 2009, or dorsal articulating facet of the ulna of Averianov, 2010) has a large horizontal falcate (sickle-shape) outline curving anteroventrally (i.e., concave posteriorly and convex anteriorly). The fovea (large basin-shaped concavity and oval cavity of Hooley, 1913) is mostly missing but concave surfaces preserved at its anterodorsal and posteroventral corners indicate that it was quite large. The ventral tuberculum (convexity and hemispherical knob of bone of Hooley, 1913, tubercle for articulation with the ulna of Wellnhofer, 1985, ulnar tubercle of Veldmeijer, 2003, or tubercle of Averianov, 2010) is only represented by part of a large knob of bone at its posterior end. A short sulcus extends ventrally from the fovea past the posterior margin of the tuberculum to reach the ventral surface. Both articular facets for the radius are preserved: the large dorsal articular facet that is an anteroventrally tapering triangle, and the small ventral articular facet that is a posteroventrally oriented semicircle, unlike the small flat subcircular facet of *Pteranodon* (Bennett, 2001a:82). The dorsal and ventral articular facets for the radius contact one another and the triangular concave area. The radial articular facets have raised rims, and where they contact they form a proximal process (pronounced tubercle of Eck et al., 2011) at the anteroventral corner of the syncarpal proximal surface. Where the dorsal radial articular facet and the dorsal ulnar articular facet contact, they form a trilateral raised prominence with the triangular concave surface. There is no distinct ridge between the dorsal and ventral radial articular facets, but the condition in *Pteranodon* is described as being separated by a step (Bennett, 2001a:82), and that is probably the most accurate characterization for *Q. northropi*. All of the proximal articular facets are weakly concave, as in *A. lancicollis* (Averianov, 2010:302) and *E. rosenfeldi* (Dalla Vecchia, 2009:168), but not as in *Q. lawsoni*.

The dorsal surface of the proximal syncarpal is restricted to the anterior half of the syncarpal due to emargination by the dorsal

intersyncarpal articular facet (large concave facet of McGowen et al., 2002). This surface slopes ventrodistally except for a horizontal proximodistally oriented sulcus in the center of the dorsal aspect of the proximal syncarpal (suboval facet that is concave in anteroposterior section of Bennett, 2001a). This dorsal sulcus is wider than long, saddle-shaped (concave anteroposteriorly, convex proximodistally), and bounded by anterior and posterior rugose flanges. It was presumably a groove for M. extensor carpi radialis tendon (Bennett, 2001b:fig. 122) that was covered by a retinaculum (Bennett, 2001a:82) attached to the flanges. A tubercle in the anterior half of the sulcus may indicate the presence of more than one tendon traversing the sulcus. There is a small foramen posterior to this dorsal sulcus, positioned between it and the dorsal intersyncarpal articular facet in a region figured to have one or two foramina in *Pteranodon* (Bennett, 2001a: figs. 77 and 80B) and two to four in *A piscator* (Kellner and Tomida, 2000:58, figs. 38 and 41). In anterodorsal view, the dorsal surface is an anteriorly expanded trapezoid: the narrow posterior margin is the dorsal sulcus, the long proximal margin is the dorsal rim of the radial dorsal articular facet, the anterior margin is the anterior process (elongated process and preaxial process of Hooley, 1913) terminating in a distal tuberculum, and the distal margin is the dorsal rim of the dorsal intersyncarpal articular facet that terminates in a sharp distal process (blunt distally-oriented process of Frey et al., 2011). The anterior process is anteroventrally oriented and forms a strong buttress for the radius on the proximal syncarpal in pterosaurs (Hooley, 1913:387). The notch between the sharp distal process and the distal tuberculum is formed by a sulcus on the ventral surface that contacts the ventral intersyncarpal articular facet (another concave facet of McGowen et al., 2002). A large foramen is present in the middle of the trapezoidal dorsal surface of the proximal syncarpal, in a similar position to a foramen present in *Pteranodon* (Bennett, 2001a:figs. 77 and 80B) and *I. latidens* (Hooley, 1913:389), as well as three large neurovascular openings described in *A. lancicollis* (Averianov, 2010:302) and apparently figured in *A. piscator* (Kellner and Tomida, 2000:fig. 38a and b).

The anterior surface has a small attenuated hastate (spearhead-shaped) outline (not figured). It is posteroventrally-oriented but curves distally (i.e., concave dorsally and convex ventrally). Its concave proximal margin is the anterior margin of the radial ventral articular facet, and its pointed distal end is the anterior process. Tubercles are present in the middle of the anterior surface near the proximal end and at the distal extremity of this surface on the anterior process.

Not much of the ventral surface is preserved. It consists of the ventral aspect of the anterior process and a portion of the proximoventral rim of the ventral intersyncarpal articular facet. A short sulcus is positioned between the process and facet distally. The ventral surface of the anterior process has a pneumatic foramen (pit of Frey et al., 2011) in *Q. lawsoni*, *Pteranodon* (Bennett, 2001a:fig. 79D), *A. piscator* (Kellner and Tomida, 2000:58, figs. 37 and 39), and *A. primordius* (Frey et al., 2011: S45), but cracks and missing cortical bone in this region of TMM 41450-3.4 preclude the identification of its presence. Bennett (2001a) and Kellner and Tomida (2000) figured a small circular foramen in the middle of the proximal end of the ventral surface of *Pteranodon* and *A. piscator* respectively, where there is a small circular area filled with plaster in TMM 41450-3.4 that could be such a foramen. Bennett (2001a) also figured two more posteriorly positioned foramina in areas covered by plaster in TMM 41450-3.4.

The posterior surface of the proximal syncarpal is almost entirely missing. A rounded posterior process projecting from the ventral articular intercondylar facet is all that is preserved.

The proximal syncarpal distal surface is dominated by the dorsal and ventral intersyncarpal articular facets (two transverse

concave surfaces of Hooley, 1913, tongue-and-groove of Padian, 1984b, two wide concavities of Padian and Wild, 1992, intersyncarpal articular surfaces and concave suboval articular surfaces of Bennett, 2001a, or intersyncarpal articulation facet of Averianov, 2010) for articulation with the distal syncarpal intersyncarpal articular surfaces. These overlap over their entire horizontal widths and most of their vertical heights. The dorsal intersyncarpal articular facet is significantly smaller than the ventral facet as in other azhdarchoids (Bennett, 2001a:83) and *Alamodactylus byrdi* Andres and Myers, 2013 (Andres and Myers, 2013:393), and it is a dorsally bowed crescent in outline (i.e., convex dorsally and concave ventrally). The articular surface of this dorsal facet is concave dorsally at its posterior end, but it twists to become concave posteriorly at its anterior end. The ventral intersyncarpal articular facet appears to be semicircular in outline, but its anteroventral margin is not preserved. It is distally concave at its posterior end becoming ventrally concave at its anterior end. It terminates posteriorly as a posterior process of the articular surface. The intersyncarpal articular facets are separated by an anteroventrally inclined crest (ridge of Hooley, 1913, diagonal ridge of Padian and Wild, 1992, smooth rounded ridge of Sangster, 2003, or oblique ridge of Averianov, 2010) that terminates in a sharp distal process at its anterior end. An accessory articular surface is reported at the anterior end of the interfacet crest in pteranodontians (Bennett, 2001a:82, fig. 79; Andres and Myers, 2013:393, fig. 4G). In *Q. northropi*, the distal process is an extension of the dorsal intersyncarpal articular facet instead of a separate articular surface, and so an accessory articular surface is not considered present in *Q. northropi*. The distal process is separated from the distal tuberculum by a notch. Averianov (2010) described a small pneumatic foramen on the distal surface opposite one on the proximal surface in *A. lancicollis* and appears to figure a foramen anterior to the intersyncarpal articular facets (Averianov, 2010:fig. 27D), where a foramen is reported in *M. minor* (McGowen et al., 2002:7, fig. 3G), *Pteranodon* (Bennett, 2001a: fig. 79D), and *A. piscator* (Kellner and Tomida, 2000:fig. 37a–b). No foramina are preserved on the distal surface of the proximal syncarpal in *Q. northropi*.

Distal Syncarpal—The distal syncarpal (distal carpal of Hooley, 1913) in pterosaurs is a squat bone with two massive intersyncarpal articular surfaces (convexities of Hooley, 1913) for contact with the proximal syncarpal, dorsal and ventral distal facets for articulation with the wing metacarpal, and an anterior process for articulation with the medial carpal (curved bar of Hooley, 1913, cranially-extended process of Kellner and Tomida, 2000, preaxial carpal process of Bennett, 2001a, curl-shaped process for the preaxial carpal of Dalla Vecchia, 2009, cranial part of the distal syncarpal of Frey et al., 2011, or nose of Dalla Vecchia, 2019). It is formed from the fusion of three bones of the distal carpal series (presumably carpals 2 through 4) (Bennett, 2001a). The distal syncarpal in *Q. northropi* (TMM 41450-3.5) remains attached to the proximal surface of the wing metacarpal but does not appear to be fused (Fig. 6). It is missing its anterior end including the medial carpal process (Table 2), but it still appears to have been rectangular in (parasagittal) cross-section, unlike the triangular cross-sections of pteranodontoids (Andres, 2021). Distal syncarpals are preserved in the azhdarchid species *Q. lawsoni* (Bennett, 2001a), *Z. linhaiensis* (Unwin and Lü, 1997), and *A. lancicollis* (Averianov, 2010), as well as the putative azhdarchid specimens MC M3929 (Buffetaut, 2008), MOR 553 (Carroll et al., 2013), TMM 45888-2.2, and YPM VPPU 002246 (Padian, 1984a). The preserved proximal surface of the distal syncarpal is taken up entirely by the proximally tall dorsal and ventral intersyncarpal articular surfaces (low raised areas of Sangster, 2003, or intersyncarpal facet and intersyncarpal articular surface of Averianov,

2010). These surfaces are right triangles in outline in proximal view, with the dorsal articular surface constituting the anterodorsal half and the ventral articular surface constituting the posteroventral half, unlike the suboval articular surfaces of *Pteranodon* (Bennett, 2001a:82). The dorsal and ventral articular surfaces increase in proximal height towards the center of the distal syncarpal, posteriorly and anteriorly, respectively. The ventral articular surface appears much larger than the incomplete dorsal articular surface and extends onto nearly the entire posterior surface. Both are bounded by sharp edges. A deep interarticular sulcus (deep diagonal depression of Padian, 1984b, groove of Bennett, 2001a, deep longitudinal slightly curved groove of Buffetaut, 2008, or deep oblique groove of Averianov, 2010) extends anteroventrally between the articular surfaces. At the midpoint of the sulcus, there appears to be a depression that excavates the ventral intersyncarpal articular surface (ventroproximal articulation facet of Frey et al., 2011). Anteroventral to the depression is an oval fovea to receive the distal process of the proximal syncarpal, in place of a concave accessory articular surface as found in *Pteranodon* (Bennett, 2001a:82). The posterodorsal end of the interarticular sulcus appears to curve around and emarginate the dorsal intersyncarpal articular surface posteriorly, so that the dorsal intersyncarpal articular surface appears to be a posteriorly curving hook in dorsal view.

The dorsal surface of the distal syncarpal is very incomplete. It can be seen to have a dorsal rise with shallow concave surfaces proximal and distal to it, unlike the concave surface of *Eoazhdarcho liaoxiensis* Lü and Ji, 2005 (Lü and Ji, 2005a:304) or the three ridges of *D. macronyx* (Sangster, 2003:70). The dorsal facet for articulation with the wing metacarpal has a straight contact, with a short anterodorsal process (hooked process of Andres et al., 2014) at the anterior end.

The anterior surface of the distal syncarpal has been broken off and is missing. The base of the medial carpal process appears to be preserved.

The ventral surface is semicircular in outline and concave ventrally. The ventral facet for articulation with the wing metacarpal is curved (i.e., concave distally and convex proximally), with a short posteroventral process at the posterior end of the contact. Dalla Vecchia (2009) described small tubercles along the distal edge of the distal syncarpal for the attachment of ligaments to the wing metacarpal in *E. rosenfeldi*. The anterodorsal and posteroventral processes of the *Q. northropi* distal syncarpal articulate with longitudinal grooves on the wing metacarpal, and so these distal processes could be homologous to the small distal tubercles of *E. rosenfeldi*. A distally projecting bony process that fits in a sulcus on the wing metacarpal to form an interlocking mechanism is reported in *A. piscator* on the posterior carpal of the distal carpal series (Kellner and Tomida, 2000:59), which may correspond to the posteroventral process in *Q. northropi*. It cannot be determined if the circular fossa at the base of the medial carpal process in *Q. lawsoni* is preserved in TMM 41450-3.5.

The posterior surface of the distal syncarpal is damaged. A ventroproximally oriented (i.e., on the ventral side of proximoventrally) ridge delineating the posterior margin of the ventral intersyncarpal articular surface is visible on this posterior surface, similar to a rugose ridge reported in *K. progenitor* (Andres et al., 2014:S14, fig. S1Fiii).

The distal articular surface of the distal syncarpal is obscured by the wing metacarpal, but it is clear in posterior view that the characteristic stair-step offset between the dorsal and ventral facets for articulation with the wing metacarpal is present. The ventral facet is dorsoventrally deeper than the dorsal facet, as in other pterosaurs except for the ornithocheiroids (Andres, 2021). There is no evidence for pneumatic fora-

mina in the distal syncarpal of *Q. northropi*, as in MC M3929 (Buffetaut, 2008:253), but the preservation would make their identification difficult, and so this absence cannot be determined for certain.

Metacarpus

The metacarpus of pterosaurs consists of a massive wing metacarpal (metacarpal IV) and the smaller manual metacarpals (metacarpals I–III, clawed digit metacarpals). Metacarpals I–III lie closely appressed to one another and to the anterior surface of the wing metacarpal with metacarpal I dorsal, metacarpal II in the middle, and metacarpal III ventral (Bennett, 2001a). In *Q. northropi*, the distal end of metacarpal III (TMM 41450-3.8) and a fragmentary wing metacarpal (TMM 41450-3.9) are preserved. The third metacarpal is present in the azhdarchid species *Q. lawsoni* (in addition to II and III) and in *E. langendorfensis* (Vremir et al., 2013b), as well as in the putative azhdarchid specimen TMP 1985.36.211 (Godfrey and Currie, 2005), and is possibly represented among other manual metacarpals in *Z. linhaiensis* (ZMNH M1323-1 and M1328), and MOR 553 is reported to have a metacarpal I or III (Carroll et al., 2013). Currie and Jacobsen (1995), Godfrey and Currie (2005), and Averianov (2014) incorrectly list TMP 1992.83.6 as a metacarpal III, but this was corrected to a metatarsal by Godfrey and Currie (2005) and Hone et al. (2019).

Metacarpal III—The single manual metacarpal preserved in *Q. northropi* (TMM 41450-3.8) is identified as the distal end of the third metacarpal (Fig. 7) based on the presence of a postero-ventral process as found in *Pteranodon* (Bennett, 2001a:90, fig. 92) and *Q. lawsoni* (TMM 41954-8.8), as well as the ventral curvature of the rim forming a concave ventral surface and greater expansion of the distal end found in TMM 41954-8.8. The shaft of this metacarpal is missing, and so it is not possible to determine its length or whether it contacted the carpus (Table 2). The cross-section of the break is trapezoidal, tapers posteriorly, and has a large circular cavity in its center. This specimen is missing cortical bone from all but its posteroventral surface. This surface is rugose and pierced by a small foramen on the anterior portion of this ventral surface. The specimen is subcircular in horizontal outline because its articular surface extends around about 225° of the distal end, turning this bone into a condyle, distinct from the wide triangular shape of *E. langendorfensis* (Vremir et al., 2013b:10). This condyle is about twice as anteroposteriorly wide as dorsoventrally deep and so is predominantly confined to the horizontal plane. The posterior half of the articular surface curves ventrally to produce the posteroventral process and a concave surface with the rest of the ventral aspect, as in *Pteranodon* (Bennett, 2001a:90, fig. 92). The anterior surface of the condyle is flattened and inclined anterior to the shaft so that it forms a slight ridge where it contacts the shaft. The dorsal surface is flat with its margins sloping down to the articular surface. The distal articular surface extends onto the posteroventral process.

Wing Metacarpal—The wing metacarpal (ulnar metacarpal of Hooley, 1913) of pterosaurs has a broad articulation with the distal syncarpal proximally and a pair of circular distal condyles for articulation with the first wing phalanx. The wing metacarpal proximal end, a shaft fragment, and the dorsal condyle of the distal end are preserved in the holotype of *Q. northropi* (TMM 41450-3.9) (Fig. 6). Their combined lengths suggest an element greater than 600 mm in length, but a substantial part of the shaft missing (Table 2). Wing metacarpals are known in the azhdarchiform species *M. minor* (Padian et al., 1995); the azhdarchid species *Q. lawsoni* (Bennett, 2001a), cf. *A. philadelphiae* (BSPG 1966 XXV 501) (Martill and Moser, 2017) possibly including NHMUK PV R 9225 and 9226

(NHMUK catalog), *Z. linhaiensis* (Cai and Wei, 1994), *E. langendorfensis* (Vremir et al., 2013b), *C. boreas* (Hone et al., 2019), possibly *M. maggii* (Vullo et al., 2018), and *A. lancicollis* (Averianov, 2010); as well as the putative azhdarchid specimens MOR 553 (Carroll et al., 2013), OMNH 22014 (Cohen et al., 2018), UMUT MV 7978 (Obata et al., 2007), ZIN PH 49/43 (Averianov, 2007), and an unnumbered specimen from near the village of Cruzy in France (Buffetaut, 2008).

The proximal surface of the wing metacarpal is obscured by the attached distal syncarpal, but the pronounced step between the dorsal articular surface (flattened oval facet of Hooley, 1913, or dorsal tuberosity of Sangster, 2003) and the ventral articular surface (medial condyle of the proximal end of Padian, 1983b) can still be observed, but this does not seem to form a notch found in other pterosaurs (Galton, 1981:1118, fig. 2; Eck et al., 2011:287, fig. 8, pl. 3A). The proximal end forms an inverted piriform in cross-section due to the bulbous proximal end and its ventral expansion (ventral crest and anteriorly concave thin triangular crest of bone of Sangster, 2003, exalted circumference around at least the ventral half of the bone of Frey et al., 2011, crista for attachment of the extensor M. digiti quarti brevis of Martill and Moser, 2017, or ventral crest and ventral flange of Dalla Vecchia, 2019), that is distinct from the rectangular cross-sections of other Lophocratia or the oval of *A. primordius* (Frey et al., 2011:S46). The metacarpal IV proximal end (proximal head of McGowen et al., 2002, or articular head of Frey et al., 2011) is enlarged both vertically and horizontally as in other Lophocratia (Andres, 2021), with an anteroposterior breadth about 80% of the dorsoventral width. Damage to the distal syncarpal reveals a massive and inflated proximal tuberculum (tuberculum and tubercle of McGowen et al., 2002; medial tuberosity, middle tuberosity, and middle prominence of Sangster, 2003; medially directed tubercle of Eck et al., 2011; or median tuberculum of Dalla Vecchia, 2019) in the middle of the anterior end of the proximal surface of the wing metacarpal that articulates with the distal fovea of the distal syncarpal.

The ventral expansion extends ventrally past the distal syncarpal to form an underhanging process. In other pterosaurs, the ventral expansion has an anteriorly curving flange (thickened lateral edge and rugose area of Galton, 1981, ventral tuberosity of Sangster, 2003, ridge arising from the caudal edge of the articular head of Frey et al., 2011) and a flexor tendon groove (deep valley and deep concavity of Hooley, 1913, channel for the extensor tendon of the flight finger of Wellnhofer, 1991b, weak sulcus for a tendon of Bennett, 2001a, groove for a tendon of Bennett, 2001b, or long oval pneumatic foramen extending along the long axis of the shaft of Frey et al., 2011) that allows M. flexor digiti quarti to traverse the carpus ventrally and functionally extend the wing digit (Bennett, 2001b, 2008), but see Frey et al. (2006) and Prondvai (2008) for alternative reconstructions. There is not such a groove or flange in *Q. northropi*, except for an anterior fossa on the ventral expansion about 5 cm from the proximal end. This is distinct from the proximal depression identified for articulation of metacarpals I–III in more basal pterosaurs (Galton, 1981:1118, fig. 2; Dalla Vecchia, 2019:37). A flexor tendon groove also seems to be absent in *E. langendorfensis* (Vremir et al., 2013b:fig. 10) and BSPG 1966 XXV 501 (Martill and Moser, 2017:fig. 2a). The ventral expansion is rather short and extends for only the first 20 cm of the metacarpal, a third of the preserved length. A large tumescence is just distal to the tuberculum on the anterior surface of the metacarpal, which may be the site of additional carpometacarpal ligaments and/or tendons (Bennett, 2001a:87). Hooley (1913) reports convexity in center of the wing metacarpal that gradually dies away distally in *I. latidens* that may be analogous to the condition in *Q. northropi*. This tumescence results in

the middle of the proximal surface being wider than the ventral end, unlike other lophocratians (Andres et al., 2014). A longitudinal groove (groove for digit extensor tendon of Galton, 1981, or slight incision of Sangster, 2003) extends dorsal to the anterior tumescence in which the anterodorsal process on the distal end of the distal syncarpal articulates. This may correspond to the longitudinal groove reported in *E. langendorfensis* by Vremir et al. (2013b), but the small subcircular depression they mention could not be located in either species. The posteroventral process on the distal end of the distal syncarpal contacts the ventral expansion posteriorly, and also appears to articulate in a sulcus. The rest of the posterior surface appears to be flat, lacking the proximal fossa found in non-lophocratian pterosaurs (Andres et al., 2014). The dorsal surface is slightly convex.

The shaft of the wing metacarpal rapidly attenuates distal to the proximal end, especially dorsoventrally, and appears to have been straight. The shaft is about two-thirds of the proximal anteroposterior breadth and almost a quarter of the proximal dorsoventral width. This decrease in width is due to the shaft becoming a flat-topped cylinder that is anteroposteriorly broader than dorsoventrally wide in its midsection, unlike the anteroposteriorly compressed oval of the non-pterodactyloid pterosaurs or the rectangular to rounded cross-section of other pterodactyloids (Andres, 2021). This semicircular cross-section is confirmed by a separate shaft fragment of this specimen. A D-shaped shaft cross-section is reported in *C. boreas* and BSPG 1966 XXV 501 (Martill and Moser, 2017:163) as well as OMNH 22014 (Cohen et al., 2018:62), but with the flattened surface identified as anterior. The dorsal ridge on the posterior surface of the shaft reported in non-pterodactyloid pterosaurs (Andres et al., 2014) and the faint grooves for the manual metacarpals reported in *M. minor* (McGowen et al., 2002:8) are absent in *Q. northropi*. The shafts of the ulna and radius of *Q. northropi* are also constricted in width so that the wing metacarpal shaft is about half the width of the combined ulna and radius shafts as in other Neopterodactyloidea. However, the combined shaft constriction and proximal expansion give *Q. northropi* the largest wing metacarpal proximal end known in pterosaurs, over three-and-a-half times wider than the mid-width of the bone and surpassing the proximal expansions of the non-pterodactyloid pterosaurs (Andres, 2021).

The dorsal condyle of the distal bicondylar articulation (obliquely placed trochlea of Hooley, 1913, pulley-like condylar area of Galton, 1981, laterally placed bicondylar joint of Padian, 1983b, distal trochlea and skewed condyles of Sangster, 2003, distal pulley-like condyle of Godfrey and Currie, 2005, or distal terminus with the articular condyle of Frey et al., 2011) with the first wing phalanx is preserved, although it is missing its posterodistal corner. The contacts among the remaining bone in this fragment was so small that it was necessary to reinforce the connection by filling around it with plaster, and so the actual connection among the parts is not visible in the restored condyle. A small part of the intercondylar sulcus (large rounded groove of McGowen et al., 2002, distal sulcus of Sangster, 2003, cleft-like groove of Averianov, 2010, or intercondylar groove of Godfrey and Currie, 2005) is preserved, and it can be seen to be flat, unlike the more V-shaped sulcus in *Pteranodon* (Bennett, 2001a:90, figs. 87 and 89). This sulcus also lacks a rounded median ridge (Bennett, 2001a) (rounded median crest or ridge of Vremir et al., 2013b), which is found in the clade including *Cearadactylus atrox* Leonardi Borgomanero, 1985, plus the Ornithocheirae. The condyle is large and circular extending over 280° of curvature. The anterior and posterior edges of the condyle curve dorsally to form a rugose dorsal fossa between them. In horizontal outline, the condyle appears to flatten at its anterior and posterior margins. The posterior end of the articular surface appears to curve dorsally to

reach the dorsal fossa of the condyle. It is not possible to determine if pneumatic foramina were present in this specimen.

Manual Digits I–III

The manual material of the *Q. northropi* holotype is unfortunately missing nearly all of the cortical bone and no element is complete (Fig. 8). Nine fragments from at least six manual phalanges can be identified (Table 2): the proximal ends of the first phalanges (TMM 41450-3.6, 3.7, and 3.12) and the distal end of the digit III first phalanx (TMM 41450-3.6), the proximal ends of the second (TMM 41450-3.13) and third digit unguals (TMM 41450-3.16), the shaft of the digit III second phalanx (TMM 41450-3.15), and a couple of phalanx midsections (TMM 41450-3.17). There are three other unidentified phalanx fragments (TMM 41450-3.17), but this material is also associated with the distal ends of the third metacarpal and third wing phalanx, and so they cannot be confirmed to be manual phalanges. Identification of elements is facilitated by comparison with *Q. lawsoni*. For the purposes of this description, pterosaurs are considered to have four digits in their hand (manual digits I–III plus wing digit) such that with their vertical arrangement, abductor tubercles are dorsal and adductor tubercles are ventral for the first two digits and reversed for the third; they are not identified in the wing digit. Manual phalanges are present in the azhdarchid species *Q. lawsoni*, *Z. linhaiensis* (Cai and Wei, 1994), *E. langendorfensis* (Vremir et al., 2013b), and *A. lancicollis* (Averianov, 2010), as well as the putative azhdarchid specimen MOR 353 (Carroll et al., 2013).

First Phalanx Digit I—The first phalanx of manual digit I specimen (TMM 41450-3.7) consists of the proximal end with a damaged dorsoproximal surface (Fig. 8I). This element has previously been identified and reconstructed as the proximal end of metacarpal II and distributed to a number of museums as a cast with this identification (TMM catalog). This bone appears to have the distal end broken off proximal to the neck. The articulation with the metacarpal is positioned posteriorly on the proximal end. The articular surface is concave and ovate (egg-shaped) in outline, similar to the concave oval reported in *Pteranodon* (Bennett, 2001a:90), and terminates posterodistally in a surface that is convex in the horizontal plane identified here as the extensor tubercle. The metacarpal articular surface has a more prominent ventral rim and is inclined slightly anterodorsally. A ventral lip for this articular surface is reported in *A. primordius* but is divided in two by a shallow but sharp incision (Frey et al., 2011:S46). The flexor tubercle can be identified on the anterior expansion, and a smaller adductor tubercle can be seen farther down on the ventral surface; the abductor tubercle was likely not preserved in this specimen. The flexor tubercles in *Quetzalcoatlus* do not form keels, such as those found in *D. macronyx* (Padian, 1983a:18). The dorsal and ventral surfaces of the phalanx are flat and converge posteriorly to form a posterior surface that is rounded in a parasagittal plane. The manual first digit first phalanx shaft lacks an anterior groove, as reported in *D. macronyx* (Sangster, 2003:74).

First Phalanx Digit II—The proximal end of the manual digit II first phalanx (TMM 41450-3.12) is preserved in *Q. northropi* (Fig. 8II). The proximal end is triangular in cross-section and is dominated by a lacriform (teardrop-shaped) proximal articular surface for metacarpal II, compared with the concave oval reported in *Pteranodon* (Bennett, 2001a:90). The articular surface is concave in the horizontal plane, is oriented proximodorsally, and projects slightly above the shaft to form a distinct rim. The anterior expansion is positioned dorsally on the anterior surface. The flexor tubercle is positioned anteroventrally. There is a strong abductor tubercle on the anterior end of the proximal surface and likely an extensor tubercle on the posterior end of

the proximal surface. The posteroventral surface is concave. The cross-section of the distal break is triangular.

Third Phalanx Digit II—TMM 41450-3.13 is the proximal end of the third phalanx ungual of the second manual digit (Fig. 8III). This element has a proximally oriented articulation with the penultimate phalanx (proximal cotyle of Frey et al., 2011), a weak and sub-horizontal intercotylar ridge (shallow mesial ridge of Kellner and Tomida, 2000, or cotylar suture of Frey et al., 2011), a narrow proximal base width (anteroposteriorly), as well as a pair of proximodistally oriented ungual grooves (shallow grooves of Bennett, 2001a, lateral sulci of Kellner and Tomida, 2000, deep furrows of Sangster, 2003, or longitudinal grooves for the attachment of the horny sheath of Dalla Vecchia, 2019) on the dorsal and ventral surfaces. These grooves give the ungual an inverted figure-eight cross-section. The dorsal and ventral proximal cotyles (deep concavities of Kellner and Tomida, 2000, or sutures of Frey et al., 2011) can be identified but the ventral cotyle is partially missing. Such an articulation is described as "saddle shaped" in *A. piscator* by Kellner and Tomida (2000:66) but is described as ginglymoid here. A prominent rim extends around this proximal articulation. Frey et al. (2011) describe a minute proximally pointing extensor tubercle posterior to the proximal articulation, which is identified here as the posterior lip of the articulation but could have also functioned as an extensor tendon insertion. The flexor tubercle (adductor tubercle of Frey et al., 2011) can be seen, but not much more can be identified in this specimen.

First Phalanx Digit III—The proximal end and distal articular surface of the left first phalanx of the third manual digit (TMM 41450-3.6) are preserved in *Q. northropi* (Fig. 8IV). The proximal end was previously reconstructed as the proximal end of metacarpal I and distributed to a number of museums as a cast with this identification (TMM catalog). It is broken off near the base and has a damaged anterior surface, probably resulting in the loss of the flexor tubercle (anterior ridge of Averianov, 2010). The proximal end of the third digit first phalanx is massively expanded as in other azhdarchids (Averianov, 2010:306, fig. 33A–E; Carroll, 2013:102). The proximal surface is trapezoidal in outline, similar to that of *A. lancicollis* (Averianov, 2010:306, fig. 33A), and oriented proximodorsally. A shallow and subcircular concave articular surface for contact with metacarpal III is positioned anteriorly on the proximal surface, as in *A. lancicollis* (Averianov, 2010:fig. 33A) and unlike the subtriangular articular facet that takes up the entire proximal surface in *Pteranodon* (Bennett, 2001a:90). A convexity identified as an extensor tubercle (posterior ridge of Averianov, 2010) is positioned posteriorly on the proximal surface of the phalanx. The base of the abductor tubercle (ventrally directed expansion of Sangster, 2003, medial ridge and flange-like ridge of Averianov, 2010, flange for the insertion of the interosseus muscle of Bennett, 2013, or abductor process of Carroll, 2013) is recognizable on the anteroventral corner of the anterior expansion of the proximal end. This is very different from the large, ventrally directed, and flange-shaped abductor tubercle reported in *Pteranodon* (Bennett, 2001a:90), and it is possible that the anterior expansion of the digit III first phalanx is a greatly expanded abductor tubercle. The abductor tubercle is described as more prominent and flange-like in *A. lancicollis* (Averianov, 2010:306), but it appears more like the condition in *Quetzalcoatlus* than that in *Pteranodon*. A smaller adductor tubercle (lateral ridge of Averianov, 2010) is visible on the anterodorsal margin in *Q. northropi*. The phalanx attenuates posteriorly, giving the broken end a triangular cross-section. The foramina reported in MOR 553 and *A. lancicollis* by Carroll et al. (2013) could not be located in TMM 41450-3.6, although its preservation would make it difficult to do so.

The distal fragment consists of a broad saddle-shaped (concave dorsoventrally, convex anteroposteriorly) articular surface for the second phalanx of digit III; this surface was indicated to be saddle-shaped to weakly ginglymoid in *Pteranodon* (Bennett, 2001a:90). The dorsal and ventral rims are missing, but the concave dorsal and ventral margins as well as the posterior narrowing of the articular surface can be seen in TMM 41450-3.6.

Second Phalanx Digit III—A small phalanx shaft fragment (TMM 41450-3.15) is identified as the third manual digit second phalanx (Fig. 8V). It is missing its proximal and distal ends as well as its dorsal surface. It is identified based on a short saddle-shaped midsection between proximal and distal expansions, a semicircular middle cross-section, and the presence of two short longitudinal ridges on the ventral surface. Not much more can be discerned on this fragment.

Fourth Phalanx Digit III—TMM 41450-3.16 is a small bone fragment with broken proximal and distal ends, a curved posterior margin, and a nearly straight anterior margin giving the entire fragment a trapezoidal outline that decreases in anteroposterior width distally (not figured). In cross-section, it has an anteriorly tapering ovate outline. The curved margin and attenuated width indicate that this is an ungual, and the nearly straight margin opposite the curved margin suggests that this fragment is from the proximal part of the midsection, or at least proximal to the higher curvature of the distal end of the claw. Nearly all the cortical bone is missing, but slight concavities on the dorsal and ventral surfaces may correspond to ungual grooves. TMM 41450-3.16 is slightly more robust and curved than the second digit third phalanx of the manus (TMM 41450-3.13), and it appears to overlap that third phalanx in preservation, so it is not considered to be another fragment of TMM 41450-3.13. Of the remaining manual unguals, the second phalanx of digit I and fourth phalanx of digit III, the more robust shape and higher curvature would indicate the latter element. TMM 41450-3.16 is tentatively identified as a left third manual digit fourth phalanx midsection.

Wing digit

The wing digit of pterosaurs consists of the hyperelongated four phalanges of the manual digit IV that support the distal portions of the wing membrane, or three phalanges in the case of *A. ammoni* (Bennett, 2007a:376). These wing phalanges are straight and parallel-sided for most of their length, with expansions at their proximal and distal ends for their articular surfaces. These expansions are both posterior and ventral, but predominantly the former, and so they are termed posterior expansions here (foot-like extension and foot-like outline of Young, 1964, posteriorly facing expansion of the articulatory surface of Frey and Martill, 1996, caudally directed projection giving it a 'shoe-like' shape of Kellner and Tomida (2000), posterior projection of Sangster, 2003, caudal projection of Dalla Vecchia, 2009, foot-like process of Zhou, 2010a, or slight expansion of the posterior margin of Eck et al., 2011); they may be termed posterior processes in other publications. These are presumably homologous with extensor insertions in other tetrapods, but they function as wing flexor insertions in pterosaurs (Bennett, 2008). Portions of the first, second, and third wing phalanges are identifiable in the left wing of *Q. northropi*, as well as a multitude of other fragments that likely include pieces of these and the fourth wing phalanx.

First Wing Phalanx—The preserved portions of the holotype left first wing phalanx (TMM 41450-3.10) include a proximal fragment and a shaft fragment in three pieces, lacking the proximal and distal articulations (Fig. 9). TMM 41450-3.10 is the longest preserved bone in the Big Bend pterosaur material,

with a length of over 1.5 meters (Table 2). It consists of an approximately 1.3 meter-long shaft fragment that has been restored but is represented by continuous bone as well as a proximally expanded 277 mm section of bone. This patchy preservation and the subsequent restoration have likely distorted the curvature of this long bone. The proximal and distal ends of the preserved portions of the phalanx have the beginnings of being expanded posteriorly and ventrally, and so they are identified as preserving the shaft near the proximal and distal ends but not the ends themselves. The proximal and shaft fragments are separated by an unknown amount of missing bone, and considering that the preserved shaft is parallel-sided and both pieces have similar widths of their broken ends, it will likely never be known. First wing phalanges are preserved in the azhdarchiform species *M. minor* (Padian et al., 1995); the azhdarchid species *Q. lawsoni*, cf. *A. philadelphiae* (SMNK 1286 and 1287 PAL) (Frey and Martill, 1996) possibly including NHMUK PV R 9227, *Z. linhaiensis* (Unwin and Lü, 1997), *C. boreas* (Hone et al., 2019), *E. langendorfensis* (Vremir et al., 2013b), *M. maggii* (Vullo et al., 2018), and *A. lancicollis* (Averianov, 2010); the questionable and tentative azhdarchid *Navajodactylus boerei* Sullivan and Fowler, 2011 (Sullivan and Fowler, 2011); and the possible azhdarchid specimens KCM VP 000,120 (Averianov, 2014), ZIN PH 13/43 (Averianov, 2014), TMM 41839-2.2, TMM 41839-3.4, TMM 41839-7, TMM 41839-8, and ZIN PH 47/43 (Averianov, 2007).

The proximal fragment shares a subtriangular cross-section with the shaft, specifically an inverted posteriorly leaning scalene triangle with rounded corners (the dorsal surface is the greatest in width, followed by the anteroventral and posteroventral surfaces). The shaft cross-section of *Pteranodon* is described as probably suboval to subtriangular (Bennett, 2001a:96), and this would encompass most of the disparity found in pterosaur first wing phalanx cross-sections. However, the triangular cross-section of this phalanx in *Q. northropi* can be distinguished from the more oval cross-sections of *Q. lawsoni*, cf. *A. philadelphiae* (SMNK 1286 PAL) (Frey and Martill, 1996:230), *E. langendorfensis* (Vremir et al., 2013b:11), *M. maggii* (Vullo et al., 2018:9), *M. minor* (Buffetaut et al., 1996:755), and ME n° FO1-20 a possible first wing phalanx from the Maastrichtian of Aude in southern France (Buffetaut et al., 1996; Buffetaut, 2008). This fragment is deeper at its proximal end and its ventral apex is closer to the midline, suggesting that it came from a portion of the shaft just distal to the position where the cross-section transitioned from the anteriorly leaning triangle of the proximal end to the posteriorly leaning triangle of the shaft. The width of the proximal fragment is not completely preserved, but it is wider than the shaft and so some of the proximal expansion is preserved. This fragment appears to curve anteriorly, but it cannot be determined whether this is anatomical or preservational due to selective bone loss of the posterior edge. The latter is suggested because such bone loss has occurred on the posterior edge of the shaft as well as the anterior edge of the preserved proximal end.

The shaft fragment has a more or less constant width and depth as well as a dorsoventrally depressed and subtriangular cross-section (2.76 aspect ratio). *Azhdarcho lancicollis* shares with *Q. northropi* a triangular shaft cross-section that becomes dorsoventrally depressed distally, although this cross-section is distally oval in *A. lancicollis* (Averianov, 2010:305). The shaft of *E. langendorfensis* is described as dorsoventrally compressed but narrows toward its distal end (Vremir et al., 2013b:11). The distal end of TMM 41450-3.10 is expanded posteriorly but appears less so than the other wing phalanx ends in this and other species, with the possible exception of the first wing phalanx distal end in *Q. lawsoni*, cf. *A. philadelphiae* (SMNK 1286 PAL) (Frey and Martill, 1996:233, fig. 5e–f), and *J. edentus* (Wang et al., 2017:16). Although the distal end is missing, the

distal preserved cross-section appears to taper to an anterior point. Even though this phalanx is incomplete, it is one of the longest bones in the skeleton with a length over 24.80 times the mid-width (compared with an average of 22.91 for this phalanx in *Q. lawsoni*).

Second Wing Phalanx—The second phalanx of the left wing digit (TMM 41450-3.11) is represented by a 312 mm-long proximal fragment and a 73 mm-long distal fragment (Fig. 10I). Second wing phalanges are reported in the azhdarchid species *Q. lawsoni* (Lawson, 1975a), cf. *H. thambema* (UBB PT2) (Averianov, 2014), *Z. linhaiensis* (Unwin and Lü, 1997), *E. langendorfensis* (Vremir et al., 2013b), *A. bostobensis* (Averianov, 2007), and *A. lancicollis* (Averianov, 2010), as well as the putative azhdarchid specimens MTM V 2010.75.1 (Ősi et al., 2005, 2011), TMM 41839-3.7, ZIN PH 10/43, ZIN PH 55/44 (Averianov, 2007), and a couple of wing phalanges from the Valencia Province of Spain (Pereda-Suberbiola et al., 2007).

The proximal end is about two-and-a-half times the width and depth of the shaft (Table 2). A proximally oriented tuberculum is present on the anterior end of the proximal surface and is distinct from the anterior point to which this proximal surface tapers. This tuberculum comprises the anterior fifth of the proximal surface with the proximal articular surface positioned posterior and ventral to it. The entire proximal surface has a ventrally leaning lacriform outline, and the deep cotyle of this articular surface is posteroventrally expanded ovate in outline, similar to that of *A. lancicollis* (Averianov, 2010:305) but dissimilar to the subcircular to suboval outline of the proximal surface and weakly concave facet in *Pteranodon* (Bennett, 2001a:93 and 96). A small posterior process is present on the proximal surface of the phalanx and is considered a distinct part of the posterior expansion. There is a dorsal rim on the proximal articular surface such that the proximal margin of the phalanx is straight in dorsal view but concave in ventral view. The proximal surface is slightly posteriorly oriented as in other pterosaurs (Andres et al., 2014:S17). There is a small rugose extensor tubercle (low proximal bulge of Frey et al., 2011) on the proximal end of the anterior surface, but the anterior flange reported in *S. wucaiwanensis* is not present (Andres et al., 2010:177).

The ventral surface of the proximal end has a deep excavation that extends distally down the shaft and comprises half of the phalanx width between the raised anterior margin and the even deeper posterior margin. Approximately 12 cm distal to the proximal end (31% of preserved length), the raised posterior margin curves onto the midline of the second phalanx to form a large ventral ridge (prominent longitudinal ridge on the ventral side and ventral median ridge of Averianov, 2010) flanked by anteroventral and posteroventral sulci with a new raised margin formed posteriorly. This produces the characteristic 'T-shaped' cross-section of azhdarchid second and third wing phalanges (Nesov, 1991), although the lowercase Greek tau (τ) would be closer in shape to this cross-section. Most pterosaur groups have suboval to subtriangular wing phalanx shaft cross-sections, with or without a posterior groove (Andres, 2021) or concavity (Hooley, 1913:392; Kellner and Tomida, 2000:68). Averianov (2010) describes this ridge as being positioned anteriorly in *Quetzalcoatlus* (Averianov, 2010:306), but the ventral ridge is actually positioned posteriorly, becoming median along the shaft, as in *A. lancicollis* (Averianov, 2010:306, fig. 32B) and *E. langendorfensis* (Vremir et al., 2013b:11). *Jidapterus edentus* has a round weakly developed ridge in the middle of its second wing phalanx ventral surface (Wu et al., 2017:17), but it lacks the flanking sulci that would give it a well-developed τ-shaped cross-section and may be an incipient stage instead. A ventral ridge is also reported on the first wing phalanx of *D. weii* (Young, 1964:246), but these authors may be just referring to the ventral apex of a triangular cross-section. The proximal

ventral excavation becomes reduced to the anteroventral sulcus with the emergence of the posteroventral sulcus but is still wider than the latter, and the anterior raised margin becomes deeper than the posterior raised margin. The deep midline ventral ridge dividing the sulci is oriented posteroventrally. The dorsal surface of the shaft is flat-topped, as in *A. lancicollis* (Averianov, 2010:305), curving ventrally just at its anterior and posterior margins. The second wing phalanx tapers gradually from the proximal end. The preserved portions of the shaft are nearly straight and parallel-sided, with a width 1.78 times the depth. The τ-shaped cross-section disappears proximal to the preserved distal fragment. At this fragment, the shaft is dorso-ventrally depressed with a slightly concave dorsal surface, as in *A. lancicollis* (Averianov, 2010:305). The ventral surface has a raised anterior margin and midline elevation, with a low sulcus between the two and another on the posteroventral surface. The pneumatic foramina reported on the proximal and distal ends of the second wing phalanx ventral surface in *Pteranodon* (Bennett, 2001a:96, fig. 99) are absent in *Q. northropi*.

These longitudinal features terminate before the distal end with the exception of the raised anterior margin, which reaches the distal end to become the anterior point of the distal surface. The distal end has a slight ventral curvature with a posterior expansion in the horizontal plane and a ventral expansion in a parasagittal plane. This produces an unusual ventrally expanded lemon-shape in outline for the distal surface, in which the deepest point is on the midline, instead of being more posteriorly positioned like the proximal end of this bone or the distal end of the first phalanx. The articular surface is convex with a posteriorly positioned apex and a slight concave area anterior to it, giving the distal margin an apparent anterior deflection in the horizontal plane (obtuse articulations between wing phalanges of Wellnhofer, 1974, or angled distal condyle of Sangster, 2003). The subcircular to slightly suboval and weakly convex distal articular surface of *Pteranodon* (Bennett, 2001a:96) as well as the ovoid ball-and-cup arrangement described in *D. macronyx* (Padian, 1983a:20 and 34) are probably more representative of other pterosaurs.

Third Wing Phalanx—Two fragments of the left third wing phalanx are preserved in the holotype of *Q. northropi* (Table 2), a portion of the proximal articulation and a portion of the distal articulation (TMM 41450-3.14) (Fig. 10II). Third wing phalanges are reported in the azhdarchid species *Q. lawsoni* (Frey and Martill, 1996), *Z. linhaiensis* (Unwin and Lü, 1997), and *A. lancicollis* (Unwin and Bakhurina, 2000); as well as the putative azhdarchid specimens TMM 41839-3.6, ZIN PH 10/43 and 55/44 (Averianov, 2007), a specimen from the Boiţa commune of Romania (Averianov, 2014), and a couple of wing phalanges from the Valencia Province of Spain (Pereda-Suberbiola et al., 2007).

The anterior end of the proximal surface of TMM 41450-3.14 is missing, so it is not possible to determine if a proximally oriented tuberculum, anterior point, or extensor tubercle were present, as found on the second wing phalanx. Similarly, damage to the posterior expansion of the proximal end precludes identification of a posterior process. The preserved proximal articular surface is rather deep, with a width only about 1.61 times the depth, compared with the 2.88 aspect ratio of the preserved distal end of this fragment. Only the posterior half of the proximal articular surface is preserved. This is a deep concave surface that would have a posteriorly expanded lacriform outline if it had the shape of the rest of the proximal end, as opposed to the more rounded cross-section of *A. lancicollis* (Averianov, 2010:305, fig. 32D). There is a dorsal rim to this surface, but it is too damaged to determine its margins. The proximal end appears to taper distally.

The shaft is not preserved and so the length and curvature of the phalanx is unknown. Its cross-section is likewise difficult to discern. The broken end of the proximal fragment has a flat dorsal surface and a ventral excavation bounded by a raised anterior margin and a deeper posterior margin on the ventral surface. This produces a cross-section similar that of to the second wing phalanx proximal to the point that the posterior margin curves onto the midline to form the midline ridge of the τ-shaped cross-section.

The broken end of the distal fragment is oval in cross-section. This distal fragment is missing its anterior margin and most of its cortical bone, obscuring its orientation. The distal articular surface is convex with a middle apex. This articular surface is subcircular in outline with a slight posterior prominence, which is likely part of a posterior expansion. It is not known if a posterior process was present on the distal end, but the distal end is significantly ventrally expanded. The pneumatic foramina suggested to be present on the proximal and distal ends of the third wing phalanx ventral surface in *Pteranodon* (Bennett, 2001a:96, fig. 99) are also absent in *Q. northropi*.

QUETZALCOATLUS cf. *NORTHROPI* Lawson, 1975b
(Figs. 9G and 11–12)

Referred Material—Right femur missing distal end (TMM 41047-1) from locality TMM 41047, left femur proximal end missing head (TMM 41398-3) and right first wing phalanx proximal end (TMM 41398-4) from locality TMM 41398, and cervical VI (TMM 42889-1) from locality TMM 42889. All sites are within the Javelina Formation.

Cervical VI—TMM 42889-1 is the only pterosaur cervical vertebra preserved in sandstone in Big Bend National Park (Fig. 11). It is also unique in being bigger than the other cervicals (the widest and only surpassed in length by the distorted TMM 41954-7) and morphologically distinct from the cervicals of *Q. lawsoni* and *W. brevirostris*. This cervical cannot be referred to either of those species, and it is instead identified as *Quetzalcoatlus* cf. *northropi* with the other stream-channel pterosaur specimens, except for TMM 44036-1 that is referred to *Q. northropi*. Sixth cervicals are present in the azhdarchid species *Q. lawsoni*, cf. *A. philadelphiae*: SMNK 1285 PAL (Frey and Martill, 1996) and BSPG 1966 XXV 508 (Martill and Moser, 2017), *W. brevirostris*, *Z. linhaiensis* (Cai and Wei, 1994), *P. mauritanicus* (Kellner, 2010; Longrich et al., 2018), *A. bostobensis* (Averianov, 2004, 2007), *A. lancicollis* (Averianov, 2010); the azhdarchiform species *M. minor*; and the putative azhdarchid specimens MPC-Nd 100/302, MC SF69, MCNA 8563 (Averianov, 2010), MGUV 2271 (Company et al., 1999), MPV TT48, and MTM V.01.51 (Averianov, 2010; Ősi et al., 2011).

TMM 42889-1 is nearly complete, missing only the prezygapophyses (processus articulares craniales of Frey and Martill, 1996, or epipophyses of Buffetaut, 2001) and cervical ribs (diminutive ribs and vestigial ribs of Godfrey and Currie, 2005, bridges of bone of Watabe et al., 2009, or vestigial cervical ribs of Vremir et al., 2015, or ventrally directed crests of Harrell et al., 2017). Length measurements have systematic importance for cervical vertebrae, and so it is important to estimate the length of the missing prezygapophyses to get the total length of the vertebra. The preserved length is >410 mm, which is essentially that of the centrum length. Extending the medial and lateral margins of the prezygapophysis bases, or scaling up *Q. lawsoni* vertebrae, adds 3 cm to the length estimate for the prezygapophysis. This produces a rather conservative 440 mm length estimate for this bone (Table 2). Most notable about this cervical is its significant dorsoventral depression, which gives it an elliptical cross-section. Some of this depression could be due to taphonomy, based on some torsion along the shaft, but taphonomy cannot account for most of the depression or the depression present at the
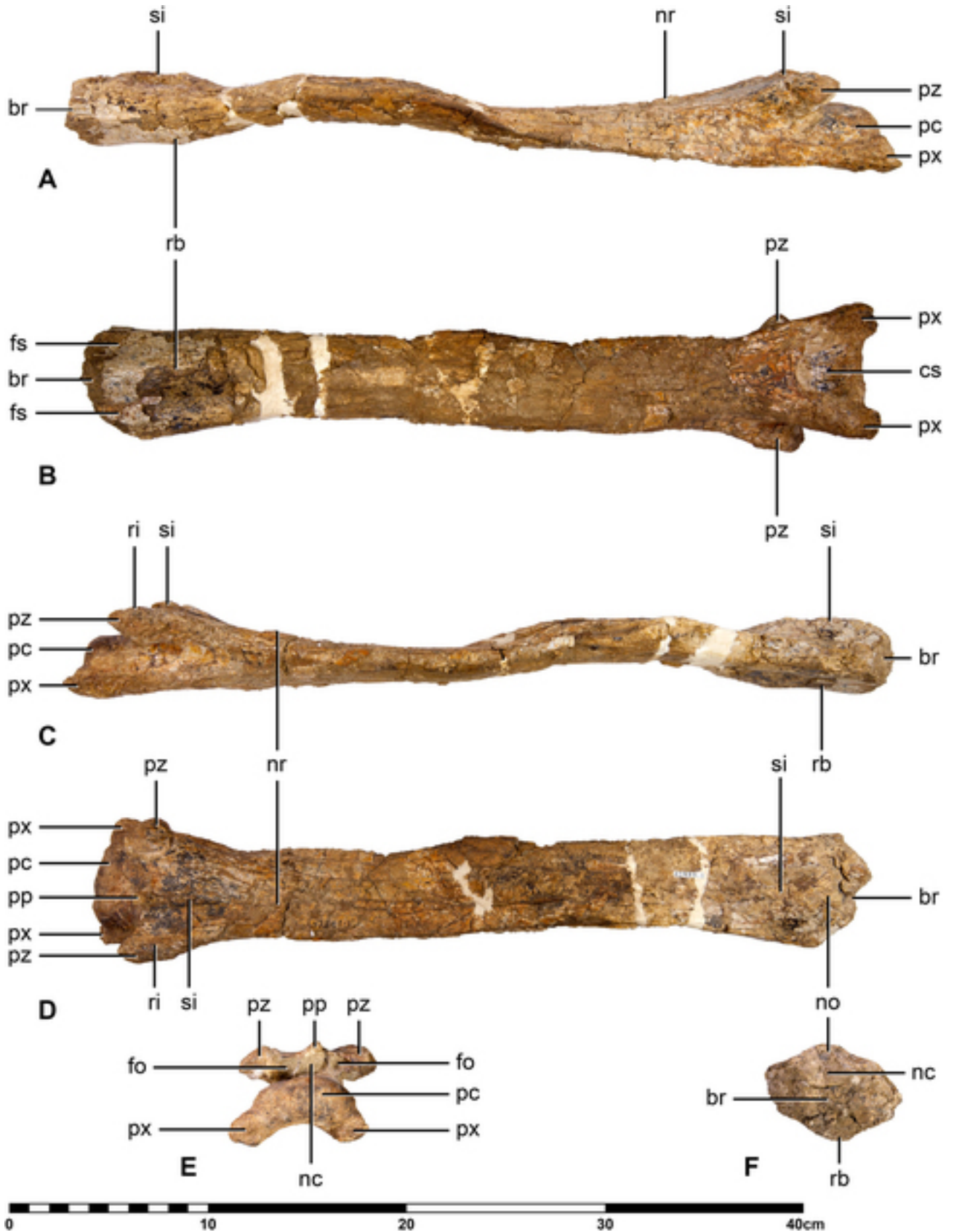
FIGURE 11. *Quetzalcoatlus* cf. *northropi* cervical VI (TMM 42889-1) photographs in **A**, left lateral; **B**, ventral; **C**, right lateral; **D**, dorsal; **E**, posterior; and **F**, anterior views. **Abbreviations: br**, break; **cs**, concave surface; **fo**, foramen; **fs**, fossa; **nc**, neural canal; **no**, notch; **nr**, neural ridge; **pc**, posterior condyle; **pp**, posterior process; **px**, postexapophysis; **pz**, postzygapophysis; **rb**, raised band; **ri**, ridge; and **si**, spinous process. Scale bar equals 40 cm.
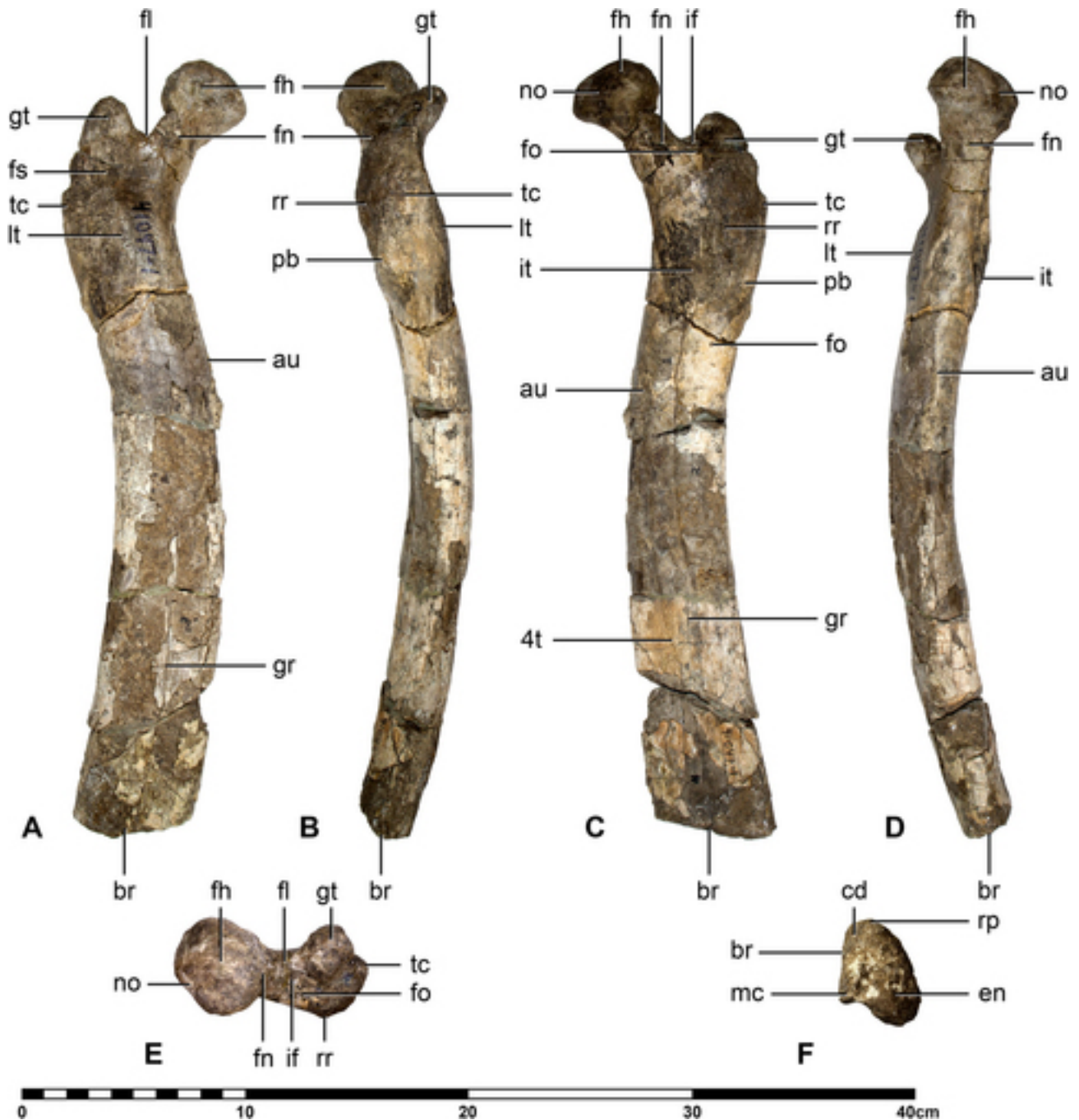
FIGURE 12. *Quetzalcoatlus* cf. *northropi* right femur proximal end and shaft (TMM 41047-1) photographs in **A**, anterior; **B**, lateral; **C**, posterior; **D**, medial; and **E**, proximal views; as well as a **F**, distal fragment in distal view. **Abbreviations: 4t**, fourth trochanter; **au**, adductor ridge; **br**, break; **cd**, circular depression; **en**, entepicondyle; **fh**, femoral head; **fl**, flange; **fn**, femoral neck; **fo**, foramen; **fs**, fossa; **gr**, groove; **gt**, greater trochanter; **if**, inter-trochanteric fossa; **it**, internal trochanter; **lt**, lesser trochanter; **mc**, medial condyle; **pb**, protuberance; **no**, notch; **rp**, raised prominence; **rr**, rugose ridge; and **tc**, trochanteric crest. Scale bar equals 40 cm.

anterior and posterior ends. Unsurprisingly, it lacks the dorsal arching of the laminae found in *Q. lawsoni* sixth cervicals. The vertebra is 9.51 times longer than its mid-width (compare with the 8.14 aspect ratio of the cervical VI in *Q. lawsoni*), but that aspect ratio increases to 21.71 when the mid-height is considered. The neural arch (arcus neuralis of Frey and Martill, 1996) and centrum (corpus and corpus vertebrae of Frey and Martill, 1996) are confluent with no trace of a suture.

The anterior end is damaged, but a ventral inflation flanked by lateral fossae matches the base of the hypapophysis (shallow keel of Bennett, 2001a) at the anterior end of the centrum in the other Big Bend pterosaurs. This inflation does not have a distinct tumescence as in the cervicals III and IV of *Q. lawsoni*, but it does continue posteriorly as a raised band (crista sagittalis ven-tralis of Frey and Martill, 1996; median ventral projection of Watabe et al., 2009; short ventral ridge along the anterior body

of the centrum of Vremir et al., 2015; or hypapophyseal 'keel', hypapophyseal ridge, carina, and tumescence of Harrell et al., 2017) adding to the depth of the anterior end, as in the cervical VI of *Q. lawsoni*. A large anterior notch present in the interzygapophyseal ridge (blunt transverse ridge of Martill et al., 1998, transverse buttress of Bennett, 2001a, dorsal edge of the neural arch of Averianov, 2004, ridge that passes posterodorsally to form the anterior rim of the low-vaulted neural arch of Godfrey and Currie, 2005, downwardly diverging laminae of Harrell et al., 2017, or laminae of Longrich et al., 2018) over the neural canal (tuba vertebralis of Frey and Martill, 1996, or cerebrospinal canal of Averianov, 2004) is also found in the sixth cervical of *Q. lawsoni*. This is the most incised dorsal margin of the neural canal opening (foramen vertebralis of Frey and Martill, 1996) found in any of the Big Bend pterosaur cervicals. It appears that the anterior end of the vertebra was sheared off just posterior to the anterior cotyle (fossa condyloidea of Frey and Martill, 1996, facies articularis cranialis of Martill et al., 1998, or anterior articular surface of the centrum of Watabe et al., 2009, or cotyla of Vremir et al., 2015). In fact, the concave ventral margin of the neural canal that would turn the anterior cotyle into a cordate (heart-shaped) outline with the hypapophysis is visible in the broken cross-section. This is all that can be seen of the anterior vestibule of the neural arch (facies anterior of the arcus neuralis of Martill et al., 1998, recess located under the V-shaped ridges of Buffetaut, 2001, interzygapophyseal area/space of Vremir et al., 2015, or vestibule of the neural canal of Harrell et al., 2017). The posterior vestibule of the neural arch is visible and roofed by the interzygapophyseal ridge. A large, wide, and subrectangular neural canal is visible in this posterior vestibule, flanked by a pair of subtriangular pneumatic foramina lateral to the neural canal (foramina pneumatica of Martill et al., 1998, or bilaterally positioned pneumatopores of Godfrey and Currie, 2005). As in other azhdarchids (Howse, 1986:317), the neural spine (neural crest of McGowen et al., 2002) is split into anterior and posterior spinous processes (processus spinosus of Frey and Martill, 1996, neural spine projection of Vremir et al., 2015, neural elevation of Harrell et al., 2017, or neural spine [anterior region] and posterior spine [posterior region] of Naish and Witton, 2017) separated by a pencil-thin ridge extending along the midline of the dorsal surface ('bifid' neural spine of Naish and Witton, 2017). This neural ridge (crista sagittalis dorsalis of Frey and Martill, 1996), as it is termed here, is visible posteriorly but is lost in its middle due to the poor preservation, and so it cannot be confirmed to reach the entire distance between the anterior and posterior processes of the neural spine. The anterior spinous process is broken off at its base and can be seen as a midline rise at the anterior end of the vertebra. The posterior spinous process is a tall ridge that overhangs the neural canal as a posterior process. There is no sign of transverse ridges (transverse processes of Howse, 1986, carinae parasagittales of Frey and Martill, 1996, transverse processes of Ikegami et al., 2000, parasagittal carinae and carinae parasagittales of Averianov, 2004, longitudinal ridges of Watabe et al., 2009, dorsolateral ridges of Harrell et al., 2017, or dorsolateral ridges and faint ridges of Longrich et al., 2018) running along the sides of this bone, but the preservation would all but preclude observing them if they are present. This cervical vertebra is also distinct in lacking a lateral constriction in its middle, similar to the reduced constriction of the *Q. lawsoni* cervical VI. However, it does have a dorsoventral constriction at a third of its length from the posterior end. The postzygapophyses (processus articulares caudales of Frey and Martill, 1996) diverge slightly laterally and expand into rounded processes. Low rounded ridges extend over their dorsal surfaces. The postzygapophyses and their articular surfaces are laterally expanded, the surfaces forming transverse ellipses. There are no traces of the epipophyses ('tubercle of the postzygapophysis'

of Wellnhofer, 1991b; or tubercular elevation, longitudinally ovate tubercle, and dorsal torus of Harrell et al., 2017). The posterior condyle (condylus vertebralis of Frey and Martill, 1996, and posterior articular surface of the centrum of Watabe et al., 2009) is a wide oval in posterior view. The postexapophyses (short obtuse processes, thick diverging apophyses, rudimental processes, and transverse processes of Owen, 1859; postexapophyses and exapophyses of Williston, 1897; posthypapophyses of Lawson, 1975a; postexapophyses and postexapophysial processes of Howse, 1986; processus ventrolaterales of Frey and Martill, 1996; or lateral exapophyses and postexapophyses of Henderson and Peterson, 2006) form long bases with the lateral margin of the centrum. There is not a lateral excavation (shallow pit at the incisura vertebralis caudalis of Frey and Martill, 1996, or fossae of Henderson and Peterson, 2006) between the base of the postexapophysis and postzygapophyses. The postexapophyses are blunt and barely extend past the posterior condyle. They are positioned at the ventrolateral edges of the posterior condyle. There is a concave surface between the postexapophyses on the underside of the posterior condyle. The length and elongated shape of TMM 42889-1 identifies it as a middle-series cervical vertebra (cervical III-VII). The relatively high aspect ratio, deep anterior centrum, ventral raised band without a tumescence, little to no lateral constriction, and presence of a large notch in the anterior interzygapophyseal ridge as found in the cervical VI of *Q. lawsoni* indicates that this is a sixth cervical.

First Wing Phalanx—TMM 41398-4 is the proximal end of the right wing phalanx 1 exposed in ventral view and still partially encased in matrix (Fig. 9G). It does not include the proximal articulation but does include a shaft fragment and a natural mold of the shaft fragment (Table 2). The subtriangular cross-section of the bone allows identification as a wing phalanx. The rapid proximal expansion, convex dorsal margin, subequal anteroventral and posteroventral surfaces, and relatively greater depth of the end allows identification as the proximal end of the first wing phalanx. This specimen comes from the proximal end but does not include the proximal surface of the first wing phalanx: the base of the posterior process is preserved in cross-section and the transition from a proximally leaning subtriangular cross-section to a more symmetrical cross-section is preserved, but the proximal cotyles and intercotylar sulcus of the proximal margin are not preserved. It is highly congruent in cross-sectional shape to the preserved first wing phalanx proximal end of the *Q. northropi* holotype (TMM 41450-3.10), but no autapomorphies could be observed to definitively refer it to this species. This specimen is about 70% of the size of the comparable region of the holotype. The many short pores in the bone grain suggest that this is not an osteologically mature individual (Bennett, 1993:95), and so the difference in size may be attributed to ontogeny.

Femur—The pterosaur femur is a long bone with a distinct head, neck, and greater trochanter on the proximal end as well as a large pair of condyles flanked by epicondyles on the distal end. TMM 41047-1 is a giant right pterosaur femur from an individual comparable in size to the holotype of *Q. northropi* (Fig. 12). It consists of the proximal half, a couple of shaft fragments (not figured), and the medial half of the distal end. Based on the expansion and preserved width of the shaft, only about half of the bone is preserved; if accurate, this would be the longest pterosaur femur by length and relative to the humerus length (Table 2). This would also be the most robust pterosaur femur, with a mediolateral mid-width about one-and-three-quarters times greater than the anteroposterior mid-breadth. It is described here in vertical orientation. Femora are reported in the azhdarchid species *Q. lawsoni*, cf. *A. philadelphiae* (BSPG 1966 XXV 506) (Martill and Moser, 2017), cf. *H. thambema* (FGGUB R.1625) (Buffetaut et al., 2003), *Z. linhaiensis* (Cai

and Wei, 1994), *C. boreas* (Hone et al., 2019), *A. lancicollis* (Nesov, 1984); and the putative azhdarchid specimens MCNA number unknown (Averianov, 2014), NJSM 18772 (Parris et al., 2004), TMM 41839-3.1 and 3.2, TMP 1991.36.616 and 92.83.6 (Godfrey and Currie, 2005), and ZIN PH 82/44 (Averianov, 2014).

The femoral head (condyle of Averianov, 2004, or caput femoris of Dalla Vecchia, 2009) is massive and medially perched on the femoral neck (femoral collum of Eck et al., 2011) such that the neck attaches to the lateral half of the base of the head in TMM 41047-1, unlike other pterosaurs. It does have an articular surface that extends more anteriorly than posteriorly, which is reported in other pterosaurs (Kellner and Tomida, 2000:75; Bennett, 2001a:101). This articular surface is hemispherical as in other ornithocheiroids (Hooley, 1913:393; Young, 1964:240; Kellner and Tomida, 2000:75; Bennett, 2001a:101; Godfrey and Currie, 2005:306; Averianov, 2010:307; Wu et al., 2017:20). A distinct notch is present on the posteromedial margin of the femoral head that is widespread in pterosaurs, with the exception of *Pteranodon* (Bennett, 2001a:104) and *Keresdrakon vilsoni* Kellner et al., 2019a. The femoral neck is long, as in other Neoazhdarchia (Young, 1964:240; Bennett, 2001a:104; Averianov, 2010:307), and constricted, as in other Novialoidea (Andres, 2021). This constriction is 46% of the diameter of the femoral head, roughly equivalent to the half diameter reported in *Pteranodon* (Bennett, 2001a:101). The neck is elliptical in cross-section, disparate from the subcircular cross-section of *Pteranodon* (Bennett, 2001a:101) and the triangular cross-section of *A. lancicollis* (Averianov, 2010:307). The head and neck are oriented anteromedially at an angle of 139°, much less than the more perpendicular angle of non-novaloid pterosaurs but less than the high angle of the pteranodontoids (Andres, 2021).

The greater trochanter (lateral trochanter of Young, 1964, trochanter externus of Wellnhofer, 1974, fourth trochanter and trochanteric process of Frey et al., 2006, or fourth trochanter and greater trochanter of Eck et al., 2011) is a massive rugose process constituting most of the mediolateral width of the proximal end. It is an anteriorly curving and hook-shaped process in TMM 41047-1 as in other neoazhdarchians (Andres, 2021), but it is oriented more dorsally and laterally expanded into a triangular outline in this specimen. A short flange extends between the femoral neck and greater trochanter. A pneumatic foramen is positioned posterior to this flange as in other ornithocheiroids, except *Anhanguera* (Andres, 2021), surrounded by an intertrochanteric fossa (deep trochanteric fossa of Hooley, 1913, deep groove of Young, 1964, marked depression of Sangster, 2003, shallow triangular sulcus of Frey et al., 2006, or intertrochanteric depression of Averianov, 2010). This foramen is slit-like, as reported in *A. bostobensis* (Averianov, 2007:195). The anterior surface of the proximal end has a fossa at the base of the greater trochanter, reminiscent of a concave area reported in *A. bostobensis* (Averianov, 2007:195) and may correspond to a deep lateral fossa reported in *D. weii* (Young, 1964:248) and DFMMh/FV 500 (Fastnacht, 2005:277), or a distinct shallow groove or depression on the anteromedial aspect of the greater trochanter reported in *A. spielbergi* (Veldmeijer, 2003:94, fig. 20B). A proximodistally oriented oval prominence on the lateral half of the proximal shaft anterior surface is identified here as the lesser trochanter (scar for the iliofemoralis internus of Averianov, 2010), and it is similar in shape to the structure in *A. bostobensis* and *A. lancicollis* (Averianov, 2007:195). Lateral to the lesser trochanter, the proximal end of the femur has a convex lateral margin in anterior/posterior view termed the trochanteric crest by Frey et al. (2011) (crest of Frey et al., 2006, and lesser trochanter of Eck et al., 2011). Frey et al. (2011) also mention a protuberance that this crest curves around that they suggest could represent a third trochanter, and there is a protuberance on the posterior surface of the

trochanteric crest in TMM 41047-1 to which this could correspond. The posterior surface of the proximal end has a massive vertical rugose ridge (wrinkled surface of Averianov, 2007, or low ridge of Averianov, 2010) connecting to the greater trochanter, extending down a quarter of the preserved shaft, and constituting the lateral half of the posterior surface. A small foramen is distal to this ridge. Averianov (2007, 2010) identified the distal portion of this ridge in *A. bostobensis* and *A. lancicollis* as the internal trochanter, the insertion for M. puboischiofemoralis externus (Bennett, 2001a). However, a ridge-like muscle scar medial to this low ridge identified in *A. lancicollis* (Averianov, 2010:309, fig. 34C) is more likely the internal trochanter, considering its similar position and orientation to the internal trochanters identified in other pterosaurs (Kellner and Tomida, 2000:75; Bennett, 2001a:103; Buffetaut et al., 2003:101). This area is damaged and missing much of its cortical bone in TMM 41047-1, but the base of a rugose eminence just lateral to this damage is identified here as the internal trochanter. A groove (well-marked groove of Kellner and Tomida, 2000, distinct shallow groove of Veldmeijer, 2003, elongate oval trough of Godfrey and Currie, 2005, or narrow longitudinal groove of Averianov, 2007) reported in this area in other ornithocheiroids (Kellner and Tomida, 2000:75; Veldmeijer, 2003:94; Godfrey and Currie, 2005:306; Averianov, 2007:195) could not be located in this specimen.

The preserved shaft is anteriorly bowed (convex anteriorly, concave posteriorly), tracing an arc of at least 40° in a parasagittal plane. Pterosaur femora are described as ranging from straight (Hooley, 1913:410, 415, and 416; Bennett, 2001a:10), to slightly curved (Wellnhofer, 1974:21; Veldmeijer, 2003:94; Lü and Ji, 2005a:305; Bennett, 2013:35; Martill and Moser, 2017:16; Wu et al., 2017:20); curved (Hooley, 1913:410; Cai and Wei, 1994:190; Fastnacht, 2005:276; Godfrey and Currie, 2005:306; Lü et al., 2008:89), slightly bowed (Bennett, 2001a:101; Buffetaut et al., 2003:10), and bowed (Huene, 1914; Padian, 1983a:21; Padian and Wild, 1992:73; Unwin and Lü, 1997:207; Kellner and Tomida, 2000:75; Padian, 2008a:102; 2008b:56; Dalla Vecchia, 2009:169; Eck et al., 2011:290; Kellner et al., 2019a:16) in the parasagittal plane, but TMM 41047-1 and *Q. lawsoni* are strongly bowed to a degree only found in the dsungaripterids (Andres, 2021). Some pterosaur femoral shafts have been described as 'sigmoidal' (Frey et al., 2006:32; Averianov, 2010:309; Dalla Vecchia, 2019:39), but this is due to the fact that the pterosaur femur is bowed in two planes (Padian, 1983a,b) and flattening/crushing of this bone can make it appear as though both curvatures are in the same plane. The femoral head and neck of TMM 41047-1 are straight in line with the shaft in medial/lateral view. In anterior/posterior view, the shaft is sinusoidal with a medial curvature of the proximal end and lateral curvature of the preserved distal shaft. This medial curvature is also reported in dsungaripterids and DFMMh/FV 500 (Fastnacht, 2005:278), but this may be widespread and recognized in rarer three-dimensionally preserved specimens. The shaft of the femur has a relatively constant diameter over its length as in *D. weii* (Young, 1964:248; Bennett, 2001a:10) and *Istiodactylus sinensis* Andres and Ji, 2006, reaching its minimum width distal to the proximal end, expanding slightly over the rest of the shaft, and lacking a distinct constriction. The shaft cross-section is an anteroposteriorly compressed oval, similar to cf. *A. philadelphiae* (BSPG 1966 XXV 506) (Martill and Moser, 2017:166, fig. 4d), *A. lancicollis* (Averianov, 2010:309), and at least the distal half of *Pteranodon* and YPM VPPU 021821 (Bennett, 2001a:103–104). A jagged ridge on the medial surface of the proximal shaft that curves distoposterolaterally is identified here as the adductor ridge (small depression with rugose surface of Kellner and Tomida, 2000, well-marked oblique ridge of Buffetaut et al., 2003, and low and blunt ridge of Frey et al., 2011) for the insertion of M. adductor femoris (Bennett, 2001a:103, fig. 107B). This ridge disappears into a

region of the shaft missing its cortical bone save for a small section on the posterior surface. The fourth trochanter of the femur is extremely reduced in pterosaurs (Sereno, 1991). There is a band of muscle scarring extending down this section of the shaft medial to the midline that is similar in position and shape to the fourth trochanter delineated in other pterosaurs (Padian and Wild, 1992:73; Kellner and Tomida, 2000:75; Bennett, 2001a:103) and is identified as such here. Despite the lack of cortical bone on the shaft, longitudinal grooves extending along the middle of the anterior and posterior surfaces can be observed. Posterior longitudinal grooves are reported in *A. bostobensis* and *A. lancicollis* (Averianov, 2007:195) as well as *A. piscator* (Kellner and Tomida, 2000:75) and *A. spielbergi* (Veldmeijer, 2003:94), but this groove is associated with the origin of M. femorotibialis in those azhdarchid species (Averianov, 2007:195) and with the fourth trochanter in those *Anhanguera* species (Kellner and Tomida, 2000:75). Two posterior fragments of the shaft (not figured) demonstrate that the cross-section becomes more elliptical distally.

Only the medial entepicondyle and partial medial condyle of the distal end is preserved. The entepicondyle is massive, taking the azhdarchoid pattern of having distinct epicondyles expanded into flanges (Andres, 2021) to the extreme with a 25 mm-wide rounded condyle in its own right, giving the distal end a convex medial outline. It is not known if it participated in the knee joint. The entepicondyle appears to form a raised prominence on the anterior surface, or this may be the medial half of the patellar sulcus. Only the medial edge of the medial condyle is preserved, and it is not separated from the epicondyle by a sulcus, which is found in *A. lancicollis* (Averianov, 2010:309) and TMP 1991.36.616 (Godfrey and Currie, 2005:306, fig. 16.10D). The medial condyle is posteriorly positioned and posteriorly angled, as in the distal condyles of other pterosaurs (Padian, 1983a:21–22; Bennett, 2001a:104; Padian, 2008b:56; Wu et al., 2017:20). A small depression is present on the anterior end of the medial condyle, matching the circular depression (shallow pit presumably for tendinous attachment of Godfrey and Currie, 2005) reported in *A. lancicollis* (Averianov, 2010) and TMP 1991.36.616 (Godfrey and Currie, 2005:306). There is no trace of a popliteal fossa (popliteal sulcus of Veldmeijer, 2003, or medial triangular depression of Fastnacht, 2005) or intercondylar fossae, but it is likely these were not preserved in this specimen. The entepicondyle is oriented posterolaterally so that if the ectepicondyle was a mirror image of it, the distal end would have a cross-section more like the D-shaped cross-section of *A. lancicollis* (Averianov, 2010:309) than the triangular cross-section of *A. piscator* (Kellner and Tomida, 2000:75).

TMM 41398-3 is the proximal end of the left femur missing most of the femoral head and greater trochanter (Table 2). This specimen has an expanded and bifurcated proximal end, with the larger medial bifurcation representing the base of the femoral neck and the smaller lateral bifurcation representing the base of the greater trochanter. The preserved base of the femoral neck forms about a 143° angle with the shaft. The base of the greater trochanter is large, constituting approximately a third of the shaft width. A posteriorly excavated flange extends between the femoral neck and the greater trochanter. Cortical bone is missing from this region and a pneumatic foramen or an intertrochanteric fossa cannot be identified. A slight fossa is present on the anterior surface of the femur between the bases of the neck and trochanter; an oval lesser trochanter is present. Damage to the cortical bone obscures the internal trochanter and posterior protuberance on the trochanteric crest. The ventral end of the rugose vertical ridge connected to greater trochanter is visible on the lateral half of the posterior surface. Only a proximal portion of the shaft is preserved, but it has a slight medial curvature over its preserved portion. The shaft cross-section is an anteroposteriorly compressed oval with a more convex posterior surface. TMM 41398-3 is similar to TMM 41047-1: there is a large greater trochanter present and directed dorsally, a fossa on the anterior surface of the proximal end, an oval lesser trochanter, a slight medial curvature of the proximal shaft, and an anteroposteriorly compressed oval shaft cross-section. TMM 41398-3 is about 70% the size of TMM 41047-1 and is characterized by a pitted and rough texture at the proximal end, so this difference in size is likely ontogenetic.

QUETZALCOATLUS LAWSONI, sp. nov.
(Figs. 1, 13–49)

Pterosaur from the Latest Cretaceous of West Texas (Lawson, 1975a:947, fig. 1) (original description).
Quetzalcoatlus northropi Lawson 1975b:678 (original name).
Quetzalcoatlus sp. (Lawson, 1975b) Langston, 1981:128, fig. 10 (new combination).

Holotype—TMM 41961-1, an associated individual comprising the following elements: cranium missing anterior end and neurocranium (TMM 41961-1.1), mandible missing anterior end (TMM 41961-1.2), cervical V (TMM 41961-1.28), cervical VI (TMM 41961-1.29), and cervical VII anterior half (TMM 41961-1.30), left ulna distal end (TMM 41961-1.8), right proximal syncarpal (TMM 41961-1.9), right distal syncarpal (TMM 41961-1.10), right medial carpal (TMM 41961-1.14), left and right pteroids (TMM 41961-1.12 and 1.11), second through fourth phalanges of right manual digit III (TMM 41961-1.18 to 20), third phalanx of right manual digit II (TMM 41961-1.21), left wing metacarpal (TMM 41961-1.3) and right wing metacarpal proximal half (TMM 41961-1.13), left first wing phalanx (TMM 41961-1.4) and right first wing phalanx without proximal end (TMM 41961-1.15), left and right second wing phalanx (TMM 41961-1.5 and 1.16), left and right third wing phalanx (TMM 41961-1.6 and 1.17), left fourth wing phalanx (TMM 41961-1.7), left femur missing proximal end (TMM 41961-1.22) and right femur shaft fragment (TMM 41961-1.24), left and right tibiotarsi (TMM 41961-1.23 and 1.25), left metatarsal I shaft (TMM 41961-1.27), right metatarsal II shaft and distal fragment (TMM 41961-1.26), and left first pedal phalanx digit I distal end (TMM 41961-1.31) (Fig. 1).

Etymology—The specific name is in honor of Douglas A. Lawson, the discoverer of *Quetzalcoatlus*, masculine genitive singular.

Localities and Horizon—Specimens were collected from the abandoned channel-lake deposits of Pterodactyl Ridge in the northeast of Big Bend National Park, Brewster County, Texas, U.S.A. These specimens were located in the unit 15 of the upper Javelina Formation, late Maastrichtian Age, latest Cretaceous Period, between 69 ± 0.9 Ma and the end of the Cretaceous (Lehman, 2021).

Diagnosis—Large azhdarchid pterosaur (wingspan 4.5 meters) that can be distinguished from *Quetzalcoatlus northropi* and other pterosaurs by the following autapomorphies: rostrum and mandible occlusal margin sinusoidal in lateral view, rostrum with inverted T-shaped cross-section, palate with foramen anterior to the nasoantorbital fenestra, nasoantorbital fenestra tall with more than 40% of height extending above orbit, premaxilla sagittal crest positioned over posterior half of nasoantorbital fenestra with humped rectangular outline in lateral view, palatines ventrally bowed, nasals extremely enlarged and conjoined, frontals vertically oriented, frontals form flat shelf at contact with premaxilla and nasal, confluent choanae with anterior expansion, pterygoid lateral process with foramen on base, quadratojugal dorsally displaced into infratemporal fenestra, quadratojugal hourglass-shaped with marginal openings,

mandible articulation with diagonal posterolateral ridge as well as anteriorly facing flat surface and notch in articular surface ventral margin, mandible anterior end dorsoventrally flattened and lacks marginal ridges, mandible symphysis occlusal surface and posterior ventral surface with circular openings, mandible symphysis posterior end with occlusal ridges that curve medially, mandible rami with sharp marginal ridges, mandible symphyseal depression without ridges, atlas neural arch with postzygapophyseal process, axis length greater than posterior width, axis neural spine vertical, axis neural spine without spinous process, axis with massive lamina, axis with robust ridge extending along postzygapophysis medial surface, axis centrum lateral surface with pneumatic foramen in deep excavation, axis neural canal posterior end ovate in outline, postaxial cervical vertebrae with preexapophyses, middle-series cervical vertebrae neural spine overhangs neural canal posterior end, cervical vertebra III neural spine tall with rectangular outline in lateral view, cervical vertebra III postzygapophyses with rhomboid outline in dorsal view, cervical vertebrae III postzygapophyses with large epipophyses, cervical vertebra III with fossa on anterior surface of the neural arch, cervical vertebra III with dorsal ridge on postzygapophyses, cervical vertebra III centrum with lateral excavation ventral to postzygapophyses, cervical vertebrae III and IV with ventral tumescences, cervical vertebra IV with concave ventral margin in lateral view and ventrally curving posterior condyle, cervical vertebra IV cross-section transitions from wider than tall to taller than wide at a posterior constriction, cervical vertebra IV posterior spinous process taller than anterior spinous process, humerus deltopectoral crest height more than twice deltopectoral crest mid-width, humerus distal surface with three pneumatic foramina*, ulna with pneumatic foramen between ulna proximal cotyles*, ulna proximal end with ridge on ventral part of anterior surface, ulna with gradual ventral expansion over distal third*, ulna distal end dorsal articular surface does not reach the anterior surface*, radius gradual ventral expansion over distal third*, proximal syncarpal with large pneumatic foramen ventral to radial dorsal articular facet*, proximal syncarpal radial dorsal articular facet with flange on ventral margin*, distal syncarpal dorsal surface with elliptical foramen at base of medial carpal process*, medial carpal with notch in medial rim of proximal cotyle, medial carpal with pit anteroventral to fovea and oriented laterally, medial carpal with large oval pneumatic foramen in center of medial surface, carpal sesamoid with circumferential ridge as well as short side process and small foramen, manual phalanx 1 digit I anterior surface with ridges on dorsal and ventral margins*, medial distal tarsal proximal articular surface constitutes 75% anteroposterior breadth and 100% mediolateral width, lateral distal tarsal with very large tendinal groove that curves posterior to medial distal tarsal, and distal intertarsal articular surface larger than proximal intertarsal articular surface. (* = diagnostic features for elements preserved in *Q. lawsoni* and *Q. northropi*).

Referred Specimens—TMM 41544-1 to 34, TMM 41545-1, TMM 41546-1 to 8, TMM 41547-1 and 2, TMM 41954-1 to 91, TMM 41961-2 and 4, TMM 42138-1 to 4, TMM 42157-2, TMM 42161-1 to 3, TMM 42180-1 to 25, TMM 42246-1 to 4, TMM 42259-1, TMM 42272-1 to 4, TMM 42297-1, TMM 42422-1 to 39, TMM 42462-1, TMM 42521-1, TMM 44037-1 and 2, TMM 44048-1, as well as TMM 45977-1 and 2, and TMM 45997-1 to 4, all from Pterodactyl Ridge.

LSID—urn:lsid:zoobank.org:act:4F1C5123-DD3F-47F9-967E-1B5422428C11.

Remarks—Common usage has considered the giant specimen (TMM 41450-3) as *Q. northropi*, and the smaller specimens found some distance away as a separate species. This practice began with Langston (1981), who restricted *Q. northropi* to the holotype and classified the smaller individuals as representing *Quetzalcoatlus* sp., an undetermined species. He noted that the two groups of *Quetzalcoatlus* were found 50 km apart (40 km in other publications) and could not be established as the same population or even living at the same time. Ultimately, Langston (1981) designated the smaller morph as *Quetzalcoatlus* sp. in the absence or proof that it was the young of *northropi* and pending new discoveries that might settle the issue definitively. Kellner and Langston (1996) were convinced that they were separate taxa based on distinctive morphological features, and they stated that a characterization of a new species of *Quetzalcoatlus* was in preparation. That characterization was never completed.

It has been common practice to refer to only the giant individual (TMM 41450-3) when discussing *Quetzalcoatlus* or *Quetzalcoatlus northropi*, and to refer to the smaller morph as *Quetzalcoatlus* sp., if it is mentioned at all. This issue has been specifically addressed only by Andres and Myers (2013). They phylogenetically analyzed all Texas pterosaur species and included *Q. northropi* and *Q.* sp. as separate terminal taxa. *Quetzalcoatlus northropi* and *Q.* sp. were recovered in a trichotomy with *A. philadelphiae*. *Arambourgiania philadelphiae* was represented by a cervical vertebra in the analysis and lacked overlapping elements with *Q. northropi*, and so its relationships with *Quetzalcoatlus* could not possibly have been resolved. Therefore, this trichotomy does not challenge the monophyly of *Quetzalcoatlus*. Without consideration of *A. philadelphiae*, *Q. northropi* and *Q.* sp. are each other's closest relatives and the monophyly of *Quetzalcoatlus* was supported. That analysis was neutral with respect to whether *Q. northropi* and *Q.* sp. belong to the same species because species taxonomy is determined a priori in a phylogenetic analysis. Later, Andres et al. (2014) subsumed character scorings of both into *Q. northropi*, but this was done more for expediency and should not be construed as a taxonomic act; *Quetzalcoatlus* or *Quetzalcoatlus* spp. would have been a more appropriate taxon label. Diagnostic apomorphies are recovered here for both *Q. northropi* and *Q.* sp. In accordance with the judgment and wishes of W.L., the latter will be erected as a new species and named *Quetzalcoatlus lawsoni* in honor of its discoverer, Douglas Lawson.

DESCRIPTION

Associated specimens

The vast majority of *Quetzalcoatlus lawsoni* material is represented by isolated elements. However, there are also associated elements that likely represent single individuals. Recognition of these individual occurrences are somewhat obscured because individual bones have historically received separate specimen numbers, and so are delineated here to avoid confusion.

Most notable and most complete of these is TMM 41961-1, represented by the most complete skull; cervicals V–VII; left ulna, pteroid, wing metacarpal, first to fourth wing phalanges, femur, tibiotarsus, first metatarsal, and first pedal digit first phalanx; as well as the right proximal and distal syncarpals, medial carpal, pteroid, wing metacarpal, second manual digit third phalanx and third manual digit except for proximal phalanx, first to third wing phalanges, femur, tibiotarsus, and second metatarsal (Fig. 1). This material is closely associated and partially articulated (Lehman, 2021:fig. 15). As the most complete individual, one of the original specimens reported by Lawson (1975a), and in accordance with the wishes of W.L., it was selected as the holotype of *Q. lawsoni*.

Although not as complete, two other *Q. lawsoni* specimens consist of associated and partially articulated elements. TMM 42180-14 includes cervicals VI and VII; the left humerus, ulna, radius, carpus except for pteroid, wing metacarpal, lateral distal

tarsal, as well as fourth and fifth metatarsals; and the proximal half of the right wing metacarpal (Lehman, 2021:fig. 15). TMM 42161-1 comprises the posterior portions of the rostrum and anterior portions of the nasoantorbital fenestra (confluent external naris and antorbital fenestra) as well as cervicals III, V, and VII (Kellner and Langston, 1996:fig. 2C). The mandible TMM 42161-2 and the cervical TMM 42161-3 were found in close association with this specimen and are likely part of the same individual.

Not as closely associated but still containing a number of elements, TMM 42138-1 includes a sternum, right scapulocoracoid, humerus, ulna, radius, wing metacarpal, second manual digit third phalanx, and the first, second, and fourth wing phalanges. TMM 41954-3 comprises some associated and likely articulated limb bones, but these are too poorly preserved to identify.

Three weathered associations include remains from more than one element that at one time may have represented the same individuals. TMM 41546-1 consists of the left postzygapophysis of cervical V associated with the right prezygapophysis of cervical III (TMM 41546-7), the posterior condyle of cervical VI (TMM 41546-8), portions of two humeri (TMM 41546-5 and 6), the distal end of a wing metacarpal and proximal end of a left first wing phalanx (TMM 41546-3), and a bone fragment (TMM 41546-4). TMM 41954-63 includes the proximal end of a right humerus associated with wing metacarpal (TMM 41954-82) and femur shaft fragments (TMM 41954-80). Finally, TMM 41954-67 is ulna fragments associated with the proximal end of a right humerus (TMM 41954-81), and distal syncarpal (TMM 41954-80).

Eight additional specimens appear to represent adjacent elements of the skeleton that remained close in position: TMM 41544-4 has portions of cervicals V and VI; TMM 41544-21 includes the left distal end of the second wing phalanx and third wing phalanx proximal end; TMM 41954-70 has right third and fourth wing phalanges as well as a right second pedal digit second phalanx (TMM 41954-87) and left third wing phalanx (TMM 41954-86); TMM 42138-2 is a left tibiotarsus and pes; TMM 42246-1 and 2 have a right proximal syncarpal and distal syncarpal that articulate in addition to first wing phalanx fragments (TMM 42246-4); TMM 42422-3 and 4 similarly comprise left proximal and distal syncarpals that can articulate; TMM 42422-6 is a left third and fourth wing phalanx in articulation; and TMM 41954-59 is a carpal sesamoid that may be associated with the distal end of a right femur.

In a few instances, two or three cervicals were found so closely associated with one another that they are presumed to belong to single individuals: TMM 41961-1 (an associated, isolated skeleton with fragmentary cervicals V, VI, and VII); TMM 41544-4, 41544-8, 41544-15, and 41544-16 (cervicals V and VI, IV, V, and III respectively); TMM 42161-1 (cervicals III, V, and VII); and TMM 42180-14 (cervicals VI and VII).

Possible associations are represented by TMM 41954-8, a right metacarpus and left pes; as well as TMM 41954-13, a left fourth pedal digit fifth phalanx and TMM 41954-78, a left first pedal digit second phalanx.

Skull

No complete skull is preserved in *Q. lawsoni* (or any of the Big Bend pterosaur material), and so its dimensions must be reconstructed from eight separate individuals (ten specimen numbers) in order to understand the skull in its entirety. Preserved skull material from *Q. lawsoni* runs the gamut from mostly complete crania and mandibles missing the anteriormost and posterior regions (TMM 41954-5.1 and 5.2, 41961-1.1 and 1.2, as well as TMM 42161-1.1 and 2), the rostrum and majority of the nasoantorbital fenestra missing the posterior

skull regions (TMM 41954-62 and 42161-1.1), the jugal-quadrato-jugal-quadrate complex and premaxillonasal bar with other skull fragments (TMM 42422-30), just the premaxillonasal bar (TMM 42180-24 and 42422-39), and a mandible missing the anterior tip (TMM 41544-22) (Table 3). Most of the skull is preserved in *Q. lawsoni* except the tip of the rostrum, chondrocranium, occiput, parietal, postorbital, squamosal, supratemporal fenestra, posttemporal fenestra, cranioquadrate opening, posterior portions of the orbit and frontal, and the dorsal portions of the quadrate and infratemporal fenestra. This largely delimits the bones around the nasoantorbital fenestra. It is not possible to discern the orientation of the occiput from the preserved material, and there is no trace of the vomers, prefrontals, or postfrontals. *Quetzalcoatlus lawsoni* is edentulous (Kellner and Langston, 1996), a trait inherited from basal Azhdarchoidea or possibly even the Ornithocheiroidea (Andres, 2021).

It is important to estimate the dimensions of the complete skull of *Q. lawsoni* for systematic purposes and to determine how much is missing (Table 3). TMM 42161-2 is a mostly complete mandible missing the anterior tip (>916 mm). A complete mandible would give the length of the skull to the jaw articulation. Extending the occlusal margins of this mandible to where these lines intersect would indicate a mandible that would have been 116 mm longer than preserved (1,032 mm), although this estimate assumes that the mandible had an extremely sharp tip. The longest preserved crania are significantly shorter than this estimate: TMM 41954-62 (>773 mm) and 42161-1.1 (>699 mm). If these crania are comparable in size to the TMM 42161-2 mandible, then they would be missing the anterior 212 and 274 mm of the cranium, respectively. This would bring the length of the rostrum (rostral part of the skull anterior to the external nares of Kellner, 1996, rostrum anterior to the nasoantorbital fenestra of Unwin, 2002, rostral part of the skull of Bennett, 2007a, prenarial rostrum of Lü et al., 2010b, or prenarial/prenasoantorbital portion of the skull of Andres et al., 2014) of TMM 41954-62 to 635 mm and TMM 42161-1.1 to 657 mm. Extending the dorsal and ventral margins of these crania to where these lines intersect produces similar rostral length estimates of 641 and 658 mm for these specimens, respectively. The rostrum length estimate based on TMM 42161-1.1 (657 mm) is put forward as the reconstructed rostrum length because of its consistency between skull and mandible estimates. This rostrum length estimate is 59% of the total skull estimate (above the 38% average for pterosaurs) inherited from the Neopterodactyloidea in which half the skull length is rostrum (Andres, 2021). This would be consistent with the descriptions of the rostrum as elongate by Lawson (1975a) and long-snouted by Kellner and Langston (1996).

Estimating the length of the missing posterior portions of the cranium is also challenging. Extending the dorsal margin of the frontal and the ventral margin of the quadrate in TMM 41961-1.1 to where these lines intersect gives an estimate of the position of the squamosal, to which cranium lengths of pterosaurs are traditionally measured. This produces an estimate of 28 missing millimeters of posterior cranium, approximately 79 mm from the posterior edge of the nasoantorbital fenestra; this is a conservative estimate. Adding this to the estimate of the skull length to the jaw articulation produces a total reconstructed skull length of 1,111 mm. This reconstruction is based on the relatively long TMM 42161 skull material and assumes a sharp tip of the skull, and so may be at the upper limit of possible estimates. Kellner and Langston (1996) estimated the skull of this species to be 1,060 mm in length, but they did not detail their method. This would be roughly equivalent to the minimum skull length that could be estimated from this material. The skull of *Q. lawsoni* is a bit more than a meter in length, and the estimates put forward vary only by a few centimeters. This skull length is large, even by pterosaur standards. Following Romer (1956), the lengths of skeletal elements are compared to the length of

TABLE 3. Measurements of *Quetzalcoatlus lawsoni*, sp. nov., cranial material. Values in millimeters. >, preserved value; <, maximum possible value; ~, approximate value; −, missing; ?, unknown; * measurements used for the skull reconstruction; a-p, anteroposterior dimension; d-v, dorsoventral dimension; lat, lateral dimension; long, long axis dimension; and short, short axis perpendicular to long axis dimension. Holotype specimen in italics.

Specimen Number: Dimension:	TMM 41954-5.1	TMM 41954-62	*TMM 41961-1.1*	TMM 42161-1.1	TMM 42180-24	TMM 42422-30	TMM 42422-39	Reconstructed
Cranium length up to squamosal (a-p)	>502	>773	>506	>699*	>341	>312	>76.17	1111
Cranium height up to height at jaw articulation (d-v)	>44.53	<178.69	157.56*	<164.79	>30.49	>54.16	>21.01	158
Cranium maximum width (lat)	>10.04	>17.60	~97.77*	>26.73	>12.57	>25.13	>8.41	98
Rostrum length up to anterior end of nasoantorbital fenestra (a-p)	>179.06	>423	>129.85	>351*	—	—	—	657
Rostrum height up to height at anterior end of nasoantorbital fenestra (d-v)	>44.76	91.12*	80.44*	85.37*	—	—	—	86
Premaxillary crest length (long)	—	134.20*	107.93	99.14	>54.50	>75.76	—	134
Premaxillary crest height (short)	—	64.25*	72.18	20.88	>9.53	27.14	—	64
Nasoantorbital fenestra length (a-p)	>323	>329	347*	>334	>341	>253	>76.17	347
Nasoantorbital fenestra maximum height (d-v)	>20.34	<147.13	104.55*	90.27	>7.48	>12.42	>4.79	105
Orbit length (a-p)	—	—	>21.68*	—	—	>14.31	—	—
Orbit height (d-v)	—	—	42.72*	—	—	>6.94	—	43
Confluent choanae length (a-p)	—	—	206–224*	>107.51	—	>117.90	—	206
Confluent choanae mid-width (lat)	—	—	24.29*	17.24	—	?	—	24
Interpterygoid vacuity length (a-p	—	—	15.88*	—	—	—	—	16
Interpterygoid vacuity width (lat)	—	—	21.07*	—	—	—	—	21
Postpalatine fenestra length (a-p)	>41.73	>48.70	51.21*	>29.01	—	48.17	—	51
Postpalatine fenestra width (lat)	>13.70	>3.12	17.87*	>9.62	—	>7.49	—	18
Suborbital fenestra length (a-p)	—	—	52.82*	—	—	45.78	—	53
Suborbital fenestra width (lat)	—	—	18.93*	—	—	>3.75	—	19
Subtemporal fenestra length (a-p)	—	—	43.25*	—	—	42.84	—	43
Subtemporal fenestra width (lat)	—	—	21.50*	—	—	>17.61	—	22
Infratemporal fenestra length (long)	—	—	—	—	—	>20.34	—	?
Infratemporal fenestra width (short)	—	—	—	—	—	>8.94	—	?
Quadrate angle	—	—	150.24°	—	—	155.96°	—	153°

a dorsal vertebra to get a dimensionless measure of size. The skull length estimate of *Q. lawsoni* is almost 40 times (39.61) the average centrum length of the preserved dorsal vertebrae, which is surpassed only by *Tupuxuara leonardii* Kellner, 1994 (43.728) and *Pteranodon sternbergi* Harksen, 1966 (43.177).

Estimates of the vertical dimensions of the skull are more straightforward. The cranium height at the nasoantorbital fenestra anterior end, which is used to calculate the rostral index of pterosaurs (aspect ratio of the prenarial rostrum), is preserved in three specimens (TMM 41954-62, 41961-1.1, and 42161-1.1). These differ by no more than a centimeter, and so the average of these heights (86 mm) is used here for the estimate. Combined with the estimate of rostrum length, this produces a rostrum aspect ratio of 7.64 (7.48°), roughly equivalent to the 7.33 estimated by Martill and Naish (2006). The cranial height of pterosaurs is traditionally measured at the jaw articulation, which is usually the highest point in the pterosaur crania (exclusive of sagittal crests). In azhdarchid pterosaurs, the highest point is anterior to the jaw articulation, over the posterior part of the nasoantorbital fenestra. This is taken to the extreme in *Q. lawsoni*, where the nasoantorbital fenestra reaches a greater height than the cranium at the jaw articulation. Therefore, it should be noted that when Kellner and Langston (1996) reported a skull height of 220 mm for *Quetzalcoatlus*, they were measuring the maximum height over the nasoantorbital fenestra and included the premaxillary sagittal crest, which is also not traditionally included in cranial measurements. The cranium of *Q. lawsoni* is still measured at the jaw articulation here to remain comparable to other pterosaur species and to distinguish changes in shape of the nasoantorbital fenestra from changes in shape of the cranium. This dimension can be directly measured in TMM 41961-1.1 (157.56 mm), which gives a skull aspect ratio of 7.05 (8.11°) that is comparable to the rostral index. TMM 41954-62 and 42161-1.1 have greater cranial height measurements, but they lack preserved jaw articulations and this represents the

maximum height over the nasoantorbital fenestra. TMM 41954-62 also appears to have an aberrantly tall cranium due to the ventral bending of the maxillojugal bar. The cranium and mandible do curve in this region in *Q. lawsoni*, but most of the curvature in this specimens is attributed to taphonomy; either the bar was bent ventrally, or it originally curved laterally and was rotated medially. Either way, the cranial height measurements of TMM 41954-62 and 42161-1.1 are presented here as maximum dimensions. The skull of *Q. lawsoni* is elongate (Kellner and Langston, 1996). Its skull aspect ratio is greater than the other neopterodactyloids and greater than the average for pterosaurs in general (5.07), but considerably less than the hyperelongated ctenochasmatids (Andres, 2021).

Skull widths are infrequently reported in pterosaurs, and so there is not a traditional dimension to measure in these specimens. The width at the jaw articulation is usually the greatest width of the cranium, just as the height at the jaw articulation is usually the greatest height, and so that measurement is reported here. TMM 41961-1.1 is the only *Q. lawsoni* specimen that preserves this width, although it has been rotated to be between the jugals, and so is reported as an approximate measurement (~97.77). This width is about 62% of the skull height, which would correspond to Langston and Kellner's (1996) characterization as a laterally compressed skull.

Mandible dimensions for the reconstructed skull are taken from the largest, most complete, and best preserved mandible —TMM 42161-2 (Table 4). Some of the mandibular dimensions can be measured in other specimens, but these specimens have much worse preservation and so averages are not reported here for these dimensions. TMM 42161-2 preserves the entire mandible except the estimated 116 mm anterior tip and the retroarticular processes. The addition of the anterior 116 mm brings the symphysis length estimate to 615 mm. Although the retroarticular processes are not preserved in this specimen, one is preserved in TMM 41961-1.2 and adds about 20 mm to the length.

TABLE 4. Measurements of *Quetzalcoatlus lawsoni*, sp. nov. mandible material. Values in millimeters. >, preserved value; * measurements used for the skull reconstruction; a-p, anteroposterior dimension; d-v, dorsoventral dimension; and lat, lateral dimension. Holotype specimen in italics.

Dimension: Specimen Number:	Length (a-p)	Symphysis length (a-p)	Symphysis posterior width (lat)	Symphysis posterior depth (d-v)	Rami depth (d-v)	Rami width (lat)
TMM 41544-22	>773	>387	38.59	22.66	34.47	11.76
TMM 41954-5.2	>664	>240	47.07	33.86	31.83	14.09
TMM 41961-1.2	>233	>95.57	48.59	20.27	27.47	10.68
TMM 42161-2	>916*	>499*	60.95*	31.90*	34.71*	21.33*
Reconstructed	1052	615	61	32	35	21

Adding these estimates to the preserved length produces a 1,052 mm estimate for the entire mandible. This is almost 95% of the estimated skull length, a percentage only surpassed by *Eopteranodon lii* Lü and Zhang, 2005, *Pterodaustro guinazui* Bonaparte, 1970, the Anurognathidae, *Fenghuangopterus lii* Lü et al., 2010, and *Qinglongopterus guoi* Lü et al., 2012 (Andres, 2021). TMM 42161-2 has the largest measurements for the mandible width at the posterior end of the symphysis (60.95 mm) as well as the height (34.71 mm) and width of the posterior ramus (21.33 mm). The only dimension for which this mandible is not the largest is the height at the posterior end of the symphysis (31.90 mm), which is a couple of millimeters shallower than TMM 41954-5.2 (33.86 mm). TMM 42161-2 is a greatly elongate mandible and symphysis, with a lateral aspect ratio (anteroposterior length versus dorsoventral depth) of 19.28 (2.97°) for the symphysis, surpassed only by *Leptostomia begaaensis* Smith et al., 2020, and *Ctenochasma elegans* (Wagner, 1861) (Andres, 2021).

Influencing the description of the skull, and the rest of the skeleton for that matter, is the possibility that there is more than one form in the *Q. lawsoni* material, which has been previously suggested (Bennett, 1992:432). These might be termed 'morphs', but that term has been used extensively to discuss the differences between *Q. northropi* and *lawsoni* (*Q.* sp. in previous literature) and so is avoided here. Two of the skulls are relatively larger with a taller nasoantorbital fenestra and a premaxillary crest with a humped lateral outline (TMM 41954-62 and 41961-1.1), whereas two other skulls are smaller with a shorter nasoantorbital fenestra and a premaxillary crest with a semicircular lateral outline (TMM 42161-1.1 and 42422-30). The remaining skulls cannot be assessed for these features. This difference in crest shape parallels the difference between the rectangular crests of *Sinopterus corollatus* Lü et al., 2006b, and *Sinopterus benxiensis* (Lü et al., 2007), and the semicircular crests of *Huaxiapterus jii* Lü and Yuan, 2005, and *Huaxiapterus atavismus* Lü et al., 2016. The two forms in *Q. lawsoni* also differ in the shape of the ventral surface of the premaxillonasal bar: the larger form is convex anteriorly and concave posteriorly, whereas the smaller form is concave anteriorly and convex posteriorly. Estimates of complete skull dimensions suggest that the smaller form has a longer and more elongate (higher aspect ratio) skull in lateral view. These forms share the diagnostic apomorphies of *Q. lawsoni* and are both referred to this species. Whether their differences are the result of variation, preservation, ontogeny, allometry, evolution, sex, or are just endpoints of a continuum is conjectural at this point. The specimens are described here and their differences noted. The causes of this variation are the purview of future work.

The skull material of *Q. lawsoni* has been previously and ably described by Kellner and Langston (1996), but new observations, discovery or preparation of new skull material (e.g., TMM 41954-5.1 and -5.2, 42180-24, elements of 42422-30, and 42422-39), and 25 years of updates in pterosaur paleobiology warrant revision of the original description.

Cranium

Seven cranium specimens (skull without mandible) are preserved in *Q. lawsoni*: TMM 41954-5.1, 41954-62, 41961-1.1, 42161-1.1, 42180-24, as well as 42422-30 and 39 (Table 3).

TMM 41954-5.1 is a very poorly preserved rostrum and left maxillojugal bar with associated mandible preserved in and incompletely prepared from calcite concretions (not figured). The premaxilla is preserved in this specimen, but only the posterior end of the occlusal margin of this bone. Most of this specimen is the maxilla, and a short dorsal process at the anterior end of the nasoantorbital fenestra that is identified here as the ascending process of the maxilla (nasal process of maxilla in basal pterosaurs). The margins of this ascending process do not appear damaged and so the premaxilla-maxilla contact may be preserved, whereas it is fused in the other specimens. The palate is obscured except about 10 cm in its midsection that reveal the left palatine. The anterior end of the left postpalatine fenestra is present, but the contact with the right palatine and the edge of the confluent choanae are obscured by concretion. The suture between maxilla and palatine is visible but not between the maxilla and jugal. The posterior 15 cm of the maxillojugal bar has been broken off and rotated dorsally.

TMM 41954-62 is the longest cranial specimen in *Q. lawsoni* (Fig. 13). It preserves nearly all of the premaxillae including the sagittal crest, the majority of the left maxilla, part of the left palatine, and the conjoined nasal process. Currently, it is in six pieces permitting cross-sectional views of the elements. This preservation delineates the majority of the nasoantorbital fenestra and left postpalatine fenestra. The preserved length of the postpalatine fenestra is nearly that of complete examples in other specimens, and so the maxillojugal bar must be broken just anterior to the ectopterygoid contact. The specimen is damaged medially posterior to the nasoantorbital fenestra anterior margin so that the lateral edge of the confluent choanae and anterior ramus of the pterygoid are not preserved. Sutures are fused but faintly visible, including one of the rare views of the premaxilla-maxilla suture. It is unlikely that the preserved end of the rostrum is the tip of the skull. Otherwise, the rostrum would come to a blunt end that is higher than wide and be much shorter than the preserved mandibles. The posterior half of the rostrum right occlusal margin has been broken off; the anterior portions are still present but rotated dorsally. This allows an internal view of the rostrum, which is trabecular in structure with curved tubular bony structures at the anterior end of the damage, the internal reticulate reinforcing ridges described in *Pteranodon* (Bennett, 2001a:9). The large amount of ventral curvature of the maxillojugal bar is attributed to taphonomic distortion. A premaxillary crest is present; its anterior and dorsal margins appear natural, but the posterior margin has been filled with plaster. It is not known if this plaster is for support or represents the outline of the crest found in situ. The frontal does not participate in the crest, and it would have been positioned just posterior to the crest. Therefore, the crest would
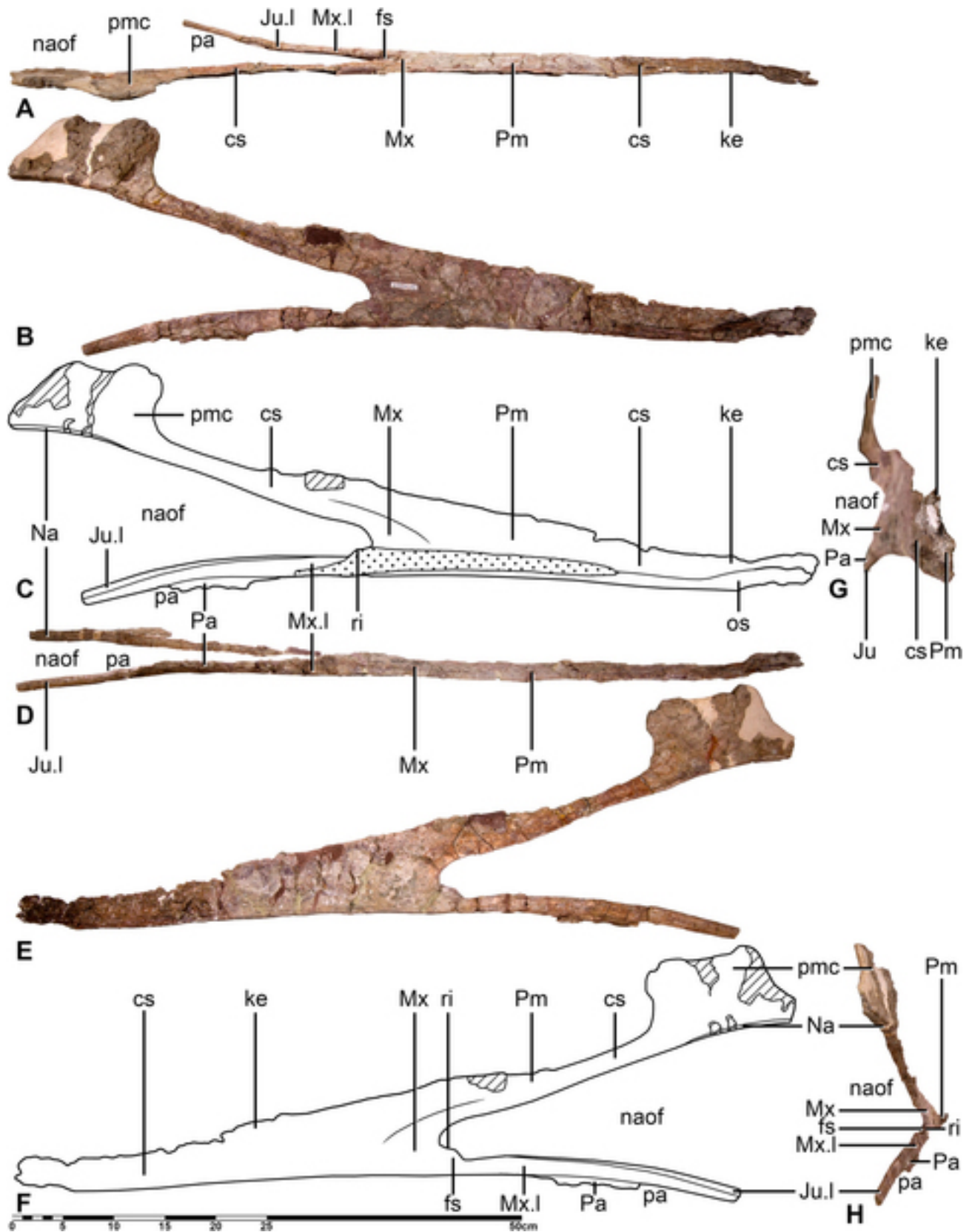
FIGURE 13. *Quetzalcoatlus lawsoni*, sp. nov., cranium left or combined left and right elements (TMM 41954-62) in **A**, dorsal photograph; **B**, right lateral photograph and **C**, line drawing; **D**, ventral photograph; **E**, left lateral photograph and **F**, line drawing; **G**, anterior photograph; and **H**, posterior photograph views. **Abbreviations: cs**, concave surface; **fs**, fossa; **Ju**, jugal; **ke**, keel; **.l**, left element; **Mx**, maxilla; **Na**, nasal; **naof**, nasoantorbital fenestra; **os**, occlusal surface; **Pa**, palatine; **pa**, postpalatine fenestra; **Pm**, premaxilla; **pmc**, premaxillary crest; and **ri**, ridge. Diagonal lines represent plaster, and dots represent matrix and/or damaged bone. Scale bar equals 50 cm.

not have been much longer than preserved. It can be confirmed to have a rectangular humped lateral outline.

TMM 41961-1.1 is the most complete cranial specimen and part of the holotype of *Q. lawsoni* (Fig. 14). It consists of anterior, dorsal, and posterior cranial fragments that enclose the nasoantorbital fenestra except for the anterodorsal portion of the premaxillonasal bar. Also missing are the anterior rostrum and nearly all of the braincase. However, most of the premaxillae, maxillae, palatines, nasals, frontals, lacrimals, jugals, pterygoids, ectopterygoids, part of the quadrates, possibly the anterior end of the basisphenoid, nasoantorbital fenestrae, anterior half of the orbit, confluent choanae, postpalatine fenestrae, suborbital fenestrae, and subtemporal fenestrae are preserved. The premaxillary sagittal crest appears unusual in this specimen—low anteriorly with a small hump followed by a tall hump with an oval opening. The anterior hump is much thicker in cross-section with a damaged dorsal margin, and so this is identified as the broken base of the anterior end of the crest. The oval opening in the posterior hump is an artifact of poor preservation (Kellner and Langston, 1996). It is put forward here that the posterior hump is not the maximum height of the crest, and the crest could have been similar in shape to that of TMM 41954-62. Although this specimen has the best-preserved palate and the only braincase material, it is significantly fractured, crushed, and distorted. Kellner and Langston (1996) called this braincase material "several other displaced bones" occurring toward the posterior end of the skull, but no description was possible owing to their fragmentary condition. The left quadrates and jugal are articulated, but the posterior end of the pterygoids and the right quadrate have been rotated from their natural position so that the right quadrate is positioned between the ascending processes of the jugals. Even so, most of our understanding of the skull of *Q. lawsoni* comes from this specimen.

TMM 42161-1.1 is a rostrum and nasoantorbital fenestra with the anterior-most preserved pieces of the rostrum (previously numbered TMM 42161-1.2) attached to TMM 42161-1.4 (cervical V) and 42161-1.5 (cervical VII) (Fig. 15). The premaxillonasal bar is supported by a metal rod glued to its left side. This specimen preserves the premaxillae, maxillae, palatines, nasals, anterior rami of the left pterygoid and left jugal, nasoantorbital fenestra, left postpalatine fenestra, and the anterior end of the confluent choanae. This specimen has the lowest preserved premaxillary sagittal crest in the *Q. lawsoni* material. Its dorsal edge is damaged, but it is only a millimeter in width, and so it was probably not much taller. The preserved portions of the crest delineate a roughly semicircular outline in lateral view. It is identified as having a crest similar in shape but lower than that of TMM 42422-30.

TMM 42180-24 and 39 are fragments of the premaxillonasal bar (not figured). TMM 42422-39 is a single poorly preserved 75 mm fragment consisting only of the premaxilla from the region anterior to the sagittal crest. TMM 42180-24 consists of 17 fragments from nearly the entire length of the bar including part of the conjoined nasals and sagittal crest. The combined length of all these fragments is nearly that of the entire nasoantorbital fenestra in TMM 41961-1.1, but it should be noted that their original linear dimension would have been much less due to the curvature of the premaxillonasal bar. The nasals form a distinct sharp process/ridge on the ventral surface of the premaxilla in TMM 42180-24. A pair of ridges running along the ventrolateral margin of this bone may correspond to the anterior tips of the lacrimals. The sagittal crest is poorly preserved and mostly detached at its base in this specimen. It is quite thin near its base and might have had a height similar to those of TMM 42161-1.1 and 42422-30.

TMM 42422-30 is a collection of seven skull fragments. The largest fragment is portions of the quadrate-quadratojugal-jugal complex attached to the posterior ramus of the maxilla and the palatine (Fig. 16). The anterior end of this fragment was broken off just posterior to the anterior termination of the jugal so that most of the ventral edge of the nasoantorbital fenestra should be preserved. Lateral edges of the palatine, suborbital, and subtemporal fenestrae are visible between the broken bases of the ectopterygoid and jugal lateral process. Kellner and Langston (1996: table 1) identified the remaining portions of this specimen as postcranial elements, but these are identified here as skull bones. A couple of parts of the premaxillonasal bar and various processes of the skull are preserved in this material. This premaxillonasal bar preserves the best example of a sagittal crest that is semicircular in outline. It is much taller than in TMM 42161-1.1 but does not reach the height of TMM 41954-62 or 41961-1.1. One unusual fragment consists of an elongate process connected to a section of converging plates of bone. It is unquestionably part of the skull, but no known part of the pterosaur skull has this configuration of bone. This fragment is identified here as a collection of skull bones connected by matrix, but the preservation prevents determining the limits of these bones, most of which are damaged, and therefore their identity.

Fenestrae—The nasoantorbital fenestra, anterior portions of the orbit, confluent choanae, interpterygoid vacuity, postpalatine fenestra, suborbital fenestra, subtemporal fenestra, and the ventral end of the infratemporal fenestra are preserved in *Q. lawsoni* (Table 3).

The nasoantorbital fenestra (antorbital aperture of Marsh, 1884, nasopreorbital fenestra of Wellnhofer, 1987, 'nasal-antorbital fenestra' and 'naso-antorbital fenestra' of Cai and Wei, 1994, or nasopreorbital and naso-preorbital opening of Unwin and Lü, 1997) is a massive opening that dominates the skull of monofenestratan pterosaurs. In the Monofenestrata, the maxilla has lost the contact with the nasal so that the external naris and antorbital fenestra become conjoined into a single fenestra, termed the nasoantorbital fenestra. The former maxillary process of the nasal (descending process of nasal) is retained as a free process in some monofenestratans, but the former nasal process of the maxilla is displaced anteriorly to contact the premaxilla over its entire length and is termed here the ascending process of the maxilla. The nasoantorbital fenestra is preserved in every specimen of *Q. lawsoni* that preserves a cranium, from nearly the entire fenestra to just pieces of the premaxillonasal bar. It is quite large, constituting over 31% of the estimated skull length (roughly equivalent to the 33% estimated by Kellner and Langston, 1996, as well as Martill and Naish, 2006) and 65% of the maximum cranium height exclusive of sagittal crests. Despite its large size, the nasoantorbital fenestra of *Q. lawsoni* is below average in terms of skull length percentage for the monofenestratans (38%) (Andres, 2021). Intuitively, this fenestra is less elongate than the skull or rostrum in *Q. lawsoni* with an aspect ratio of 3.32 (17.13°) (equivalent to the height 30% of the length reported by Kellner and Langston, 1996), which would be above average for the monofenestratans (3.26) (Andres, 2021). Again, TMM 41954-62 has an aberrantly tall nasoantorbital fenestra due to the presumed taphonomic ventral bending of the maxillojugal bar; its height is presented as a maximum measurement (<147.13 mm) and probably would have been about 110 mm, based on the preservation of the anterior end of the fenestra. The lateral outline of the nasoantorbital fenestra is half-cordate (bisected heart-shape) due to an inclined posteroventral edge and concave dorsoposterior edges. The dorsal and ventral edges of the nasoantorbital fenestra form an acute angle as in other non-moganopterine monofenestratans (Andres, 2021), but the posterodorsal corner is concave, mirroring the dorsal convexity of the skull in this region. This contrasts with the more typical subtriangular to suboval nasoantorbital fenestra described in *Pteranodon* (Bennett, 2001a:9).
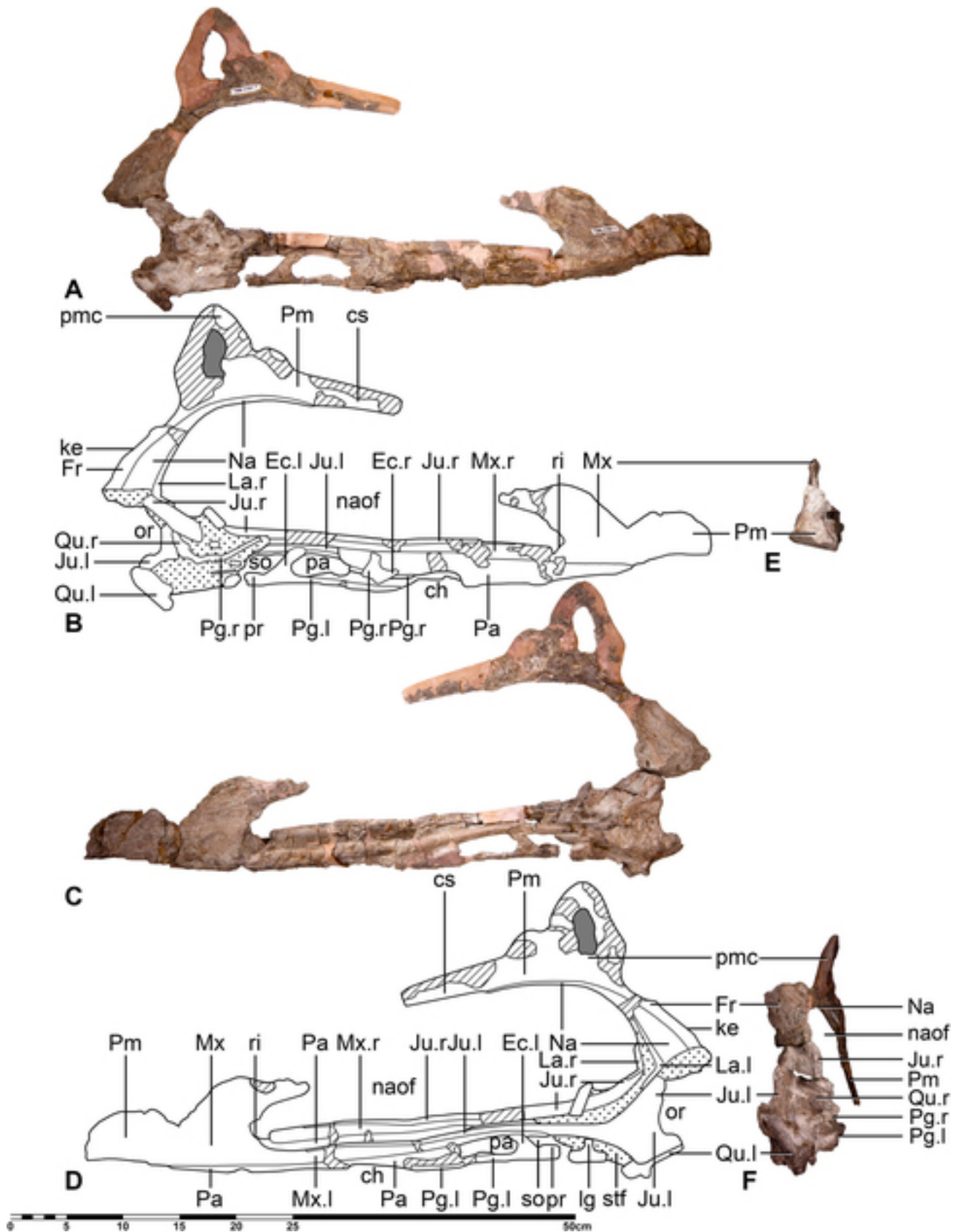
FIGURE 14. *Quetzalcoatlus lawsoni*, sp. nov., cranium (TMM 41961-1.1) in **A**, right lateral photograph and **B**, line drawing; **C**, left lateral photograph and **D**, line drawing; **E**, anterior photograph; and **F**, posterior photograph views. **Abbreviations: ch**, confluent choanae; **Ec**, ectopterygoid; **Fr**, frontal; **itf**, infratemporal fenestra; **Ju**, jugal; **ke**, keel; **.l**, left element; **La**, lacrimal; **lg**, pterygoid lateral process; **Mx**, maxilla; **Na**, nasal; **naof**, nasoantorbital fenestra; **or**, orbit; **Pa**, palatine; **pa**, postpalatine fenestra; **Pg**, pterygoid; **Pm**, premaxilla; **pmc**, premaxillary crest; **pr**, process; **Qu**, quadrate; **.r**, right element; **ri**, ridge; **so**, suborbital fenestra; and **stf**, subtemporal fenestra. Diagonal lines represent plaster, dark gray represents an unfilled hole in the bone, and dots represent matrix and/or damaged bone. Scale bar equals 50 cm.
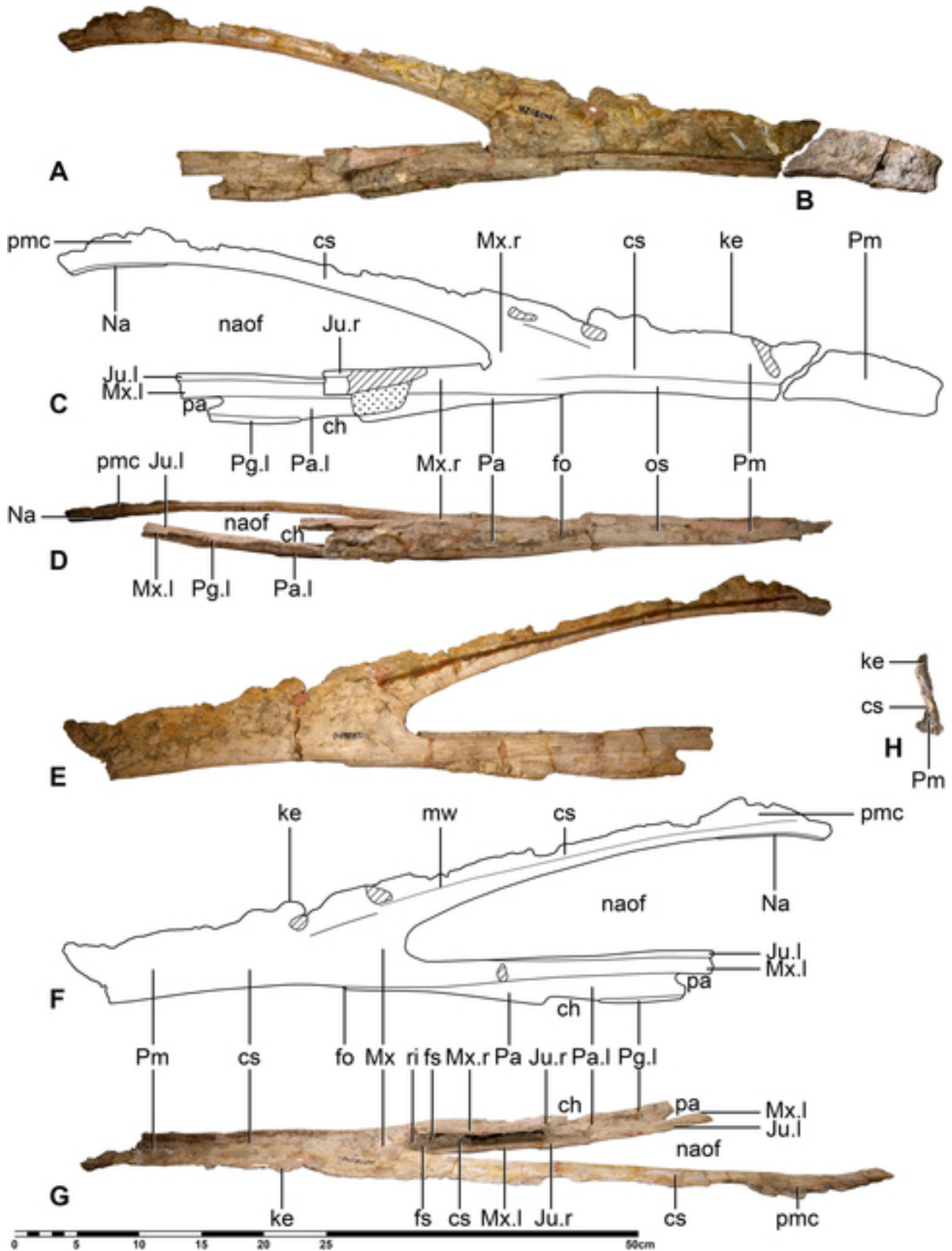
FIGURE 15. *Quetzalcoatlus lawsoni*, sp. nov., cranium (TMM 42161-1.1) in **A**, right lateral photograph; **B**, rostrum fragment attached to cervical vertebrae right lateral photograph; **C**, right lateral line drawing; **D**, ventral photograph; **E**, left lateral photograph; **F**, left lateral line drawing; **G**, dorsal photograph; and **H**, anterior photograph views. **Abbreviations: ch**, confluent choanae; **cs**, concave surface; **fo**, foramen; **Ju**, jugal; **ke**, keel; **.l**, left element; **mw**, metal wire; **Mx**, maxilla; **Na**, nasal; **naof**, nasoantorbital fenestra; **os**, occlusal surface; **Pa**, palatine; **pa**, postpalatine fenestra; **Pg**, pterygoid; **Pm**, premaxilla; **pmc**, premaxillary crest; **.r**, right element; and **ri**, ridge. Diagonal lines represent plaster, and dots represent matrix and/or damaged bone. Scale bar equals 50 cm.
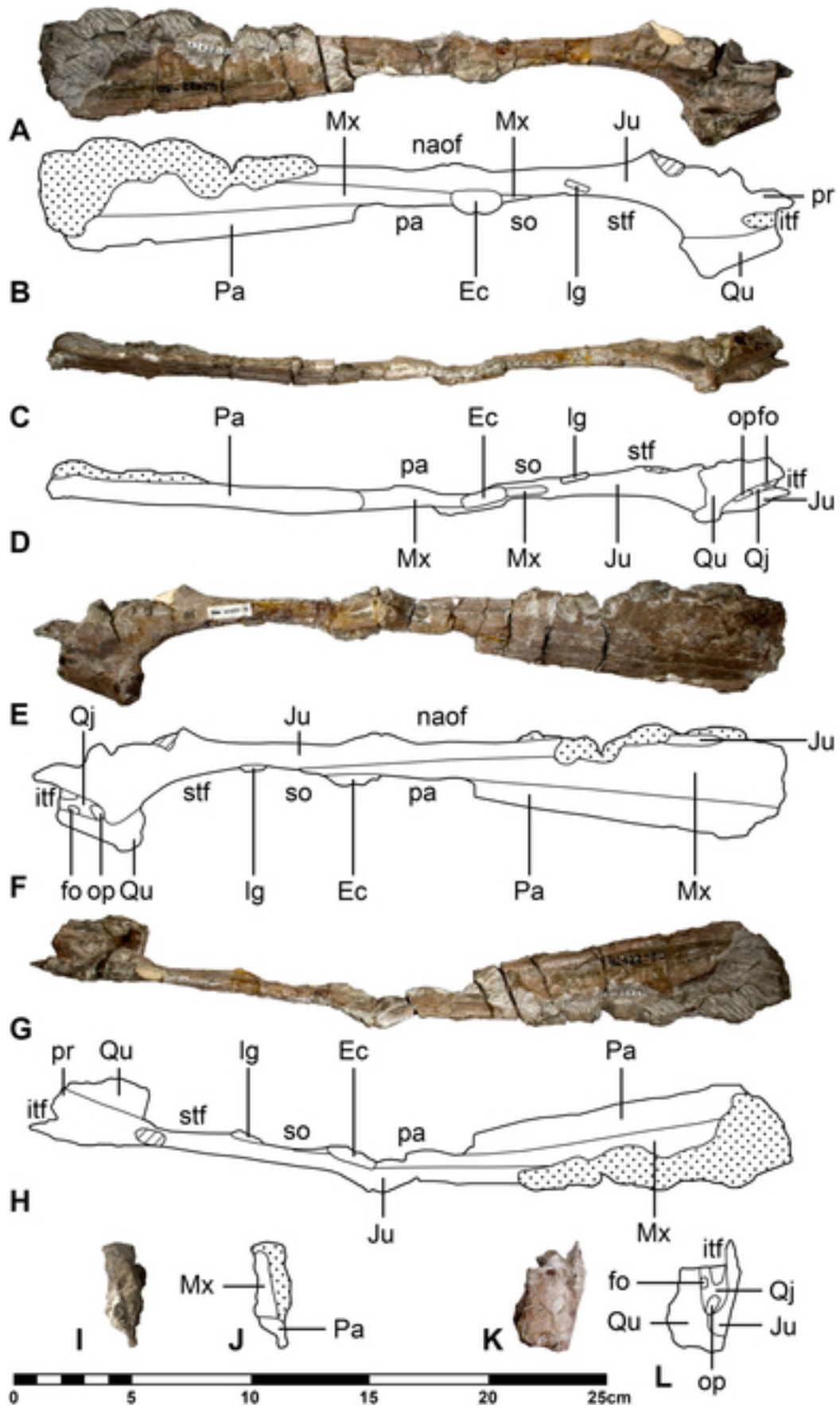
The orbit varies in shape and position over the Pterosauria. In *Q. lawsoni*, it is positioned roughly 7 cm below the dorsal margin of the nasoantorbital fenestra. This ventral position of the orbit is unique to the Azhdarchoidea (Andres, 2021). Its shape is more difficult to discern. Both TMM 41961-1.1 and 42422-30 preserve the orbit in *Q. lawsoni*, but only the anteroventral tip of the orbit is preserved in 42422-30. TMM 41961-1.1 preserves the dorsal edge of the orbit on the nasal and frontal, the anterior edge of the orbit on the ascending process of the jugal, and the ventral end at the base of the jugal postorbital process. No other circumorbital bones can be identified. Only the anterior half of the orbital shape can be determined. The orbital outline has a curved dorsal edge, a vertical and slightly concave anterior edge, and a narrow anteroventral end. This orbit was described as piriform (pear-shaped) by Kellner and Langston (1996), but there is no visible constriction at the narrow end reminiscent of a pear. If the missing posterior half mirrored the anterior half, the shape would be closer to obovate (inverted egg-shape) and about as wide as tall (1.02 aspect ratio), which is close to average for pterosaurs in general (1.13 aspect ratio). Inverted piriform to obovate orbits have been lumped together because of their similarity for systematic purposes and are synapomorphic for Ornithocheiroidea, although several groups have reverted back to subcircular orbits within this clade (Andres, 2021).

Only the ventral end of the infratemporal fenestra (lower temporal fenestra of Bennett, 2001a) is preserved in the *Q. lawsoni* material (TMM 42422-30). Its narrow ventral edge would suggest the elongate elliptical outline plesiomorphic for the Monofenestrata (Andres, 2021), instead of the elongated oval outline found in *Pteranodon* (Bennett, 2001a:9). However, not enough of the fenestra is preserved to rule out an elongate triangular outline. It is identified as being inclined and reaching under the orbit as in Novialoidea (Andres, 2021). There is no trace of the supratemporal fenestra in *Q. lawsoni*.

On the palate, the confluent choanae (posterior narial vacuity of Marsh, 1884, posterior nares of Woodward, 1902, choana of Kellner and Langston, 1996, or choanae of Veldmeijer, 2003) is a midline fenestra formed from the combined left and right choanae in pterosaurs. No vomer, median process, or arcuate elements are identified in *Q. lawsoni* that would form part of an interchoanal septum. Portions of the confluent choanae are preserved in TMM 42161-1.1, and 42422-30, but the length is only complete in TMM 41961-1.1 (Kellner and Langston, 1996). This fenestra is positioned posterior to the anterior margin of the nasoantorbital fenestra and anterior to the jaw articulation, unlike the relatively larger confluent choanae of *Pteranodon* (Bennett, 2001a:21). The anterior 5 cm of the lateral edges of this fenestra are delineated by the posterior rami of left and right palatines, and so the confluent choanae do not contact the maxillae, unlike the anurognathids (Andres, 2021). Posterior to this area, the left and right palatal rami of the pterygoids contact the posterior rami of the palatines medially and constitute the rest of the confluent choanae lateral edges. Because the pterygoids and palatines do not form a straight medial edge for the confluent choanae, this fenestra has an anterior expansion. The two skulls that preserve the lateral edges of the confluent choanae appear to be laterally crushed in this region and are missing one of the palatal rami of the pterygoids. TMM 42161-

1.1 provides a width measurement for the anterior expansion of the confluent choanae between the palatine posterior rami, and TMM 41961-1.1 provides a posterior width estimate between the pterygoid palatal rami. The latter is put forward as the mid-width for this fenestra because it would have been approximately the same for most of the length of the confluent choanae. The posterior edge of the confluent choanae would be delineated by the pterygoids, presumably by the median process of the pterygoids (conjoined left and right pterygoid medial processes) and/or the ectopterygoids, and so a range of lengths for the choanae are listed in Table 3 to reflect either condition.

In TMM 41961-1.1, there is a base of a process on the medial surface of the right pterygoid palatal ramus that may be the right base of a pterygoid medial process. This base would define the border between the confluent choanae and the interpterygoid vacuity (interpterygoid opening of Kellner, 1996, or interpterygoid fenestra of Kellner, 2013), and so it is used here to measure the length of these fenestrae. Only part of the interpterygoid opening is preserved in this specimen. It is surrounded laterally by the pterygoid palatal rami, and likely contacted the basisphenoid posteriorly as well as the pterygoid median process anteriorly. Based on its length estimate, it is considerably shorter than the subtemporal fenestra, as in other Caelicodracones (Andres, 2021), but much larger than the reduced interpterygoid opening of *Pteranodon* (Bennett, 2001a:22, fig. 14). It is not known if the pterygoid fenestra (pterygoid fenestra and fenestra pterygoidalis of Kellner, 2013, or foramen of Chen et al., 2020) between the ectopterygoid base, pterygoid median process, and pterygoid palatal ramus that is reported in *Caupedactylus ybaka* Kellner, 2013, was present in *Q. lawsoni*. A parasphenoid process (parasphenoid rostrum of Bennett, 2001a) is not preserved in this material.

The postpalatine fenestra (posterior palatine vacuity of Williston, 1902, 'postpalatine perforation' of Huene, 1914, postpalatinal fenestra of Wellnhofer and Kellner, 1991, palatine and palatal fenestra of Bennett, 2001a, postpalatal and post-palatal fenestra of Gasparini et al., 2004, or suborbital fenestra of Ősi *et al.*, 2010) is an opening in the palate of pterosaurs between the palatines and ectopterygoids. Ősi et al. (2010) identified this as the suborbital fenestra and identified the suborbital fenestra as a new opening they called the 'pterygoectopterygoid fenestra'. This was based on the identification of the palatine as a 'palatal plate of the maxilla' and the palatal ramus of the pterygoid as the palatine. However, this identification is not supported in *Q. lawsoni* or other pterosaurs, and so this opening is reidentified as the postpalatine fenestra here. It is preserved in TMM 41954-5.1 and 62, 41961-1.1, 42161-1.1, and 42422-30. Its edges are delineated by the palatine anteriorly and medially, the pterygoid posteromedially, the maxilla laterally, and the ectopterygoid posteriorly in *Q. lawsoni*. Its anteromedial edge is the posterolateral margin of a pterygoid process of the palatine, which tapers posteriorly to give the fenestra a triangular outline, described as piriform by Kellner and Langston (1996). The palatine does not reach the ectopterygoid, and so the pterygoid palatal ramus constitutes a few millimeters of the posteromedial edge of the postpalatine fenestra. The ectopterygoid is oriented anterolaterally, and so the outline of this fenestra would be most accurately described as an obtuse scalene triangle. The ectopterygoid lies in

←FIGURE 16. *Quetzalcoatlus lawsoni*, sp. nov., right quadrate-quadratojugal-jugal complex (TMM 42422-30) in **A**, medial photograph and **B**, line drawing; **C**, ventral photograph and **D**, line drawing; **E**, lateral photograph and **F**, line drawing; **G**, dorsal photograph and **H**, line drawing; **I**, anterior photograph and **J**, line drawing; and **K**, posterior photograph and **L**, line drawing. **Abbreviations: Ec**, ectopterygoid; **fo,** foramen; **itf,** infratemporal fenestra; **Ju**, jugal; **lg,** pterygoid lateral process; **Mx**, maxilla; **naof**, nasoantorbital fenestra; **op**, opening; **Pa**, palatine; **pa**, postpalatine fenestra; **pr**, process; **Qj**, quadratojugal; **Qu**, quadrate; **so**, suborbital fenestra; and **stf**, subtemporal fenestra. Diagonal lines represent plaster, and dots represent matrix and/or damaged bone. Scale bar equals 25 cm.

the plane of the palatines and pterygoids instead of dorsal to it, and so the postpalatine fenestra is not virtually incorporated into the subtemporal fenestra as in *Pteranodon* (Bennett, 2001a:22). The maxillary ramus of the jugal reaches the level of the postpalatine fenestra, but a ridge that specifically delineates the lateral edge of this fenestra is present only on the maxilla, and so the jugal is not identified as contacting the postpalatine fenestra. This ridge is an expansion of the more ventral of two ridges that flank the maxilla-jugal contact in this area.

The suborbital fenestra (infraorbital vacuity of Woodward, 1902, infraorbital fenestra of Gasparini et al., 2004, pterygoectopterygoid fenestra of Ősi *et al.*, 2010, or secondary subtemporal fenestra of Kellner, 2013) of pterosaurs is an opening between the ectopterygoid and a lateral process of the pterygoid, when the process contacts the jugal. The pterygoid lateral process is not always present in pterosaurs and does not always reach the jugal when present. When the pterygoid lateral process does not contact the jugal to divide the suborbital fenestra from the subtemporal fenestra, the confluent opening is typically termed the subtemporal fenestra (pterygo-jugal vacuity of Williston, 1902, division of subtemporal fenestra of Kellner and Langston, 1996, subtemporal fenestra of Bennett, 2001a, or subtemporal fenestra + pterygoectopterygoid fenestra of Ősi et al., 2010). The edges of the suborbital fenestra are preserved in TMM 41961-1.1 and 42422-30. TMM 42422-30 preserves only the right maxillojugal bar in this region, and so only the lengths of this and other palatal fenestrae can be determined by measuring distances between the broken bases of the ectopterygoid and pterygoid lateral process as well as the palatine and quadrate. TMM 41961-1.1 has much better preserved suborbital fenestra on its left side, missing only a small section of the medial edge. The pterygoid constitutes the entirety of the medial and posterior edges, the ectopterygoid constitutes the anterior edge, and the jugal constitutes the lateral edge. The posterior ramus of the maxilla reaches the level of the suborbital fenestra, but a ridge that delineates the specific lateral edge of the fenestra is present only on the jugal and so the maxilla is not identified as contacting the suborbital fenestra. This ridge is an expansion of the more dorsal of two ridges that flank the maxilla-jugal contact in this area, mirroring the condition of the postpalatine fenestra. The suborbital fenestra is oval in outline with a sharp anterolateral corner due to the anterolateral orientation of the ectopterygoid at the front of this fenestra.

The subtemporal fenestra (infratemporal vacuity of Woodward, 1902) is identified as the most posterior fenestra of the palate found in pterosaurs, whether a pterygoid lateral process is present or not. TMM 42422-30 preserves the lateral and posterior margins of the right subtemporal fenestra, and TMM 41961-1.1 preserves a nearly complete left and possibly present right subtemporal fenestra. In *Q. lawsoni*, this is an oval opening bounded by the pterygoid lateral process anteriorly, the pterygoid palatal ramus medially, the jugal laterally, and the quadrate posteriorly (Kellner and Langston, 1996). An oval subtemporal fenestra is also reported in *Pteranodon*, but this incorporates the suborbital fenestra and postpalatinal fenestra in that shape (Bennett, 2001a:22). The suborbital fenestra of *Q. lawsoni* is a little over twice as long as wide, below the 2.77 average aspect ratio for pterosaurs, but typical for azhdarchids. The posterior pterygoid fenestra reported in *Cacibupteryx caribensis* Gasparini et al., 2004, is not present in *Q. lawsoni*.

Premaxilla—The premaxilla dominates both the skull and taxonomy of pterosaurs, such that the greatest numbers of species and taxonomic characters are based on this large bone. This is unsurprising considering that this element comprises almost the entire rostrum, nasoantorbital fenestra, sagittal crest and dentition if present, as well as overlapping the neurocranium and taking up a portion of the palate. It is also robust by pterosaur skull bone standards, and so it tends to be preserved more often. Pterosaur premaxillae are long scalene triangles that contact at least the maxillae and nasals. In all but the most basal pterosaurs, the premaxilla lacks a maxillary process and also extends over the nasals to contact the frontals (Andres, 2021). Every *Q. lawsoni* cranial specimen preserves the premaxilla, but no specimen preserves the entire bone. Most notably, the anterior tip of the premaxilla has not been preserved, but specimens reveal the three-dimensional shape of the rostrum just posterior to the tip. Premaxillae are preserved in the azhdarchid species *Z. linhaiensis* (Cai and Wei, 1994), *A. tharmisensis* (Solomon et al., 2020), *A. sudamericanus* (Novas et al., 2012), *M. maggii* (identified as a mandible in original publication), and *A. lancicollis* (Averianov, 2010), and the putative azhdarchid specimen ZIN PH 48/43 (Averianov, 2007).

One aspect of the three-dimensional shape of the rostrum in *Q. lawsoni* is a sinusoidal curve to the occlusal margins of the cranium and mandible in lateral view. This is most readily visible in the mandible TMM 42161-2 (Fig. 17). Kellner and Langston (1996) described the posterior ventral curvature of the maxilla and mandible in this species. However, articulating the fragments of TMM 42161-2 reveals that the anterior end of the mandible curves dorsally as well. The TMM 41954-62, 41961-1.1, and 42161-1.1 crania demonstrate that the ventral curvature of the posterior skull reaches anterior to the nasoantorbital fenestra. TMM 41951-62 also preserves the anterior dorsal curvature. Although damage in this region of this specimen appears to accentuate the curvature into a dorsal deflection, it is a gentle curvature. The lateral margins of the occlusal surfaces (triturating surfaces of Averianov, 2010) parallel this curvature, and so *Q. lawsoni* is not considered to have a reflected dental/occlusal margin as found in the Lanceodontia (Andres, 2021). The anterior ends of the rostrum and mandible occlusal margins in *A. lancicollis* are convex and concave, respectively (Averianov, 2010:271, fig. 5), and the occlusal margin of the *A. sudamericanus* anterior rostrum is described as convex as well (Novas et al., 2012:1448), and so these species may have had a sinusoidal curvature as well, at least in part. *Bakonydraco galaczi* Ősi et al., 2005, is described as having sinusoidal occlusal margins (Averianov, 2010:272), but it curves in the opposite pattern due to a dorsal eminence on it symphysis (Andres, 2021).

The anterior tip of the rostrum is not preserved in *Q. lawsoni* (Kellner and Langston, 1996), and so it is not possible to assess the shape of the anterior margin or determine if a rostral process was present. However, enough of the rostrum is preserved to determine that an upturned, downturned, or laterally expanded anterior end is absent. Preserved portions show the cross-sectional shape of the rostrum: the anterior half of the rostrum has an inverted T-shaped cross-section that becomes more triangular ventrally to resemble an inverted golf tee (fat 'Y' of Ibrahim et al., 2010, wine glass of Averianov, 2010, or Y-shaped of Novas et al., 2012) at the nasoantorbital anterior margin, contra the narrowly triangular cross-section described by Kellner and Langston (1996). This is distinct from the 'V'-to 'D'-shaped cross-section of *A. sudamericanus* (Novas et al., 2012:1448) or the subtriangular cross-section of *A. tharmisensis* (Solomon et al., 2020:5–6, fig. 2D–E), *A. lancicollis* (Averianov, 2010:270), and *Pteranodon* (Bennett, 2001a:10). This inverted golf tee cross-section can also be seen in the rostra of the thalassodromine *Alanqa saharica* Ibrahim et al., 2010 (Wellnhofer and Buffetaut, 1999:fig. 4; Ibrahim et al., 2010:5–6, fig. 2). In *Q. lawsoni*, this cross-sectional shape forms concave lateral surfaces that continue for the entire length of the premaxilla, but they are not lateral sulci and are not pierced by foramina in a row parallel to the occlusal margin, as found in non-novialoid pterosaurs (Andres, 2021). Foramina are positioned in a row parallel to the occlusal margin of the jaw lateral surfaces in *A. tharmisensis*, *A. sudamericanus*, and *M. maggii* (Andres,

2021), but these are not contained within a sulcus. In addition, other pterosaurs have foramina in a row but parallel to the dorsal margin of the rostrum or ventral margin of the mandible (Novas et al., 2012:1448; McPhee et al., 2020:1, fig. 4). Foramina are widespread on the lateral surfaces of the jaws in most azhdarchoid species, but there are no traces of foramina in the jaws of *Q. lawsoni*.

The lateral margins of the rostrum occlusal surface are sharp ridges anteriorly (elevated crests and thick lateral edges of Novas et al., 2012), as in other non-lanceodontian ornithocheiroids (Andres, 2021), that transition to rounded margins posteriorly, as in other non-pteranodontoids (Andres, 2021), at a point about 3 cm anterior to the nasoantorbital fenestra. The rostrum is laterally attenuated towards the tip of the skull but not laterally flattened, which is found in a couple of azhdarchine and tapejarine species (Andres, 2021). *Quetzalcoatlus lawsoni* lacks the middle expansion of the rostrum present in the Tapejaridae (Andres, 2021). The premaxilla has a dorsal keel for its entire length up to the sagittal crest. This keel is tall anteriorly and decreases in height posteriorly. However, the rest of the cranium increases in height at the same rate so that the skull keeps a straight dorsal margin to the premaxillary crest. Similar structures are described as a long low crest in *Pteranodon* (Bennett, 2001a:13), a dorsal crest in *A. lancicollis* (Averianov, 2010:270), or absent in *Z. linhaiensis* (Cai and Wei, 1994:182), but they are identified here as dorsal keels. Posterior to the sagittal crest, the dorsal margin of the skull curves ventrally so that the skull is convex in its entirety, as inherited from the Quetzalcoatlinae (Andres, 2021). The exceedingly thin keel is damaged along its dorsal margin in most *Q. lawsoni* specimens. The keel dorsal margin appears to delineate a sagittal crest in TMM 41954-62, but this is due to damage in this specimen and is not mirrored in the better preserved TMM 42161-1.1. Cross-sections also do not reveal trabeculae in this keel. The rostral surfaces are smooth in texture, lacking the longitudinal striations and numerous small pits of *A. sudamericanus* (Novas et al., 2012:1448).

The occlusal surface of the rostrum anterior end is flat, similar to that of *A. lancicollis* (Averianov, 2010:271, fig. 5B) and *M. maggii* (Vullo et al., 2018:4, fig. 1G), and unlike the concave surface of *A. sudamericanus* (Novas et al., 2012:1448) and *A. tharmisensis* (Solomon et al., 2020:5, fig. 2B). There is no trace of the median palatal ridge (Kellner and Langston, 1996; Bennett, 2001a) found in *M. maggii*, the Dsungaripteromorpha, Ornithocheiromorpha, and *Darwinopterus modularis* Lü et al., 2010 (Andres, 2021). A weak median ridge has been reported in the anterior portion of the rostrum in *A. lancicollis* (Bennett, 2001a:15; Averianov, 2010:271), but this appears to be a weak rise between grooves along the occlusal margins that narrows toward the tip of the rostrum until it was regarded as a ridge, and so it is considered here as distinct from a palatal ridge. Similarly, the occlusal surface of *A. sudamericanus* was described as having a low and well-defined median longitudinal eminence by Novas et al. (2012:1448, fig. 2H), but no ridge-like projection could be located in their figure even though it is labeled, and so it is considered here as having a condition similar to *A. lancicollis*. There is a strip of bone present at the posterior end of the *A. sudamericanus* rostrum fragment, but this area is damaged, covered by matrix, and not labeled the median eminence by Novas et al. (2012:fig. 2H). Confusingly, the keel-shaped palatal ridge present in rostra of *A. saharica* and *M. maggii* (identified as mandibles in the descriptions but are rostra based on the preponderance of anatomical evidence) were also termed eminences (Ibrahim et al., 2010:1, 6, and 7, fig. 3B; Vullo et al., 2018:1, 4, 10, and 13, fig. 1). Palatal keels were previously only known in thalassodromids, *Lonchodraco*, and orthithocheirines (Andres, 2021), and the elements of *A. saharica* and *M. maggii* are only thought to be "likely belonging to a single immature individual" (Vullo et al., 2018:1). It is also possible that the rostra of *M. maggii* is a late surviving thalassodromid that does not belong to the same species as some or all of the other elements, and palatal keels are also not found in azhdarchids. The anterior palatal fossa of the tapejarids, *Coloborhynchus clavirostris* Owen, 1874, and *Coloborhynchus wadleighi* Lee, 1994, and *Ludodactylus colorhinus* (Seeley, 1870) is also absent in *Q. lawsoni* (Andres, 2021).

The texture of the occlusal surface is smooth, lacking a suture between the left and right premaxillae or foramina, which are present in most other azhdarchoid species. The two faint irregular grooves extending along lateral margins of the occlusal surface mentioned previously are present in *Q. lawsoni* and are not identified as sutures. Similar structures have been attributed to sulci for blood vessels (Bennett, 2001a:10) or a keratinous sheath (Chen et al., 2020:1) in *D. weii*. On the occlusal surface near the anterior margin of the nasoantorbital fenestra is a protuberance that appears to house an anteriorly oriented foramen (larger foramen of Kellner, 1989, medial foramen entering the maxilla-palatines of Wellnhofer and Kellner, 1991, or foramen incisivum and incisive foramen of Ősi et al., 2010). Posterior to this, there is a difference in bone texture between the middle and sides of the palate, and the palate begins to bow ventrally. The bone in the middle of the palate is identified here as the palatines, and the edges are identified as the maxillae. The medial foramen appears to be where the palatines contact the premaxillae and/or maxillae on the occlusal surface, which has also been reported in *T. wellnhoferi* (Kellner, 1989:443, fig. 8; Wellnhofer and Kellner, 1991:94, fig. 2a) and *D. banthensis* (Ősi et al., 2010:248, fig. 8). Openings in this region have been suggested to be apertures for the vomeronasal organ (Ősi et al., 2010:255 and 257, fig. 8), or this may be a feature due to the confluence of up to six bones of the palate.

There is no trace of a contact or suture between the left and right premaxillae. The premaxilla-maxilla suture is also tightly fused, but it is visible in TMM 41954-62 and 42161-1.1. Breaks in this region present in TMM 41954-5.1 and 41961-1.1 possibly represent disarticulation at the premaxilla-maxilla contact, but poor preservation precludes confirmation of this. The anterior end of this suture disappears into damaged regions of specimens, and it appears to totally fuse on both the occlusal surface and premaxillonasal bar. Therefore, it is not possible to tell how much the maxilla constitutes to the palate or premaxillonasal bar.

The premaxillary bar (premaxillary posterodorsal process of Sereno, 1991, process separating external nares of Kellner, 1996, or posterodorsal extension of premaxilla of Witton, 2012, premaxillary bar and internasal process of Andres and Myers, 2013, or premaxilla posterior process of Longrich et al., 2018) of *Q. lawsoni* conjoins ventrally with the thin anterior projection of the nasals to form a structure we term here the premaxillonasal bar, which appears to be present in both *Z. linhaiensis* (Cai and Wei, 1994:fig. 1) and *A. lancicollis* (Averianov, 2010:269, fig. 2). However, it should be noted that nasals meeting at the midline and being overlapped by the premaxillae is the normal condition for pterosaurs (Bennett, 2001a). This premaxillonasal bar maintains the inverted golf tee cross-section of the posterior rostrum over its length, unlike the inverted V- to U-shaped cross-section of *Pteranodon* (Bennett, 2001a:16) or the triangular cross-section of *A. lancicollis* (Averianov, 2010:269). In TMM 41954-62 and 41961-1.1, the anterior end of the premaxillonasal bar ventral surface is slightly convex, becoming flat and then concave posteriorly. TMM 42161-1.1, however, has a premaxillonasal bar ventral surface that is concave anteriorly becoming convex posteriorly. The bar is oriented posterodorsally at the anterior end of the nasoantorbital fenestra, but it curves posteriorly and ventrally over its length to form a long and curved process that contacts the neurocranium dorsally. This gives the cranium a convex dorsal margin and the nasoantorbital fenestra a concave dorsal edge. This premaxillonasal bar is rather wide by

pterosaur standards, significantly wider than the Anurognathidae or Chaoyangopteridae (Andres, 2021).

The premaxilla contacts the nasal dorsally. The conjoined anterior projection of the nasals runs along the underside of the premaxilla in the nasoantorbital fenestra (Kellner and Langston, 1996) and reaches to the level of the sagittal crest anterior margin. This anterior projection of the nasals is flanked by grooves on the premaxilla ventral surface, like in *A. lancicollis* (Averianov, 2010:269), that appear to be a suture in some areas. The main body of the nasals and the anterior process of the frontals combine to form a small horizontal surface for articulation with the posterior end of the premaxillae. In dorsal view, the premaxillae divide the nasals to contact the frontals as in other macronychopterans (Andres, 2021), but this premaxilla-frontal contact is only a couple of centimeters in length.

The presence of premaxillary crests is quite variable in pterosaurs, and the premaxillary crest of *Q. lawsoni* was only inherited from its last common ancestor with *W. brevirostris* (Andres, 2021). A premaxillary crest is present in all of the *Q. lawsoni* crania that preserve the appropriate region of the skull (TMM 41954-62, 41961-1.1, 42161-1.1, 42180-24, and 42422-30), but they differ in shape and preservation among them. These crests are thin plates of bone without a trace of internal space or tissue in cross-section, unlike the trabeculae-filled crests of the rest of the Ornithocheiroidea (Andres, 2021). They are about a millimeter in width at their dorsal margin (Kellner and Langston, 1996), but not much thicker at their base and so have nearly parallel lateral surfaces. These surfaces are smooth in texture without the striae of the non-ornithocheiroids, dsungaripterids, *Tupandactylus*, and *Hamipterus tianshanensis* Wang et al., 2014, or the branching networks of grooves of the thalassodromids (Andres, 2021). In lateral outline, TMM 41954-62 and 41961-1.1 have a "humped appearance" (Kellner and Langston, 1996:225) with height expansions positioned anteriorly and posteriorly in TMM 41954-62 or preserved only posteriorly in TMM 41961-1; not to be confused with the dorsal spine found in *Caiuajara dobruskii* Manzig et al., 2014, plus *Tupandactylus* (Andres, 2021). TMM 42161-1.1 and 42422-30 have a semicircular outline instead. The crest is quite low in TMM 42161-1.1, and this may be due in part to damage along its dorsal edge, but this crest is as thin in cross-section as the dorsal margins of the other crests and so it is improbable that it reached their height. Two forms of crests are identified in the *Q. lawsoni* individuals: a larger crest that is rectangular in outline with anterior and posterior humps as exemplified by TMM 41954-62 (the anterior hump of the 41961-1.1 crest is identified as missing), and a smaller crest that is semicircular in outline as exemplified by TMM 42422-30 (the TMM 42161-1.1 crest is identified as being the same shape but lower in height). Therefore, *Q. lawsoni* is polymorphically coded in the phylogenetic analysis with both rectangular and semicircular premaxillary crests, as well as subvertical and posteriorly inclined crest anterior margins, respectively (Andres, 2021). Enough of these crests are preserved to delineate their overall lateral outline, but not their exact lengths. However, the crests found in *Q. lawsoni* are positioned at the posterior end of the nasoantorbital fenestra (Kellner and Langston, 1996), as inherited from the Ornithocheiroidea (Andres, 2021). The frontal is located just posterior to the preserved portion of the crests and does not participate in the crest, and so they could not have been much longer.

Maxilla—The pterosaur maxilla is a long bone consisting of a triradiate/triangular anterior end and a long posterior ramus forming the ventral portions of the maxillojugal bar. The entire structure has the outline of a halberd in lateral view. The maxilla is preserved in TMM 41954-5.1 and 62, 41961-1, 42161-1.1, and 42422-30, where it takes up a large portion of the rostrum. Its contact with the premaxilla is a tight suture that curves up onto the premaxillonasal bar, giving the anterior

maxilla dorsal margin a convex outline. This dorsal curvature forms the ascending process of the maxilla, which is here identified as homologous with the nasal process of the maxilla in non-monofenestratan pterosaurs. The anterior end of the maxilla on the rostrum and the most posterior extent of the maxilla on the premaxillonasal bar are not visible in *Q. lawsoni* specimens. It is not known how much the maxilla contributes to the occlusal surface or the premaxillonasal bar. Maxillae are reported in the azhdarchid species *Z. linhaiensis* (Cai and Wei, 1994) and one fused premaxilla-maxilla specimen (ZIN PH 112/44) of *A. lancicollis* (Averianov, 2010:fig. 4).

The anterior ends of the nasoantorbital fenestrae terminate in a pair of fossae under the ascending process of the maxillae that may correspond to the antorbital fossae, found in non-macronychopteran pterosaurs (Andres, 2021), but displaced medially instead. Lateral ridges separate the fossae from the lateral surfaces of the rostrum in TMM 42161-1.1, but more rounded borders are present in TMM 41954-62 and TMM 41961-1.1. Either way, these fossae do not reach onto the lateral surfaces of the rostrum. In all specimens, these fossae are confluent with a large concave surface formed by the dorsal surface of the ventrally bowed palatines and medial surfaces of the maxillae posterior rami. The left and right fossae are separated by a median ridge with midline suture, identified as the contact between left and right maxillae. This ridge is a continuation of the ventral convexity of the premaxillonasal bar in TMM 41954-62 and 41961-1.1, but it terminates dorsally in a concavity in TMM 42161-1.1.

The vast majority of the maxilla length consists of its posterior ramus (jugal process of Dalla Vecchia, 2019), which contacts the maxillary ramus of the jugal ventrally to form the maxillojugal bar as well as the ventral edge of the nasoantorbital fenestra (Kellner and Langston, 1996). The maxillojugal bar transitions from being slightly broader horizontally with an L-shaped cross-section at its anterior end to being much taller vertically with an elliptical cross-section at its posterior end. This is due to the interplay between bones in this region. The anterior L-shaped cross-section is the vertical posterior ramus of the maxilla articulating with the horizontal palatine (and so this would technically be the maxillopalatojugal bar). The maxilla partially surrounds the palatine in this region, and a faint groove extending along the ventral surface delineates this contact (Kellner and Langston, 1996). Posteriorly, the palatine thins and displaces ventrally as the bowing of the palate increases posteriorly (Kellner and Langston, 1996). The maxilla has an oval cross-section posterior to the palatine. The anterior end of the jugal maxillary ramus appears about 5 cm from the nasoantorbital anterior edge as a sharp process. Posteriorly, the jugal maxillary process expands vertically as the maxilla posterior ramus attenuates vertically so that the maxillojugal bar keeps the same approximate shape and diameter over its length. The maxilla lacks a ventral expansion of the posterior end found in the Dsungaripteridae (Andres, 2021). Where the ectopterygoid contacts the maxillojugal bar, the bar is equal parts maxilla and jugal, and the ectopterygoid contacts both equally. The ectopterygoid also contacts both the maxilla and jugal in *Pteranodon* (Bennett, 2001a:17), but they are positioned medially and laterally as opposed to ventrally and dorsally, respectively. The posterior ramus of the maxilla almost reaches the posterior end of the nasoantorbital fenestra. It terminates at a constriction anterior to the main body of the jugal. This can be seen in a cross-section of the maxillojugal bar in TMM 41961-1.1. The maxilla therefore forms the majority of occlusal margin, including the transition from anterior marginal ridges to posterior rounded margins.

The suture between left and right maxillae is only visible under the premaxillonasal bar in the anterior end of the nasoantorbital fenestrae. A tight curved suture between the premaxilla and maxilla is visible in the posterior rostrum of TMM 41954-62

and TMM 42161-1.1, contra Kellner and Langston (1996). This contact appears to fuse without a trace before reaching both the occlusal surface and premaxillonasal bars, and so it is not possible to determine the maxillary component of those elements. This is quite disparate from the straight (and apparently horizontal) premaxilla-maxilla suture described and figured in *Z. linhaiensis* (Cai and Wei, 1994:183, fig. 1). The maxilla-palatine suture is visible wherever preservation permits. Although the maxilla and jugal tightly fuse, it is possible to trace their contacts along a slight constriction in the maxillojugal bar and in cross-sections at breaks in the specimens. This constriction is flanked by a pair of parallel ridges in some places. There is an expanded contact with the ectopterygoid, which appears to fuse equally to the maxilla and jugal. It is not possible to determine whether the left and right maxillae contact along the midline of the occlusal surface.

Palatine—The palatines are very long palatal bones with medial and lateral emarginations for the confluent choanae and postpalatine fenestrae, respectively. Ősi et al. (2010), Pinheiro and Schultz (2012), and O'Sullivan and Martill (2017) have suggested that these bones are instead palatal plates of the maxilla. However, contacts between these palatines and the maxillae are visible on the bones and in cross-sections of *Q. lawsoni* and other pterosaurs with sufficient preservation. It is most defensible that these authors are pointing out ontogenetic fusion of the palatines to the maxillae. The palatal process of the maxilla has instead been displaced dorsally onto its medial surface, at least in basal pterosaurs (Andres et al., 2010).

The palatines are present and preserved in TMM 41954-5.1 and 62, 41961-1.1, 42161-1.1, and 42422-30. These are broad and flat bones that are triangular in outline as in all pterosaurs, save for the anurognathids in which they are reduced to thin bars of bones (Andres, 2021). The left and right palatines appear to be ventrally bowed in all specimens, and this bowing increases posteriorly. This convex posterior palate is shared with *W. brevirostris*, but is also present in *Tupuxuara*, *T. wellnhoferi* plus *Europejara olcadesorum* Vullo et al., 2012, the Istiodactylidae, and the Archaeopterodactyloidea (Andres, 2021). The palatines in *Q. lawsoni* terminate anteriorly at the putative medial foramen. They contact the maxillae with sutures for almost their entire length, contra Kellner and Langston (1996). The ventral bowing of the palatines and their lateral contact with the maxillae forms a half-pipe for the anterior 10 cm of the nasoantorbital fenestra length. The left and right palatines are confluent anteriorly and diverge posteriorly as posterior rami. They delineate the lateral edges of the confluent choanae anterior end for about 5 cm. Posterior to this, the palatal processes of the pterygoids contact the posterior rami of the palatines to take up the lateral boundaries of the confluent choanae. Unlike the arc-shaped palatine-pterygoid contacts of *Pteranodon* (Bennett, 2001a:22, fig. 8), these contacts are straight. The posterior end of the palatine is a process in the postpalatine fenestra that extends along the lateral margin of the pterygoid palatal ramus to almost contact the ectopterygoid; it is termed here the pterygoid process of the palatine. There is also a parallel ridge that extends along the lateral edge of the postpalatine fenestra, but a cross-section of the maxillojugal bar in TMM 42161-1.1 demonstrates that this is part of the maxilla instead of a process of the palatine. Sutures are visible with the maxillae and between the left and right palatines where preservation permits.

Nasal—The nasal is a triangular or triradiate bone that partially divides the external naris and antorbital fenestra in non-monofenestratan pterosaurs, or the nasoantorbital fenestra and orbit in monofenestratan pterosaurs. It is preserved in TMM 41954-62, 41961-1.1, 42161-1.1, and 42180-24. However, it is most complete in TMM 41961-1.1 and so most of the description

here details that specimen. Nasals are reported in the azhdarchid species *Z. linhaiensis* (Cai and Wei, 1994) and in one fused premaxillonasal bar (ZIN PH 59/44) of *A. lancicollis* (Averianov, 2010:fig. 2).

The nasals of *Q. lawsoni* are highly derived. They form a large, anteriorly curving, and tapering wedge with the frontals that extends from the anterodorsal margin of the orbit to the anterior margin of the premaxillary sagittal crest, quite distinct from the small and elongate nasals of other pterosaurs such as *Pteranodon* (Bennett, 2001a:17). A similar wedge appears to be present in *Z. linhaiensis* (Cai and Wei, 1994:fig. 1), but it was identified as the frontal and parietal instead of the nasal and frontal (Cai and Wei, 1994:183). The left and right nasals conjoin into a thin anterior projection (opposing nasals are fused ventrally and form a sagittal ridge that lies underneath the premaxilla of Kellner and Langston, 1996, anterior end of confluent nasals of Averianov, 2010), but the posterior end of their contact is obscured by matrix, and so it is not known if they are fused over their entire length. The prefrontal is not identified in *Q. lawsoni*, and so the nasals contact the orbit. The nasals are expanded posteriorly, forming over half of the cross-section of the bar between the orbit and premaxillary crest. The conjoined projection of the nasals attenuates greatly over its length so that it forms a sharp needle over its anterior half. The nasals are nearly vertical at their posterior/orbital margin and curve almost 90° to be horizontal under the crest. They extend under the frontals over their posterior half and under the premaxillae over their anterior half. The lacrimals extend along the lateral margins of the nasals dorsal to the orbit, forming a median space. This corresponds to the median pneumatic space of Bennett (2001a) that presumably contained diverticula of the nasal passages, but this space cannot be identified as pneumatic in TMM 41961-1.1 due to its infilling with matrix. There are no foramina preserved on the body of the nasals of *Q. lawsoni*, such as have been reported in some *Pteranodon* specimens (Bennett, 2001a:17). A raised ridge marks the contact between the nasals and frontals so that between the lacrimals and frontals, the lateral surfaces of the nasals are concave.

No contact is visible between the left and right nasals. Parallel grooves mark the lateral boundaries of the nasal under the premaxillae that appear sutured in some areas. The nasals do suture to the lacrimals, but only ridges define the boundary with the frontals. The nasals and frontals combine to form a horizontal surface for contact with the posterior end of the premaxillae. The nasals lack a free descending process (Kellner and Langston, 1996) as in a number of ornithocheiroid clades, but *Q. lawsoni* inherited its absent process from the Neoazhdarchia (Andres, 2021).

Lacrimal—The lacrimal is a triradiate/triangular bone in most pterosaurs that forms part of the posterior margin of the nasoantorbital fenestra, as well as part of the preorbital bar with the nasal and jugal. Lacrimals are preserved in TMM 41961-1 and possibly TMM 42180-24 as well as in *Z. linhaiensis* (Cai and Wei, 1994). In *Q. lawsoni*, however, they are long crescent-shaped bones that form the anterior margin of the preorbital bar. The lacrimals contact the ascending process of the jugal posteriorly and extend down only half of its length. They taper dorsally to extend along the lateral margins of the nasals, forming raised ridges (Kellner and Langston, 1996) with the median space between them. The vertically oriented hooked lacrimal process and the lacrimal fossa of *Pteranodon* (Bennett, 2001a:19, fig. 7) is not present in *Q. lawsoni*. The lacrimal contacts the nasals and jugal with sutures, but it does not contact the orbit, contra Kellner and Langston (1996). This is a rather unusual configuration for a pterosaur lacrimal, and it is possible that they fused to the nasal without a trace of their margins to form nasolacrimals as reported in *I. sinensis* (Andres and Ji, 2006:72).

However, a very similar gracile and curved bone is identified in the same position in *Z. linhaiensis*, although it was identified as the nasal and the jugal ascending process was identified as the lacrimal (Cai and Wei, 1994:183, fig. 1). The lacrimal foramen of non-neoazhdarchian pterodactyloids and the orbital process of lanceodontians are absent in *Q. lawsoni* (Andres, 2021).

Frontal—In pterosaurs, the combined frontals are trullate (trowel-shaped) in dorsal view with lateral postorbital processes and a posterior process that overlaps the parietals posteriorly. They are midline bones, which have their anterior end divided by the posterior end of the premaxillae in all but the Eopterosauria (Andres, 2021). The frontal forms the dorsoposterior edge of the orbit and the dorsoanterior edge of the supratemporal fenestra. Frontals are only preserved in TMM 41961-1.1, and only the anterior half of the frontals is present in this specimen. Frontals are also reported in the azhdarchid species *Z. linhaiensis* (Cai and Wei, 1994).

The frontals in *Q. lawsoni* match the nasals and lacrimals in forming an anteriorly curving and tapering process dorsal to the orbit. The frontals extend anterior to the preorbital bar as in other azhdarchoids (Andres, 2021). Only a small portion of the dorsal rim of the orbit is preserved on the frontal in TMM 41961-1.1. Left and right frontals are divided anteriorly by the posterior end of the premaxillae, but only for about a centimeter. This contact is a flat horizontal surface formed by the frontals posteriorly and the nasals anteriorly. The frontals do not participate in a sagittal crest, unlike the non-azhdarchiform azhdarchoids, but this can only be assessed in *Z. linhaiensis* (Andres, 2021). Instead, the frontals have a slight dorsal keel between the left and right elements in *Q. lawsoni*. Ridges form the border with the nasals, and there is no trace of sutures on the frontals.

Jugal—The jugal is a tetraradiate bone in basal pterosaurs, but it loses its posterior process to become triradiate in the Pterodactylomorpha (Andres, 2021). Portions of the remaining three processes are preserved in *Q. lawsoni* (Kellner and Langston, 1996): the maxillary ramus (TMM 41954-5.1 and 62, 41961-1.1, 42161-1.1, 42422-30), the ascending process (TMM 41961-1.1 and 42422-30), and the base of the postorbital process (TMM 42422-30). These processes delineate the edges of the nasoantorbital, orbital, infratemporal, postpalatine, suborbital, and subtemporal fenestrae. The left jugal of TMM 41961-1.1 is the most completely preserved, but the main body of its right jugal has been largely destroyed. A jugal is also reported in the azhdarchid species *H. thambema* (Buffetaut et al., 2003), *Z. linhaiensis* (Cai and Wei, 1994), and *A. bostobensis* (CCMGE 41/11915) (Averianov, 2004).

The jugal is oriented horizontally in line with the occlusal margin of *Q. lawsoni*. Its main body is quite large due to the expansion of the base of the ascending process (lacrimal process of Kellner and Langston, 1996, or lacrimal ramus of Bennett, 2001a) as well as an expansion of the area ventral to the orbit between the ascending and postorbital process, which is also found in *Z. linhaiensis* and several other pterosaur clades (Andres, 2021). The ascending process is more expanded anteriorly, giving it an inclined appearance. However, the posterior margin of this process is vertical, and so the ascending process is identified here as being subvertical, as in most non-pterodactylomorphs (Andres, 2021). The jugal forms a concave/beveled posteroventral edge for the nasoantorbital fenestra (ridge extending posterodorsally from the ventral margin of the NAOF to the ventral corner of the orbit of Bennett, 2001a), shared with *W. brevirostris* but also present in pteranodontians and ornithocheiriforms (Andres, 2021). There is no nasoantorbital fossa on the jugal (jugal depressed 2–3 mm below the level of the bone ventral to the ridge of Bennett, 2001a, or pronounced ridge on the lateral side of the jugal of Wang et al. 2012), which has been found in the Eopterosauria

and Pteranodontoidea (Andres, 2021). *Aralazhdarcho bostobensis* also has a fossa on the jugal (deep lateral depression of Averianov, 2004), but this is positioned between the ascending and postorbital processes of the jugal and is separated from the nasoantorbital fenestra by a ridge (thick subvertical crest and ventral ridge of Averianov, 2004) (Averianov, 2004:432, fig. 7). The triangular area of smooth bone reported on the jugal ascending process of *Pteranodon* and possibly *Eudimorphodon* (Bennett, 2001a:20–21) is not preserved in *Q. lawsoni*. In TMM 42422-30, there is a bony process lying on the medial surface of the jugal main body near the base of the postorbital process. It cannot be confirmed whether this process is attached to the jugal, and it is not found on the medial aspects of TMM 41961-1.1 jugals.

The jugal maxillary ramus ('anterior projection' of Cai and Wei, 1994, maxillary process of the jugal of Kellner and Langston, 1996, anterior ramus and maxillary ramus of the jugal of Bennett, 2001a, or anterior process of jugal of Wang et al., 2009) is present in all pterosaurs but *Campylognathoides* (Andres, 2021). In *Q. lawsoni*, it overlaps the posterior ramus of the maxilla dorsally to form the maxillojugal bar. This overlap is so extensive that the jugal constitutes only a few centimeters of the occlusal margin in front of the mandible articulation, but it also constitutes all but the anterior 5 cm of the nasoantorbital ventral edge. Hence, this is termed the maxillojugal bar. The jugal maxillary ramus extends along the dorsal margin of the bar and terminates anteriorly with a sharp tip posterior to the nasoantorbital fenestra anterior margin, unlike the Pteranodontia and the clade containing the Ornithocheirae and *Ludodactylus sibbicki* Frey et al., 2003a (Andres, 2021). A thickened ventral margin of the maxillojugal bar anterior to the left jugal main body in TMM 41961-1.1 is identified as the posterior extent of the maxilla, and this is confirmed in cross-section. The maxillary process of the jugal is oval in cross-section over its length, lacking the subrectangular posterior cross-section reported in *A. bostobensis* (CCMGE 41/11915) (Averianov, 2004:432). The lateral process of the pterygoid contacts the jugal maxillary ramus between this posterior terminus of the maxilla and the jugal main body to divide the suborbital fenestra from the subtemporal fenestra. The ectopterygoid contacts the maxilla and jugal equally to divide the postpalatine fenestra from the suborbital fenestra in *Q. lawsoni*.

The jugal main body expands rapidly posterior to the constriction at posterior end of the maxillary ramus. Here, the ventral margin of the jugal main body curves ventrally to contact a ventrally positioned mandibular articulation on the quadrate, forming a concave ventral margin for the cranium in this region found in breviquartossans (Andres, 2021). The contact with the quadrate on its lateral surface is an inclined crevice in TMM 41961-1.1 that may have previously held the quadratojugal. A crevice is not present on TMM 42422-30, which does appear to preserve the quadratojugal. The ascending process has a broad triangular base that attenuates dorsally (Kellner and Langston, 1996), as in most pterosaurs (Andres, 2021). The postorbital process is broken off at its base in the specimens (Kellner and Langston, 1996), but it can be seen to form a narrow but not sharp anteroventral corner for the orbit. Needless to say, the jugal postorbital process does not contact the lacrimal to form an orbital bar, such as found in the Dsungaripteridae (Andres, 2021). The posterior process of the jugal is absent as in other pterodactylomorphs (Andres, 2021), but it does have a ventrally oriented convexity at its contact with the mandible articulation. The jugal fuses with all the bones it contacts.

Quadratojugal—The quadratojugal lies between the quadrate and jugal below the infratemporal fenestra in most pterosaurs; however, it is displaced dorsally and loses contact with the occlusal margin in some pterodactyloids. TMM 41961-1.1 and 42422-30 preserve the quadrate and jugal, but the quadratojugal is

not obtrusively apparent between them. TMM 41961-1.1 preserves the most ventral end of the infratemporal fenestra, and it has a crevice extending anteroventrally from it between the quadrate and jugal, giving the appearance that the quadratojugal has become dislodged. TMM 42422-30 preserves more of this region. The crevice is not present in this specimen. Instead, posterodorsal to the mandible articulation is an hourglass-shaped bone with three openings positioned anteroventrally, posterodorsally, and posteroventrally. Kellner and Langston (1996) identified this bone as part of the quadrate, and three openings (termed X, Y, and Z) as possible pneumatic foramina or tooth perforations. They favored the latter hypothesis, but it should be noted that these openings are not arranged linearly as they would be in a jaw. Although the largest and most dorsal opening (Y) is incomplete and both the postorbital process of the jugal and the ascending process of the quadrate are present, the infratemporal fenestra was not identified in TMM 42422-30 by Kellner and Langston (1996). Also, the most ventral opening (X) is confluent with the contact between the quadrate and jugal. The most defensible explanation is that the hourglass-shaped bone is a quadratojugal that has been dorsally displaced so that the quadrate contacts the jugal ventrally: X is an opening at the anteroventral margin of the quadratojugal that contacts the quadrate and jugal, Y is the anteroventral edge of the infratemporal fenestra, and Z is a de novo foramen between the quadrate and quadratojugal. A quadratojugal is reported in the azhdarchid species *H. thambema* (Buffetaut et al., 2003), *Z. linhaiensis* (Cai and Wei, 1994), and possibly *A. lancicollis* (Averianov, 2010).

Dorsally displaced quadratojugals are common in pterodactyloids, but *Quetzalcoatlus lawsoni* differs in being even more dorsally positioned. An hourglass-shaped quadratojugal is also reported in *D. macronyx* (Sangster, 2003:29), but this is not recovered as homologous with the *Q. lawsoni* condition (Andres, 2021). The posteroventral opening (Z) is a foramen of unknown origin. It could be related to the attenuated margins of the quadratojugal like the anteroventral opening (X), or to a foramen found on the anterior surface of some pterosaur quadrates (Bennett, 2001a:24; Andres et al., 2010:171, fig. 4D) that are obscured in these specimens, but this remains conjectural. The quadratojugal of *Q. lawsoni* is a thin plate of bone that laps onto the jugal and quadrate laterally as in *Pteranodon* (Bennett, 2001a:21), but it does not participate in the mandibular articulation as in *Pteranodon* (Bennett, 2001a:12). It is fused to the quadrate and jugal, forming the narrow ventral corner of the infratemporal fenestra in *Q. lawsoni*. The quadratojugal is also reduced in *H. thambema* and *Z. linhaiensis* (Cai and Wei, 1994:183; Buffetaut et al., 2003:94), and reconstructed as dorsally displaced in the latter (Cai and Wei, 1994:fig. 1).

Quadrate—The pterosaur quadrate is a posteriorly to dorsally oriented plate of bone that contacts the jugal/quadratojugal anteriorly, pterygoid/basipterygoid medially, and squamosal/occiput dorsally, as well as forming most of if not all of the mandibular articulation. Although it contacts the lateral surface of the skull, it belongs to the posterior surface and articulates with the posteromedial margin of the jugal at a right angle. The ventral end of the quadrates including the mandibular articulation (transverse bar of Averianov, 2010) is preserved in TMM 41961-1.1 and 42422-30. The mandibular articulation of TMM 42422-30 was described as completely restored by Kellner and Langston (1996), but it appears to be completely preserved today. The articulation in TMM 42422-30 is better preserved than in TMM 41961-1.1, and so most of the description here pertains to TMM 42422-30. The lateral angle that the long axis of the quadrate forms with the occlusal margin of the skull varies greatly over the Pterosauria. In *Q. lawsoni*, the preserved portion of the quadrates delineates an approximate 153° angle

with the occlusal margin (Table 3), which is high for the eupterodactyloids in which it is typically closer to 120°, but the articulation is positioned under the anterior end of the orbit as in other eupterodactyloids (Andres, 2021). Quadrates are preserved in the azhdarchid species *H. thambema* (Buffetaut et al., 2003), *Z. linhaiensis* (Cai and Wei, 1994), and *A. lancicollis* (Averianov, 2010).

The mandibular articulation (condyloid process of the jaw articulation of Bennett, 2001a, or quadrate condyle of Averianov, 2010) in this species has been identified as helical in structure (Kellner and Langston, 1996). However, it has a diagonal ridge (sharp edge of Kellner and Langston, 1996) extending posterolaterally from the anterior end of the medial condyle to the posterior end of the lateral condyle, instead of an intercondylar groove (diagonal groove of Bennett, 2001a, or oblique groove of Buffetaut et al. 2002) in this position and orientation found in other ornithocheiroids (Andres, 2021). *Azhdarcho lancicollis* has a thickened medial edge of the lateral condyle (Averianov, 2010:269) in place of the diagonal ridge. The intercondylar groove is also present in *Q. lawsoni*, but it is displaced posteriorly so that it extends from the posterior half of the medial condyle to posterior to the lateral condyle, as in *A. lancicollis* (Averianov, 2010:fig. 3). A ridge extending from the posterior end of the medial condyle defines the posterior border of the intercondylar groove. This groove has been interpreted by Kellner and Langston (1996) as a notch to receive the posterolateral process of the cranial articulation of the mandible to serve as a bony stop during jaw abduction. This groove likely performed this function, but it also articulates with the intercotylar ridge on the mandible and so is identified here as homologous with the intercondylar groove of other ornithocheiroids. *Hatzegopteryx thambema* was described as lacking this notch (Buffetaut et al., 2002:181), but it has an intercondylar groove and so is interpreted as not having the unusual posterior displacement of the groove found in *Q. lawsoni*.

The diagonal ridge is the ventral margin of an anteriorly facing flat surface (Kellner and Langston, 1996), which constitutes the majority of the lateral articular surface. This articular surface is triangular in outline with a distinct process at its dorsomedial corner, contrasting with *A. lancicollis*, which has a pointed angle at the posterolateral corner of the lateral articular surface instead (Averianov, 2010:269, fig. 3). Both would probably be considered to have 'angular condyles' sensu Buffetaut et al. (2003). The diagonal ridge and triangular articular surface articulates with the lateral cotyle of the mandible, and the dorsomedial process extends dorsally over the mandible lateral cotyle at its medial end where it is narrowest. A groove lateral to this process on the dorsal surface of the quadrate receives the midpoint of the dorsal lip of the cranial articulation on the mandible, and likely corresponds to the transverse groove of *A. lancicollis* (Averianov, 2010:269, fig. 3). The medial condyle is positioned slightly ventral to the lateral condyle (Kellner and Langston, 1996) and contacts the intercondylar groove, giving the ventral margin of the articular surface a cleft appearance in anterior view. The medial condyle is slightly larger than the lateral condyle, unlike in *A. lancicollis* (Averianov, 2010:269), and the medial margin is thicker than the lateral margin. Although *Q. lawsoni* has a unique construction of the mandibular articulation, it is identified here as helical in shape and homologous with the other ornithocheiroids. The condyles diverge slightly anteriorly in their orientations but are subparallel to the long axis of the skull as in other ornithocheiroids. This is unlike the helical articulation in *H. thambema* and the rhamphorhynchines, in which rounded oval condyles are oriented anteromedially-posterolaterally (Buffetaut et al., 2003:94, fig, 4; Andres et al., 2010:171, fig. 4C) and positioned almost laterally to one another, giving them an arrangement described as 'offset' (Buffetaut et al., 2002:181).

The quadrates preserved in *Q. lawsoni* are missing the majority of their ascending processes, which have been described as rod-like (Kellner and Langston, 1996:226), but they can be seen to not be thin and cylindrical as found in the anurognathids (Andres, 2021). The ventral end of the quadrate lateral margin contacts the posterior margin of the jugal with a suture. The quadratojugal has been displaced dorsally into the infratemporal fenestra, where it fuses to the jugal postorbital process and the base of the quadrate ascending process. The quadrate-quadratojugal contact has an anterior opening and a posterior foramen along its border. The three openings (X, Y, and Z) identified in the quadrate by Kellner and Langston (1996) are instead on the margins of the quadratojugal. The right quadrate appears to have a medial process and contact with the pterygoid in TMM 41961-1.1, but the preservation is not sufficient to determine the nature of that contact.

Pterygoid—The pterygoid is a complicated and variable bone in pterosaurs. In its simplest construction, it is a long bone that contacts the palatine medially with a palatal ramus (pterygoid dorsolateral branch of Buffetaut et al., 2003, or palatine and rostral process of the pterygoid of Ősi et al., 2010), that contacts the quadrate and basisphenoid/basipterygoid posteriorly, and that contacts the other pterygoid with a medial process (pterygoid medial branch of Buffetaut et al., 2003). It can have a separate process for the posterior contact (basipterygoid of Wellnhofer, 1970) and can contact the jugal with a lateral process (transverse bone of Goldfuß, 1831; transpalatine of Newton, 1888; or pterygoid process, laterally directed process, and bony process from the pterygoid of Kellner and Langston, 1996). The medial processes can fuse into a single median process of the pterygoids (median process and anterior median process of Bennett, 2001a, or medial pterygoid process of Kellner et al., 2003). The palatal ramus can contact the ectopterygoid, the median process of the pterygoids can contact the ectopterygoid with the ectopterygoid overlying the palatal ramus dorsally, or the palatal ramus and median process of the pterygoids can both contact the ectopterygoid with the ectopterygoid changing orientation between the two. Aspects of all of these appear to be present in *Q. lawsoni*. A pterygoid has been reported in *H. thambema* (Buffetaut et al., 2003).

Only the anterior end palatal ramus of the left pterygoid is preserved in TMM 42161-1.1, but both left and right pterygoids are preserved in TMM 41961-1.1. The pterygoid has a complex shape made more problematic in TMM 41961-1.1 by the fragmentation and displacement of its pieces, although this remains the best preserved example of the pterygoids in *Q. lawsoni*. The left pterygoid is preserved except for a small section near the base of the palatal ramus between the lateral process and ectopterygoid contact. The right pterygoid appears to be in at least four pieces: the anterior end of the palatal ramus is identified as still attached to the right palatine, a triradiate bone fragment preserved lying on the posterior end of the right palatine is identified as the contact between the right pterygoid and ectopterygoid, the posterior process of the pterygoid with its contact with the right quadrate and possibly the basisphenoid is identified, and a broken process touching the right pterygoid and jugal is identified as the lateral process of the pterygoid.

Although the preserved crania of *Q. lawsoni* are somewhat distorted, it appears that the pterygoids are shifted ventrally with respect to the occlusal margins as a continuation of the ventral bowing of the palate to form a half-pipe structure. The shifting of the pterygoids ventral to the occlusal margin is also shared with *H. thambema* (Buffetaut et al., 2003:95), as well as thalassodromids and ornithocheirans (Andres, 2021). The palatal ramus of the pterygoid contacts the ectopterygoid on its lateral surface and contacts the process of another bone, or possible continuation of the ectopterygoid, on its medial surface more posteriorly. The exact margins cannot be discerned and so are not

depicted in Fig. 14. Posterior to this, the lateral process of the pterygoids divides the suborbital fenestra from the subtemporal fenestra. This is best seen on the left side of TMM 41961-1.1. The left lateral process of the jugal has a tubercle at its base on its ventral surface with a small foramen medial to it. Similar foramina are found in other pterosaurs. The medial process of the pterygoid is severely damaged in TMM 41961-1.1, if present at all. A blunt protuberance on the medial surface of the right palatal process is suggested here to be the base of a medial process that may or may not fuse with its counterpart to form the median process of the pterygoids, a condition found in some ornithocheiroids (Bennett, 2001a:22, fig. 8). There is also a long fragment, in addition to other small fragments, that lies anterior to the blunt process that may represent the median process, but they are not connected and so this cannot be confirmed.

The palatal ramus of the pterygoid forms distinct sutures with the palatine, but it is tightly fused to the ectopterygoid with no sign of sutures. The lateral process of the pterygoid contacts the jugal and does not fuse with it in TMM 41961-1, but it appears to be fused in TMM 42422-30. The posterior process of the pterygoid contacts the quadrate and/or the basisphenoid, but this region in TMM 41961-1.1 is not preserved well enough to resolve the contacts. Buffetaut et al. (2002, 2003) considered this a pterygoid/rostrodorsal process of the quadrate in the *H. thambema* holotype, but the sutures cannot be resolved in this specimen either. Buffetaut et al. (2003) also reports a well-marked ventral ridge and two subparallel dorsal ridges on this process, but the preservation in *Q. lawsoni* is not sufficient to ascertain if they were present in this species.

Ectopterygoid—There are two structures in pterosaurs identified as the ectopterygoid: a bar of bone (ectopterygoid bar of Chen et al., 2020) that extends from the lateral surface of the pterygoid palatal ramus to the medial surface of the maxillojugal bar, and a slender rod that extends from the median process of the pterygoids over the dorsal surface of the pterygoid palatal ramus (free part of ectopterygoid between the median process of the pterygoid and the palatal ramus of pterygoid of Bennett, 2001a) in ornithocheiroids. The ectopterygoid bar and rod are considered to be the same bone by previous authors (Bennett, 2001a:22, fig. 14; Pinheiro and Schultz, 2012:7–8, figs. 4–5; Kellner, 2013:6, fig. 5; Chen et al., 2020:9, fig. 1). In *Q. lawsoni* (TMM 41961-1.1), there is a bone that extends from the lateral surface of the jugal palatal ramus to the maxillojugal bar that is identified here as the ectopterygoid bar. The base of a broken process is present posterior to the ectopterygoid bar on the medial surface of the jugal palatal ramus that is likely the ectopterygoid rod. It cannot be definitively known whether this broken process contacted the median process of the pterygoids. However, the posterior surface of the ectopterygoid bar bifurcates at its medial end, forming a posterior fossa at the ectopterygoid bar-pterygoid contact, and the dorsal part of this bifurcation contacts the broken base on the medial surface of the pterygoid, suggesting that it corresponds to the rod that contacts the pterygoid median process. The ectopterygoid in *Q. lawsoni* may represent the contact of two processes/bones that meet at different orientations at the palatal ramus of the pterygoid. This is mirrored by the condition in *Thalassodromeus sethi* Kellner and Campos, 2002 (Pêgas et al., 2018:fig. 8), *T. leonardii* (Pinheiro and Schultz, 2012:fig. 4), *D. weii* (Chen et al., 2020:fig. 1), and *C. ybaka* (Kellner, 2013:fig. 5) in which the ectopterygoid sensu lato appears to change trajectory, deflecting anteriorly when it contacts the pterygoid palatal ramus. The small foramen that divides the ectopterygoid bar in some specimens of *Pteranodon* (Bennett, 2001a:23) may also represent the contact/fusion of the ectopterygoid bar and the rod. The palate is a complex region of the skull visible in few pterosaur species. *Quetzalcoatlus lawsoni* does not resolve the

homology of all its various elements, but it does provide information toward that end.

The left and right ectopterygoids are identified in TMM 41961-1.1. The right ectopterygoid bar-jugal palatal ramus contact is preserved in a triradiate bone fragment lying on the right palatine. The left ectopterygoid bar is complete and divides the post-palatine fenestra from the suborbital fenestra in the plane formed by the pterygoids, unlike in *Pteranodon* (Bennett, 2001a:23). The ectopterygoid bar is an anterolaterally oriented process in horizontal outline that tapers laterally but has an expanded oval contact with the maxillojugal bar in *Q. lawsoni*. In the transverse plane, it is oriented dorsolaterally with an expanded foot at the maxillojugal contact. Although this contact is expanded dorsally, the ectopterygoid contacts the maxilla and jugal equally with a dorsal protuberance extending above the maxillojugal border. The small process reported on the dorsal margin of the jugal maxillary ramus in *Pteranodon* (Bennett, 2001a:20) corresponds to this protuberance. A number of small fragments preserved near the palatal ramus of the right pterygoid in TMM 41961-1.1 may be part of the ectopterygoid rod that could have extended from the median pterygoid process to the ectopterygoid bar, but these are poorly preserved and inordinately small. The ectopterygoid is fused with all the elements it contacts.

Basisphenoid—In TMM 41961-1.1, there is some poorly preserved bone material medial to the right quadrate and pterygoid posterior process. This would correspond to the anterior/ventral-most end of the basisphenoid in other pterodactyloids. The dorsal surface of this area is visible on the left side of the specimen under the main body of the left jugal, and a couple of tubercles can be seen that could be the contact for the pterygoid and/or quadrate or for a meshwork of bone struts extending up to the interorbital septum, which is reported in *Pteranodon* (Bennett, 2001a:27, fig. 17). Basipterygoid processes appear to be absent in this specimen, and the long basipterygoid processes of the non-pterodactyloid pterosaurs are almost certainly absent (Andres, 2021). There are no visible bone contacts in this area, and so the extent, shape, or even the presence of the basisphenoid in this specimen cannot be confirmed.

Mandible

Mandible material is known from TMM 41544-22, 41954-5.2, 41961-1.2, and 42161-2 in *Q. lawsoni* (Table 4). These are not well-preserved specimens; a lot of the contacts between bones have been obscured and regions have been filled in with plaster. Each of these specimens preserves all of the mandible bones, but they need to be considered altogether to determine the shape of those bones. When the fragments of these mandibles are articulated, they mirror the sinusoidal curve of the cranium occlusal margin. The mandibular rami curve ventrally but are oriented posterodorsally at their anterior contact with the symphysis so that they are dorsally bowed over their length, and the symphysis is straight over its posterior half but curves slightly dorsally over its anterior half (Fig. 17). The rami are long and nearly straight in dorsal/view, which is quite disparate from the short, deep, and laterally bowed mandibular rami of *Pteranodon* (Bennett, 2001a:9 and 29, figs. 21 and 22). The mandible of *Q. lawsoni* is elongate (Lawson, 1975a), with a length over 30 times the depth of the rami, a value only surpassed by a few cte-nochasmatid pterosaurs (Andres, 2021). Mandibles are reported in the azhdarchid species cf. *H. thambema* (LPB R.2347) (Averianov, 2014), *W. brevirostris*, *Z. linhaiensis* (Cai and Wei, 1994), *A. bostobensis* (ZIN PH no. 37/43) (Averianov, 2007), cf. *A. bostobensis* (WDC Kz-001) (Averianov, 2014; Averianov et al., 2015) formerly *Samrukia nessovi* Naish et al., 2011, *A. tharmisensis* (Solomon et al., 2020), *A. lancicollis* (Nesov,

1984); and the azhdarchiform species *M. minor* (McGowen et al., 2002).

TMM 41544-22 is a mostly complete mandible in five fragments that fit into two pieces. It is missing the anterior tip, right retroarticular process, and about 7 cm of the anterior end of the left ramus. Kellner and Langston (1996) figured the left ramus attached to the symphysis (Kellner and Langston, 1996: fig. 5B). However these pieces do not fit, and this would necessitate that the jaw rami be different lengths.

TMM 41954-5.2 is a very poorly preserved mandible in four pieces whose surfaces have largely been obliterated by the concretion in which it is preserved and not completely prepared from. It is missing only the anterior end of the rostrum. A large and long plate of bone in two pieces is associated with this mandible in the collections. It is most likely that this is part of the cranium that shares this specimen number, possibly the right palatine.

TMM 41961-1.2 is a slightly better preserved mandible in two pieces missing most of the symphysis and the left cranial articulation and retroarticular process (Kellner and Langston, 1996: fig. 5A). The right cranial articulation is the best preserved in *Q. lawsoni*. However, a medial plate just anterior to this articulation is identified as the displaced ventral margin of the ramus. The rest of the mandible has been crushed, distorted, and infilled with plaster. The ventral end of the symphysis has broken off, permitting a view of the symphyseal cavity. This is also one of the best specimens to see the concave lateral margin of the skull in the horizontal plane found in the ornithocheiroids or azh-darchoids (Andres, 2021).

TMM 42161-2 is the best-preserved mandible in *Q. lawsoni* (Fig. 17). It is in four pieces that preserve the entire length of this element except the anterior tip and cranial articulations. It is also the only specimen to preserve the circular openings in the occlusal and ventral surface of the mandible.

Dentary—The dentary comprises the entire mandible except the posterior end of the rami in pterosaurs. The anterior tip is not preserved in the *Q. lawsoni* specimens, and so it is not possible to determine whether a sharp tip, blunt terminus, odontoid process, or prow was present. The symphysis is fused in the *Q. lawsoni* specimens, as in all non-anurognathid breviquartos-sans (Andres, 2021). It extends for 58% of the total length of the mandible, typical for the Azhdarchidae and a bit above the average (about 50%) for the Ornithocheiroidea (Andres, 2021).

The preserved anterior end of the mandible projects anteriorly as in most pterosaurs (Andres, 2021). The symphysis of cf. *H. thambema* (LPB R.2347) has been described as curved slightly downward (Vremir et al., 2018:6), but this is from the posterior end of the symphysis instead of the anterior end and was more likely part of a sinusoidal curve as in *Q. lawsoni*. Both species share a dorsoventrally depressed cross-section of the symphysis (Andres, 2021), with a width about five times the depth in *Q. lawsoni* specimens (TMM 41544-22, 41954-5.2, and 42161-2). All *Q. lawsoni* mandibles are damaged, but this dorsoventral depression is identified as reflecting the original anatomy. The occlusal surface of the mandibular symphysis is flat (Kellner and Langston, 1996) with no trace of foramina, pits, fossae, ridges, keels, grooves, sulci, or even a suture between the left and right dentaries. No anterior expansion such as found in *S. wucaiwanensis*, gnathosaurines, and non-boreopterid ornitho-cheiriforms is present in *Q. lawsoni* (Andres, 2021), contra Lawson (1975a). Likewise, the dorsal eminence of eudimorpho-dontoids, the *D. banthensis* plus *Dolicorhamphus* clade, and the Tapejaridae is also absent (Andres, 2021). The mandible anterior end lacks occlusal ridges, but these ridges appear posteriorly about halfway down the length of the symphysis and continue onto the rami. This is opposite to the normal neopterodactyloid condition in which the ridges are only positioned anteriorly (Andres, 2021), which was how cf. *H. thambema* (LPB R.2347)
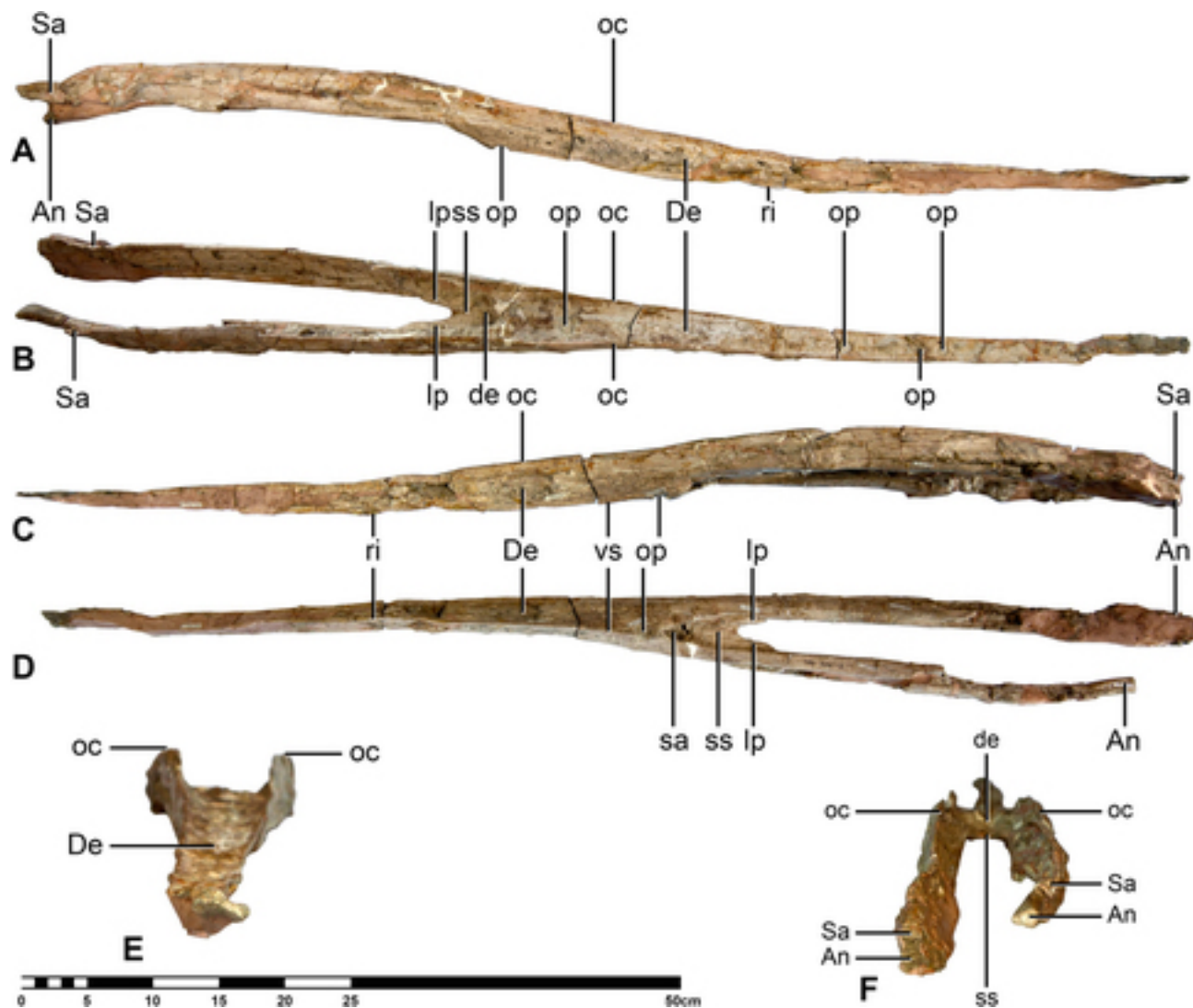
FIGURE 17. *Quetzalcoatlus lawsoni*, sp. nov., mandible (TMM 42161-2) photographs in **A**, right lateral; **B**, dorsal; **C**, left lateral; **D**, ventral; **E**, anterior; and **F**, posterior views. **Abbreviations: An**, angular; **De**, dentary; **de**, depression; **lp**, lateral process; **oc**, occlusal ridge; **op**, opening; **ri**, ridge; **Sa**, surangular; **sa**, symphyseal cavity; **ss**, symphyseal shelf; and **vs**, ventral symphysis. Scale bar equals 50 cm.

was described (Vremir et al., 2018:4). However, the symphysis of LPB R.2347 is also described as anteriorly deepening (Vremir et al., 2018:4, 6, and 7) but without a ventral crest that would account for this increased depth. It is put forward here that the orientation of LPB R.2347 is the reverse of that described, and it has posteriorly positioned ridges and a posteriorly increased depth as in *Q. lawsoni*. The marginal ridges project above the posterior symphysis to form a concave occlusal surface in *Q. lawsoni* (Kellner and Langston, 1996). They curve medially at the posterior end of the symphysis in TMM 42161-2. There is no expansion in the middle of the mandible, such as found in the Tapejaridae (Andres, 2021).

The symphyseal region of the mandible in *Q. lawsoni* is triangular in cross-section (Lawson, 1975a) as in other edentulous pterosaurs (Bennett, 2001a:29; Vremir et al., 2018:4). The ventral margin of the symphysis has a sharp ridge identified as a keel (Kellner and Langston, 1996:228), inherited from the Ornithocheiroidea (Andres, 2021). This keel is the intersection of the straight lateral surfaces, but it does not project below the symphysis or form concave lateral surfaces, or convex surfaces

as is the case in *Pteranodon* (Bennett, 2001a:29). Therefore, a crest is not identified in the mandible of *Q. lawsoni* (Kellner and Langston, 1996:228). This triangular cross-section increases in depth to the ventral symphysis; the keel terminates just anterior to the symphysis end but becomes sharper posteriorly as in LPB R.2347, contra Vremir et al. (2018). Crushing can give the impression of lateral concave surfaces in some areas, but these are not mirrored on the other side or in other specimens. The mandible symphysis is unusually shallow for the neopterodactyloids, in which it typically forms a much deeper angle in lateral view (Andres, 2021). The lateral taper of the symphysis in the horizontal plane is likewise narrow, but it does not become subparallel as in LPB R.2347 (Vremir et al., 2018) and some other pterosaurs with long mandibles (Andres, 2021). The lateral sulci of the non-novialoids, the large foramina of the Raeticodactylidae, and the pits of the Anurognathidae are not present on the mandible (Andres, 2021).

The symphysis bifurcates posteriorly into a ventral symphysis and a dorsal symphyseal shelf, forming a symphyseal cavity (anteriorly directed cavity in the symphysis of Kellner and

Langston, 1996) between the two, found in the azhdarchoids and pteranodontians (Andres, 2021). The symphyseal shelf extends posterior to the ventral symphysis (Kellner and Langston, 1996), unlike in *Noripterus* and *Pteranodon* (Andres, 2021). The damaged ventral margin of TMM 41961-1.2 allows an internal view of this symphyseal cavity. It is a triangular space in horizontal and transverse planes. The cross-section of the preserved anterior end of this specimen reveals no trace of this cavity, and so it would have been about 9 cm in total length. The posterior end of the symphyseal shelf has a depression below the occlusal surface for reception of the ventral bowing of the palate. The posterior end of the occlusal surface extends as lateral processes along the medial surfaces of the rami. There are no parallel ridges in this depression for contact with the ventral keel of the palate, as found in the thalassodromines (Andres, 2021). The anterior end of the depression does not appear to contact the symphyseal cavity in TMM 42161-2, and the dorsal surface of the symphyseal cavity appears flat with no representation of the depression in TMM 41961-1.2. This means that the symphyseal shelf is much deeper anterior to the depression. The posterior end of the symphyseal shelf in this depression extends for 4 cm along the midline, but it extends laterally as the paired processes along the medial surfaces of the rami for about another 4 cm, reminiscent of the occlusal surface posterior end. These lateral processes are not part of the splenials, and there is no splenial shelf.

The mandible rami present an inverted comma-shape (or 6-shape) in cross-section with concave medial and convex lateral surfaces, contrasting with the probably suboval cross-section of *Pteranodon* (Bennett, 2001a:29). The ventral margin is expanded into a rounded cross-section with the rest of the cross-section consisting of a medially curving plate of bone confluent with the sharp occlusal ridge. The medial surface flattens posteriorly. The rami have convex dorsal margins in medial/lateral view as in other neoazhdarchians but curve ventrally, uniquely for this group (Andres, 2021). A pair of ridges extending ventral to the cranial articulation on the lateral surface may represent a thin process of the posterior end of dentary, such as the thin posterior process of the dentary reported in *Pteranodon* (Bennett, 2001a:33, figs. 22A and 28A). In this case, the dentary would separate the surangular from the angular as in other macronychopterans (Andres, 2021). In *Pteranodon*, it appears that the surangular and angular do contact one another internally but are overlain laterally by the dentary posterior process (Bennett, 2001a:33, figs. 22A and 27A), which also is a possibility in *Q. lawsoni*. These ridges diverge anteriorly to enter an area of damaged bone found in all specimens, and so most of the lateral contacts of the dentary with the surangular and angular would not be visible.

A series of four circular openings pierce the occlusal surface of the symphysis, and a fifth pierces the posterior end of the ventral surface of the symphysis in TMM 42161-2. Kellner and Langston (1996) illustrated these openings but did not mention them. Eighteen centimeters from the preserved anterior end of the mandible is an 8 mm in diameter circular opening in the occlusal surface. Another opening of the same size is positioned 8 cm posterior to it. This opening is damaged posteriorly, and there is an unnatural knob of bone just to its posterior. Five centimeters posterior to the second opening is a third of the same size. Twenty centimeters posterior to the third opening is a fourth that is twice the size of the others. A fifth hole pierces the ventral surface of the mandible near the posterior end of the ventral symphysis about a centimeter posterior to the fourth. These openings are of unknown origin. They do not appear to be present on the other mandibles, but their preservation does not preclude them being present, possibly fewer in number. These openings do not appear to be post-mortem alterations. Their margins are nearly perfect circles, and they do not

appear to be damaged. If these were borings, they would not be positioned exactly on the midline and they would all show up on the ventral surface. The fifth and sixth openings are dorsal and ventral to one another, but they are offset by a centimeter. If something did bore through the posterior symphysis at an oblique angle to form these openings, they would be elliptical in outline. They also coincide with the mandible anatomy: the ventral keel terminates at the ventral opening, and the largest openings are posterior where the symphysis is larger. The origin and function of these openings is unknown, but they are identified as anatomical.

Surangular—The surangular is a large dorsally bowed bone in medial/lateral view that ramps into a convex dorsal edge that merges evenly with the rest of the ramus in *Q. lawsoni*. A rugose area on the lateral surface of the top of this curve may be the insertion for the M. adductor mandibulae and possibly M. pterygoideus anterior (Bennett, 2001a:30). Posterior to this, the dorsal margin loses its sharp occlusal ridge and expands toward the jaw articulation. Damage on the dorsal surface of this bone in TMM 41961-1.2 appears to delineate a dorsal eminence (coronoid of Wild, 1979, or coronoid process of Dalla Vecchia, 2003a), but this is not found in any other mandible specimen and so *Q. lawsoni* is like other novialoid pterosaurs in lacking a dorsal eminence on the mandible rami (Andres, 2021). The surangular is deep in the region of the adductor fossa on its medial and lateral surfaces, and it appears to constitute the surface of the fossa down to its ventral lip. Anterior to the adductor fossa, the surangular attenuates into an elongate ramus that is a sliver on the lateral surface and almost as narrow on its medial surface. It terminates about 12 cm from the symphyseal shelf. There is no sign of a small foramen for the external mandibular artery, reported in *Pteranodon* (Bennett, 2001a:33, figs. 22A, 27A, and 28A).

The adductor fossa is a long slit with a convex dorsal margin, which is convex because the surangular is dorsally bowed. The anterior half is horizontal and the posterior half curves ventrally. A deeper part of the posterior end of the fossa may be a foramen for the chorda tympani, which has been reported in *Pteranodon* (Bennett, 2001a:30, fig. 26). The ventral lip of the adductor fossa is a raised ridge that expands posteriorly to merge with the medial lip of the articulation. The surangular does not appear to contribute to the cranial articulations, as it does in *Pteranodon* (Bennett, 2001a:33, fig. 22).

Angular—The angular is a long bone that forms the ventral portion of the posterior ramus and probably the retroarticular process as well. Its medial contact with the prearticular and lateral contact with the probable posterior process of the dentary can be seen, but its anterior and posterior contacts cannot be resolved. The retroarticular process is short and triangular in lateral outline as inherited from the Monofenestrata, and subparallel in orientation to the preceding ramus as in most pterosaurs (Andres, 2021). In cross-section, it is a triangular crescent because its dorsal surface is concave. A foramen pierces the medial part of this concave surface posterior to the medial cotyle. Kellner and Langston (1996) identified this foramen as a fossa depresssoria, but it is identified as a pneumatic foramen here. Similar structures in the cranial articulation that are likely foramina are reported in many pterosaurs (Wellnhofer, 1985:116; 1987:18; Bennett, 2001a:31–32; Ősi et al., 2005:780; Myers, 2010:28; Buffetaut, 2011:134, fig. 2A; Britt et al., 2018:4). The sharp ridge along the lateral margin of the retroarticular process described in *A. lancicollis* (Averianov, 2010:272, fig. 6) also appears to be present in *Q. lawsoni*. The articular is fused to the dentary, surangular, angular, and prearticular with no trace of sutures. It is not known how much the articular contributes to the retroarticular process in *Q. lawsoni*.

Splenial—The middle of the mandible rami medial surface has a rougher texture than the dorsal and ventral margins, and it is set

apart from those margins by faint sutures. The medial surface of the rami is identified here as the splenial and possibly the prearticular posteriorly. There is a possible anterior Meckelian foramen (Meckelian fossa of Bennett, 2001a) on the right ramus of TMM 42161-2 that would mark the anterior end of the splenial and adductor canal. However, this foramen is not found on the left ramus or any other specimen, and so it is not identified as present in *Q. lawsoni*. The splenial does not contribute to the symphyseal shelf in this or any other pterosaur species.

Prearticular—The area ventral to the adductor fossa is poorly preserved in all specimens. The prearticular appears to reach the anterior end of the adductor fossa, but this cannot be confirmed. The contact with the splenial is not discernable (Kellner and Langston, 1996). There is no trace of the irregular foramina reported in the prearticulars of some *Pteranodon* specimens (Bennett, 2001a:34, fig. 25).

Articular—The articular comprises the cranial articulation (glenoid fossa of Kellner and Langston, 1996, or 'fossa articularis mandibulae' of Wellnhofer, 1980) and at least part of the retro-articular process in the mandible of pterosaurs. In *Q. lawsoni*, the cranial articulation expands equally medially and laterally, unlike the large medial projection of *A. lancicollis* (Averianov, 2010:272, fig. 6), but it is anteroposteriorly broader medially because of a horizontal flange attached to the medial cotyle (expanded medial edge of the medial cotyle of Kellner and Langston, 1996). A similar vertical flange (thickened and projecting edge of Kellner and Langston, 1996) is attached to the lateral cotyle. The dorsal lip of the articulation (transverse ridge of Averianov, 2010) extends most posteriorly at its midpoint due largely to the anterolateral curvature of the lateral cotyle at this midpoint. The cranial articulation of the mandible complements the mandible articulation of the cranium: a diagonal intercotylar ridge (diagonal ridge of Bennett, 2001a, sharp diagonal ridge of Averianov, 2010, ridge and oblique ridge of Buffetaut et al., 2011, or anteromedially-posterolaterally oriented ridge and oblique ridge of Buffetaut, 2011) that extends posterolaterally from the anterior end of the medial cotyle to the posterior end of the lateral cotyle for articulation with a similar intercondylar groove on the quadrate. The medial and lateral articular surfaces are conical in shape expanding medially and laterally, respectively, as found in *A. lancicollis* (Averianov, 2010:272, fig. 6). The lateral cotyle is positioned anterior and dorsal to the medial cotyle (Kellner and Langston, 1996), but they overlap greatly over their length and width. The lateral cotyle is directed posteriorly, whereas the medial cotyle is directed posterodorsally. There is a notch (broad triangular notch of Kellner and Langston, 1996) between the vertical flange of the lateral condyle and the intercotylar ridge, turning the lateral end of the intercotylar ridge into the posterolateral process (small triangular area, peg-like structure, peg-like process, and posterolateral process at the edge of the glenoid fossa of Kellner and Langston, 1996) also reported in cf. *A. bostobensis* (WDC Kz-001) (Averianov, 2014:7). There is no similar process on the anteromedial end of the intercotylar ridge.

Cervical Vertebrae

The cervical vertebrae of *Q. lawsoni* have not been found in articulation, but all of the nine cervical vertebrae present in pterosaurs, sensu Bennett (2004, 2014), have been identified in this material. These vertebrae are procoelous as in all pterosaurs (Sereno, 1991). In a few instances, two or three cervicals were found so closely associated with one another that they are presumed to belong to single individuals: TMM 41961-1 (an associated skeleton with fragmentary cervicals V, VI, and VII); TMM 41544-4, 41544-8, 41544-15, and 41544-16 (and cervicals VI, IV, V, and III respectively); TMM 42161-1 (cervicals III, V, and VII); and TMM 42180-14 (cervicals VI, V, and VII).

TABLE 5. Measurements of *Quetzalcoatlus lawsoni*, sp. nov., cervical material. Values in millimeters. >, preserved value; <, maximum possible value; ~, approximate value; a-p, anteroposterior dimension; d-v, dorsoventral dimension; and lat, lateral dimension. Holotype specimen in italics.

Dimension: Element: Specimen Number:	Total length (a-p)	Mid-width (lat)	Mid-depth (d-v)
Atlantoaxis			
TMM 41954-39	68.47	16.20	56.46
TMM 42180-5	>48.10	23.47	>25.95
Atlas			
TMM 41954-39	8.81	18.45	~24.62
TMM 42180-5	>7.51	21.25	~25.91
Axis			
TMM 41954-39	57.86	16.20	56.46
TMM 42180-5	>40.79	23.47	>25.95
Cervical III			
TMM 41544-16	166.34	28.13	32.50
TMM 41546-2	>147.34	34.20	31.05
TMM 41546-7	>35.06	>36.21	>24.17
TMM 42161-1.3	170.71	25.38	29.49
TMM 42180-1	198.11	33.60	30.54
TMM 42422-24	173.48	24.29	40.68
Cervical IV			
TMM 41544-8	258	37.74	30.34
TMM 42462-1	>68.32	35.28	<46.73
Cervical V			
TMM 41544-4	>147.65	>33.68	>21.45
TMM 41544-15	412	37.03	22.79
TMM 41546-1	>56.17	>23.20	>29.90
TMM 41954-7	484	47.80	26.48
TMM 41954-31	>87.72	>33.97	>22.60
TMM 41961-1.28	341	28.07	34.67
TMM 42161-1.4	412	29.48	19.88
TMM 42180-2	395	35.75	21.90
TMM 42422-22	417	35.63	27.03
TMM 42422-32	388	35.72	27.90
Cervical VI			
TMM 41544-4	>264	>24.22	~37.58
TMM 41544-12	>61.58	~39.79	25.56
TMM 41546-8	>39.72	>51.80	>26.75
TMM 41954-10	>119.80	38.92	28.04
TMM 41954-30	>117.00	40.17	>14.46
TMM 41954-65	348	38.40	24.29
TMM 41961-1.29	>276	38.95	28.03
TMM 42161-3	>183.54	52.62	>13.23
TMM 42180-3	>104.58	46.63	26.36
TMM 42180-14.10	329	37.49	30.79
TMM 42180-19	368	40.12	33.95
TMM 42259-1.1	>82.13	<68.47	<45.99
TMM 42422-20	336	44.89	26.04
Cervical VII			
TMM 41954-41	278	31.48	26.62
TMM 41954-88	>96.72	41.21	>20.14
TMM 41961-1.30	>159.55	41.91	23.23
TMM 42161-1.5	264	43.79	34.60
TMM 42180-14.11	229	39.90	33.73
TMM 42259-1.2	280	44.56	29.28
TMM 42422-31	>175.01	32.37	35.57
TMM 45997-4	>64.05	>52.08	>22.71
Cervical VIII			
TMM 41954-42	87.20	86.69	>47.68
TMM 42422-8	78.60	64.78	70.79
Cervical IX			
TMM 41954-40	48.95	99.67	>38.46
TMM 42422-7	45.03	91.70	64.71

Wellnhopterus brevirostris preserves cervicals IV–VIII in articulation and provides some aid in these identifications. Mostly complete and most identifiable *Q. lawsoni* cervicals comprise: atlantoaxis (n=2), cervical III (n=5), cervical IV (n=1), cervical V (n=7), cervical VI (n=4), cervical VII (n=5), cervical VIII (n=2) cervical IX (n=2), and a number of cervical fragments

(n=5+) whose sequential positions are identified with less certainty (Table 5).

As in other pterosaurs, the cervical vertebrae of *Q. lawsoni* are divided into three morphological regions: the atlantoaxis (fused atlas-axis complex), the middle-series cervicals III–VII, and the posterior-series cervicals VIII and IX. Cervicals IX and possibly VIII used to be regarded as dorsal vertebrae in some pterosaur species in the past, owing to their resemblance to vertebrae of the trunk and the presence of large, bicipital ribs. Following the definition of Bennett (2004, 2014), cervicals VIII and IX are considered posterior-series cervicals here.

Postatlantal cervicals bear a wider posterior condyle that is a slightly reniform (kidney-shaped) oval in cross-section in *Q. lawsoni*, as in other pterodactyloids (Andres et al., 2010). The posterior condyle is flanked by a massive pair of posterolaterally directed processes termed postexapophyses. Postexapophyses are present in the Ornithocheiroidea, Ctenochasmatidae, and Wukongopteridae pterosaurs (Andres, 2021), but they appear different in each taxon: distinct ventrolateral processes in ornithocheiroids, lateral flanges in ctenochasmatids, and posterolateral processes in wukongopterids (Andres et al., 2010). These are not to be confused with the postlateral projections (exapophyses of Bonde and Christiansen, 2003, and Padian, 2008a) of most non-pterodactyloid pterosaurs (Andres et al., 2010). The repeated evolution of postexapophyses may be an example of parallel evolution from these postlateral projections (Andres et al. 2010). In *Q. lawsoni*, the postexapophyses have well-defined articular surfaces continuous with but separated by a groove from the articular surface of the posterior condyle. The postexapophyses articulate with the preexapophyseal articulations (exapophyses of Williston, 1897, or lateral accessory articular surfaces of Vremir et al., 2013b) of the following vertebra. The postexapophyses of *Q. lawsoni* are robust, but their pedestals have been described as considerably smaller than in *C. boreas* (Hone et al., 2019:8).

Postaxial cervicals have a wide anterior cotyle that is cordate to subtriangular in outline, with the lateral ends curving ventrally to varying degrees. This shape is due to a midline notch/emargination (shallow depression adjacent to the concavity of the dorsal margin of the facies articularis cranialis of Martill et al., 1998, small groove present on the middle portion of the dorsal rim of the cotyle of Vremir et al., 2013b, or cotyle higher than neural canal and distinct dorsal incision of Andres et al., 2010) in the dorsal cotyle rim (two sharp carinae slightly diverging anteriorly of Martill et al., 1998, or supracotylar shelf of Vremir et al., 2015) where it contacts the neural canal as well as an anterior projection in the ventral rim of the cotyle, termed a hypapophysis by Howse (1986). Hypapophyses are present on middle- and posterior-series cervicals, and likely provided the origin of hypaxial muscles (Bennett, 2001a). They are expressed as broad-based, anteriorly directed, and triangular processes that articulate with the ventral surface of the posterior condyle between the postexapophyses. The hypapophysis is flanked by a pair of shallow ventral fossae. The width of the cotyle varies from 6.1 to 7.5 times its depth. The dorsal rim of the anterior cotyle and interzygapophyseal ridge turn the anterior end of the neural arch into an anterior vestibule. The anterior vestibule connects to lateral sulci (shallow sulci of Harrell et al., 2017) that extend medial and then ventral to the prezygapophyses to contact the transverse foramina. The prezygapophyses are positioned lateral to and project past the anterior cotyle (except cervical IX), often described as horn-like (Pereda-Suberbiola et al., 2003:82; Godfrey and Currie, 2005:294 and 299; Henderson and Peterson, 2006:192; Vremir et al., 2015:9). None of the postaxial postzygapophyses extend past the posterior condyle. Two midline ridges on the dorsal surface of the anterior cotyle separate the neural canal opening from the lateral sulci. The laminae of the neural arch

also constitute a dorsal rim on the posterior end of the neural arch to form a posterior vestibule, but not in all cervicals. The postaxial cervicals also have preexapophyses (pre-exapophyses and pre-expophysial processes of Howse, 1986, prezygapophysial tubercles and prezygapophyseal tubercles of Ősi et al., 2005, accessory articular processes and preexapophyses of Watabe et al., 2009, ventral prezygapophyseal tubercles of Vremir et al., 2015, or ventral prezygapophyseal tubercle [fused cervical rib] of Naish and Witton, 2017) where preservation permits their identification. It should be noted that previous reports of preexapophyses have referred to accessory articular surfaces on the underside of lateral projections of the anterior cotyle, instead of separate processes (Bennett, 2001a). These accessory articular surfaces are continuous with the articular surface of the anterior cotyle and articulate with the postexapophyses, and so have been termed preexapophyseal articulations by Bennett (2001a). The postaxial cervical vertebrae of *Q. lawsoni* have both preexapophyseal articulations as well as distinct processes anterolateral to these articulations on the underside of the prezygapophyses, which are identified here as preexapophyses. Preexapophyses have also been reported in the azhdarchid species *E. langendorfensis* (Vremir et al., 2013b:7) and *A. lancicollis* (Averianov, 2010:275).

The middle-series cervicals (middle-series cervical vertebrae of Howse, 1986, mid-series cervicals and mid-cervicals of Company et al., 1999, midcervical series and midcervicals of Bennett, 2001a, middle-series cervicals and mid-cervicals of Andres and Ji, 2008, or midseries cervical vertebrae of Vremir et al., 2015) in *Quetzalcoatlus* and all other azhdarchid pterosaurs are known for being extremely elongated, reaching lengths of up to 17 times the length of a dorsal vertebra with aspect ratios approaching ten (Andres, 2021). However, cervicals III and VII are notably distinct from the other middle-series cervicals, and so the term 'mid-cervical' should probably be used to refer to the more similar and more elongate cervicals IV–VI. It should be noted that Rodrigues et al. (2011) considered cervicals IV–VII to be the middle series. In undistorted specimens, they are constricted in their midsections (waisted in mid-section of Harrell et al., 2017, maximum lateral constriction of Averianov, 2010, and narrow-waisted region and distinct "waist" of Vremir et al., 2015). The middle-series cervicals differ from one another in elongation, position of constriction, and development of the neural spine. The prezygapophyses are oriented anteriorly in lateral view, and the postexapophyses extend posterior to the posterior condyle. Their articular surfaces are oval in outline and oriented anterodorsomedially, mirrored by posteroventrolateral articular surfaces on the postzygapophyses. They lack the pneumatic foramina on the lateral surfaces of the centra that are found in other non-neopterodactyloid ornithocheiroids and ctenochasmatids, as well as on the neural arch in non-pterodactyloid pterosaurs (Andres, 2021). The neural arch is low, merged fully with the centrum, and lack lateral excavations (lateral concavities of Harrell et al., 2017) creating tubular midsections, as in other neopterodactyloids (Andres, 2021). The middle-series cervicals have reduced and fused C-shaped ribs, as in other non-ctenochasmatine caelicodracones. The fused rib bridges the transverse foramen (vertebrarterial canal of Williston, 1903, foramen pneumaticum of Frey and Martill, 1996, foramen transversarium of Martill et al., 1998, transverse canal of Henderson and Peterson, 2006, transverse foramen and vertebrocostal canal of Watabe et al., 2009, or canal for housing of the vertebral artery of Averianov, 2010) on either side of the anterior cotyle. Extending posteriorly from the transverse foramen on the ventrolateral surface of the centrum is a distinct sulcus (narrow sulcus and sulcus ventralis of Frey and Martill, 1996, sulcus and lateral sulcus of Martill et al., 1998, longitudinal oval sulcus of Pereda-Suberbiola et al, 2003, vertebrocostal sulcus of Averianov, 2010, shallow trough of Watabe et al., 2009, longitudinal

sulcus and ventrolateral sulcus of Rodrigues et al., 2011, ventral sulcus and prezygapophyseal sulcus of Vremir et al., 2013b, or vertebrarterial sulcus of Harrell et al., 2017). There is a midline emargination in the interzygapophyseal ridges above the anterior end of the neural canal. In the anterior and posterior vestibules of the neural arch, a pair of well-defined pneumatic foramina are located lateral to the neural canal between the cotyle/condyle and zygapophyses, inherited from the Ornithocheiroidea (Andres, 2021). No trace of bony canals can be seen extending between these foramina in broken sections of the centra, and so these passages may have simply emptied into the lumen of the centrum. A foramen is not present in the neural arch above the neural canal (median pneumatic foramen of Bennett, 2001a, third pneumatopore of Godfrey and Currie, 2005, dorsal pneumatic foramen of Averianov, 2010, or accessory pneumatopore and accessory dorsal pneumatopore of Hone et al., 2019), which is commonly present in the ornithocheiroids (Unwin, 1991:452; Wellnhofer, 1991a:fig. 4–8; Bennett, 2001a:43, fig. 39; Andres and Norell, 2005:4, fig. 2B; Godfrey and Currie, 2005:298, fig. 16.1–16.2; Averianov, 2010:275, fig. 8; Rodrigues et al., 2011:151, fig. 3A). It should be noted that pterosaur taxa with dorsal pneumatic foramina may not have them present on all of their middle-series cervicals; *A. lancicollis* lacks them in cervicals III and IV (Averianov, 2010:275, fig. 8), for example. However, some of the neural canals in *Q. lawsoni* are clithridiate (keyhole-shaped), suggesting that the neural canal and dorsal pneumatic foramen have become confluent, and it has been suggested by Nesov (1984) that these openings are incipiently confluent in some *A. lancicollis* specimens.

In *Q. lawsoni* cervicals IV–VII, the neural spine is bifid: split into elevated anterior and posterior processes with a pencil-thin ridge extending between them. For this unusual configuration of the neural spine, the anterior and posterior spine elevations are termed here the anterior spinous process and posterior spinous process, respectively, and the ridge between them is termed the neural ridge. In addition, the posterior condyle extends posterior to the postzygapophyses in cervicals IV–VII.

The mid-cervical vertebrae (IV–VI) are a wider than tall ellipse in cross-section in *Quetzalcoatlus* and cf. *H. thambema* (LPB R.2395) (Andres, 2021), except toward the ends where they are rhombohedral anteriorly and trapezoidal posteriorly. Non-giant azhdarchids have an oval cross-section (Averianov, 2010:275). *Arambourgiania philadelphiae* has an oval cross-section, but it is laterally compressed instead (Andres, 2021). The mid-cervical neural spines form ridges in the neopterodactyloids, but only become extremely reduced in the azhdarchids (Andres, 2021). The posterior neural spine overhangs the end of the neural canal as a posterior process in *Q. lawsoni*. Low transverse ridges the size and shape of the neural ridge extend posteriorly along the lateral surfaces of the vertebrae, but differ in their length and dorsal position among vertebrae. They are weakly expressed, and so cannot be detected in the more crushed and poorly preserved vertebrae. The neural canal is well defined at each end of the neural arch, but it can rarely be seen in cross-sections. In TMM 42180-2, grinding at the broken ends of the middle and posterior segments of this fifth cervical has revealed the sub-rounded cross-section of a matrix-filled neural canal with a diameter of approximately 7 mm. The walls of this canal are composed of compact bone no more than 0.1 mm thick, confirming the presence of an ossified neural canal in the Azhdarchidae (Nesov, 1984:49). The spinal cord would have passed through the vertebra in this delicate tube of bone suspended from the neural arch by trabeculae, presumably within the hollow lumen of the centrum.

Quetzalcoatlus lawsoni is like other azhdarchid pterosaurs in having very elongate middle-series cervicals, but it is distinct in having cervicals V–VII as the longest vertebrae instead of cervicals IV–VI. The ratio of the average lengths of the cervicals (I/II–IX) to the atlantoaxis in this species is 1 : 2.59 : 3.77 : 5.82 : 5.03 : 3.83 : 1.15 : 0.66, following the pterodactyloid pattern of increasing length to cervical V and then decreasing in length (Howse, 1986; Bennett, 2001a; Averianov, 2010).

The posterior-series cervicals consist of cervicals VIII and IX. They are the shortest, widest, and tallest of the cervicals and bear features found in both the cervical (e.g., hypapophyses and postexapophyses) and dorsal vertebrae (e.g., transverse processes, tall neural spines, tall neural arches, large ribs, and a clear distinction between centrum and neural arch). Only two specimens of each are preserved in *Q. lawsoni* and likely belong to two individuals: TMM 41954-40 and 42 as well as TMM 42422-7 and 8. The TMM 41954 posterior-series cervicals articulate well with each other, as do the TMM 42422 cervicals, but the TMM 41954 and 42422 cervicals do not articulate with the other. These pairs of vertebrae have the greatest number of differences among specimens of the same element. Some of this variation could be explained by deformation, but not all. Their common features are used to describe these elements, but they may represent two forms in *Q. lawsoni*.

Atlantoaxis—The only atlas and axis material in *Q. lawsoni* is represented by TMM 41954-39 and 42180-5 (Table 5). The atlas and axis in this material are fused into a common element termed an atlantoaxis (atlanto-axis of Howse, 1986, atlas-axis and atlas/axis of Cai and Wei, 1994, or atlas-axis complex of Bennett, 2001a) without sutures, found in both the ornithocheiroids and darwinopterans (Andres, 2021). TMM 41954-39 is the better preserved of the two, although it is missing the right postzygapophysis and postexapophysis, has damage to the left diapophysis and the dorsal tip of the axis, and has distorted curvature to the right (Fig. 18). TMM 42180-5 is notable for being significantly larger and more robust, but it is much less complete: missing the rim of the anterior cotyle (cotyle for articulation with the cranial condyle of Averianov, 2010, cotyle of the atlas for articulation with the occipital condyle and condyloid fossa of Watabe et al., 2009) and presumably most of the axis, as well as the neural arch and most of the right postexapophysis. The atlantoaxis is shorter than all of the cervicals except for the cervical IX in *Q. lawsoni*. It is comparable in size to the atlantoaxis of *Z. linhaiensis* (Cai and Wei, 1994:183, fig. 1) and *A. lancicollis* (Averianov, 2010:274, fig. 7), but it does not approach the short atlantoaxis of *Pteranodon* (Bennett, 2001a:39, fig. 34C). Atlantoaxes are reported in the azhdarchid species *Z. linhaiensis* (Cai and Wei, 1994), possibly *E. langendorfensis* (UBB specimen) (Vremir et al., 2013b:9, fig. 4-10), *A. bostobensis* (Averianov, 2007), *M. maggii* (Vullo et al., 2018), and *A. lancicollis* (Nesov, 1984), as well as the putative azhdarchid specimen MPC−Nd 100/302 (Watabe et al., 2009).

Atlas—Although the atlas and axis are fused, it is possible to discern their boundaries (Table 5). This is most readily done in the region of the atlas neural arch, which is partially separated from the atlas arch by a fissure-like intervertebral foramen (intervertebral foramen, spinal foramen, and spinal nerve foramen of Averianov, 2010) (Fig. 18), also reported in *A. lancicollis* (Averianov, 2010) and MPC−Nd 100/302 (Watabe et al., 2009:234). This foramen delineates a Z-shaped pedicle for the axis neural arch in *Q. lawsoni*. The angles of this Z-shape are reminiscent of pre- and postzygapophyses, with an anterior process located dorsomedially and a posterior process located ventrolaterally, and so they are identified as such here. The intervertebral foramen is also positioned just posterior to the maximum expansion of the anterior end of the atlantoaxis and just anterior to the constriction of the axis centrum (distinct groove of Averianov, 2010), which is missing in *Pteranodon* that widens posteriorly from the anterior cotyle instead (Bennett, 2001a:40). On TMM 42180-5, where the anterior margin has lost its cortical bone, the point of
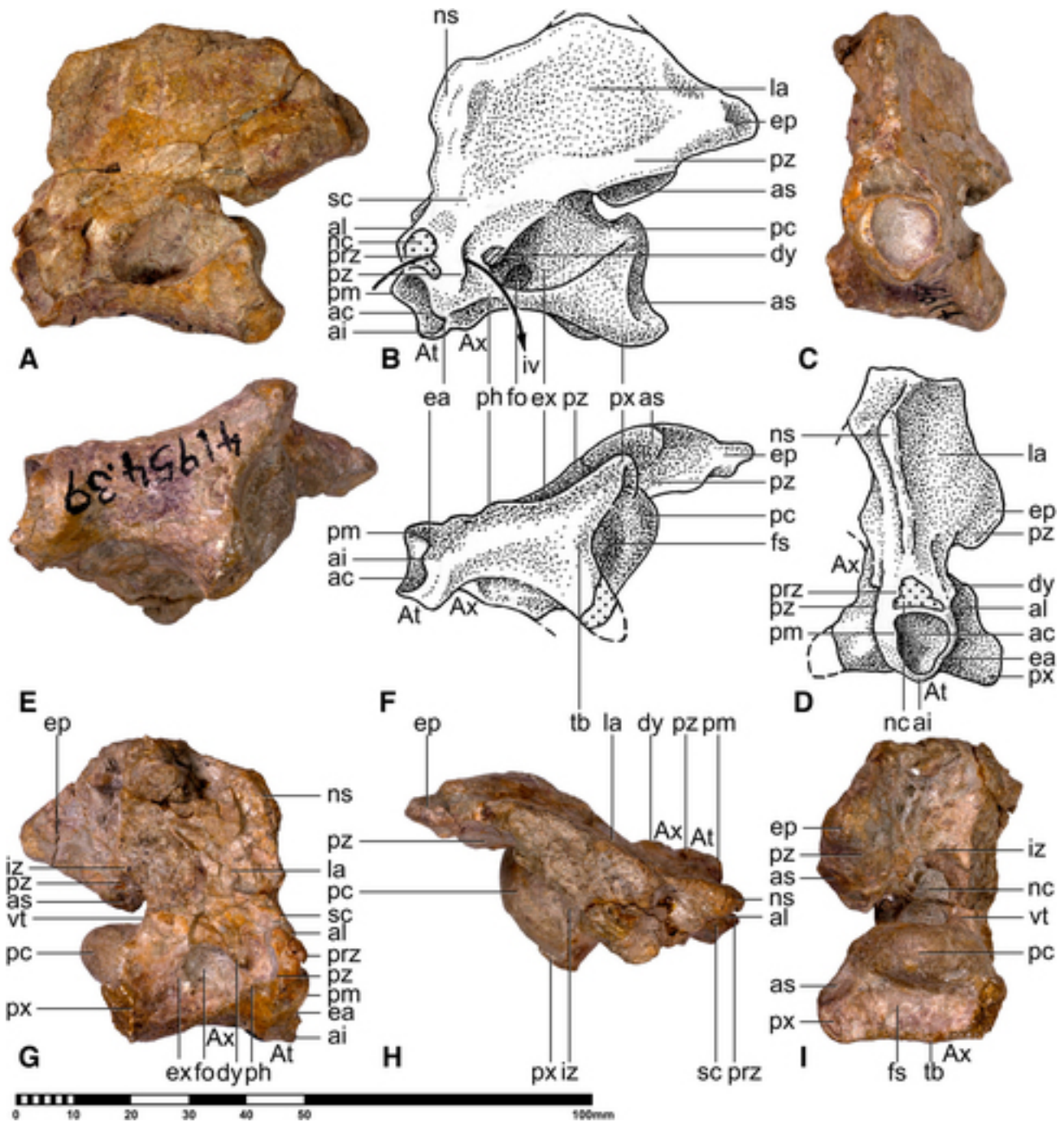
FIGURE 18. *Quetzalcoatlus lawsoni*, sp. nov., atlantoaxis (TMM 41954-39) in **A**, left lateral photograph and **B**, line drawing; **C**, anterior photograph and **D**, line drawing; **E**, ventral photograph and **F**, line drawing; **G**, right lateral photograph; **H**, dorsal photograph; and **I**, posterior photograph views. **Abbreviations: ac**, anterior cotyle; **ai**, atlas intercentrum; **al**, atlas neural arch; **as**, articular surface; **At**, atlas; **Ax**, axis; **dy**, diapophysis; **ea**, emargination; **ep**, epipophysis; **ex**, excavation; **fo**, foramen; **fs**, fossa; **iv**, intervertebral foramen; **iz**, interzygapophyseal ridge; **la**, lamina; **nc**, neural canal; **ns**, neural spine; **pc**, posterior condyle; **ph**, parapophysis; **pm**, prominence; **prz**, prezygapophysis; **px**, postexapophysis; **pz**, postzygapophysis; **sc**, scar; **tb**, tuberosity; and **vt**, vestibule. Dots represent matrix and/or damaged bone. Scale bar equals 100 mm.

maximum anterior expansion is characterized by a delineation separating slightly different bone textures. This delineation is mirrored by a thickened ridge on TMM 41954-39. The region anterior to the maximum expansion of the atlantoaxis and the intervertebral foramen is identified here as the atlas. This delineates an atlas that is more robust than in *Pteranodon* but not as robust as in *Pterodactylus antiquus* (Sömmerring, 1812)

(Bennett, 2001a:40–41). However, Watabe et al. (2009) labeled the entire anterior expansion in MPC–Nd 100/302 as the atlas.

Three atlanteal elements can be recognized in *Q. lawsoni*: a dorsal pair of neural arches and a ventral intercentrum. On the lateral surface, ventral to the atlas neural arch is a slight groove at the level of the axis parapophysis that reaches the anterior cotyle at an emargination of the cotyle perimeter; this

is identified as the demarcation between the atlas neural arch and intercentrum. The atlas intercentrum is a semicircular crescent in anterior view, forming the ventral margin of the anterior cotyle. This lateral emargination is also present in *A. lancicollis* (Averianov, 2010:fig. 7D), but the entire anterior cotyle was identified as the atlas intercentrum by Averianov (2010). A midline process is present on the anteroventral margin of the intercentrum in *Q. lawsoni*, termed a hypapophysis by Averianov (2010).

The left and right halves of the atlas neural arch may meet at subtle midline emarginations present on both the dorsal margin of the anterior cotyle and the dorsal margin of the neural canal, but no sutures are visible to confirm this. The atlas neural arches of *A. lancicollis* and *Nyctosaurus gracilis* (Marsh, 1876) are described as meeting at the midline dorsal to the anterior cotyle but not dorsal to the neural canal (Bennett, 2001a:41) to form C-shaped structures. Averianov (2010) instead reconstructs a plate-like proatlas fusing with the neural arches over the neural canal in *A. lancicollis*. There is no trace of an atlas neural spine as reported in *P. antiquus* (Bennett, 2001a:41) or a wing-like process of the atlas neural arch as reported in MPC–Nd 100/302 (Watabe et al., 2009:234). The left and right atlas neural arch are triradiate: a Z-shaped dorsal process delineated by the intervertebral foramen that forms the dorsal and lateral margins of the neural canal, a medial process that forms both the ventral margin of the neural canal and the dorsal margin of the anterior cotyle, and a ventral process that forms the dorsolateral margin of the anterior cotyle. This ventral process creates a prominence on the anterior cotyle. This is a much more complex atlas than the three crescent-shaped atlanteal elements that form the margins of just the anterior cotyle in *Pteranodon* (Bennett, 2001a:39–40, fig. 35). The anterior opening of the neural canal is broadly triangular and wider than tall (11.83 mm by 5.53 mm in TMM 41954-39), as in *A. lancicollis* (Averianov, 2010:274, fig. 7A), and contrasting with the semicircular outline of MPC–Nd 100/302 (Watabe et al., 2009:figs. 5 and 6). The anterior cotyle is hemispherical and almost perfectly round (average diameter of 10.97 mm in TMM 41954-39) with three prominences, two dorsolateral and one ventral.

Axis—The axis (epistropheus and axis of Averianov, 2007) of TMM 41954-39 is large compared with the atlas and dorsal vertebrae, although it is dwarfed by the other cervicals (Table 5). Much of its size comes from a massive pair of postzygapophyses and epipophyses (Fig. 18). The enlargement of the postzygapophyses appears to have shifted the axis neural spine (vertical ridge for the origin of muscles of Bennett, 2001a) anteriorly into a nearly vertical orientation dorsal to the atlas. This neural spine is a blade-shaped flange in lateral outline and apparently lacks a spinous process. MPC–Nd 100/302 has a more traditional neural spine with an almost horizontal spinous process that is triangular in the transverse plane (Watabe et al., 2009:234, figs. 5 and 6; Averianov, 2010:274), whereas *A. lancicollis* seems to combine both a blade-shaped flange and a triangular spinous process into an anteriorly inclined neural spine (Averianov, 2010:274, fig. 7). *Azhdarcho lancicollis* also has a notch between the neural spine and neural canal (Averianov, 2010:274, fig. 7D) shared with MPC–Nd 100/302 (Watabe et al., 2009:figs. 5 and 6), contra Averianov (2010), that is absent in *Q. lawsoni*. There is some damage to the dorsal tip of the axis in TMM 41954-39, but this is posterior to posterior/dorsal margin of the neural spine and so it is unlikely that the neural spine continued or had a spinous process. The postzygapophyses can also be seen to bifurcate by this point, separated by a vertical flat surface that overhangs the posterior neural canal opening. This vertical surface is separated by an interzygapophyseal ridge between the postzygapophyses (pronounced ridge of Bennett, 2001a, interzygapophyseal ridge of Watabe et al., 2009, or transverse ridge of Averianov, 2010) from a horizontal surface that overhangs the neural canal, also reported in

A. lancicollis (Averianov, 2010:274). The vertical flat surface has a median ridge in *Pteranodon* (Bennett, 2001a:40, fig. 35) and MPC–Nd 100/302 (Watabe et al., 2009:234–235) that intersects the interzygapophyseal ridge, or a prominent depression in *A. lancicollis* (Averianov, 2010:274, fig. 7B), that are presumably for the attachment of an intervertebral/interspinal ligament (Watabe et al., 2009:234–235; Averianov, 2010:274), but it is too poorly preserved in *Q. lawsoni* to ascertain if either was present. The lateral surface between the neural spine and the epipophyses is identified as a massive lamina of the neural arch. The epipophysis is likewise large, constituting half of the postzygapophysis and extending far beyond the posterior condyle of the centrum. The main body of the postzygapophysis is oriented posterodorsally, but the epipophysis is oriented posteriorly, giving the entire postzygapophysis a curved appearance in dorsal/ventral view. The proximal half of the postzygapophysis is taken up by a flat posteroventrally oriented oval articular surface for the prezygapophysis of cervical III, similar in shape to *A. lancicollis* (Averianov, 2010:274) and probably *E. langendorfensis* (Vremir et al., 2013b:8), but distinct from the lacriform outline of MPC–Nd 100/302 (Watabe et al., 2009:235, figs. 5 and 6). A robust ridge extends along the ventral margin of the medial aspect of the postzygapophysis. A deep lateral notch in the pedicle of the neural arch separates the postzygapophysis from the posterior condyle. In posterior view, pneumatic foramina lateral to the neural canal are absent, as in *A. lancicollis* (Averianov, 2010:274), but they are reported in MPC–Nd 100/302 (Watabe et al., 2009:235) and *Pteranodon* (Bennett, 2001a:40, figs. 34 and 35). The neural canal is ovate in outline posteriorly in *Q. lawsoni* (7.90 mm by 11.79 mm in TMM 41954-39) as opposed to lacriform in *M. maggii* (Vullo et al., 2018:5), round in *A. lancicollis* (Averianov, 2010:274, fig. 7B), and clithridiate in MPC–Nd 100/302 (Watabe et al., 2009:figs. 5 and 6). There is no demarcation between the axis neural arch and centrum.

The axis centrum expands rapidly from an anterior constriction, terminating in a pair of robust ventroposterolaterally oriented postexapophyses, and giving the centrum a triangular outline in ventral view. A suboval articular surface forms a concave facet for the preexapophyseal articulation of cervical III on the dorsal surface of postexapophysis and contacts the posterior condyle. A posteriorly oriented fossa (deep concavity of Watabe et al., 2009) is positioned between the postexapophyses and ventral to the posterior condyle for the reception of the hypapophysis of cervical III, and appears to be present in *A. bostobensis* (Averianov, 2007:pl. 9, fig. 1), *M. maggii* (Vullo et al., 2018:5, fig. 2), *A. lancicollis* (Averianov, 2010:274, fig. 7B), and MPC–Nd 100/302 (Watabe et al., 2009:figs. 5 and 6). A low median tuberosity occurs at the ventral edge of this fossa. The posterior condyle is oval in outline in TMM 41954-39 (25.52 by 10.03 mm); the condyle is more ventrally bowed in TMM 42180-5 (28.63 by 11.72 mm), and the sulcus of the neural canal reaches the posterior margin of the condyle. The posterior condyle extends well past the neural canal. The axis centrum has a concave ventral margin in lateral view, as in *A. lancicollis* (contra Averianov, 2010) and MPC–Nd 100/302 (Watabe et al., 2009:fig. 5B), that differs from the convex centrum of *A. bostobensis* (Averianov, 2007:193, pl. 9, fig. 1b), the flat centrum of *M. maggii* (Vullo et al., 2018:4, fig. 2A and D), and the centrum of *Pteranodon* that is only concave between the postexapophyses (Bennett, 2001a:40). The lateral surface of the centrum has a deep excavation (lateral concavity of Watabe et al., 2009) with a circular pneumatic foramen positioned at the anterior end, much as in *A. bostobensis* (Averianov, 2007:195, pl. 9, fig. 1b), *M. maggii* (Vullo et al., 2018:5, fig. 2A and D), *A. lancicollis* (Averianov, 2010:fig. 7D), and *Pteranodon* (Bennett, 2001a:40, figs. 33–35). However, the lateral surface of the centrum in MPC–Nd 100/302 is described as slightly
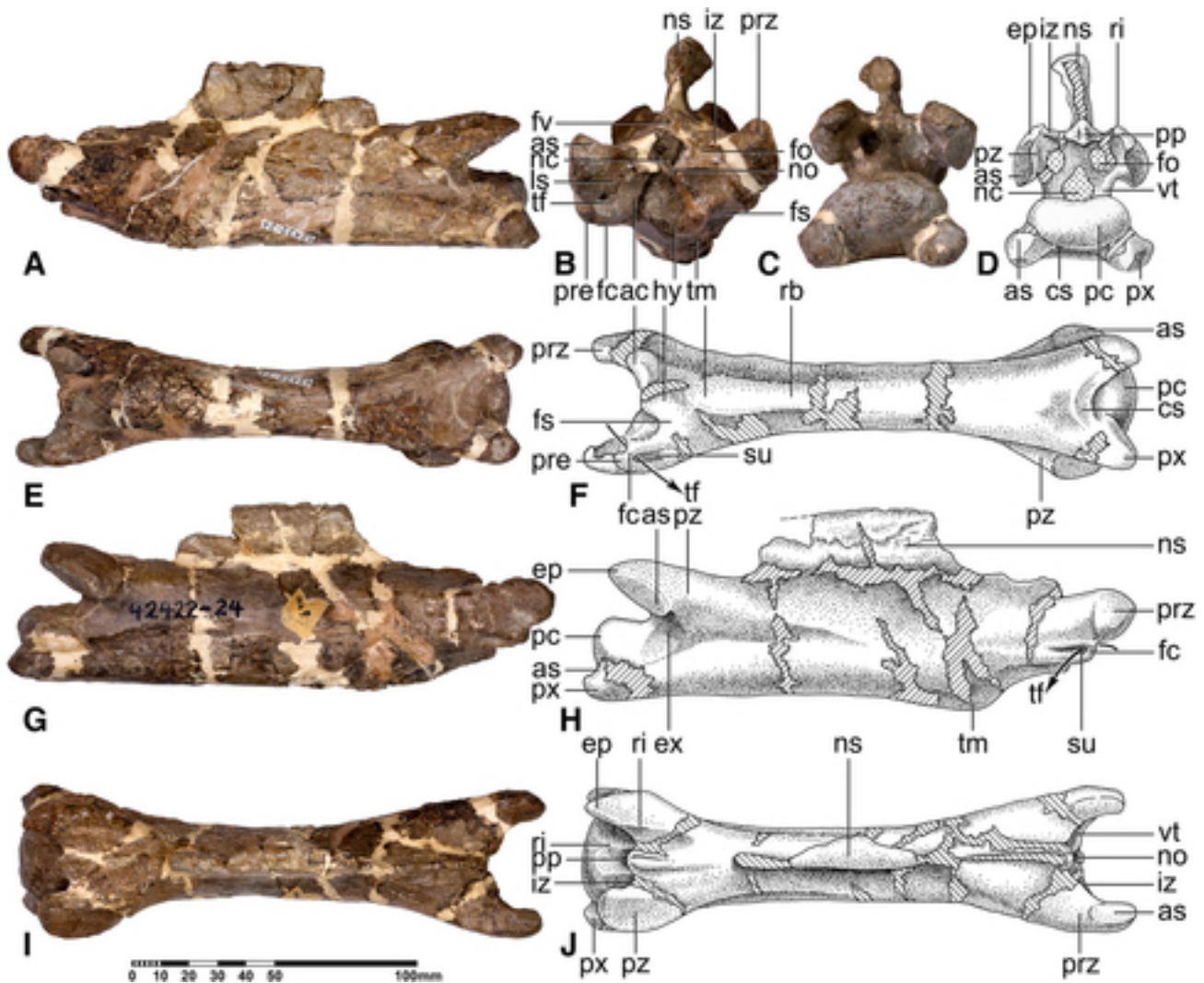
FIGURE 19. *Quetzalcoatlus lawsoni*, sp. nov., cervical III (TMM 42422-24) in **A**, left lateral photograph; **B**, anterior photograph; **C**, posterior photograph and **D**, line drawing; **E**, ventral photograph and **F**, line drawing; **G**, right lateral photograph and **H**, line drawing; **I**, dorsal photograph and **J**, line drawing views. **Abbreviations: ac**, anterior cotyle; **as**, articular surface; **cs**, concave surface; **ep**, epipophysis; **ex**, excavation; **fc**, fused cervical rib; **fo**, foramen; **fs**, fossa; **fv**, fovea; **hy**, hypapophysis; **iz**, interzygapophyseal ridge; **ls**, lateral sulcus; **nc**, neural canal; **no**, notch; **ns**, neural spine; **pc**, posterior condyle; **pp**, posterior process; **pre**, preexapophysis; **prz**, prezygapophysis; **px**, postexapophysis; **pz**, postzygapophysis; **rb**, raised band; **ri**, ridge; **su**, sulcus; **tf**, transverse foramen; **tm**, tumescence; and **vt**, vestibule. Diagonal lines represent plaster, and dots represent matrix. Scale bar equals 100 mm.

concave and lacking a foramen (Watabe et al., 2009:235). Anterior to the excavation are a diapophysis and parapophysis, suggesting the presence of a bicipital axial rib, but none is preserved in the Big Bend material. Although damaged, the diapophysis is much larger and positioned dorsoposteriorly relative to the parapophysis. It terminates in a sharp point on a dorsoposterior ridge (anteroventrally-extending shelf-like diapophysis of Watabe et al., 2009, or marked oblique ridge with bump-like extension of Averianov, 2010). The parapophysis is a small tubercle located just posterior to the contact with the atlas.

Cervical III—The third cervical is the first and traditionally least elongated of the middle-series cervicals; in *Q. lawsoni* it only reaches an aspect ratio of 6.08. It can be distinguished from the other middle-series cervicals by its smaller size, less elongation, narrow anterior articulation for the atlantoaxis, blunt hypapophysis, large ventral tumescence, elongate epipophyses, and most obviously by a tall single neural spine that is rectangular in lateral outline (Fig. 19). Cervical III is preserved

in TMM 41544-16, 41546-2, 42161-1.3, 42180-1, and 42422-24, in addition to a right prezygapophysis attributed to this cervical (TMM 41546-7) presumably because of the anterior orientation of the zygapophysis. The complete lengths of all these elements are preserved except for the TMM 41546-7 prezygapophysis and TMM 41546-2, which is missing part of the anterior cotyle and prezygapophyses as well as the posterior half of the centrum. They average 177 mm in length, but this is somewhat increased by the unusually long (198.11 mm) and distinct TMM 42180-1 (Table 5). Third cervicals are present in the azhdarchid species *Z. linhaiensis* (Cai and Wei, 1994), *E. langendorfensis* (Vremir et al., 2013b), *P. mauritanicus* (Kellner, 2010), and *A. lancicollis* (Averianov, 2010), as well as the putative azhdarchid specimen MPC–Nd 100/302 (Watabe et al., 2009).

The neural spine is the most distinguishing feature of the *Q. lawsoni* cervical III. Only the base of the neural spine is preserved in most specimens, with the notable exception of TMM 42422-24 that is just missing a chunk from the posterodorsal

corner. This neural spine is tall and rectangular in lateral outline, but it quickly drops off in height to a tall ridge anteriorly and posteriorly. This seems unusual for a species in a clade known for their unusually reduced cervical neural spines (Azhdarchidae). However, rectangular or blade-like cervical III neural spines are present in the azhdarchids *Z. linhaiensis* (ZMNH M1324 and M1328), *E. langendorfensis* (Vremir et al., 2013b:8–9), *A. lancicollis* (Averianov, 2010:276), and MPC–Nd 100/302 (Watabe et al., 2009:236; Averianov, 2010:286), and so this is likely the pervasive condition in Pterosauria. It should be noted that *Q. lawsoni* has a taller cervical III neural spine than the other azhdarchids. This spine is inflated at its dorsal margin, although it appears to be more thickened on the left side than the right, which may be pathological. It also has a greater thickness towards the mid-length of the neural spine. An inflated top of the cervical III neural spine is also reported in *Pteranodon* (Bennett, 2001a:43), and so this is not unique to *Q. lawsoni*. The spine extends for the entire length of the neural canal and overhangs the neural canal posteriorly as a relatively blunt posterior process.

Another distinguishing feature of the third cervical is a ventral tumescence (Harrell et al., 2017) posterior to a blunt hypapophysis and continuing posteriorly as a raised band. A small hypapophysis has also been put forward as a diagnostic character for an azhdarchid cervical III by Averianov (2010) and Vremir et al. (2015). The tumescence continues posteriorly as a raised band to the midsection, giving the vertebra a convex to slightly sinusoidal ventral margin in lateral view, apparently also present in *E. langendorfensis* (Vremir et al., 2013b:8), *A. lancicollis* (Averianov, 2010:276, fig. 9), and MPC–Nd 100/302 (Averianov, 2010:286). The prezygapophyses are also oriented more anteriorly and the articular surfaces oriented more dorsally than in the other cervicals. A pair of pneumatic foramina flank the neural canal in the anterior and posterior vestibules of the vertebra. The posterior foramina are significantly larger than the anterior foramina and are positioned dorsally with respect to a neural canal. This canal is circular in outline anteriorly and triangular in outline posteriorly, but it appears to be clithridiate posteriorly in 41544-16. There is a small fovea (fovea for elastic ligament of Harrell et al., 2017) in the center of the anterior end of the neural arch visible in TMM 41544-16 and 42180-1. The interzygapophyseal ridges are described in *A. lancicollis* as more prominent in cervical III than the other cervicals (Averianov, 2010:276), but they appear comparable in *Q. lawsoni*. Preexapophyses are present on the third cervical as in *E. langendorfensis* (Vremir et al., 2013b:7). The preexapophysis is attached to the anterolateral edge of the fused cervical rib. The middle cross-section is roughly as tall as wide and rounded. A transverse ridge extending from the base of the prezygapophysis along the lateral edge of the vertebra to the midpoint of the vertebra is visible on TMM 41544-16 and seems to be present in MPC–Nd 100/302, but this specimen has a second more ventral ridge as well (Watabe et al., 2009:236–237). The midsection is narrower than the articular ends but is largely parallel-sided and does not have a distinct constriction, as has been put forward for azhdarchid third cervicals (Vremir et al., 2015). Lateral excavations are present on the centrum between the postzygapophyses and postexapophyses bases. Lateral excavations are prevalent in pterosaurs, but in non-azhdarchids they are positioned in the midsection of the vertebra instead. There is a concave surface between the postexapophyses and ventral to the posterior condyle that does not form a distinct fossa, as in MPC–Nd 100/302 (Watabe et al., 2009:237); this area is described as flat in *A. lancicollis* (Averianov, 2010:276). The postzygapophysis has a posteroventrolaterally oriented articular surface but has a straight posterior centimeter-long epiphysis, giving the zygapophysis a curved appearance in lateral view and a rhomboid outline in dorsal view. The combined postzygapophysis with epiphysis length reaches the posterior margin of the posterior condyle. A dorsal ridge is also present on the postzygapophysis. The postexapophyses are not as robust, have longer bases reaching the midsection of the vertebra, and are oriented straight posteriorly in lateral view compared with the other cervical vertebrae.

Cervical IV—Cervical IV is the first of the mid-cervicals (cervicals IV–VI), which are traditionally the longest vertebrae in pterosaurs. *Quetzalcoatlus lawsoni* is unusual in that its cervical IV is slightly shorter than cervical VII (Table 5). It is also less wide in its midsection while still being longer than the cervical IV of *C. boreas*, and so has been described as less robust than *C. boreas* (Hone et al., 2019:8). Cervical IV in *Q. lawsoni* can be identified by its small ventral tumescence, tall and ventrally deflected posterior end, narrow posterior condyle, tall posterior spinous process, and postexapophyses positioned ventrally and closer to the midline (Fig. 20). There are two fourth cervicals preserved in *Q. lawsoni*: TMM 41544-8 is distorted but nearly complete, missing the anterior tip of the right postzygapophysis, both postzygapophyses, and the posterior process of the neural spine; TMM 42462-1 is the left half of the posterior end including the neural canal, left lateral pneumatic foramen and postexapophysis, and the left half of the posterior condyle. The fourth cervical is midway between cervical III and V in length (258 mm), slightly shorter than cervical VII, with an aspect ratio of 6.85. Fourth cervicals are present in the azhdarchid species cf. *A. philadelphiae* (MPPM 2000.23.1 and BSPG 1966 XXV 503), *W. brevirostris*, *Z. linhaiensis* (Cai and Wei, 1994), *E. langendorfensis* (Vremir et al., 2013b), *P. mauritanicus* (Kellner, 2010), *C. boreas* (Hone et al., 2019), *A. tharmisensis* (Solomon et al., 2020), and *A. lancicollis* (Averianov, 2010), as well as the putative azhdarchiform specimens LINHM 014 (Averianov, 2014), LPB R.2395 (Vremir et al., 2015), MPC–Nd 100/303 (Averianov, 2014), and MTM V 2010.100.1 (Averianov, 2010; Ősi et al., 2011), as well as TMM 42538-1 and TMM 45888-2.1.

The anterior cotyle of the fourth cervical appears more triangular in outline and the prezygapophyses more laterally oriented than in the third cervical. The MPPM 2000.23.1 anterior cotyle has a similar outline but is more laterally compressed into a 'rhomboidal' shape (Harrell et al., 2017:100 and 102). The neural canal and a pair of small circular lateral pneumatic foramina can be seen in the anterior vestibule of TMM 41544-8, but only a neural canal can be distinguished in the poorly preserved posterior end. A pneumatic foramen dorsal to the neural canal is absent in this and other azhdarchid fourth cervicals, with the exception of *C. boreas* (Godfrey and Currie, 2005:298, figs 16.1–16.2). This cervical has a rudimentary ventral tumescence (slight ridge of Vremir et al., 2015, or smooth median ridge of Solomon, 2020), which is constricted on its anterior end by the lateral fossae posterior to the anterior cotyle and does not continue posteriorly in *Q. lawsoni*. These fossae are said to be absent in LPB R.2395 (Vremir et al., 2015:10) and MPPM 2000.23.1 (Harrell et al., 2017:100), but apparently have become pneumatic foramina in LINHM 014 (Rodrigues et al., 2011:151, fig. 4D). Damage at the anterior end of TMM 41544-8 prevents determining if a hypapophysis or preexapophyses were present, but hypapophyses (Godfrey and Currie, 2005:295, figs. 16.1–16.2; Ősi et al., 2005:780, fig. 4A; Averianov, 2010:277; Rodrigues et al., 2011:151; Vremir et al., 2015:8, fig. 3; Harrell et al., 2017:fig. 4; Solomon et al., 2020:6, fig. 3B) and preexapophyses (Ősi et al., 2005:780. fig. 4A; Averianov, 2010:277; Vremir et al., 2013b:7–8) are reported in other azhdarchiform fourth cervicals. The sulcus for the transverse foramen is present but not the fused cervical rib that encloses it into a foramen in TMM 41544-8; damage to this area implies that the rib has been detached. The dorsal prezygapophyseal tubercle present in LPB R.2395 is absent in TMM 41544-8 (Vremir et al., 2015).
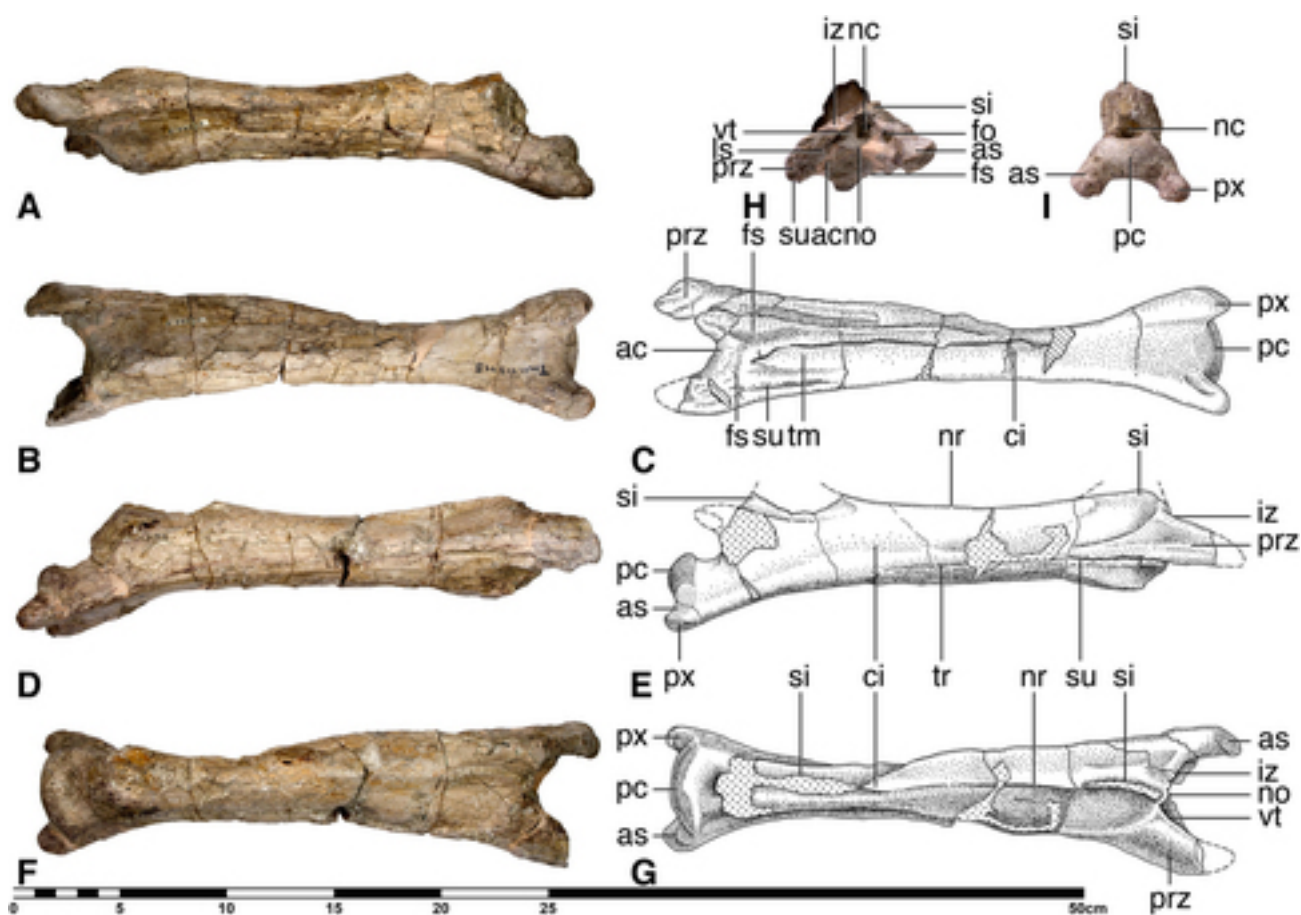
FIGURE 20. *Quetzalcoatlus lawsoni*, sp. nov., cervical IV (TMM 41544-8) in **A**, left lateral photograph; **B**, ventral photograph and **C**, line drawing; **D**, right lateral photograph and **E**, line drawing; **F**, dorsal photograph and **G**, line drawing; **H**, anterior photograph; and **I**, posterior photograph views. **Abbreviations: ac**, anterior cotyle; **as**, articular surface; **ci**, constriction; **ea**, emargination; **fo**, foramen; **fs**, fossa; **iz**, interzygapophyseal ridge; **ls**, lateral sulcus; **nc**, neural canal; **no**, notch; **nr**, neural ridge; **pc**, posterior condyle; **prz**, prezygapophysis; **px**, postexapophysis; **si**, spinous process; **su**, sulcus; **tm**, tumescence; **tr**, transverse ridge; and **vt**, vestibule. Diagonal lines represent plaster, and dots represent damaged bone. Scale bar equals 50 cm.

Cervical IV is the first middle-series cervical to have a bifid neural spine split into anterior and posterior spinous processes, as also reported in the fourth cervicals of *A. lancicollis* (Averianov, 2010:276), *C. boreas* (Godfrey and Currie, 2005:298, figs. 16.1–16.2), and LPB R.2395 (Vremir et al., 2015:8, fig. 3). The anterior spinous process is a high ridge with a broken dorsal margin that is triangular in cross-section in TMM 41544-8. A fovea is reported on the anterior surface of the spine in MPPM 2000.23.1 (Harrell et al., 2017:fig. 4), but preservation precludes its identification in *Q. lawsoni*. The posterior spinous process is damaged in both specimens, but from the broken bases it can be seen to have been wider and higher than the anterior process, also suggested in MPPM 2000.23.1 (Harrell et al., 2017:100) but reversed in *A. tharmisensis* (Solomon et al., 2020:13–14, fig. 3C–D), MPC−Nd 100/303 (Watabe et al., 2009:232, figs. 3–4), and LPB R.2395 (Vremir et al., 2015:8, fig. 3). The fourth cervical neural spine of *E. langendorfensis* is described as blade-like and less reduced than in other azhdarchids, but it is still divided into anterior and posterior ridges separated by a long gap (Vremir et al., 2013b:8–9). The neural spine of LINHM 014 is similarly described as low but not vestigial (Rodrigues et al., 2011:157) or unreduced as an obviously primitive feature (Averianov, 2014:6). These neural spines are less derived than those in

A. lancicollis and may indicate that they are more basal azhdarchiforms.

TMM 41544-8 has a constriction at a third of the distance from the posterior end, as in *A. lancicollis* (Averianov, 2010:277) and LPB R.2395 (Vremir et al., 2015:5). At this point the cross-section in this specimen transitions from being a dorsoventrally depressed ellipse anteriorly to being taller than wide oblong posteriorly, which is also found in MPPM 2000.23.1 (Harrell et al., 2017:100, fig. 4) and BSPG 1966 XXV 503 (Martill and Moser, 2017:fig. 3), but not in *E. langendorfensis*, *A. tharmisensis*, or *A. lancicollis* that instead have an oval cross-section over their length (Solomon et al., 2020:13). TMM 42462-1 consists of only this posterior section, and it is identified based on its posterior height as well as postexapophyses positioned ventrally and close to the midline. Ventrally and closely positioned postexapophyses are also present in MPPM 2000.23.1 but are much smaller and extend only slightly past the posterior condyle (Harrell et al., 2017:99, fig. 4). A lateral transverse ridge extends posteriorly from the base of the prezygapophysis in TMM 41544-8 but does not extend posterior to the constriction, also reported in *E. langendorfensis* (Vremir et al., 2013b:9), MPC−Nd 100/303 (Watabe et al., 2009:233), and MTM V 2010.100.1. (Ősi et al., 2005:780; Ősi et al., 2011). This transverse ridge is more ventrally positioned than in the other middle-series cervicals. The ventral

margin of the centrum in TMM 41544-8 is distinctly concave in lateral view, due largely to the ventral deflection of the posterior end, unlike the convex margin of LPB R.2395 (Vremir et al., 2015:5, fig. 2). This deflection and a narrow posterior condyle are also shared with *A. tharmisensis* (Solomon et al., 2020:fig. 3D), MPPM 2000.23.1 (Harrell et al., 2017:98, fig. 4), and presumably BSPG 1966 XXV 503 (Martill and Moser, 2017:fig. 3), allowing these isolated vertebrae to be identified as fourth cervicals. However, *A. lancicollis* is concave ventrally but seems to lack a posterior ventral deflection, which is present on the cervical VI instead (Averianov, 2010:276–277, figs. 10 and 13).

The dorsolateral tubercles reported on the postexapophyses of LINHM 014 (Rodrigues et al., 2011:152–153, fig. 4) are absent in *Q. lawsoni*. The area between the postexapophyses is flattened in *Q. lawsoni*, as in *A. lancicollis* (Averianov, 2010:277), MPPM 2000.23.1 (Harrell et al., 2017:100), and BSPG 1966 XXV 503 (Martill and Moser, 2017:164), but unlike the small depression of *A. tharmisensis* (Solomon et al., 2020:6, fig. 3B) and the concave area of LINHM 014 (Rodrigues et al., 2011). The fourth cervical shares an elongate base of the postexapophysis with the third in *Q. lawsoni*, but it lacks a lateral excavation dorsal to it on the centrum (TMM 41544-8 is damaged on the left side) and its postexapophyses are larger and oriented more medially and ventrally. A lateral excavation may be the structure identified as a pneumatic foramen in BSPG 1966 XXV 503 (Martill and Moser, 2017:164). TMM 42462-1 has a tall clithridiate posterior neural canal and an elongate oval lateral pneumatic foramen. Harrell et al. (2017) report an elongate oval posterior neural canal in MPPM 2000.23.1, which may instead be a lateral pneumatic foramen that they state is lacking. *Quetzalcoatlus lawsoni* has a posterior condyle with a reniform outline, unlike the subhemispherical posterior condyle with faint annular sulcus reported in MPPM 2000.23.1 (Harrell et al., 2017:98–99, fig. 4B) or the oval condyle of *A. tharmisensis* and *A. lancicollis* (Solomon et al., 2020:13).

Cervical V—Cervical V is the longest and most variable cervical in the *Quetzalcoatlus* material. It can be identified by its extreme length and aspect ratio, tubular elliptical midsection, three tiny parallel ridges on the dorsal surface, and a posterior almost fossa ventral to the posterior condyle (Fig. 21). Complete or nearly complete fifth cervicals are found in TMM 41544-15, 41954-7, 41961-1.28, 42161-1.4, 42180-2, 42422-22, and 42422-32 for *Q. lawsoni*. An anterior cotyle and posterior condyle (TMM 41544-4), posterior neural arch including a left postzygapophysis (TMM 41546-1), and a right prezygapophysis (TMM 41954-31) are also referred to cervical V. They average about 405 mm in length (11.08 in aspect ratio) but vary from 341–484 mm (Table 5). Fifth cervicals are present in the azhdarchid species *A. philadelphiae* (Lawson, 1975a), *W. brevirostris*, *Z. linhaiensis* (Cai and Wei, 1994), *P. mauritanicus* (Kellner, 2010), *C. boreas* (Hone et al., 2019), *M. maggii* (Vullo et al., 2018), *A. lancicollis* (Bakhurina and Unwin, 1995), as well as the putative azhdarchiform specimens BMR P2002.2 (Henderson and Peterson, 2006), CMN 50801 (Rodrigues et al., 2011), FSAC-OB 14 (Longrich et al., 2018), MDM 349 (Averianov, 2010), ME1 04 (Averianov, 2010), MTM V. 2003.21 (Ősi et al., 2005, 2011), a Senegalese specimen (Averianov, 2010), and UCMP 114286 (Averianov, 2010).

The anterior cotyle is very broad and subtriangular in outline, with only a slight midline notch in the dorsal rim in *Q. lawsoni*. The fifth cervical of BMR P2002.2 (Henderson and Peterson, 2006:figs. 1–2) and *A. lancicollis* seem to lack this notch altogether and instead have a convex dorsal margin of the cotyle (Averianov, 2010:277, fig. 11), whereas *A. philadelphiae* has a larger notch and a narrower cotyle to form a cordate outline (Martill et al., 1998:66, figs. 5–6). The cervical V has the shortest hypapophysis of the *Q. lawsoni* cervical series and is flanked by much shallower fossae, unlike the prominent

hypapophyses of *P. mauritanicus* (Pereda-Suberbiola et al., 2003:82; Longrich et al., 2018:21), BMR P2002.2 (Henderson and Peterson, 2006:192, figs. 1–2), CMN 50801 (Rodrigues et al., 2011:151, fig. 2D), and ME1 04 (Buffetaut et al., 1997:554). *Quetzalcoatlus lawsoni* lacks a tumescence or raised band posterior to the hypapophysis. A ventral keel (crista sagittalis ventralis of Frey and Martill, 1996, or ridge-like hypophyseal process of Henderson and Peterson, 2006) is instead reported in this area in *A. philadelphiae* (Frey and Martill, 1996:229, fig. 4b) but see Martill et al. (1998), as well as *P. mauritanicus* (Pereda-Suberbiola et al., 2003:82) and BMR P2002.2 (Henderson and Peterson, 2006:192, figs. 1–2). Both preexapophyses and preexapophyseal articulations are present in the cervical V of *Q. lawsoni*, but the preexapophysis is located more anterior on the prezygapophysis than in other vertebrae and does not contact the fused cervical rib. Preexapophyses are reported in the fifth cervicals of *P. mauritanicus* and MTM V. 2003.21, but they are termed prezygapophysial tubercles or medial processes (Pereda-Suberbiola et al., 2003:82; Ősi et al., 2005:783). The anterior neural canal is largely obscured in all *Q. lawsoni* specimens, but large circular pneumatic foramina lateral to the canal can be seen in TMM 42422-32. A dorsal pneumatic foramen is absent in *Q. lawsoni* and *M. maggii* (Vullo et al., 2018:8, fig. 3D and H), but present in *A. lancicollis* (Averianov, 2010:277, fig. 11) and CMN 50801 (Rodrigues et al., 2011:151). In *C. boreas*, TMP 1981.16.107 lacks a dorsal foramen, but TMP 1996.12.369 has a small pit in this location (Godfrey and Currie, 2005:298, fig. 16.3D) labeled an accessory pneumatopore by Hone et al. (2019).

The neural spine is bifid, and the tiny neural ridge between the anterior and posterior spinous processes almost disappears in the midsection of the *Q. lawsoni* fifth cervical. The anterior spinous process is much taller than the posterior one, and it forms a vertical flange with a vertical anterior margin. CMN 50801 has the primitively unreduced and blade-like neural spines extending along the whole length of the neural arch, also found in the LINHM 014 cervical IV (Rodrigues et al., 2011:151 and 157; Averianov, 2014:6), which indicate that these specimens are basal to the Azhdarchidae. Transverse ridges extend almost the entire length of the fifth cervical terminating just anterior to the base of the postzygapophyses in *Q. lawsoni*. Notably, these ridges are reflected dorsally to become positioned on the dorsal surface of the neural arch about a centimeter from the neural ridge to form three parallel ridges, shared with *A. philadelphiae* (Andres, 2021). Previously, these three parallel ridges were thought to be present only in *A. philadelphiae* (Lawson, 1975a:947), but they are also present in *Q. lawsoni*, FSAC-OB 14 (Longrich et al., 2018:21), and MDM 349 (Ikegami et al., 2000:167, fig. 3). The middle cross-section of *Q. lawsoni* is a dorsoventrally depressed ellipse in shape, unlike the laterally compressed oval cross-section of *A. philadelphiae* (Frey and Martill, 1996:229) and possibly BMR P2002.2 (Henderson and Peterson, 2006:figs. 1–2) or the diamond-shaped outline in other azhdarchids (Vullo et al., 2018:7). The *Q. lawsoni* cervical V is greatly constricted about a fifth of its length from the posterior end, as in FSAC-OB 14 (Longrich et al., 2018:21, fig. 14), but it is just posterior to the middle in *A. lancicollis* (Averianov, 2010:277) and apparently absent in *P. mauritanicus* (Pereda-Suberbiola et al., 2003:figs. 2–3; Longrich et al., 2018:fig. 13).

The posterior process in *Q. lawsoni* is a low eminence that the spinous process traverses, and that barely overhangs the posterior neural canal. Henderson and Peterson (2006) report a fovea possibly for an elastic ligament in this region in BMR P2002.2, but this is not observed in *Q. lawsoni* and may be related to the pit reported in *C. boreas* (TMP 1996.12.369) (Godfrey and Currie, 2005:298, fig. 16.3D). The posterior vestibule of the neural arch is visible in TMM 42161-1.4: the posterior
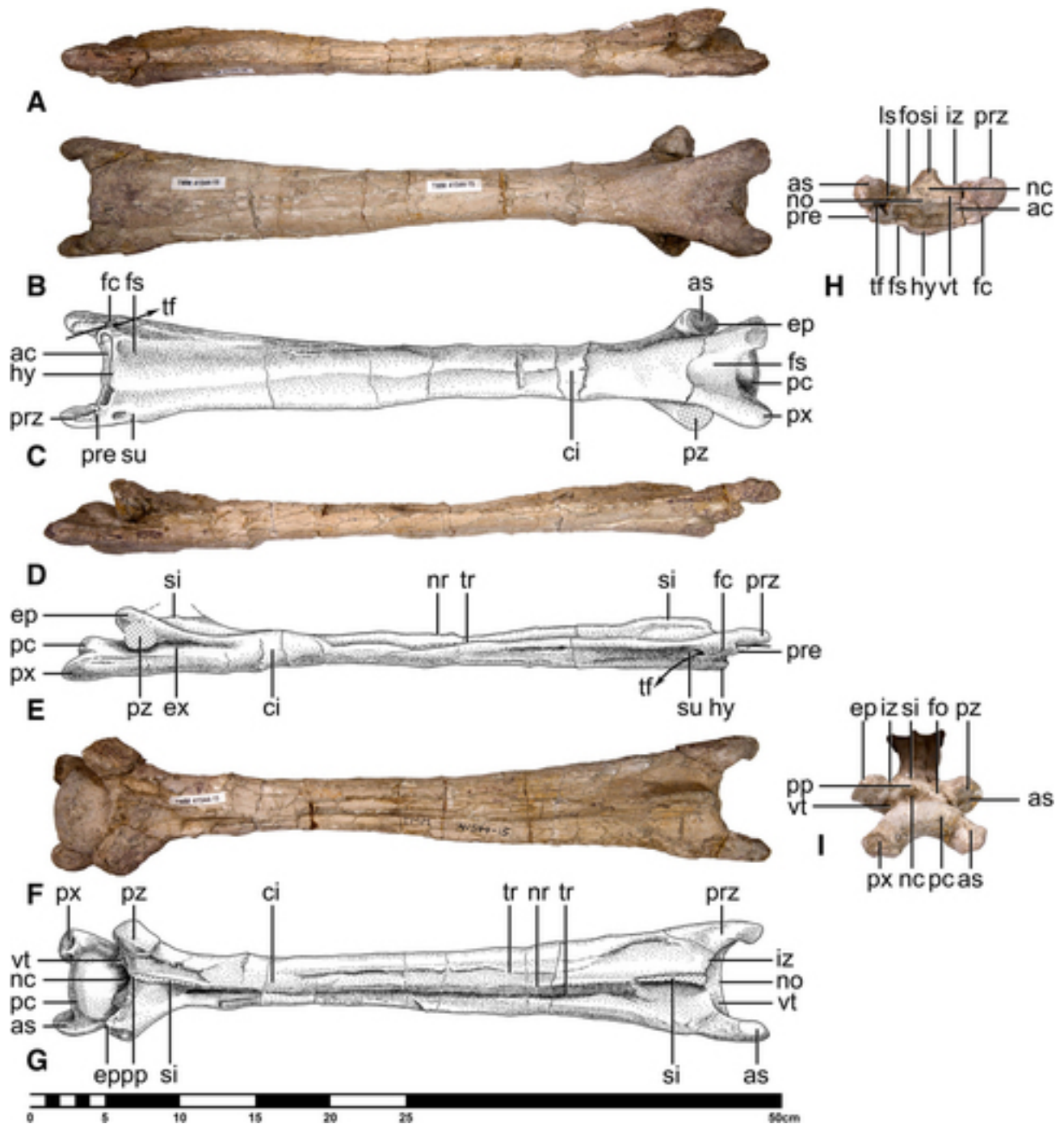
FIGURE 21. *Quetzalcoatlus lawsoni*, sp. nov., cervical V (TMM 41544-15) in **A**, left lateral photograph; **B**, ventral photograph and **C**, line drawing; **D**, right lateral photograph and **E**, line drawing; **F**, dorsal photograph and **G**, line drawing; **H**, anterior photograph; and **I**, posterior photograph views. **Abbreviations: ac**, anterior cotyle; **as**, articular surface; **ci**, constriction; **ep**, epiphysis; **ex**, excavation; **fc**, fused cervical rib; **fo**, foramen; **fs**, fossa; **hy**, hypapophysis; **iz**, interzygapophyseal ridge; **ls**, lateral sulcus; **nc**, neural canal; **no**, notch; **nr**, neural ridge; **pc**, posterior condyle; **pp**, posterior process; **pre**, preexapophyses; **prz**, prezygapophysis; **px**, postexapophysis; **pz**, postzygapophysis; **si**, spinous process; **su**, sulcus; **tf**, transverse foramen; and **vt**, vestibule. Dots represent damaged bone. Scale bar equals 50 cm.

neural canal opening is clithridiate in outline and is flanked by circular pneumatic foramina slightly larger than the anterior pneumatic foramina. The posterior neural canal is ovate (slit-like anteriorly) in BMR P2002.2 (Henderson and Peterson, 2006:192–193) and circular in MTM V. 2003.21 (Ősi et al., 2005:783, fig. 5B; 2011). The postzygapophyses are

ventrolaterally expanded into a more rounded process with a slight proximal constriction in *Q. lawsoni*. Short blunt epiphyses are located medially on the postzygapophyses. Lateral excavations are present between the postzygapophyses and postexapophyses. A vertical slit-like opening interpreted as a pneumatic foramen is reported in this excavation of BMR P2002.2

(Henderson and Peterson, 2006:192), in a similar position to the foramina reported in the cf. *A. philadelphiae* fourth cervical (BSPG 1966 XXV 503), and may just be a deeper part of the excavation. The posterior condyle is a symmetrical oval in *Q. lawsoni*, except in the slightly reniform TMM 42422-22. The postexapophyses have the shortest bases of the middle-series cervicals and are positioned ventrolaterally. The dorsolateral tubercles on the postexapophyses reported in CMN 50801 (Rodrigues et al., 2011:151, fig. 2) and the long troughs on the postexapophyses ventral surfaces reported in *C. boreas* (Godfrey and Currie, 2005:299) could not be located in *Q. lawsoni*. Although all the middle-series cervicals of *Q. lawsoni* are a variation on a tube, the fifth cervical can be identified by a posterior median fossa (broad groove of Buffetaut et al., 1997, ovoid concavity of Godfrey and Currie, 2005, broad shallow groove of Henderson and Peterson, 2006, shallow depression of Rodrigues et al., 2011, or deep ventral depression of Longrich et al., 2018) ventral to the posterior condyle and medial to the postexapophyses, also reported in *P. mauritanicus* (Longrich et al., 2018), FSAC-OB 14 (Longrich et al., 2018), BMR P2002.2 (Henderson and Peterson, 2006:192), CMN 50801 (Rodrigues et al., 2011:151, fig. 2D), and ME1 04 (Buffetaut et al., 1997:554). A similar but more posteriorly facing fossa is present on the axis and presumably also articulated with the hypapophysis of the succeeding vertebra. This fossa is bordered by a distinct rim except in TMM 42161-1.4, which has a shallower fossa. *Azhdarcho lancicollis* (Averianov, 2010:277) and MDM 349 (Ikegami et al., 2000:167) have a flat ventral surface in this area instead.

Cervical VI—Cervical VI is the second longest cervical vertebra, approaching the fifth in length (the largest sixth cervical is longer than the smallest fifth cervical) but with much less variation in *Q. lawsoni* (Table 5). It can be identified by this more moderate length, dorsal arching of the laminae, increased anterior depth, and a less distinct posterior constriction (Fig. 22). Mostly complete sixth cervicals include TMM 41954-65, 41961-1.29, 42180-14.10, 42180-19, and 42422-20. Also identified as cervical VI are the anterior end of a vertebra (TMM 41544-4, 41954-30, TMM 42161-3, 42180-3, and 42559-1.1), posterior condyle (TMM 41546-8 and 41954-10), and a pair of postzygapophyses (TMM 41544-12). The cervical VI of *Q. lawsoni* is large (346 mm average) and elongate (8.14 aspect ratio), but not as much as the hyperelongate fifth cervical. However, it is considerably more elongate than the cervical VI of *A. lancicollis* (Averianov, 2010:277, fig. 13). It is also less variable: it has a range of only about 4 cm, but there are only four complete sixth cervicals compared with seven fifth cervicals, and so this may be affected by sampling.

The cervical VI anterior cotyle has a slight emargination in the center of its dorsal lip, instead of a notch as in *A. lancicollis* (Averianov, 2010:277, fig. 13A) and *A. bostobensis* (Averianov, 2004:433, fig. 8), and so it has a slightly convex anterior cotyle dorsal margin. Combined with a prominent hypapophysis, this gives the anterior cotyle a triangular outline, similar to MC SF69 (Buffetaut, 2001:359, fig. c). This is distinct from the cordate outline of *A. bostobensis* (Averianov, 2004:433, fig. 8), and probably cf. *northropi* (TMM 42889-1), or the dorsoventrally depressed oval of *P. mauritanicus* (Pereda-Suberbiola et al., 2003:82). The hypapophysis is positioned more ventrally in the fifth cervical than in the other cervicals of *Q. lawsoni*, increasing the depth of the anterior centrum. It extends posteriorly for a few centimeters as a raised band, giving the vertebra midsection a slightly concave ventral margin in lateral view. *Aralazhdarcho bostobensis* shares this relatively large hypapophysis but lacks the raised band (Averianov, 2004:433, fig. 8), MC SF69 has both (Buffetaut, 2001:360, fig. c), and MPV TT48 has a hypapophysis followed by parallel striae (Company et al., 1999:328, fig. 2). The fossae lateral to the hypapophysis extend for half of the length of the band in *Q. lawsoni*. The anterior vestibule is

recessed so that the small circular lateral pneumatic foramina appear as elliptical openings more anteriorly. *Aralazhdarcho bostobensis* lacks these lateral pneumatic foramina and has very small and shallow fossae in their place (Averianov, 2004:433, fig. 8), a feature shared with *P. mauritanicus* (Pereda-Suberbiola et al., 2003:fig. 3f; Longrich et al., 2018:fig. 13D; Andres, 2021). *Azhdarcho lancicollis* retains a dorsal pneumatic foramen in the anterior vestibule of cervical VI (Averianov, 2010:277, fig. 8A). Cervical VI has the largest midline notch in the interzygapophyseal ridge over the anterior vestibule in *Q. lawsoni*, as in cf. *northropi* (TMM 424889-1). Preexapophyses do not contact the transverse foramina and are instead completely on the ventral surface of the prezygapophyses (not preserved in TMM 42180-19), which may be why they are sometimes termed as prezygapophyseal tubercles (Ősi et al., 2005:780, fig. 4A; Vremir et al., 2015:5; Naish and Witton, 2017:19, fig. 1B). The laminae roofing the neural arch are dorsally arched forming a slight angular dorsal surface, contrasting with the rounded dorsal surfaces of other cervicals, and described as a roof-like dorsal margin of the neural canal in *P. mauritanicus* (Pereda-Suberbiola et al., 2003:82). This arching increases anteriorly, further adding to the height of the anterior end. This gives the elliptical cross-section a slight inverted lacriform outline, contrasting with the oval cross-section of cf. *A. philadelphiae* (SMNK 1285 PAL) (Frey and Martill, 1996:238). This likely also produces the largest neural ridge in the *Q. lawsoni* cervicals, albeit only a millimeter in width. The spinous processes are flanges; the anterior one is taller and longer, described as low and crest-like in MTM V.01.51 (Ősi et al., 2005:781, fig. 4B; 2011).

Transverse ridges extend almost the entire length between the zygapophyses and are positioned on the lateral surfaces of the vertebra, as in *A. bostobensis* (Averianov, 2004:433, fig. 8e). The reduced constriction is positioned at the posterior quarter of the vertebra, roughly between the positions of cervicals IV and VII of *Q. lawsoni*. This is in a similar position to *A. lancicollis* (Averianov, 2010:280, fig. 13), but it is posterior to the middle constriction of *P. mauritanicus* (Pereda-Suberbiola et al., 2003:82). In *Q. lawsoni*, the postzygapophysis is laterally expanded with a distinct epiphysis and an indistinct constriction producing a rhomboid horizontal outline with rounded edges. The epiphysis is large and triangular in outline curving posteromedially, similar to the condition in MPC−Nd 100/302 (Watabe et al., 2009:237, figs. 9–10). Between the postzygapophyses and postexapophyses is a lateral excavation. There are three presumably pneumatic elongate pits in this area of cf. *A. philadelphiae* (SMNK 1285 PAL) (Frey and Martill, 1996:234–236, fig. 8d) that are not present in *Quetzalcoatlus*. Similar to the fourth cervical, the posterior condyle is laterally narrow and the postexapophyses are larger and positioned more ventrally in the sixth cervical. Whereas the posterior condyle is broad with a dorsal concavity and lateral postexapophyses in *A. lancicollis* (Averianov, 2010:277, fig. 13E), MPC−Nd 100/302 appears to be intermediate between these two species (Watabe et al., 2009:figs. 9–10). The postexapophyses of the sixth cervical extend more posteriorly than the other vertebrae. The posterior condyle is oriented posteriorly, unlike the posteroventral orientation of *A. lancicollis* that gives it its concave ventral margin in lateral view more akin to the fourth cervical of *Q. lawsoni* (Averianov, 2010:277, fig. 13C). The area ventral to the posterior condyle between the postexapophyses is concave in *Q. lawsoni*, as in MPC−Nd 100/302 (Watabe et al., 2009:277, figs. 9–10) and unlike the convex area reported in *A. lancicollis* (Averianov, 2010:277, fig. 13). In *Q. lawsoni*, the posterior opening of the neural canal is a large trapezoid, as opposed to the lacriform outline in *A. lancicollis* (Averianov, 2010:277, fig. 13E), that is flanked by dorsally positioned and oval lateral pneumatic
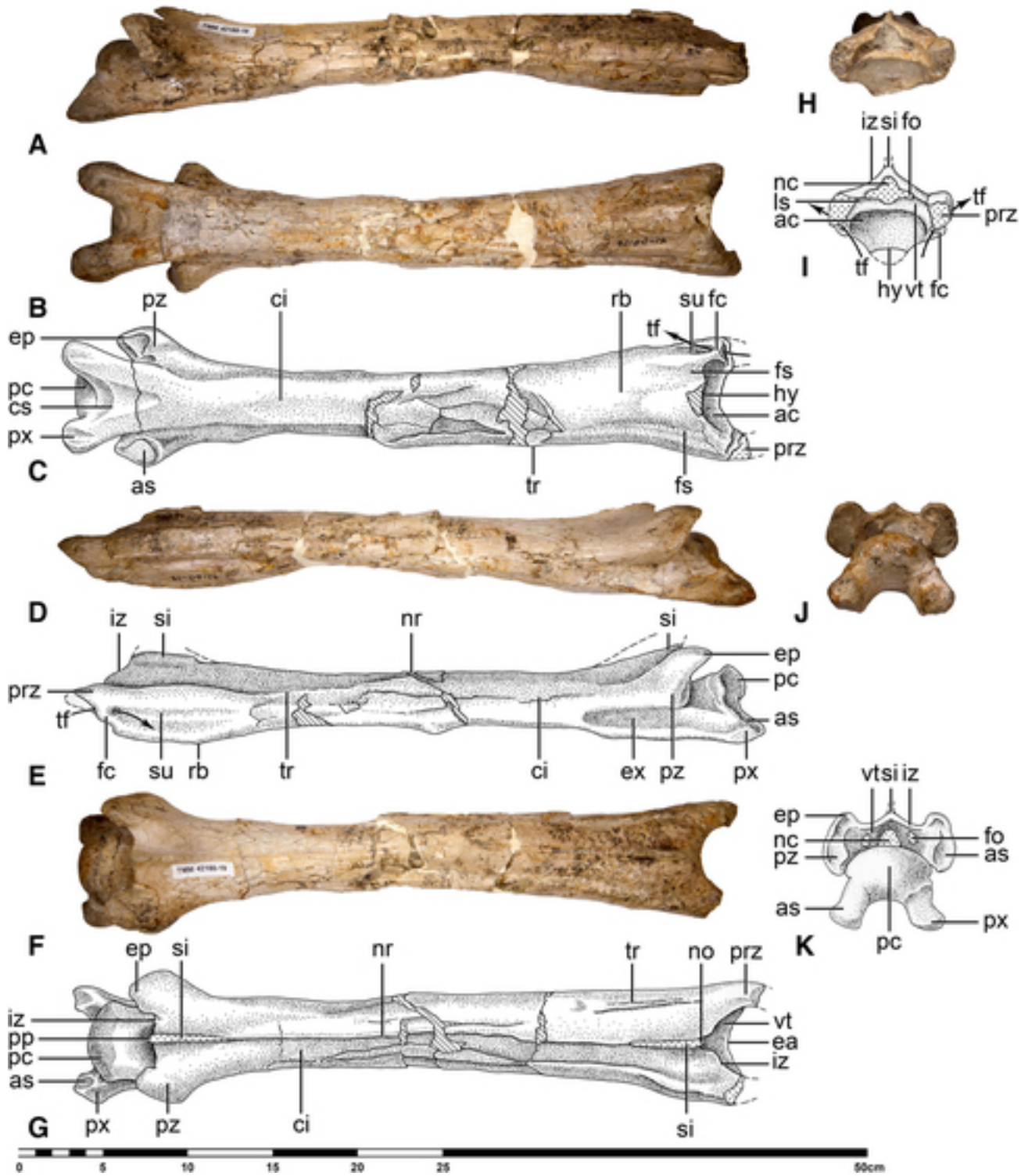
FIGURE 22. *Quetzalcoatlus lawsoni*, sp. nov., cervical VI (TMM 42180-19) in **A**, right lateral photograph; **B**, ventral photograph and **C**, line drawing; **D**, left lateral photograph and **E**, line drawing; **F**, dorsal photograph and **G**, line drawing; **H**, anterior photograph and **I**, line drawing; **J**, posterior photograph; and **K**, line drawing views. **Abbreviations: ac**, anterior cotyle; **as**, articular surface; **ci**, constriction; **cs**, concave surface; **ea**, emargination; **ep**, epipophysis; **ex**, excavation; **fc**, fused cervical rib; **fo**, foramen; **fs**, fossa; **hy**, hypapophysis; **iz**, interzygapophyseal ridge; **ls**, lateral sulcus; **nc**, neural canal; **no**, notch; **nr**, neural ridge; **pc**, posterior condyle; **pp**, posterior process; **prz**, prezygapophysis; **px**, postexapophysis; **pz**, postzygapophysis; **rb**, raised band; **si**, spinous process; **su**, sulcus; **tf**, transverse foramen; **tr**, transverse ridge; and **vt**, vestibule. Diagonal lines represent plaster, and dots represent matrix and/or damaged bone. Scale bar equals 50 cm.
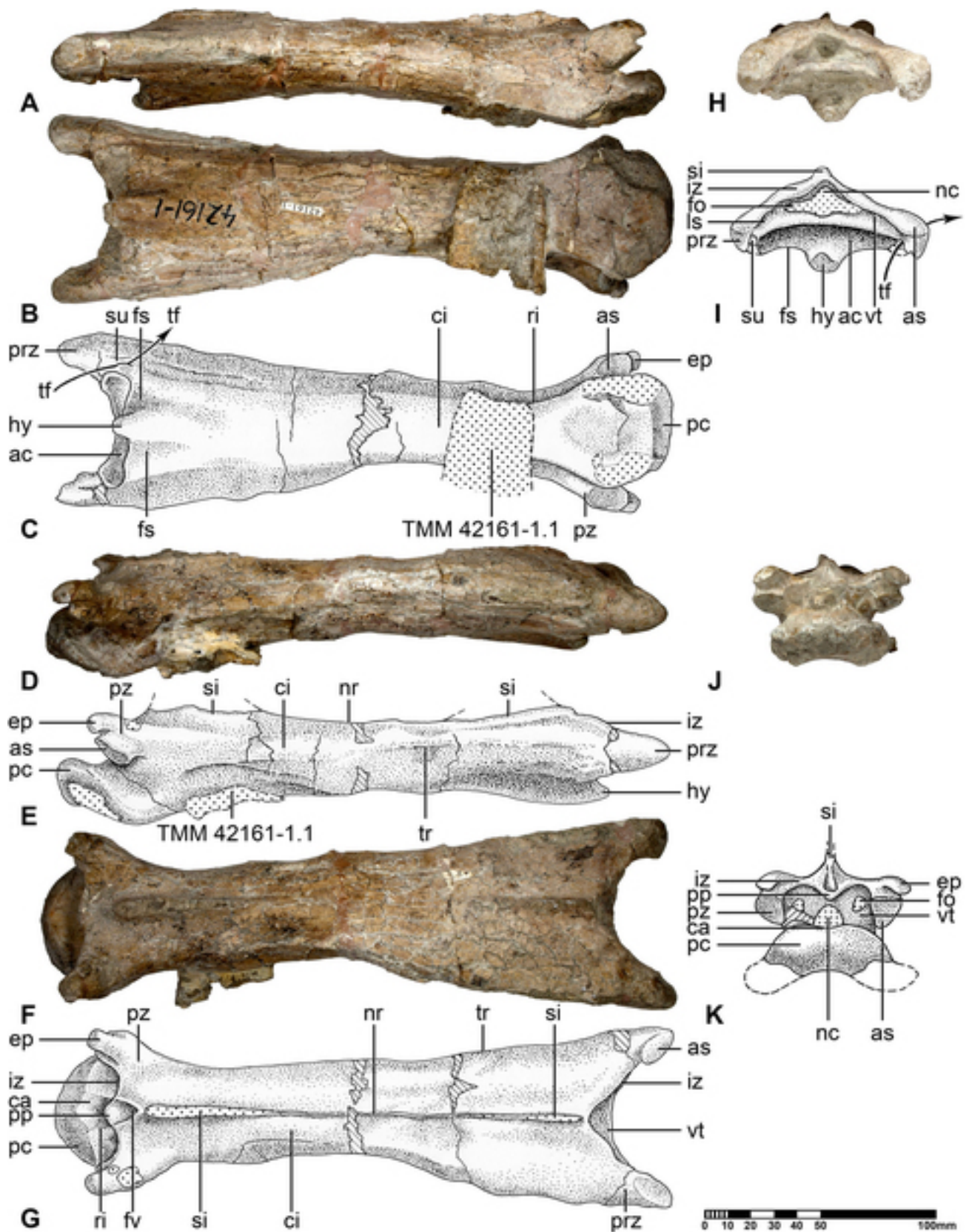
FIGURE 23. *Quetzalcoatlus lawsoni*, sp. nov., cervical VII (TMM 42161-1.4) in **A**, left lateral photograph; **B**, ventral photograph and **C**, line drawing; **D**, right lateral photograph and **E**, line drawing; **F**, dorsal photograph and **G**, line drawing; **H**, anterior photograph and **I**, line drawing; **J**, posterior photograph; and **K**, line drawing views. **Abbreviations: ac**, anterior cotyle; **as**, articular surface; **ca**, concavity; **ci**, constriction; **ep**, epipophysis; **fo**, foramen; **fs**, fossa; **fv**, fovea; **hy**, hypapophysis; **iz**, interzygapophyseal ridge; **ls**, lateral sulcus; **nc**, neural canal; **nr**, neural ridge; **pc**, posterior condyle; **pp**, posterior process; **prz**, prezygapophysis; **pz**, postzygapophysis; **ri**, ridge; **si**, spinous process, **su**, sulcus; **tf**, transverse foramen; **tr**, transverse ridge; and **vt**, vestibule. Diagonal lines represent plaster, and dots represent matrix and/or damaged bone. Scale bar equals 100 mm.

foramina about twice the size of the anterior pneumatic foramina. The posterior process barely overhangs the posterior neural canal.

Cervical VII—The seventh cervical is a robust bone at the transition between the more elongate mid-cervicals and the stouter posterior-series cervicals. It is unusually long in *Q. lawsoni*, surpassing the fourth in length but much more robust (Table 5). This vertebra can be identified by this robust construction, posterior constriction with rapid lateral anterior expansion and widely spaced prezygapophyses, anteroventrally projected hypapophysis, posterior spinous process not extending onto the posterior process of the neural arch, and hook-shaped epiphyses (Fig. 23). Seventh cervicals are relatively less common in the *Q. lawsoni* material; complete examples are represented by TMM 41954-41, 42161-1.5, 42180-14.11, TMM 42259-1.2, and 42422-31. Anterior ends are preserved in TMM 41961-1.30 and 45997-4, and a posterior end in TMM 41954-88. Although cervical VII is the third longest middle-series cervical (263 mm average), it is the second stoutest (6.68 aspect ratio) behind cervical III. It is much longer than the short cervical VIIs of *A. lancicollis* (Averianov, 2010:280, fig. 14), EME 315 (Naish and Witton, 2017:fig. 1), and MTM V 2010.101.1. (Ősi et al., 2005:781, fig. 5A; 2011). The cervical VII is preserved in azhdarchid species cf. *H. thambema* (EME 315) (Naish and Witton, 2017), *W. brevirostris*, *Z. linhaiensis* (Cai and Wei, 1994), *P. mauritanicus* (Kellner, 2010), *A. lancicollis* (Averianov, 2010), as well as the putative azhdarchiform specimen MTM V 2010.101.1 (Averianov, 2010; Ősi et al., 2011).

In the seventh cervical of *Q. lawsoni*, the anterior cotyle dorsal rim lacks a notch and curves down laterally, giving the cotyle a convex dorsal margin. The rest of the cotyle is wide and shallow with a large hypapophysis, matching the morphology of *A. lancicollis* (Averianov, 2010:280), to form an arbelos (three-point crescent) in outline. Cervical VII has the largest and most ventrally directed hypapophysis in the vertebrae. Large lateral fossae sculpt the hypapophysis into a relatively narrow process. In the anterior vestibule of TMM 42259-1.2, the neural canal appears lacriform in outline; its lateral pneumatic foramina ventrally positioned with the same shape but inverted. The right pneumatic foramen in TMM 41954-41 appears to be a more traditional circle, and so the outlines in TMM 42259-1.2 may be due to the outline being more posterior as a result of breakage at the anterior end of this bone. In the posterior vestibule of the neural arch, the neural canal appears to be clithridiate in outline and flanked by smaller circular pneumatic foramina. *Azhdarcho lancicollis* has anterior and posterior dorsal pneumatic foramina above the neural canal (Averianov, 2010:280, fig. 14) that are absent in *Q. lawsoni*. An anterior dorsal pneumatic foramen is reported in EME 315 by Naish and Witton (2017), but this opening is confluent with the neural canal in a clithridiate outline and so is not considered a separate pneumatic foramen here; it is also not figured by Vremir (2010). Preexapophyses and preexapophyseal articulations appear present in some *Q. lawsoni* specimens but are damaged. The prezygapophyses are widely spaced, separated by a distance equal to about one-third of the length of the centrum. The entire anterior end of the cervical VII is laterally wide and dorsoventrally depressed. The prezygapophysis articular surface is oriented only slightly medially. The neural spine is separated into anterior and posterior spinous processes by a thin neural ridge, as in the mid-cervicals. The anterior spinous process is a low ridge and the posterior process is a taller ridge, which is reported in MTM V 2010.101.1. (Ősi et al., 2005, 2011). This contrasts with the tall cervical VII neural spines in EME 315 (Naish and Witton, 2017:6), *Z. linhaiensis* (ZMNH M1328), *W. brevirostris*, and *P. mauritanicus* (Pereda-Suberbiola et al., 2003:82, fig. 3d), but not preserved in *A. philadelphiae* or *A. lancicollis* (Averianov,

2010:280, fig. 14). A tall cervical VII neural spine is likely the plesiomorphic condition for the Azhdarchidae, and a reduced spine is likely an apomorphic feature for *Quetzalcoatlus*.

There appear to be two faint transverse ridges on the lateral surface of the cervical VII in *Q. lawsoni*: a dorsally reflected one extending posteriorly from the base of the prezygapophysis and a more ventral one extending anteriorly from the base of the postexapophysis. EME 315 also appears to have two transverse ridges, but these are more ventrally positioned and do not reach the dorsal surface. The lateral constriction is positioned a third of the total distance from the posterior end, unlike the middle constriction of *A. lancicollis* (Averianov, 2010:281). At this constriction in *Q. lawsoni*, the cross-sectional shape transitions from an anterior ellipse to a posterior trapezoid. The postzygapophysis is a stout lump of a process. It is characterized by a large posteriorly curving and hook-shaped epiphysis. The postzygapophysis articular surface is circular and oriented nearly ventrally. Cervical VII has the widest and shallowest posterior condyle, and it is also the most reniform in outline because of a midline dorsal concavity that is demarcated by lateral ridges. The posterior condyle is wide and shallow in *A. lancicollis* but also convex dorsally (Averianov, 2010:281, fig. 14D). In *Q. lawsoni*, the postexapophyses are large and bulbous, with very distinct postexapophyseal articulations bordered by sharp ridges. The posterior spinous process uncharacteristically does not extend onto the posterior process that overhangs the neural canal. This posterior process is blunt and in TMM 42161-1.5 appears to have a small triangular fovea on its dorsal surface. Ősi et al. (2005) reported a pneumatic foramen ventral to the posterior condyle in MTM V 2010.101.1. and suggested that a similar unreported cavity is also present in *T. wellnhoferi* (AMNH 24440), but this is more likely a posteriorly directed fossa between the postexapophyses. Neither a foramen nor a fossa is present ventral to the posterior condyle in *Q. lawsoni*.

Cervical VIII—Cervical VIII is the first of the two posterior-series cervical vertebrae. It is longer (78.69 mm average) and more elongated (1.21 aspect ratio) than the ninth cervical (Table 5). Two eighth cervicals are present in the *Q. lawsoni* material: TMM 41954-42 and 42422-8. TMM 42422-8 is nearly complete, with slight damage to its left transverse process and side (Fig. 24). TMM 41954-42 is missing the dorsal portions of its neural arch including the spine. Even without considering the missing neural spine, TMM 41954-42 is a much shallower and wider vertebra. Eighth cervicals are preserved in the azhdarchid species *W. brevirostris*, *Z. linhaiensis* (Cai and Wei, 1994), *P. mauritanicus* (Kellner, 2010), and *A. lancicollis* (Averianov, 2010), as well as the putative azhdarchid specimen MPC-D 100/118 (Tsuihiji et al., 2017).

The anterior cotyle of the *Q. lawsoni* cervical VIII has a significant dorsal notch in the middle of the dorsal rim. The lateral ends of the cotyle curve ventrally to a great degree, forming a bifalcate outline (double sickle-shaped) and a convex dorsal margin, as in *A. lancicollis* (Averianov, 2010:284, fig. 15). Large preexapophyseal articulations are present under the lateral ends of the cotyle, as in *A. lancicollis* and *Pteranodon* (Bennett, 2001a:45, fig. 41; Averianov, 2010:fig. 15A). The hypapophysis is large and projects anteroventrally (Bennett, 2001a). Distinct lateral fossae incise into the hypapophysis and anterior cotyle. Combined with the wide posterior condyle, the centrum has a trapezoidal outline in ventral view due to a constriction posterior to the fused cervical rib, also found in *Pteranodon* (Bennett, 2001a:45) but contrasting with the squarish outline of *A. lancicollis* (Averianov, 2010:284, fig. 15). A very subtle ventral midline ridge extends along this ventral surface from hypapophysis to posterior condyle. A hypapophysis is reported as absent in *A. lancicollis* (Averianov, 2010:284, fig. 15). In *Q. lawsoni*, the anterior end of the neural arch has a distinct anterior vestibule that curves ventrolaterally to contact the lateral sulci. In TMM 42422-8, a
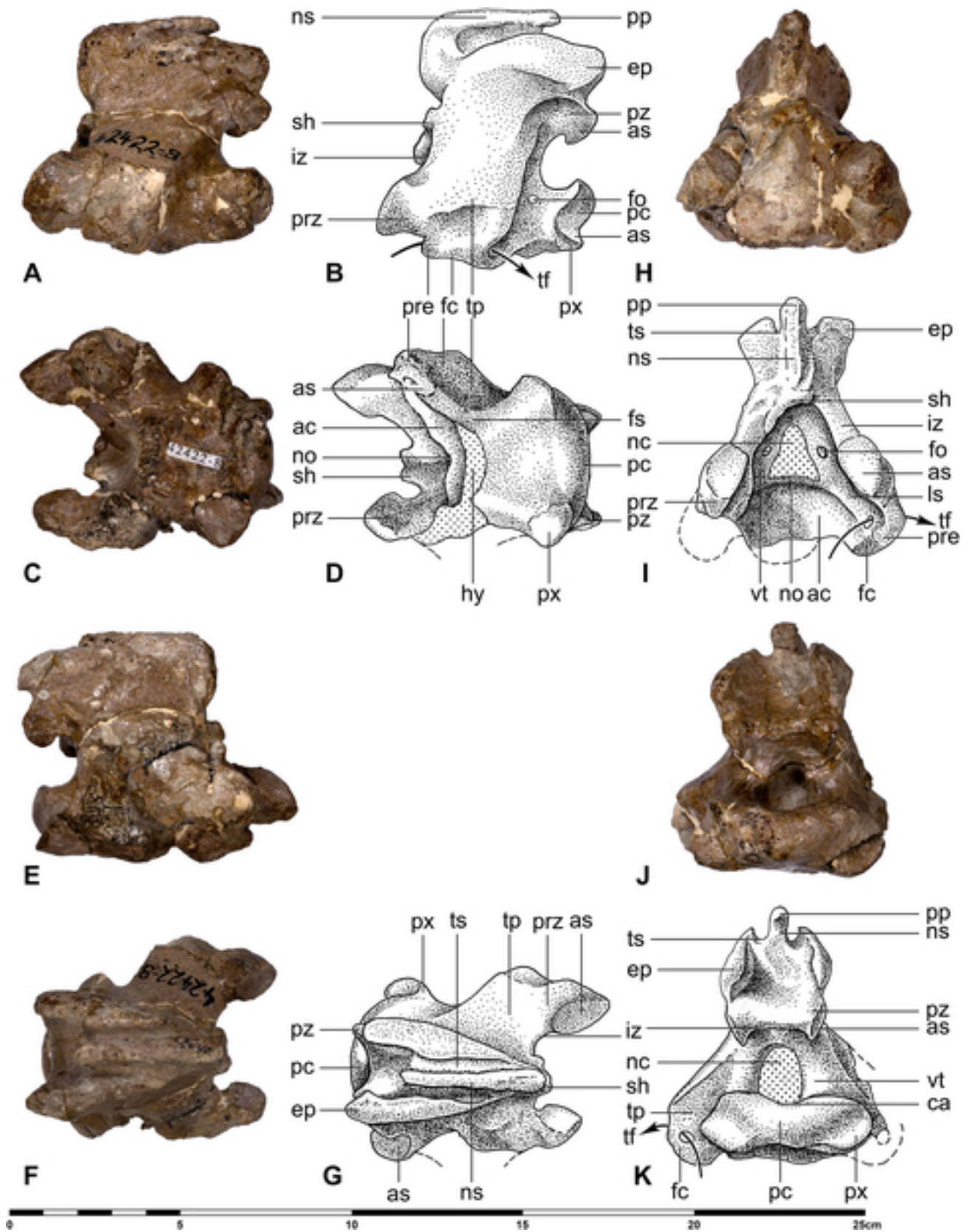
FIGURE 24. *Quetzalcoatlus lawsoni*, sp. nov., cervical VIII (TMM 42422-8) in **A**, left lateral photograph and **B**, line drawing; **C**, ventral photograph and **D**, line drawing; **E**, right lateral photograph; **F**, dorsal photograph and **G**, line drawing; **H**, anterior photograph and **I**, line drawing; **J**, posterior photograph; and **K**, line drawing views. **Abbreviations: ac**, anterior cotyle; **as**, articular surface; **ca**, concavity; **ep**, epipophysis; **fc**, fused cervical rib; **fo**, foramen; **fs**, fossa; **hy**, hypapophysis; **iz**, interzygapophyseal ridge; **ls**, lateral sulcus; **nc**, neural canal; **no**, notch; **ns**, neural spine; **pc**, posterior condyle; **pp**, posterior process; **pre**, preexapophysis; **prz**, prezygapophysis; **px**, postexapophysis; **pz**, postzygapophysis; **sh**, shelf; **tf**, transverse foramen; **tp**, transverse process; **ts**, transverse sulcus; and **vt**, vestibule. Dots represent matrix and/or damaged bone. Scale bar equals 25 cm.

dorsal shelf is present, albeit broken, above the neural canal. In TMM 41954-42, the neural canal is piriform and flanked by ventrally positioned circular pneumatic foramina in the vestibule. MPC-D 100/118 has an anterior pneumatic foramen dorsal to the anterior cotyle that was likely lateral to the neural canal (Tsuihiji et al., 2017:5, fig. 4), but it does not appear to be in the vestibule. The anterior vestibule of TMM 42422-8 is not as well preserved, and so the shape of the neural canal opening cannot be resolved. However, a piriform neural canal can be seen in the posterior vestibule of TMM 42422-8, and there is no trace of posterior lateral pneumatic foramina, as in *Pteranodon* (Bennett, 2001a:45). This area is obscured by matrix in TMM 41954-42, and so it is a possibility that they were present in this specimen. The pneumatic foramina lateral to the neural canal apparently reach the posterior surface in *A. lancicollis* (Averianov, 2010:284). Cervical VIII is the first vertebra in the column to be identified with transverse processes instead of transverse ridges in *Q. lawsoni*. Large C-shaped cervical ribs are fused to the lateral ends of the cotyle and the underside of these transverse processes to enclose a large transverse foramen in TMM 41954-42; the rib and foramen are smaller in TMM 42422-8. On the left side of both specimens, an anterior process is present where the rib contacts the transverse process. This is identified as a preexapophysis (mound-like anterior process of Tsuihiji et al., 2017) although it is possibly part of the fused rib. The prezygapophyses are attached to the anterior ends of the transverse processes. The prezygapophyseal articular surfaces are dorsomedially oriented expanded ovals. The combined prezygapophyses and transverse processes are large anterolaterally curving rectangular processes, but they are smaller and oriented more ventrally in TMM 42422-8. The prezygapophyses are level with or even slightly lower than the neural canal, unlike *Pteranodon* in which they are dorsal to the canal (Bennett, 2001a:45, fig. 41A), but the postzygapophyses are higher than the prezygapophyses in both.

The centrum in the *Q. lawsoni* cervical VIII is a low and transversely wide oval in cross-section. Whereas the neural arch is very tall, constituting most of the height of the vertebra. A pneumatic foramen pierces the posterior end of the ventral surface of the transverse process near its base in TMM 41954-42. In TMM 42422-8 the foramen appears to be on the lateral surface of the vertebral centrum near where the transverse process contacts the centrum instead. *Azhdarcho lancicollis* and MPC-D 100/118 appear to have a foramen in the latter position (Averianov, 2010:284; Tsuihiji et al., 2017:5, fig. 4E), whereas *Pteranodon* lacks pneumatic foramina on the centrum altogether (Bennett, 2001a:45, fig. 41). The neural spine of the eighth cervical is tall, as in non-monofenestratan and ornithocheiroid pterosaurs (Andres, 2021). In lateral view, the neural spine is rectangular in outline with a vertical anterior margin that projects anterior to the rest of the neural arch. The dorsal margin of the spine is inflated and continues as a posterior process that overhangs the posterior surface of the neural arch. The neural spine is separated laterally from a giant pair of epipophyses by a pair of transverse sulci. These epipophyses begin at almost the anterior end of the neural arch and extend posterolaterally to be level with the posterior margin of the postzygapophyses. The small round postzygapophyses have a proximal constriction and appear to hang down from the ventral margin of the epipophyses. The postzygapophyses are vertically oriented and the articular surfaces face nearly horizontally. A horizontal interzygapophyseal ridge extends between the postzygapophyses. This delineates the ventral margin of a large sloping posterior face between the postzygapophyses, epipophyses, and neural spine. The interzygapophyseal ridge forms a horizontal shelf bordering the dorsal margin of the posterior vestibule and reaches a couple of centimeters

posterior to the neural canal. A midline ridge extends along the underside of the horizontal shelf to the canal. The posterior condyle is crescent-shaped in outline with a wide dorsal concavity extending to the neural canal. Distinct postexapophyses extend posterolaterally from the posterior condyle, but they are positioned anteriorly about a centimeter from the posterior end of the condyle. The postexapophyseal articular surfaces are flat so that they have a semicircular outline in posterior view.

Cervical IX—Cervical IX is the second of the two posterior-series cervical vertebrae. Of the cervicals, this vertebra most closely resembles the dorsal vertebrae, and previously has been considered a cervicalized dorsal in the ornithocheiroids (e.g., Williston, 1903; Bennett, 2001a), but it is now considered the posterior-most cervical in all pterosaurs (Bennett, 2004; 2014). It is by far the shortest (45.03 mm average) and broadest (0.49 aspect ratio) of the cervical vertebrae in *Q. lawsoni* with the possible exception of the atlantal and axial components of the atlantoaxis (Table 5). TMM 41954-40 and 42422-7 are the only ninth cervicals in the *Q. lawsoni* material. They are similar in preservation to the eighth cervicals: TMM 42422-7 is nearly complete (Fig. 25) and TMM 41954-40 is missing its neural spine and upper neural arch, further suggesting that these pairs come from the same individuals (e.g., TMM 41954-40/42 and 42422-7/8). Ninth cervicals are present in the azhdarchid species *Z. linhaiensis* (Cai and Wei, 1994), *P. mauritanicus* (Pereda-Suberbiola et al., 2003), and *A. lancicollis* (Averianov, 2020), as well as the putative azhdarchid specimens MPC-D 100/116 and 100/117 (Tsuihiji et al., 2017).

The anterior cotyle is a flattened M-shape in outline with a midline notch in its dorsal rim in *Q. lawsoni*; the lateral ends project anteroventrally as large processes, also reported in *A. lancicollis* (Averianov, 2010:284, fig. 16A). Only a small portion of the anterior cotyle is preserved in MPC-D 100/116, but it appears to share this midline notch (Tsuihiji et al., 2017:fig. 2E). In *Q. lawsoni*, the preexapophyseal articular surfaces (preexapophyseal surfaces of Averianov, 2010, or accessory articular surface ventrolateral to the cotyle of Tsuihiji et al., 2017) are present on the anteroventral surfaces of the anterior cotyle processes and continuous with its articular surface, and so they are not preexapophyses sensu Bennett (2001a). They are also reported in *A. lancicollis* and MPC-D 100/117 (Averianov, 2010:284, fig. 15A; Tsuihiji et al., 2017:2, fig. 3A). Another pair of tubercles (anterolaterally facing rugose muscle scars of Bennett, 2001a, or distinct tubercles of Averianov, 2010) extend anteriorly from the ventral surface of the centrum in *Q. lawsoni*. These are not topologically similar to the preexapophyses on the other cervical vertebrae, and so are considered here de novo structures. They are also present in *A. lancicollis* (Averianov, 2010:284, fig. 16G) and stated to be absent in MPC-D 100/116, but Tsuihiji et al. (2017) label a low process in this location. The rib for this vertebra is missing in TMM 41954-40 and 42422-7, and it is possible that a preexapophysis was present on that element. The hypapophysis is wide but short, and is also present in *A. lancicollis* (Averianov, 2010:284). Its lateral fossae are delineated by the margins of the hypapophysis, preexapophyseal articulation processes, and the ventral processes in *Q. lawsoni*. A ridge in the middle of the centrum ventral surface (single median muscle scar of Bennett, 2001a, or subtle mid-sagittal ridge with scarring of Tsuihiji et al., 2017) trifurcates into a median ridge on the hypapophysis and two lateral ridges that curve anterior to the ventral processes. The anterior end of the neural arch does not have a vestibule in TMM 42422-7, but one appears to be present in TMM 41954-40. The anterior neural canal opening is clithridiate in outline. Pneumatic foramina are not located lateral to the neural canal. However, there is a pair of pits
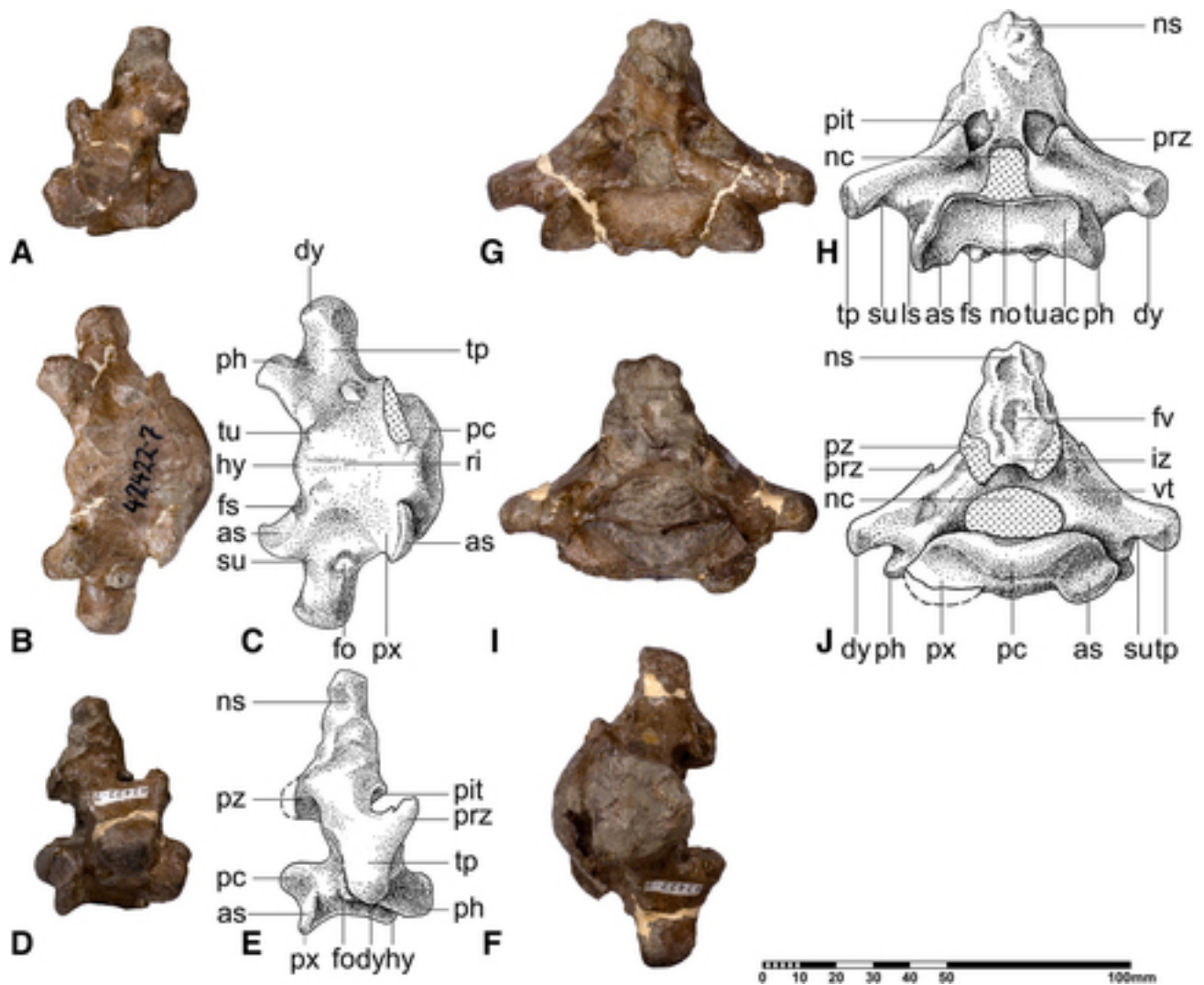
FIGURE 25. *Quetzalcoatlus lawsoni*, sp. nov., cervical IX (TMM 42422-7) in **A**, left lateral photograph; **B**, ventral photograph and **C**, line drawing; **D**, right lateral photograph and **E**, line drawing; **F**, dorsal photograph; **G**, anterior photograph and **H**, line drawing; and **I**, posterior photograph and **J**, line drawing views. **Abbreviations: ac**, anterior cotyle; **as**, articular surface; **dy**, diapophysis; **fo**, foramen; **fs**, fossa; **fv**, fovea; **hy**, hypapophysis; **iz**, interzygapophyseal ridge; **ls**, lateral sulcus; **nc**, neural canal; **no**, notch; **ns**, neural spine; **pc**, posterior condyle; **ph**, parapophysis; **pit**, pit; **pre**, preexapophysis; **prz**, prezygapophysis; **px**, postexapophysis; **pz**, postzygapophysis; **su**, sulcus; **tp**, transverse process; **tu**, tubercle; and **vt**, vestibule. Dots represent matrix and/or damaged bone. Scale bar equals 100 mm.

posteromedial to the prezygapophyses that could be the termination of pneumatic diverticula. A deep pneumatic excavation is also reported in MPC-D 100/117 (Tsuihiji et al., 2017:5, fig. 3E) but on the opposite side of the prezygapophysis. *Azhdarcho lancicollis* has the more traditional condition of anterior and posterior lateral pneumatic foramina ventral to the zygapophyses in the vestibules (Averianov, 2010:286, fig. 16). The prezygapophyses are extensions of the neural arch and positioned more medially than in the preceding cervicals of *Q. lawsoni*. The prezygapophyseal articular surface is subvertical and oriented medially, compared with the dorsomedial orientation of MPC-D 100/117 (Tsuihiji et al., 2017:2, fig. 3A). Dorsal to the anterior neural canal opening *Q. lawsoni* has a posteriorly sloping face that merges with the neural spine.

The transverse processes are well developed ventrolateral knobs in TMM 42422-7, but they are lateral wings that are rectangular in horizontal outline in TMM 41954-40. There are no ribs preserved and therefore no transverse foramina are preserved in these specimens, but TMM 41954-40 appears to have diapophyses and parapophyses for their articulation. The parapophysis is located immediately posterolateral to the preexapophyseal articular surface (Tsuihiji et al., 2017), and the diaphysis is on the anteroventral margin of the tip of the transverse process. A small and presumably pneumatic foramen pierces the posterior end of the ventral surface of the transverse process base, in a position similar to the pair of foramina described in MPC-D 100/116 (Tsuihiji et al., 2017:2–3, fig. 3). The top of the neural spine is missing in TMM 41954-40 and 42422-7, but it can be seen to be a tall and wider than long process, similarly described as swollen in *P. mauritanicus* (Pereda-Suberbiola et al., 2003:84, fig. 3e) but contrasting with the slender spine with a large anterior ridge of *Pteranodon* (Bennett, 2001a:46, fig. 42). The posterior surface of the spine is damaged in the *Q. lawsoni* material but appears to have a

TABLE 6. Measurements of *Quetzalcoatlus lawsoni*, sp. nov., dorsal and sacral vertebra material. Values in millimeters. >, preserved value; <, maximum possible value; ~, approximate value; a-p, anteroposterior dimension; d-v, dorsoventral dimension; lat, lateral dimension; p-d, proximodistal dimension.

Dimension: Element: Specimen Number:	Centrum length (a-p)	Centrum width at anterior cotyle (lat)	Centrum mid-width (lat)	Total width (lat)	Total height (d-v)
Dorsal I					
TMM 41954-60.1	32.93	56.60	30.14	87.66	>39.66
TMM 41954-73	>32.77	>31.13	>22.17	>40.76	>30.20
TMM 42246-3	29.68	42.29	>19.13	>52.44	>36.80
Dorsal II					
TMM 41954-60.1	31.79	39.62	25.06	76.60	>33.85
TMM 42246-3	>25.09	>11.95	>12.07	>46.08	55.62
Dorsal III					
TMM 41954-60.1	25.80	33.38	20.64	74.69	>39.77
TMM 42246-3	24.87	>10.49	>7.69	>42.08	64.86
Dorsal IV					
TMM 41954-60.1	23.26	26.75	18.57	77.03	>46.45
TMM 42246-3	23.81	>10.14	>4.96	51.26	59.72
TMM 41954-57					
Free dorsal	26.02	14.98	13.14	17.95	50.88
Synsacral I	28.99	15.76	>8.47	>28.09	>46.45
Synsacral II	26.16	15.34	12.04	>19.19	>40.30
Synsacral III	20.11	17.24	>14.19	>17.81	>31.28
Sacral I	19.44	~15.93	>9.40	>30.35	>25.17
Notarial rib I	Length (p-d)	Mid-width (a-p)	Mid-depth (d-v)		
TMM 41954-60.1	>34.99	17.99	<11.81		
TMM 41954-60.3	>68.82	17.81	4.73		
Notarial rib II					
TMM 41954-60.2	86.94	9.17	3.79		
TMM 41954-76	>54.69	9.13	5.62		
TMM 42246-3	>29.72	<13.09	<6.72		
Dorsal ribs					
TMM 42521-1	>41.86	5.72	?		

fovea, reported as an oval depression with thick vertical edges in *P. mauritanicus* (Pereda-Suberbiola et al., 2003:84, fig. 3e) or thin rugose plates in *Pteranodon* (Bennett, 2001a:46, fig. 42B). The pneumatic foramen in this area reported in *Pteranodon* (Bennett, 2001a:46, fig. 42B) is absent in *Q. lawsoni*. The postzygapophyses have been broken off at their bases in TMM 42422-7. Like the eighth cervical, a horizontal shelf with the interzygapophyseal ridge (transverse ridge of Bennett, 2001a) extending between the ventral margins of the postzygapophyses forms the dorsal margin of the posterior vestibule of the neural arch. The postzygapophyses are described as missing in *P. mauritanicus*, but they appear to have the same arrangement as *Q. lawsoni* (Pereda-Suberbiola et al., 2003:84, fig. 3e) and *A. lancicollis* for that matter (Averianov, 2010:fig. 16C). The posterior opening of the neural canal is a broad oval in outline, compared with the circular opening of *P. mauritanicus* (Pereda-Suberbiola et al., 2003:84, fig. 3e). There are also no traces of posterior pneumatic foramina lateral to the neural canal. The posterior condyle is a sharp-edged crescent in outline, as in *P. mauritanicus* (Pereda-Suberbiola et al., 2003:84, fig. 3e) and MPC-D 100/116 (Tsuihiji et al., 2017:2, fig. 2F). Postexapophyses resemble the condition in cervical VII as well: positioned anterior to the posterior condyle with a flat articular surface and semicircular outline. MPC-D 100/116 has a similar postexapophyseal outline, but it is concave instead (Tsuihiji et al., 2017:2 fig. 2F). They differ from the eighth cervical in *Q. lawsoni* by being positioned more ventrally.

Dorsal Vertebrae

Pterosaurs have between 11 and 15 dorsal vertebrae (Bennett, 2007a). The skeleton of the dorsal vertebral column of *Q. lawsoni* is known from two notaria (TMM 41954-60.1 and 42246-3), a first notarial vertebra (TMM 41954-73), and the posterior-most free dorsal associated with a synsacrum (TMM 41954-57) (Table 6). A fragment identified as rib, TMM 41954-76, might be a free rib posterior to the notarium, but the broad width of this proximal end suggests that it was anterior in the vertebral series and likely the first notarial rib broken off the notarium. It is unknown how many free vertebrae lie between the fused notarial and synsacral vertebrae and the exact number of synsacral vertebrae (Padian et al., 2021). These vertebrae are rather squat. Their centra are only slightly longer than their maximum width across the anterior cotyle (1.06 aspect ratio). This is significantly broader than the 1.44 average for pterosaurs and the 1.13 aspect ratio present in *A. lancicollis* that is plesiomorphic for the Azhdarchiformes.

Notarium—Ornithocheiroid pterosaurs typically have several anterior dorsal vertebrae fused into a notarium (Andres, 2021). The notarial material of *Q. lawsoni* includes the complete and relatively well preserved TMM 41954-60.1 and 42246-3, and the right half of dorsal vertebra I in TMM 41954-73. TMM 41954-60.1 is complete except for the neural spines of the first two dorsal vertebrae and the top of the spines in the second two dorsal vertebrae (Fig. 26). It is almost completely prepared, although matrix still adheres between the vertebrae. The proximal end of a rib is fused to the left side of dorsal vertebra II. A distal rib fragment was previously numbered TMM 41954-24, but it fits with the proximal rib fragment fused to TMM 41954-60.1 and so was given the number TMM 41954-60.2 with that fused fragment. Another rib associated with this notarium was numbered TMM 41954-60.3. TMM 42246-3 is less complete and less prepared, but it does preserve the neural spines and supraneural plate for dorsals II–IV. The left half of this specimen is damaged, and so it is missing the left intertransverse ossification and most of the left transverse processes as well as the left half of the centra of dorsals III and IV. TMM 41954-60.1 is significantly larger than TMM 42246-3. Notarial vertebrae are reported
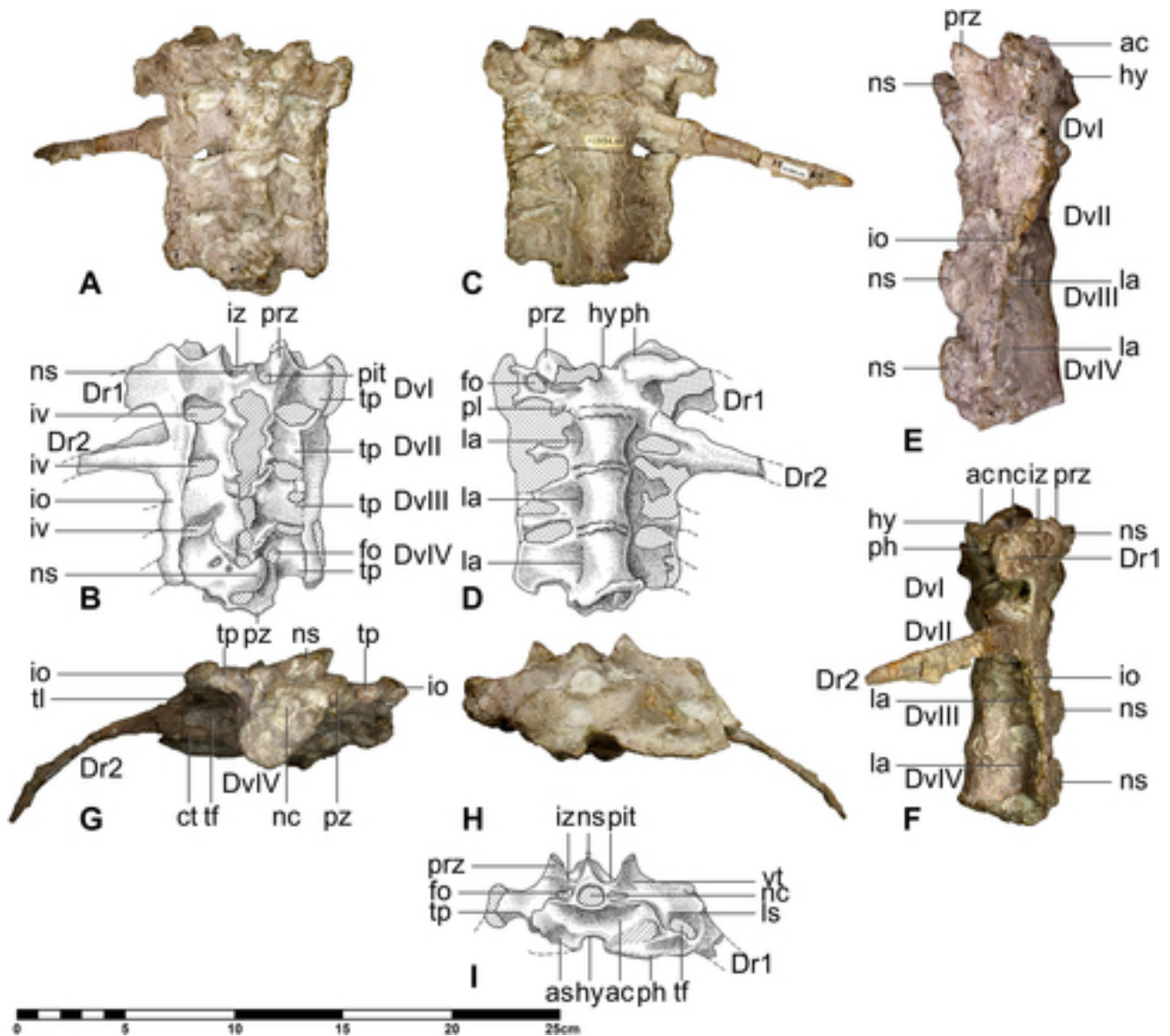
FIGURE 26. *Quetzalcoatlus lawsoni*, sp. nov., notarium (TMM 41954-60.1) and left second dorsal rib (TMM 41954-60.2) in **A**, dorsal photograph and **B**, line drawing; **C**, ventral photograph and **D**, line drawing; **E**, right lateral photograph; **F**, left photograph; **G**, posterior photograph; **H**, anterior photograph and **I**, line drawing views. **Abbreviations: ac**, anterior cotyle; **as**, articular surface; **ct**, capitulum; **DrX**, dorsal rib X; **DvY**, dorsal vertebra Y; **fo**, foramen; **hy**, hypapophysis; **io**, intertransverse ossification; **iv**, intervertebral foramen; **iz**, interzygapophyseal ridge; **la**, lamina; **ls**, lateral sulcus; **nc**, neural canal; **ns**, neural spine; **pit**, pit; **pl**, posterolateral projection; **ph**, parapophysis; **prz**, prezygapophysis; **pz**, postzygapophysis; **tf**, transverse foramen; **tl**, tuberculum, **tp**, transverse process, and **vt**, vestibule. Dots represent matrix and/or damaged bone. Another dorsal rib (TMM 41954-60.3) associated with this notarium is not figured. Scale bar equals 25 cm.

in the azhdarchid species *Z. linhaiensis* (Cai and Wei, 1994), *A. bostobensis* (Averianov, 2010), and *A. lancicollis* (Nesov, 1984), as well as the putative azhdarchid specimens MCNA 8564 (Averianov, 2014) and RBCM.EH.2009.019.0001C (Martin-Silverstone et al., 2016).

Both notaria consist of four fused vertebrae with complete and unfused articular surfaces at both ends. Therefore, *Q. lawsoni* is identified as having four notarial vertebrae, the four anterior-series dorsals forming the transition between wide cervical vertebrae and the narrower free dorsal vertebrae (Bennett, 2001a). Ornithocheiroids can have up to seven dorsal vertebrae fused into a notarium (Gilmore, 1928:343; Aires et al., 2014:4). *Zhejiangopterus linhaiensis* is reported to have six notarial vertebrae and a supraneural plate (Cai and Wei,

1994:32), whereas *A. lancicollis* and MCNA 8564 have four known notarials (Astibia et al., 1990:fig. 5; Averianov, 2010:288 and 291). These vertebrae are fully fused at their centra, zygapophyses, transverse process distal ends, and neural spines in *Q. lawsoni*. At least the first two ribs are fused to the notarium. Fused notarial ribs are also present in *D. weii* and *Nyctosaurus*, with at least four (and possibly more) in *Pteranodon* (Bennett, 2001a:48, figs. 46–47). The centra are the best preserved portions of these elements in TMM 41954-60.1 and 42246-3, allowing measurement of both the centrum length and width (Table 6). These centra are wider than long, with an average aspect ratio of 0.80 when measured at the anterior cotyle. The centra are significantly constricted at their midsections (60% average), and so they appear

longer than wide at that dimension (1.66 average aspect ratio). Both anterior and mid-widths are reported for clarity. These dorsals form the transition from the cervical series to the free dorsal series (unfused vertebrae between the notarium and synsacrum). The notarial vertebrae are decrease in size posteriorly: 78% of anterior width, 85% of mid-width, and 90% of length is lost between successive vertebrae on average.

In *Q. lawsoni*, the first dorsal/notarial vertebra shares some features with the cervical series and specifically cervical IX: preexapophyseal articulations, hypapophysis, crescent-shaped anterior cotyle, lateral sulci connecting the anterior vestibule of the neural arch to transverse foramina, pits posteromedial to the prezygapophyses, pneumatic foramina at the bases of transverse processes, large prezygapophyses connected by the interzygapophyseal ridge, and medially-oriented prezygapophyseal articulations. Many of these features are obscured in subsequent vertebrae, but the postexapophyses, hypapophysis, and foramina medial to the prezygapophyses are not present in the second dorsal. Pneumatic foramina on the transverse processes and a broad anterior articulation persist to the third dorsal vertebra. Dorsals I and II have laterally-oriented transverse processes, whereas III and IV have successively more dorsolaterally oriented processes, as also present in *Pteranodon* (Bennett, 2001a:50). The second and third dorsal transverse processes of *Q. lawsoni* also appear to have a slight posterolateral component to their articulation. The fourth dorsal vertebra, the last of the notarial series, resembles the free dorsal in having a centrum about as wide as long and circular in cross-section as well as dorsolaterally oriented transverse processes. In posterior view, dorsal IV has a tall oval neural canal and a circular centrum in outline, described as round in *A. lancicollis* (Averianov, 2010:289, fig. 18E).

The first dorsal/notarial vertebra is the largest vertebra of the post-cervical series in *Q. lawsoni*. It has a broad crescentic anterior cotyle, matching the posterior condyle of cervical IX. It lacks postexapophyses, but the posterior margin of the centrum has a lateral structure termed posterolateral projections by Bennett (2001a). It shares with *A. lancicollis* a ventral surface flatter than succeeding vertebra (Averianov, 2010:288). The preexapophyseal articular surface is large, reaching from the anterior cotyle to the base of a ventral process. This ventral process is fused to the capitulum of the first notarial rib on the left side of TMM 41954-60, and so it is identified as the parapophysis. Preexapophyseal articular surfaces on the parapophyses are also reported in *Pteranodon* (Bennett, 2001a:48). There is a space between these parapophyses below the anterior cotyle in which a small blunt hypapophysis is located in *Q. lawsoni*, termed a concavity in *A. lancicollis* but lacking a hypapophysis (Averianov, 2010:288). The tuberculum is fused to the lateral end of the transverse process/diapophysis to enclose an oval transverse foramen, but their margins cannot be resolved. The lateral sulcus connecting the transverse foramen to the anterior vestibule is wide laterally and constricts at the contact with the vestibule, which is rather small and less distinct than in the cervical series. A large circular neural canal constitutes most of the anterior vestibule. The dorsal margin of the anterior cotyle is concave at the midline to accommodate this opening, as in *A. lancicollis* (Averianov, 2010:288, fig. 17A). The neural canal is flanked laterally by tiny elliptical openings identified as pneumatic foramina. There is a pair of openings posteromedial to the prezygapophyses that may be pneumatic. However, they do not appear to communicate with an internal chamber in the vertebra, and so are identified as pits similar to those on cervical IX. The prezygapophyses project anteriorly, but their articular surfaces are oriented dorsomedially. The postzygapophyses are much smaller and positioned more medially than the prezygapophyses, but they are fused to the subsequent vertebra so it is difficult to resolve their boundaries. Only the base of the neural spine is

preserved in both specimens and would have likely been incorporated into a supraneural plate. The transverse process is a broad rectangle with slight distal expansion in horizontal outline. It is a deep process in anterior view, and it is an anteriorly expanded trapezoid in parasagittal cross-section. A large oval pneumatic foramen constitutes most of the ventral surface of the transverse process.

The transverse processes of the notarium in *Q. lawsoni* are connected at their distal ends by an intertransverse ossification (intertransverse ossification and longitudinal ossifications of Bennett, 2001a) that encloses a series of openings between the processes, termed intervertebral foramina here. Intertransverse ossifications are reported in *D. weii*, *Pteranodon*, and *Nyctosaurus* (Bennett, 2001a:50–51). This ossification appears to extend over the dorsal surface of the transverse processes, and so it is identified as ossified intertransverse ligaments (Bennett, 2001a) instead of lateral expansions of the processes contacting one another. In dorsal view, the intervertebral foramina of *Q. lawsoni* are large and oval in outline anterior in the series, becoming smaller and elliptical in outline posterior in the series. In ventral view, they keep roughly the same size, but they become more elongated and elliptical posterior in the series due in large part to the dorsal deflection of the transverse processes. These transverse processes become dorsoventrally thinner posteriorly in the series as well. The ventral pneumatic foramen present on the transverse process is a smaller triangle on the second dorsal, an elongate ellipse on the third dorsal, and absent on the fourth dorsal. The fourth dorsal vertebra instead has pneumatic foramen on the dorsal surface of the transverse process posterolateral to the prezygapophysis. A rib is fused to the second dorsal in both specimens. Unlike in dorsal I, the capitulum of the rib is fused to a parapophyseal process on the lateral surface of the centrum. No parapophyseal articulations are visible on the centra of dorsals III and IV. Diapophyseal articulations appear to be present on the distal ends of their transverse processes.

The neural spines of dorsals II-IV are preserved in TMM 42246-3. They become laterally thinner posteriorly in the series, and they expand dorsally to where they fuse together in a supraneural plate. The neural spines expand anteriorly and posteriorly and so this plate appears to be the fusion of the spines contacting one another, as in *D. weii* and *I. latidens* (Bennett, 2001a:51) but contrasting with the ossified ligaments of *Pteranodon* (Bennett, 2001a:50–51). Supraneural plates are preserved in *Z. linhaiensis* and MCNA 8564 (Cai and Wei, 1994:32; Averianov, 2010:291). The supraneural plate is tallest and widest over the third dorsal, where there is a 2 cm long rugose surface that marks the articulation with the scapula. There is not a distinct facet for the scapular articulation, whereas there is a scapular facet in *D. weii*, *I. latidens*, and *Pteranodon* that is positioned primarily over the fourth and part of the third dorsals (Bennett, 2001a:50–51).

Free dorsal—The only vertebrae posterior to the notarium preserved in the *Q. lawsoni* material consists of five vertebrae associated with the left pelvic plate of TMM 41954-57 (Fig. 27). The most anterior vertebra of this series is not fused to the subsequent vertebrae and is rotated slightly with respect to them. It is therefore identified as the last of the free dorsals located between the fused notarium and synsacrum (Table 6). It is also not part of a fused pair of free dorsals, which has been reported in some specimens of *Pteranodon*, *D. weii*, and *A. lancicollis* (Bennett, 2001a:47–48, fig. 46; Averianov, 2010:289, fig. 18C–F). Its right side is damaged, but it can be seen to be tall and laterally compressed. The centrum is strongly procoelous with a deep anterior cotyle and a substantial lateral constriction in its middle. The centrum is elliptical in cross-section with a height almost twice the width. The surface of the centrum is strongly scarred. No rib facets are visible, which may have been entirely on the transverse processes that have been broken off near
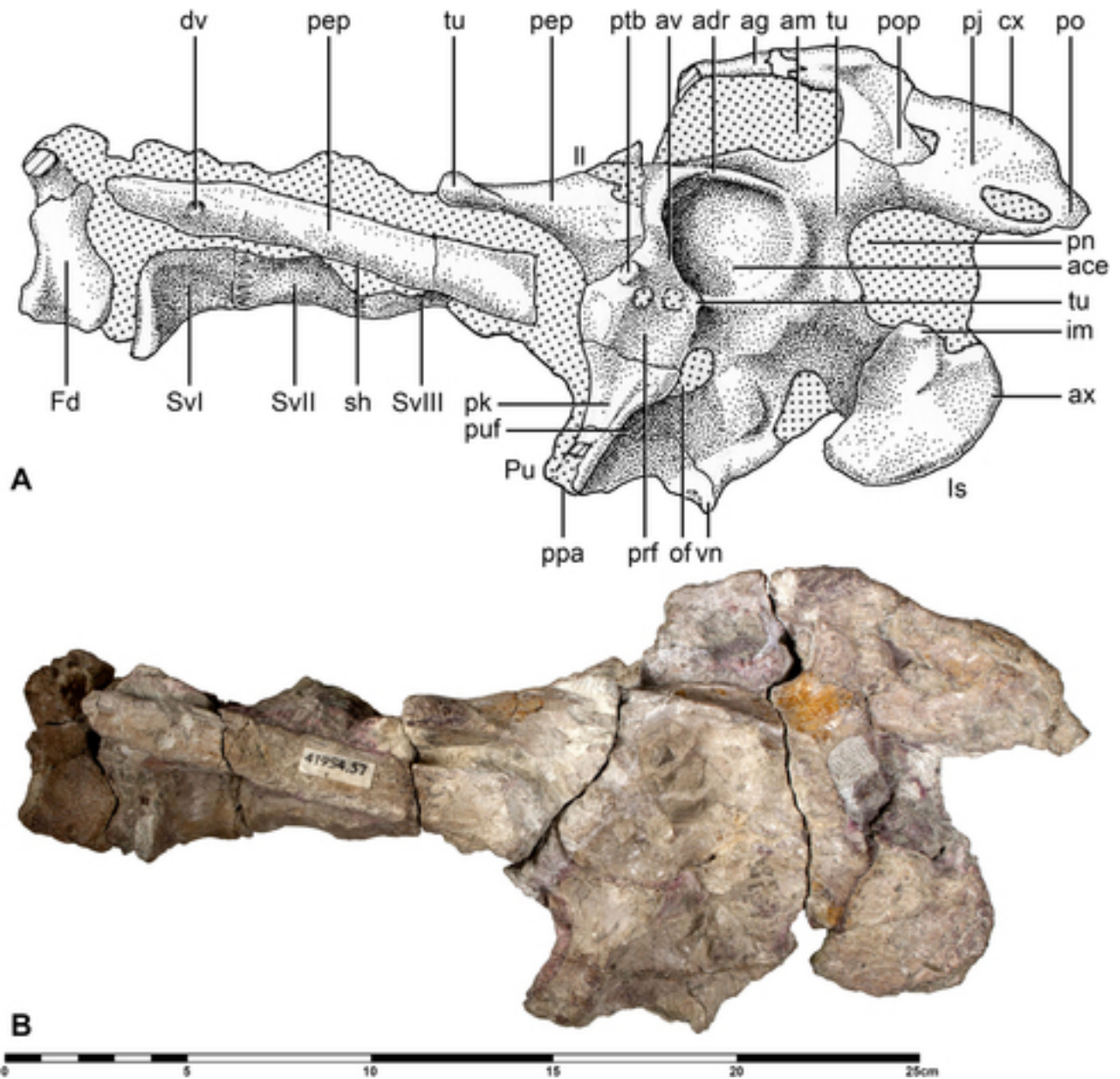
FIGURE 27. Q*uetzalcoatlus lawsoni*, sp. nov., left pelvis (TMM 41954-57) **A**, line drawing; and **B**, photograph in left lateral view. **Abbreviations: ace**, acetabulum; **adr**, anterodorsal ridge; **ax**, angular extremity; **ag**, angular process; **am**, anterior emargination; **av**, anteroventral prominence; **cx**, convexity; **dv**, divot; **Fd**, free dorsal; **Il**, ilium; **im**, ischial eminence; **Is**, ischium; **of**, obturator foramen; **pep**, preacetabular iliac process; **pj**, posterior projection; **pk**, pubic stalk; **pn**, posterior emargination; **po**, posterior tip; **pop**, postacetabular process; **ppa**, prepubic articulation; **prf**, preacetabular fossa; **ptb**, pubic tubercle; **Pu**, pubis; **puf**, pubic fossa; **sh**, shelf; **SvX**, synsacral vertebra X; **tu**, tubercle; and **vn**, ventral process. Dots represent matrix. Scale bar equals 25 cm.

their bases. The neural arch is positioned only on the anterior half of the centrum. It has tall laminae enclosing a circular neural canal with a small process overhanging its anterior margin. Although broken, the transverse processes can be seen to be oriented dorsolaterally. The prezygapophyses are missing and so were also likely attached to the transverse processes. The left postzygapophysis is preserved. It is short and robust with an articular surface oriented about 70° from the horizontal plane. The neural spine is also broken off at its base. Free dorsal vertebrae are reported in the azhdarchid species *Z. linhaiensis* (Cai and Wei, 1994), *A. bostobensis* (Averianov, 2007), and

A. lancicollis (Averianov, 2010), as well as the putative azhdarchid specimens MOR 553 (Carroll et al., 2013), RBCM.EH.2009.019.0001D and E (Martin-Silverstone et al., 2016), ZIN PH 54/43 (Averianov, 2007), ZIN PH 55/43 (Averianov, 2014), and ZIN PH 46/43 (Averianov et al., 2015).

Synsacral Vertebrae—The sacrum of pterosaurs consists of up to six sacral vertebrae and up to four dorsal or caudal vertebrae fused to it to form the synsacrum; these fused dorsals and sacrals are termed synsacral vertebrae. The synsacral vertebrae do not contact the main body of the ilium with sacral ribs but instead contact the anterior or posterior iliac processes with transverse

processes (Bennett, 2001a). Four vertebrae fused at their centra and zygapophyses are associated with the left pelvis of TMM 41954-57 (Fig. 27). They are identified as the three anterior synsacral and the first sacral vertebra (Table 6). Their right sides have been damaged and remain largely encased in matrix, but much of their anatomy can be observed. Their neural spines have been broken off at their bases and so it is not possible to directly ascertain if a supraneural plate was present. The synsacral vertebrae are articulated but do not appear to be fused with the ilium. The preacetabular process of the ilium has become detached and displaced ventrally in TMM 41954-57.

The right side of TMM 41954-57 has been much damaged, but this has permitted an internal view of the neural canal in the third synsacral. The three synsacrals resemble the free dorsal in being laterally compressed with dorsolaterally oriented transverse processes, but they lack the rugose centrum of the free dorsal. In this specimen, the anterior end of the first synsacral has been rotated to the left and this change in position appears accommodated by a break in the neural arch. The centra of the synsacrals are constricted both ventrally and laterally. The transverse processes transition from being oriented dorsolaterally to laterally along the series matching the descent in height of the anterior iliac process of the pelvis. The transverse processes themselves are horizontally wide, although the preserved process of the third synsacral appears narrower than the others. The fused postzygapophysis of the third synsacral and prezygapophysis of the first sacral are visible. The prezygapophysis is slightly medial to the postzygapophysis so that the articular surfaces are about 45° from the sagittal plane in dorsal view and 70° from the horizontal plane in medial view.

At least one poorly preserved sacral vertebra is preserved in TMM 419544-57. It is identified as the first sacral (fourth of the synsacrum) by the bases of a pair of posterolateral processes on the centrum that correspond to the united sacral ribs and transverse processes in pterosaurs. Fragments of three and possibly four other vertebrae can be observed posterior to the first sacral. These appear to be left zygapophyses of successive vertebrae. The posterior two or three are positioned under the three neural spine contacts on the medial flange of the posterior iliac process. There is enough room for another vertebra between these remains and the first sacral, and so this specimen may provide evidence for nine synsacrals in *Q. lawsoni*. It is not possible to ascertain if any caudals were incorporated into the posterior synsacrum, but if one were present it would match the condition of ten vertebrae in synsacrum of *Pteranodon* (Bennett, 2001a), the maximum number in pterosaurs (Andres, 2021).

Ribs—Evidence of ribs in *Q. lawsoni* are found in all cervical vertebrae, the notaria TMM 41954-60 and 42246-3, the likely isolated notarial rib TMM 41954-76, and possibly multiple dorsal ribs in the fragments of TMM 42521-1 (Table 6). Dorsal ribs are reported in the azhdarchid species cf. *H. thambema* (LPB R.2397) (Vremir et al., 2018), *Z. linhaiensis* (Cai and Wei, 1994), *C. boreas* (Hone et al., 2019), and *A. lancicollis* (Averianov, 2010), as well as the putative azhdarchid specimens MOR 553 (Carroll et al., 2013), ZIN PH 51/44 (Averianov, 2014), and ZIN PH 81/44 (Averianov, 2007).

Caelicodraconian pterosaurs typically lack traditional bicipital ribs with a shaft on their cervical vertebrae. Instead, they have transverse foramina formed by the fusion of small C-shaped ribs consisting of only the capitulum and tuberculum. This is reversed in the Ctenochasmatinae in which the shaft has reappeared. Cervicals III–VII in *Q. lawsoni* contain minute (~2 mm wide) transverse foramina beneath the base of the prezygapophyses presumably formed by the fusion of these cervical ribs. On the axis, there are two small tuberosities located laterally on the centrum that are likely the diapophysis and parapophysis (Fig. 18). They probably indicate the presence of a small bicipital

axial rib, but no examples of such a rib have been found. The transverse foramen in cervical VIII is oval and much larger than in the preceding vertebrae (5 mm by 11 mm in TMM 41954-42) and also likely represents the fusion of a larger C-shaped rib (Fig. 24). A slightly thickened area distally on the parapophysis may represent the zone of fusion with the capitulum of the rib in TMM 41954-42. Cervical IX clearly possessed a large bicipital rib that freely articulated with the large and well developed diapophysis and parapophysis (Fig. 25), but no example of this rib has been found.

The dorsal ribs in *Q. lawsoni* are represented only by notarial ribs and possibly the multiple rib fragments of TMM 42521-1. The first two dorsal ribs fuse to the notarium. In TMM 41954-60, the proximal end of the left first notarial rib (included with the vertebrae in TMM 41954-60.1), the presumably complete left second notarial rib (TMM 41954-60.2 in two pieces, the broken off shaft was previously numbered TMM 41954-24), and the disarticulated proximal rib end identified as the right first notarial rib (TMM 41954-60.3) are preserved (Fig. 26). TMM 42246-3 preserves the proximal end of the second notarial rib. The first notarial rib capitulum is fused to the preexapophyseal articulation of the first notarial vertebra and the tuberculum is fused to the transverse process and intertransverse ossification with no trace of a suture (Fig. 26). A rib shaft (TMM 41954-60.3) is identified as the right first notarial rib based on its size (not figured). It is about twice the width of the other ribs and curves more posteroventrally. It is deeper posteriorly with a thin anterior flange that gives it a comma-shaped cross-section. A pneumatic foramen pierces the dorsal surface of its proximal end. It appears to preserve a short, wide, and unfused tuberculum with a missing capitulum. This identification/morphology is not precluded by the left first rib fused to TMM 41954-60.1, although the fusion of just one side remains unlikely. This left rib encloses a large oval transverse foramen. Although fused, the second notarial rib can be seen to support a short and wide tuberculum with a much longer capitulum. The tuberculum does have a distinct process and the capitulum fuses with a process on the lateral surface of the centrum. Articulating the two pieces of the TMM 41954-60.2 rib reveals a rather short and tapering shaft. Either this specimen had its ribs continue as cartilage, or the two pieces erroneously match. The second notarial rib encloses a more elongated and elliptical transverse foramen. TMM 41954-76 is a proximal rib fragment that corresponds well to the second left notarial rib in shape and size. It may be an unfused third notarial rib considering that it lacks a capitulum and the third notarial vertebra lacks a diapophysis.

TMM 42521 consists of 15 concretions with fragments of bones. A couple of these consist of two long, thin, and parallel shafts. These and the rest of the concretions likely preserve fragments of dorsal ribs. The dimensions of the longest fragment are reported in Table 6.

Pectoral Girdle

The pectoral girdle of pterosaurs consists of three elements: a scapula and coracoid that fuse over ontogeny into the scapulocoracoid as well as the sternum. The scapulocoracoid is rotated laterally in the Eupterodactyloidea and articulates with the vertebral column dorsally in the non-nyctosaurid ornithocheiroids (Andres, 2021). Therefore, the positional terms of proximal and distal are used here to refer to the ramus and glenoid regions of the scapula and coracoid, respectively. Seven scapulocoracoids and three sternum fragments are preserved in the *Q. lawsoni* material.

Scapulocoracoid—The pterosaur scapulocoracoid is a V- to U-shaped element constructed from the conjoined scapula and coracoid. They are oriented at an oblique angle to the vertebral column so that the medial end of the coracoid contacts the

sternum ventrally, both scapula and coracoid contact the humerus laterally at the glenoid fossa, and the medial end of the scapula (dorsolateral end in most tetrapods) contacts the ribcage or the dorsal vertebral column medially. All of the scapulocoracoids in the *Q. lawsoni* material are completely fused with only a slight trace of the contact. TMM 41544-25 and 42138-1.1 are complete right scapulocoracoids, TMM 42422-12 is a right scapulocoracoid missing the coracoid proximal end, TMM 41544-26 is a left scapulocoracoid missing both the scapula proximal end and coracoid ramus, TMM 42180-9 is a right glenoid, TMM 41954-29 is a left coracoid, and TMM 42180-10 comprises fragments of a left scapulocoracoid (Table 7). Scapulocoracoids are reported in the azhdarchid species cf. *H. thambema* (LPB R.2396) (Csiki-Sava et al., 2016), *Z. linhaiensis* (Cai and Wei, 1994), *A. bostobensis* (Averianov, 2007), *C. boreas* (Hone et al., 2019), and *A. lancicollis* (Averianov, 2010); the azhdarchiform species *M. minor* (Padian et al., 1995); and the putative azhdarchid specimens NZGS CD 547 (Averianov, 2014) as well as ZIN PH 52/43 and 53/43 (Averianov, 2007).

The scapulocoracoid in *Q. lawsoni* is a broad U-shaped structure in anterior/posterior view with a 45° kink in the scapula and a 135° bend in the coracoid so that the U leans ventrolaterally (Fig. 28). The scapula is slightly longer than the coracoid (1.12 ratio) at the end of a trend of scapula length reduction in the Azhdarchoidea, although this is dwarfed by a greater reduction in the Pteranodontoidea (Andres, 2021). The scapula and coracoid rami have different orientations in the horizontal plane: the scapula is oriented about 20° more medial than the coracoid. Therefore, the scapula would have articulated with the supraneural plate at an angle of about 66°, and the coracoid would have articulated with the sternum at an angle of about 45°.

The glenoid dominates the scapulocoracoid with massive dorsal and ventral lips (ridges of Godfrey and Currie, 2005). These lips are directed dorsolaterally so that the articular surface is an inverted crescent in lateral view. They are positioned in the posterior half of the articular surface. The glenoid as a whole is a roughly cylindrical structure that is about as tall as it is wide, with a saddle-shaped articulation (concave dorsoventrally, convex anteroposteriorly) incised into its lateral surface. The articular surface is oriented slightly posterior to a straight lateral orientation, and in natural articulation (with some movement) its orientation is much closer to posterior (Padian et al., 2021). The coracoid constitutes the majority of the glenoid, unlike in *A. lancicollis* and *M. minor* (McGowen et al., 2002:2; Averianov, 2010:293). A large and dorsoventrally elongate pneumatic foramen (bridge of Molnar and Wiffen, 1994, slender vertical ridge of Godfrey and Currie, 2005, or deep furrow and large canal opening of Averianov, 2010) pierces the medial surface of the glenoid in *Q. lawsoni*, which is widespread in pterosaurs. Damage to the anteromedial surface of TMM 42138-1 makes this foramen appear to pierce through the bone, but this is preservational. The other end of this pneumatic diverticulum is likely a pneumatic foramen on the other side of the glenoid just proximal to a large biceps tubercle, which is also widespread in pterosaurs. In TMM 41544-25, the posterior end of the articular surface terminates on a tubercle just lateral to the medial pneumatic foramen that may function as a bony stop; the morphology of the less well preserved specimens appear to confirm this structure. The anterior end of the articular surface reaches the anterior pneumatic foramen. TMM 42422-25 is unusual in having a circular opening in the middle of its glenoid. This is not natural and a similar opening is on the opposite side of the bone, and so this may represent a boring or puncture.

Scapula—The scapula is a dorsomedially curved bone with its distal end expanded for the glenoid. In *Q. lawsoni* and most pterosaurs, the scapula forms an elongate process (Fig. 28), unlike the stout and constricted shape found in the Lanceodontia (Andres,

2021). The lanceodontians have a distinct kink at this constriction, whereas the pteranodontians and *Haopterus gracilis* Wang and Lü, 2001, have essentially straight shafts, and the azhdarchoids and non-eupterodactyloids have a gentle curvature. In *Q. lawsoni*, the medial margin of the scapula ramus has a relatively gentle curve, whereas the lateral margin has more of an angular flexure due to a large supraglenoid tubercle (small inflation of dorsal margin of Cai and Wei, 1994, large tubercle for the origin of a muscle probably M. triceps brachii of Bennett, 2001a, or triceps tubercle of McGowen et al., 2002). This tubercle continues as a ridge distally for about 5 cm to contact the supraglenoid buttress as a thin ridge (sharp ridge of Averianov, 2010) flanked and excavated by a pair of small fossae on the dorsal surface of the buttress. Averianov (2010) reports a deep vertical groove in *A. lancicollis* and *Quetzalcoatlus*, but such a groove is not present in *Q. lawsoni*. The supraglenoid buttress contacts a vertically oriented ridge on the anterior surface that extends to the coracoid process/biceps tubercle (acromion of Molnar and Wiffen, 1994). The distal end is triangular in cross-section, flattening proximally to become a flat-topped semicircle on the scapular ramus, contrasting with the subcircular cross-section of *Pteranodon* (Bennett, 2001a:69). In *Q. lawsoni*, the proximal articulation with the notarium supraneural plate maintains this semicircular outline of the ramus. The articular surface is dorsoventrally depressed (elongate and compressed in the horizontal plane) and not significantly expanded, unlike the expanded suboval of the pteranodontoids (Andres, 2021). This matches closely the articular surface of *A. bostobensis* (Averianov, 2007:195, pl. 9, fig. 3) and possibly *A. lancicollis* (Bennett, 2001a:293), except that *A. bostobensis* appears to be more lacriform in outline. In medial view, there is a clockwise torsion of the scapula along the ramus in *Q. lawsoni*. There is an elongate tubercle on the anterior margin of the proximal end of the scapular ramus, best seen in TMM 42422-25.

Coracoid—The pterosaur coracoid is an elongate process articulating with the scapula and sternum. It has a broad shaft in the Eopterosauria but is narrow in *Q. lawsoni* and other macronychopterans (Andres, 2021). In *Q. lawsoni*, the coracoid traces a 90° arc along its length, transitioning from being vertical and laterally compressed to being horizontal and dorsoventrally depressed (Fig. 28). A much smoother and smaller curvature is found in *Pteranodon* (Bennett, 2001a:69, fig. 66–67). The distal end is triangular in cross-section at the glenoid in *Q. lawsoni*, as in the distal end of the scapula. The ventral glenoid lip on the coracoid (infraglenoid buttress of Averianov, 2010) does not curve around a depressed area, which was reported in *A. lancicollis* (Averianov, 2010:293). The coracoid process and biceps tubercle are combined into a single rounded blunt process, for the origin of M. biceps brachii (Bennett, 2001a:71). It is pierced on its dorsolateral surface by a pneumatic foramen. The coracoid has a massive ventral crest (sharp crest and cristiform projection of Molnar and Wiffen, 1994, ventrally directed flange of Bennett, 2001a, ventral flange of McGowen et al., 2002, or coracoid flange of Averianov, 2007) along most of its length and depth, present in azhdarchoids and pterodaustrins but modified into a broad tubercle within the dsungaripteromorphs (Andres, 2021). This crest protrudes ventrally as a large semicircle in outline that curves anteriorly, for the origin of the supracoracoideus (Bennett, 2001a). In *Q. lawsoni*, it terminates three-quarters down the length from the distal end, tapering in depth and width along its length. In total, the ventral crest takes up 58% of the coracoid length, only matched by *M. minor* (McGowen, 2002:figs. 2–3). The remaining proximal coracoid ramus is oval in cross-section, compared with the rhomboidal cross-section of *A. lancicollis* (Averianov, 2010:293). A ridge (flange of McGowen et al., 2002) extends along the posterior margin of the ramus, forming a dorsal groove in *Q. lawsoni*. This ridge terminates on the posterior margin of
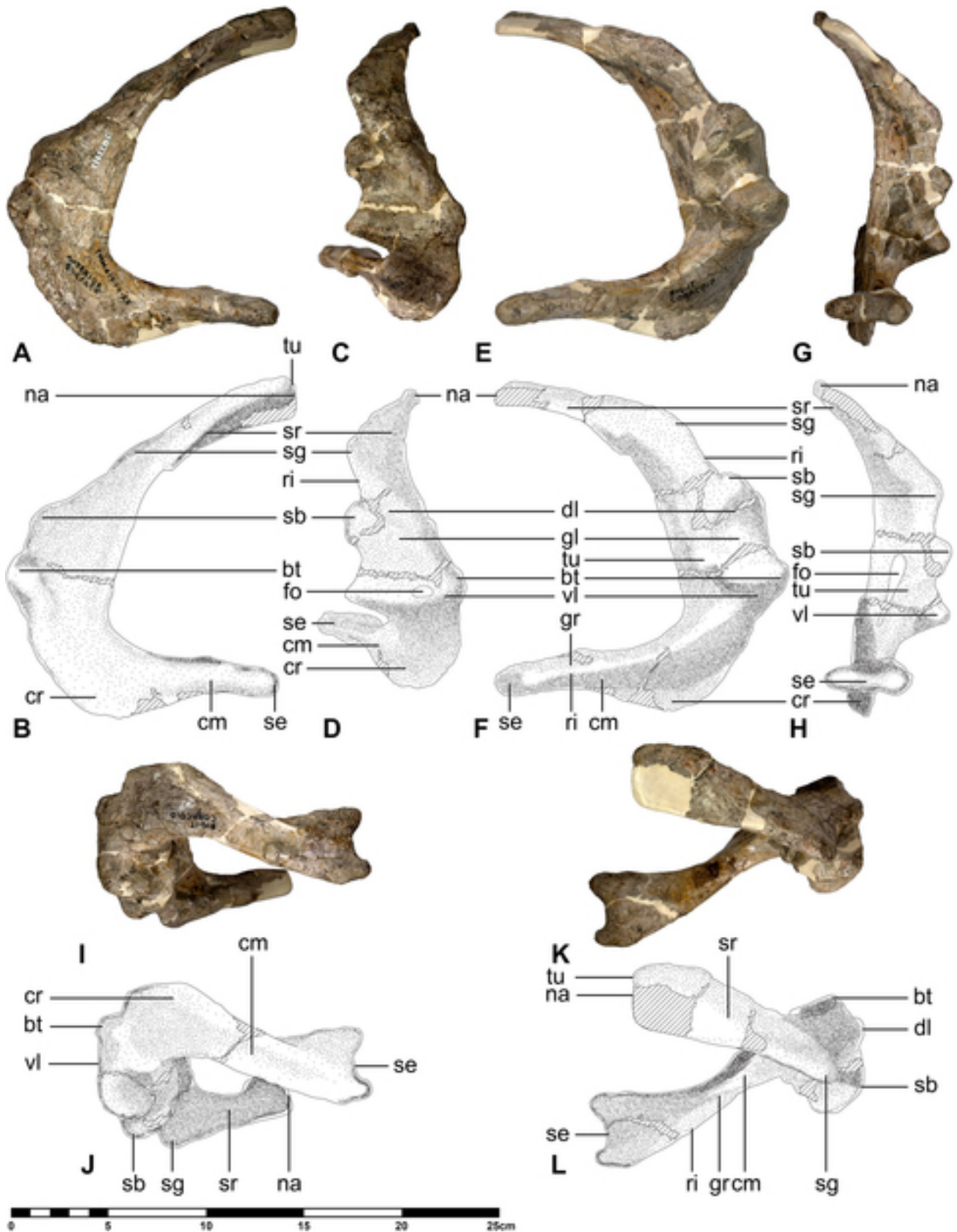
FIGURE 28. *Quetzalcoatlus lawsoni*, sp. nov., right scapulocoracoid (TMM 41544-25) in **A**, anterior photograph and **B**, line drawing; **C**, lateral photograph and **D**, line drawing; **E**, posterior photograph and **F**, line drawing; **G**, medial photograph and **H**, line drawing; **I**, ventral photograph and **J**, line drawing; and **K**, dorsal photograph and **L**, line drawing views. **Abbreviations: bt**, biceps tubercle; **cr**, crest; **cm**, coracoid ramus; **dl**, dorsal lip; **fo**, foramen; **gl**, glenoid; **gr**, groove; **na**, notarium articulation—**ri**, ridge; **sb**, supraglenoid buttress; **se**, sternum articulation; **sg**, supraglenoid tubercle; **sr**, scapula ramus; **tu**, tubercle; and **vl**, ventral lip. Diagonal lines represent plaster. Scale bar equals 25 cm.
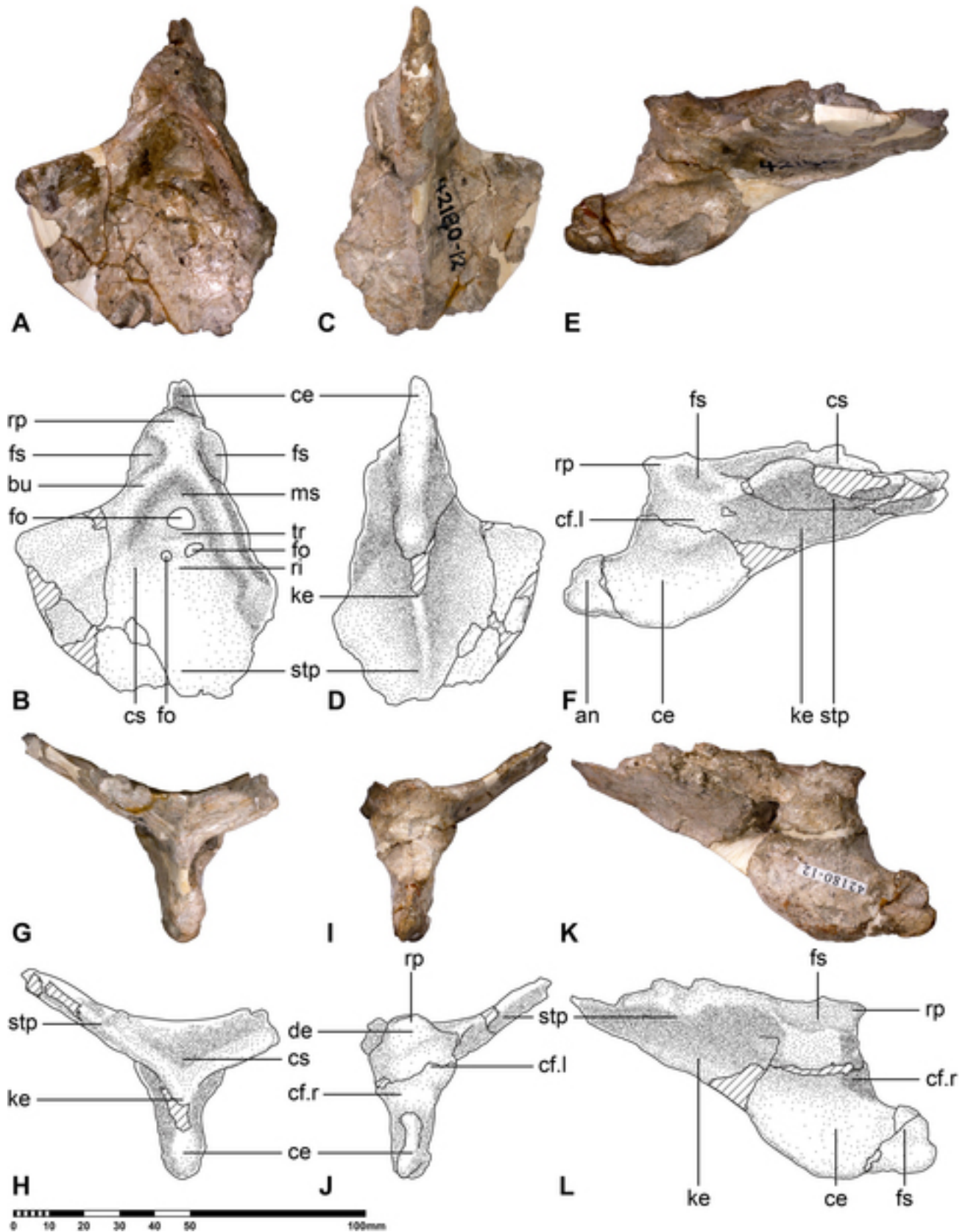
FIGURE 29. *Quetzalcoatlus lawsoni*, sp. nov., sternum (TMM 42180-12) in **A**, dorsal photograph and **B**, line drawing; **C**, ventral photograph and **D**, line drawing; **E**, left lateral photograph and **F**, line drawing; **G**, posterior photograph and **H**, line drawing; **I**, anterior photograph and **J**, line drawing; and **K**, right lateral photograph and **L**, line drawing views. **Abbreviations: an**, anterior process; **bu**, buttress; **ce**, cristospine; **cf**, coracoid facet; **cs**, concave surface; **de**, depression; **fo**, foramen; **fs**, fossa; **ke**, keel; **.l**, left element; **ms**, median fossa; **.r**, right element **ri**, ridge; **rp**, raised prominence; **stp**, sternal plate; and **tr**, transverse ridge. Diagonal lines represent plaster. Scale bar equals 100 mm.

the sternal articulation, and was a likely insertion for M. sternocoracoideus (Bennett, 2001a:71). This ridge and groove are reported in *A. lancicollis* except that the ridge is positioned dorsally and the groove anteriorly (Averianov, 2010:293, fig. 22E). The sternal articulation is only preserved in TMM 41544-25 and 42138-1.1. It is forked into two processes with a horizontal saddle-shaped articular surface between them (concave mediolaterally, convex dorsoventrally), a morphology that is widespread but variable in pterosaurs. In TMM 41544-25, the sternal articulation is a simple rounded and rugose crescent at the end of the ramus. In TMM 42138-1.1, the sternal articulation is smaller and twisted, likely due to damage caused by reverse telescoping of the proximal ramus in this specimen; its articular surface is distinct, with facets bordered by distinct ridges. The small nutrient foramina below the glenoid reported in *Pteranodon* (Bennett, 2001a:71, fig. 67) could not be located in *Q. lawsoni*.

Sternum—The sternum in pterosaurs is a broad plate with a large process on the anterior part of its ventral surface (the cristospine) and with articular facets for the coracoids on its dorsal surface where the cristospine contacts the plate. Three *Q. lawsoni* sternal fragments are known: TMM 42138-1.5 including the coracoid facets, base of cristospine, and an anteromedial portion of the left sternal plate; TMM 42180-12 including the undistorted anterior third of the sternum and cristospine (Fig. 29); and TMM 42422-29 including the coracoid facets as well as the anterior edge and left lateral edge of the sternal plate (Table 7). Sterna are preserved in the azhdarchid species *Z. linhaiensis* (Cai and Wei, 1994) and *A. lancicollis* (Averianov, 2010), as well as the azhdarchiform species *M. minor* (MOR 691).

TMM 42422-29 is the only sternal specimen that gives an idea of the entire shape of the sternal plate (posterior plate of Bennett, 2001a). It has straight anterolateral margins and a straight left posterolateral margin preserved with an approximate 120° angle between the two. If the entire plate continues this outline, it would be rhombic in outline. The sternal plate is thicker anteriorly, but there is no general thickening at the edges. At the contact between anterolateral and posterolateral margins, there is a slight dorsoventral thickening that reaches the lateral margin to form a small elliptical expansion, bounded posteriorly by a short emargination in the posterolateral margin; this is identified as a costal articulation. In the transverse plane, the sides of the sternal plate diverge dorsolaterally to form a V-shape. However, the angle of divergence of the sides of the sternal plate varies among specimens: TMM 42422-29 is about 150°, TMM 42180-12 is about 120°, and TMM 42138-1.5 is about 90°. TMM 42180-12 is the least distorted of these elements and seems to have the most accurate shape. This divergence of sternal sides turns the plate into a concave dish that deepens anteriorly toward the coracoid facets. At its deepest point is a large median fossa (large depression of Bennett, 2001a) pierced by a number of foramina. TMM 42180-12 preserves two pneumatic foramina and an incipient third foramen. A single foramen can be seen in TMM 42138-1.5 and 42422-1.5, but this does not preclude the presence of others. The anteriormost pneumatic foramen has a large funnel shape with a triangular outline. It is bounded posteriorly by a transverse ridge. A transverse ridge is also reported in *Pteranodon*, but it is anterior to the pneumatic foramen and immediately posterior to the coracoid facets instead (Bennett, 2001a:66, fig. 63A). Posterior to this ridge on the right side is a smaller elliptical pneumatic foramen in *Q. lawsoni*. Complementing it on the left side is a small fossa with a small circular foramen, which is also likely pneumatic. The two posterior foramina are separated by a low ridge that contacts the transverse ridge at a right angle.

The anterior edges of the sternal plate converge and rise medially as two large buttresses to form a raised knob-like prominence anterior to the median fossa. The anterior surface of the raised

TABLE 7. Measurements of *Quetzalcoatlus lawsoni*, sp. nov., pectoral girdle material. Values in millimeters. >, preserved value; <, maximum possible value; ~, approximate value; a-p, anteroposterior dimension; d-v, dorsoventral dimension; lat, lateral dimension; and p-d, proximodistal dimension. Holotype specimen in italics.

Coracoid

Specimen Number	Length (p-d)	Crest length (p-d)	Crest depth (d-v)	Ramus depth (d-v)	Ramus breadth (lat)
TMM 41544-25	151.76	87.10	36.54	17.37	17.30
TMM 41544-26	>60.16	—	—	—	—
TMM 41954-29	149.50	~88.28	31.07	14.91	19.08
TMM 42138-1.1	147.60	82.84	36.78	16.35	11.70
TMM 42180-9	>82.72	>35.99	>12.50	<31.42	<17.52
TMM 42180-10	>93.20	—	—	>25.76	18.55
TMM 42422-12	>133.22	93.49	30.57	33.71	16.87
TMM 42422-25	>80.57	>40.25	19.35	—	—

Scapula

Specimen Number	Length (p-d)	Ramus depth (p-d)	Ramus breadth (lat)	Glenoid height (d-v)	Glenoid breadth (lat)
TMM 41544-25	155.90	13.14	28.98	52.61	47.07
TMM 41544-26	>127.08	11.03	37.68	49.28	45.68
TMM 41954-29	—	—	—	47.34	44.07
TMM 42138-1.1	176.56	16.55	33.25	42.63	42.98
TMM 42180-9	>56.26	—	—	48.19	48.44
TMM 42180-10	>151.20	15.66	34.55	53.42	48.31
TMM 42422-12	>80.57	>40.25	19.35	—	—
TMM 42422-25	175.18	17.98	31.64	49.70	44.92

Sternum

Specimen Number	Plate length (a-p)	Plate width (lat)	Plate depth (d-v)	Cristospine length (a-p)	Cristospine depth (d-v)
TMM 42138-1.5	>38.82	>42.68	5.29	>53.09	34.61
TMM 42180-12	>61.52	>74.21	7.53	90.94	36.92
TMM 42422-29	>86.07	138.34	6.29	>20.29	>7.34

prominence has a concavity, and so the prominence and concavity may be homologous with the median tubercle and subtriangular depression posterior to the coracoid facets in *Pteranodon* (Bennett, 2001a:66, fig. 62). There is no constriction between the coracoid facets and sternal plate in *Q. lawsoni*, as in the other non-pteranodontoids (Andres, 2021), but the prominence is laterally excavated by a pair of fossae on its dorsal surface.

The cristospine is only complete in TMM 42180-12 and gives the entire sternum a Y-shaped cross-section in the transverse plane. The cristospine rises from the ventral margin of the sternal plate as a keel to become about twice as dorsoventrally deep as the lateral width of its base. At the level of the anterior margin of the plate, the cristospine expands ventrolaterally to accommodate the coracoid facets. The tip of the cristospine is a laterally compressed process that is rectangular in lateral view and extends anterior to the facets. The dorsal half of the tip is excavated by a fossa on its right side. Taken as a whole, the cristospine is a deep and stout anteriorly curving hook with vertically arranged coracoid facets, highly similar to the cristospines in *A. lancicollis* (Averianov, 2010:293, fig. 21C) and *M. minor* (MOR 691). Deep cristospines are present in the ornithocheiroids and a number of other pterosaur groups (Andres, 2021). Bennett (2001a) reports dorsal and ventral median ridges on the cristospine of *Pteranodon* anterior to the coracoid facets, but the anterior process of the cristospine in *Q. lawsoni* is so laterally compressed that it is not possible to ascertain if they are absent or if the entire process is just a pair of expanded dorsal and ventral median ridges.

The coracoid facets are positioned just anterior and ventral to the anterior margin of the sternal plate in *Q. lawsoni*. They are asymmetrically arranged (Bennett, 2001a) and stacked on top of one another, such that the right end of the left facet overlies the left end of the right facet along the midline. The left coracoid facet is also slightly anterior to the right facet. The facets are not positioned lateral to one another, a condition inherited from the Azhdarchoidea or possibly the Ornithocheiroidea (Andres, 2021). They overlap over about half of their width and about a third of their height. The left facet is slightly larger than the right, but both facets are saddle-shaped with a short concave outline in the sagittal plane and a longer convex outline in the horizontal plane. The articular surfaces are oriented anterolaterally. The left coracoid articular surface is a laterally tapering lacriform in outline, whereas the right articular surface is a scalene triangle because its anterior end extends onto the anterior process of the cristospine. The tubercles below the coracoid articulations for the sternocoracoid ligaments in *Pteranodon* (Bennett, 2001a:66, fig. 63B) could not be located in *Q. lawsoni*.

Forelimb

Every element of the upper arm, forearm, carpus, metacarpus, manual digits, and wing digit are preserved in *Q. lawsoni*. With the possible exception of the tips of a couple of manual unguals, all of these elements are represented by at least one complete bone. There are no traces of ossified tendons in the arm or the rest of the forelimb of *Q. lawsoni*, which have been found in the *A. byrdi* plus Nyctosauridae clade (Bennett, 2003:63; Frey et al., 2006:21; Andres and Myers, 2013:10–11, fig. 4). The forelimb bones are also the only elements that overlap between *Q. lawsoni* and the holotype of *Q. northropi* (TMM 41450-3). These forelimb bones are quite similar in the *Quetzalcoatlus* species, and so the following description is presented to distinguish them.

Humerus—The humerus is among the best represented elements in *Quetzalcoatlus* and one of the few found in both species. Twelve specimens are known from the *Q. lawsoni* material: TMM 42138-1.2 (Fig. 30) and 42422-18 are complete right humeri, TMM 42180-14.1 and 42422-23 are left humeri

missing their deltopectoral crests, TMM 41954-81 is a right humeral head, TMM 41544-9 and 41954-27 are left proximal ends, TMM 41954-26 and 63 as well as 42180-11 are right proximal ends, TMM 41546-6 is a dozen left shaft fragments, TMM 41544-10 is the right distal end, and TMM 41546-5 is four fragments (Table 8). The humerus has a middle attenuation like *Q. northropi*, but it is narrowed along a greater length of its shaft and reaches only three-quarters of the proximal width and half of the distal width. The humerus of *Q. lawsoni* does not approach the hourglass shape of *Q. northropi*; it is stout but not as stout as in *Q. northropi*. The humerus of *Q. lawsoni* is relatively small, at least as measured with respect to the dorsal vertebra length used here as a proxy for body size. Pterosaur humeri vary from about 6 to 18.5 times the length of a dorsal vertebra (Andres, 2021). *Quetzalcoatlus lawsoni* has a humerus to dorsal vertebra length ratio of 8.5, down from a plesiomorphic 11 for the Pterodactyloidea. This ratio is not known in *Q. northropi* because it lacks preserved dorsal vertebrae.

The articulation of the humerus with the scapulocoracoid is semicircular, saddle-shaped (concave anteroposteriorly, convex dorsoventrally), expanded anteriorly, lacking depressions and constrictions, and is dorsoventrally deep with a height only about half the width, roughly between *H. thambema* (Buffetaut et al., 2003:fig. 5) and *Q. northropi*. The humeral head is also less bowed dorsally (concave ventrally, convex dorsally) and so has a relatively smaller ventral concavity, but this concavity reaches past the distal margin of the deltopectoral crest to contact a slightly concave surface posterior to the rise between the deltopectoral crest and ulnar condyle. The humeral head is also positioned on the long axis of the humerus. There is a distinct crease between the articular surface and the dorsal surface, instead of the fossa pair in *Q. northropi*. The scapulocoracoid articular surface terminates anteriorly at the vertical flange, but there is no fossa on the posterior surface of the flange in the ventral concavity of the humeral head, such as found in *Q. northropi*. A pneumatic foramen is present on the ventral surface of the proximal end in this region, but it is exceedingly small, as in the azhdarchoid humerus CMN 50814 (Rodrigues et al., 2011:155, fig. 6A). No foramen is present on the dorsal surface of the proximal end, including the nutrient foramen found at the distal margin of the ulnar crest in *Q. northropi*.

Quetzalcoatlus lawsoni shares a ventrally curving, bulbous, and oblong ulnar crest reaching the proximal margin of the humerus and separated from the head by a constriction with *Q. northropi*, albeit less massive. The deltopectoral crest is likewise similar in both species and azhdarchids: large, elongate with a length greater than its base, rectangular in anterior/posterior view, positioned farther down the shaft, ventrally thickened but lacking a bulbous tip, and 'torted' such that it is more curved posteriorly at its ventrodistal corner. *Quetzalcoatlus lawsoni* differs from *Q. northropi* in having a slightly smaller and ventrally curved deltopectoral crest. The base of the crest extends down only 27% of the humerus length. The posterior aspect of the deltopectoral crest lacks both the midline ridge and proximal shelf of *Q. northropi*, but it does taper toward its margins with a raised rugose middle area, which may be the insertion for M. pectoralis (Bennett, 2001a:69–70).

The humeral shaft in *Q. lawsoni* is straight and constricted distal to the deltopectoral crest, but it is attenuated for a greater length of the shaft than *Q. northropi* before it expands distally to terminate in a rectangular distal cross-section. This shaft has a subcircular cross-section as in *Q. northropi* but with a flattened ventral margin. A low rise of bone also extends from the deltopectoral crest base to the ulnar condyle in both species, but it is paralleled by another low rise on the posterior margin of the ventral surface defining a slightly concave surface and forming the flattened ventral margin of the shaft in
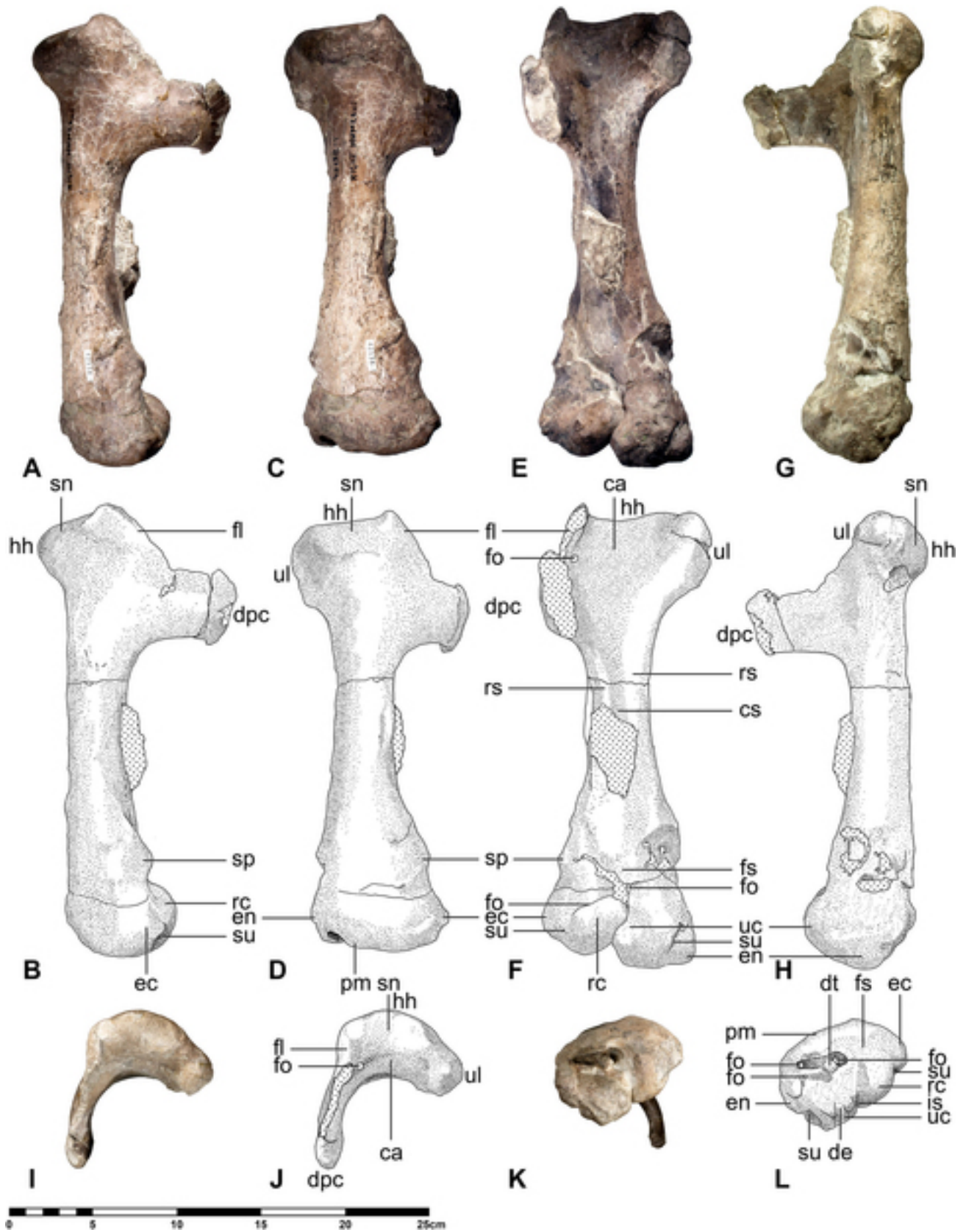
FIGURE 30. *Quetzalcoatlus lawsoni*, sp. nov., right humerus (TMM 42138-1.2) in **A**, anterior photograph and **B**, line drawing; **C**, dorsal photograph and **D**, line drawing; **E**, ventral photograph and **F**, line drawing; **G**, posterior photograph and **H**, line drawing; **I**, proximal photograph and **J**, line drawing; and **K**, distal photograph and **L**, line drawing. **Abbreviations: ca**, concavity; **cs**, concave surface; **de**, depression; **dpc**, deltopectoral crest; **dt**, distal tubercle; **ec**, ectepicondyle; **en**, entepicondyle; **fl**, flange; **fo**, foramen; **fs**, fossa; **hh**, humeral head; **is**, intercondylar sulcus; **pm**, prominence; **rc**, radial condyle; **rs**, rise; **sn**, scapulocoracoid articulation; **sp**, supracondylar process; **su**, sulcus; **uc**, ulnar condyle; and **ul**, ulnar crest. Dots represent matrix and/or damaged bone. Scale bar equals 25 cm.

TABLE 8. Measurements of *Quetzalcoatlus lawsoni*, sp. nov., humerus material. Values in millimeters. >, preserved value; <, maximum possible value; ~, approximate value; a-p, anteroposterior dimension; d-v, dorsoventral dimension; max, maximum dimension perpendicular to long axis of bone; min, minimum dimension perpendicular to long axis of bone; and p-d, proximodistal dimension.

Specimen Number: Dimension:	TMM 41544-9	TMM 41544-10	TMM 41546-5	TMM 41546-6	TMM 41954-26	TMM 41954-27	TMM 41954-63	TMM 41954-81	TMM 42138-1.2	TMM 42180-11	TMM 42180-14.1	TMM 42422-18	TMM 42422-23
Length (p-d)	>86.64	>84.24	>76.65	>113.10	>117.32	>107.68	>132.11	>35.46	227	>62.46	232	246	246
Mid-width (a-p)	38.69	—	>54.05	<58.04	44.51	48.26	51.11	—	35.30	33.17	35.78	37.40	40.00
Mid-depth (d-v)	25.32	—	21.88	30.22	34.90	34.93	42.91	—	34.24	16.37	32.45	26.39	30.17
Proximal articulation width (a-p)	52.47	—	—	>43.60	56.23	>43.43	53.00	61.44	59.66	>38.85	58.40	53.11	59.01
Proximal articulation depth (d-v)	34.99	—	—	>30.50	28.81	~33.23	25.92	35.12	33.26	>27.05	31.88	42.88	30.70
Deltopectoral crest base length (p-d)	56.31	—	—	>41.57	>49.68	64.44	89.30	—	58.07	52.71	54.41	64.34	69.17
Deltopectoral crest height (max)	61.36	—	—	>31.75	71.94	85.25	81.71	—	41.41	>45.13	>15.01	77.60	>16.60
Ulnar crest base length (p-d)	43.69	—	—	—	51.81	44.53	?	—	49.23	—	39.16	53.77	52.63
Ulnar crest height (max)	26.23	—	—	—	>10.28	—	?	—	23.60	—	28.76	25.70	27.16
Distal end width (max)	—	77.04	—	—	—	—	—	—	49.15	—	81.03	74.30	84.58
Distal end breadth (min)	—	33.26	—	—	—	—	—	—	53.71	—	54.87	59.44	56.63
Entepicondyle breadth (max)	—	10.68	—	—	—	—	—	—	12.24	—	15.08	?	21.24
Ectepicondyle breadth (max)	—	—	—	—	—	—	—	—	9.98	—	13.38	11.46	13.28

Q. lawsoni. The supracondylar process is a rounded knob. *Quetzalcoatlus lawsoni* has a relatively smaller triangular fossa proximal to the distal condyles that does not contact the supracondylar process or the lateral margins of the humerus, but it does still surround the radial condyle. A pneumatic foramen pierces the anteroproximal surface of the radial condyle and another is positioned proximal to the intercondylar sulcus in the triangular fossa, as in *Q. northropi*. The distal condyles are large but not to the extent of *Q. northropi*. The radial condyle is larger than the ulnar condyle, but both extend to about the same level proximally and distally, taking the anterior deflection of the distal end into account. The radial condyle is oval in outline with a flat distal surface like *Q. northropi*, but the ulnar condyle is anteroposteriorly expanded so that it is about the same size and subparallel to the radial condyle unlike *Q. northropi*. The ulnar condyle has a depression on its distal surface that may be comparable to the groove of *A. lancicollis* (Averianov, 2010:296). There is no anterior fovea exclusive of the triangular fossa. The ent- and ectepicondyles have raised prominences on the dorsal and ventral surfaces of the distal end separated by sulci from the condyles to create distinct epicondylar ridges. The entepicondyle is bump-like and positioned on the posterior corner of the distal end as in *Q. northropi* and *A. lancicollis* (Averianov, 2010:297, fig. 24). The ectepicondyle is significantly larger than the entepicondyle as in most pterosaurs, but not in *Q. northropi* (Andres, 2021). It does terminate in a proximally-curving hook like *Q. northropi*. The posterior surface of the distal end lacks a deep longitudinal groove.

The distal surface of the humerus in *Q. lawsoni* is best seen in TMM 42138-1.2 (Fig. 30). It is torsioned 45° and has a rectangular outline like *Q. northropi* and most azhdarchoids. A posterior prominence extends over the width of the distal surface, much shorter than the equivalent in *Q. northropi*. The radial condyle dominates the anterodorsal corner of the distal surface, the ulnar condyle constitutes the anteroventral corner of the distal surface, and the posterodorsal portion is taken up by an oblong distal fossa. The intercondylar sulcus extends to the distal surface to contact this fossa as in *M. minor* (McGowen et al., 2002:6). A prominent distal tubercle rises from the middle of the distal surface. It is connected to the ulnar condyle and entepicondyle by anterior and ventral crests of bone, respectively, that divide the posteroventral portion of the distal surface into a smaller ventral opening and a larger dorsal elliptical opening. One of these elliptical openings is likely homologous to the distal transverse groove found in *R. langstoni* (Murry et al., 1991:167, fig. 2–4) and *M. minor* (McGowen et al., 2002:6). The ventral elliptical opening in *Q. lawsoni* shares a pneumatic foramen at its posterior end with the distal transverse groove of *R. langstoni* (Andres and Myers, 2013:390, fig. 3F) and *M. minor* (McGowen et al., 2002:6); the position and orientation are the same in *Q. lawsoni* and *R. langstoni* (Andres and Myers, 2013:fig. 3F). The transverse groove extends more dorsally to contact the radial condyle in *M. minor* (McGowen et al., 2002: fig. 1), and so its distal transverse groove may be homologous with the dorsal elliptical opening in *Q. lawsoni*. The dorsal elliptical opening is deeper than the ventral opening and appears to have two pneumatic foramina flanking the distal tubercle. *Azhdarcho lancicollis* lacks a distal transverse groove but does have a thin constriction of the distal fossa and numerous posteriorly positioned small foramina (Averianov, 2010:297, fig. 24C). These openings have been filled with plaster in the holotype of *Q. northropi* if they are preserved at all, and the area covered could accommodate all of these grooves or openings. Distal surface pneumatic foramina are present in azhdarchiforms and lanceodontians (Andres, 2021); a distal surface pneumatic fossa/foramen has been reported in *T. regalis* (Longrich et al., 2018:9, fig. 2) and *Alcione elainus* Longrich et al,. 2018 (Longrich et al., 2018:13) but these are just part of the distal fossa. The

humerus distal epiphyses appear to be fused in all specimens of *Q. lawsoni*.

Ulna—The ulna of *Q. lawsoni* is a much more cylindrical bone with less expanded ends than *Q. northropi*. It rapidly tapers distal to the proximal end, and it gradually expands starting at a point two-thirds down the shaft. This is a rather robust shaft. It is about half the width and about 60% of the height of the proximal and distal ends, which is much less of a constriction than in *Q. northropi* but still rather attenuated among pterosaurs. The terminal expansions are predominantly ventral. The entire ulna is essentially straight in the transverse plane, but it has a slight anterior expansion proximally and a slight posterior expansion/deflection distally in the horizontal plane. This ulna is also relatively longer than in *Q. northropi*, with a relative length about one-and-a-half times the humerus length on average, roughly the same as the other azhdarchiforms. Complete ulnae include TMM 42180-14.3 and 42422-13 from the left as well as TMM 42138-1.3 from the right side (Fig. 31). The TMM 41544-11 right ulna has a small portion of the shaft removed for sectioning and replaced with a plaster cast, but it is otherwise complete. TMM 41954-36 is a left ulna proximal end. TMM 41544-24 and 41954-4 are left and 41954-55 and 67 are right ulnae missing their proximal ends. Finally, TMM 41961-1.8 and 42422-26 are distal left ulnae, and TMM 45997-1.5 is a distal right ulna end (Table 9).

The proximal end of the ulna in *Q. lawsoni* has a similar cross-section to the semicircular cross-section of *Q. northropi* but more crescentic. The dorsal cotyle forms a dorsal process, but the dorsal expansion as a whole is smaller than the ventral expansion. The dorsal cotyle is a dorsoanteriorly oriented hook-shape and is projected above the shaft, but not to the degree found in *Q. northropi*. Its articular surface is oriented proximoanteriorly, is saddle-shaped (concave dorsoventrally, convex anteroposteriorly) as in *A. lancicollis* (Averianov, 2010:298) and *C. boreas* (Godfrey and Currie, 2005:302), and only appears to have a distinct lip in TMM 42138-1.3 where it is best preserved. The dorsal and ventral cotyle slightly overlap vertically, unlike *Q. northropi*, with the dorsal articular surface anterior to the ventral articular surface. The intercotylar crest is the coalesced borders of the cotyles on the anterior surface of the ulna and forms a knob-like protuberance on the proximal surface. The ventral cotyle is approximately the same size as the dorsal cotyle, concave like the ulna cotyles of *Q. northropi*, and lacriform in outline with a ridge-like proximal prominence that contacts the intercotylar ridge. This prominence was reported in TMM 42138-1.3 as a small tubercle and suggested to be a bony stop for hyperextension by McGowen et al. (2002). The ventral cotyle projects more anteriorly to the shaft with an anteroproximally oriented articular surface. A pneumatic foramen is present on the proximal surface of the ulna posterior to the intercotylar crest, in a similar position to a pneumatic foramen reported in *A. piscator* (Kellner and Tomida, 2000:56, fig. 34). Posterior to the foramen and ventral cotyle prominence is an oblong fossa in *Q. lawsoni*. A tuberosity on the posterior margin of the proximal end is identified as the olecranon. It does not project posteriorly, and so the proximal cross-section is semicircular in outline like *Q. northropi*. In TMM 42138-1.3, there appears to be a process dorsal to the identified olecranon, but this shape is exacerbated by damage to the dorsal cotyle. In other specimens (e.g., TMM 42422-13), it is more similar to the eminence described in *Q. northropi* and is so termed here. There are no traces of separate ulnar epiphyses in *Q. lawsoni*.

A pneumatic foramen is present between the cotyles on the anterior surface of the proximal ulna (contra Bennett, 2001a, and Averianov, 2010), as reported in numerous ornithocheiroids (Wild, 1990:fig. 4; Bennett and Long, 1991:437, fig. 3; Kellner and Tomida, 2000:57–58; Bennett, 2001a:76–79; McGowen et al., 2002:7, fig. 2; Godfrey and Currie, 2005:303, fig. 16.7; Averianov,

TABLE 9. Measurements of *Quetzalcoatlus lawsoni*, sp. nov., forearm material. Values in millimeters. >, preserved value; <, maximum value; a-p, anteroposterior dimension; d-v, dorsoventral dimension; and p-d, proximodistal dimension. Holotype specimen in italics.

Dimension: Element: Specimen Number:	Length (p-d)	Mid-width (d-v)	Mid-breadth (a-p)
Ulna			
TMM 41544-11	>344	33.92	19.87
TMM 41544-24	>351	33.77	20.32
TMM 41954-4	>74.62	36.99	29.74
TMM 41954-36	>100.35	<45.95	18.14
TMM 41954-55	>188.42	30.71	15.26
TMM 41954-67	>241	31.82	15.82
TMM 41961-1.8	>91.76	<56.07	<26.86
TMM 42138-1.3	380	32.99	25.93
TMM 42180-14.3	360	81.90	32.73
TMM 42422-13	363	34.22	22.17
TMM 42422-26	>68.89	<48.51	23.18
TMM 45997-1.5	>77.41	<85.97	>10.10
Radius			
TMM 41544-28	>224	19.70	11.93
TMM 41954-20	>114.87	31.22	10.45
TMM 41954-33	>310	28.73	14.14
TMM 41954-52	367	21.11	9.31
TMM 41954-85	>226	22.99	13.20
TMM 42138-1.4	>80.96	23.32	16.06
TMM 42180-14.2	341	19.82	11.23
TMM 42422-1	360	18.66	16.09
TMM 45997-1.4	>61.67	<50.51	18.72

2010:298; Eck et al., 2011:287). It has a proximoventrally/distodorsally oriented elliptical outline in TMM 42138-1.3 and 42422-13 but is circular in TMM 41544-11 and 42180-14.3, and it may be two foramina in TMM 42422-13 (and possibly 42138-1.3). Variable numbers of foramina in this region have been reported in *Pteranodon* (Bennett, 2001a:76, figs. 74–75) and *A. lancicollis* (Averianov, 2010:298). Distal to the dorsal cotyle is a concave surface for articulation with the radius proximal end. This concave surface terminates distally at a rugose elliptical tubercle, which may be an attachment for a radioulnar ligament (Bennett, 2001a:76). Ventral to this tubercle and distal to the ventral cotyle on the ulna anterior surface is the larger oval biceps tubercle. Dalla Vecchia (2014) identified a 'C-shaped groove' in this region, which likely corresponds to a slightly rugose muscle scar surrounding the biceps tubercle in some *Pteranodon* specimens (Bennett, 2001a:76). A thin corrugated ridge extends distally from just dorsal to the biceps tubercle along the ventral half of the anterior surface of the ulna, and may be an attachment for an interosseus membrane (Bennett, 2001a:76). A longitudinal ridge on the anterior surface of the ulna is present in azhdarchoids and istiodactylids (Andres, 2021), but in the latter the ridge is identified as a platform for the radius and an insertion for the biceps brachii (Bennett, 2001a:78). The nutrient foramina described in *Pteranodon* distal to the biceps tubercle and on the proximal ventral expansion (Bennett, 2001a:76) are not preserved in *Q. lawsoni*. There is no trace of a groove on the proximal end of the anterior surface of the shaft, which has been reported in *E. rosenfeldi* (Dalla Vecchia, 2009:167).

The shaft of the ulna is straight and parallel-sided up to its midpoint in *Q. lawsoni*. Specimens have a vertically oriented oval shaft cross-section as in most pterosaurs, except for TMM 42138-1.3 that has a more subcircular cross-section. *Quetzalcoatlus lawsoni* has a smaller ventral expansion than *Q. northropi* on the ulna distal end, which expands gradually over the distal half of the ulna length in *Q. lawsoni*. The ventral tubercle on the ventral expansion of the ulna distal end present in *Q. northropi* and *A. lancicollis* (Averianov, 2010:fig.

FIGURE 31. *Quetzalcoatlus lawsoni*, sp. nov., right ulna (TMM 42138-1.3) in **A**, anterior photograph and **B**, line drawing; **C**, ventral photograph and **D**, line drawing; **E**, posterior photograph and **F**, line drawing; **G**, dorsal photograph and **H**, line drawing; **I**, proximal photograph and **J**, line drawing; and **K**, posterior photograph and **L**, line drawing views. **Abbreviations: bt**, biceps tubercle; **cr**, crest; **cs**, concave surface; **da**, dorsal articular surface; **do**, dorsal cotyle; **du**, distal tuberculum; **em**, eminence; **fg**, flexor tendon groove; **fo**, foramen; **fs**, fossa; **fv**, fovea; **ic**, intercotylar crest; **ol**, olecranon; **pm**, prominence; **pr**, process; **ri**, ridge; **rs**, rise; **sl**, styloid prominence; **su**, sulcus; **tu**, tubercle; **ve**, ventral expansion; and **vo**, ventral cotyle. Dots represent matrix and/or damaged bone. Scale bar equals 25 cm.

25) is less distinct in *Q. lawsoni*. The nutrient foramina reported on the dorsal surface of the distal end in *M. minor* are not observed in *Q. lawsoni*. The anterior surface of the ventral expansion is concave for articulation with the radius and the posterior surface is convex, giving the entire distal surface a question-mark shape with the posteriorly projected dorsal articular surface forming the crook of that punctuation. This distal outline has a dorsal emargination of the posterior surface and a ventral emargination of the anterior surface, but these do not continue proximally as sulci as in *Q. northropi* but instead contact concave surfaces. There does not appear to be a notch in the outline of the distal end in anterior/posterior view, which is found in *Q. northropi*. The posterior circular facet of *I. latidens* (Hooley, 1913:388, pl. XXXIX, fig. 6) is also absent. The flexor tendon groove is present on the dorsal half of the anterior surface of the distal end and is bounded by the dorsal crest and ventral rugose ridge in *Q. lawsoni*. Although the position and size are variable, there appears to be a pneumatic foramen in the middle of the distal end posterior surface, as also reported in *A. lancicollis* (Averianov, 2010:298–300), *M. minor* (McGowen et al., 2002:7), *T. wellnhoferi* (Eck et al., 2011:fig. 7, pl. 2), *Pteranodon* (Bennett, 2001a:77, fig. 76), and BSPG 1982 I 89 (Wellnhofer, 1985:fig. 8). There is possibly another foramen on the anterior surface of the distal end in some of these specimens, as has been reported in BSPG 1982 I 89 (Wellnhofer, 1985:fig. 9), but none are preserved well enough to be identified here as such.

Quetzalcoatlus lawsoni has the three distal articular surfaces of other pterosaurs: the dorsal articular surface, distal tuberculum, and ventral fovea. The dorsal articular surface is semicircular in distal view. It does not reach the anterior surface but does extend more onto the posterior surface to contact a rise of bone extending along the dorsal half of the ulna posterior surface. The distal tuberculum is a large round knob that contacts both anterior and posterior surfaces on the ventral half of the distal end. The ventral fovea is posteriorly positioned on the distal surface and slightly excavates the distal tuberculum; it is elliptical to circular in outline. The styloid prominence extends distally ventral to these articular surfaces.

Radius—The radius of *Q. lawsoni* is similar to the ulna, a straight cylindrical bone with an abrupt expansion of the proximal end and a parallel-sided shaft that gradually expands over the distal half of its length. Complete left radii are known in TMM 42180-14.2 and 42422-1 (Fig. 32), a complete right radius in TMM 41954-52, a left crushed proximal end in TMM 41954-20, a right proximal end in TMM 42138-1.4, a left radius missing the proximal end in TMM 41954-33, a right radius distal half in TMM 41544-28 and 41954-85, and a right distal end in TMM 41544-28 for *Q. lawsoni* (Table 9). There is a modest expansion to the distal ends: the shaft is about 40% the width of the ends and 70% of their heights, more than in *Q. northropi* but less than in *A. lancicollis* (Averianov, 2010:300). The radius midsection width is about 68% of the ulna mid-width, less than the azhdarchid and pterosaur average of 75% and much less than the 81% of *Q. northropi* (Andres, 2021).

The proximal end of the radius has a boot-shaped outline in the anterior/posterior view due to its dorsal expansion, as in other pterosaurs (Andres, 2010). A rugose tubercle is present on the anterior surface of the dorsal expansion, and another tubercle is present on the anterior surface of the ventral end. The posterior aspect of the proximal radius is a concave surface, unlike the flatter surface found in *Q. northropi*. Some specimens have a small tubercle in the middle of the posterior rim of the proximal cotyle, but all *Quetzalcoatlus* specimens have at least some convexity here. This proximal cotyle expands ventrally, forming a lacriform outline for the articular surface and entire proximal surface, as in *A. lancicollis* (Averianov, 2010:300) but unlike the oval cotyle of *Pteranodon* (Bennett, 2001a:79), semi-lunar articular face of

A. primordius Frey et al. (2011), or concave ellipse of YPM VPPU 002246 (Padian and Smith, 1992:89). The cotyle is positioned more posteriorly on the ventral three-quarters of the proximal surface with a more distinct anterior rim, because the radial condyle of the humerus is shared between the radius cotyle and the dorsal cotyle of the ulna (Andres, 2010). It reaches the ventral margin of the radius, unlike *S. wucaiwanensis* (Andres, 2010:176). Bennett (2001a) reported but did not figure a second articular surface on the anterior surface of the dorsal expansion in *Pteranodon* for articulation with the humerus radial condyle during extension (Bennett, 2001a:79), and Averianov (2010) labeled such an articular surface in *A. lancicollis*. There is no obvious second articular surface on the proximal radius in *Q. lawsoni*, but there is a slightly concave area dorsal to the tubercle on the dorsal expansion that would correspond to the surface labeled in *A. lancicollis*. The dorsal expansion continues distally as a thin ridge, as *A. lancicollis* (Averianov, 2010:300) and *Q. northropi*. There is no trace of a proximal epiphysis, as suggested to be present in *E. rosenfeldi* (Dalla Vecchia, 2009:167).

A small crest is positioned on the ventral margin of the radius proximal half, found in *A. lancicollis* (Averianov, 2010:fig. 26A–B) and in *Q. northropi*. Also shared by the *Quetzalcoatlus* species, three tiny rugose ridges extend distally from the ventral crest to a third of the way down the shaft in TMM 41954-52 and 42422-1: one along the ventral end of the anterior surface, one along the ventral surface, and one along the ventral end of the posterior surface. These may correspond to the U-shaped muscle scar in this region of *Pteranodon* (Bennett, 2001a:79). There is about 33° of counterclockwise torsion along the radius shaft. This shaft has a vertical oval cross-section as in *A. lancicollis* (Averianov, 2010:300), *T. wellnhoferi* (Eck et al., 2011:287), and BSPG 1966 XXV 507 (Martill and Moser, 2017:166), but unlike the subcircular cross-section of *Q. northropi*.

The dorsal expansion of the distal end is not as distinct a process as the proximal expansion, and the shaft appears to widen more ventrally over the distal third of the shaft. A ridge on the anterior surface of the shaft extends over this distance to contact the anterior tuberosity on the ventral half of the distal end. This anterior tuberosity is much smaller than the anterior crest of *Q. northropi*, with the possible exception of TMM 41544-28 in which it seems to form a crest. This produces a distal cross-section that is a right triangle in outline, as found in other azhdarchoids (Andres, 2021). The anterior surface of the distal end has a midline sulcus bounded ventrally by the anterior tuberosity and dorsally by a small tubercle, as in *Q. northropi*. There is no apparent sulcus dorsal to this tubercle. The posterior surface of the distal end is flat, becoming slightly concave at its extremity, but it lacks a depression or a bony stop in this region. There are two articular surfaces on the distal surface of the radius. The dorsal articular surface is oval in outline and constitutes two-thirds of the distal end. The ventral articular surface is small and subtriangular, different from the subcircular ventral articular surface reported in *Pteranodon* (Bennett, 2001a:79). In *Q. lawsoni*, it extends onto the posterior surface as a tubercle, as reported in *A. lancicollis* (Averianov, 2010:300), YPM VPPU 002246 (Padian and Smith, 1992:89–90) and *A. primordius* (Frey et al., 2011:S45), but it does not continue proximally as a crest as in *Q. northropi*. The ventral articular surface also does not contact the anterior tuberosity, as found in *A. lancicollis* (Averianov, 2010:300). A small foramen is present on the distal end of the posterior surface that may be a nutrient foramen, but it is in a position where pneumatic foramina are reported in azhdarchids (Nesov, 1984:pl. VII, fig. 8b; McGowen et al., 2002) and *Pteranodon* (Bennett, 2001a:79–80, fig. 75B). *Montanazhdarcho minor* has both nutrient foramina and a pneumatic foramen identified in this area (McGowen et al., 2002:7, fig. 2D). The distal margin of the radius in *Q. lawsoni* is convex in anterior/posterior view, described as a slight ridge on the distal face in YPM VPPU 002246 (Padian, 1984a:518).
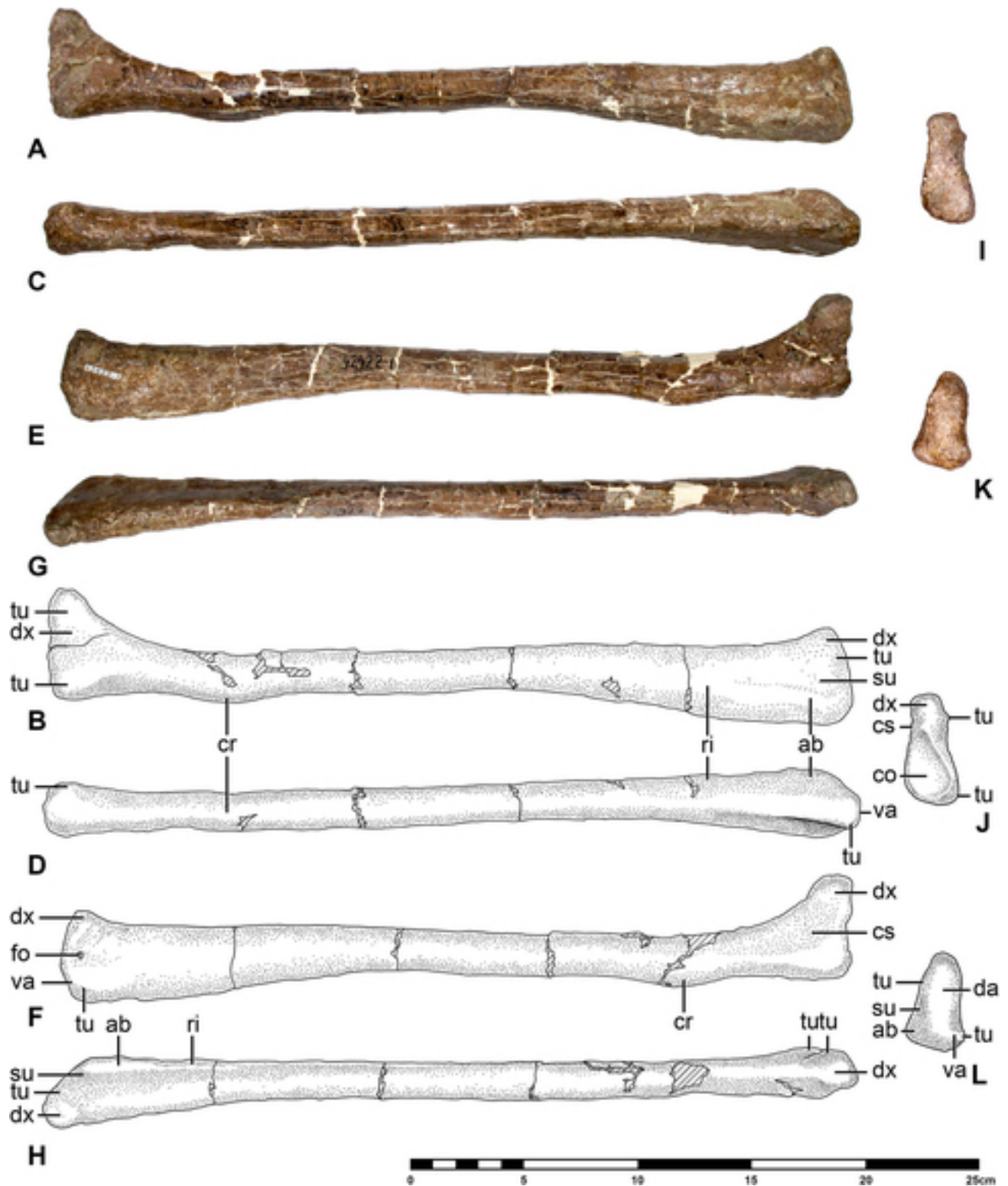
FIGURE 32. *Quetzalcoatlus lawsoni*, sp. nov., left radius (TMM 42422-1) in **A**, anterior photograph and **B**, line drawing; **C**, ventral photograph and **D**, line drawing; **E**, posterior photograph and **F**, line drawing; **G**, dorsal photograph and **H**, line drawing; **I**, proximal photograph and **J**, line drawing; and **K**, distal photograph and **L**, line drawing views. **Abbreviations: ab**, anterior tuberosity; **co**, cotyle; **cr**, crest; **cs**, concave surface; **da**, dorsal articular surface; **dx**, dorsal expansion; **fo**, foramen; **ri**, ridge; **su**, sulcus; **tu**, tubercle; and **va**, ventral articular surface. Diagonal lines represent plaster. Scale bar equals 25 cm.

Carpus

Quetzalcoatlus lawsoni has the typical pterosaur condition of interlocking proximal and distal syncarpals formed from the fusion of two proximal series and three distal series carpals, respectively, a medial carpal from the distal series that articulates with the anterior surface of the distal syncarpal, a sesamoid that articulates in the fovea of the medial carpal (Bennett, 2001a), and the pteroid that articulates with the anterior surface of the medial carpal. No trace of the original carpals or their sutures are visible in the *Quetzalcoatlus* material. Proximal and distal syncarpals are articulated but poorly preserved in TMM 42180-14. TMM 45997-1 is the only specimen in which the carpals are significantly distorted, but these elements also appear to be somewhat smaller than in other *Q. lawsoni* specimens, and so this may reflect a less mature individual. TMM 419544-43 and 48, 41961-1.9 and 1.10, 42180-6 and 8, 42422-3 and 4, and 42246-1 and 2 are proximal and distal syncarpals with separate specimen numbers but that articulate and likely came from the same individuals.

Proximal Syncarpal—In *Q. lawsoni*, left proximal syncarpals are the specimens TMM 41954-34, 42180-14.12, and 42422-4 (Fig. 33); and right proximal syncarpals are the specimens TMM 41545-1, 41954-48, 41954-74, 41961-1.9, 42180-8, 42246-2, and 45997-1.6. These bones are well preserved, with the exception of the incomplete TMM 41954-74 as well as the proximodistally crushed TMM 41954-34 and 48. These are wider syncarpals than in *Q. northropi* with widths about twice the length and height (Table 10).

The proximal view of the proximal syncarpal has a trapezoidal outline in *Q. lawsoni* and almost entirely consists of articular surfaces: three ulnar and two radial. The two surfaces that are not articular are pneumatic: a large deep circular foramen (small concavity of Hooley, 1913, or pneumatic foramen in volcano-shaped pit of McGowen et al., 2002) is positioned ventral to the dorsal radial articular facet, posterior to the ventral radius articular facet, and anterior to the ulnar fovea; and a smaller reniform foramen is positioned in a small triangular surface ventral to the border between the ulnar dorsal articular facet and fovea. Both of these pneumatic surfaces contact sulci that extend ventrally onto the proximal syncarpal ventral surface to contact anterior and posterior notches, which are presumably for the passage of the wing digit extensor and flexor tendons, respectively (Bennett, 2001b, 2008). The posterior-most sulcus does contact the flexor tendon groove on the ventral surface, but it does not extend dorsally on the proximal surface as a vertical groove as described in *A. byrdi* (Andres and Myers, 2013:393, fig. 4G) and figured in *Pteranodon* (Bennett, 2001a: fig. 79D). The dorsal ulnar articular facet is the largest articular surface, taking up most of the height and the posterior third of the proximal surface in *Q. lawsoni*. It is a dorsodistally/ventroproximally inclined concave surface that is semicircular in outline and terminates proximally in a prominence at the posteroventral corner of the proximal surface in a similar manner as described for *I. latidens* (Hooley, 1913:389). The articular surface on this prominence would have articulated with the posterior extension of the ulna dorsal articular surface. The ulnar fovea contacts both the dorsal articular facet and tuberculum for the ulna without demarcations, and it also contacts the dorsal radial articular facet with a high ridge, as in *A. lancicollis* (Averianov, 2010:302). This fovea is a circular concavity positioned in the middle of the ventral half of the proximal syncarpal. The ulnar tuberculum is a subspherical knob of bone on the ventral margin of the proximal surface a third of the distance from the anterior margin. The dorsal and ventral radial articular facets constitute the anterior half of the dorsal margin and the anterior margin of the proximal syncarpal proximal surface, respectively. They contact one another and form an L-shape without a ridge between the two, as in *Q. northropi*.

One or two pneumatic foramina divide the radial articular facets in *Pteranodon* (Bennett, 2001a:81, fig. 79C), but the two foramina in *A. piscator* (Kellner and Tomida, 2000:fig. 36a–b) as well as the circular foramen in *M. minor* (McGowen et al., 2002:7) and *Q. lawsoni* lie adjacent to these facets without dividing them. *Montanazhdarcho minor* is figured with two pneumatic foramina on the proximal surface, but the other foramen is located near the contact between the dorsal ulnar and radial articular facets (McGowen et al., 2002:fig. 3F). The dorsal articular facet is deeply concave in *Q. lawsoni*, unlike *Pteranodon* (Bennett, 2001a:81–82) and *Q. northropi*, with a distinct rim that becomes a flange between the cotyle and ulnar fovea. The ventral radial articular facet is triangular in outline, does not have a distinct rim, and is positioned on the edge of the proximal and anterior surfaces.

The dorsal surface of the proximal syncarpal is confined to the anterior two-thirds of the proximal syncarpal and is inclined anteroventrally in *Q. lawsoni*. There is a shallow proximodistal sulcus in the middle of the dorsal aspect, as in *Q. northropi*, that is likely for M. extensor carpi radialis (Bennett, 2001b:fig. 121). Unlike *Q. northropi*, it is bounded by rugose tubercles instead of flanges but still likely anchored a retinaculum. Preservation in this region makes it difficult to determine if another tubercle was present in the sulcus, as found in *Q. northropi*. In TMM 41545-1, there are two foramina posterior to the dorsal sulcus. This area is not well preserved in all *Q. lawsoni* specimens, and so these foramina may have been present in the entire species. In anterodorsal view, the dorsal surface is a trapezoid that is a mirror image of the proximal surface. The proximal margin of the dorsal surface is the dorsal rim of the dorsal radial facet; the distal margin is the dorsal rim of the dorsal intersyncarpal articular facet; the posterior margin is the dorsal groove; and the anterior end is the anterior process (blunt process of Andres and Ji, 2008). This anterior process has two tubercles at its anterodistal corner. The more posterodistal of the two is the distal tuberculum, and the more anteroproximal is a tubercle on the distal extremity of the anterior surface. A large foramen in the middle of the dorsal surface of the proximal syncarpal appears to contain the three neurovascular openings reported in *A. lancicollis* (Averianov, 2010:302), and so these openings may be present in more specimens but hidden by matrix infilling the foramen.

The anterior surface is a relatively small, subhorizontal, and ventrally convex semicircle in outline in *Q. lawsoni*. The proximal margin is the ventral radial articular facet, and the anterior end is a tubercle anteroproximal to the distal tuberculum.

The ventral surface of the proximal syncarpal is divided into anterior and posterior sections by an emargination formed by the ventral intersyncarpal articular facet in *Q. lawsoni*. The anterior section is the ventral aspect of the anterior process. It is perforated in its middle by a pneumatic foramen and possibly some nutrient foramina. The ventral sulcus from the large circular proximal foramen is present on the proximal end, and the distal tuberculum is present on the distal end of the anterior process. The distal tuberculum is separated from a distal process at the anterior end of the dorsal intersyncarpal articular facet by a notch formed by a sulcus. The posterior section of the ventral surface is a triangle in outline, with most of its area consisting of a proximodistal flexor tendon groove connecting with the ventral sulcus from the small reniform proximal foramen. This groove is likely for the wing digit flexor, bounded by rugose ridges likely for the attachment of a retinaculum.

The posterior surface of the proximal syncarpal is an inverted comma-shape in outline due to the rounded margin of the wing flexor tendon groove and a posterior process formed by the posterior end of the ventral intersyncarpal articular facet in *Q. lawsoni*. A foramen on the posterior surface of the proximal syncarpal is reported in *D. banthensis* (Padian and Wild,
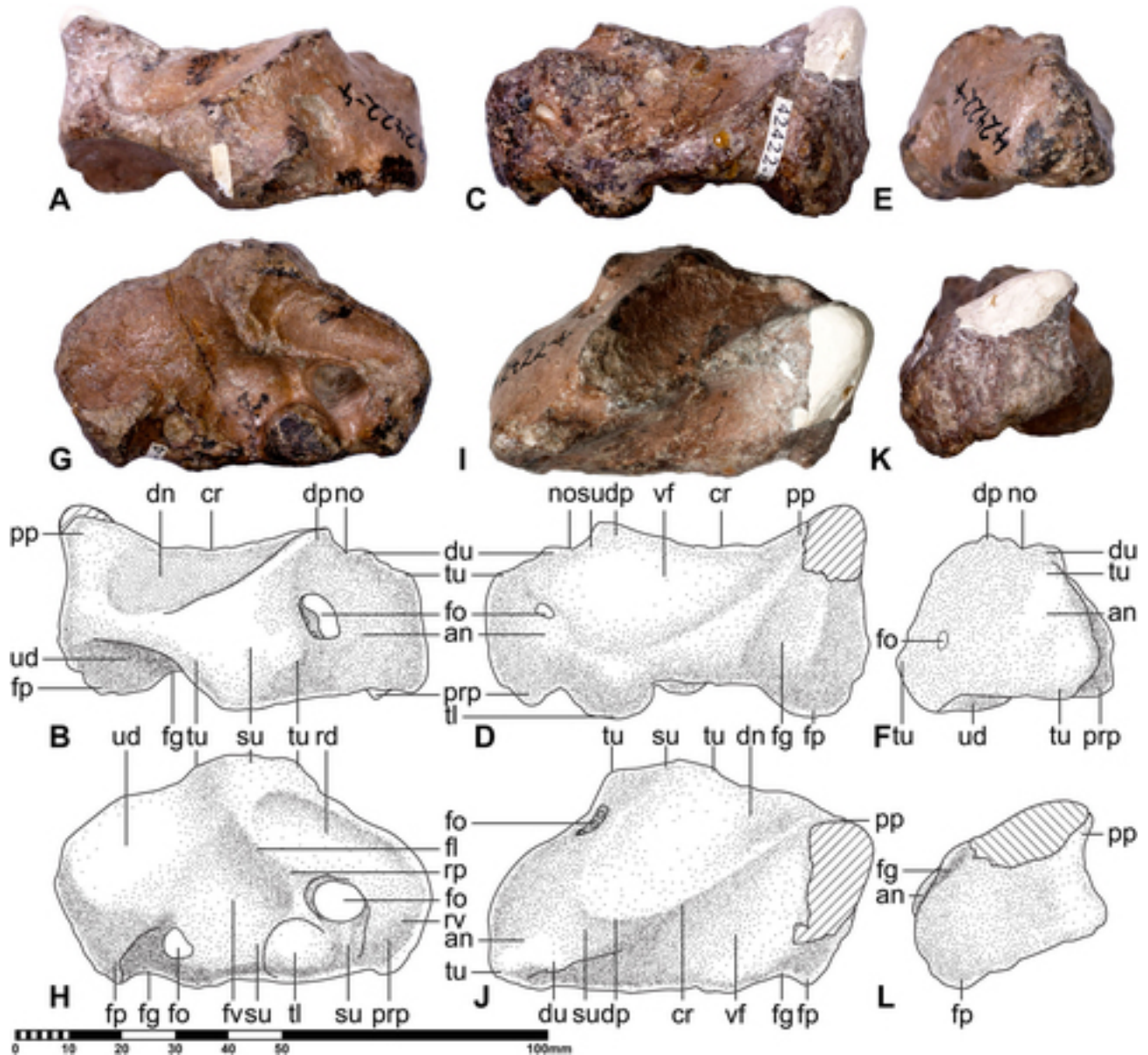
FIGURE 33. *Quetzalcoatlus lawsoni*, sp. nov., left proximal syncarpal (TMM 42422-4) in **A**, dorsal photograph and **B**, line drawing; **C**, ventral photograph and **D**, line drawing; **E**, anterior photograph and **F**, line drawing; **G**, proximal photograph and **H**, line drawing; **I**, distal photograph and **J**, line drawing; and **K**, posterior photograph and **L**, line drawing views. **Abbreviations: an**, anterior process; **cr**, crest; **dn**, dorsal intersyncarpal articular facet; **dp**, distal process; **du**, distal tuberculum; **fg**, flexor tendon groove; **fl**, flange; **fo**, foramen; **fp**, flexor tendon process; **fv**, fovea; **no**, notch; **pp**, posterior process; **prp**, proximal process; **rd**, radial dorsal articular facet; **rp**, raised prominence; **rv**, radial ventral articular surface; **su**, sulcus; **tl**, tuberculum; **tu**, tubercle; **ud**, ulnar dorsal articular surface; and **vf**, ventral intersyncarpal articular facet. Diagonal lines represent plaster. Scale bar equals 100 mm.

1992:67, pl. 4, fig. 5). Divots in the middle of the posterior surface in TMM 41545-1 and 41961-1.9 may be foramina, but preservation obscures this determination.

The distal surface of the proximal syncarpal is dominated by the dorsal and ventral intersyncarpal articular facets. In *Q. lawsoni*, they are about equal in height, but the ventral facet extends nearly the entire width of the syncarpal, whereas the dorsal facet is confined to the posterior two-thirds of the width. The great width of the ventral facet is due in part to the large posterior process at its posterior end. The intersyncarpal facets are separated by a crest that terminates in the distal process at its anteroventral end, separated from the distal tuberculum by a notch formed by a ventral sulcus, as in *Q. northropi*. The rest

of the distal surface of the proximal syncarpal consists of the distal end of the flexor tendon groove at the posteroventral corner as well as a sulcus between the distal tuberculum and the distal process at the anteroventral corner. No foramina are preserved on the distal surface of the proximal syncarpal in *Q. lawsoni* or *Q. northropi*.

Distal Syncarpal—The distal syncarpal is rectangular in cross-section in *Q. lawsoni*, like MC M3929 (Buffetaut, 2008:253) and most pterodactyloids but unlike the more triangular pteranodon-toids (Andres, 2021), with a height about three-quarters of the width and an anteroventrally sloping dorsal margin. Both left distal syncarpals: TMM 42180-6 and 14.13, and 42422-3 (Fig. 34); and right syncarpals: TMM 41544-19, 41954-43 and

TABLE 10.   Measurements of *Quetzalcoatlus lawsoni*, sp. nov., carpal material. Values in millimeters. >, preserved length; ~, approximate length; a-p, anteroposterior dimension; d-v, dorsoventral dimension; lat, lateral dimension; p-d, proximodistal dimension. Holotype specimen in italics.

Dimension: Element: Specimen Number:	Length (p-d)	Width (a-p)	Depth (d-v)
Proximal syncarpal			
TMM 41545-1	36.81	78.87	44.37
TMM 41954-34	30.47	77.74	54.43
TMM 41954-48	~23.53	75.31	43.48
TMM 41954-74	>25.53	>61.74	>43.39
TMM 41961-1.9	36.80	71.27	48.79
TMM 42180-8	32.45	70.70	45.51
TMM 42180-14.12	~23.26	70.25	41.82
TMM 42246-2	31.45	68.92	44.13
TMM 42422-4	37.99	75.61	45.91
TMM 45997-1.6	31.45	58.17	~25.59
Distal syncarpal	Length (p-d)	Width (a-p)	Height (d-v)
TMM 41544-19	38.24	>53.88	44.20
TMM 41954-43	30.52	64.54	51.64
TMM 41954-80	>23.61	>24.94	46.33
TMM 41961-1.10	48.12	65.74	41.57
TMM 42157-2	37.50	64.85	50.83
TMM 42180-6	30.49	60.90	49.93
TMM 42180-14.13	~28.87	73.85	44.71
TMM 42246-1	35.73	63.41	48.54
TMM 42422-3	31.54	60.46	48.95
TMM 45997-1.3	30.62	46.67	28.52
Medial carpal	Length (a-p)	Depth (d-v)	Breadth (lat)
TMM 41954-61	41.24	39.24	15.96
TMM 41961-1.14	37.26	34.29	16.01
TMM 42180-14.4	40.52	34.28	15.50
TMM 44048-1.1	>32.94	31.73	16.59
Carpal sesamoid	Long axis	Medium axis	Short axis
TMM 41954-59.1	22.08	18.18	9.23
TMM 42422-37	26.89	24.73	14.48
TMM 44048-1.2	18.53	13.15	5.21
Pteroid	Length (p-d)	Mid-depth (d-v)	Mid-width (a-p)
TMM 41954-21	206	8.13	4.73
TMM 41954-22	>193.48	7.47	4.82
TMM 41954-69	216	7.49	5.84
TMM 41961-1.11	>182.73	5.66	5.53
TMM 41961-1.12	>131.88	5.27	5.77

80, 41961-1.10, 42157-2, 42246-1, 45997-1.3 are preserved in the *Q. lawsoni* material (Table 10). These are all complete or nearly so with the exception of TMM 41954-80, which is just a posterodistal corner of a right distal syncarpal.

The intersyncarpal articular surfaces comprise over half of the width of the proximal surface of the proximal syncarpal in *Q. lawsoni*, positioned just posterior of center. They form complementary right triangles in proximal view and are separated by an anteroventrally oriented interarticular sulcus. They are comparable in size, unlike the narrower ventral intersyncarpal articular surface found in MC M3929 (Buffetaut, 2008:253) and *K. progenitor* (Andres et al., 2014:S14, fig. S1Fvii), although the ventral intersyncarpal articular surface is a bit wider because it reaches onto the posterior and anterior surfaces. The dorsal intersyncarpal articular surface increases in proximal height posteriorly, whereas the ventral intersyncarpal articular surface increases in proximal height anteriorly; both reach their maximum height at the same point in the middle of the syncarpal, as in other pterosaurs (Averianov, 2010:302). The interarticular sulcus reaches the dorsal margin of the syncarpal to emarginate the dorsal surface posteriorly. The intersyncarpal articular surfaces contact anteriorly extending flanges that are in turn connected by a thin vertical ridge on the anterior end of the distal syncarpal, which do not appear to be preserved in *Q. northropi*. This ridge is not present in *K. progenitor*, allowing the ventral flange to contact the medial carpal process (Andres et al., 2014:S14, fig. S1Fvii). The vertical ridge separates the articular surface for the medial carpal from the proximal

syncarpal articular surfaces in *Q. lawsoni*. The medial carpal articular surface is convex, as reported in *Pteranodon* (Bennett, 2001a:83) and MC M3929 (Buffetaut, 2008:253). The medial carpal process itself is bluntly rounded in proximal/distal view, as described in *Pteranodon* (Bennett, 2001a:83) and *A. lancicollis* (Averianov, 2010:302, fig. 28), but with a shorter length and the base confined to the ventral half of the distal syncarpal. On the proximal surface of the medial carpal process, there is a fovea dorsal to the ventral anteriorly extending flange for the reception of the distal process of the proximal syncarpal. The dorsal anteriorly extending flange terminates anteriorly in a tubercle. The result of this arrangement of articular surfaces, flanges, and ridge is that the interarticular sulcus contacts a vertical sulcus on the anterior end of the syncarpal to produce a checkmark-shaped continuous groove. A small circular foramen is present at the intersection of these sulci on the anteroventral corner of the proximal surface in some specimens, as in *A. lancicollis* (Averianov, 2010:302), in a similar position to an irregularly shaped foramen reported in *Pteranodon* (Bennett, 2001a:82, fig.79B). Similarity in the shape, slope, and arrangement of the intersyncarpal articular facets on the proximal surface of the distal syncarpal in *Quetzalcoatlus* and MC M3929 was used to refer the latter to the Azhdarchidae by Buffetaut (2008).

The dorsal surface of the distal syncarpal in *Q. lawsoni* consists of a posteriorly leaning convex proximal margin, an emarginated posterior margin with a posterior expansion on the distal end, a flat distal margin with an anterodorsal process on the anterior
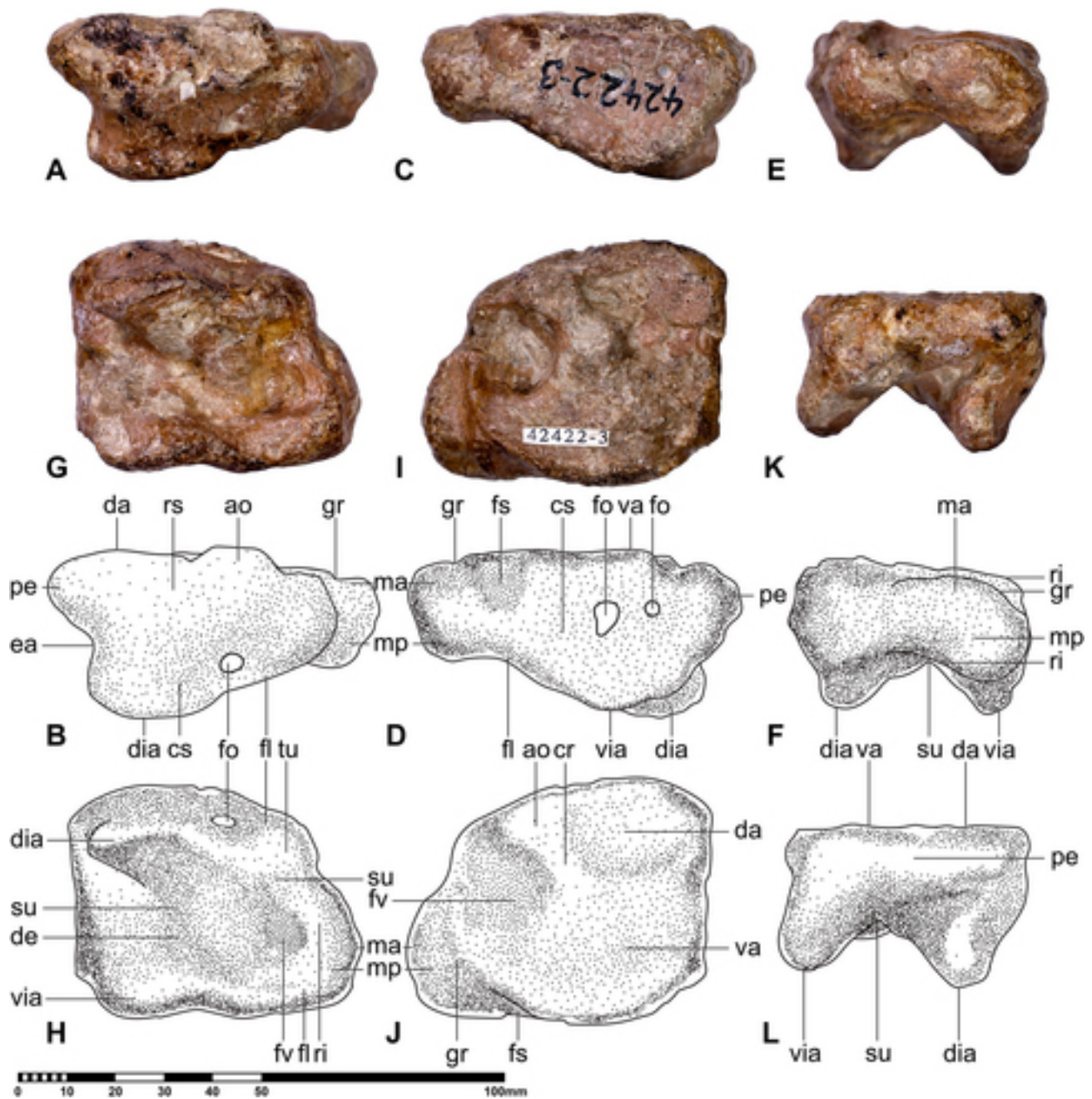
FIGURE 34. *Quetzalcoatlus lawsoni*, sp. nov., left distal syncarpal (TMM 42422-3) in **A**, dorsal photograph and **B**, line drawing; **C**, ventral photograph and **D**, line drawing; **E**, anterior photograph and **F**, line drawing; **G**, proximal photograph and **H**, line drawing; **I**, distal photograph and **J**, line drawing; and **K**, posterior photograph and **L**, line drawing views. **Abbreviations: ao**, anterodorsal process; **cr**, crest; **cs**, concave surface; **da**, dorsal articular surface; **de**, depression; **dia**, dorsal intersyncarpal articular surface; **ea**, emargination; **fl**, flange; **fo**, foramen; **fs**, fossa; **fv**, fovea; **gr**, groove; **ma**, medial carpal articular surface; **mp**, medial carpal process; **pe**, posterior expansion; **ri**, ridge; **rs**, rise; **su**, sulcus; **tu**, tubercle; **va**, ventral articular surface; and **via**, ventral intersyncarpal articular surface. Scale bar equals 100 mm.

half, and a medial carpal process with a constricted base on the anterior margin. A medial carpal process with a constricted base (constricted neck of Bennett, 2001a) is also reported in *Pteranodon* (Bennett, 2001a:82) and *E. prolatus* (Andres and Ji, 2008:459). The dorsal surface is roughly semicircular in outline in *Q. lawsoni*, disparate from the subrectangular outline in *Pteranodon* (Bennett, 2001a:83, figs. 77 and 80B) and the subtriangular outline of *E. prolatus* (Andres and Ji, 2008:459). The dorsal surface is concave proximally but bulges in a dorsal rise

distally, lacking the distal concave surface found in *Q. northropi*. An elliptical foramen pierces the proximal end of the dorsal surface at the base of the medial carpal process; pneumatic foramina on the dorsal surface of the distal syncarpal are reported in *Pteranodon* (Bennett, 2001a:83), *E. prolatus* (Andres and Ji, 2008:459), and *E. rosenfeldi* (Dalla Vecchia, 2009:168).

The posterior emargination of the distal syncarpal by the interarticular sulcus restricts the posterior surface to a triangular

sliver at the ventrodistal corner in *Q. lawsoni*. This restricted posterior surface is part of the thickened lip of the ventral articular surface for the wing metacarpal.

In *Q. lawsoni*, the ventral surface of the distal syncarpal is a larger version of the dorsal surface, with a thickening of the medial carpal process and no posterior emargination instead. The medial carpal process is wider ventrally but does not approach the transversely oval condition described in *A. primordius* (Frey et al., 2011:S45). The ventral surface is mostly concave as in *Q. northropi* and also lacks the irregular groove and pit of *A. primordius* (Frey et al., 2011:S45). The distal margin is straight as in *Pteranodon* (Bennett, 2001a:83), unlike the concave margin in *Q. northropi*. A circular fossa (shallow cotyle of Frey et al., 2011) is present at the distal margin of the medial carpal process base and connects to the groove on the distal surface; this fossa has been identified as an articulation facet for the pteroid in *A. primordius* (Frey et al., 2011:S45). In *Q. lawsoni*, there is a posterior expansion instead of the posteroventral process found in *Q. northropi*. One to three pneumatic foramina pierce the middle of the ventral surface, similar to the three small pneumatic foramina reported in *Pteranodon* (Bennett, 2001a:83).

The anterior surface of the distal syncarpal is taken up entirely by the medial carpal articulation in *Q. lawsoni*. This consists of a convex elliptical articular surface bounded proximally by the vertical ridge on the proximal surface. More oval articular surfaces are reported in pteranodontoids, BSPG 1980 I 121, and MC M3929 (Bennett, 2001a:83; Buffetaut, 2008:253), and a lacriform articular surface is reported in *A. lancicollis* (Averianov, 2010:302).

The distal surface of the *Q. lawsoni* distal syncarpal consists of a raised platform in the outline of an inverted mushroom. This platform has a dorsal crest (prominent ridge of Padian, 1984c, or distinct rounded rim of Bennett, 2001a) separating a deep anterodorsal circular fovea (very large and deep circular pit and central cavity of Hooley, 1913, smaller deep circular pit of Padian, 1984c, fovea carpalis of Kellner and Tomida, 2000, or deep pit and fovea of Buffetaut, 2008) from a recessed posterodorsal rectangular facet (quadrangular articular facet of Hooley, 1913, or smaller recessed kidney-shaped area of Padian, 1984c). The ventral half of the raised platform is a flat articular surface for the ventral wing metacarpal articulation (socket of Hooley, 1913, or prominent kidney-shaped platform and tripartite topography of Padian, 1984c). The dorsal crest extends from the ventral articular surface to form the posterior rim for the circular fovea and to contact the anterodorsal process of the dorsal surface. Posterior to this crest is a square sunken facet for the wing metacarpal dorsal articular surface, creating a pronounced step between the articular surfaces found in other pterosaurs (Bennett, 2001a:83), but without the ridge found in *K. progenitor* (Andres et al., 2014:S14, fig. S1Fviii). The dorsal articular surface for the wing metacarpal is considerably smaller than the ventral articular surface (Bennett, 2001a). The flat ventral articular surface and deeply concave dorsal articular surface of *A. lancicollis* (Averianov, 2010:302) and *Q. lawsoni* contrast with the weakly concave articular surfaces of *Pteranodon* (Bennett, 2001a:83) as well as the concave ventral and flat dorsal articular surfaces of *A. piscator* (Kellner and Tomida, 2000:59). The circular fovea articulates with the proximal tuberculum of the wing metacarpal (or metacarpal III according to Padian, 1984a), and is reported to have a pneumatic foramen in *A. lancicollis* (Averianov, 2010:302), but such a foramen could not be confirmed in *Q. lawsoni*. This fovea has a strong rim except for its anterodorsal margin, as in *Nyctosaurus* but unlike the weaker rim with the ventral articular surface described in *Pteranodon* (Bennett, 2001a:83). The fovea is positioned anterodorsally in *Q. lawsoni*, as in MC M3929 (Buffetaut, 2008:253, fig. 3b), instead of being

more centrally located as in *Pteranodon* (Bennett, 2001a:83, fig. 79A), *I. latidens* (Hooley, 1913:390), and *K. progenitor* (Andres et al., 2014:S14, fig. S1Fviii). In *Q. lawsoni*, a groove separates the ventral articular surface for the wing metacarpal from the medial carpal process on the distal surface. Padian (1984b) reported a row of three faint depressions (divots of Andres et al., 2014, or sockets of Sangster, 2003) near the anterior edge of the YPM VPPU 002246 distal surface and suggested that they were where the metacarpals I–III originated, but this has not been confirmed. In *Q. lawsoni*, this would be on the distal surface of the medial carpal process, which is much smaller and restricted to the ventral half of the distal syncarpal. There are no depressions or other traces of the metacarpal I–III proximal articulations on the distal syncarpal of *Q. lawsoni*, and there does not appear to have been room for them. Metacarpals I–III are identified here as not articulating with the carpus in *Q. lawsoni* as in most ornithocheiroids, but it should be noted that this condition is quite variable in the Ornithocheiroidea (Andres, 2021).

Medial Carpal—The medial carpal (lateral carpal of Hooley, 1913, distal lateral carpal of Wellnhofer, 1985, preaxial carpal of Bennett, 2001a, or lateral distal carpal of Kellner and Tomida, 2000) is a distal series carpal (likely distal carpal 1 according to Bennett, 2001a) that articulates with the anterior end of the distal syncarpal and the proximal end of the pteroid. See Frey et al. (2006) for a discussion of the pteroid articulating with the proximal syncarpal, and see Frey et al. (2011) for a discussion of the pteroid articulating with the distal syncarpal. There is considerable debate over its orientation and how it articulates with the pteroid and the sesamoid (Frey and Riess, 1981; Wilkinson et al., 2006; Bennett, 2007b; Palmer and Dyke, 2010). The *Q. lawsoni* material supports Bennett (2007b) in that the medial carpal fovea (emargination of Hooley, 1913, medial carpal glenoid of Unwin et al., 1996, dorsally orientated pit of Frey et al., 2006, or subcircular pit and notch of the preaxial carpal of Frey et al., 2011) is oriented dorsally with the carpal sesamoid articulated in it, and the pteroid articulates with the anteromedial surface of the medial carpal anterior (distal) end. It is described here according to this orientation. This bone is oriented anteriorly so that its posterior (proximal) end is at right angles to the proximal ends of most of the wing bones. In the interest of clarity, the side of the medial carpal that faces the midline of the pterosaur body is termed the medial side, and the opposite side that points away from the midline is the lateral side. There are two left, TMM 42180-14.4 and 44048-1.1, as well as two right, TMM 41954-61 (Fig. 35) and 41961-1.14 medial carpals preserved in *Q. lawsoni* (Table 10). These are relatively well preserved with the exception of TMM 44048-1.1, which is incomplete and distorted, but it is also the only specimen with the sesamoid (TMM 44048-1.2) articulated in the fovea. Medial carpals are preserved in the azhdarchid species *Q. lawsoni* (Bennett, 2007b) and *A. lancicollis* (Averianov, 2010) as well as the azhdarchiform species *M. minor* (Padian et al., 1995). The *A. lancicollis* medial carpal (ZIN PH 183/44) described by Averianov (2010) has since been identified as an ulna fragment (Averianov, 2014), but Averianov (2010) mentioned that there are several other very incomplete specimens.

The medial carpal of *Q. lawsoni* is a rounded right triangle in medial/lateral view (in the parasagittal plane) as found in most pterosaurs, as compared with being shovel-shaped in *I. latidens* (Hooley, 1913:390), quadrangular in *E. prolatus* (Andres and Ji, 2008:459, fig. 4A), rhomboid in *K. progenitor* (Andres et al., 2014:S14), semicircular in *D. macronyx* (Sangster, 2003:71, fig. 3.9D), or crescent-shaped in *E. rosenfeldi* (Dalla Vecchia, 2009:168). It is squat with an anteroposterior length slightly more than its dorsoventral width as in most pterosaurs (Andres, 2021), and it is laterally compressed with a dorsoventral width over twice that of its mediolateral breadth.

The posterior (proximal) surface consists entirely of the distal syncarpal articular surface in *Q. lawsoni*, a concave vertical ellipse with a distinct rim, different from the subcircular articular surface reported in *Pteranodon* (Bennett, 2001a:83) and the long oval of BPG 1980 I 121 (Bennett, 2001a:84). The medial rim is higher in elevation with a medial deflection at its middle, giving its medial margin the appearance of two rims separated by a notch in *Q. lawsoni*, but not to the extreme found in *K. progenitor* in which these rims are expanded into two flanges (Andres et al., 2014:S15). This articular surface articulates with the distal syncarpal medial carpal process, and the raised medial rim articulates with the vertical ridge on the proximal surface anterior end of the distal syncarpal in *Q. lawsoni*. The middle deflection of the medial rim accommodates the ventral expansion of the medial carpal process.

The dorsal surface of the medial carpal consists of a dorsal expansion proximally and the fovea distally. *Quetzalcoatlus lawsoni* lacks the dorsal foramina separated by thin struts of bone reported in *Pteranodon* (Bennett, 2001a:83, fig. 81A). The fovea is a circular concave surface, contrasting with the flat circular surface in *K. progenitor* (Andres et al., 2014:fig. S1i and vii). The fovea in *Q. lawsoni* has raised medial and lateral rims that give it the appearance of an anterolaterally/posteromedially oriented groove. Anterior and ventral to the fovea is a small pit that is also oriented anterolaterally, and does not appear to contain the irregular small foramina reported in *Pteranodon* (Bennett, 2001a:83, fig. 81A). This pit may have contained a ligament that attached to the carpal sesamoid.

In *Q. lawsoni*, the medial surface of the medial carpal has a large oval pneumatic foramen in its center with a distinct rim, instead of the two figured in *Pteranodon* (Bennett, 2001a:fig. 82A). A process for articulation with the pteroid (terminal process and triangular process of Bennett, 2001a, or short straight round process of Andres and Ji, 2008) extends anterior to the fovea of *Q. lawsoni*. This process is relatively short by pterosaurs standards, especially compared with the elongated pteroid process of *Nyctosaurus* (Bennett, 2001a:84). The pteroid articular surface (indistinctly marked convex oval of Bennett, 2007b) is present on the medioventral surface of this process in *Q. lawsoni*, between the position on the medial surface found in most pterosaurs and the ventral surface in *Nyctosaurus* (Bennett, 2007b:887). The articular surface itself consists of anteroventral and posterodorsal semicircular facets separated by a slight anterodorsally/posteroventrally oriented sulcus to form a weak saddle-shaped articular surface. A saddle-shaped pteroid articular surface also has been reported in *Anhanguera* sp. (AMNH FR 22555) (Bennett, 2007b:887). The strong ridge present on the medial carpal medial surface of *E. rosenfeldi* (Dalla Vecchia, 2009:168) could also not be found in *Q. lawsoni*.

The ventral surface of the medial carpal in *Q. lawsoni* consists of a rugose ventral ridge that extends between a tubercle at the posteroventral corner, also reported in *Pteranodon* (Bennett, 2001a:83, figs. 81 and 82), and the base of the pteroid process. Bennett (2001a) identified this posteroventral tubercle as the articular surface for the pteroid, but the articular surface was later corrected to be more anterior on the medial surface by Bennett (2007b). The foramina figured on the ventral surface of the medial carpal of *Pteranodon* (Bennett, 2001a:fig. 81B) are not present in *Q. lawsoni*.

The medial carpal lateral surface is flat and predominantly featureless in *Q. lawsoni*. It lacks the multiple foramina identified in *Pteranodon* (Bennett, 2001a:fig. 82B).

The anterior (distal) surface of the medial carpal consists of the pteroid process in *Q. lawsoni*. A vertical groove appears to be present on the anterior end of the TMM 41961-1.14 medial carpal, but this is attributed here to preservation.

Carpal sesamoid—The carpal sesamoid (distal carpal 1 of Wellnhofer 1975a, carpal of Wild, 1979, small round sesamoid bone of Padian, 1983b, sesamoid of unknown position of Wellnhofer, 1985, developed sesamoid of Kellner and Tomida, 2000, sesamoid A of Bennett, 2001a, sesamoidal element of an extensor tendon of Frey et al., 2006, subglobular sesamoid and sesamoid bone of Frey et al., 2011, or pisiform of Bennett, 2018b) articulates in the fovea of the medial carpal and is associated with the M. flexor carpi ulnaris tendon (Bennett, 2001a, 2007b). Three specimens are identified as carpal sesamoids in the *Q. lawsoni* material: TMM 41954-59.1, 42422-37, and 44048-1.2 (Table 10). TMM 41954-59.1 is the best preserved and is the specimen specifically described here. TMM 42422-37 is the worst preserved and is tentatively identified based on its overall shape. TMM 44048-1.2 includes a slightly better preserved and smaller carpal sesamoid articulated in a left medial carpal fovea; its shape allows the identification of TMM 41954-59.1 as a left sesamoid. The carpal sesamoid is oval in horizontal outline, as in *Pteranodon* (Bennett, 2001a:85, fig. 84C and D), but with a short side process. The articular surface is a convex mound that constitutes the entire proximal surface in *Q. lawsoni*, unlike the smaller and ventrally offset articular surface of *Pteranodon* (Bennett, 2001a:85, fig. 84C). A small foramen pierces this convex surface between the side process and the closest terminal end (ventral end of Bennett, 2001a). The articular surface increases in height toward this end. The non-articular surface is nearly flat but curves upward toward the terminal end with the foramen. This forms a deflection in a ridge that extends around the circumference of the sesamoid. The coarse striations reported in *Pteranodon* (Bennett, 2001a:85, fig. 84D) are not visible in *Q. lawsoni*. The carpal sesamoids are larger than the fovea of the medial carpals, and it is not readily apparent how they articulate because they can fit together in a number of ways. The sesamoids B and C of Bennett (2001a) could not be located in the *Q. lawsoni* material. *Quetzalcoatlus lawsoni* is the only azhdarchiform currently with a reported carpal sesamoid (Bennett, 2007b:883), and the closest taxon to preserve one appears to be the chaoyangopterid *J. edentus* (Wu et al., 2017:14, fig. 6A and B).

Pteroid—The pteroid is a elongate neomorphic bone (vestigial digit I of Goldfuß, 1831; calcified tendon of Quenstedt, 1855; modified carpal of Williston, 1904; distinct ossification of Hooley, 1913; or either the first distal carpal, metacarpal I, or neomorph digit of Unwin et al., 1996) attached to the propatagium (membranous forewing). As with the medial carpal, there is considerable debate over its orientation. The morphology of *Q. lawsoni* supports Bennett (2007b) in that the pteroid extends medially from the medial carpal to form the distal leading (anterior) edge of the propatagium, and it is described here accordingly. Two left pteroids: TMM 41954-21 and TMM 41961-1.12; and three right pteroids: TMM 41954-22, 41954-69, and 41961-1.11; are identified in *Q. lawsoni* (Table 10). TMM 41954-21 (Fig. 36) is complete but has some damage on its proximal and distal ends, TMM 41954-22 is missing its proximal and distal ends, TMM 41954-69 has the surfaces of its shaft damaged and remains in its field jacket, as well TMM 41961-1.11 and 1.12 are missing their ends and remain attached to the sixth and fifth cervicals, respectively. Pteroids are known in the azhdarchid species *Z. linhaiensis* (Unwin and Lü, 1997), *C. boreas* (Hone et al., 2019), and *M. maggii* (Vullo et al., 2018).

The pteroid in *Q. lawsoni* is a proximally-curved slender rod, as found in the Pterodactylomorpha (Andres, 2021). Its length is about 28 times its width. It reaches a little over half the length of the ulna, as inherited from the Lophocratia. The pteroid shaft is oval in cross-section with a rounder anterior margin and a dorsoventral width about one-and-a-half times
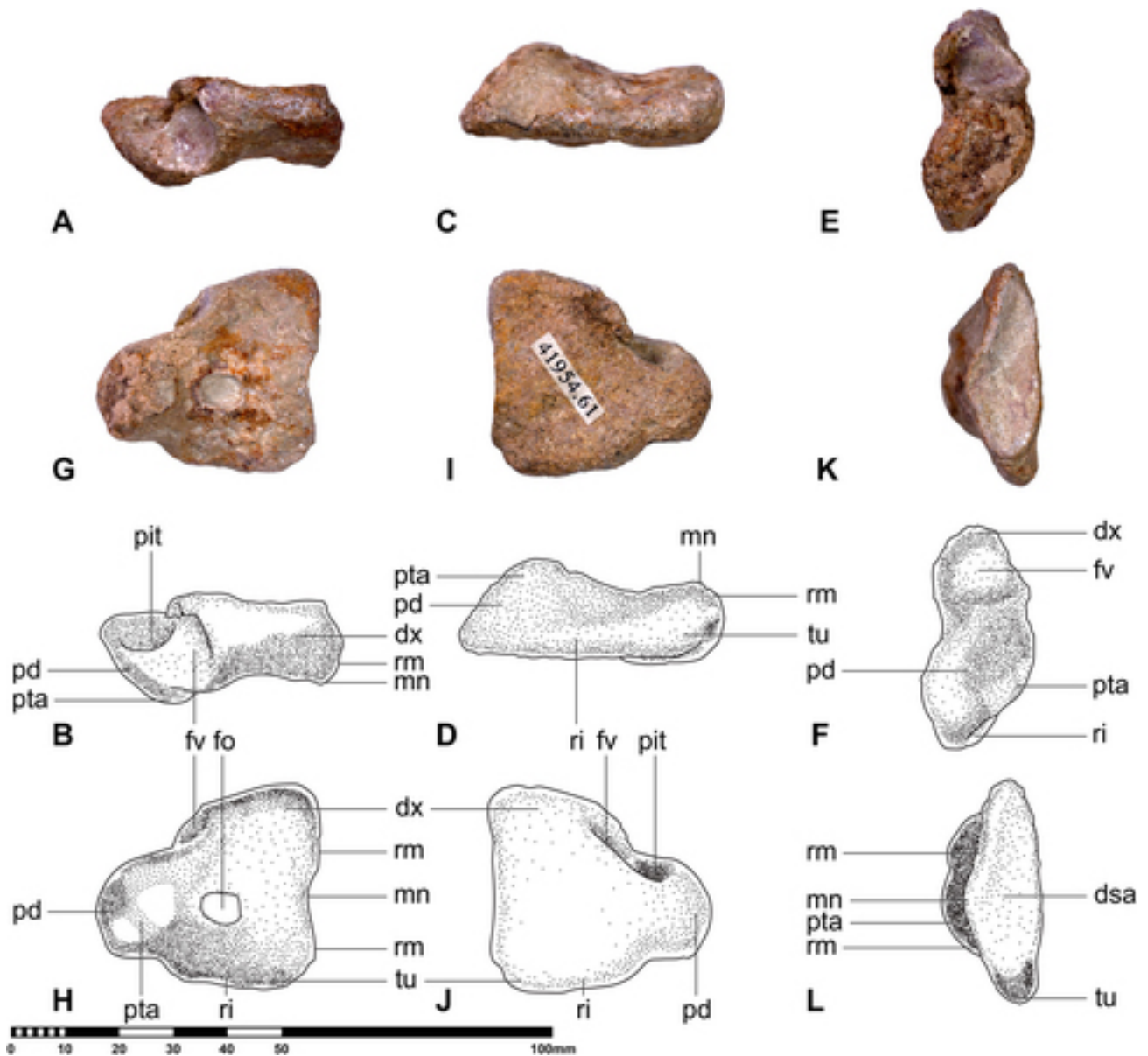
FIGURE 35. *Quetzalcoatlus lawsoni*, sp. nov., right medial carpal (TMM 41954-61) in **A**, dorsal photograph and **B**, line drawing; **C**, ventral photograph and **D**, line drawing; **E**, anterior (distal) photograph and **F**, line drawing; **G**, medial photograph and **H**, line drawing; **I**, lateral photograph and **J**, line drawing; and **K**, posterior (proximal) photograph and **L**, line drawing views. **Abbreviations: dsa**, distal syncarpal articular surface; **dx**, dorsal expansion; **fo**, foramen; **fv**, fovea; **mn**, medial deflection; **pd**, pteroid process; **pit**, pit; **pta**, pteroid articular surface; **ri**, ridge; **rm**, rim; and **tu**, tubercle. Scale bar equals 100 mm.

the anteroposterior breadth of the shaft, not subcircular as in the azhdarchid *C. boreas* or flattened as in the basal pterosaurs *Scaphognathus crassirostris* (Goldfuß, 1831) (Bennett, 2014:333), *E. rosenfeldi* (Dalla Vecchia, 2009:168), and *S. venieri* (Dalla Vecchia, 2019:35). In *Q. lawsoni*, the pteroid is oriented anteromedially for the proximal fifth of its length, and then it curves about 35° and is straight in the horizontal plane for the remainder of its length. In the transverse plane, the pteroid is slightly sinusoidal with a proximal ventral arch (concave dorsally, convex ventrally) followed by a dorsal arch (convex dorsally, concave ventrally) and a ventral expansion at the distal end. The pteroid in *M. maggii* is described as slightly sigmoidal, but this is in the horizontal plane (Vullo et al., 2018:8, fig. 6). The dorsal curvature of the proximal end allows

the pteroid to articulate with the ventromedial surface of the medial carpal pteroid process, and this facilitates the identification of left and right elements in isolation.

The proximal articulation with the medial carpal (head of the pteroid of Wilkinson et al., 2006, articular head of Frey et al., 2011, or proximal articular head of Dalla Vecchia, 2019) is preserved in TMM 41954-21 and 69. In TMM 41954-21, the proximal surface is an inclined square in outline with a ventral keel (flattened expansion at the proximal end of Hooley, 1913, lateral facet and thinner roller-shaped articular facet of Unwin et al., 1996, large crest of Bennett, 2001a, or protuberance of Frey et al., 2011), as compared with the asymmetrical subtriangular proximal outline described in *Anhanguera robustus* (Wellnhofer, 1987) (SMNK PAL 1133)
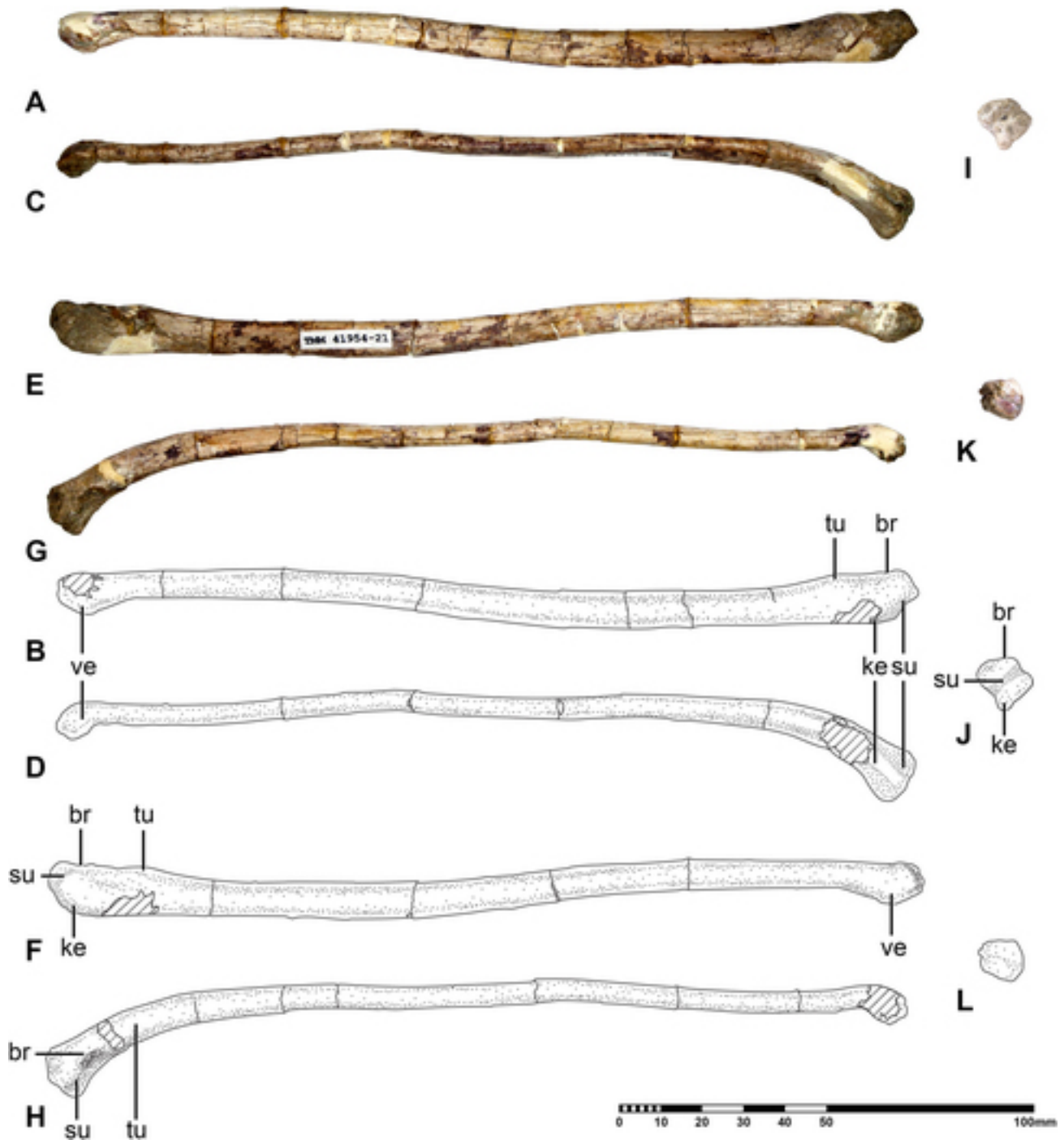
FIGURE 36. *Quetzalcoatlus lawsoni*, sp. nov., left pteroid (TMM 41954-21) in **A**, anterior photograph and **B**, line drawing; **C**, ventral photograph and **D**, line drawing; **E**, posterior photograph and **F**, line drawing; **G**, dorsal photograph and **H**, line drawing; **I**, proximal photograph and **J**, line drawing; and **K**, distal photograph and **L**, line drawing views. **Abbreviations: br**, break; **ke**, keel; **su**, sulcus; **tu**, tubercle; and **ve**, ventral expansion. Diagonal lines represent plaster. Scale bar equals 100 mm.

(Unwin et al., 1996:47, fig. 2f). A slight sulcus extends antero-ventrally/posterodorsally around it giving the slight appearance of condyles. In fact, this proximal articulation of the pteroid is termed an articular condyle in *A. robustus* (Unwin et al., 1996:47), and two slightly vaulted condyles of equal size are described in *A. primordius* (Frey et al., 2011:S45). In *Q. lawsoni*, this creates a weak saddle-shaped articular surface (shallow intercondylar fossa of Unwin et al., 1996, bound proximally by two protuberances of Sangster, 2003, or shallow cotyle of Frey et al., 2011), also reported in *Anhanguera* (Bennett, 2007b:886–887), that complements the medial carpal articular surface with its anterodorsally/postero-ventrally oriented sulcus. These can be contrasted with the convex oval proximal articular surfaces of *Pteranodon*

(Bennett, 2001a:84) and *P. antiquus* (Bennett, 2007b:886), or the small convex surface of *Nyctosaurus* (Bennett, 2001a:85) and *I. latidens* (Hooley, 1913:408). The proximal end of TMM 41954-69 also has a dorsal expansion (medial facet of Unwin et al., 1996) found in other pterosaurs. The dorsal surface of the proximal end of TMM 41954-21 is damaged, and so the most defensible explanation is that both specimens were proximally expanded but that TMM 41954-21 was damaged. A fossa on the posterior surface of the pteroid proximal end (very shallow concavity of Hooley, 1913, elongate ventral concavity of Unwin et al., 1996, or scooped out posterior surface of Sangster, 2003) reported in *I. latidens* (Hooley, 1913:392) and *D. macronyx* (Sangster, 2003:72), as well as fossae on the posterior and anterior surfaces (wide shallow tongue-shape semicircular facet of Unwin et al., 1996) reported in *A. robustus* (Unwin et al., 1996:47, fig. 2) and *Anhanguera* sp. (AMNH FR 22555) (Wilkinson et al., 2006:121) may be expansions of the slight sulcus found in *Q. lawsoni*, although this area is damaged in TMM 41954-21.

The inclined quadrangular cross-section of the proximal end transitions at the medial curvature to the oval cross-section of the shaft, much like the inclined trapezoidal to oval transition in *A. robustus* (Unwin et al., 1996:46) but without the neck reported in that species, *Muzquizopteryx coahuilensis* Frey et al., 2006 (Frey et al., 2006:35), and *S. venieri* (Dalla Vecchia, 2019:fig. 20). *Quetzalcoatlus lawsoni* lacks the large process (wing-like projection at right angles to the shaft of Hooley, 1913, or blade-like extension of the laterally facing margin of the neck of Frey et al., 2006) on the proximal end of the pteroid in *Nyctosaurus* (Bennett, 2001a:84–85). There is a tubercle on the anteroventral surface of the medial curvature in the *Q. lawsoni* pteroid that is near the position of a muscle scar in *Pteranodon* (Bennett, 2001a:84, fig. 83), a low and blunt protuberance with a rugose surface in *A. robustus* and BSPG 1980 I 121 (Unwin et al., 1996:47, fig. 2a), a blunt ridge in *N. gracilis* (Frey et al., 2006:35), and a tuberosity in 'ornithocheirids' (Frey et al., 2006:36) (roughly equivalent to the Ornithocheiriformes) that are likely insertions for extensor and/or depressor muscles (Bennett, 2001a) in these taxa. There is no trace of foramina on the proximal end of the pteroid in *Q. lawsoni*, which have been reported in *C. boreas* (Godfrey and Currie, 2005:303, fig. 16.8), *M. maggii* (Vullo et al., 2018:8, fig. 6), *Pteranodon* (Bennett, 2001a:84, fig. 83), *I. latidens* (Hooley, 1913:392), *A. robustus* (Unwin et al., 1996:47–49, fig. 2), BSPG 1987 I 1 (Wellnhofer, 1991a:fig. 37a), as well as *A. piscator* and BSPG 1982 I 89 (Kellner and Tomida, 2000:62).

On the pteroid shaft, a posterior groove (ventral groove and furrow of Unwin et al., 1996) is reported in *A. robustus*, BSPG 1980 I 121, BSPG 1987 I 1, and *N. gracilis* (Williston, 1903:pl. XLII, fig. 5; Unwin et al., 1996:48–49; Frey et al., 2006:35); a dorsal groove (longitudinal shallow groove of Lü and Ji, 2005a, or shallow groove along the axis of Frey et al., 2006) is reported in *E. liaoxiensis* (Lü and Ji, 2005a:304) and *M. coahuilensis* (Frey et al., 2006:30, fig. 5A); and both anterior and posterior grooves are reported in the "Santana formation ornithocheirids" (Frey et al., 2006:35), but these are absent in *Q. lawsoni*. The striae reported in *C. boreas* (Godfrey and Currie, 2005:303) and *I. latidens* (Hooley, 1913:392) are also not preserved in *Q. lawsoni*. The distal end is best preserved, albeit still damaged, in TMM 41954-21. Most of the less well preserved pteroids in *Q. lawsoni* appear to come to a blunt and rounded terminus, as in *Pteranodon* (Bennett, 2001a:84) and most pterosaurs. TMM 41954-21 instead has a ventral expansion at its distal end. The very tip of the pteroid in this specimen is oriented posteroventrally. In distal view, the tip has what appears to be an incipient sulcus surrounded by a rugosity.

Metacarpus

The metacarpus varies greatly in length over the Pterosauria. The metacarpals transition from being some of the shortest bones of the wing in the non-pterodactyloid pterosaurs to being some of the longest, if not the longest, in the wing of the pterodactyloids (Andres et al., 2014). In the hyperelongated metacarpals of the ornithocheiroids, some or all of the manual metacarpals (metacarpals I–III) do not reach to contact the carpus proximally (Andres, 2021). The manual metacarpals of *Q. lawsoni* taper to points, and therefore are not thought to articulate with the carpus. The distal ends expand horizontally into asymmetric paddle-shaped condyles, unlike the condyles separated by a sulcus (rounded bulbs with ligamentous grooves of Padian, 1983b, two condyles separated by a deep and prominent sulcus or flexor tendon groove of Sangster, 2003, or ginglymi with broad intercondylar sulci of Dalla Vecchia, 2019) of basal pterosaurs (Padian, 1983a:15–1; Dalla Vecchia, 2019:36). The shafts are more or less constant in diameter with an anteroposteriorly wider oval cross-section. There are no articulated metacarpals in *Q. lawsoni* and so it is not known if their distal ends reached the same distal position, but they are assumed to be positioned at the distal end of the wing metacarpal as in other pterosaurs. These manual metacarpals are only a quarter of the wing metacarpal length (Table 11), between the tenth reported in *Nyctosaurus* (Bennett, 2001a:90) and the third in other pterosaurs in which the manual metacarpals do not reach the carpus (Lü and Ji, 2005a:304; Wu et al., 2017:16). Fifteen wing metacarpals are known in *Q. lawsoni*, but only six manual metacarpals. Fortunately, all three manual metacarpals are preserved in TMM 41954-8 (Fig. 37), allowing their identification as metacarpals I–III. These manual metacarpals are approximately the same length and about the same length as in *Pteranodon* (Bennett, 2001a). They are assumed to be positioned concave down as in other pterosaurs. The shafts are also approximately the same size, unlike most pterosaurs in which the third metacarpal is more robust (Bennett, 2001a:89; 2007a:385). However, the distal ends increase in size and amount of ventral curvature from metacarpals I to III so that they can nest on top of one another. They must have not totally overlapped or have been imbricated because they have pneumatic foramina on the ventral surface of their distal ends, as found in *Pteranodon* (Bennett, 2001a:90, figs. 91–93), which would otherwise have been obstructed. In dorsal view, the straighter posterior margins for articulation with the wing metacarpal are on the right side and the distal expansions for articulation with the manual digits are on the left side of the TMM 41954-8 metacarpals, and so these are identified as right metacarpals in this specimen.

Metacarpal I—Only one metacarpal I is preserved in *Q. lawsoni* (Table 11), the right TMM 41954-8.6 (Fig. 37I). This bone is dorsoventrally depressed, expands more gradually over its entire length, and lacks a large distal expansion, unlike the other manual metacarpals. The proximal end is a blunt and poorly formed tip that may have continued proximally as cartilage or missing bone. The shaft has a slight sinusoid in the horizontal plane with a proximal posterior arch (concave anteriorly, convex posteriorly) and a distal anterior arch (concave posteriorly, convex anteriorly). It is only ventrally curved at its distal tip in the form of a slight flange, and so the distal end ventral surface is essentially flat. A separate thin flange extends along the distal half of the posterior margin, giving the metacarpal an anteriorly leaning semicircular cross-section distally, distinct from the oval distal cross-section of *Pteranodon* (Bennett, 2001a:90). An elongate pneumatic foramen pierces the ventral surface of the flange near its distal terminus in *Q. lawsoni*. The distal condyle has its articular surface for the first manual digit positioned dorsally and oriented anterodorsally.
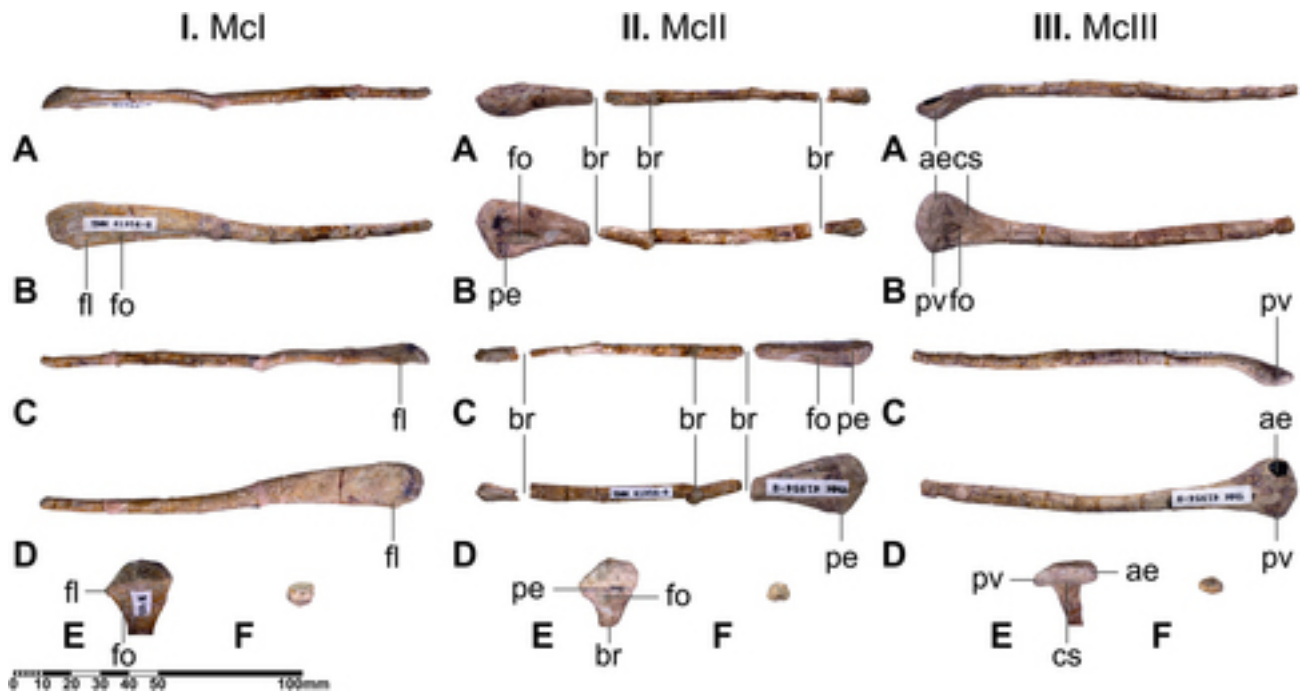
FIGURE 37. *Quetzalcoatlus lawsoni*, sp. nov., right metacarpals I–III (TMM 41954-8). **I**. metacarpal I (TMM 41954-8.6); **II**. metacarpal II (TMM 41954-8.7); and **III**. metacarpal III (TMM 41954-8.8) in **A**, anterior; **B**, ventral; **C**, posterior; **D**, dorsal; **E**, proximal; and **F**, distal views. **Abbreviation:** **ae**, anterior expansion; **br**, break; **cs**, concave surface; **fl**, flange; **fo**, foramen; **pe**, posterior expansion; and **pv**, posteroventral process. Scale bar equals 100 mm.

Metacarpal II—Neither of the two right second metacarpals is complete in the *Q. lawsoni* material. TMM 41954-50.1 is missing its distal half and TMM 41954-8.7 is missing a couple of parts of its shaft (Fig. 37II). Fortunately the dimensions of TMM 41954-8.7 were measured *in situ* and reconstructed in the plaster cradle in which they are stored (Table 11). The proximal end of metacarpal II terminates in an expanded bulb. The shaft is the thinnest of the metacarpals, dorsoventrally depressed proximally becoming nearly circular in cross-section at its mid-length. It is weakly sinusoidal, arching posteriorly (concave anteriorly, convex posteriorly) over most of its length to expand and arching anteriorly (concave posteriorly, convex anteriorly) at its distal quarter. This expansion is predominantly posterior, roughly between the posterior flange of metacarpal I and the posteroventral process of metacarpal III in shape. The distal end attenuates posteriorly, mirroring the distal cross-section of the first metacarpal but deeper, and also distinct from the oval cross-section of *Pteranodon* (Bennett, 2001a:90). The distal condyle is curved ventrally to create an inverted spoon-shape in *Q. lawsoni*, unlike the wide triangular shape of *E. langendorfensis* (Vremir et al., 2013b:10). An oval pneumatic foramen pierces the posterior half of the distal end ventral surface. The articular surface is positioned ventrodistally on the distal end.

Metacarpal III—Three right third metacarpals are complete or nearly so: TMM 41954-8.8 (Fig. 37III), 50.2, and 56. TMM 41954-8.8 is missing its proximal end, but an impression in its plaster cradle indicates that it tapered to a rounded point as in the other two specimens (Table 11). The entire bone traces a slight dorsoventral sinusoid over its length with a proximal ventral arch (concave dorsally, convex ventrally) followed by a dorsal arch (convex dorsally, concave ventrally). It curves anteriorly as in the manual metacarpals of basal pterosaurs (Padian, 1983a:15; Dalla Vecchia, 2003b:27; 2009:169). The

shaft is oval in cross-section, as compared with the subtriangular to suboval cross-section of *E. langendorfensis* (Vremir et al., 2013b:10). Short ridges are visible on the dorsal and ventral surfaces of the proximal end of TMM 41954-50.2. Metacarpal III greatly expands and curves ventrally over its distal fifth in *Q. lawsoni*. This expansion is primarily anterior with a smaller posteroventral process. A large circular pneumatic foramen opens into a perforated surface inside the bone on the posterior half of the distal end ventral surface; TMM 41954-56 and *Q. northropi* (TMM 41450-3.8) have a small foramen in this area instead. The distal end is oriented distoventrally with the distal condyle positioned ventrally. The articular surface extends onto the posteroventral process in a crescent shape giving the distal end of metacarpal III a concave ventral surface, as in *Q. northropi* and *Pteranodon* (Bennett, 2001a:90, fig. 92).

Wing Metacarpal—The wing metacarpal (metacarpal IV) marks the transition between forearm to wing digit and facilitates the transition between terrestrial locomotion and flight. Its morphology is centered on these transitions: a broad proximal contact with the distal syncarpal transfers the forces of walking and flying, and a distal pulley-shaped hinge folds the wing digit away to use the manual digits for walking and manipulation. Unsurprisingly, this is one of the most variable bones in the pterosaur wing and some of the most variable specimens in *Quetzalcoatlus*. This may be due in part to its sampling; the wing metacarpal is one of the most common and poorly preserved elements: only TMM 41954-71 (right), 41961-1.3 (left) (Fig. 38), 42138-1.6 (right), and possibly the smaller 45997-1.1 (right) preserve the entire length, but these nearly all have their proximal ends crushed; TMM 42180-14.5 (left) and 17 (right) are missing their proximal ends; TMM 41961-1.13 (right) and 42180-14.6 (right) are missing their distal ends; TMM 41954-2 (right), 41954-9 (right), 41954-12 (right), 41954-

TABLE 11. Measurements of *Quetzalcoatlus lawsoni*, sp. nov., metacarpal material. Values in millimeters. >, preserved value; ~, approximate length; a-p, anteroposterior dimension; d-v, dorsoventral dimension; and p-d, proximodistal dimension. Holotype specimen in italics.

Dimension: Element: Specimen Number:	Length (p-d)	Mid-width (a-p)	Mid-depth (d-v)
Metacarpal I			
TMM 41954-8.6	118.13	5.53	4.04
Metacarpal II			
TMM 41954-8.7	119.30	3.88	3.26
TMM 41954-50.1	>63.17	3.80	2.76
Metacarpal III			
TMM 41954-8.8	117.76	5.23	4.40
TMM 41954-50.2	112.24	5.19	4.14
TMM 41954-56	103.08	5.04	4.06

Metacarpal IV	Length (p-d)	Proximal width (d-v)	Mid-width (d-v)	Mid-breadth (a-p)
TMM 41546-3.1	>40.04	—	—	—
TMM 41954-2	>233	—	35.08	19.52
TMM 41954-9	>416	—	34.45	15.15
TMM 41954-12	>105.15	—	23.98	14.81
TMM 41954-66	>347	—	42.16	27.25
TMM 41954-71	457	58.41	35.80	17.28
TMM 41954-82	>254	—	52.55	29.17
TMM 41961-1.3	473	48.12	30.68	15.87
TMM 41961-1.13	>307	58.66	31.79	21.20
TMM 42138-1.6	485	>28.98	24.34	18.51
TMM 42180-14.5	>423	—	23.56	20.49
TMM 42180-14.6	>448	58.18	33.74	26.33
TMM 42180-15	>88.67	—	21.56	18.29
TMM 42180-17	>215	—	26.70	17.02
TMM 45997-1.1	~371	52.28	27.18	12.00

66, and 41954-82 are shaft fragments; and TMM 41546-3.1 (left) and 42180-15 (right) are just distal ends (Table 11).

The wing metacarpal in *Q. lawsoni* has a length about 15 times the dorsoventral mid-width, up to 25 times if the mid-breadth is considered. The wing metacarpal is about twice the length of the humerus in *Q. lawsoni*, which appears to be the condition in the Azhdarchidae although some chaoyangopterids approach and reach this length (Andres, 2021). This is also almost twice the average relative length in pterosaurs, reaching almost three times the humerus length in *N. gracilis* (Andres, 2021). The mid-width of the wing metacarpal is roughly half that of the combined ulna and radius widths, as in *Q. northropi* and the Neopterodactyloidea (Andres, 2021). The wing metacarpals in *Q. lawsoni* taper very gradually along their lengths and have a slight ventral expansion on their proximal ends, as in other pterodactyloids (Andres, 2021). Their mid-widths are about one-and-two-thirds their proximal widths, as in other lophocratians and considerably less than the extreme condition in *Q. northropi*.

The proximal surface is uncrushed in only a couple of specimens, but the morphology can be seen in TMM 41961-1.3 (Fig. 38); even then, only the most apparent of structures can be resolved. The proximal surface is roughly rectangular in outline, as in other lophocratians (Andres, 2021), although it appears more like a parallelogram in TMM 41961-1.3. Unlike *Q. northropi*, the middle of the wing metacarpal proximal surface does not appear to be significantly broader than the rest. The proximal tuberculum of the wing metacarpal is positioned on the anterior margin of the proximal surface and is relatively low, as in non-pterodactyloid pterosaurs (Andres et al., 2014). A crescentic sulcus encircles the proximal tubercle as in the other pterodactyloids (Andres et al., 2014). This sulcus contacts the flexor tendon groove on the anterior surface ventrally, and it separates the proximal tuberculum from a dorsal rim on the proximal surface dorsally. There is no posterior rim on the proximal surface of the wing metacarpal. A small dorsal articular surface and a larger flat semicircular ventral articular surface can be identified, but their margins and elevations are difficult to resolve due to preservation. A circular opening at the proximal end of the anterior surface of TMM 42180-14.6 is attributed to damage to the specimen rather than being a pneumatic foramen. The proximal tumescence on the anterior surface of the metacarpal in *Q. northropi* is absent in *Q. lawsoni*.

The ventral expansion of the proximal end extends below its articulation with the distal syncarpal, but it appears to extend distally for only about one-sixteenth of the length in *Q. lawsoni*. It is a possibility that the ventral expansion actually stretches for half or even the entire length of the shaft, but that it tapers so smoothly that its distal termination is obscured. The former hypothesis is put forward because there is a wing digit flexor tendon groove, functional extensor (Bennett, 2008), that extends for that one-sixteenth length on the ventral half of the proximal end anterior surface. This groove is bound ventrally by a robust ridge, instead of the larger anteriorly curving flange in other lophocratians (Andres et al., 2014). The dorsal longitudinal groove of *Q. northropi* could not be identified in *Q. lawsoni*. The posterior surface of the proximal end is convex and lacks a proximal fossa, the dorsal surface is a flat continuation of the dorsal rim, and the ventral surface appears to be a distorted extension of the convex posterior surface in *Q. lawsoni*.

The wing metacarpal shaft is an anteriorly flat cylinder of bone with a semicircular cross-section that is dorsoventrally wider than anteroposteriorly broad, similar to the conditions in cf. *A. philadelphiae* (BSPG 1966 XXV 501) (Martill and Moser, 2017:fig. 2b), *M. maggii* (Vullo et al., 2018:8, fig. 7), *A. lancicollis* (Cohen et al., 2018:63), and OMNH 22014 (Cohen et al., 2018:62). It lacks the faint grooves for the articulation of the manual metacarpals reported in *M. minor* (McGowen et al., 2002:8). Most of the shaft is straight until about 15% of the length from the distal end, where there is a 15° ventral deflection of the distal shaft. There is a complementary dorsal bend (dorsally deflected metacarpal distal end of Averianov, 2010) just proximal to the neck (constricted neck of Bennett, 2013, characteristic waist of the diaphysis of Averianov, 2010, or diaphyseal constriction and constriction just behind the condyle of Martill
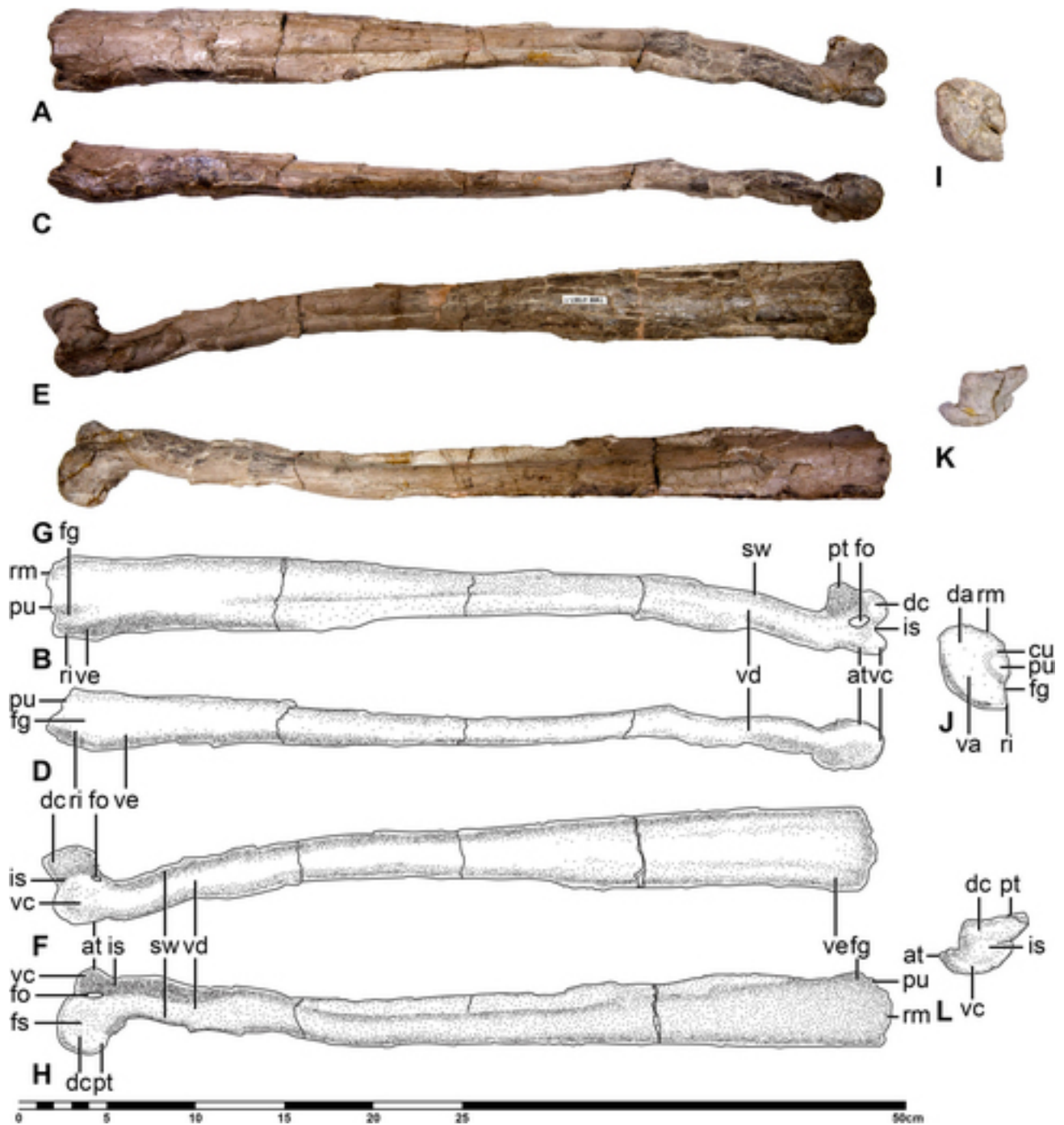
FIGURE 38. *Quetzalcoatlus lawsoni*, sp. nov., left wing metacarpal (metacarpal IV) (TMM 41961-1.3) in **A**, anterior photograph and **B**, line drawing; **C**, ventral photograph and **D**, line drawing; **E**, posterior photograph and **F**, line drawing; **G**, dorsal photograph and **H**, line drawing; **I**, proximal photograph and **J**, line drawing; and **K**, distal photograph and **L**, line drawing views. **Abbreviations: at**, anterior tubercle; **cu**, crescentic sulcus; **da**, dorsal articular surface; **dc**, dorsal condyle; **fg**, flexor tendon groove; **fo**, foramen; **is**, intercondylar sulcus; **pt**, posterior tubercle; **pu**, proximal tuberculum; **ri**, ridge; **rm**, rim; **sw**, swelling; **va**, ventral articular surface; **vc**, ventral condyle; **vd**, ventral deflection; and **ve**, ventral expansion. Scale bar equals 50 cm.

et al., 2013, or dorsoventral constriction in shaft diameter of Cohen et al., 2018) at the distal end so that the distal articulation is parallel to the shaft. This ventral kink (bent shaft of Averianov, 2010, or ventral deflection of Cohen et al., 2018) is distinct from the ventral curvatures of some pterodactyloid specimens (Bennett, 2001a:87; Eck et al., 2011:287, fig. 8, pl. 3), the gentle anterior curvature of *C. boreas* (Godfrey and Currie, 2005:303), or the posterior curvature of *A. ammoni* (Bennett, 2007a:385, fig. 6). This kink is also present in *C. boreas* (Godfrey and Currie, 2005:fig. 16.9A), OMNH 22014 (Cohen et al., 2018), and ZIN PH 49/43 (Averianov, 2010:305). There is a rugose swelling of bone (weak prominent and rough surface of Young, 1964,

rugose area of Galton, 1981, oval muscle or ligament attachment scar and tuberculum of Bennett, 2001a, bony ridge of Dalla Vecchia et al., 2001, low but clearly visible diagonal ridge of Godfrey and Currie, 2005, extensive muscle scar along the dorsal edge of the shaft and oval scar with rugose sculpture of Averianov, 2010, or rugose tubercle of Andres and Myers, 2013) on the posterodorsal surface of the ventral deflection, which may be the attachment for a ligamentous pulley for a long flexor tendon (Bennett, 2001a, 2008). This appears to be analogous but not homologous with the dorsal crest (crista metacarpi of Wild, 1979, prominent roughened area along most of the posteromedial edge and rugose area of Galton, 1981, dorsal ridge and long wide ridge of Sangster, 2003, or prominent lip-like crest of Dalla Vecchia and Cau, 2015) on the posterior surface of the shaft in non-pterodactyloids (Sangster, 2003; Dalla Vecchia and Cau, 2015). Cohen et al. (2018) reports a dorsal ridge in this area on *C. boreas* and OMNH 22014, but on the anterior surface and extending to the ventral distal condyle.

The distal articulation consists of a trochlea/pulley formed from two large circular condyles separated by a deep sulcus. These condyles are oriented subhorizontally with the posterior margin slightly elevated dorsally. The dorsal and ventral condyles are about the same size, as in OMNH 22014 (Cohen et al., 2018:63), whereas the dorsal condyle is at times larger in pterosaurs (Galton, 1981:1119; Bennett, 2001a:88; Godfrey and Currie, 2005:fig. 16.9E; Bennett, 2007a:385; Dalla Vecchia, 2009:168; Eck et al., 2011:287; Dalla Vecchia, 2019:37). The dorsal condyle (lateral condyle of Galton, 1981) is slightly rectangular in horizontal outline and positioned more posteriorly whereas the ventral condyle (medial condyle of Galton, 1981) is slightly circular in outline and offset more anteriorly as in other pterosaurs (Bennett, 2001a:88, figs. 88, 90A, and 98B; 2013:30; Cohen et al., 2018:62, fig. 2), with the possible exceptions of the anteroposteriorly aligned condyles of *A. lancicollis* (Cohen et al., 2018:63) and the circular condyles of OMNH 22014 (Cohen et al., 2018:63). The dorsal condyle also extends more distally than the ventral condyle, as reported in *M. minor* (McGowen et al., 2002:8), and is oriented slightly distodorsally giving the distal articulation an asymmetrical 'offset' appearance (dorsally deflected of Cohen et al., 2018), which has been suggested to be indicative of azhdarchoids by Martill et al. (2013) but is more likely a neoazhdarchian feature. The intercondylar sulcus (intercondylar notch of Cohen et al., 2018) widens posteriorly and is U-shaped in cross-section, lacking the median ridge at its bottom found in ornithocheiriforms more closely related to *Ornithocheirus simus* Owen, 1861, than *H. tianshanensis* (Andres, 2021). An oval pneumatic foramen (intercondylar notch of Godfrey and Currie, 2005) pierces the posterior surface where the sulcus contacts the shaft, as in *A. lancicollis* (Averianov, 2010:304, fig. 30D), *T. wellnhoferi* (Eck et al., 2011:287), *Pteranodon* (Bennett, 2001a:89, figs. 87B and 89B), *A. piscator* (Kellner and Tomida, 2000:64, fig. 42d), ZIN PH 49/43 (Averianov, 2007:pl. 8, fig. 4a), and *C. boreas* (Godfrey and Currie, 2005:fig. 16.9D), but without the second foramen found in some of the *Pteranodon* specimens (Bennett, 2001a:89, figs. 87B and 89B). Another elliptical pneumatic foramen pierces the base of the dorsal condyle on its anterior surface in *Q. lawsoni*, as also found in *M. minor* (MOR 691), *A. piscator* (Kellner and Tomida, 2000:64, fig. 42b), *C. boreas* (Cohen et al., 2018:63–64), BSPG 1980 I 122 (Wellnhofer, 1985:fig. 20), BSPG 1987 I 1 (Wellnhofer, 1991a:fig. 38), and BSPG 1987 I 66 (Wellnhofer, 1991a:fig. 39). The outer margins of the dorsal condyle project dorsally above the shaft to form a dorsal fossa. The proximal end of the posterior part of this condyle projects much higher than the shaft so that the condyle terminates in a posterior tubercle (posterior lip of dorsal condyle is more expanded at the proximal end of Averianov, 2010), absent in *C. boreas* (Cohen et al., 2018:63). The dorsal condyle has about

300° of curvature, with a flattened distal margin. The ventral condyle is more circular but only has about a 270° curvature. Its ventral surface is much less concave and does not have a distinct tubercle at the proximoposterior end of the condyle, unlike the incipient hook developed in OMNH 22014 (Cohen et al., 2018:62). The extension of the ventral condyle onto the anterior surface does form an anterior tubercle, as reported in *M. minor* (McGowen et al., 2002:8) and *Pteranodon* (Bennett, 2001a:88, figs. 87A, 89A, and 90), but absent in *C. boreas* (Cohen et al., 2018:63).

Manual Digits I–III

The phalangeal formula of the pterosaur manus is 2-3-4-4-X with few exceptions (e.g., three phalanx wing digit of *A. ammoni*), and all the manual material found in *Q. lawsoni* fits into this formulation (Table 12). A complete first digit is found in TMM 42422-15 (Fig. 39A) and the three distal phalanges of the third digit are found in TMM 41961-1.1 (Fig. 39G), which greatly facilitates the identification of other manual phalanges in isolation. The first phalanx of the third manual digit is very distinctive and can be easily recognized in *Q. lawsoni* (Fig. 39E). This leaves the phalanges of the second digit (Fig. 39B–D), which are identified by comparison with other pterosaurs and the process of elimination. Identification of left or right elements is facilitated because double condyles/cotyles have larger and more convex ventral condyles/cotyles. Singular proximal cotyles of the proximal phalanges are similarly ventrally expanded with ventral adductor/abductor tubercles on the bone.

The manual digits increase in size from digit I to III. This is mostly due to the increase in phalanx number from digit I to III, but comparable elements are usually larger in subsequent digits. The manual phalanges are many times larger than the pedal phalanges in *Q. lawsoni* as in other breviquartossans (Andres, 2021). The terminal phalanges of the manual digits are elongate, strongly curved, dorsoventrally compressed, and proximally expanded unguals with distinct flexor tubercles and (anteroposteriorly) deep bases. The penultimate phalanges are similar in length and shape to each other—an anterior expansion on the proximal end followed by a constricted neck and a posteriorly positioned double condyle ginglymus—and do not appear to have the oblique condyles or curvature reported in *A. lancicollis* (Averianov, 2010:307, fig. 33K–P) or the collateral ligament pits (circular foramina piercing the sides of Sangster, 2003) reported in *S. venieri* (Dalla Vecchia, 2019:37) and *D. macronyx* (Sangster, 2003:76). The remaining phalanges have unique constructions: the first phalanx of the second digit is a stout bone with expanded ends, the first phalanx of the third digit is a massive anteriorly curving bone, and the second phalanx of the third digit is extremely short and wide. Unlike *Pteranodon*, the manual unguals of *Quetzalcoatlus* lack foramina between the articular surface and the flexor tubercle (Bennett, 2001a). *Quetzalcoatlus lawsoni* also lacks foramina in the ungual grooves, unlike *E. prolatus* (Andres and Ji, 2008:459). Pneumatic foramina absent on the manual unguals is also reported in *A. piscator* (Kellner and Tomida, 2000:66) but is widespread in pterosaurs. The manual sesamoids reported in non-novialoid pterosaurs (Wild, 1979:212 and 230; 1994:105; Sangster, 2003:77; Dalla Vecchia, 2009:169; 2019:37) and *D. banthensis* (Padian, 2008b:55) could not be located in *Quetzalcoatlus* either.

First Phalanx Manual Digit I—TMM 42422-15.1 (Fig. 39A) is the only first phalanx of manual digit I (left) preserved in the *Q. lawsoni* material (Table 12). It is articulated with the second and ultimate phalanx (ungual) of the first digit (TMM 42422-15.2). It is dorsoventrally depressed with its articular surfaces oriented in the horizontal plane. The phalanx is slightly

TABLE 12. Measurements of *Quetzalcoatlus lawsoni*, sp. nov., manual material. Values in millimeters. >, preserved value; a-p, anteroposterior dimension; d-v, dorsoventral dimension; p-d, proximodistal dimension. Holotype specimen in italics.

Dimension: Element: Specimen Number:	Length (p-d)	Mid-width (a-p)	Mid-depth (d-v)
First phalanx digit I			
TMM 42422-15.1	44.38	7.12	4.09
Second phalanx digit I (ungual)	Length (p-d)	Base-width (a-p)	Base-breadth (d-v)
TMM 41544-5	40.04	16.28	7.60
TMM 41954-51	34.14	15.74	7.49
TMM 42422-15.2	>32.70	18.07	7.19
First phalanx digit II	Length (p-d)	Mid-width (a-p)	Mid-depth (d-v)
TMM 42422-19	36.59	8.70	4.22
TMM 45997-3	>18.74	8.22	5.96
Second phalanx digit II	Length (p-d)	Mid-width (a-p)	Mid-depth (d-v)
TMM 42138-3	33.80	8.07	5.42
Third phalanx digit II (ungual)	Length (p-d)	Base-width (a-p)	Base-breadth (d-v)
TMM 41961-1.21	>29.01	12.61	6.73
TMM 42138-1.9	>32.54	17.03	6.13
TMM 42422-14	>20.80	14.25	8.04
First phalanx digit III	Length (p-d)	Mid-width (a-p)	Mid-depth (d-v)
TMM 41544-31	59.40	12.22	12.75
TMM 41954-25	67.95	13.29	14.67
TMM 41954-49	57.37	12.79	13.36
TMM 41954-72	>41.31	13.94	14.04
TMM 42138-4	53.54	12.65	12.84
TMM 42422-21	53.02	11.07	12.34
Second phalanx digit III	Length (p-d)	Mid-width (a-p)	Mid-depth (d-v)
TMM 41544-7	19.04	8.49	9.69
TMM 41961-1.18	19.86	11.85	11.32
Third phalanx digit III	Length (p-d)	Mid-width (a-p)	Mid-depth (d-v)
TMM 41961-1.19	43.88	10.36	8.45
Fourth phalanx digit III (ungual)	Length (p-d)	Base-width (a-p)	Base-breadth (d-v)
TMM 41544-6	>14.51	12.79	6.15
TMM 41961-1.20	43.88	10.36	8.45

dorsoventrally constricted in the middle so that the dorsal and ventral margins are concave in anterior/posterior view, not unlike the shape described in *A. primordius* (Frey et al., 2011: S46). There is a slight ventral curvature along the shaft. A proximal cotyle for articulation with the distal condyle of metacarpal I is present on the posteroproximal corner of the phalanx and constitutes about two-thirds of the proximal end. The articular surface is a ventrally expanded oval in outline, similar to the concave oval reported in *Pteranodon* (Bennett, 2001a:90), with a more prominent ventral rim, similar to the ventral lip in *A. primordius* but undivided (Frey et al., 2011:S46). The rest of the proximal end is an anterior expansion containing a flexor tubercle. A much smaller adductor tubercle is present on the ventral surface of the anterior expansion. The abductor tubercle could not be located, and so the proximal end of this phalanx in *Q. lawsoni* is different from *D. macronyx* in which this end is dominated by three tubercles. The anterior expansion forms a concave anterior margin for the rest of this phalanx in dorsal/ventral view. The anterior surface of the phalanx consists of dorsal and ventral ridges flanking a middle concave surface, comparable to the continuous groove reported in *D. macronyx* (Sangster, 2003:74). The posterior surface of the phalanx is straight in dorsal/ventral view and consists of a longitudinal ridge that terminates at a convex surface proximal to the distal condyles. The ventral surface is concave proximally, becoming convex at the neck. The dorsal surface is flat and is pierced on its proximal end by an elliptical pneumatic foramen. The midsection of the phalanx consists of a neck constricted to about half the (anteroposterior) width and (dorsoventral) height of the proximal end and oval in cross-section. The distal end expands into a posteriorly positioned double-condyle ginglymus, compared with the more anteriorly expanded ginglymus of *A. primordius* (Frey et al., 2011:S46). These condyles curve about 225° and are

separated by a deep sulcus (ginglymal groove of Padian, 1983b). The ventral condyle is significantly larger than the dorsal condyle and is oriented slightly dorsally. A small tubercle is present on the anteroproximal end of the ventral condyle. Averianov (2010) reported an elongate curved penultimate phalanx with a subrectangular proximal cross-section and an oval neck cross-section in *A. lancicollis* (ZIN PH 230/44) that is most likely a first phalanx of manual digit I. However, it has pneumatic foramina on both its dorsal and ventral surfaces as well as being flat ventrally and convex dorsally (Averianov, 2010:307, fig. K–L), as opposed to concave ventrally and flat dorsally as in *Q. lawsoni*. *Eurazhdarcho langendorfensis* has a penultimate manual phalanx (EME VP 312/7) with a subrectangular proximal end, concave proximal articular surface, and a slightly curved shaft with an oval cross-section, but lacks preserved foramina (Vremir et al., 2013b:11, fig. 14); it is also identified here as a first digit first phalanx.

Second Phalanx Manual Digit I—The second phalanx of manual digit I is known from the left (TMM 42422-15.2) and right sides (TMM 41544-5 and 41954-51) in *Q. lawsoni* (Table 12). TMM 42422-15.2 is missing its distal tip (Fig. 39A), and TMM 41544-5 is damaged at its distal tip but the end is identified as present. This phalanx can be identified as the longest and most falcate in shape of the preserved unguals. The claw curves over at least 123° of arc. The proximal articulation comprises the posterior half of the proximal end and is oriented proximoposteriorly. It consists of asymmetrical dorsal and ventral cotyles separated by a posteroventrally oriented intercotylar ridge. The ventral cotyle is wider, deeper, more concave, and has less of a lip than the dorsal cotyle. A prominent flexor tubercle is present on the anterior end of the proximal surface. It is positioned slightly dorsally, with a groove extending around its base that becomes deeper ventrally. The proximal

FIGURE 39. *Quetzalcoatlus lawsoni*, sp. nov., manual elements: **A**, Left first (TMM 42422-15.1) and second (TMM 42422-15.2) phalanx of digit I in ventral view; **B**, right first phalanx of digit II (TMM 42422-19) in dorsal view; **C**, right second phalanx of digit II (TMM 42138-3) in dorsal view; **D**, left third phalanx of digit II (TMM 42138-1.9) in ventral view; **E**, left first phalanx of digit III (TMM 42138-4) in ventral view; **F**, left second phalanx of digit III (TMM 41544-7) in dorsal view; and **G**, right second through fourth phalanx of digit III (TMM 41961-1.18 to 1.20) attached to right tibiotarsus proximal end (TMM 41961-1.25). **Abbreviations: abd**, abductor tubercle; **as**, articular surface; **ad**, adductor tubercle; **ae**, anterior expansion; **br**, break; **cs**, concave surface; **cx**, convexity; **dl**, dorsal lip; **do**, dorsal cotyle; **et**, extensor tubercle; **fl**, flange; **fo**, foramen; **ft**, flexor tubercle; **gi**, ginglymus; **gr**, groove; **FXdY**, manual phalanx X of digit Y; **ir**, intercotylar ridge; **ls**, flat surface; **mu**, metacarpal articular surface; **ne**, neck; **pm**, prominence; **prp**, proximal process; **ri**, ridge; **rm**, rim; **sd**, saddle-shaped articulation; **su**, sulcus; **tu**, tubercle; **ug**, ungual groove; **vl**, ventral lip; and **vo**, ventral cotyle. Scale bar equals 100 mm.

groove contacts a concave ventral surface, which is not present on the dorsal surface. The ventral concavity tapers anteriorly into the ungual groove extending along the center of the ventral surface of the claw; in contrast, the proximal groove contacts the dorsal ungual groove directly. The ungual tapers to a dorsoventrally flattened blade instead of a sharp point, which may be what Bennett (2001a) was referring to when he described the unguals of *Quetzalcoatlus* as more slender towards the tips.

First Phalanx Manual Digit II—The right first phalanx of digit II of TMM 42422-19 (Fig. 39B) and the distal end of the left first phalanx of digit II of TMM 45997-3 are preserved in *Q. lawsoni* (Table 12). This is a stout phalanx and the second shortest bone in the manus. It has a distinctly constricted shaft (or expanded ends) that is dorsoventrally flattened. Whereas the mid-width is about 60% of the proximal width, the mid-depth is only about a third of the proximal depth. The proximal end is expanded anteriorly with a flexor tubercle at its tip, giving it an ovate proximal cross-section. The distal articulation is also anteriorly expanded so that the shaft of the bone has a more concave anterior margin than posterior margin in dorsal/ventral view.

This shape is similar to that described for *A. primordius* (Frey et al., 2011:S46). In *Q. lawsoni*, the proximal articular surface for the metacarpal II is positioned on the posterodorsal corner of the proximal end. The articular surface is a slightly concave cotyle that is oval in outline, as in *Pteranodon* (Bennett, 2001a:90). The adductor tubercle is on the anterior end of the ventral surface of the proximal end about a fifth of the total length from the proximal margin. A smaller abductor tubercle is present in a similar position on the dorsal surface, as also figured by Eck et al. (2011:fig. 8, pl. 4B) in *T. wellnhoferi*. As in the manual digit I first phalanx, a pair of ridges extend along the dorsal and ventral margins of the anterior surface, but they only reach the midpoint of the shaft. There is also a concave surface between them as in the first digit first phalanx, but it is restricted to the proximoventral corner of the anterior surface ventral to the flexor tubercle. Also like the digit I first phalanx, the posterior surface is a longitudinal ridge. This ridge is oriented posterodistally because of torsion present in the phalanx; the distal end has about a 33° counterclockwise rotation in distal view. The dorsal surface of the proximal end has a pneumatic foramen on its proximal third. The distal end consists of a massive saddle-shaped articular surface (concave dorsoventrally, convex anteroposteriorly) with sharp distally oriented dorsal and ventral rims, which probably corresponds to the saddle-shaped to weakly ginglymoid non-ungual interphalangeal joints described in *Pteranodon* (Bennett, 2001a:90). However, all the manual interphalangeal joints are described as ginglymoid (distal roller and proximal trochlea joints of Frey et al., 2011) in *A. primordius* (Frey et al., 2011:S46–S47), *D. macronyx* (Sangster, 2003:76), and *E. rosenfeldi* (Dalla Vecchia, 2009:169). These rims converge posteriorly in *Q. lawsoni*, producing a hastate outline in distal view. A small tubercle is present on the anterior end of the intercondylar sulcus. Another tubercle is found on the anterodistal part of the ventral lip.

Second Phalanx Manual Digit II—The second phalanx of the manual digit II is only represented by the right TMM 42138-3 (Fig. 39C) in *Q. lawsoni* (Table 12). It is similar to the first phalanx of the first digit except that it is smaller and more triangular in dorsal/ventral view due to a flat proximal margin, unlike the convex proximal margin in that phalanx or the concave proximal margin found in *D. macronyx* (Sangster, 2003:76). The second digit second phalanx is a straight bone with a broad anterior expansion in *Q. lawsoni*, but there appears to be a slight dorsal curvature along the shaft, which has also been reported in *D. macronyx* (Sangster, 2003:76). The proximal surface is unusual in shape, likely due to its mixed saddle-shaped and ginglymoid articulation with the first phalanx. This surface is a dorsally curved hastate in proximal view (concave dorsally, convex ventrally). This is due to a larger and more curved crescentic ventral cotyle as well as a smaller and more anteriorly positioned dorsal cotyle for articulation with the first phalanx, different from the symmetrical cotyles (cotylar notches of Frey et al., 2011) of *A. primordius* (Frey et al., 2011:S46). There is a weak intercotylar ridge that becomes stronger posteriorly. It terminates anteriorly at a tiny tubercle, identified here as the flexor tubercle and terminates posteriorly at a more distinct extensor tubercle. The anterior expansion is split into a pair of dorsal and ventral flanges on the anterior surface that terminate at the midsection. The adductor tubercle is present on the ventral flange, and a short sulcus lies between the two flanges. The posterior surface is another longitudinal ridge that becomes rounded and convex at the midsection. The dorsal surface is flat with a middle ovate pneumatic foramen on its proximal quarter. The ventral surface is convex. The distal ginglymus is small and posteriorly positioned. The distal condyles are semicircular in horizontal outline and converge posteriorly. The intercondylar sulcus is deep anteriorly and terminates on the posterior end of the distal surface. The dorsal

condyle appears larger but damage to the posterior end of the ventral condyle obscures their relative sizes. Eck et al. (2011) reported an unusual manual phalanx with a subtriangular proximal outline with two large tubercles on the anterior surface separated by a pronounced sulcus in *T. wellnhoferi*, which is likely a manual second digit second phalanx based on its similarity to TMM 42138-3.

Third Phalanx Manual Digit II—Three third phalanges of the manual digit II ungual are known, the left TMM 42138-1.9 (Fig. 39D) as well as the right TMM 41961-1.21 and 42422-14 (Table 12). These are the straightest and narrowest of the manual unguals in *Q. lawsoni*. They are all missing their distal tips, but the preserved portions average a minmum 95° of curvature. The proximal articulation is oriented proximally and has a weak subhorizontal intercotylar ridge, which cannot even be seen in TMM 41961-1.21 and 42422-14. The base of the ungual is relatively (anteroposteriorly) narrow with the majority taken up by the proximal cotyles. These are barely asymmetrical: the smaller dorsal cotyle is positioned slightly anteriorly and the ventral cotyle has a more prominent rim. The flexor tubercle is positioned more anteriorly than in the other unguals. In anterior view, the proximal end of the tubercle curves slightly dorsally. The groove around the base of the flexor tubercle connects with the ungual grooves extending along the middle of the dorsal and ventral surfaces of the claw. These grooves expand proximally, but concavities are not present on these surfaces.

First Phalanx Manual Digit III—The first phalanx of the third digit is the most commonly preserved manual phalanx in *Q. lawsoni*, probably because it is a larger and blockier element (Table 12). Six of these phalanges are preserved: the left TMM 41544-31, 41954-25, 41954-49, 42138-4 (Fig. 39E), and 42422-21, as well as the right TMM 41954-72 proximal end. This is the longest and largest manual phalanx in *Q. lawsoni*, unlike in the non-pterodactyloid pterosaurs in which it is the third or even second shortest phalanx (Bennett, 2007a:386, fig. 6; Dalla Vecchia, 2009:169; Bennett, 2014:33, figs. 1 and 6; Dalla Vecchia, 2019:37, fig. 21). This bone is unique among the manual phalanges in having a massively expanded proximal end as well as curving dorsally and anteriorly over its length, as found in *A. lancicollis* (Averianov, 2010:306). The proximal surface is poorly preserved but it can be seen to be square in outline with a shallow subcircular fossa in proximal view, also found in *A. lancicollis* (Averianov, 2010:fig. 33A), as well as having a slight dorsal lip for articulation with metacarpal III. The proximal half of the phalanx is greatly expanded anteriorly and maintains its square cross-section to the distal half, which constricts to a narrow neck with an anteriorly flattened round cross-section, as compared with the triangular cross-section of *A. lancicollis* (Averianov, 2010:307, fig. 33G–J). This flat anterior aspect results from a pair of ridges extending along the dorsal and ventral edges of the anterior surface in *Q. lawsoni*, as opposed to the single anterior ridge of *A. lancicollis* (Averianov, 2010:307, fig. 33G–J). These ridges diverge proximally to contact a dorsoventrally broad flexor tubercle, although this appears to be two separate tubercles in TMM 41954-72. Ventral to the flexor tubercle is the abductor tubercle in the form of an anteriorly directed flange. Just posterior to this tubercle on the ventral surface is a circular pneumatic foramen that can open into a perforated surface inside the bone, reminiscent of the foramen in the third metacarpal. This foramen varies in size in the third digit first phalanges, but it can be quite large. A similar foramen is reported in *Pteranodon* but on the posterior surface of the abductor tubercle flange (Bennett, 2001a:90–91, fig. 96B), although it is possibly on the ventral surface instead. *Azhdarcho lancicollis* has both ventral and dorsal pneumatic foramina on the proximal half of this phalanx (Averianov, 2010:306, fig. 33B–E). An adductor tubercle is present on the anterodorsal edge of the proximal end in *Q. lawsoni*, separated from the flexor

tubercle by a sulcus. A pneumatic foramen is present on the anterior surface of the neck just proximal to the distal articulation, accompanied by a small foramen ventral to it in some specimens. A similar foramen is figured in *A. lancicollis* (Averianov, 2010:307, fig. 33I) and *Pteranodon* (Bennett, 2001a:fig. 96B) but on the posterior surface of the neck. In *Q. lawsoni*, a large tubercle is present in the middle of the dorsal surface. The distal end is torsioned about 45° counterclockwise in distal view with respect to the proximal end. The distal articulation is similar to the first phalanx of the second digit in that it is saddle-shaped (concave dorsoventrally, convex anteroposteriorly) to ginglymoid in the horizontal plane, as in *Pteranodon* (Bennett, 2001a:90), but more saddle-shaped with less distinct rims and the dorsal rim is relatively thicker. A large tubercle is present on the anterior part of the distal end dorsal surface, and a more central tubercle is present on the ventral surface, giving the distal end a subcircular cross-section. The articular surface narrows posteriorly but reaches the posterior surface of the phalanx. The articular surface is crescentic in distal view (concave ventrally, convex dorsally). A median sulcus and a pair of two variably developed foramina are reported in this phalanx in *A. lancicollis* (Averianov, 2010:307, fig. 33F), but these may be taphonomic artifacts.

Second Phalanx Manual Digit III—The second phalanx of the third manual digit is the smallest phalanx in the pterosaur manus, but it becomes exceedingly short in the Pterodactylomorpha. This phalanx is represented by the left TMM 41544-7 (Fig. 39F) and right TMM 41961-1.18 (Fig. 39G) in *Q. lawsoni* (Table 12). This is a squat bone that is almost as wide as long with a substantial middle constriction, described as nubbin-like in *J. edentus* (Wu et al., 2017:16) and as a subrounded bony disk in *A. piscator* (Kellner and Tomida, 2000:66). The proximal surface is a posteriorly leaning semicircle in outline, with anterior and posterior expansions (lips that pivot around the distal trochlea of phalanx 1 of digit III of Sangster, 2003) containing the flexor and extensor tubercles, respectively. The proximal articular surface is more ginglymoid than saddle-shaped, divided by a horizontal intercotylar ridge into a smaller elliptical dorsal cotyle and a larger crescentic ventral cotyle. The anterior expansion is large and constitutes almost half of the proximal width, containing the flexor tubercle on its anterodistal corner. An oval pneumatic foramen is positioned distal to the flexor tubercle in the center of the anterior surface. A ridge extends from the flexor tubercle to the distal articulation ventral to this foramen. The ventral surface has a pair of parallel ridges extending from the proximal ventral cotyle to the distal articulation, as in *Q. northropi*. The rest of the midsection is convex dorsally, giving the short shaft a semicircular cross-section. The distal articular surface is more saddle-shaped (concave dorsoventrally, convex anteroposteriorly) than ginglymoid. It has a prominent distally oriented lip ventrally, and it tapers to a dorsally oriented prominence dorsally. The posterior end of the articular surface has a very distinct rim, and the anterior end curves dorsally. The distal articular surface of this manual phalanx is described in *Pteranodon* as a ginglymoid joint of unusual form that would allow only limited flexion and extension (Bennett, 2001a:90), but this may be due to that phalanx being described as oriented 90° (Bennett, 2001a:fig. 95D–G) from the orientation put forward here.

Third Phalanx Manual Digit III—The penultimate phalanx of the third digit in *Q. lawsoni* is preserved only in the right TMM 41961-1.19 (Fig. 39G). It is poorly preserved and partially obscured by the right tibiotarsus (TMM 41961-1.25). The digit III third phalanx resembles a wider version of the digit I first phalanx, and the digit II second phalanx to a slightly lesser degree (Table 12): it has flat proximal and posterior margins, a large anterior expansion of the proximal end, dorsally and ventrally positioned ridges extending along the length of the anterior surface, a posterior ridge, and the entire bone is dorsoventrally

depressed. It differs from the first phalanx of manual digit I in lacking a concave anterior margin in dorsal/ventral view, distinct neck, posteriorly positioned distal articulation, small tubercle on the anteroproximal end of the distal end ventral condyle, and distal intercondylar sulcus (shallow groove of Veldmeijer, 2003) reaching the posterior surface of the ginglymus. The proximal surface is largely obscured but appears to be hastate in proximal view, terminating posteriorly in an extensor tubercle. The flexor tubercle and most of the anterior expansion is obscured by the digit III second phalanx (TMM 41961-1.18). TMM 41961-1.19 is similar to the manual third digit third phalanx reported in *A. spielbergi* but with a larger anterior expansion on the proximal end. Averianov (2010) reported a curved manual phalanx with a subtriangular cross-section and a single pneumatic foramen near its proximal end (ZIN PH 231/44) that would be a penultimate phalanx of the second or third digit. The saddle-shaped proximal surface of this phalanx (Averianov, 2010:fig. 33M–P) corresponds most closely to the distal surface of the manual digit III second phalanx in *Q. lawsoni*, and so ZIN PH 231/44 is identified as a third digit third phalanx of the manus.

Fourth Phalanx Manual Digit III—The ungual of the third manual digit in *Q. lawsoni* is preserved from the right side: TMM 41544-6 and 41961-1.20 (Fig. 39G). It can be identified as the shortest (Table 12) and most highly curved ungual, averaging 140° of preserved curvature. The third digit fourth phalanx is the most dorsoventrally depressed of the manual unguals. The proximal articulation is posteroproximally oriented and constitutes the majority of the proximal surface. It is surrounded by an expanded rim around its periphery that terminates in a proximal process. The intercotylar ridge is concave dorsally so that the dorsal cotyle is (dorsoventrally) deeper than the ventral cotyle, but the ventral cotyle is (anteroposteriorly) wider than the dorsal cotyle. The flexor tubercle is positioned at the proximal margin of the anterior surface and is slightly expanded ventrally. A groove constricts the base of this tubercle and contacts dorsal and ventral concave surfaces. These surfaces attenuate into thin ungual grooves in the middle of the phalanx extending down the claw. The tip of the ungual is a dorsoventrally flattened blade as in the first manual digit ungual.

Wing Digit

The pterosaur wing digit consists of the extremely elongated four phalanges of manual digit IV, which form the distal portions of the wing skeleton (Table 13). These are bracket-shaped bones in dorsal/ventral view due to the posterior expansions of the interphalangeal articulations (moderate condyles of Sangster, 2003). The outline in anterior/posterior view is similar with ventral expansions of the proximal and distal ends, but these are smaller and expand more gradually over their lengths than the posterior expansion. The proximal and distal ends of the entire wing digit are different from these interphalangeal articulations. The proximal end of the first wing phalanx is enlarged and fuses with the extensor tendon process to form a hook-shaped olecranon with a pair of circular cotyles to manipulate the wing digit in flight and fold it out of the way for terrestrial locomotion. At the other end of the wing digit, the distal end of the fourth wing phalanx terminates in a nub or sharp point in pterosaurs. All four phalanges are identified with putative complete examples in *Q. lawsoni*. Many of the phalanges appear curved, but these vary in direction and degree and so at least some of the curvature is likely taphonomic. There is some flexure at the interphalangeal joints, and so there would have been a slight posterior curvature over the entire wing digit, as in other pterosaurs (Bennett, 2001a; Padian et al., 2021). The wing phalanges in *Q. lawsoni* decrease and vary greatly in length along the digit. The relative lengths of the wing phalanges with respect to the first phalanx are 1 : 0.52 : 0.30 : 0.07. With the

exception of the fourth phalanx, they all have about the same degree of elongation. Their aspect ratios of length to mid-width equal 22.91 : 22.80 : 22.03 : 8.43 for the successive phalanges.

First Wing Phalanx—The first wing phalanx is the most common of the wing digit elements in the *Q. lawsoni* material (Table 13). Complete left (TMM 41961-1.4 and 42422-2, Fig. 40) and right (TMM 41544-3 and 41954-6) phalanges, left (TMM 41546-3.2 and 42180-4) and right (TMM 45997-1.2) proximal ends, left (TMM 41954-14) and right (TMM 41544-29 and 41961-1.15) phalanges missing their proximal ends, a right phalanx missing its distal end (TMM 42138-1.7), as well as left (TMM 41954-84, 42272-4, and 42422-17) and right (TMM 41961-2 and 42246-4) shaft fragments are preserved in *Q. lawsoni* (Table 13). All of these phalanges have their extensor tendon processes (olecranon of Goldfuß, 1831, olecranon process of Owen, 1870, usual epiphysis of Hooley, 1913, strong anterior process of Wellnhofer, 1974, olecranon-like process of Young, 1964, processes tendinis extensoris of Wellnhofer, 1978, proximal articular process on the first flight phalanx of Wellnhofer, 1991b, hooklike prominence or snoutlike proximal process of Padian and Wild, 1992, sesamoid bone and isolated sesamoidal mineralization of the tendo extensoris of the wing digit of Frey and Martill, 1998, extensor tendon projects of Averianov, 2010, olecranon process of Frey et al., 2011, or extensor tendinal process of Vremir et al., 2013b) fused to their proximal ends without a trace of suture. This process is a secondary ossification center that fuses to the proximal surface of the first wing phalanx late in ontogeny (Bennett, 1993; Frey and Martill, 1998) and forms the anterior margin of the ventral cotyle. TMM 41544-29 and 42180-4 are missing their extensor tendon processes, but this is due to damage at their proximal ends rather than a lack of fusion. The first wing phalanx is the longest element in the postcranium and slightly more elongate than other wing phalanges (22.91 aspect ratio). The first wing phalanx of *Q. lawsoni* is also rather long by pterosaur standards. It is almost two-and-a-half times the length of the humerus, as in the pteranodontians, whereas the corresponding elements in other azhdarchids and the Eupterodactyloidea are plesiomorphically only about twice the length, with the average for all pterosaurs being about one-and-three-quarters (Andres, 2021).

In *Q. lawsoni* and other pterosaurs, the proximal end of the first wing phalanx is expanded to form a large bicotylar articulation (small and deep semicircular emargination of Hooley, 1913, bipartite articular socket Wellnhofer, 1974, concave articular facet of Padian and Wild, 1992, facies articularis proximalis of Frey and Martill, 1996, trochlea of Frey and Martill, 1998, deep concavity for articulation of Sangster, 2003, or articular concavity of Dalla Vecchia, 2009) for the distal condyles of the wing metacarpal. This metacarpophalangeal articulation consists of: a dorsal cotyle (radius facet of Young, 1964, fossa dorsalis of Wellnhofer, 1991b, facies articularis dorsalis and sulcus dorsalis of Frey and Martill, 1996, facies articularis proximalis pars dorsalis of Frey and Martill, 1998, or dorsal concavity and dorsal articular surface of Sangster, 2003) on the proximal surface of the posterior process (short process of Wellnhofer, 1974, caudal projection of Kellner and Tomida, 2000, or caudal articular process of Frey et al., 2011) as well as a ventral cotyle (ulnar facet of Young, 1964, fossa ventralis of Wellnhofer, 1991b, facies articularis ventralis and sulcus ventralis of Frey and Martill, 1996, facies articularis proximalis pars ventralis of Frey and Martill, 1998, ventral concavity and ventral articular surface of Sangster, 2003, or ventral articular cotyle of Vremir et al., 2013b) that is shared between the posterior surface of the extensor tendon process and the middle of the ventral margin of the proximal surface. A ridge (sharp ridge of Young, 1964, blunt ridge of Frey and Martill, 1998, distinct ridge of Sullivan and Fowler, 2011, or short narrow ridge of Vullo et al., 2018) extends from the dorsal margin of the ventral cotyle to the ventral margin of

TABLE 13. Measurements of *Quetzalcoatlus lawsoni*, sp. nov., wing digit material. Values in millimeters. >, preserved value; <, maximum possible value; a-p, anteroposterior dimension; d-v, dorsoventral dimension; and p-d, proximodistal dimension. Holotype specimen in italics.

Dimension: Element: Specimen Number:	Length (p-d)	Mid-width (a-p)	Mid-depth (d-v)
First wing phalanx			
TMM 41544-3	570	25.03	10.82
TMM 41544-29	591	23.84	8.58
TMM 41546-3.2	>41.87	29.19	13.33
TMM 41954-6	619	26.35	12.01
TMM 41954-14	>529	28.93	10.92
TMM 41954-84	>234	32.49	9.14
TMM 41961-1.4	585	22.35	8.91
TMM 41961-1.15	>402.34	27.88	10.40
TMM 41961-2	>226.68	27.48	14.69
TMM 42138-1.7	>415	23.84	14.09
TMM 42180-4	>72.35	26.42	12.45
TMM 42246-4	>57.97	>40.95	>13.98
TMM 42272-4	252	21.92	16.21
TMM 42422-2	579	23.15	13.72
TMM 42422-17	>270	24.98	10.69
TMM 45997-1.2	>107.28	21.54	8.57
Second wing phalanx			
TMM 41544-20	>294	13.54	5.97
TMM 41544-21	>80.97	11.51	5.91
TMM 41544-23	>116.61	11.39	4.66
TMM 41547-1	>308	15.83	7.12
TMM 41547-2	>49.02	12.42	6.26
TMM 41954-11	>287	16.26	7.01
TMM 41954-54	307	13.20	7.47
TMM 41961-1.5	306	12.68	6.55
TMM 41961-1.16	301	13.46	6.96
TMM 42138-1.8	>288	13.51	6.58
TMM 42180-21.1	>22.46	13.01	6.24
TMM 42422-5	307	12.89	7.16
Third wing phalanx			
TMM 41544-21	>51.22	6.45	3.57
TMM 41954-70.1	182.47	6.45	4.08
TMM 41954-86	188.32	7.22	4.74
TMM 41961-1.6	181.98	6.37	4.73
TMM 41961-1.17	181.64	6.89	4.63
TMM 42180-21.2	>23.92	9.36	4.27
TMM 42422-6.1	158.20	6.05	4.86
TMM 45997-2	>12.80	<11.71	3.80
Fourth wing phalanx			
TMM 41954-70.2	>9.23	5.08	2.36
TMM 41961-1.7	>14.59	3.70	2.46
TMM 42138-1.10	>15.32	7.38	4.80
TMM 42422-6.2	39.38	2.52	2.32

the dorsal cotyle in *Q. lawsoni*, but it does not separate the two as reported in *N. boerei* (Godfrey and Currie, 2005:305).

The dorsal cotyle of the first wing phalanx proximal articulation is a deep concavity in *Q. lawsoni*, unlike the relatively flat face found in *Pteranodon* (Bennett, 2001a:94), but it and the posterior process of the proximal end curve slightly posteroventrally. This cotyle is falcate in proximal view, giving the proximal end of the phalanx a convex dorsal margin, distinct from the oval dorsal cotyle of cf. *A. philadelphiae* (SMNK 1286 PAL) that twists dorsally at its posterior end. The proximal outline of this cotyle in *Q. lawsoni* is similar to the outline of the dorsal cotyle in SMNK 1135 PAL, except that its anterior margin is rounded and its posterior margin is pointed, opposite that of SMNK 1135 PAL. The dorsal cotyle constitutes the posterior two-thirds of the proximal width of the first wing phalanx in *Q. lawsoni*, with the remaining third taken up by the extensor tendon process. The cotyle lacks the prominent dorsal boss on its dorsal margin as well as the well developed depression anterior to it, found in *N. boerei* (Sullivan and Fowler, 2011:395).

In proximal view, the extensor tendon process curves posteroventrally. In ventral view, this process forms a ventrally exposed semicircular cotyle for the distal ventral condyle of the wing metacarpal, different from the narrow and more constant radius of the *Pteranodon* ventral cotyle (Bennett, 2001a:94–95) or the oval outline of SMNK 1135 PAL (Frey and Martill, 1998:590). The two foramina reported on the ventral cotyle of *N. boerei* (Sullivan and Fowler, 2011:395) could not be located in *Q. lawsoni*, the smaller of which may correspond to the nutrient foramen between the proximal cotyles reported in *Pteranodon* (Bennett, 2001a:95, fig. 89B). Likewise, the pneumatic foramen on the anterior end of the proximal ventral surface reported in *K. vilsoni* (Kellner et al., 2019a:15) could also not be located in *Q. lawsoni*. The distal part of this ventral cotyle continues onto the ventral surface of the first wing phalanx main body for about a centimeter to form a small ventral prominence, as in *Pteranodon* (Bennett, 2001a:94, fig. 98A). This prominence does not extend distally as a ridge (anterior wall of the fossa triangularis of Frey and Martill, 1998), as reported in *S. wucaiwanensis* (Andres et al., 2010:177). A large longitudinal intercotylar sulcus (fossa of Frey and Martill, 1996, fossa triangularis of Frey and Martill, 1998, or large concavity on the caudal half of Kellner and Tomida, 2000) extends down the midline of the ventral surface from the proximal cotyles. This produces an elliptical cross-section lacking a posteroventral quadrant. A large oval pneumatic foramen (triangular foramen pneumaticum of Frey and Martill, 1996) pierces the midpoint of the intercotylar sulcus, inherited from the Ornithocheiroidea (Andres, 2021). A second pneumatic foramen pierces a fossa on the posterodorsal surface of the extensor tendon process, as found in *Pteranodon* (Bennett, 2001a:95, as well as figs. 89B, 90A, and 98A) and *N. boerei* (Sullivan and Fowler, 2011:395 and fig. 4B); *A. piscator* has a second foramen anterior to this one on the extensor tendon process (Kellner and Tomida, 2000:66, fig. 43b). The subcircular tubercle reported on the posteroventral margin of the proximal end in *M. maggii* and *N. boerei* (Sullivan and Fowler, 2011:fig. 3d; Vullo et al., 2018:9, fig. 8A–D) could not be located in *Q. lawsoni*.

The distal contacts of the extensor tendon process are difficult to discern due to its fusion, but in specimens that have been damaged to reveal internal structure (e.g., TMM 41544-3), the process can be seen to have a straight vertical contact with the rest of the first wing phalanx at the position of its greatest width and depth. This gives the extensor tendon process an elongate trapezoidal outline in dorsal/ventral view with a notch (distal groove of Frey and Martill, 1998, deep groove of Averianov, 2010, or saddle of Sullivan and Fowler, 2011) on its anteroproximal margin. In TMM 41961-1.4, this process is squarer in outline with a notch on the proximal margin. In pterosaurs, the extensor tendon process varies greatly in shape: from a hook (Andres and Ji, 2006:75), square (Andres and Ji, 2008:459; Averianov, 2010:305), rectangle (Sangster, 2003:78), trapezoid (Andres and Myers, 2013:393), cone (Frey and Martill, 1998:587), circle (pers. obs.), sub-triangle (Elgin and Frey, 2011: S27; Elgin, 2014:27, figs. 2, 17), to a right triangle (Andres and Ji, 2008:177; Vremir et al., 2013b:11, fig. 12) both with (Andres and Ji, 2006:75; Averianov, 2010:305; Sullivan and Fowler, 2011:395 and 400) and without a notch (Andres and Ji, 2008:177). *Quetzalcoatlus lawsoni* lacks a proximal groove (two expanded regions on top of Kellner and Tomida, 2000) as reported in SMNK 1135 PAL (Frey and Martill, 1998:592, fig. 4A) and *A. piscator* (Kellner and Tomida, 2000:66, fig. 43). In anterior or posterior view, the extensor tendon process is a ventrally leaning oblong process with a slight mid-constriction.

The anterior margin of the *Q. lawsoni* first wing phalanx proximal end is an expanded horizontal flange (extension for attaching the extensor tendon of the first flight phalanx Wellnhofer,

FIGURE 40. Q*uetzalcoatlus lawsoni*, sp. nov., left first wing phalanx (TMM 42422-2) in **A**, anterior; **B**, ventral; **C**, posterior; **D**, dorsal; **E**, proximal; and **F**, distal views. **Abbreviations: ca**, concavity; **di**, distal condyle; **do**, dorsal cotyle; **etp**, extensor tendon process; **fl**, flange; **fo**, foramen; **fs**, fossa; **in**, intercotylar sulcus; **no**, notch; **pe**, posterior expansion; **pp**, posterior process; **ri**, ridge; **vo**, ventral cotyle; and **vp**, ventral prominence. Scale bar equals 50 cm.

1991b, anterior crest and angular thin crest of Sangster, 2003, tuberosity of Godfrey and Currie, 2005, broad cranial crest of Dalla Vecchia, 2009, blunt projection of Lü and Ji, 2005a, rounded longitudinal flange of Andres et al., 2010, anterior boss for muscle attachment of Sullivan and Fowler, 2011, cranial articular process of Frey et al., 2011, anterior flange of Andres et al., 2014, crest for additional insertion of the extensor tendon of the wing phalanx 1 of Dalla Vecchia, 2014, or broad preaxial crest of additional insertion of the extensor tendon of the phalanx of Dalla Vecchia, 2019). A groove running along the proximal anterior surface of *M. minor* (McGowen et al., 2002:8) could not be located in that species or *Q. lawsoni* and may represent damage in the holotype of *M. minor*.

Bennett (2001a) is followed in terming the posteroproximal tip of the first wing phalanx proximal a posterior process, although some publications term all posterior expansions of the wing phalanges posterior processes. This process on the first wing phalanx is similar to the posterior expansions on the other wing phalanx

proximal ends, and it likely functioned as a flexor tubercle as well. It is not termed a posterior expansion on the first wing phalanx because it lacks the ventral expansions of those other ends, and the proximal end of the first phalanx is expanded equally anteriorly and posteriorly.

The first wing phalanx shaft is parallel-sided in *Q. lawsoni* with a nearly constant width and a distal end that is slightly expanded over a fifth of the entire length. This slight posterior expansion of the distal end over a considerable distance is shared with *Q. northropi*. There is some variation in the curvature of the shaft among specimens, but this is attributed to taphonomic variation of a straight shaft. The proximal shaft cross-section is oval in outline (Buffetaut et al., 1996), similar to cf. *A. philadelphiae* (SMNK 1286 PAL) (Frey and Martill, 1996:230) but with a deeper anterior end and flatter dorsal margin, which transitions to a posteriorly deeper oval for the rest of the shaft, unlike the more triangular cross-section of *Q. northropi*. The mid-shaft cross-section is about 2.40 times wider than deep. The slight expansion of the distal end is entirely in the ventral and posterior directions. The tubercle for collateral ligaments on the dorsoanterior surface of the distal end in *E. rosenfeldi* (Dalla Vecchia, 2009:169) could not be located in *Q. lawsoni*. The distal articular surface (oval facies articularis of Frey and Martill, 1996) is substantially convex with a middle apex and a concave area anterior to it, unlike the weakly convex surfaces of most pterosaurs (Young, 1964:246; Bennett, 2001a:96; Sangster, 2003:78; Lü and Ji, 2005a:305; Wu et al., 2017:16), although this appears to be exacerbated by damage in TMM 42422-2. The distal articular surface is a slightly posteriorly deeper oval in distal view like the preceeding shaft, which may also be consistent with the subcircular to slightly suboval outline of *Pteranodon* (Bennett, 2001a:96). This distal outline lacks the anterior point likely present in *Q. northropi*. The faint longitudinal striations and 'humpy' surface reported in cf. *A. philadelphiae* (SMNK 1286 PAL) (Frey and Martill, 1996:233) also cannot be identified in *Q. lawsoni*.

Second Wing Phalanx—The second wing phalanx of *Q. lawsoni* is represented by the complete left (TMM 41961-1.5 and 42422-5, Fig. 41) and right (TMM 41954-54 and 41961-1.16), the left (TMM 41544-20 and 41954-11) and right (TMM 41547-1 and 42138-1.8) majorities missing their distal ends, left (TMM 41544-23) and right (TMM 41547-2) shaft and distal end fragments, and the left (TMM 41544-21) and right distal ends (TMM 42180-21.1) (Table 13). This is an elongate bone that has an aspect ratio almost that of the first wing phalanx (22.80) but only half its length (52%). With a length of a little over half of the first wing phalanx, the second wing phalanx of *Q. lawsoni* is the relatively shortest second wing phalanx found in pterosaurs, but this is somewhat accentuated by the very long first wing phalanx in this species. On average, the second wing phalanx is only slightly shorter than the first wing phalanx in pterosaurs (Andres, 2021).

A proximally oriented tuberculum is present in the center of the anterior fifth of the proximal surface in *Q. lawsoni*, distinct from the anterior point of the proximal end and giving the proximal margin a concave outline in dorsal/ventral view, as in *Q. northropi*. The proximal articular surface is positioned posterior to this tubercle, producing a slight posterior orientation for the entire surface, also as in *Q. northropi*. This articular surface is concave, oval in outline, and expanded more ventrally than dorsally. It has a distinct lip around its periphery, instead of just the dorsal rim found in *Q. northropi*. A large posterior expansion is present on the proximal end, but it lacks the small posterior process found in *Q. northropi*. A slight extensor tubercle is present on the proximal end of the anterior surface.

An excavation on the ventral surface with a raised anterior margin begins a centimeter from the proximal end in *Q. lawsoni*. Unlike *Q. northropi*, this raised margin disappears

where the excavation turns into the anteroventral sulcus and the azhdarchid τ-shaped cross-section of the second wing phalanx begins. This cross-sectional shape consists of a posteroventrally oriented midline ventral ridge separating the concave anteroventral and posteroventral sulci from one another. The posteroventral sulcus is a couple of centimeters shorter on both its proximal and distal ends, and it is about half the width of the anteroventral sulcus. Unlike *Q. northropi*, the midline ventral ridge does not merge with a raised posterior margin and instead connects directly to the expansion of the proximal end. There is no raised posterior margin and only a slightly deeper anterior margin on the shaft. The dorsal surface of the shaft has a slightly concave midline, whereas this area is flat-topped in *Q. northropi*. The second wing phalanx is straight in anterior/posterior view, although TMM 42422-5 has some dorsal curvature that may be attributed to taphonomy. The second wing phalanx is straight to slightly curved posteriorly in the horizontal plane. The shaft is twice as wide as deep becoming more dorsoventrally depressed distally. It rapidly tapers from the proximal margin and then subtly attenuates over the remaining shaft.

The distal end of the third wing phalanx is expanded dorsally and ventrally in *Q. lawsoni*, but more in the ventral direction. A small posterior expansion is also present. The distal articular surface is convex with an anterior point, a central apex, and a semicircular outline. Like *Q. northropi*, the distal surface reaches its greatest depth at the midline, but this surface has only a slight anterior deflection in the horizontal plane. The tubercle for collateral ligaments on the anteroventral surface of the distal end reported in *E. rosenfeldi* (Dalla Vecchia, 2009:169) is not present in *Q. lawsoni*.

Third Wing Phalanx—Eight third wing phalanges are found in *Q. lawsoni* (Table 13): three complete left (TMM 41954-86, 41961-1.6, and 42422-6.1), two complete right (TMM 41954-70.1, Fig. 42, and 41961-1.17), a left proximal end (TMM 41544-21), and a couple of right proximal ends (TMM 42180-21.2 and 45997-2). The TMM 41961-1.17 phalanx is unusual in having an approximate 33° anterior bend about a quarter of the length down the shaft; this is identified as a broken and healed bone as opposed to a taphonomic break. The third wing phalanx is similar to the second phalanx, differing mainly in its dimensions. It is substantially shorter than the second wing phalanx (58% length), slightly less elongate (22.03 aspect ratio), significantly deeper (mid-width 1.60 times mid-depth), and has a more gradual taper proximally and over the entire length. The third phalanx in *Q. lawsoni* is also the relatively shortest third wing phalanx in pterosaur species, with a length only 30% of the first wing phalanx length. This is part of a trend of reduction of the length of this wing phalanx largely occurring over the history of the Pterosauria (Andres, 2021).

The third wing phalanx of *Q. lawsoni* lacks the proximally oriented tuberculum on the anterior end of the proximal surface found on the second phalanx, but the proximal margin is still concave in dorsal/ventral view and the articular surface does not reach onto the anterior fifth of the proximal surface. Instead the anterior margin of the shaft extends past the rest of the proximal surface to form a proximally projecting anterior point. The entire proximal margin is slightly posteriorly deflected to complement the anterior deflection of the third phalanx distal margin. The proximal surface is a Reuleaux triangle (guitar pick-shaped) in outline that is expanded a bit more ventrally than dorsally. The posterior expansion of the proximal end lacks a distinct posterior process and instead smoothly transitions to the taper of the shaft in the horizontal plane. An extensor tubercle on the proximal end of the anterior surface can only faintly be seen in the third wing phalanx, with the exception of TMM 41961-1.17 in which it may be related to the broken and healed shape. The ventral surface of the proximal end lacks the distinct ventral

excavation found in the second wing phalanx, or in the third wing phalanx of *Q. northropi*.

The cross-section of the third wing phalanx shaft is τ-shaped in *Q. lawsoni*, but less developed than the second phalanx: the midline ventral ridge is not as deep and is oriented more ventrally, the anteroventral and posteroventral sulci are shallower and subequal in width in the midsection, raised anterior and posterior margins on the ventral surface are absent, and the shaft is flat-topped sloping ventrally only on the anterior margin. Like the second wing phalanx, the posteroventral sulcus is a few centimeters shorter than the anteroventral sulcus, and the midline ventral ridge contacts the ends of the bone directly instead of the posterior margin. The anteroventral sulcus extends from the proximal end, where it is not expanded into an excavation, to near the distal end. The minimum width of the shaft is about one-seventh the length from the distal end, similar to the distal constriction found in *J. edentus* (Wang et al., 2017:17). The shaft of this phalanx varies greatly in curvature in this material due to taphonomic variation, and so the original curvature is unknown.

The distal end is quite small, only slightly larger than the shaft, and is a flat-topped in *Q. lawsoni*. The distal surface is convex and ventrally expanded at the midline. TMM 41954-70.1 appears to have a distinct posterior process instead of a posterior expansion on the distal end. Whereas in TMM 41961-1.6 and -1.17, the distal articular surfaces are subcircular in outline and lack a posterior process. In less well-preserved distal ends, there is a slight posterior process or at least a subtriangular distal outline. *Quetzalcoatlus lawsoni* is identified as having a posterior process on the distal end of the third wing phalanx, as in *Q. northropi*.

Fourth Wing Phalanx—There are only four fourth wing phalanges known in the *Q. lawsoni* material, the left TMM 41961-1.7 and 42422-6.2 (Fig. 43) as well as the right TMM 41954-70.2 and 42138-1.10 (Table 13). These are proximal end fragments with the exception of TMM 42422-6.2, which remains partially embedded in matrix but is likely complete. This specimen preserves a shaft that tapers to a rounded tip or blunt point, as in most pterosaurs (Sangster, 2003:79; Dalla Vecchia, 2009:16; Frey et al., 2011:S47; Bennett, 2014:333–334) but unlike the small knob (nub of Andres et al., 2010, or golf club-like distal end of Averianov, 2010) found in *A. lancicollis* (Averianov, 2010:305), *Pteranodon* (Bennett, 2001a:96), *E. prolatus* (Andres and Ji, 2008:460), and *S. wucaiwanensis* (Andres et al., 2010:177). There is a small amount of matrix adhering to its distal end, implying that the terminus is preserved. This distal end is about a millimeter in diameter and could not have become much thinner and still provided support for the wing membrane, especially the very distal tip of the wing. If this bone is not complete, it could not have been much longer. The fourth wing phalanx is rather stout with a length a little over ten times the width, disparate from the rod-like phalanx of *A. lancicollis* (Averianov, 2010:305), *E. liaoxiensis* (Lü and Ji, 2005a:305), and *J. edentus* (Wu et al., 2017:305). It is also exceedingly small, only 7% the length and 15% the mid-width of the first wing phalanx. This is considerably less than the average 59% of first wing phalanx length for pterosaur species (Andres, 2021). Only the fourth wing phalanx of *Microtuban altivolans* Elgin and Frey, 2011, is shorter with a length 3% the length of the first wing phalanx (Andres, 2021). Fourth wing phalanges are preserved in the azhdarchid species *E. langendorfensis* (Vremir et al., 2013b) and *A. lancicollis* (Averianov, 2010).

The fourth wing phalanx of *Q. lawsoni* is a straight bone, unlike the curved fourth phalanges found in most pterosaurs (Wellnhofer, 1974:20; Bennett, 2001a:93; Sangster, 2003:79; Lü and Ji, 2005a:305; Andres and Ji, 2008:46; Dalla Vecchia, 2009:169; Frey et al., 2011:S47; Bennett, 2014:333–334; Kellner et al., 2019b). However, it seems to share a nearly constant diameter over much of its length with *Pteranodon* (Bennett,
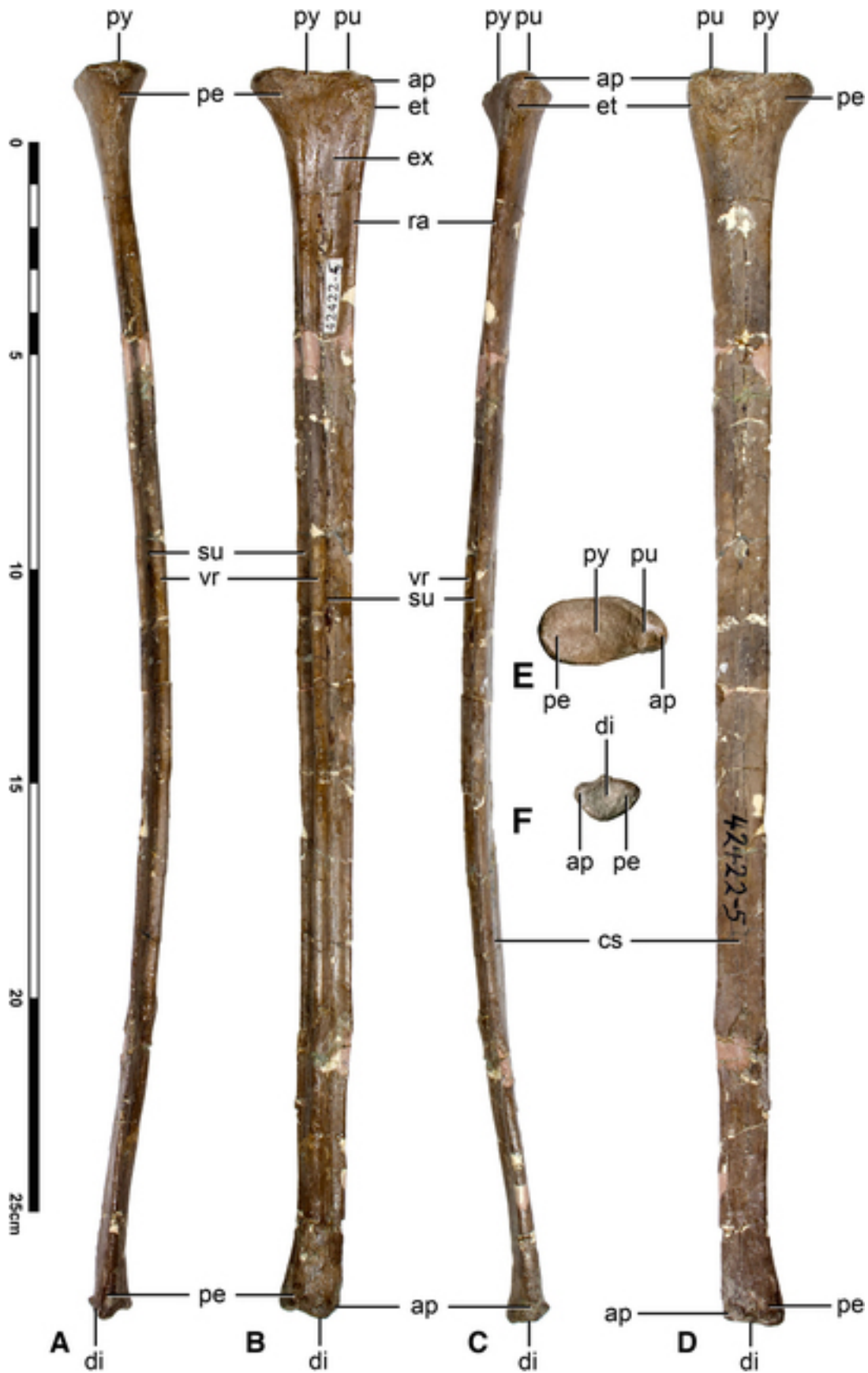
FIGURE 41. Q*uetzalcoatlus lawsoni*, sp. nov., left second wing phalanx (TMM 42422-5) photographs in **A**, posterior; **B**, ventral; **C**, anterior; **D**, dorsal; **E**, proximal; and **F**, distal views. **Abbreviations: ap**, anterior point; **di**, distal condyle; **et**, extensor tubercle; **ex**, excavation; **pe**, posterior expansion; **pu**, proximal tubercle; **py**, proximal cotyle; **ra**, raised margin; **su**, sulcus; and **vr**, ventral ridge. Dorsal curvature is likely taphonomic. Scale bar equals 25 cm.
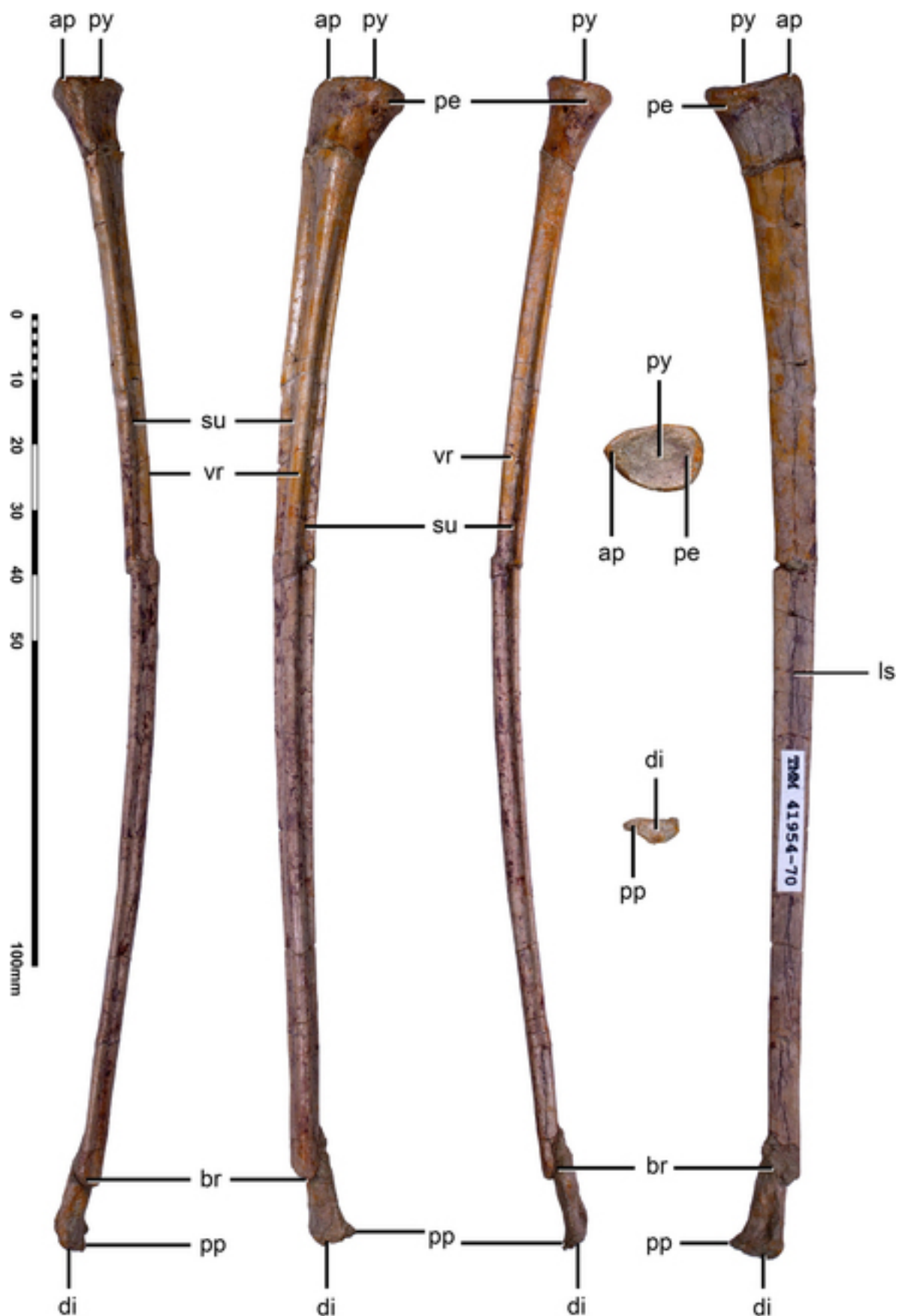
FIGURE 42. *Quetzalcoatlus lawsoni*, sp. nov., right third wing phalanx (TMM 41954-70) in **A**, anterior; **B**, ventral; **C**, posterior; **D**, dorsal; **E**, proximal; and **F**, distal views. **Abbreviations: ap**, anterior point; **br**, break; **di**, distal condyle; **ls**, flat surface; **pe**, posterior expansion; **pp**, posterior process; **py**, proximal cotyle; **su**, sulcus; **vr**, ventral ridge. Dorsal curvature is likely taphonomic. Scale bar equals 100 mm.

2001a:96). Although TMM 41961-1.7 appears to be posteriorly curved, this is attributed to taphonomy or possibly damage. The proximal end is about one-and-a-half-times the mid-width. There is a slight posterior expansion on the proximal end formed by the ventroposterior extension of the articular surface, absent in *D. macronyx* (Sangster, 2003:79). Some specimens reach their greatest proximal depth on the midline, others more posterior, and this may be related to the variable formation of a posterior process on the distal end of the third wing phalanx. The articular surface does not extend onto the anterior quarter of the proximal surface. A flange is present on the anterior margin of the fourth wing phalanx proximal end, as reported in *S. wucaiwanensis* (Andres et al., 2010:177), that reaches the proximal margin to form an anterior point and may have functioned as an extensor tubercle. The proximal surface is slightly concave and subtriangular in outline, unlike the circular outline of *Pteranodon* (Bennett, 2001a:93 and 96) or the semi-circular outline of *K. progenitor* (Andres et al., 2014:S17). The shaft of the fourth wing phalanx is dorsoventrally depressed in *Q. lawsoni* with a width about one-and-a-half times the depth. The dorsal surface of the shaft is flat, whereas there is a slight concave area on the ventral surface at the base of the anterior flange. The shaft cross-section is a posteriorly expanded lacriform that becomes circular distally and terminates in a blunt tip. This is disparate from both the triangular (Averianov, 2010:305) and 'T-shaped' cross-section of *A. lancicollis* (Averianov, 2010:306), the subtriangular becoming oval cross-section of *E. langendorfensis* (Vremir et al., 2013b:12) and *A. piscator* (Kellner and Tomida, 2000:68), the subcircular to oval cross-section becoming lacriform at the distal end with a posteriorly directed terminal crest in *Pteranodon* (Bennett, 2001a:96), the circular cross-section of *E. prolatus* (Andres and Ji, 2008:460), and the possibly ovoid cross-section of *D. macronyx* (Padian, 1983a:20). The posterior longitudinal groove reported in *D. weii* (Young, 1964:246–247) is not present in *Q. lawsoni*. The nutrient foramen on the posterior surface of the fourth wing phalanx in *Pteranodon* (Bennett, 2001a:96) could also not be located in *Q. lawsoni*.

Pelvis

The pelvis of *Q. lawsoni* has the typical pterosaur condition of a coalesced ilium, pubis, and ischium that fuses with the synsacrum medially to enclose the pelvic canal (puboischial arch of Molnar and Wiffen, 1994) and that articulates with the prepubis anteroventrally. Within pterosaurs, the ilium projects anterior and posterior processes to varying degrees, the pubis is an anteroventrally oriented process with different amounts of anterior curvature, the ischium becomes a large plate that fuses with the pubis, and the prepubis articulates with a mobile joint at the ventral end of the pubis. *Quetzalcoatlus lawsoni* takes these features to an extreme as the culmination of over 150 million years of pterosaur pelvic evolution. The pelvis is represented in the *Q. lawsoni* material by the left pelvic plate articulated with part of a synsacrum, TMM 41954-57 (Fig. 27), and the left prepubis, TMM 41954-58, which are probably from different individuals (Table 14). Unfortunately, TMM 41954-57 is fractured, heavily encrusted with concretionary material, and this matrix is often stained a similar color to the bone. The medial surfaces are obscured by matrix so that only a few features can be seen, such as the base of the first sacral rib. Pelvic material is reported in the azhdarchid species *Z. linhaiensis* (Cai and Wei, 1994:4) although it is very poorly preserved, and the putative azhdarchid specimen MOR 553 is reported to have pelvic elements (Carroll et al., 2013). A specimen from the Dinosaur Park Formation of Canada (UALVP 56200) was first identified as a partial pelvis and tentatively referred to the Azhdarchidae (Funston et al.,

2017), but it was later reidentified as a badly broken tyrannosaurid squamosal (Funston et al., 2018).

The pelvic plate (ischiadic plate of Owen, 1870, or innominate bone of Williston, 1903) of pterosaurs fuses over ontogeny (Williston, 1903; Wellnhofer, 1975b; Bennett, 1993, 1995, 2001a) so that the entire structure could be termed the iliopuboischium, but it is usually just discussed in terms of the ilium and puboischiadic plate (ischium of Plieninger, 1894, ischio-pubis of Williston, 1903, ischiopubis of Wellnhofer, 1974, puboischial plate of Molnar, 1987, ischiopubic plate of Wellnhofer, 1988, or ischiadic plate of Fastnacht, 2005). The lack of visible sutures in the TMM 41954-57 pelvis suggests that it belongs to an adult individual. Either way, this fusion makes it not possible to ascertain what portions the ilium, pubis, and ischium contribute to the acetabulum.

The acetabulum in *Q. lawsoni* is large, as in other pterosaurs (Bennett, 2001a:99; Sangster, 2003:84; Hyder et al., 2014:113–116), and subcircular in outline with a height almost that of the width, as in other pterodactyloids (Andres, 2021). It is rather shallower in (mediolateral) depth than typically reported in pterosaurs (Wellnhofer, 1988:9; Bennett, 2001a:81,99; Eck et al., 2011:289; Bennett, 2013:34) with the possible exception of *D. macronyx* (Sangster, 2003:84), but it is still imperforate as in all pterosaurs (Hyder et al., 2014). It is also positioned slightly posterior on the pelvic plate, unlike the more centrally located acetabula of ctenochasmatoids and anteriorly located acetabula of rhamphorhynchids (Hyder et al., 2014).

The acetabulum is somewhat obovate in outline due to a slight ventral point and a rather straight anterodorsal ridge (sharp dorsal rim and projection of the upper rim of Wellnhofer, 1988; rugose tubercle and possible origin of the ambiens muscle of Bennett, 2001a; deep wall, deeper anterior margin, and anterior wall of acetabulum firmly buttressed of Sangster, 2003; iliofemoralis origin of Fastnacht, 2005; raised knob of Padian, 2008a; or strong upper margin of Bennett, 2013), which is distinguished from the supra-acetabular crest of dinosaurs (Sangster, 2003; Padian, 2008b). This contrasts with the oval (Bennett, 1990:81; Kellner and Tomida, 2000:69; Bennett, 2001a:99; Eck et al., 2011:289; Naish et al., 2013b:8,11; Bennett, 2014:334), subcircular to circular (Sangster, 2003:84; Fastnacht, 2005:276; Zhou, 2010b:281; Naish et al., 2013b:3,11), or even rounded square outlines (Young, 1964:247) of other pterosaur acetabula. In addition to the anterodorsal ridge, the acetabular rim of TMM 41954-17 has an anteroventral prominence (very pronounced lower rim of Wellnhofer, 1988, cranioventral margin of Kellner and Tomida, 2000, rugose and thick pubic acetabular margin as well as prominent ventral-anterior rim of Sangster, 2003, or acetabular rim that projects further laterally at the anterior end than at the posterior end of Naish et al. 2013a). The acetabular rim lacks the dorsal emargination reported in *Pteranodon* (Bennett, 2001a:97, 99), AMNH FR 22569 (Bennett, 1990:81), and *S. crassirostris* (Bennett, 2014:334) as well as the ventral emargination reported in *Pteranodon* (Bennett, 2001a:97, 99), AMNH FR 22569 (Bennett, 1990:81), and *D. macronyx* (Sangster, 2003:84, fig. 3.15B). However, a notch is present between the anterodorsal ridge and the anteroventral prominence, unlike *D. macronyx* in which they are continuous (Sangster, 2003:83). The remaining posteroventral half of the acetabular rim is a low rugose lip, as in *D. macronyx* (Sangster, 2003:83). The posterodorsal ridge (considerable elevation forming a thick part of Young, 1964, thickened posterodorsal to the acetabulum of Veldmeijer, 2003, posteroventrally-oriented ridge and posteroventrally-oriented overhanging ridge of Naish et al. 2013a, iliofemoralis externus origin of Costa et al., 2013, or small ridge upon the postero-dorsal margin of the acetabulum and iliofemoralis origin of Frigot, 2017) and posterior subtriangular concavity (concavity posterodorsal to the acetabulum, subtriangular concavity, and shallow triangular notch of Naish

TABLE 14. Measurements of *Quetzalcoatlus lawsoni*, sp. nov., pelvic material. Values in millimeters.

Dimension:	Specimen Number: TMM 41954-57	Dimension:	Specimen Number: TMM 41954-58
Element	Left pelvis	Element	Left prepubis
Acetabulum anteroposterior length	29.47		
Ilium anterior process length	157.15	Anteroposterior length	71.84
Ilium posterior process length	64.38		
Ilium posterior process expansion length	109.11	Mediolateral width	53.67
Pubis dorsoventral depth	64.36		
Pubis anteroposterior length	13.97	Dorsoventral depth	8.52
Pubis mediolateral width	10.46		

et al. 2013a) are absent in *Q. lawsoni*. The acetabulum is deepest dorsoanteriorly, unlike the greatest central depth reported in *A. piscator* (Kellner and Tomida, 2000:69).

Much ink has been used in the discussion of the orientation of the pterosaur acetabulum with hypotheses ranging from lateral (Wellnhofer, 1975a, 1978; Bennett, 2001a:100), lateroventral (Padian, 1983b), laterodorsal (Wellnhofer and Vahldiek, 1986; Unwin, 1987; Wellnhofer, 1988:4), anterodorsal (Unwin, 1988), posterolateral (Bennett, 1990:80; Kellner and Tomida, 2000; Bennett, 2001a:97,99–100), to laterodorsoposterior (Molnar, 1987; Wellnhofer, 1988:3,9; Bennett, 1990; 2001a:99). Considering that the point of greatest depth is positioned dorsoanteriorly within the acetabulum of TMM 41954-57, it would be most defensible that the acetabulum of *Q. lawsoni* is oriented ventroposteriorly. However, this pelvic plate is not preserved well enough to decisively determine its orientation with respect to the vertebral column, and so the acetabulum could have had a somewhat different orientation.

The puboischiadic plate is generally described as broad (Dalla Vecchia, 2009:169; Andres et al., 2010:175; Zhou, 2010b:282), large (Bennett, 2001a:99; Hyder et al., 2014:116 and 121), massive (Hyder et al., 2014:118), or otherwise expanded (Hyder et al., 2014:119) in pterosaurs. Its relative size is generally discussed with respect to its dorsoventral depth (e.g., Bennett, 1992, 2001a; Hyder et al., 2014), quantified as the ratio of its depth ventral to the acetabulum (pubis length) to the acetabulum (anteroposterior) length by Naish et al. (2013b). By this metric the pubis of *Q. lawsoni* is 2.18 times the acetabulum length, which is more or less average for pterosaurs (2.24), but this dimension varies greatly over the entire group (Andres, 2021). The entire shape of the puboischiadic plate is somewhat obscured in TMM 41954-57 by a large crack and a missing portion of the ventral margin, but it resembles a quarter circle in medial/lateral view. This has been described as posteroventrally expanded in azhdarchoids (Hyder et al., 2014:119), but it seems to be prevalent in all pterosaurs except for the trapezoidal plates of basal pterosaurs (Sangster, 2003:fig. 5.10; Dalla Vecchia, 2009:169; Hyder et al., 2014:113) and the narrower and posteriorly deflected plates (Hyder et al., 2014:118) of the ornithocheiriforms more closely related to *O. simus* than *H. tianshanensis*.

In pterosaurs, the contact between the pubis and ischium in the puboischiadic plate is sometimes partially open (deep notch of Hooley, 1913, incisure of Molnar, 1987, or ventral interosseous space of Naish et al. 2013a) in the form of either a ventral separation (deep sinus of Wellnhofer, 1974, fenestration and splitting of Sangster, 2003, deep emargination of Bennett, 2013, embayment of Bennett, 2014, or ventral partition and division of Hyder et al., 2014) due to the taphonomic separation of the pubis and ischium in osteologically immature individuals, or in the form of a larger oval opening (fissure of Molnar, 1987, wide gap of Wellnhofer, 1988, recessus puboischidiacum of Frey and Martill, 1994, lateral opening and oval opening of Kellner and Tomida, 2000, ischiopubic fenestra of Veldmeijer,

2003, or large opening and ischiopubic foramen of Hyder et al., 2014) present in lanceodontians (Andres, 2021), which was likely filled by an ischiopubic ligament (Frigot, 2017). Although there is a substantial crack and missing section of bone in the puboischiadic plate of TMM 41954-57, this is positioned more posteriorly on the plate, and the pubis and ischium are confluent along their length without a ventral separation or oval opening (Andres, 2021).

Taken as whole, the pelvis of TMM 41954-57 is a comparatively large structure, assuming the rest of this individual was comparable in size to the other *Q. lawsoni* specimens. Large pelves have been intermittently reported in pterosaurs, usually in reference to sexual dimorphism (Bennett, 1992, 1994; Lü et al., 2011) and usually in reference to the depth of the puboischiadic plate (Bennett, 1992) or the size of the pelvic canal (Bennett, 1992, 1994; Frey et al., 2011; Lü et al., 2011), with the deeper plates and larger canals attributed to females to facilitate the passage of eggs. This has predominantly been done in relative terms, but Bennett (1992) quantified this magnitude relative to other pelvic dimensions. Unfortunately, none of the dimensions put forward are preserved in TMM 41954-57. Bennett (1992) also mentioned the pelvic girdle posterior emargination (angle at the base of the posterior process of the ilium of Williston, 1903, recessus ilioischia dicum of Frey and Martill, 1994, postacetabular-ischiadic recess of Hyder, 2012, or angle between the ventral margin of the postacetabular process and the posterodorsal margin of the ischium of Hyder et al., 2014) as being anteroposteriorly deeper and lacking a posterior upward curve in the ischia in putative females. This would correspond to the morphology of TMM 41954-57. In this specimen, the pelvic posterior emargination is an acute rounded angle, as described in *N. gracilis* (Williston, 1903:148), but at such a depth that the angle of the entire emargination is 13.85°, the smallest angle reported in pterosaurs (Hyder et al., 2014: table 5.1). In addition, there is no trace of a pelvic symphysis (symphysial line, median symphysis, and median suture of Williston, 1903; median symphysis of Padian, 1983b; puboischiadic symphysis of Wellnhofer, 1988; or ventral symphysis of Bennett, 2007a) or a median keel in TMM 41954-57. The pelvic plates of the putative *D. modularis* (Lü et al., 2011:23) and *A. robustus* (Frey et al., 2011:S49) females do not meet along the ventral midline and lack a keel, although it should be noted that pelvic symphyses are present in *Pteranodon* irrespective of putative sex (Bennett, 1992). Ventrally open pelves are also reported in *Anhanguera* sp. (AMNH FR 22555) (Wellnhofer, 1988:9, fig. 6), *A. piscator* (Kellner and Tomida, 2000:69), DFMMh/FV 500 (Hyder et al., 2014:115–116), *A. ammoni* (Bennett, 2007a:386), *R. muensteri* (Wellnhofer, 1975b:fig. 10; 1988:11), *Campylognathoides* sp. (Wellnhofer and Vahldiek, 1986:fig. 4), and *Campylognathoides liasicus* (Quenstedt, 1858) (Wellnhofer, 1974:20, fig. 9). However, the open pelvis in *C. liasicus* was later determined to be a break by Padian (1983b). It has been suggested that this ventral opening was bridged by cartilage (Kellner and Tomida, 2000:72, 74) or a ligament (Zhou, 2010b:282) and that a ventral process on the

ischium, such as is present on TMM 41954-57, may have been an attachment area for such a ligamentous or cartilaginous connection (Zhou, 2010b:282). The small area of bone between the ischia of *Cycnorhamphus suevicus* (Quenstedt, 1855) (Bennett, 2013:34, fig. 5) may be an ossified example of this. Possible sexual dimorphism has been suggested to be present in *Quetzalcoatlus* (Bennett, 1992:432), but this appears to be in reference to the difference in sizes between the two morphs that are erected here as *Q. northropi* and *Q. lawsoni*. The large pelvis, deep posterior emargination, and lack of preserved pelvic symphysis in TMM 41954-57 would be indicative of a putative female individual under the rubric put forward by previous authors, but this remains conjectural until more and better preserved pelvic material of this species is discovered. Putative sexual differences in pelvic structure have been reported in *Pteranodon* (Bennett, 1992, 1994, 2001a) and *Darwinopterus* (Lü et al., 2011); possibly in *D. weii*, *Anhanguera*, *Nyctosaurus*, and QM F12982 (Bennett, 1992); but not in *Rhamphorhynchus* or *Pterodactylus* (Bennett, 1992).

Ilium—The ilium of *Q. lawsoni* is dominated by giant anterior and posterior processes in TMM 41954-57 (Fig. 43): the preacetabular process (anterior process of Williston, 1903, slender pointed blade of Wellnhofer, 1974, rodlike process of Padian, 1983b, antacetabular portion of Molnar, 1987, pre-acetabular iliac blades of Wellnhofer, 1988, anterior blade of Bennett, 1990, cranial process of Frey et al., 2006, or anterior iliac process of Eck et al., 2011) and the postacetabular process (obtuse process and projection of the ilium of Williston, 1903, posterior projection of Young, 1964, rodlike process of Padian, 1983b, postacetabular portion of Molnar, 1987, posterior process and postacetabular ilium of Sangster, 2003, caudal part of the ilium of Frey et al., 2006, or posterior iliac process of Frigot, 2017) that take up 78% of the total ilium length (Table 14). These processes produce the long and slender (Kellner and Tomida, 2000:69; Bennett, 2001a:100; 2014:334) or elongate (Bennett, 2001a:97–99; Kellner et al., 2019a:15) ilia reported in pterosaurs. The dorsal surface of the ilium between these processes is smooth, as reported in *D. macronyx* and was likely just covered by integument (Sangster, 2003:81). There is no trace of the pneumaticity in the ilium reported in *Anhanguera* sp. (AMNH FR 22555) by Claessens et al. (2009) and *Vectidraco daisymorrisae* Naish et al., 2013b, by Naish et al. (2013b).

The preacetabular process of the ilium has been broken off about 4 cm from its base and displaced below it in TMM 41954-57. The respective breaks between the preacetabular process and the rest of the ilium match, and they demonstrate that the surface of the process exposed in Fig. 27 is the ventral surface. The only other possible identification for the process is the first sacral rib, the base of which is already preserved in this specimen. The base of the preacetabular process has also been fractured and rotated slightly counterclockwise in lateral view. Restoring the orientation of the base restores the two halves of the pubic tubercle positioned anteroventral to the acetabulum. This restoration produces a hyperelongate preacetabular process angled dorsally about 30° from the vertebral column with a slight ventral curvature but otherwise straight. TMM 41954-57 has the longest preacetabular process known in pterosaurs, but when its length is converted into a shape factor (dimensionless value that describes shape independent of size) by division with the postacetabular process length, it is only above average in relative length (Andres, 2021). This preacetabular process is dorsoventrally depressed as in other pterosaurs (Williston, 1903:147; Molnar, 1987:89; Kellner and Tomida, 2000:69; Eck et al., 2011:289; Naish et al., 2013b:3; Bennett, 2014:334), but it is more rod-like than blade-like, similar to *V. daisymorrisae* (Frigot, 2017) and *D. macronyx* (Padian, 1983a; Andres, 2021). In *Q. lawsoni*, this process tapers to an anterior point with straight medial and lateral margins, but

lacks the triangular pointed tip found in *Campylognathoides* (Andres, 2021). The lateral margin forms a sharp-edged ridge in TMM 41954-57, as in *V. daisymorrisae* (Naish et al., 2013b:3), instead of a rugose margin as reported in *Pteranodon* (Bennett, 2001a:100), *D. macronyx* (Sangster, 2003:80–81), and *A. piscator* (Costa et al., 2014:16). This ridge may be the origin of M. iliotibialis (Sangster, 2003:fig. 5.35; Frigot, 2017:48, fig. 2a) or MM. iliotibialis and iliofemoralis (Bennett, 2001a:100; Sangster, 2003:80–81; Costa et al., 2014:13–16), or the origin(s) may be an oblong tubercle just proximal to the break on the lateral surface. A swelling just distal to the break on the detached process may indicate a similar structure on the medial surface. A small divot on the anterior end of the preacetabular process ventral surface may be taphonomic, or correspond to the origin of M. puboischiofemoralis internus (Frigot, 2017:48, 53). The dorsiflexion of the preacetabular process is apomorphic for the Breviquartossa (Andres, 2021), but the slight ventral curvature has only been reported in *Darwinopterus robustodens* Lü et al., 2011 (Hyder et al., 2014:114). The transverse processes of the synsacral vertebrae would have contacted the preacetabular process, and a medial shelf on the preacetabular process appears to extend ventral to where they would have articulated.

Quetzalcoatlus lawsoni also has the largest postacetabular process of the ilium known in pterosaurs. The postacetabular process of pterosaurs consists of a posteriorly/posterodorsally oriented shaft that elevates a horizontal to posteroventrally oriented terminus, the dorsal and posterior margin of which is termed the apex (Naish et al., 2013b). The terminus of TMM 41954-57 is about 5.5 times the anteroposterior length of the shaft. In non-pterodactyloid pterosaurs and *Germanodactylus* this terminus consists of just the posterior projection (posterodorsal process and posteroventral extension of Naish et al., 2013a, or ventral process of Wu et al., 2017). In the other pterodactyloids, however, the terminus is expanded anteriorly due to the formation of an angular process (angular expansion and angular process of Williston, 1903; iliofibularis origin of Sangster, 2003; hook-like process and dorsal process of Zhou, 2010a; anterior-facing projection and anterior projection of Hyder, 2012; anterodorsal edge of postacetabular process of Naish et al. 2013a; anterodorsal extension of Hyder et al., 2014; or anteriorly directed prominence, angular process, and iliofibularis origin of Frigot, 2017) on the anterodorsal edge of the terminus. In *Q. lawsoni* and neoazhdarchians such as AMNH FR 22569 (Bennett, 1990:fig. 1B), EH2 (Hyder et al., 2014:fig. 8C), MN 6588-V (Sayão and Kellner, 2006:fig. 8), and possibly *K. vilsoni* (Kellner et al., 2019a), the angular process is very large and rivals the posterior projection in length. The angular process of TMM 41954-57 surpasses these other specimens, reaching the anterior margin of the acetabulum as a sharp horizontal process. The posterior projection is even larger in this specimen, extending posteroventrally past the ischium posterior margin. The posterior projection is described as hook-shaped in azhdarchoids (Hyder, 2012:119,121; Naish et al., 2013b:3), but in this specimen it is rather straight, with dorsal and ventral convexities terminating before a blunt rounded posterior tip (caudal tip of Kellner and Tomida, 2000, iliocaudalis insertion of Sangster, 2003, flexor tibialis internus 2 origin of Costa et al., 2014, or flexor tibialis internus origin of Frigot, 2017). The ventral convexity on the posterior projection may be the origin of the caudofemoralis brevis, reconstructed in a similar position in *D. macronyx* (Sangster, 2003:fig. 5.35A) and *V. daisymorrisae* (Frigot, 2017:51, fig. 2a). The lateral surface of the terminus is slightly concave as in many pterosaurs, but not in the form of a depression as found in DFMMh/FV 500 (Fastnacht, 2005:275–276) or a series of depressions/fossae as found in *V. daisymorrisae* (Naish et al., 2013b:3, 12). The preservation of this lateral surface is not sufficient to determine whether it was smooth as in *J. edentus* (Wu et al., 2017:20) and some other pterosaurs (Naish et al.,

2013b:12), or rugose for the attachment of epaxial musculature and the M. caudofemoralis (Bennett, 2001a:100); iliofemoralis, iliofibularis, flexor tibialis externus, and flexor tibialis internus 2 (Sangster, 2003:fig. 5.35A); iliofibularis and flexor tibialis (Fastnacht, 2005:fig. 16); iliofibularis, flexor tibialis externus, and flexor tibialis internus 2 (Costa et al., 2014:16–19, fig. 1A); flexor tibialis externus (Frigot, 2017:48, fig. 2a); or unspecified muscles (Kellner and Tomida, 2000:69). The terminal expansion in TMM 41954-57 is further emphasized by the constriction of the shaft of the postacetabular process found in azhdarchoids (Andres, 2021), (anteroposteriorly) deepening the posterior emargination between the posterior projection and the ischium as well as the anterior emargination between the angular process and the ilium main body. This produces the hatchet or T-shaped postacetabular processes reported in azhdarchoids (Naish et al., 2013b:3; Hyder et al., 2014:116, 121; Wu et al., 2017:20). *Quetzalcoatlus lawsoni* has a quite short shaft for the postacetabular process, unlike the longer shafts of *V. daisymorrisae* (Naish et al., 2013b:3, 8), *J. edentus* (Wu et al., 2017:20), and more basal pterosaurs. The shaft in TMM 41954-57 is oriented at about a 35° angle from the axial column, significantly higher than the subhorizontal orientation of non-novialoid, darwinopteran, and archaeopterodactyloid pterosaurs. The postacetabular process apex/terminus dorsal edge (dorsal border of Veldmeijer, 2003; or dorsal surface, dorsal edge, platform, and dorsoposterior margin of Naish et al., 2013a) is convex in azhdarchoids (Andres, 2021). In TMM 41954-57, there is a convexity on the dorsal edge of the posterior projection and another on the angular process with an emargination between the two. There may have been a missing section of bone uniting the two, except that the posterior convexity curves medially and the anterior torus curves laterally. This contrasts with the prominent medial and lateral edges on the apex found in *V. daisymorrisae* (Naish et al., 2013b:3). The short tubercle present on the apex of the *T. wellnhoferi* (SMNK PAL 1137) postacetabular process (Eck et al., 2011:290, fig. 9; Naish et al., 2013b:fig. 10) is absent in *Q. lawsoni*. A broad shelf extends along the medial surface of the anterior two-thirds of the apex; the posterior third appears to be mediolaterally compressed. In anterior/posterior view, the postacetabular process is oriented nearly straight dorsally, and there is no indication that it contacted or fused with either the sacral neural spines or the other postacetabular process, as in the Pteranodontia (Williston, 1903:148; Bennett, 2001a:100; Frey et al., 2006:30; Naish et al., 2013b:7; Hyder et al., 2014:115–116).

Pubis—The entire shape of the pubis in TMM 41954-57 (Fig. 43) is difficult to discern because the suture between it and the ischium is not visible, and so it is difficult to compare their relative sizes (Table 14). There is a demarcation between the lateral width of the pubic stalk (angular process and pectineal process of Williston, 1903; stalk of the pubis and stalklike element of Padian, 1983b; projection of the pubis of Kellner and Tomida, 2000; shaft and central ridge of the pubis of Sangster, 2003; thickened ridge and main body of the pubis of Andres et al., 2010; or dorsoventrally-aligned thickened anterior ridge, anterolateral ridge, pillar- or vertical ridge-like structure, vertical ridge, and pillar of Naish et al., 2013a) and the thinner portion of the puboischiadic plate, but this contact would assume absence of a posterior lamina in the pubis (delicate lamina of Naish et al., 2013a, laminar plate of Wu et al., 2017, or thin bony plate of Kellner et al., 2019a). The posterior lamina of the pubis is present in many (and debatably all) pterosaurs, but this can be obscured by taphonomic flattening of the laterally oriented pubic stalk, making the pubis appear anteroposteriorly longer than it was in life. The position of the obturator foramen (ischiadic foramen of Williston, 1903, foramen obturatorium of Arthaber, 1921, pubic foramen of Young, 1964, or obdurator foramen of Sangster, 2003) has been

suggested by Naish et al. (2013b) to provide an indication of the pubis-ischium contact, and the obturator foramen is present on this demarcation in TMM 41954-57. However, the pubis-ischium contact could be posterior to the obturator foramen as in *Anhanguera* (Wellnhofer, 1991a:fig. 21c; Kellner and Tomida, 2000:fig. 44; Veldmeijer, 2003:fig. 10A), and this foramen can be rather large so that a pubis-ischium contact at its anterior margin would indicate a much smaller pubis than if the contact was on its posterior margin. When the contact occurs on the posterior margin of the obturator foramen in pterosaurs, the foramen divides the main body of the posterior lamina from the dorsally positioned horizontal bar (pubic base under the acetabulum of Padian, 2008a, or comparatively thick bony bar of Kellner et al., 2019a). The obturator foramen is large in *Q. lawsoni* and lacriform in outline, unlike the rounded (Williston, 1903:148; Wu et al., 2017:19), circular (Molnar, 1987:91; Wellnhofer, 1988:8), subcircular (Eck et al., 2011:290), oval (Molnar, 1987:91), suboval (Bennett, 2001a:99; Sangster, 2003:8), or even heart-shaped (Molnar, 1987:91) obturator foramina reported in other pterosaurs. However, an irregular ventral margin suggests that only the dorsal half may be original in this specimen. The obturator foramen is positioned ventral to the anterior half of the acetabulum, as in other azhdarchoids and basal pterosaurs (Hyder et al., 2014:116). The pubis is also fused to the ilium so that it is not possible to ascertain if an anterodorsal process (articular surface facing dorsally for the preacetabular process of Kellner and Tomida, 2000, dorsal part of the pubis forming the anteroventral part of the acetabulum of Veldmeijer, 2003, second bar orientated dorsally of Eck et al., 2011, pubis thickened and extended anterodorsally along the acetabulum of Wu et al., 2017, or stout dorsal portion that contacts the ilium of Kellner et al., 2019a) was present at the anterior end of the contact with the ilium.

The pubic stalk is deflected laterally in pterosaurs, creating a larger pelvic brim (opening of the pelvis and pelvic brim of Williston, 1903, anterior margin of the pelvic canal of Bennett, 2001a, or pelvic aperture of Frey et al., 2011) and forming a concave lateral surface on the puboischiadic plate termed the pubic fossa (depression or fossa of Young, 1964, facet on the anterior margin of the pubis immediately below the acetabulum of Molnar, 1987, slightly depressed area of Veldmeijer, 2003, or pubic fossa and puboischiofemoralis externus origin of Frigot, 2017). This stalk is usually just described as an anterior thickening of the pubis in pterosaurs (Williston, 1903:148; Wellnhofer, 1988:8; Kellner and Tomida, 2000:72; Dalla Vecchia, 2009:169; Zhou, 2010b:282–283; Naish et al., 2013b:3–4, 9; Wu et al., 2017:17–19), but this is predominantly or entirely due to the lateral orientation of the pubic stalk. The stalk varies in orientation in pterosaurs from anteroventral (Williston, 1903:147; Naish et al., 2013b:3; Wu et al., 2017:19), ventral (Padian, 1983a:35; Bennett, 2001a:97–99; Sangster, 2003:83; Padian, 2008b:55; Eck et al., 2011:289; Naish et al., 2013b:3–4; Hyder et al., 2014:118), to posteroventral (Molnar, 1987:91; Veldmeijer, 2003:90; Hyder et al., 2014:120), with *Q. lawsoni* in the anteroventral category. Similar variation exists for the curvature of the pubic anterior margin, with *Q. lawsoni* curving slightly anteroventrally, as inherited from the Ornithocheiroidea (Andres, 2021).

The dorsal end of the pubic stalk is deflected posterolateraly in TMM 41954-57, accentuating the depth of the pubic fossa in the region of the obturator foramen. Anterior to the foramen and stalk is the preacetabular fossa (subtle concavity of Naish et al., 2013a, preacetabular fossa and puboischiofemoralis internus origin of Costa et al., 2014, or ventral iliac fossa and puboischiofemoralis internus origin of Frigot, 2017) found in azhdarchoids (Sayão and Kellner, 2006:fig. 8A; Naish et al., 2013b:3; Costa et al., 2014:fig. 8C; Frigot, 2017:48, fig. 1c). The pubic tubercle (small tuberosity and ambiens tubercle of Sangster, 2003, small
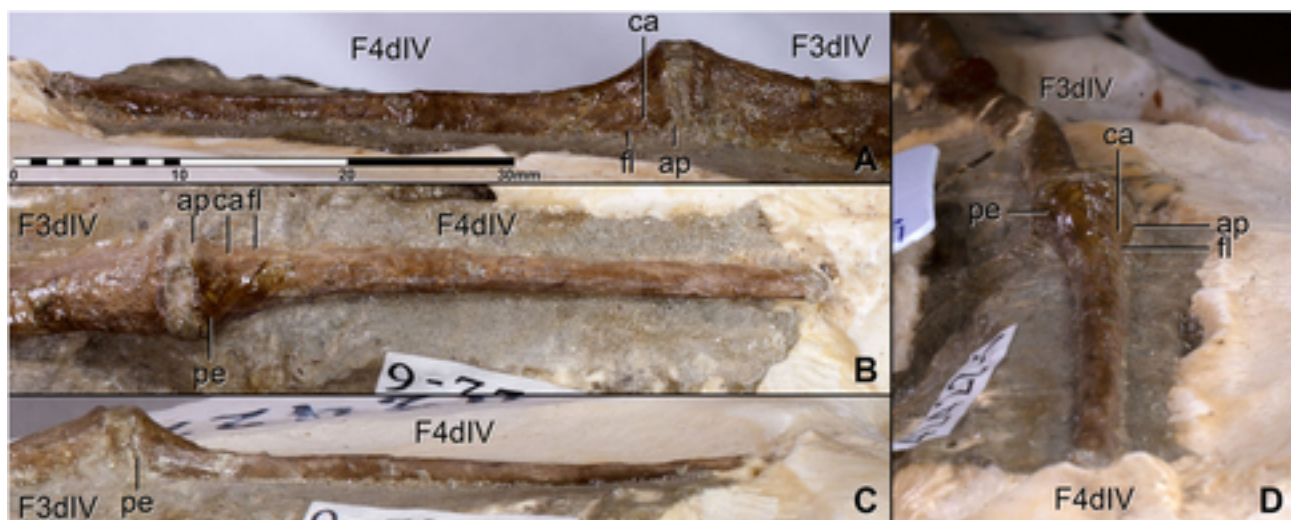
FIGURE 43. *Quetzalcoatlus lawsoni*, sp. nov., left fourth wing phalanx (TMM 42422-6.2) and distal end of third wing phalanx (TMM 42422-6.1) in **A**, anterior; **B** ventral; **C**, posterior; and **D**, distal views. **Abbreviations: ap**, anterior point; **ca**, concavity; **fl**, flange; **FXdIV**, phalanx X of wing digit; and **pe**, posterior expansion. Scale bar equals 30 mm.

distinct tubercle of Veldmeijer, 2003, or pubic tubercle and ambiens origin of Frigot, 2017) is positioned dorsal to the preacetabular fossa and anterior to the acetabulum in this specimen. This is distinct from a small tubercle (third rugose tubercle of Bennett, 2001a) on the anteroventral part of the acetabular rim.

The pubic stalk expands in mediolateral width ventrally in TMM 41954-57, as in other pterosaurs (Williston, 1903:148; Molnar, 1987:91; Wellnhofer, 1988:9; Bennett, 2001a:100; Sangster, 2003:83). Sangster (2003) reconstructed the M. pubiosichiofemoralis externus as originating both on the lateral surface of the stalk and posterior to it on the plate, whereas Costa et al. (2014) reconstructed the insertion of M. puboischiofemoralis externus 2 posterior to the pubic stalk. The prepubic articular surface (cranioventral joint of Claessens et al., 2009) is positioned at the ventral end of the pubis in *Q. lawsoni* as in all pterosaurs, save for some *Anhanguera* specimens in which it is suggested to be on a projection of the pubis anterior margin (Wellnhofer, 1988:fig. 3; Kellner and Tomida, 2000:72, fig. 44; Veldmeijer, 2003:fig. 10). This articular end is lacriform in ventral view, as in *V. daisymorrisae* Naish et al. (2013b). There is no trace of a pubic symphysis in this specimen. The foramina reported in QM F12982 by Molnar (1987) and the pneumaticity reported in *Anhanguera* sp. (AMNH FR 22555) by Claessens et al. (2009) could not be located in *Q. lawsoni*.

Ischium—The pubis-ischium contact is not visible in TMM 41954-57 (Fig. 27), and so it is not possible to determine the exact position and orientation of the ischium. However, it can be seen to be a large laterally compressed semicircular plate, which shares a convex ventral margin with the novialoids (Andres, 2021). The ischium is likewise fused to the ilium so that it is not possible to ascertain if a posterodorsal process (spur of Hooley, 1913) was present at the posterior end of the contact with the ilium. The ischium as a whole is approximately equal in depth to the pubis but does extend as far posteriorly as the postacetabular process of the ilium. The ventral margin is damaged and deeply incised by a wedge-shaped crack, approximately where Fastnacht (2005) reconstructed the puboischiofemoralis origin and Costa et al. (2014) reconstructed the adductor femoris 2 and flexor tibialis internus 1 origins. Likewise, the adductor femoris and puboischiotibialis origins reconstructed

along the ventral margin of the ischium by Sangster (2003) cannot be assessed. Between this crack and pubic stalk is a ventral process, which is also reported in *E. prolatus* (Zhou, 2010b:282–283) and *Austriadraco dallavecchiai* Kellner, 2015 (Dalla Vecchia, 2019, fig. 23), and appears to be natural in this specimen. This may be the attachment area for a ligament or cartilage (Zhou, 2010b:282), but Fastnacht (2005) reconstructed the adductor femoris origin and Costa et al. (2014) reconstructed the adductor femoris 2 origin in this area. The angular extremity (distal projection of Kellner and Tomida, 2000, laterally projecting point and ischiocaudalis origin of Sangster, 2003, caudal projection of Dalla Vecchia, 2009, posteroventral corner of Naish et al., 2013a, posterior extension and posteroventral margin of Hyder et al., 2014, or 'caudal process' of Dalla Vecchia, 2014) at the posteroventral corner of the ischium is rounded, as in most pterosaurs in which it is described (Kellner and Tomida, 2000:74; Sangster, 2003:83–84; Dalla Vecchia, 2019:38). It curves slightly laterally, as in *A. piscator* (Kellner and Tomida, 2000:74) and *D. macronyx* (Sangster, 2003:83). The posterior margin of the ischium (in the posterior emargination) is oriented posteroventrally/anterodorsally and is slightly concave in medial/lateral view, as is common in pterosaurs (Kellner and Tomida, 2000:74; Sangster, 2003:83; Naish et al., 2013b:4; Dalla Vecchia, 2019:38). This margin is interrupted in its middle by a low ischial eminence (short rounded process, prominent tubercle, ischial tubercle, flexor tubercle, and flexor tibialis internus 3 origin of Sangster, 2003; tubercle of Eck et al., 2011; ischial tuberosity and flexor tibialis internus 3 origin of Costa et al., 2014; dorsal caudal process of Dalla Vecchia, 2014; or ischial tubercle, potential flexor tibialis internus 3 origin, and ischial eminence of Frigot, 2017). Sangster (2003) reconstructed the origin of the flexor tibialis internus 1 and Costa et al. (2014) reconstructed the origin of the flexor tibialis internus 3 between the angular extremity and ischial eminence, but preservation is not sufficient to determine if these are present in *Q. lawsoni*. The diagonal ridge (subtle and faint diagonal ridge of Naish et al., 2013a, or diagonal prominence of Frigot, 2017) dividing the ischium lateral surface into a dorsal ischial fossa (flexor tibialis internus origin, postero-dorsal fossa, and dorsal ischial fossa of Frigot, 2017) and a ventral ischial fossa (adductores femores origins

and ventral ischial fossa of Frigot, 2017) as well as the shallow sub-rounded concavity posteroventral to the acetabulum reported in *V. daisymorrisae* are not visible in TMM 41954-57. Likewise, the small foramina reported in *Pteranodon* (Bennett, 2001a:99, fig. 103A) and *K. vilsoni* (Kellner et al., 2019a:16, fig. 8d) also cannot be located in this specimen. However, a tubercle posterior to the acetabulum (second rugose tubercle of Bennett, 2001a, and raised node of Sangster, 2003) found in *Pteranodon* (Bennett, 2001a:99, fig. 103) and *D. macronyx* (Sangster, 2003: fig. 3.15A) is present in TMM 41954-57. There is no trace of an ischial symphysis or keel in this specimen.

Prepubis—The prepubis (pubis of Owen, 1870; prepubic bone of Seeley, 1901; praepubis of Arthaber, 1921; distal half of the pubis or prepubis of Padian, 1983a; prepubis or prepubic process of Sangster, 2003; or praepubis, epipubis, or os marsupial Claessens and Vickaryous, 2008) is either a neomorphic element or a distal segment of the pubis that articulated with the pubic stalk through a syndesmotic or synovial joint (Claessens and Vickaryous, 2008). It likely served as an origin for a hepatic piston muscle (Padian, 1983a) for the expansion and contraction of the abdominal cavity through its posteroventral-anterodorsal rotation during respiration (Carrier and Farmer, 2000; Claessens et al., 2009; Geist et al., 2014). The pterosaur prepubis consists of the blade (bony plate of Wellnhofer, 1974, median blade of Padian, 1983a, prepubic plate of Carrier and Farmer, 2000, paddle and blade of Sangster, 2003, apron of Padian, 2008a, lamina of Zhou, 2010b, ala of Frey et al., 2011, and prepubic blade of Dalla Vecchia, 2019) and the shaft (posterior flattened portion of Williston, 1903, stick-like base of Wellnhofer, 1974, posterior ramus of Bennett, 2001a, corpus of Frey et al., 2006, stalk of Padian, 2008a, peduncle of Frey et al., 2011, or prepubic stalk and stem of Dalla Vecchia, 2019), which articulates with the pubis. In the Macronychoptera, the shaft has a constriction such that it forms a process distinct from the blade (Andres, 2021). The only prepubis preserved in *Q. lawsoni* is a left element, TMM 41954-58 (Fig. 44), and is complete (Table 14). Prepubes are reported in the azhdarchid species *Z. linhaiensis* (Cai and Wei, 1994).

TMM 41954-58 is slightly below average in aspect ratio for prepubes in pterosaurs with a length about 1.4 times its maximum width (Andres, 2021). The blade is relatively flat, characteristic for pterosaurs (Geist et al., 2014), but the entire structure forms a dorsally concave dish. It has concave medial and convex lateral margins in dorsal/ventral view so that the bone curves anteromedially, as in many pterosaurs (Bennett, 2001a:68; Sangster, 2003:84; Frey et al., 2006:30; Padian, 2008b:55). There is a medial contact for the symphysis with the right prepubis, but it is unfused in this specimen. This contact is straight but oriented at an angle to the proximal articulation. If the median symphysis was positioned on the midline, then the entire bone would be oriented anteromedially and the shaft would be oriented posterolaterally, a shaft orientation suggested to be found in putative female specimens by Bennett (2001a). The prepubis is also not fused with the gastralia, which occurs in the pteranodontians (Williston, 1903:149; Bennett, 2001a:68, 97; Frey et al., 2006:27, 30–31; Geist et al., 2014:2243). The posteromedially directed muscle scar reported on the ventral side of the prepubis in *Pteranodon* (Bennett, 2001a:68) could not be located in TMM 41954-58.

The prepubic blade of pterosaurs consist of a medial process (angularly expanded median symphysis of Williston, 1903, medial ramus of Bennett, 2001a, symphysis of Sangster, 2003, cranially directed ramus of Frey et al., 2006, medial prepubic prong of Claessens et al., 2009, or medial part of the ala of Frey et al., 2011) and a lateral process (anterior process of Williston, 1903, craniolateral process of Carrier and Farmer, 2000, anterior ramus of Bennett, 2001a, divergent stump of Sangster, 2003, cranially directed ramus of Frey et al., 2006, or laterally directed rounded process of Frey et al., 2011). In *Q. lawsoni*

and most macronychopterans, the medial and lateral processes are united to form a flabellate (fan shape) outline in dorsal/ventral view (Andres, 2021). The medial process tapers along its length with the same medial curvature found in the rest of the pubis. The orientation of the median symphysis implies that the medial process contacted its counterpart at an obtuse angle, as reported in some *Pteranodon* specimens (Bennett, 2001a:68). The lateral process bows outward in a flange, similar to *A. primordius* (Frey et al., 2011:S43, fig. 2–4) and *S. crassirostris* (Bennett, 2014:334, fig. 1), and is thickest at its lateral-most point in TMM 41954-58. A notch in the posterior end of the lateral process at its contact with the shaft is infilled with plaster, making it appear to have a posterior tubercle, such as the one reported in *A. primordius* (Frey et al., 2011: S43, figs. 2–4). However, this plaster is believed to be a fairly accurate restoration because a flange can be seen to be present on at least part of the prepubis shaft lateral surface. The dorsal surface of the lateral process has a linear muscle scar. The circular fenestra (large foramen of Sangster, 2003) reported in the prepubic blade of *C. liasicus* is absent in TMM 41954-58.

The prepubic shaft is short and robust as in other ornithocheiroids. It is the only thick portion of the entire prepubis and expands proximally, which seems to be true of well preserved pterosaur prepubes (Williston, 1903:149; Sangster, 2003:84). The proximal articular surface is oblong in outline and is not angled with respect to the shaft, as found in pteranodontians (Bennett, 2001a:68; Frey et al., 2006:30). In pterosaurs, the proximal articular surface of the prepubis is described as either flat (Sangster, 2003:84; Frey et al., 2006:30) or concave (Bennett, 2001a:68; Frey et al., 2011:S43). TMM 41954-57 falls in the latter category. The dorsal ridge ('dorsal crest' of Dalla Vecchia, 2014) of *E. rosenfeldi* (Dalla Vecchia, 2014:11, fig. 4.1.124) as well as the dorsal and ventral ridges of *D. macronyx* (Sangster, 2003:84, fig. 3.16) found on the prepubic shaft of these species are not present in *Q. lawsoni*.

Hind Limb

The hind limb of pterosaurs consists of the femur, a tibiotarsus formed from the fusion of the tibia with the fibula and a couple of proximal tarsals, the medial and lateral distal tarsals, five metatarsals, and 14–16 pedal phalanges. It has been reconstructed in various positions for flight, but without a clear consensus. None of these positions, however, make intuitive sense in descriptions and are not comparable with the relatives of pterosaurs, which are terrestrial with erect or at least semierect posture. Therefore, the hind limb in *Q. northropi* is described here in a standing position with the leg vertical and the pes plantigrade.

Femur—The femur is one of the most robust yet poorly preserved bones in *Q. lawsoni*. A complete right femur (TMM 41544-2), left femur missing the proximal end (TMM 41961-1.22), right femur missing the proximal end (TMM 41544-27), right femur missing the head and much of distal end (TMM 42422-28), left femur proximal end missing the head (TMM 42272-1), right femur proximal end (TMM 42422-27), right femur shafts (TMM 41544-17, 41954-83, 41961-1.24, and 42297-1), and a right femur distal end (TMM 41954-59.2) are preserved (Table 15). TMM 41544-2 is the best preserved specimen in the material and so is described here in detail, although it has a crushed and distorted distal end (Fig. 45), and compared with TMM 41047-1 (*Quetzalcoatlus* cf. *northropi*). *Quetzalcoatlus lawsoni* has one of the longest femora relative to the humerus (162%), surpassed only by *S. benxiensis* (Andres, 2021).

The large femoral head is set on a constricted neck, which is about half of the diameter of the head in *Q. lawsoni*. This constriction is slightly more pronounced medially so that the neck
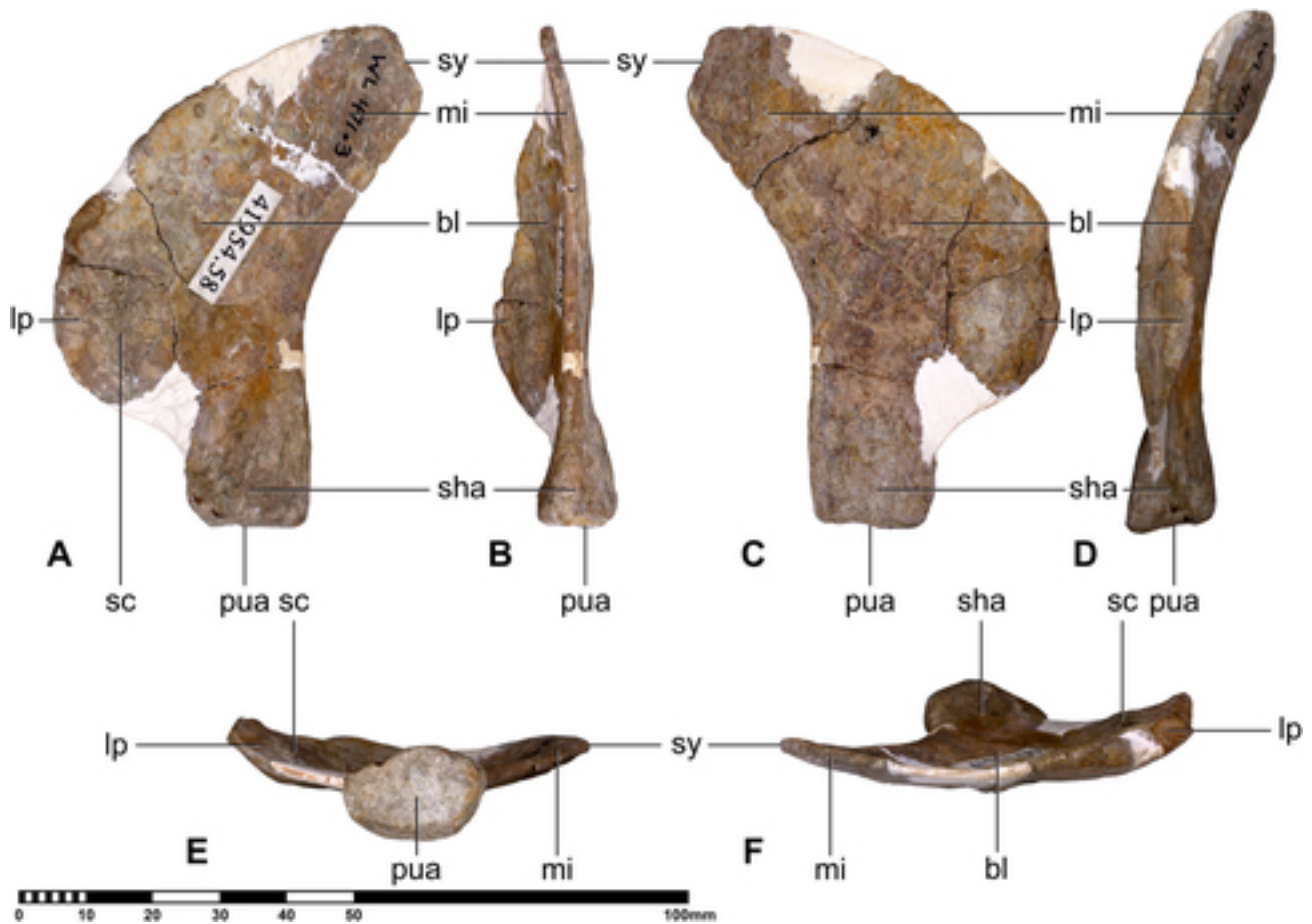
FIGURE 44. *Quetzalcoatlus lawsoni*, sp. nov., left prepubis (TMM 41954-58) in **A**, dorsal; **B**, medial; **C**, ventral; **D**, lateral; **E**, proximal; and **F**, distal views. **Abbreviations: bl**, blade; **lp**, lateral process; **mi**, medial process; **pua**, pubis articulation; **sc**, scar; **sha**, shaft; and **sy**, symphysis. Scale bar equals 100 mm.

contacts the head more laterally, similar to TMM 41047-1. The head is hemispherical with a subcircular cross-section. It has an articular surface positioned slightly more anteriorly than posteriorly. The cross-section is not entirely circular because there is a slight notch on the posteromedial surface. The femoral head and neck are angled anteromedially 136° with respect to femoral shaft, three degrees less but essentially the same angle as in TMM 41047-1. However, it appears to be directed more anteriorly than in TMM 41047-1. The femoral neck is ovate in cross-section, tapering posterolaterally due to a flange extending laterally between the neck and greater trochanter, contrasting with the more elliptical cross-section of TMM 41047-1. The flange itself is posteriorly excavated by the intertrochanteric fossa which contains a large oval pneumatic foramen, distinct from the relatively smaller slit-like foramen of TMM 41047-1. The foramen in *Q. lawsoni* is oriented dorsally and positioned posteriorly to the humeral neck and greater trochanter. This greater trochanter is a massive, anteriorly curving, rugose, and hook-shaped process. Anteriorly, there is a subtle fossa at the base of the process bounded ventrolaterally by the lesser trochanter in the form of a rugose tubercle. A thin jagged ridge extends from the dorsal margin of the lesser trochanter down the proximal 5 cm of the middle of the anterior surface that is likely a muscle scar. Posteriorly, the greater trochanter continues ventrally as a rugose ridge for about the same distance. Lateral to

this rugose ridge, the femur expands outward in a convex trochanteric crest. The internal trochanter is positioned medial to the distal end of the rugose ridge on the posterior surface of the femur. A slight sulcus separates the internal trochanter from the rugose ridge, as reported in *A. bostobensis* and *A. lancicollis* (Averianov, 2007:195), *C. boreas* (Godfrey and Currie, 2005:306), as well as *A. piscator* (Kellner and Tomida, 2000:75) and *spielbergi* (Veldmeijer, 2003:94, fig. 20A). The posterior protuberance found in TMM 41047-1 cannot be distinguished from the trochanteric crest in *Q. lawsoni*.

The femur is bowed anteriorly with a curvature of 57° (concave posteriorly, convex anteriorly) in *Q. lawsoni*, matching the strong curvature of TMM 41047-1 and the dsungaripterids. However, it is straight in anterior/posterior view with a slight lateral curvature of the distal end, as in *D. macronyx* (Padian, 1983a:22), but damaged in TMM 41544-2. The femoral shaft is constricted just distal to the proximal end, unlike in TMM 41047-1. The shaft expands gradually over its length, but it expands in different directions in different specimens: TMM 41954-83, 41961-1.22 and 24, 42297-1, 42422-28 are expanded anteroposteriorly, whereas TMM 41544-2, 7, and 27 are expanded mediolaterally. These differences in cross-sectional shape are attributed to preservation. The shaft cross-section appears to transition from oval to more D-shaped along its shaft, as in *A. lancicollis* (Averianov,

TABLE 15. Measurements of *Quetzalcoatlus lawsoni*, sp. nov., hind limb material. Values in millimeters. >, preserved value; <, maximum possible value; ~, approximate value; a-p, anteroposterior dimension; lat, lateral dimension; and p-d, proximodistal dimension. Holotype specimen in italics.

Dimension: Element: Specimen Number:	Length (p-d)	Mid-width (lat)	Mid-breadth (a-p)
Femur			
TMM 41544-2	385	28.45	18.10
TMM 41544-17	>255	15.03	29.48
TMM 41544-27	>342	22.95	23.15
TMM 41954-59.2	>19.75	34.49	38.06
TMM 41954-83	>155.57	22.78	18.14
TMM 41961-1.22	>315	22.81	25.67
TMM 41961-1.24	>166.20	25.07	33.49
TMM 42272-1	>132.62	19.67	21.74
TMM 42297-1	>188.89	17.43	22.92
TMM 42422-27	>66.42	24.26	>12.57
TMM 42422-28	345	23.47	26.75
Tibiotarsus			
TMM 41954-79	>28.07	26.15	<39.45
TMM 41961-1.23	553	14.11	25.77
TMM 41961-1.25	548	18.50	26.04
TMM 42180-20	>494	18.33	22.11
TMM 42272-2	>144.70	14.77	23.16
TMM 42422-9	601	19.90	27.38
TMM 42422-10	570	22.28	28.06
TMM 42422-11	575	19.27	26.76
Fibula			
TMM 41961-1.23	121.54	4.89	4.34
TMM 41961-1.25	125.39	?	4.65
TMM 42180-20	122.25	5.40	4.30
TMM 42422-9	145.70	5.49	4.99
TMM 42422-10	138.54	5.99	5.74
TMM 42422-11	~112.93	?	4.66

2010:309). A long and jagged ridge identified as the adductor ridge extends from the femur medial surface a quarter of the length from the proximal end to the posterior surface at the mid-length in *Q. lawsoni*. This ridge is expanded at its preserved distal end, which is identified as the fourth trochanter. The anterior and posterior longitudinal grooves found in TMM 41047-1 are not present in *Q. lawsoni*.

The distal end of the *Q. lawsoni* femur is expanded due to two large semicircular condyles and epicondyles that appear to reach the same point distally, unlike in *A. spielbergi* (Veldmeijer, 2003:94) and *D. macronyx* (Padian, 1983a:22) in which the lateral condyle extends slightly farther posterodistally. Instead the medial condyle and epicondyle are substantially larger than the lateral in *Q. lawsoni*, as reported in *Pteranodon* (Bennett, 2001a:104), *A. spielbergi* (Veldmeijer, 2003:94), and *D. banthensis* (Padian, 2008b:56). The distal condyles of *Q. lawsoni* are expanded onto the posterior surface as in other pterosaurs (Padian, 1983b), but they do not reach the anterior surface of the distal end. Instead there is a pair of raised prominences divided by the intercondylar sulcus (central notch of Godfrey and Currie, 2005, or medial groove of Fastnacht, 2005) positioned at the distal end of the anterior surface. There appears to be an intercondylar fossa (patellar sulcus of Veldmeijer, 2003) for the attachment of the quadriceps femoris tendon (Wellnhofer, 1974:21) or the triceps femoris tendon (Bennett, 2001a:104), but this region is not preserved well in any *Q. lawsoni* specimen. The wide intercondylar sulcus extends from the anterior surface over the condyles to contact a large but shallow popliteal fossa posteriorly, as in other pterosaurs (Bennett, 2001a:104; Veldmeijer, 2003:95; Averianov, 2010:309). A short transverse ridge in the posterior part of the intercondylar sulcus reported in *A. lancicollis* (Averianov, 2010:309) is not present in *Q. lawsoni*. The sulcus deeply divides the condyles,

which is usually described as shallow in pterosaurs (Kellner and Tomida, 2000:75; Bennett, 2001a:104; Godfrey and Currie, 2005:306; Averianov, 2010:309). The intercondylar sulcus posteriorly turns the condyles into a pair of posterior processes in *Q. lawsoni*, which can also be seen in *A. lancicollis* (Averianov, 2010:fig. 34) and TMP 1991.36.616 (Godfrey and Currie, 2005: fig. 16.10D). The epicondyles of *Q. lawsoni* are greatly expanded constituting the entire medial and lateral surfaces of the distal end. These are prominent flanges separated from the condyles by sulci; they extend from the anterior end of the distal surface to the posterior surface of the femur to form the medial and lateral margins of the popliteal fossa. The entepicondyle is larger, unlike in *Pteranodon* (Bennett, 2001a:104), and more distolaterally oriented than the smaller and more laterodistally oriented ectepicondyle. The condyles and epicondyles are oriented at a slight acute angle with respect to one another, forming a trapezoidal distal cross-section that tapers anteriorly. A circular depression is present on the anterior end of the medial condyle on the femur distal surface as in TMM 41047-1.

Tibiotarsus—The crus of pterosaurs consists of the tibia, the fibula, and the proximal tarsals (astragalus and calcaneum) that fuse together ontogenetically. This element would therefore technically be the tibiofibulotarsus, but it will continue to be termed the tibiotarsus here to maintain consistency in the literature (Padian et al., 2021). These elements are surprisingly well preserved in *Q. lawsoni*. A complete left tibiotarsus is present in TMM 41961-1.23, and a complete right tibiotarsus is preserved in TMM 41961-1.25 as well as 42422-9 (Fig. 46) and 42422-11; TMM 42180-20 and 42422-10 (impression of distal end preserves total length) are left tibiotarsi just missing their distal ends; TMM 42272-2 is a left shaft fragment in two pieces; and TMM 41954-79 is a left distal end attached to a cervical V (TMM 41954-7) (Table 15). The proximal tarsals are fused to the tibia with no trace of a suture in all specimens. Tibiotarsi are also preserved in the azhdarchid species *C. boreas* (Hone et al., 2019), *Z. linhaiensis* (Cai and Wei, 1994), possibly *M. maggii* (Vullo et al., 2018), and *A. lancicollis* (Averianov, 2010), as well as the putative azhdarchid specimens TMM 41839-3.3 (pers. obs.) and YPM VPPU 021821 (Baird and Galton, 1981).

The length of the tibiotarsus is 30 times its mid-width in *Q. lawsoni*, about one-and-a-half times the femur length as in other neoazhdarchians (Andres, 2021). It is straight in anterior/posterior view, but it has a slight anterior curvature in medial/lateral view (concave anteriorly, convex posteriorly). This is unlike the straight tibiotarsi of most pterosaurs (Young, 1964:248; Bennett, 2001a:104; 2007a:387; Dalla Vecchia, 2009:169; Bennett, 2013:35), the posteriorly curved tibiotarsi of *S. crassirostris* (Bennett, 2014:334) and the ornithocheiriforms (Kellner and Tomida, 2000:78; Veldmeijer, 2003:95, fig. 21, pl. 16; Lü and Ji, 2005b:160), the medial curvature also found in the tibiotarsi of *Anhanguera* (Kellner and Tomida, 2000:fig. 53; Veldmeijer, 2003:fig. 21, pl. 16), or the slight lateral curvature in the tibiotarsus of *A. primordius* (Frey et al., 2011:S48). The proximal 15% of the tibiotarsus in *Q. lawsoni* is slightly and gradually expanded, but the remainder of the shaft is approximately the same diameter until the expanded distal condyles, similar to the proximal quarter expansion of *Pteranodon* (Bennett, 2001a:104) and *E. rosenfeldi* (Dalla Vecchia, 2009:169), but contrasting with the constant width of *D. macronyx* (Sangster, 2003:87) and the gradually tapered widths of *Z. linhaiensis* (Cai and Wei, 1994:8) and other pterosaurs (Young, 1964:248; Kellner and Tomida, 2000:78; Veldmeijer, 2003:fig. 21, pl. 16; Eck et al., 2011:290; Frey et al., 2011: S48; Wu et al., 2017:20). The proximal end of the tibiotarsus is flared for the cotyles as in other pterosaurs (Young, 1964:248; Bennett, 2007a:387; Dalla Vecchia, 2009:169; Frey et al., 2011: S48) as well as posteriorly inclined as in *D. macronyx* (Padian,
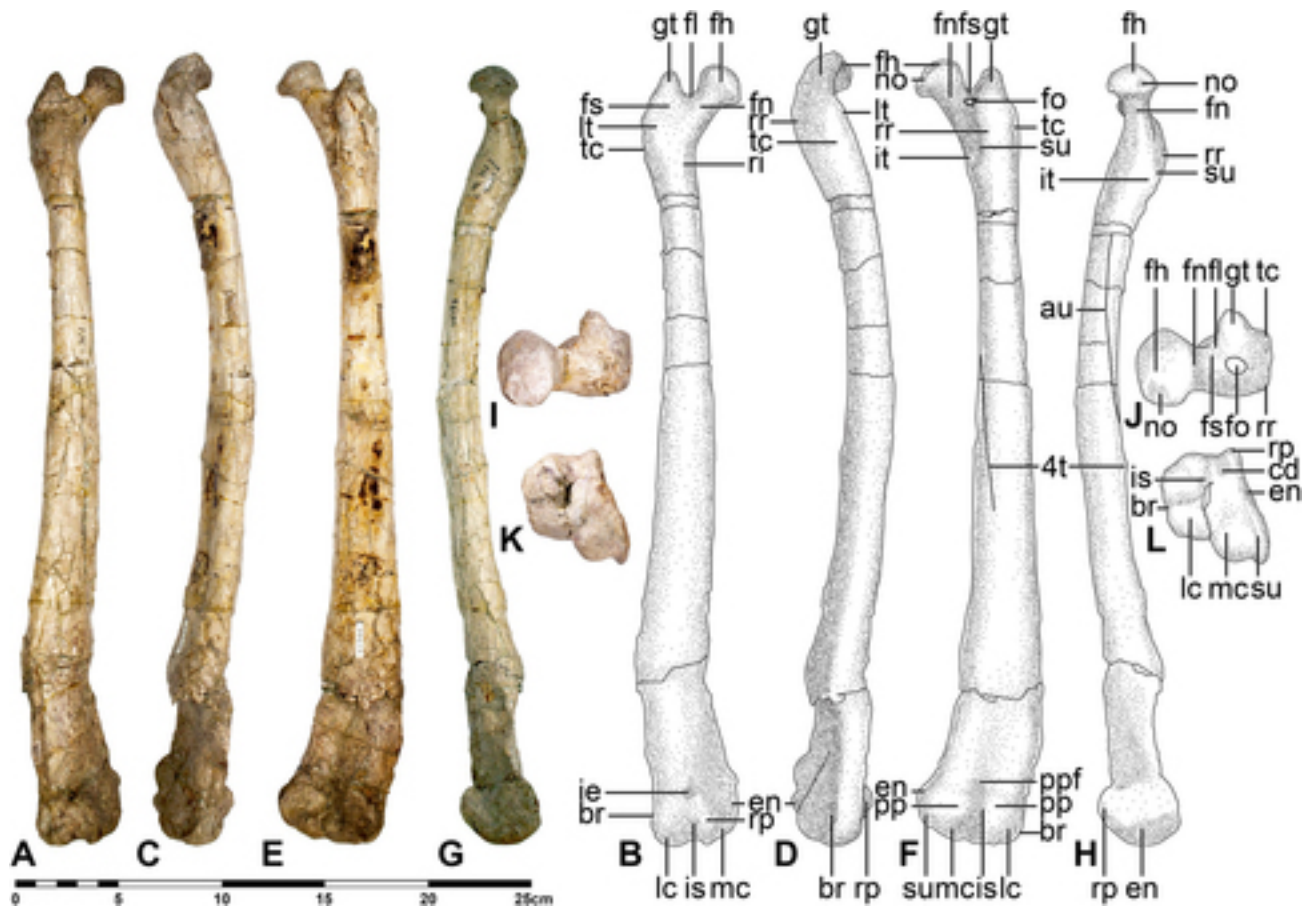
FIGURE 45. *Quetzalcoatlus lawsoni*, sp. nov., right femur (TMM 41544-2) in **A**, anterior photograph and **B**, line drawing; **C**, right lateral photograph and **D**, line drawing; **E**, posterior photograph and **F**, line drawing; **G**, left medial photograph and **H**, line drawing; **I**, proximal photograph and **J**, line drawing; and **K**, posterior photograph and **L**, line drawing views. **Abbreviations: 4t**, fourth trochanter; **au**, adductor ridge; **br**, break; **cd**, circular depression; **en**, entepicondyle; **fh**, femoral head; **fl**, flange; **fn**, femoral neck; **fo**, foramen; **fs**, fossa; **gt**, greater trochanter; **ie**, intercondylar fossa; **is**, intercondylar sulcus; **it**, internal trochanter; **lc**, lateral condyle; **lt**, lesser trochanter; **mc**, medial condyle; **no**, notch; **pp**, posterior process; **ppf**, popliteal fossa; **ri**, ridge; **rp**, raised prominence; **rr**, rugose ridge; **su**, sulcus; and **tc**, trochanteric crest. Scale bar equals 25 cm.

1983a:22; Sangster, 2003:87). This proximal flare forms a sulcus with the shaft posteriorly, which has been identified in *D. macronyx* for the attachment of lower leg flexors (Sangster, 2003:87).

The proximal surface of the tibiotarsus is readily visible in TMM 41961-1.23 as well as 42422-9 (Fig. 46) and 42422-10, although TMM 41961-1.23 appears to have been anteroposteriorly compressed taphonomically. The proximal surface has a lemon-shaped outline with small anterior and posterior processes, comparable to the mediolaterally compressed suboval of pteranodontoids (Kellner and Tomida, 2000:78; Bennett, 2001a:104) but less so the anteroposteriorly compressed ovals of other pterosaurs. The anterior and posterior processes in *Q. lawsoni* are the cnemial boss (Padian, 2008b) and posterodorsal eminence, respectively. The cnemial boss (incipient expansion and tuberosity of Padian, 1983a, extensor tubercle of Unwin, 1991, large protuberance of Kellner and Tomida, 2000, incipient cnemial crest of Sangster, 2003, small knob of Dalla Vecchia, 2009, or proximal tubercle of Aires et al., 2014) has been identified as the insertion for knee extensor musculature (Sangster, 2003), specifically M. triceps femoris (Bennett, 2001a). It is positioned slightly medially as in other pterosaurs (Bennett, 2001a: fig. 109; Dalla Vecchia, 2009:170; Frey et al., 2011:S48), unlike

the anterolateral position of *A. piscator* (Kellner and Tomida, 2000:78). Shallow but distinct medial and lateral cotyles for articulation with the distal femur condyles are present on the proximal surface of the *Q. lawsoni* tibiotarsus. The medial cotyle is positioned more anteriorly, as reported in *Pteranodon* (Bennett, 2001a:104). A midline intercotylar ridge (low bony ridge of Kellner and Tomida, 2000, slight elevation of Sangster, 2003, or process on the cranial edge of the proximal articular surface of Dalla Vecchia, 2009) separates these articulations in *Q. lawsoni*, unlike the combined concave facet of pteranodontians (Bennett, 2001a:104; Frey et al., 2006:32). In *Q. lawsoni*, the lateral cotyle is a semicircle and the medial cotyle is an ellipse in outline, which are both disparate from the laterally compressed articular surfaces of the pteranodontoids (Kellner and Tomida, 2000:fig. 54; Bennett, 2001a:fig. 109C; Veldmeijer, 2003:fig. 21, pl. 16) or the subcircular cotyles of more basal pterosaurs (Padian, 1983a:fig. 20; Sangster, 2003:87). The lateral cotyle is broader than the medial cotyle in *Q. lawsoni*, as in other pterosaurs (Dalla Vecchia, 2009:169). The fibula does not participate in the knee joint, unlike in *Pteranodon* (Bennett, 2001a:104) and *D. macronyx* (Seeley, 1901:60; Padian, 1983a:22; Sangster, 2003:87). A large circular opening appears to be present in the middle of the medial cotyle in *Q. lawsoni*, but it

FIGURE 46. *Quetzalcoatlus lawsoni*, sp. nov., right tibiotarsus (TMM 42422-9) in **A**, anterior photograph and **B**, line drawing; **C**, right lateral photograph and **D**, line drawing; **E**, posterior photograph and **F**, line drawing; **G**, left medial photograph and **H**, line drawing; **I**, proximal photograph and **J**, line drawing; and **K**, distal photograph and **L**, line drawing views. **Abbreviations: bt**, biceps tubercle; **cb**, cnemial boss; **cc**, cnemial crest; **cn**, cnemial sulcus; **de**, depression; **ea**, emargination; **em**, eminence; **Fi**, fibula; **fs**, fossa; **ir**, intercotylar ridge; **is**, intercondylar sulcus; **lc**, lateral condyle; **le**, lateral epicondyle; **lf**, ligamentous fossa; **lo**, lateral cotyle; **mc**, medial condyle; **me**, medial epicondyle; **mf**, medial distal tarsal fossa; **mi**, missing section; **mo**, medial cotyle; **nd**, node; **no**, notch; **op**, opening; **ot**, oval tubercle; **ri**, ridge; and **su**, sulcus. Outlines courtesy of John Conway and modified by first author. Scale bar equals 50 cm.

is not known how deep it extends into the bone or if it is natural. The medial rim of the proximal surface has a raised margin anteriorly and an emargination posteriorly forming a sinusoid in medial view. The intercotylar ridge has a depression at its posterior end that contacts this emargination. The lateral rim of the lateral cotyle rises slightly anterolaterally at the fibula articulation with a notch between it and the cnemial boss. There is a notch in the posterolateral rim of TMM 42422-10, but this is not visible in other specimens. The posterodorsal eminence is positioned on the posterior end of the proximal margin.

The cnemial boss of the proximal tibiotarsus continues straight down the anterior margin of the shaft as the cnemial crest in *Q. lawsoni*, as in other pterodactyloids (Bennett, 2001a:104; Frey et al., 2011:S48). It extends for the length of the proximal expansion with a concave lateral cnemial sulcus (elongate depression of Frey et al., 2011) and a convex medial surface. An articular facet for the fibula on the tibiotarsus as reported in *Anhanguera* (Kellner and Tomida, 2000:80, fig. 54; Veldmeijer, 2003:fig. 21) is not present in *Q. lawsoni*, but this may instead be

the cnemial sulcus in *Anhanguera* instead. Neither is the tibiotarsus convex and the fibula concave, as reported present in *D. macronyx* (Padian, 1983a:22). However, there is a groove between the fibula and tibiotarsus on the proximal surface, as in *D. macronyx* (Sangster, 2003:87). The tibiotarsus fibular crest reported in *A. primordius* by Frey et al. (2011:48) is not present in *Q. lawsoni*. The shaft has a flattened medial surface giving its cross-section the shape of an anteriorly leaning triangle with rounded corners, similar to the rounded triangular cross-section described in *D. weii* (Young, 1964:248) but dissimilar to the laterally compressed oval cross-section of *A. lancicollis* (Averianov, 2010:310), the putative subcircular cross-section of *Pteranodon* (Bennett, 2001a:105), or the laterally compressed elliptical cross-section of *A. piscator* (Kellner and Tomida, 2000:78). This cross-sectional shape allows TMM 42272-2 to be identified as fragments of a left tibiotarsus shaft. There is an oval tubercle on the posteromedial surface of the tibiotarsus about 7 cm down the shaft, in a similar position to a rugose scar found in *Pteranodon* (Bennett, 2001a:104–105) and a well

pronounced tuberosity in *A. piscator* (Kellner and Tomida, 2000:79), but which is absent in *A. spielbergi* (Veldmeijer, 2003:95). A small node proximal to the biceps tubercle in some specimens is in a similar position to a muscle scar on the tibiotarsus of *Pteranodon* identified as a possible additional insertion of M. biceps femoris (Bennett, 2001a:104). The anterior curvature of the tibiotarsus is located in the middle of the shaft with slight posterior deflections at the proximal and distal ends, giving the entire bone a weak sinusoid shape. The longitudinal grooves described by Kellner and Tomida (2000:78) on the tibiotarsus shaft of *A. piscator* could not be located in *Q. lawsoni*. The shaft cross-section becomes a mediolaterally compressed rectangle distally, as compared with the anteroposteriorly compressed ellipse of *A. piscator* (Kellner and Tomida, 2000:78–79) or the oval of other pterosaurs. Bennett's (2001a:105) muscle scar for the attachment of a pes extensor or digit flexor on the medial surface of the distal shaft in *Pteranodon* cannot be seen in *Q. lawsoni*. A short rugose ridge on the anterior surface of the shaft distal end may be an extensor retinaculum or oblique ligament, as suggested for *Pteranodon* (Bennett, 2001a:105) and *D. macronyx* (Padian, 1983a:fig. 19), respectively. There is not a ligamentous groove as reported in *D. macronyx* (Padian, 1983a:23), but a small fossa (shallow depression for foot flexors and digit extensors of Sangster, 2003) is present on the anterior surface just proximal to the distal condyles.

The distal end of the tibiotarsus is well preserved in TMM 41954-79 as well as in TMM 42422-9 (Fig. 46) and 42422-11. The distal condyles (fused astragalus and calcaneum) are anteriorly expanded, as in other pterosaurs (Padian, 1983a:23; Sangster, 2003:87; Averianov, 2010:fig. 35), and greatly mediolaterally compressed as in other neoazhdarchians with an anteroposterior breadth over 1.6 times the mediolateral width. The lateral condyle articular surface is more convex than the medial condyle in anterior/posterior view, as in other pterosaurs (Bennett, 2001a:105). The medial and lateral epicondyles (medial and lateral ligamentous prominences of Padian, 1983a) are not distinct flanges, but they are instead represented by round swellings at the base of the condyles. The lateral epicondyle is larger and positioned more proximally than the medial epicondyle, opposite to the condition in *D. macronyx* (Sangster, 2003:88), whereas in *Pteranodon* the medial epicondyle is larger but also positioned more distally (Bennett, 2001a:106). The rest of the medial and lateral surfaces of the condyles exclusive of the epicondyles are concave and form a distinct rim at the border with the articular surfaces. These concavities may correspond to depressions for ligament attachments and the lateral curved groove reported in *D. macronyx* (Sangster, 2003:88), or to depressions on the anterior or posterior corners of the medial condyle reported in *A. piscator* and *Tapejara* (Kellner, 2004b:28), respectively. These areas are not well preserved in *Q. lawsoni* but appear to be pierced by nutrient foramina, as in *Tapejara* (Kellner, 2004b:27) and *Pteranodon* (Bennett, 2001a:106), but also appear to have larger circular openings of unknown depth anterior to the lateral epicondyle and posterior to medial epicondyle. Although unreported, *A. lancicollis* appears to have a similar circular opening posterior to its medial epicondyle as well (Averianov, 2010:fig. 35); the condition on its lateral surface has not been described or figured. The distal condyles are subcircular in medial/lateral view in *Q. lawsoni*, curving over 240°. They are subterminally positioned on the distal end of the tibiotarsus such that the articular surfaces reach the anterior surface of the shaft but extend up the posterior surface. A shallow and slightly V-shaped intercondylar sulcus (incisura of Padian, 1983a, intertrochlear sulcus of Sangster, 2003, or intercondylar incision of Frey et al., 2011) separates the medial and lateral distal condyles. There are anterior and posterior shallow depressions on the distal surface of this sulcus. The anterior depression corresponds to the ligamentous

fossa of Bennett (2001a) (deep oval depression of Sangster, 2003) identified in *A. lancicollis* (Averianov, 2010:309), *Pteranodon* (Bennett, 2001a:105–106, fig. 110A), and *D. macronyx* (Sangster, 2003:88, fig. 3.20). The posterior depression is present and larger in *A. lancicollis* (Averianov, 2010:fig. 35), and both contact the medial tarsal fossa of Bennett (2001a). In medial/lateral view, the lateral condyle is slightly larger, more circular in outline, and reaches more distally than the more proximodistally compressed oval medial condyle in *Q. lawsoni*, as in other pterosaurs (Padian, 1983a:23; Dalla Vecchia, 2003b:37–38, 2009:170; Sangster, 2003:88). The medial condyle protrudes more anteriorly and is mediolaterally narrower than the lateral condyle with its flatter anterior margin, unlike in basal pterosaurs (Padian, 1983a:23; Dalla Vecchia, 2003b:37; Sangster, 2003:88). In *Q. lawsoni*, there is an incipient groove on the anterior surface between the medial condyle and tibiotarsus shaft that might correspond to the groove for the M. extensor digitorum longus identified in *D. macronyx* (Padian, 1983a:fig. 19). The groove for the M. peroneus profundus found in *D. macronyx* (Padian, 1983a:fig. 19) cannot be seen on the proximal end of the lateral condyle in *Q. lawsoni*. The lateral condyle protrudes more posteriorly, as in *A. lancicollis* (Averianov, 2010:309). The distal condyles of *Q. lawsoni* do not contact anterior flanges on the shaft, unlike the non-ornithocheiroid pterosaurs (Frey et al., 2011:S48). In *Q. lawsoni*, there is a distal emargination in the middle of the medial condyle that corresponds to the medial tarsal fossa of *Pteranodon* (Bennett, 2001a:106, fig. 110A) and also appears to be present in *A. lancicollis* (Averianov, 2010:fig. 35). The distal condyles are subparallel in *Q. lawsoni*. They converge, are deflected medially, and decrease in width posteriorly to combine into a dorsal rim on the posterior surface of the shaft so that the condyles do not contact posterior flanges on the shaft as in other ornithocheiroids. The posterior end of the intercondylar sulcus has been identified for the passage of the M. gastrocnemius (Sangster, 2003:87–88) and/or digit flexor tendons (Bennett, 2001a:106) in pterosaurs. The medial deflection and change in the orientation of the posterior intercondylar sulcus for these tendons may form the posterior distal fossa in *Q. lawsoni*, which is also found in *A. lancicollis* (Averianov, 2010:fig. 35).

Fibula—The fibula is a slender splint of a bone attached to the lateral surface of the tibiotarsus in pterosaurs, about one-fifth the mid-width of the tibiotarsus in *Q. lawsoni* (Table 15). It does not reach the ankle joint in pterosaurs but comes close in some basal species. Its length is variable but shortens over phylogeny, becoming less than a quarter of the tibiotarsus length in the least inclusive clade including *Q. lawsoni* and *Z. linhaiensis* as well as in a few other species (Andres, 2021). The fibula reaches the proximal margin of the tibiotarsus in *Q. lawsoni*, unlike in *J. edentus* (Wu et al., 2017:20) and *T. wellnhoferi* (Eck et al., 2011:290). The fibula is commonly fused to the tibiotarsus in pterosaurs, and likely does so ontogenetically (Bennett, 2001a; Dalla Vecchia, 2003b; Bennett, 2013, 2014). In *Q. lawsoni*, it is fused proximally, at the biceps tubercle, and distally on the lateral surface of the tibiotarsus, as in *Pteranodon* (Bennett, 2001a:104). The space between the fused parts of the fibula and tibiotarsus is termed the interosseus space (interosseal space of Padian, 1983a, interosseus gap of Sangster, 2003, spatium interosseum of Dalla Vecchia, 2009, or interosseal foramen of Frey et al., 2011). Often a section of the fibula is missing between the proximal fusion and the biceps tubercle in *Q. lawsoni* as in TMM 42422-9 (Fig. 46). The fibula is present in all the listed tibiotarsi except TMM 42422-11, where it is likely broken off. However, its length can be traced in that specimen because the proximal and distal articulations can be identified. In the place of the fibula, there are two tubercles on the proximal end that would flank it and may correspond to a fibular process

(trochanter of Padian, 2008a, or fibular tubercle of Frey et al., 2011) found in more basal pterosaurs, as well as a round eminence in the region of the biceps tubercle. The biceps tubercle (node of Sangster, 2003) is a rugose tumescence on the midpoint of the fibula, identified as an insertion for the biceps femoris (Bennett, 2001a) or iliofibularis (Sangster, 2003), and apparently widespread in pterosaurs (Bennett, 2001a:104; Sangster, 2003:87; Dalla Vecchia, 2009:170). The proximal end of the fibula is positioned on the anterior surface of the tibiotarsus lateral to the cnemial crest in *Q. lawsoni*. It does not have a significant proximal expansion, unlike *Pteranodon* (Bennett, 2001a:104) and *S. crassirostris* (Bennett, 2014:334). The fibula of *Q. lawsoni* does not participate in the articular surface of the knee, also unlike *Pteranodon* (Bennett, 2001a:104) and *D. macronyx* (Padian, 1983a:22; Sangster, 2003:87). The fibula in *Q. lawsoni* is curved anteroproximally, as in other ornithocheiroids (Bennett, 2001a:fig. 108–109; Eck et al., 2011:fig. 10, pl. 2). From its anterior end, the fibula is bowed anteriorly (concave posteriorly, convex anteriorly) and then posteriorly (concave anteriorly, convex posteriorly), with the biceps tubercle at the inflection point to trace a sinusoid on the lateral surface of the tibiotarsus shaft. It has a relatively constant diameter proximal to the biceps tubercle, but it attenuates until about one-fifth down the shaft distally. The fibula tapers to a point, as in most other pterosaurs (Bennett, 2001a:104; Dalla Vecchia, 2003b:27–28; Sangster, 2003:87; Padian, 2008b:56; Dalla Vecchia, 2009:170; Frey et al., 2011:S48; Bennett, 2013:35), and unlike the spatulate shape found in some *D. banthensis* specimens (Padian, 2008b:56) or the rounded expansion in *Campylognathoides* (Wellnhofer, 1974:21; Dalla Vecchia, 2003b:33; Padian, 2008a:94) and *Eudimorphodon* cf. *ranzii* (BSPG 1994 I 51) (Wellnhofer, 2003:17; Dalla Vecchia, 2009:Appendix 2). The distal end of the fibula does not terminate in a small lateral furrow, as suggested by Sangster (2003:87), which possibly would have indicated a missing portion of a longer unfused fibula (Kellner and Tomida, 2000:79–80).

Tarsus

The pterosaur tarsus consists of four or (more rarely) five elements: two proximal series tarsals and two to three distal series tarsals (Wellnhofer, 1970, 1975b, 1978, 1991b; Padian, 2017). The proximal tarsals (astragalus and calcaneum) fuse to the distal end of the tibia early in ontogeny to form the distal condyles of the tibiotarsus (Seeley, 1901; Wellnhofer, 1978; Padian, 1983a; Unwin, 1988; Bennett, 1993; Dalla Vecchia, 2003b). When they are unfused, they are usually a pair of indistinct disk- or lozenge-shaped elements found in juvenile pterosaurs preserved in laminated deposits (e.g., Solnhofen Limestone). When they are fused, they tend to fuse first with each other into an astraglocalcaneum before fusing with the distal tibia (Padian, 2008b) (e.g., second specimen of *A. ammoni*, Bennett, 2007a:387). In a handful of specimens, the contact between the calcaneum and astragalus can still be observed. In non-pterodactyloid pterosaurs, the astragalus constitutes the majority of the distal tibiotarsal surface, with the smaller calcaneum forming the lateral condyle (contra Dalla Vecchia, 2003b). In the pterodactyloids, the calcaneum is reduced even further to form only the anterior corner of the lateral condyle, which has previously been suggested to be the condition for the Ornithocheiroidea by Kellner (2004b) (i.e., *A. piscator* and *Tapejara* according to Kellner, 1995), but it is confirmed here as a synapomorphy for the Pterodactyloidea. The fusion of the proximal tarsals to the tibia necessitates that the movement of the ankle is between the proximal and distal tarsals in an advanced mesotarsal joint, and because the astragalus and calcaneum articulate with a concavoconvex locking joint with the distal concavity on the astragalus, this has been identified as the advanced mesotarsal-reversed

joint of Chatterjee (1982) (Kellner, 2004b). All the proximal tarsals found in *Q. lawsoni* have fused to the tibia without a trace of a suture and so this material does not reveal any new details about the proximal tarsal series (Padian, 2017).

The distal tarsal series of pterosaurs consists of the medial and lateral distal tarsals, identified as the distal tarsal 3 and 4 of other archosaurs, respectively (Kellner, 2004b; Padian, 2017). When a third tarsal rarely appears in pterosaurs, it is sometimes interpreted as an intermedium or centrale (Schaeffer, 1941; Romer and Parsons, 1977). This tarsal is thought to either be a distal tarsal 2 that fuses with the distal tarsal 3 to form the medial distal tarsal (Padian, 2017) or a separate element that is lost over phylogeny (Kellner, 2004b). There are only a handful of specimens in other pterosaurs in which the distal tarsals are isolated and three-dimensionally preserved with which to compare with *Q. lawsoni*: *Dimorphodon macronyx*—YPM VP 00350M, 00350R, and 009182 (Padian, 1983a), as well as NHMUK 41212 and R.1034 (Sangster, 2003); *Pteranodon*—YPM VP 002462 (Bennett, 2001a); and *Tapejara* sp.—MN 6532-V, which is a juvenile specimen and may not be indicative of adult morphology (Kellner, 2004b). Comparable material is present in *Dimorphodon weintraubi* Clark et al., 1998, *Noripterus complicidens* Young, 1973, *P. guinazui*, and MOR 553 (Carroll et al., 2013), but these await formal description.

The remains of seven distal tarsi are preserved in *Q. lawsoni* (Table 16), of which three are articulated lateral and medial distal tarsals (TMM 41544-34.1 and 41544-34.2, 41954-64.3 and 41954-64.4, 42138-2.3 and 42138-2.4, respectively). One of these articulated pair of distal tarsals, TMM 41954-64.3 and 4 (Fig. 47), was prepared so that their internal articulated surfaces are visible, but it appears that they were more recently glued together in the past and so their orientation to one another may not be original. It is warranted to compare with TMM 42138-2.3 and 2.4 (Padian, 2017:figs. 5–6) that are still attached by matrix. The TMM 41954-89 right lateral distal tarsal is associated with some crushed bone that might be the medial distal tarsal, but it is on the lateral side of that lateral distal tarsal. Also, isolated left lateral distal tarsals (TMM 41954-8.5 and -28 as well as 42180-14.7) and a right lateral distal tarsal (TMM 41954-89) are preserved. All of these elements are rather well preserved, except the proximodistally flattened TMM 41544-34.1 and 34.2.

The medial and lateral distal tarsals in *Q. lawsoni* are blocky in shape, as in *Pteranodon* (Bennett, 2001a:fig. 113) and *Tapejara* (Kellner, 2004b:fig. 2.4), but unlike the more wedge-shaped distal tarsals of *D. macronyx* (Padian, 1983a:25–26; Bennett, 2001a:109; Sangster, 2003:88; Kellner, 2004b:30) or the discoidal tarsals of juvenile pterosaurs. These tarsals tightly articulate with each other with their proximal surfaces meeting at a 210° angle in anterior/posterior view. This configuration creates a midline elevation on their combined proximal surface, which likely functions as an intercotylar ridge to articulate with the intercondylar sulcus of the tibiotarsus, as in *Pteranodon* (Bennett, 2001a:107), but at a shallower angle. The cotyles for the articulation with the tibiotarsus distal condyles are concave fossae on the proximal surfaces of the distal tarsals, unlike the rimmed facets in *D. macronyx* (Padian, 1983a:26; Sangster, 2003:90). The medial and lateral cotyles are oriented slightly proximomedially and proximolaterally to contact the tibiotarsus condyles laterally and medially, respectively. These proximal articulations are anteroposteriorly longer than mediolaterally wide (Padian, 2017). Anterodistally, the two distal tarsals combine to form a wide continuous convex distal surface for articulation with the metatarsals. The distal concave articular grooves separated by ridges of *D. macronyx* (Padian, 1983a:25; Bennett, 2001a:109; Kellner, 2004b:30; Padian, 2017:6) are absent in *Q. lawsoni*. Metatarsal V articulates with the lateral surface on the lateral distal tarsal as in other pterosaurs (Padian, 2017). The lateral distal tarsal is significantly larger than the medial distal tarsal in both the

proximodistal and anteroposterior dimensions, unlike the subequal distal tarsals of *Tapejara* (Kellner, 2004b:29) and *Pteranodon*. The medial distal tarsal constitutes the majority of the proximal articular surface as in other pterosaurs, but the lateral distal tarsal constitutes the majority of the distal metatarsal articular surface as in *Tapejara* (Kellner, 2004b). In *Q. lawsoni*, this is due to a mediodistally curving contact between the tarsals—the intertarsal contact is predominantly vertical except at its distal end, where the distal shelf of the lateral distal tarsal curves medially below a corresponding shelf on the medial distal tarsal. The intertarsal articulation surfaces of the distal tarsals consist of proximal and distal shelves on the medial distal tarsal contacted distolaterally by similar articular shelves on the lateral distal tarsal. In TMM 42138-2, the anterior end of the intertarsal contact on the proximal surface appears to have a minute peg on the medial distal tarsal with a complementary notch on the lateral distal tarsal, but these are not observed in other specimens. At the posterior end of the intertarsal contact, a small peg is visible in TMM 41954-64 on the medial surface of the lateral distal tarsal tendinal groove, and it appears to articulate with a small depression on the lateral surface of the medial distal tarsal posterior end. In TMM 41954-64 and 42138-2, another peg is on the lateral (intertarsal) surface of the distal ridge of the medial distal tarsal, and it appears to articulate with a small depression on the medial surface of the lateral distal tarsal distal process. It is not known how these small structures would have affected motion, considering their variable preservation among specimens.

Medial Distal Tarsal—The left medial distal tarsal is present in the specimen TMM 41954-64.4 (Fig. 47), and the right medial distal tarsal is present in the specimens TMM 41544-34.2 and 42138-2.4 in *Q. lawsoni* (Table 16). This tarsal is semicircular in proximal view and is a wedge from 60° and 120° of a circle in anterior and lateral views, respectively, quite disparate from the complicated shape of *Pteranodon* (Bennett, 2001a:106). In proximal view, pterosaur medial distal tarsals tend to be a rounded quadrangle as in *D. macronyx* (Padian, 2017:25) or a rectangle with anterior and posterior expansions as in *Tapejara* (Kellner, 2004b:29) and *Pteranodon* (Bennett, 2001a:fig. 113).

The medial distal tarsal is a much smaller and more compact bone than the lateral distal tarsal in *Q. lawsoni*, and nearly its entire proximal surface consists of a shallow fossa for articulation with the medial condyle of the tibiotarsus, as in *D. macronyx* (Padian, 1983a:26, fig. 20). This surface slopes slightly mediodistally and lacks a distinct rim. There is an anterior tubercle on the proximal surface anterior margin (tubercle-like process of Wu et al., 2017), suggested to be an attachment for ligaments in *Pteranodon* (Bennett, 2001a), but it is much smaller and blunter in *Q. lawsoni*. Another tubercle is present on the proximal surface medial margin. A small ridge between the two tubercles delineates the proximal margin of an anteromedial facet on this tarsal. This facet also appears to be present in *J. edentus* where it contacts the metatarsal I (Wu et al., 2017:fig. 7), which was thought not to articulate with the tarsus in pterosaurs because they lack a distal tarsal I (Wellnhofer, 1978; Padian, 1983a; Sangster, 2003; Padian, 2017) but see Bennett (2001a) and (Kellner, 2004b). The anteromedial facet is semicircular in outline, similar to the proximal outline of the metatarsal I in TMM 41954-8.1. A small foramen is present on the anterior end of the anteromedial facet. *Dimorphodon macronyx* (NHMUK 41212) is reported to have a small anterior foramen (Sangster, 2003:90), which is figured on what appears to be an anteromedial facet (Sangster, 2003:fig. 3.21), but neither the foramen or facet were reported by Padian (1983a, 2017). *Pteranodon* has a large irregular foramen on the medial surface of the medial distal tarsal but this is positioned more posteriorly (Bennett, 2001a:106).

Quetzalcoatlus lawsoni lacks the posterior prominence on the medial distal tarsal proximal surface found in *Pteranodon*

(Bennett, 2001a:106). In fact, *Pteranodon* has the entire posterior half of the medial distal tarsal expanded, especially proximodistally, and bears the flexor tendon grooves on its posterior surface (Bennett, 2001a:106) instead of on the lateral distal tarsal, as in other pterosaurs (Padian, 2017). The medial distal tarsal in *Q. lawsoni* instead tapers to a posterior tubercle and has a triangular outline in posterior view, unlike the subrectangular outline in *Pteranodon* (Bennett, 2001a:106). The large tendinal groove is located on the lateral distal tarsal in *Q. lawsoni* as in other pterosaurs, but it has been figured as contacting the medial distal tarsal on its posterior surface in TMM 41954-64.4 (Padian, 2017:fig. 5L). The main body of the tendinal groove does not contact the medial distal tarsal in this specimen, but there is a proximomedially/distolaterally oriented depression on the posterior surface of the medial distal tarsal. This depression is aligned with an emargination between the medial peg and the tendinal groove on the lateral distal tarsal. This configuration suggests that the tendons in the two grooves of *Pteranodon* share a groove distally in *Q. lawsoni* and split proximally, with the medial one traversing the posterior surface of the medial distal tarsal.

The posterior tubercle of the medial distal tarsal delineates the posterior margin of a large mediodistally facing concave area, previously termed the mediolaterally oriented depression in *Q. lawsoni* (Padian, 2017) (diagonal mediolateral depression in *Tapejara* of Kellner, 2004b, or concave area in *Pteranodon* of Bennett, 2001a); it is not reported in *D. macronyx*. The concave area is trapezoidal in outline, it is bounded distally by a ridge that connects the anterior metatarsal articulation to the posterior end of the tarsal, and it forms most of the posterior half of the medial and distal surfaces of the medial distal tarsal. The distal ridge bears the medial distal tarsal peg on its lateral (intertarsal surface). The anterior half of the distal surface is an articular surface for the metatarsals that extends onto the anterior surface of the medial distal tarsal. This is the medial third of the total articular surface for the metatarsals on the distal tarsals. There is a divot on the mediodistal part of this articular surface that may contain a foramen, which would limit the space for articulating metatarsals on the medial distal tarsal. The thin and curved proximal surface of metatarsal II would most certainly fit on this articular surface and likely the thinner metatarsal III as well (Padian, 2017), which may have been shared between the distal tarsals. The second metatarsal appears to be shared between the tarsals in *J. edentus* (Wu et al., 2017:fig. 7), although it is only reported as being preserved against the medial distal tarsal (Wu et al., 2017:20). The second and third metatarsals are shared between the distal tarsals in *Pteranodon* (Bennett, 2001a:fig. 115), and the fourth is shared between the tarsals in in *D. macronyx* (Padian, 1983a:26; Sangster, 2003:90, fig. 3.21; Padian, 2017:6), but see Kellner (2004b). Padian (2017) suggested that the mediodistal concave area on the medial distal tarsal received metatarsals II and III, and it is possible that the ventral end of the proximal surfaces of these metatarsals reached this area.

The lateral (intertarsal) surface of the medial distal tarsal is taken up mostly by the articulations for the lateral distal tarsal. These consist of proximal (dorsal) and distal (ventral) semicircular, anteroposteriorly elongate, and subequal in size articular surfaces. They are located on the distal surfaces of laterally projecting shelves, which are separated by a horizontal sulcus that is perforated by a number of foramina in middle and posterior depressions. Two elongate articular surfaces with the bone between them pierced by nutrient foramina has also been reported in *Pteranodon* (Bennett, 2001a:106–107), but with the proximal surface greatly larger than the distal. The lateral (intertarsal) surface of the medial distal tarsal in *Tapejara* is just described as flat with a cavity bearing a large foramen (Kellner, 2004b:30).

Lateral Distal Tarsal—The left lateral distal tarsal is present in the *Q. lawsoni* specimens TMM 41954-8.5 (Fig. 48A), 41954-28, and 41954-64.3 (Fig. 47), as well as 42180-14.7. The right lateral distal tarsal is present in TMM 41544-34.1, 41954-89, and 42138-2.3 (Table 16). It is pisciform (fish-shaped) in medial/lateral view, specifically a semicircular outline with large proximal and distal processes on the posterior end. This is similar to other pterosaurs except for the relatively larger expansion of the posterior end, and contrasts greatly with the wedge shape of *Pteranodon* (Bennett, 2001a:106). In proximal view, the lateral distal tarsal is a 'q' shape—anterolateral and posteromedial expansions with the latter including a medially curving posterior process—described as a 'P' or comma shape in this species and *D. macronyx* (Padian, 2017:8). This is disparate from the more rectangular outline of the lateral distal tarsals of *Tapejara* (Kellner, 2004b:fig. 2.4) and *Pteranodon* (Bennett, 2001a: fig.113). *Quetzalcoatlus lawsoni* shares a slight lateral emargination with *Tapejara* and *D. macronyx*, attributed to a concavity for articulation with the metatarsal V and accentuated by a protruding point (protruding corner of Sangster, 2003) on the lateral surface of *D. macronyx* (Sangster, 2003:90) and *Q. lawsoni*. The lateral distal tarsal is significantly larger (predominantly anteroposteriorly broader) than the medial distal tarsal due to the large posterior process (tuberous posterior process of Padian, 1983a, or a talus-shaped prominence and 'tail' of Padian, 2017). This posterior process bears the tendinal groove (Padian, 2017) and may also have been the site of tendinous attachments (Padian, 1983a:26). The tendons that transect the tendinal grooves of the distal tarsals in pterosaurs have been identified as plantar flexors (Bennett, 2001a:106; Padian, 2017:8, fig. 5) and/or pedal digit flexors (Bennett, 2001a:106).

The proximal fossa for articulation with the lateral tibiotarsal condyle constitutes the anterior three-quarters of the proximal surface and all of the width of the lateral distal tarsal in *Q. lawsoni*. It is an anterolaterally sloping concave articular surface bounded by the intercotylar ridge medially, the protruding point at its anterolateral corner, and a distinct rim on its posterior border. This rim defines a small fossa on TMM 42138-1 between it and the posterior process that is not found on the more poorly preserved lateral distal tarsals. TMM 41954-64.3 appears to have an anterior prominence on its proximal surface, but this is due to a crack running through the tarsal. Posterior to the proximal fossa is the posterior process of the lateral distal tarsal. In *Q. lawsoni*, the posterior process curves medially around the posterior end of the medial distal tarsal (Padian, 2017). The proximal end of the tendinal groove divides the tip of the posterior process into a sharp posterior point, which may have been the site of tendon attachments suggested by Padian (1983a), and a medially-curving flange that contacts the medial distal tarsal posteriorly.

The posterior surface of the lateral distal tarsal consists of the large tendinal groove and the medial and lateral rims that delineate its margins in *Q. lawsoni*. In TMM 41954-28 and 42138-1, this groove is oriented subvertically, but in TMM 41954-64.3 there is a much larger and better preserved posterior process in which the groove is proximomedially/distolaterally oriented. In this latter specimen, the lateral rim of the tendinal groove is oriented proximomedially/distolaterally whereas the medial rim is oriented subvertically, so that the groove takes the three-dimensional shape of a distally expanded cone. The lateral rim of the tendinal groove is larger and forms the distal margin of the projection that terminates in the tip of the posterior process. *Pteranodon* (Bennett, 2001a:107) and *Tapejara* (Kellner, 2004b:fig. 2.5B) have subtriangular posterior surfaces on their lateral distal tarsals, but this is the entire surface and they lack tendinal grooves, described as flat in *Tapejara* (Kellner, 2004b:29). In *Q. lawsoni* the medial rim of the tendinal groove bears a medial peg that apparently articulates with a

depression on the posterior end of the medial distal tarsal lateral (intertarsal) surface. The tendinal groove is oriented anterodistally/posteroproximally in the parasagittal plane, curving slightly anteriorly down its length.

The tendinal groove extends past the rest of the distal surface of the lateral distal tarsal on a distal process in *Q. lawsoni*. A large mediolateral sulcus separates the distal process from the articular surface for the metatarsals on the anterior half of the distal surface, and may have provided a bony stop for the metatarsals. *Pteranodon* and *D. macronyx* have a concave area bounded by a ridge in this region, but these are oriented laterally and identified as the articular surface for metatarsal V (Bennett, 2001a:109; Sangster, 2003:90); *Tapejara* just has a large central depression in this region (Kellner, 2004b:29). *Quetzalcoatlus lawsoni* lacks the two foramina on the distal surface reported in *Pteranodon* and *Tapejara* (Bennett, 2001a:107; Kellner, 2004b:29). The contact with the metatarsals is an anterodistally oriented convex articular surface that terminates at a horizontal anterior ridge, which may have served as another bony stop for the metatarsals. This contrasts with the anterior tubercle found in *Pteranodon* (Bennett, 2001a:106). A couple of foramina are present on the anterior aspect of this bone in *Q. lawsoni*, whereas *A. piscator* (Kellner and Tomida, 2000:81) and *D. macronyx* (Sangster, 2003:90) have a single foramen. The metatarsal articular surface on the lateral distal tarsal of *Q. lawsoni* has a raised prominence on its posteromedial corner, around which the large triangular proximal end of metatarsal III may have articulated. The protruding point lies at the posterolateral corner of this articular surface.

The articulation for the metatarsal V in *Q. lawsoni* is positioned posterior to the protruding point on the lateral surface of the lateral distal tarsal. In TMM 41954-64.3 this articulation is a deep depression, but in all other specimens it is a large circular socket surrounded by a distinct rim formed by the protruding point, proximal cotyle, posterior process, and ridge on the lateral margin of the mediolateral sulcus. The articulation with the metatarsal V lacks a clear facet in *Tapejara* (Padian, 2017:7), is a concave area in *Pteranodon* (Bennett, 2001a:109), and is a notch in *D. macronyx* (Padian, 1983a:26). The metatarsal V articulation is oriented almost straight laterally in *Q. lawsoni*, unlike the distolaterally oriented facets of *Tapejara* (Kellner, 2004b:29), *Pteranodon* (Bennett, 2001a:109), and *D. macronyx* (Padian, 2017:6).

The medial (intertarsal) articular surface of the lateral distal tarsal comprises the same anterior three-quarters length as the proximal tibiotarsus articular surface in *Q. lawsoni*. The entire surface is a semicircle with two articulations for the medial distal tarsal. These consist of a smaller semicircular proximal (dorsal) articular surface and a longer crescentic distal (ventral) articular surface, the reverse of the condition found in *Pteranodon* (Bennett, 2001a:fig. 112). A curving sulcus (proximally concave, distally convex) is positioned between the two articular surfaces. A number of foramina pierce this non-articular area in *Pteranodon* (Bennett, 2001a:106), but they cannot be seen in *Q. lawsoni*, although were likely present considering the similar foramina on the medial distal tarsal. The articular surfaces are on the proximal portions of proximal and distal shelves, the latter of which are responsible for the greater distal width of the lateral distal tarsal.

Pes

Partially articulated pedes are present in TMM 41954-8 and 41954-64 as well as 42180-14 in the *Q. lawsoni* material. TMM 41954-8.1–8.5 includes the complete left metatarsals I–IV, except for the missing metacarpal III distal end, and the associated lateral distal tarsal (Fig. 48A). This specimen was partially prepared from the concretion in which it was preserved, and so
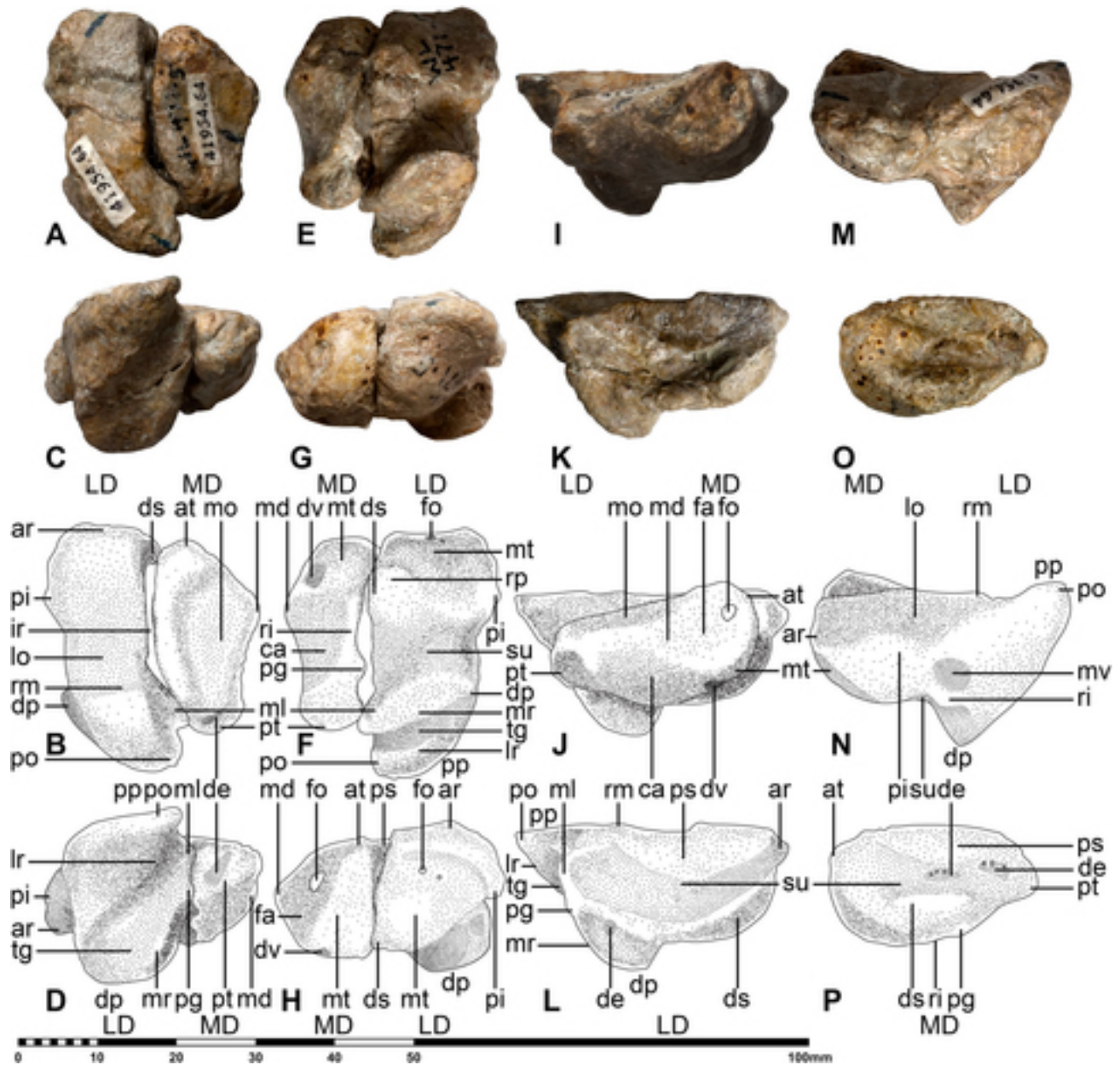
FIGURE 47. *Quetzalcoatlus lawsoni*, sp. nov., left medial (TMM 41954-64.4) and lateral distal tarsals (TMM 41954-64.3) in **A**, proximal photograph and **B**, line drawing; **C**, posterior photograph and **D**, line drawing; **E**, distal photograph and **F**, line drawing; **G**, anterior photograph and **H**, line drawing; **I**, medial photograph and **J**, line drawing; **K**, medial view of lateral distal tarsal photograph and **L**, line drawing; **M**, lateral photograph and **N**, line drawing; and **O**, lateral view of medial distal tarsal photograph and **P**, line drawing views. **Abbreviations: ar**, anterior ridge; **at**, anterior tubercle; **ca**, concavity; **de**, depression; **dp**, distal process; **ds**, distal shelf; **dv**, divot; **fa**, facet; **fo**, foramen; **ir**, intercotylar ridge; **LD**, lateral distal tarsal; **lo**, lateral cotyle; **lr**, lateral rim; **md**, medial tubercle; **MD**, medial distal tarsal; **ml**, medial flange; **mo**, medial cotyle; **mr**, medial rim; **mt**, metatarsal articulation; **mv**, metatarsal V articulation; **pg**, peg; **pi**, protruding point; **po**, posterior tip; **pp**, posterior process; **ps**, proximal shelf; **pt**, posterior tubercle; **ri**, ridge; **rm**, rim; **rp**, raised prominence; **su**, sulcus; and **tg**, tendinal groove. Outlines courtesy of John Conway and modified by first author. Scale bar equals 100 mm.

it retains the arrangement of bones in a semi-articulated arrangement. This facilitates the identification of the other metatarsals in the *Q. lawsoni* material, but the crushing of the proximal ends obscures some of their three-dimensional shape. In addition, the shafts of the first two metatarsals appear to have been broken before fossilization. TMM 41954-8 is exposed in ventral view, as confirmed by the dorsal arching of the shafts and the ventrally positioned distal condyles/subterminal flange of the metatarsals. It is corroborated as belonging to the left side by Padian (2017) and the association of the left lateral distal tarsal. TMM 41954-64.1–64.5 is a left metatarsal I missing its distal end and a metatarsal II missing part of its distal shaft still embedded in matrix, lateral and medial distal tarsals, and possibly a poorly preserved proximal end of metatarsal V. In this
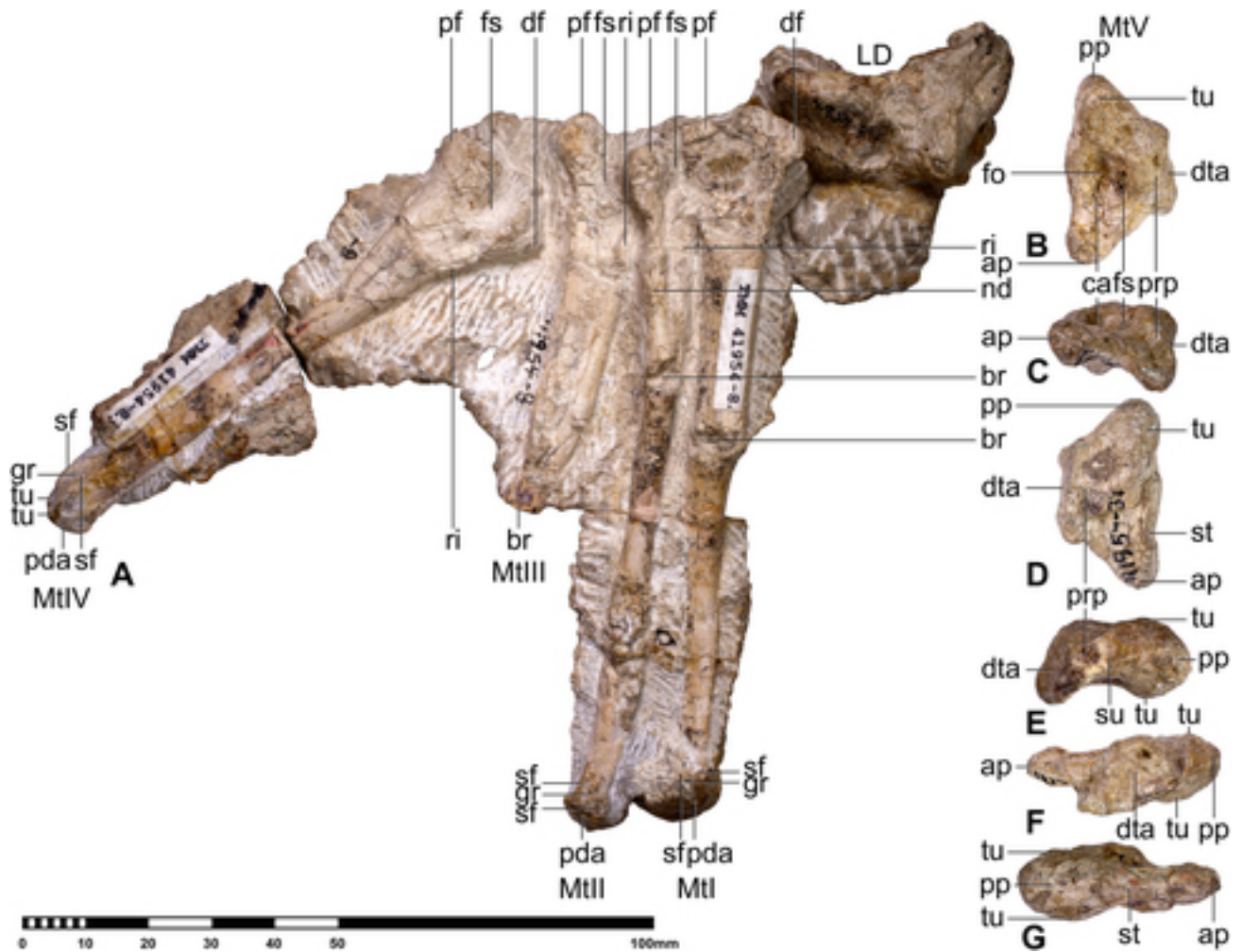
FIGURE 48. *Quetzalcoatlus lawsoni*, sp. nov., left metatarsals I (TMM 41954-8.1), II (TMM 41954-8.2), III (TMM 41954-8.3), IV (TMM 41954-8.4), and lateral distal tarsal (TMM 41954-8.5) in **A**, ventral view; and right metatarsal V (TMM 41954-37) in **B**, dorsal; **C**, anterior (distal); **D**, ventral; **E**, posterior; **F**, proximal (medial); and **G**, lateral views. **Abbreviations: ap**, anterior point; **br**, break; **ca**, concavity; **df**, dorsiflexor tubercle; **dta**, distal tarsal articulation; **fo**, foramen; **fs**, fossa; **gr**, groove; **LDT**, lateral distal tarsal; **MtX**, metatarsal X; **nd**, node; **pda**, pedal digit articulation; **pf**, plantar flexor tubercle; **pp**, posterior process; **prp**, proximal process; **ri**, ridge; **sf**, subterminal flange; **st**, striae; and **tu**, tubercle. Scale bar equals 100 mm.

specimen, the tarsus and metatarsus are preserved as separate articulated units. The metatarsals were partially left in their original matrix so that the length of the second metatarsal can be measured despite the missing portion. TMM 42180-14.7–14.9 is the left lateral distal tarsal, the metatarsal IV proximal end, the metatarsal V, and three possible pedal phalanx fragments. The elements of this specimen are fully articulated and illustrate how these elements fit together.

Metatarsus

In addition to the associated material (TMM 41954-8, 41954-64, and 42180-14), an isolated left metatarsal I shaft fragment (TMM 41961-1.27), a proximal portion of the right metatarsal II shaft and a poorly preserved metatarsal distal end in matrix given the same number (TMM 41961-1.26), a left metatarsal III (TMM 42180-18), left metatarsal IV proximal end with a mold of the distal end (TMM 41544-30), and right metatarsal V (TMM 41954-37 and 42422-16) are preserved in *Q. lawsoni* (Table 17). The metatarsals of TMM 41954-8 appear splayed

(Fig. 48A), as has been reported in some pterosaurs, but this splay has been attributed to partial disarticulation of the metatarsals with the proximal ends held together by strong ligaments and tendons that resisted deterioration (Padian, 2017). These metatarsals I–IV would articulate and fit together but would not be closely appressed/tightly bound, as in most pterosaurs (Padian, 1984b) that can be distinguished by their flat and beveled lateral and medial sides (Padian, 1983a,b). Short longitudinal ridges extending along the dorsal end of the medial surface of the metatarsals II–III (ligament attachment scar of Bennett, 2001a, or ligament bump of Averianov, 2010) are likely attachment sites for ligaments that bound the metatarsus together proximally. *Zhejiangopterus linhaiensis* was described by Cai and Wei (1994) as having metatarsals I–IV that are tightly associated proximally but diverge distally, and this would seem to apply to *Q. lawsoni* as well. Metatarsal material is reported in the azhdarchid species *C. boreas* (Hone et al., 2019), *Z. linhaiensis* (Cai and Wei, 1994), and *A. lancicollis* (Averianov, 2010), as well as the putative azhdarchids TMM 41839-10 to 41839-12, YPM 21821 (Averianov, 2014), and a Senegalese specimen (Averianov, 2010).

TABLE 16. Measurements of *Quetzalcoatlus lawsoni*, sp. nov., tarsal material. Values in millimeters. ~, approximate value; a-p, anteroposterior dimension; lat, lateral dimension; and p-d, proximodistal dimension.

Dimension: Element: Specimen Number:	Length (p-d)	Width (lat)	Breadth (a-p)
Medial distal tarsal			
TMM 41544-34.2	~9.68	13.47	31.22
TMM 41954-64.4	13.25	15.55	25.92
TMM 42138-2.4	13.15	14.19	21.82
Lateral distal tarsal			
TMM 41544-34.1	~8.52	16.07	36.34
TMM 41954-8.5	15.77	17.90	37.98
TMM 41954-28	15.58	13.97	33.77
TMM 41954-64.3	14.85	14.56	32.36
TMM 41954-89	12.84	12.29	24.97
TMM 42138-2.3	13.17	16.10	26.62
TMM 42180-14.7	13.54	13.77	25.38

TABLE 17. Measurements of *Quetzalcoatlus lawsoni*, sp. nov., metatarsal material. Values in millimeters. >, preserved value; ~, approximate value; d-v, dorsoventral dimension; lat, lateral dimension; and p-d, proximodistal dimension. Holotype specimen in italics.

Dimension: Element: Specimen Number:	Length (p-d)	Mid-width (lat)	Mid-depth (d-v)
Metatarsal I			
TMM 41954-8.1	103.02	8.05	6.90
TMM 41954-64.1	>82.69	5.64	4.59
TMM 41961-1.27	>32.56	5.85	4.30
Metatarsal II			
TMM 41954-8.2	107.16	5.04	5.48
TMM 41954-64.2	113.41	4.19	5.10
TMM 41961-1.26	>88.94	4.34	6.33
Metatarsal III			
TMM 41954-8.3	>63.55	3.53	6.38
TMM 42180-18	83.24	3.75	6.35
Metatarsal IV			
TMM 41544-30	80.04	7.48	7.71
TMM 41954-8.4	90.91	5.46	5.81
TMM 42180-14.8	>24.42	~8.13	~6.24
Metatarsal V			
TMM 41954-37	31.17	17.54	10.78
TMM 41954-64.5	~16.18	~11.99	~8.29
TMM 42138-2.2	28.18	15.09	7.22
TMM 42422-16	21.38	14.30	8.87
TMM 42180-14.9	27.98	17.86	14.32

The metatarsus of *Q. lawsoni* is rather small compared with that of other pterosaurs. The length of the third metatarsal is traditionally used as a proxy for the metatarsus size and varies from almost half the length of the tibiotarsus in basal pterosaurs to almost one-tenth the length of the tibiotarsus in *Zhenyuanopterus longirostris* Lü, 2010 (Andres, 2021). There is a decrease in relative metatarsal length over phylogeny, with the azhdarchoids having metatarsals about one-quarter to one-fifth of the tibiotarsus length and the lanceodontians even less (Andres, 2021). *Quetzalcoatlus lawsoni* has the third shortest metatarsal III in pterosaurs after *Z. longirostris* and *Nurhachius ignaciobritoi* Wang et al., 2005, with a length almost 15% of the tibiotarsus (Andres, 2021). The only complete metatarsal III in the *Q. lawsoni* material (TMM 42180-18) may be from a smaller individual, but even the largest metatarsal in the material would only be 20% of the tibiotarsus length. *Azhdarcho lancicollis* has one incomplete metatarsal preserved, and the only other azhdarchid with metatarsus material, *Z. linhaiensis* (ZMNH M1328), has metatarsals 23% the length of the tibiotarsus. *Quetzalcoatlus* is the culmination of a long trend of metatarsal reduction in azhdarchoids.

The second metatarsal is the longest followed by the first, fourth, and fifth in TMM 41954-8 (metatarsals II>I>IV>V), as in most pterosaurs (Bennett, 2001a:111; Lü and Ji, 2005b:table 1; Dalla Vecchia, 2009:170; Wu et al., 2017:table 1), with notable exceptions for *M. coahuilensis* (Frey et al., 2006:32–33) and *D. macronyx* (Padian, 1983a:26) in which the first metatarsal is shorter than the fourth. The third metatarsal is missing its distal half in TMM 41954-8, and the length of the only complete third metatarsal (TMM 42180-18) is between that of the two complete fourth metatarsals (TMM 41544-30 and 41954-8.4). However, TMM 41954-8.3 appears significantly larger than the metatarsal III of TMM 42180-18 and the metatarsal IV of TMM 41954-8.4, and so the metatarsal III is likely to be at least the length of the metatarsal IV in TMM 41954-8 as in other pterosaurs.

The metatarsals are constructed with dorsoventrally expanded and laterally compressed proximal ends, dorsally arched shafts, and slightly expanded distal ends in *Q. lawsoni*. This proximal dorsoventral expansion is significantly larger than in other pterosaurs. The first metatarsal is the most curved, as in *A. primordius* (Frey et al., 2011:S48), followed by the second and third with the fourth metatarsal being essentially straight, as found in *Pteranodon* (Bennett, 2001a:111). The metatarsal proximal ends are concave medially so that the concave medial surface of a metatarsal fits onto a convex lateral surface of the preceding metatarsal, not unlike the ventrally cupped proximal

ends described in *D. macronyx* (Sangster, 2003:91). These ends appear to be medially imbricated in TMM 41954-8 such that metatarsal IV overlies III, metatarsal III overlies II, and metatarsal II overlies I, as in other pterosaurs (Bennett, 2001a:111; Frey et al., 2006:32; Frey et al., 2011:S48). The proximal ends of metatarsals II and III are much more laterally compressed than metatarsals I and IV, also found in *J. edentus* (Wu et al., 2017:20) and *Pteranodon* (Bennett, 2001a:111). In *Q. lawsoni*, metatarsals I–III appear to articulate with the medial distal tarsal and metatarsal IV appears to articulate with the lateral distal tarsal, with the articulation for the laterally compressed metatarsal III proximal end possibly shared between the two. Dorsiflexor and plantar flexor tubercles are present on the dorsal and ventral margins of the proximal end of the metatarsals, respectively. *Pteranodon* only has small subcircular muscle scars on the dorsal surface in this area (suggested tibialis anterior or other ankle flexor insertions) (Bennett, 2001a:111). Foramina are not apparent on the proximal ends of the metatarsals in *Q. lawsoni*, as has been found in *A. lancicollis* (Averianov, 2010:310) and *Pteranodon* (Bennett, 2001a:fig.114), but preservation of this material would make their identification difficult if present.

The metatarsal lengths reach to over 20 times their shaft widths in *Q. lawsoni*. These shafts are taller than wide, except for the first metatarsal in which this condition is reversed. TMM 42180-14.8 is the only non-metatarsal I in which the cross-section of the shaft is also wider than tall, unlike the other fourth metatarsals (TMM 41544-30 and TMM 41954-8.4), but only the proximal end is present in TMM 42180-14.8 and so the midsection of the shaft could have a different aspect ratio. The beveled medial and lateral metatarsal surfaces reported in *D. macronyx* (Padian, 2017:5) are not present in *Q. lawsoni*. The muscle scars on the ventral surface of the metatarsals reported in *Pteranodon* (suggested digit flexor interosseus muscle origins) (Bennett, 2001a:11) are also not visible. In *Q. lawsoni*, the distal articulation with the pedal phalanges is slightly convex and square in outline, not unlike the simple convex-concave metatarsophalangeal joints reported in *Pteranodon* (Bennett, 2001a). Two small round flanges are present on either side of the ventral surface of the distal end

with a short median groove between them (ginglymal groove of Padian, 1983a, broad groove of Clark et al. 1998, or deep fossa and intercondylar sulcus of Sangster, 2003). This groove terminates at the distal margin, instead of extending up the distal surface to form an intercondylar sulcus as in *S. wucaiwanensis* (Andres et al., 2010:178). These subterminal flanges have been identified as modified distal condyles by Andres et al. (2010) that may have served to brace the metatarsophalangeal joint ventrally. Well shaped condyles, however, have been reported in the basal pterosaurs *D. macronyx* (Padian, 1983a:37; Sangster, 2003:91; Frey et al., 2011:S48) and *E. rosenfeldi* (Dalla Vecchia, 2009:170). The subterminal flanges on the first metatarsal are the lowest and widest, with the other metatarsals having successively taller and thinner flanges.

Averianov (2010) reported an *A. lancicollis* metatarsal missing its distal end (ZIN PH 200/44) and identified it as either a right metatarsal II or III. Its proximal surface is triangular in outline with a ventral fossa, and it has a nearly straight shaft with a circular cross-section (Averianov, 2010:310, fig. 36) like the fourth metatarsal of *Q. lawsoni*. However, the proximal outline is mediolaterally compressed with a middle constriction, the proximal end has medial and lateral concavities with depressions in them (containing foramina in *A. lancicollis*), and is elongate and slender (Averianov, 2010:310, fig. 36) like the third metatarsal of *Q. lawsoni*. The mediolateral compression of the second and third metatarsal seems to be conserved across the Pterosauria, and so this is most likely a metatarsal III. *Cryodrakon boreas* includes an element identified as a right metatarsal III or IV (TMP 1992.83.6) that was described as a metacarpal III in Currie and Jacobsen (1995) (Godfrey and Currie, 2005). It shares a slightly convex subrectangular distal articulation with a ventral groove (depression in Godfrey and Currie, 2005) with the metatarsals of *Q. lawsoni*, although it also has depressions on the medial and lateral surfaces of the distal end (Godfrey and Currie, 2005:307). Its triangular proximal outline (Godfrey and Currie, 2005:307) and nearly straight shaft support its identification as a metatarsal IV, but its 126 mm length would make it larger than any *Q. lawsoni* metatarsal.

Metatarsal I—The first metatarsal includes a left complete element (TMM 41954-8.1, Fig. 48A), a left element missing the distal end (TMM 41954-64.1), and a probable left shaft fragment (TMM 41961-1.27) in the *Q. lawsoni* material (Table 17). The mid-shaft is laterally wider than tall and curves more ventrally than the other metatarsals, allowing the referral of TMM 41961-1.27. This specimen is identified as a left element based on it having a flattened lateral surface on its left, where it would contact the metatarsal II. In TMM 41954-8.1, the proximal end has been broken, rotated, and laterally crushed. In proximal view, it is a laterally convex semicircle in outline with a raised median section terminating in a point. This raised median section is not found in other specimens, and it is interpreted here as a lateral expansion crushed onto the proximal surface in TMM 41954-8.1. Both dorsiflexor and plantar flexor tubercles are recognizable. TMM 41954-64.1 has a damaged proximal surface that is convex, ovate in outline, and inclined proximoventrally. Despite their difference in proximal outlines, TMM 41954-8.1 and 64.1 are both wider ventrally. TMM 41954-64.1 is smaller and more poorly preserved, and so the semicircular proximal outline of TMM 41954-8.1 is likely more accurate, with the differences attributable to taphonomy and ontogeny in TMM 41954-64.1. It is likely that the damaged dorsal end of the proximal margin has been sheared off in TMM 41954-64.1 (including dorsiflexor tubercle), producing a proximoventrally inclined cross-section similar to that seen in the proximal shaft of TMM 41954-8.1. This is distinct from the subtriangular proximal outline of *Pteranodon* (Bennett, 2001a:111). The rest of the metatarsal I shaft is arched dorsally with a semicircular cross-section becoming subrectangular distally, unlike the circular

cross-section of metatarsals I–II in *T. wellnhoferi* (Eck et al., 2011:290). The distal surface is damaged in TMM 41954-8.1, but it appears to have a slight medial orientation with a longer medial subterminal flange extending more proximally than the lateral flange, as in *D. macronyx* (Sangster, 2003:91). The subterminal flanges appear wider and more like condyles than in the other metatarsals.

Metatarsal II—Metatarsal II is represented by the complete left TMM 41954-8.2 with a largely obscured and crushed proximal end (Fig. 48A), the left proximal and distal ends of TMM 41954-64.2 embedded in matrix, and the right proximal shaft fragment TMM 41961-1.26 associated with a metatarsal distal end in matrix in *Q. lawsoni* (Table 17). The proximal end is a laterally compressed crescent in cross-section due to a medially curving dorsal flange and a medially expanded ventral tubercle. The latter is likely the plantar flexor tubercle, but the dorsiflexor tubercle is obscured in TMM 41954-8.2 and not preserved in TMM 41954-64.2. There is a small tubercle on the dorsal flange located more distally on TMM 41954-64.2 that may possibly have served this purpose. Distal to this is a short longitudinal ridge extending along the dorsal end of the medial surface, visible in TMM 41954-8.2, which is likely a ligament attachment site. The medially concave crescentic shape of the metatarsal II proximal end articulates with the laterally convex semicircular–ovate proximal end of metatarsal I. There is a thin ridge extending along the middle of the medial surface of TMM 41954-64.2 proximal end, which seems to delimit a ventral facet for articulation with the ventral half of metatarsal I. A slight node on the proximal portion of the shaft may be a muscle attachment. The shaft itself is subcircular in cross-section, as in *T. wellnhoferi* (Eck et al., 2011:290), and curves ventrally with the curvature increasing distally, allowing the identification of TMM 41961-1.26 as a metatarsal II. The distal end is somewhat expanded mediolaterally, as in other pterosaur metatarsals (Dalla Vecchia, 2009:170; Frey et al., 2011:S48), but it is still square in cross-section with a slight lateral orientation of the distal surface, which might be taphonomic. The subterminal flanges are thin and low, separated by a flat groove, and the lateral flange is slightly taller with the medial flange slightly more distal. The metatarsal distal end fragment associated with TMM 41961-1.26 corresponds with this shape, although the flanges are more tubercular in shape.

Metatarsal III—Metatarsal III is represented by the complete and three-dimensional left TMM 42180-18 and the proximal half of left TMM 41954-8.3 (Fig. 48A) in *Q. lawsoni* (Table 17). The proximal end of this metatarsal is laterally compressed with a slight middle constriction, reminiscent of *Pteranodon*'s metatarsal proximal ends that are concave in lateral view (Bennett, 2001a:111). It has a figure-of-eight outline in proximal view due to the medial and lateral expansion of the dorsiflexor and plantar flexor tubercles, respectively. In medial or lateral view, the proximal end appears to have dorsal and proximoventral projections with a fossa between them. The fossa on the medial surface presumably articulates with the lateral convexity of the second metatarsal. Smaller depressions lie within the center of the medial fossa and at the dorsal end of the lateral fossa, which may correspond to depressions with nets of small foramina reported in *A. lancicollis* (Averianov, 2010:310). Another short longitudinal ridge extending along the dorsal end of the medial surface is present in TMM 41954-8.3, presumably for the attachment of a ligament. The metatarsal III shaft is laterally compressed and quite straight, like the metatarsals identified in *S. wucaiwanensis* (Andres et al., 2010:177), which might also be third metatarsals. The shaft cross-section is oval, like metatarsals III–IV in *T. wellnhoferi* (Eck et al., 2011:290). The slight curvature of the shaft that is present in metatarsal III of *Q. lawsoni* is positioned proximally, unlike the other metatarsals. The distal surface is more convex than in other metatarsals and is a

laterally compressed rectangle in distal view. It appears to be oriented straight distally, unlike the slight lateral inclination in *D. macronyx* (Sangster, 2003:91). The subterminal flanges are small and quite thin. They are equal in length, but the lateral flange is much taller.

Metatarsal IV—A complete left metatarsal IV (albeit in two pieces) is preserved in TMM 41954-8.4 (Fig. 48A), a left proximal end with its distal end preserved as an impression in matrix is preserved in TMM 41544-30, and an articulated left proximal end is preserved in TMM 42180-14.8 for *Q. lawsoni* (Table 17). This is a straight bone, lacking the lateral curvature at the proximal and distal ends reported in *D. macronyx* (Padian, 1983a:26). The proximal end of metatarsal IV is more complex than the other metatarsals of *Q. lawsoni*. It is mediolaterally wider like metatarsal I, but it is subtriangular in proximal view with a ventromedial emargination that continues as a fossa on the medial surface. A subtriangular proximal outline for metatarsal IV is also reported in *Pteranodon* (Bennett, 2001a:111). This fossa would presumably articulate with the ventral mediolateral expansion of the third metatarsal. Like TMM 41954-8.1, there is a raised median section terminating in a point on the proximal surface of TMM 41954-8.4 not found in other specimens, which is also interpreted here as a lateral expansion crushed onto the proximal surface. The rest of the proximal end of TMM 41954-8.4 is obscured by matrix and so much of the information about metatarsal IV comes from TMM 41544-30 and to a lesser extent, TMM 42180-14.8. There is a fossa on the exposed ventral part of the TMM 41954-8.4 proximal end, which can be seen to extend to the center of the proximal surface in TMM 41544-30. The dorsiflexor and plantar flexor tubercles form the dorsal and ventral corners of a triangular outline for the proximal surface, respectively. The lateral and longest margin of the triangle is flat in TMM 41544-30 to slightly concave in TMM 42180-14.8, the dorsomedial margin is slightly convex in TMM 41544-30 to flat in TMM 42180-14.8, and the ventromedial margin is concave due to the presence of the fossa. In articulation with the tarsus, this triangular proximal surface would presumably cover most or all of the distal articular surface of the lateral distal tarsal, and the concave ventromedial margin would wrap around the raised prominence on the distomedial corner of the lateral distal tarsal. A short ridge on the dorsal end of the medial surface is also present in TMM 41954-8.4, presumably for the attachment of a ligament. A nutrient foramen figured on the dorsal surface of the metatarsal IV proximal end in *Pteranodon* (Bennett, 2001a:fig. 114) is not apparent in the *Q. lawsoni* material, but it may just not be preserved. The shaft of metatarsal IV is nearly straight with a subcircular cross-section, like the metatarsals of *Pteranodon* (Bennett, 2001a:111) and *A. ammoni* (Bennett, 2007a:387) but unlike the oval metatarsals III–IV in *T. wellnhoferi* (Eck et al., 2011:290). The distal end is only preserved in TMM 41954-8.4, and it appears to have a slight mediolateral expansion. The distal articular surface also appears to have a slight lateral orientation, as in *D. macronyx* (Sangster, 2003:91). The subterminal flanges reach the distal end of the metatarsal to form tiny tubercles at the ventral corners of the distal surface. This is somewhat similar in shape to the distal end associated with TMM 41961-1.26 and so this may be a metatarsal IV fragment, but its poor preservation precludes its identification. The distal flanges are asymmetrical: the lateral flange is taller, longer, thinner, and reaches more proximally than the medial flange. The metatarsals are all roughly the same length in basal pterosaurs, but the metatarsal IV becomes significantly shorter in the Breviquartossa (Andres, 2021). The complete third metatarsal is not preserved in TMM 41954-8, but the fourth metatarsal is significantly shorter than the first two metatarsals, and so it is identified here as having the same short fourth metatarsal as in the other breviquartossans.

Metatarsal V—The fifth metatarsal is the shortest and most robust of the metatarsal elements in pterosaurs (Sangster, 2003; Bennett, 2007a; Dalla Vecchia, 2009; Bennett, 2014). In *Q. lawsoni*, right fifth metatarsals are present in TMM 41954-37 (Fig. 48B–D) and 42422-16 (missing distal end), and left fifth metatarsals are present in TMM 42138-2.2 and 42180-14.9 specimens (Table 17). Padian (2017) identified an element associated with TMM 41954-64 as the proximal end of metatarsal V. This element (TMM 41954-64.5) is associated but not articulated with the left lateral distal tarsal (TMM 41954-64.3), as evidenced by a black line drawn on its surface (similar to other marks made on the distal tarsals in this specimen) that aligns with a mark on the field jacket in which it is still stored. It is poorly preserved and appears to be a single triangular bone in 'dorsal' view but has two breaks on the 'ventral' surface dividing it into three possible segments. Whether these breaks are cracks or contacts is not known. If separate, these segments would be so small that they could correspond to the second and third phalanges of pedal digit IV in addition to another fragment. The entire structure has a triangular outline similar to a metatarsal V, but is much smaller than the others with a reduced proximal articulation and expanded posterolateral tubercle. Padian (2017) is likely correct that this is a poorly preserved part of a larger metatarsal V, but whether it includes the proximal end is uncertain.

Metatarsal V varies greatly in shape over pterosaur phylogeny, but it is triangular in dorsal/ventral view in *Q. lawsoni*, *T. wellnhoferi* (Eck et al., 2011:290), and *A. primordius* (Frey et al., 2011:S48), unlike the less robust and more hook-shaped fifth metatarsals of the pteranodontoids (Kellner and Tomida, 2000:81; Bennett, 2001a:111–112; Frey et al., 2006:32, fig. 3) or the middle-constricted fifth metatarsals of basal pterosaurs (Padian, 1983a:fig. 26; Sangster, 2003:92; Dalla Vecchia, 2009:170). It has a proximal (medial) process (ventral tuberosity of Sangster, 2003) to articulate with the lateral distal tarsal. The proximal articular surface is slightly concave, lacriform in outline, and inclined ventrally at a 40° angle (with respect to the anterior process). This articular surface is described as suboval in *Pteranodon* (Bennett, 2001a:112), but it essentially has the same outline as in *Q. lawsoni*. In TMM 42180-14.9, the posterior end of this articulation appears to fit into the circular depression on the lateral surface of the lateral distal tarsal. The entire bone attenuates anterodistally, with a straight distal (lateral) margin. It lacks the middle constriction, torsion, and the distal trochlea of basal pterosaurs (Sangster, 2003:92). The metatarsal V is nearly straight in distal (lateral) view, instead of curved anteriorly as in *Pteranodon* (Bennett, 2001a:112). It has a dorsal expansion of the anterior process (rugose prominence of Padian, 1983a) forming a dorsal concave area. A small, presumably nutritive foramen is present in this concavity, in a similar position to a foramen found in *Pteranodon* (Bennett, 2001a:112), along with a more posteroproximally-positioned fossa. A distinct posterior process (dorsal tuberosity of Sangster, 2003, or proximally pointing process of Frey et al., 2011) is present on the posterodistal corner and includes a tubercle on its dorsal surface (node of Sangster, 2003) with a much larger tubercle present on its ventral side, presumably for tendon or muscle attachment (Sangster, 2003:92). These combined tubercles form an expansion of the posterior tip. A saddle-shaped sulcus (well-marked groove of Padian, 1983a) is positioned between the proximal articulation and the posterior expansion on the posterior surface, evidently for the passage of tendons (Padian, 1983a:37). The ventral surface is visible in TMM 41954-37 and 42180-14.9, but they have disparate preservation: smooth and convex in TMM 42180-14.9 but weathered with a pair of divots in TMM 41954-37. TMM 42180-14.9 is the better preserved of these and so is viewed as having the more accurate morphology. Rough striations extend distally from the ventral tubercle to the anterior

expansion, as reported in *Pteranodon* (Bennett, 2001a:112). The metatarsal V of *Quetzalcoatlus* has been described as similar to that of *Pteranodon* except that it appears to be more robust, suggesting that it was more terrestrial in habits than was *Pteranodon* (Bennett, 2001a).

Pedal Digits

The phalangeal formula of the pterosaur pes is 2-3-4-5-2/1/0, with the lophocratian pterodactyloids losing one or both of the fifth pedal digit phalanges (Andres, 2021). Eleven pedal phalanges are preserved in the *Q. lawsoni* material (Fig. 49): five ungual (TMM 41954-13, 41954-68, and 41954-78, as well as 42138-2.8 and 42138-2.9) and six non-ungual phalanges (TMM 41954-32 and 41954-87, 41961-1.31, and 42138-2.5 to 42138-2.7), and so most but not all of the pedal phalanges are preserved (Table 18). There are four or five tiny bone fragments associated with the TMM 42180-14 pes that may be sesamoids or pedal phalanx fragments; possibly the highly reduced (nubbin-like of Wu et al., 2017) third digit second phalanx or fourth digit second and third phalanges found in monofenestratans (Bennett, 2001a; Wu et al., 2017), but they are too fragmentary to be identified with certainty. There is no trace of fifth pedal digit phalanges and the fifth metatarsal does not appear to have a distal articulation. None of this material is articulated, but five left pedal phalanges are associated with one another in the left pes of TMM 42138-2 (Fig. 49I); the rest are isolated specimens. This makes their identification challenging, and so what it is presented here represents the most defensible identifications, facilitated by comparison with more complete pterosaur pedes, especially those of *Z. linhaiensis* (ZMNH M1323 and M1328) and *J. edentus* (RCPS-030366CY). Only the first two phalanges of pedal digit III, and the first three phalanges of pedal digit IV are not preserved in the *Q. lawsoni* material.

Pterosaurs have four pedal digits (I–IV) with unguals. The TMM 42138-2.8 and 2.9 pedal unguals are preserved in association in matrix (Fig. 49I), TMM 41954-13 and 78 are three-dimensionally preserved (Figs. 49VII and IV, respectively), and TMM 41954-68 is an isolated phalanx that was too fragile to remove from the surrounding matrix without risk of damage (Fig. 49II). The two three-dimensional pedal unguals are the best preserved and the most disparate pedal unguals in the material: TMM 41954-13 is deep and highly curved with a large proximal flexor tubercle (adductor tubercle of Frey et al., 2011), whereas TMM 41954-78 is elongate and straighter, with a small more distal flexor tubercle (note that these specimens were originally both numbered TMM 41954-13 at the time they were photographed, but TMM 41954-78 was given a new number). The two associated pedal unguals (TMM 42138-2.8 and 2.9) morphologically fall between these two: TMM 42138-2.9 is more elongate and straighter with a smaller and more distal flexor tubercle similar to TMM 41954-78, and TMM 42138-2.8 is deeper and more curved with a larger proximal flexor tubercle similar to TMM 41954-13. These four distinct unguals likely represent the unguals for all four pedal digits in *Q. lawsoni*. The remaining pedal phalanx, TMM 41954-68 (Fig. 49II), is most similar to TMM 42138-2.8 and so is identified as the same phalanx of the pes. In pterosaurs, the pedal unguals typically transition from more elongate and less curved to deeper and more curved along the series: digit I to IV (*Z. linhaiensis*: ZMNH M1328; *J. edentus*: RCPS-030366CY), although Sangster (2003) described the ungual of pedal digit IV in *D. macronyx* as not as tightly curved as the previous digits but still deep. This facilitates the identification of these as the unguals for pedal digits I (TMM 41954-78), II (TMM 42138-2.9), III (TMM 41954-68 and 42138-2.8), and IV (TMM 41954-13) in decreasing elongation and increasing curvature. It should also be noted that this transition mirrors an increase in

disparity between the medial and lateral condyles/cotyles of the penultimate phalanx-ungual articulation along the series in *Q. lawsoni*, wherein the lateral condyle/cotyle becomes larger and more dorsally positioned than the medial condyle/cotyle from pedal digits I to IV. Also, there is a concomitant ventral migration and disparity in the medial and lateral ungual groove along the series. This would suggest a medial rotation of the pedal ungual in the lateral digits, but whether that was actually the case and what the functional implications would be are open questions.

The pedal unguals of *Q. lawsoni* are smaller than the manual unguals, but they are large by pterosaur standards and similar to basal pterosaurs in being robust and significantly curved. Most breviquartossan pterosaurs have manual unguals over twice the length of the pedal unguals (Andres, 2021), which are generally reduced to small triangular elements. In *Q. lawsoni*, the manual unguals average 1.67 times the length of the pedal unguals. This is due in part to high curvature of the manual unguals in this species. If the arc lengths of these unguals are measured, the manual unguals are 1.75 times the length of the pedal unguals. A pair of ungual grooves (lateral sulcus of Kellner and Tomida, 2000, deep furrow of Sangster, 2003, deep longitudinal groove of Dalla Vecchia, 2009, sulcus of Frey et al., 2011, or narrow groove of Eck et al., 2011) extend down the medial and lateral surfaces of the pedal unguals, absent in the pteranodontoids *A. piscator* and *Pteranodon* (Kellner and Tomida, 2000:81, fig. 55; Bennett, 2001b:fig. 126). *Quetzalcoatlus lawsoni* has well developed pedal unguals with elongate moderately curved claws and distinct flexor tubercles. These are less developed than the tightly curved sharp unguals with strong flexor tubercles reported in tapejarids (Lü et al., 2006a:fig. 4; Wang et al., 2008:1985; Eck et al., 2011:290–291; Wu et al., 2017:fig. 9), but more developed than the mildly curved unguals with weakly developed flexor tubercles reported in chaoyangopterids (Lü et al., 2008:894; Wu et al., 2017:22) and the slender and weakly curved unguals lacking flexor tubercles reported in *Pteranodon* (Bennett, 2001a:112).

No example of the reduced (nubbin-like) pedal phalanges represented by the third digit second phalanx or the fourth digit second and third phalanges were found in the *Q. lawsoni* material. Therefore all of the non-ungual pedal phalanges preserved are either proximal or penultimate phalanges (or both in the case of the pedal digit I phalanx 1). Five of these have semi-circular distal bicondyles that would have articulated with the pedal ungual proximal cotyles, and so these can be identified as penultimate phalanges: TMM 41954-87, 41961-1.31, and 42138-2.5–2.7. The remaining phalanx (TMM 41954-32) lacks these distal condyles, indicating it is from the proximal series. It also lacks the saddle-shaped (ginglymal of Padian, 1983a, ginglymoid of Bennett, 2001a, or sulcate of Sangster, 2003) interphalangeal joints reported in pterosaur pedals (Padian, 1983a). All but one of the non-ungual interphalangeal joints of the pes involve the reduced (nubbin-like) phalanges of pedal digits III and IV that have these saddle-shaped articulations, leaving the first phalanx of pedal digit II as the best candidate for having a different articulation and for being TMM 41954-32. This is supported by its small size (Wu et al., 2017:22) and a similar interphalangeal articulation as the second phalanx of pedal digit II (TMM 41954-87).

The identification of the five penultimate phalanges is aided by three of them being associated in TMM 42138-2. The shortest penultimate pedal phalanx is in the fourth digit of pterosaurs (Bennett, 2001b:fig. 126; Sangster, 2003; Wu et al., 2017:table 1; ZMNH M1328), and it typically is the most constricted of the series. Both characteristics are found in TMM 42138-2.6, which is also the shortest complete pedal phalanx found in *Q. lawsoni* and appears to have a saddle-shaped proximal articulation for the reduced third phalanx of the fourth digit.
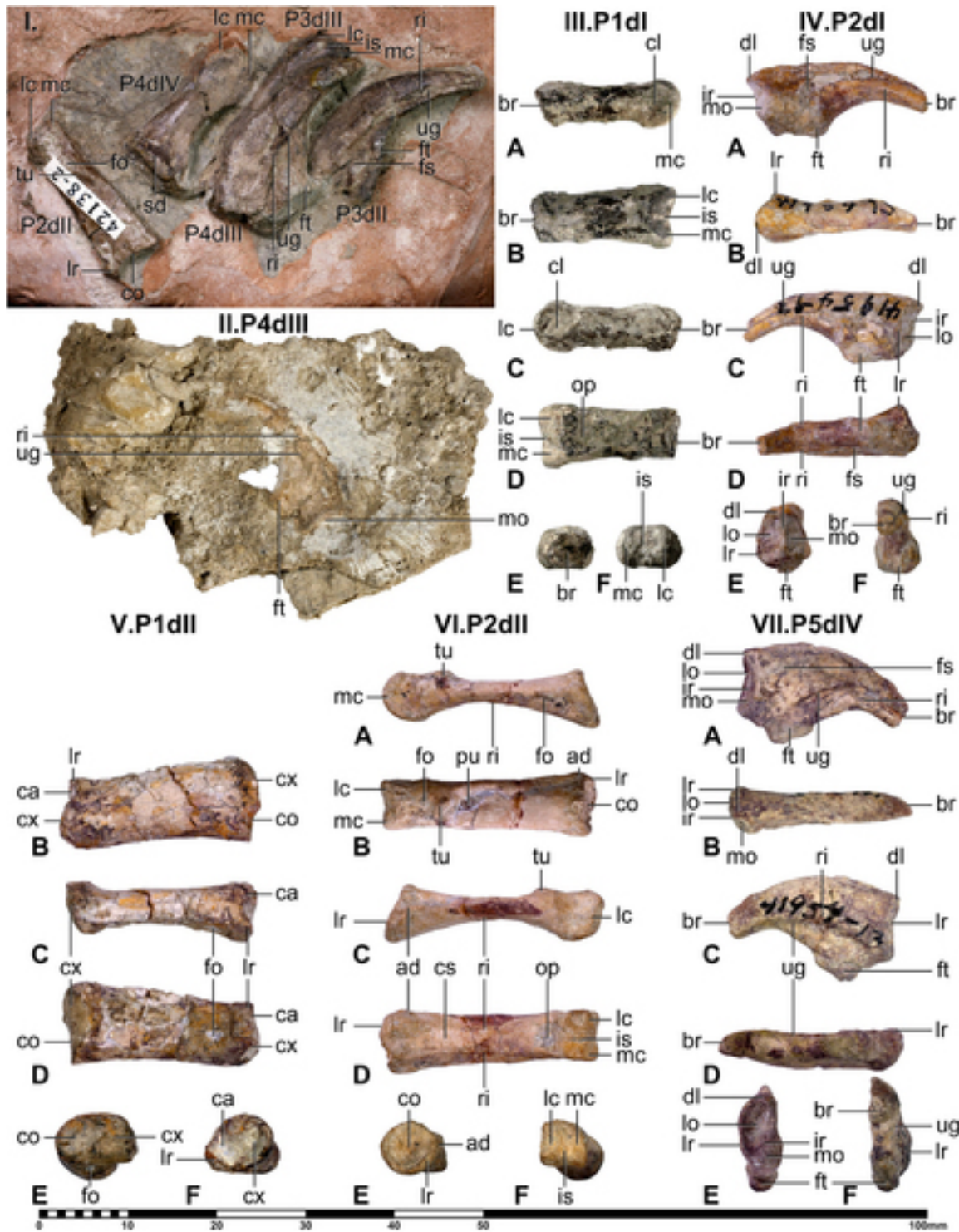
FIGURE 49. Q*uetzalcoatlus lawsoni*, sp. nov., pedal phalanges: **I**, left pedal phalanges including second phalanx pedal digit II in dorsal view (TMM 42138-2.5), fourth phalanx pedal digit IV in dorsal view (TMM 42138-2.6), third phalanx pedal digit III in dorsal view (TMM 42138-2.7), fourth phalanx pedal digit III in medial view (TMM 42138-2.8), and third phalanx pedal digit II in medial view (TMM 42138-2.9), **II**, right fourth phalanx pedal digit III (TMM 41954-68) in medial view; **III**, left first phalanx pedal digit I distal end (TMM 41961-1.31); **IV**, left second phalanx pedal digit I (TMM 41954-78); **V**, right first phalanx pedal digit II (TMM 41954-32); **VI**, right second phalanx pedal digit II (TMM 41954-87); and **VII**, left fifth phalanx pedal digit IV (TMM 41954-13) in **A,** medial, **B**, dorsal; **C**, lateral; **D**, ventral; **E**, proximal; and **F**, distal views. Note that the medial view of TMM 41954-32 could not be photographed in time for publication. TMM 41954-13 was originally a specimen number for two pedal unguals, one of which (IV) has since been renumbered TMM 41954-78, but it was marked with the original number at the time it was photographed. **Abbreviations: ad**, adductor tubercle; **br**, break; **ca**, concavity; **cl**, collateral ligament pit; **co**, cotyle; **cs**, concave surface; **cx**, convexity; **fo**, foramen; **fs**, fossa; **ft**, flexor tubercle; **ir**, intercotylar ridge; **is**, intercondylar sulcus; **lc**, lateral condyle; **lo**, lateral cotyle; **lr**, lateral rim; **mc**, medial condyle; **mo**, medial cotyle; **op**, opening; **PxdY**, pedal phalanx X of Digit Y; **pu**, puncture; **ri**, ridge; **sd**, saddle-shaped articulation; **tu**, tubercle, and **ug**, ungual groove. Scale bar equals 100 mm.

TABLE 18. Measurements of *Quetzalcoatlus lawsoni*, sp. nov., pedal material. Values in millimeters. >, preserved value; ~, approximate value; d-v, dorsoventral dimension; lat, lateral dimension; and p-d, proximodistal dimension. Holotype specimen in italics.

Dimension: Element: Specimen Number:	Length (p-d)	Mid-width (lat)	Mid-depth (d-v)
First phalanx pedal digit I			
TMM 41961-1.31	>16.15	5.49	4.30
Second phalanx pedal digit I (ungual)	Length (p-d)	Base-depth (d-v)	Base-breadth (lat)
TMM 41954-78	>20.07	8.88	5.80
First phalanx pedal digit II	Length (p-d)	Mid-width (lat)	Mid-depth (d-v)
TMM 41954-32	21.64	7.76	4.31
Second phalanx pedal digit II	Length (p-d)	Mid-width (lat)	Mid-depth (d-v)
TMM 41954-87	24.39	5.46	2.55
TMM 42138-2.5	24.13	6.52	?
Third phalanx pedal digit II (ungual)	Length (p-d)	Base-depth (d-v)	Base-breadth (lat)
TMM 42138-2.9	24.20	9.43	?
Third phalanx pedal digit III	Length (p-d)	Mid-width (lat)	Mid-depth (d-v)
TMM 42138-2.7	19.28	5.56	?
Fourth phalanx pedal digit III (ungual)	Length (p-d)	Base-depth (d-v)	Base-breadth (lat)
TMM 41954-68	19.82	8.83	3.66
TMM 42138-2.8	22.22	10.90	?
Fourth phalanx pedal digit IV	Length (p-d)	Mid-width (lat)	Mid-depth(d-v)
TMM 42138-2.6	18.47	?	4.65
Fifth phalanx pedal digit IV (ungual)	Length (p-d)	Base-depth (d-v)	Base-breadth (lat)
TMM 41954-13	>21.52	12.35	5.26

In addition, the high asymmetry of the distal condyles matches the proximal end of the fourth pedal digit ungual (TMM 41954-13). The longest pterosaur pedal phalanx is traditionally the first phalanx of the first digit (Padian, 2008b). Such an elongate phalanx is not preserved in *Q. lawsoni*, but the distal fragment of a phalanx associated with the TMM 41961-1.31 number is almost the length of some of the complete pedal phalanges and shows no sign of a proximal expansion on its shaft, indicating that it would be a significantly longer phalanx. The small amount of asymmetry of the TMM 41961-1.31 distal end also matches the proximal end of the first digit ungual (TMM 41954-78), supporting its identification as the first phalanx of the first pedal digit. It is evident that TMM 42138-2 does not preserve this long first phalanx of the first pedal digit, necessitating that the two remaining penultimate phalanges (TMM 42138-2.5 and 2.7) are from the second and third digit, matching the preserved second and third digit unguals (TMM 42138-2.8 and 2.9) in this specimen. TMM 42138-2.7 is largely obscured by TMM 42138-2.8 such that its greater length (longest pedal phalanx in TMM 42138-2) and significant asymmetry of the distal condyles are about the only recognizable features. The penultimate phalanges of pterosaur second and third pedal digits are often nearly equal in length, but when there is disparity, the third digit penultimate phalanx is typically the longer. Also, the asymmetry of the distal end is more similar to the fourth digit ungual than the first digit ungual, supporting the identification of TMM 42138-2.7 as the third pedal digit third phalanx. In this manner, the resting of the third digit ungual (TMM 42138-2.9) on top of the third digit penultimate phalanx (TMM 42138-2.5) would not be coincidental. TMM 42138-2.5 and 41954-87 are almost identical in shape and are put forward here as the same phalanx. The three-dimensional preservation of TMM 41954-87 supports their identification as the second pedal digit second phalanx: the proximal end lacks a saddle-shaped articulation for a third or fourth digit reduced phalanx, but instead has a circular rimmed cotyle that matches the distal convexity of the second digit first phalanx (TMM 41954-32), and the slighter asymmetry of the distal condyles is also more similar to the first digit ungual than the fourth digit ungual.

The non-ungual pedal phalanges of pterosaurs are generally described as slender and gently curved in lateral view (Bennett, 2001a:112; Sangster, 2003:92–94; Eck et al., 2011:290),

However, the non-ungual pedal phalanges of *Q. lawsoni* have straight shafts and are only concave ventrally, as in *J. edentus* (Wu et al., 2017:fig. 7) and *A. lancicollis* (Averianov, 2010:311). The shafts of the *A. lancicollis* non-ungual phalanges are triangular in cross-section (Averianov, 2010:fig. 37), unlike the more oval cross-section of *Q. lawsoni*. In general, the non-ungual pedal phalanges of *Q. lawsoni* appear more robust and less elongate than other pterosaurs.

First Phalanx Pedal Digit I—TMM 41961-1.31 (Fig. 49III) includes a fragment identified here as the distal end of the left pedal digit I phalanx 1 (Table 18). It is not well preserved; much of its cortical bone is damaged and indistinguishable from matrix. It can be recognized as a penultimate phalanx based on the distinct semicircular distal condyles for articulation with the proximal cotyles of a pedal ungual. Although incomplete, it is about the same length as the pedal digit II and III penultimate phalanges and shows no sign of the proximal expansion at its break. Therefore, it would be significantly longer than those phalanges, and the first phalanx of digit I is traditionally the longest penultimate phalanx in the pterosaur pes (Padian, 2008b). The first phalanx of the fourth pedal digit is slightly longer in *J. edentus* (Wu et al., 2017:22), but it lacks distal condyles. Not enough of the shaft of TMM 41961-1.31 is preserved to determine curvature. The shaft cross-section is circular, becoming oval distally. A matrix-filled opening similar to one present in TMM 41954-87 appears to be present just proximal to the distal condyles on the ventral surface that may contain a foramen. A foramen may also be present in a similar position on the dorsal surface as in TMM 41954-87, but the poor preservation precludes its observation. The distal condyles are positioned slightly ventrally and have collateral ligament pits (collateral ligament fossae of Bennett, 2001a, or foramen of Sangster, 2003) in the center of their lateral surfaces. The distal condyles are similar in shape differing in that the medial condyle is about three-quarters the size of the lateral condyle, and the lateral condyle protrudes slightly more distally. The intercondylar sulcus between the two does not form a deep groove. It is identified as a left element (like the rest of the TMM 41961-1 pedal material) based on its slightly larger and distally-positioned lateral condyle.

Individual pedal phalanges are rarely described in pterosaurs, and even then the description is limited to their relative lengths. Sangster (2003) does describe a first phalanx of pedal digit I in

D. macronyx (NHMUK 41212), but this element has a deep intercondylar sulcus and a narrower lateral condyle on its distal end. It is possible that the TMM 41961-1.31 phalanx with its wider lateral condyle could be from the right side instead. However, the NHMUK 41212 left pedal digit I phalanx 1 lateral condyle is partially obscured by its ungual (Padian, 1983a:fig. 22; Sangster, 2003:fig. 3.22). The distally positioned TMM 41961-1.31 lateral condyle also gives the distal end a slight medial deflection, like the metatarsal I distal end and the medial deflection of the first pedal digit reported in the *Dimorphodon* species (Clark et al., 1998:887). Averianov (2010) reported a single proximal pedal phalanx (ZIN PH 240/44) in the *A. lancicollis* material that appears to have distal condyles (Averianov, 2010:fig. 37), and the digit I phalanx 1 is the only proximal pedal phalanx with distal condyles. This identification is supported by its greater length than the other preserved pedal phalanges and the undivided proximal articular surface (Averianov, 2010:310–311, fig. 37), which would articulate with a metatarsal. ZIN PH 240/44 differs from the TMM 41961-1.31 phalanx in having a triangular cross-section, sharp medial and lateral edges on the ventral surface, distal condyles that project dorsally above the shaft, and possibly lacking foramina/openings. It is possible that the sharp edges of the ventral surface did not reach the distal end and would not have been preserved in TMM 41961-1.31, in which case both species would share a flat ventral surface. Alternatively, Sangster (2003) figured the first phalanx of pedal digit III as having distal condyles that project dorsally above the shaft (Sangster, 2003:fig. 3.24) and described it as dorsally bowed in *D. macronyx*, or it may just be upside down.

Second Phalanx Pedal Digit I—TMM 41954-78 (Fig. 49IV) is the straightest and narrowest of the pedal unguals in the *Q. lawsoni* material (Table 18). The tip is missing, but the preserved portion curves over an arc of only 75°. It has a flat medial surface, larger lateral proximal cotyle with a prominent lateral rim, and a medially positioned flexor tubercle, allowing it to be identified as a left ungual. This flexor tubercle is distinct, but shallower and positioned farther down the shaft than in the other pedal unguals. Both proximal cotyles (dorsally-situated concavity on the proximal edge of Sangster, 2003, or ungual trochlea of Frey et al., 2011) are piriform in outline, with the lateral cotyle larger and reaching more ventrally than the medial cotyle. They are separated by a distinct intercotylar ridge. The proximal end is expanded both dorsoventrally and mediolaterally, largely due to the expanded lateral and dorsal rim of the articular cotyles. This dorsal rim was termed a projecting process by Sangster (2003:92–94) and identified as the insertion for the claw extensors. The convex surface dorsal to this rim, separated from the convex dorsal surface of the claw by a slight notch, would be a more likely candidate for an extensor insertion site. The flat medial surface of this pedal ungual has a proximally positioned fossa. The ungual grooves extend down the midline of the medial and lateral surfaces of the claw. The distal half of the preserved ungual has a pair of medial and lateral ridges merging with the ventral margin to form a flat ventral surface and a semicircular cross-section distally. A flattened ventral surface has also been reported in the pedal digit II and III unguals of *A. piscator* (Kellner and Tomida, 2000:81).

No unguals are reported in the *A. lancicollis* material and only the base of this phalanx is preserved in *Z. linhaiensis* (ZMNH M1328), but this can be seen to be the narrowest ungual in the latter species. It is both the longest and narrowest pedal ungual in *J. edentus* (Wu et al., 2017:33, fig. 7). TMM 41954-78 is missing its distal tip and so could possibly be the longest ungual in *Q. lawsoni* if it came to a sharp point. A pedal digit I second phalanx is preserved in *D. macronyx* (NHMUK 41212) but was described as deep and trenchant (Sangster, 2003:94).

First Phalanx Pedal Digit II—TMM 41954-32 (Fig. 49V) is identified as a pedal digit II first phalanx based on its squat shape (although not as short as the greatly reduced second phalanx of digit III or the second and third phalanges of digit IV), lack of distal condyles or ginglymus (suggesting that it did not articulate with an ungual or reduced pedal phalanx), and that its distal articular surface is a mirror-image of the second phalanx pedal digit II proximal articular surface (Table 18). It also shares a medial deflection of the shaft with other pterosaur second digit first phalanges (Bennett, 2001b:126; Sangster, 2003:94; Wu et al., 2017:fig. 7; ZMNH M1323 and M1328). The proximal and distal articular surfaces are parallel to one another and so the entire bone is slightly sinusoidal (concave medially, convex laterally). Whether this medial deflection would have accommodated a slight lateral orientation present in the TMM 41954-8.2 metatarsal II (Fig. 48A), or this angle was taphonomic, the curvature of this first phalanx would have positioned the second digit between the first and third digits. The proximal articulation has a large medially positioned oval cotyle constituting at least two-thirds of the proximal surface, bordered by a ventrolateral convexity that may have functioned as a flexor and/or adductor tubercle. This gives the proximal end a concave medial and convex lateral outline in dorsal/ventral view. The shaft is crushed, but it appears to have been semicircular in cross-section. A tiny elliptical foramen pierces the ventral surface of the distal half, and an even smaller foramen may be present on the medial surface of the proximal end, but the preservation is not sufficient to identify its presence with certainty. The distal end has a slight ventral orientation. The distal surface is the reverse of the proximal end, a medial convexity and a lateral concave area with rim. The cortical bone of the distal articular surface does not appear to be preserved. In distal view, the distal end appears torsioned about 45° counterclockwise. The medial deflection of the shaft, larger lateral articular surfaces, and distal lateral rim allow this element to be identified as a right element.

The first phalanx of the second pedal digit is preserved in *Z. linhaiensis* (ZMNH M1323 and M1328) and *J. edentus* (RCPS-030366CY). They share a deflection of the shaft and same general outline with *Q. lawsoni*, but not much more can be discerned. *Jidapterus edentus* appears to have a normal ginglymoid distal articulation (Wu et al., 2017:fig. 7) but this condition is difficult to determine in *Z. linhaiensis* (ZMNH M1328), and so the unusual pedal digit II first and second phalanx articulation of *Q. lawsoni* may be unique to the Azhdarchidae or one of its subgroups.

Second Phalanx Pedal Digit II—TMM 41954-87 (Fig. 49VI) and TMM 42138-2.5 (Fig. 49I) are penultimate phalanges based on the presence of distal semicircular condyles for articulation with an ungual (Table 18). They are almost identical except that they come from different sides of the body and TMM 41954-87 is three-dimensionally preserved, and so they are identified as the same element. The proximal end of this element is unusual in that it lacks a saddle-shaped or ginglymoid articulation and instead has a single circular cotyle with a lateral rim. This would imply that this is a metatarsal articulation for the first pedal digit I phalanx (the only penultimate pedal phalanx that articulates with a metatarsal in pterosaurs), except that it is exceedingly short for that phalanx and would imply an aberrantly short first pedal digit for *Q. lawsoni*. The most defensible identification for this element is that it is the second pedal digit II phalanx, that its proximal medial concave facet articulated with the distal medial convex facet of the first pedal digit II phalanx, and that its proximal lateral rim articulated with the lateral concave facet of that first phalanx. This is also the only pedal phalanx in the material that has a ventrally sloping proximal end with a concomitant posterodorsally oriented proximal articulation surface to match the slight ventral orientation of

the distal end of the second pedal digit first phalanx. Sangster (2003:94) identified a similar articulation in the pes of *D. macronyx*, but said it was true of all the phalanges in the pes. The moderate asymmetry of the distal condyles support that these specimens come from the second pedal digit (slightly more asymmetric than the pedal digit I penultimate phalanx condyles), and their slightly larger lateral condyles identify TMM 41954-87 and 42138-2.5 as right and left elements, respectively. In addition, there is a slight lateral expansion of the proximal end and a tiny adductor tubercle present on the proximal end of the lateral surface. A tiny elliptical foramen is present on the other side on the proximal end of the medial surface. The second pedal digit second phalanx is a straight bone with a dorsoventrally depressed midsection. A hole in the middle of the TMM 41954-87 dorsal surface (not present in TMM 42138-2.5) that has a crack running through it is identified as a puncture mark. Distal to this puncture is a dorsal tubercle about a quarter of the length from the distal end, which is found in both specimens. Its function is not known but its dorsal position implies that it was involved in extension/dorsiflexion. Between the dorsal tubercle and distal condyles is a small circular foramen. Two parallel ridges extend along the entire ventral surface of the phalanx to contact the rims of the distal condyles, creating a slightly concave surface between them on the proximal half. This is very similar to the ventral longitudinal shallow groove reported in *A. primordius* that is most transversely concave on its proximal third (Frey et al., 2011:S49), except that the structure was reported on all non-ungual pedal phalanges of *A. primordius*. A trapezoidal opening of unknown depth is present on the ventral surface just proximal to the distal condyles. The second pedal digit second phalanx of *Q. lawsoni* is mediolaterally constricted at its distal third, instead of at its middle, as in the non-ungual phalanges of *A. primordius* (Frey et al., 2011:S49). This creates concave outlines for the dorsal and ventral surfaces in medial/lateral view, with the ventral concavity being more developed. The distal semicircular condyles taper in (mediolateral) width on the dorsal surface and lack both a deep intercondylar groove and collateral ligament pits.

The dorsal features found in the *Q. lawsoni* second pedal digit second phalanx are obscured or not preserved in *Z. linhaiensis* (ZMNH M1323 and M1328, respectively). This phalanx is visible in ventral view in *J. edentus* (RCPS-030366CY) and appears to have a ventral concave surface bounded by ridges as in TMM 41954-87. Averianov (2010) reported three and described two penultimate phalanges in the *A. lancicollis* material. The shortest of the figured phalanges, ZIN PH 241/44 (Averianov, 2010:fig. 37F–J), shares with the pedal digit II phalanx 2 of *Q. lawsoni* a ventrally sloping proximal end, a lateral adductor tubercle (peculiar outgrowth on one side of Averianov, 2010), a medial proximal foramen, ventral ridges flanking a concave surface (sulcus along the ventral side of Averianov, 2010), and a lack of collateral ligament pits. In addition, Averianov (2010) described the proximal articulation of ZIN PH 241/44 as subdivided into two parts, but not saddle-shaped as in other penultimate phalanges, which would be consistent with the concave and convex facets of the pedal digit II first and second phalanx articulation of *Q. lawsoni*. This unusual articulation is likely a synapomorphy of the Azhdarchidae. ZIN PH 241/44 differs from TMM 41954-87 and 42138-2.5 in being triangular in cross-section, like the other *A. lancicollis* pedal phalanges (Averianov, 2010:311), and in lacking a dorsal foramen, but it may have a ventral opening (Averianov, 2010: fig. 37F–J). ZIN PH 241/44 is identified here as a left pedal digit II second phalanx.

Third Phalanx Pedal Digit II—TMM 42138-2.9 (Fig. 49I) is one of the two moderately-curved and elongate two-dimensional pedal unguals with medium-sized and distally positioned flexor tubercles preserved in TMM 42138-2 (Table 18). TMM 42138-2.9 is closer in morphology to the pedal digit I ungual than 42138-2.8 and so is identified as the pedal digit II ungual. Its lateral crushing and partial obstruction by TMM 42138-2.8 have obscured much of its features. A partial rim of the medial cotyle is all that can be observed of the proximal margin. A low flexor tubercle that is not offset laterally from the exposed surface is positioned about a third down the phalanx. A shallow fossa appears to be present on its identified flat medial surface. The ungual groove extends down the ventral half of the medial surface of the claw, bounded dorsally by a midline ridge. This ungual appears to be complete and lacks a sharp tip. It is identified here as a left phalanx, as is the rest of the TMM 42138-2 pes, based on its flat medial surface and a medially positioned fossa and flexor tubercle.

The pedal digit II ungual is not preserved in *Z. linhaiensis* or *A. lancicollis*. It is preserved in *J. edentus* (Wu et al., 2017:fig. 7) and shares with TMM 42138-2.9 the broad outline of a moderately elongate and curved ungual.

Third Phalanx Pedal Digit III—TMM 42138-2.7 (Fig. 49I) is largely obscured by the overlying TMM 42138-2.8 pedal ungual (Table 18). Not much more than its length and its distal articulation can be observed. It is identified as phalanx 3 of pedal digit III in part by the process of elimination: the distal condyles necessitate it is a penultimate phalanx, the elongate pedal digit I penultimate phalanx is not preserved in TMM 42138-2, the pedal digit II penultimate phalanx (TMM 42138-2.5) has a distinctive proximal articulation in *Q. lawsoni*, the pedal digit IV penultimate phalanx is much shorter with a distinct constriction (TMM 42138-2.6), and *Q. lawsoni* has no pedal digit V phalanges. TMM 42138-2.7 is also the longest pedal phalanx in the TMM 42138-2 material, and the third digit third phalanx is often the longest penultimate phalanx after the first digit penultimate/proximal phalanx. However, it should be noted that the penultimate phalanges of pedal digits II and III are nearly equal in length in other neopterodactyloids (*Z. linhaiensis*: ZMNH M1328 and *J. edentus*: RCPS-030366CY). The large asymmetry of the distal end of this phalanx is also closer to the fourth pedal digit than to the other digits. Lastly, the fourth phalanx of pedal digit III (TMM 42138-2.8) is lying on top of this phalanx, and whereas this is not proof of its identification as the third phalanx of pedal digit III, it is correlated with it. The shaft of the TMM 42138-2.7 phalanx appears to have some distal curvature. The distal condyles are rather small; the lateral condyle is larger and reaches more dorsally onto the shaft, supporting the identification of this pedal phalanx as a left element. A slight intercondylar sulcus extends between the condyles. At the proximal end of this sulcus on the dorsal surface is a tiny matrix-filled hole that may be a foramen. No collateral ligament pits are visible.

The pedal digit III third phalanx is preserved in both *Z. linhaiensis* (ZMNH M1323 and M1328) and *J. edentus* (Wu et al., 2017:fig. 7), but the poor preservation of TMM 42138-2.7 limits comparisons to length and that *Z. linhaiensis* (ZMNH M1328) also lacks collateral ligament pits. The third phalanx of pedal digit III is also long in *D. macronyx*, but collateral ligament pits are present (Sangster, 2003:94). The longest of the penultimate phalanges identified by Averianov (2010) appears to have a tiny foramen on the distal end of the dorsal surface (Averianov, 2010:fig. 37N–O) and may be a pedal digit III third phalanx as well.

Fourth Phalanx Pedal Digit III—TMM 41954-68 (Fig. 49II) and 42138-2.8 (Fig. 49I) share a similar curvature, position and shape of the flexor tubercle, and position of the ungual groove and ridge, and so are identified as the same element but from different sides of the body, right and left, respectively (Table 18). TMM 42138-2.8 is one of the two pedal unguals that

morphologically falls between the identified first (TMM 41954-78) and fourth (TMM 41954-13) pedal unguals in the TMM 42138-2 material. TMM 41954-68 and 42138-2.8 are certainly more similar to TMM 41954-13. They share with the fourth digit ungual a greater curvature, larger and more proximal flexor tubercle, and larger fossa on the proximal end of the medial surface, but to a lesser extent. They also share a flexor tubercle that is pointed, but TMM 41954-13 has a divided flexor tubercle in which the proximal end is pointed. In addition, they share an ungual groove on one side that does not reach the distal end of the claw but that terminates at the ventral margin about a third from the end, with the more dorsal ridge merging with the ventral surface to form a flat ventral surface. However, the ventral termination of the ungual groove occurs on the medial surface of TMM 41954-68 and 42138-2.8 but on the lateral surface of TMM 41954-13, with the other side having a midline ridge and an ungual groove on the ventral half of the claw reaching the distal end. TMM 41954-68 and 42138-2.8 are identified here as digit III fourth phalanx unguals, based on their intermediate morphology between the digit II and IV unguals, as well as their great similarity to the latter. TMM 42138-2.8 is also lying on top of the identified third pedal digit third phalanx. TMM 41954-68 and 42138-2.8 are identified here as right and left elements, respectively, based on their medial fossae and medially positioned tubercles. The proximal articulations are largely obscured but can be seen to have a rim. This pedal phalanx has the sharpest of tips preserved in the unguals.

A flattened ventral surface on the distal end is present in the TMM 41954-78 second digit ungual, the TMM 41954-13 fourth digit ungual, the pedal unguals of *A. piscator* (Kellner and Tomida, 2000:81), and so may have been present in all *Q. lawsoni* pedal unguals. The third digit fourth pedal phalanx is present but poorly preserved in *Z. linhaiensis* (ZMNH M1328), but it can be seen to be substantially curved. The pedal unguals of *J. edentus* have relatively less curvature, but those of the third digit can still be noted to have higher curvature than the medial digits (Wu et al., 2017:fig. 7). The third digit pedal ungual of *D. macronyx* is just described as being roughly subequal in size to those of the other digits (Sangster, 2003:94).

Fourth Phalanx Pedal Digit IV—TMM 42138-2.6 (Fig. 49I) is the shortest and most highly constricted pedal phalanx in the *Q. lawsoni* material (Table 18). The fourth phalanx of the fourth pedal digit is traditionally the shortest penultimate phalanx in pterosaurs, and often the shortest phalanx outside the reduced intermediate phalanges of digits III and IV. This phalanx also often has the highest constriction, but this constriction is medial (i.e., the shaft is concave medially) in TMM 42138-2.6 forming proximal and distal medial expansions, whereas it seems to be lateral in other pterosaurs. This constriction is located in the middle of its length, as in non-ungual pedal phalanges of *A. primordius* (Frey et al., 2011:S49). The proximal articulation is saddle-shaped but dorsally crushed to the point that it is not possible to determine whether it is also ginglymoid. The shaft is triangular in cross-section with a flat dorsal surface as it is preserved. The distal condyles confirm that this is a penultimate phalanx. These condyles are highly asymmetrical. The lateral condyle is larger, indicating this is a left phalanx (like the rest of TMM 42138-2), and primarily ventrally positioned but with the anterior end reaching the dorsal surface to give it a comma-shaped outline in lateral view. The medial condyle is less developed and entirely ventrally positioned so that it does not reach the dorsal surface. This matches the shape of the proximal cotyles of the pedal digit IV ungual (TMM 41954-13). No intercondylar sulcus is visible, but it may be present on the ventral surface and obscured from view.

The fourth pedal digit fourth phalanx is short and constricted in *Z. linhaiensis* (ZMNH M1328) and *J. edentus* (Wu et al.,

2017:fig. 7), but not to the degree found in *Q. lawsoni*. In addition, this phalanx in those taxa is concave laterally, instead of concave medially in *Q. lawsoni*. It is possible that TMM 42138-2.6 is preserved upside down, but the distal articulation matches the proximal articulation of the digit IV ungual as is.

Fifth Phalanx Pedal Digit IV—TMM 41954-13 (Fig. 49VII) is identified as a fourth pedal digit ungual based on its deep shape, high curvature, large proximally positioned flexor tubercle, and highly asymmetrical proximal cotyles (Table 18). These cotyles are so asymmetrical that the greatly expanded lateral cotyle is positioned dorsal to the smaller medial cotyle with the intercotylar ridge between the two oriented at 45°. These match the highly asymmetrical condyles of the pedal digit IV penultimate phalanx. In addition, the proximal cotyles have a raised lateral rim that contacts both cotyles and reaches onto the dorsal margin to form a dorsal lip. The large proximal flexor tubercle is divided into two prominences, a deeper and sharper proximal one and a lower and more rounded distal one. The proximal half of the medial surface is dominated by a large fossa, giving the entire proximal end a crescentic cross-section. This fossa grades into the ungual groove that extends along the entire midline of the preserved medial surface. A ridge on the ventral half of the medial surface appears two-thirds of the length down the ungual and merges with the ventral margin. On the lateral surface, the ridge extends along the midline, with the ungual groove ventral to it. The medial and lateral ridges form a flat ventral surface on the distal end of the pedal ungual where they merge with the ventral margin of the claw.

Flat-bottomed pedal unguals are reported in *A. piscator* (Kellner and Tomida, 2000:81) and at the distal end of the other *Q. lawsoni* unguals with three-dimensional preservation. The fifth phalanx of the fourth pedal digit is the most highly curved ungual, with the deepest flexor tubercle in *Z. linhaiensis* (ZMNH M1328) and *J. edentus* (Wu et al., 2017:fig. 7). In *D. macronyx*, this ungual is described as deep but not as tightly curved as in the other digits (Sangster, 2003:94). However, it does appear to be as curved as the other unguals and has a sharp flexor tubercle in the figures (Sangster, 2003:fig. 3.24).

Other Material

As in any large collection of fossil material, there are specimens too poorly preserved to be identified. Most of these are limb bone shaft fragments (TMM 41544-32, 41954-35, 42180-13, 42272-3, 44037-1, 44037-2, and 45977-1). TMM 41954-3 represents associated fragmentary limb bones, presumably from the same individual. A number of surface fragments were also collected, which cannot be identified but have been useful at times for more destructive sampling (TMM 41544-1, 41954-1, and 41954-53). Random bone fragments include TMM 41954-23, 42180-16, and a specimen in the box of 41544-25 and 26. Finally, specimen TMM 41544-18 has gone missing, but it is possibly TMM 41544-21, which shares the same field number.

WELLNHOPTERUS BREVIROSTRIS, gen. et sp. nov.
(Figs. 1 and 50)

'small' *Quetzalcoatlus* sp. Wellnhofer, 1991a:144, fig. 437 (original description).
short-faced animal (Kellner and Langston, 1996:320).
possible tapejarid (Kellner, 2004a:523, fig. 7).
Javelina *Tupuxuara* (Martill and Naish, 2006:929, table 2, fig. 5).
Thalassodromidae (Elgin and Frey, 2011:S30).
basal azhdarchid (Andres and Myers, 2013:391, table 1, fig. 1).
unnamed azhdarchid (Naish and Witton, 2017:fig. 8).
'Javelina azhdarchid' (Vremir et al., 2018:6).

Holotype—TMM 42489-2, associated skeleton comprising the anterior portions of the rostrum including a possible anterior process of right jugal (TMM 42489-2.1) and the mandible in articulation (TMM 42489-2.2), cervical IV anterior end and fragments in concretions (TMM 42489-2.8), cervical IV posterior end to cervical VIII in articulation (TMM 42489-2.3 to 42489-2.7), and a long bone with other fragments in concretions (TMM 42489-2.9).

Etymology—One of us (W.L.) wished to erect a new genus for the specimen and name it in honor of Peter Wellnhofer, the great pterosaur expert at the BSPG. However the genus name he chose, *Wellnhoferia*, is preoccupied and previously used to denote a genus of archaeopterygid bird (Elżanowski, 2001). To honor these wishes, Wellnhofer's name is combined with the Greek *pteron*, meaning wing and also a traditional ending for pterosaur names, to create the masculine nominative singular generic epithet *Wellnhopterus*. The specific epithet is a combinatorial name of the Latin words *brevis*, meaning short, and *rostrum*, meaning beak, in reference to its description in the literature as a "short-faced animal" (Kellner and Langston, 1996:320), also in the masculine nominative singular.

Locality and Horizon—The specimen was collected from the abandoned channel-lake deposit of locality TMM 42489 at Pterodactyl Ridge in northeast Big Bend National Park, Brewster County, Texas, U.S.A. These specimens were located in unit 10 of the Javelina Formation, Maastrichtian Stage, latest Cretaceous Period, more than 69 ± 0.9 Ma in age (Lehman, 2021).

Diagnosis—Moderate-sized azhdarchid (wingspan 3 meters) that can be distinguished from *Quetzalcoatlus* and other pterosaurs by the following autapomorphies: deep skull with length to height aspect ratio of approximately 2.59, premaxilla sagittal crest short and low with blade-like shape, nasoantorbital fenestra deep with 1.38 aspect ratio, rostrum cross-section triangular without dorsal keel but keel present on premaxillary bar, rostrum lateral surfaces concave only at anterior end, postpalatine fenestra with triangular anterior margin tapering to sharp point on maxilla, mandible symphysis deep with 6.39 aspect ratio, mandible rami cross-section deep with 4.55 aspect ratio, small middle-series cervical vertebrae with circular middle cross-section, middle-series cervical vertebrae with laterally constricted postexapophysis bases, cervical vertebra IV postexapophyses positioned ventrally near the midline, cervical vertebra V with medially curving epipophyses, cervical vertebra V with shallow fossa ventral to posterior condyle, cervical vertebra IX with pair of processes on ventral surface, cervical vertebra IX with trifurcate ridge on ventral surface, and cervical vertebra IX pits posteromedial to prezygapophyses.

Remarks—TMM 42489-2 represents a third pterosaur species from Big Bend National Park, from the same area as *Q. lawsoni* but lower in the Javelina Formation. Previously, elements of this one unambiguous individual were erroneously cataloged under separate numbers (TMM 42489-1 and 42489-2). This publication corrects the record and details the cataloging of all the elements under TMM 42489-2. Photographs and field sketches made during the collection of this material confirm that the skull and cervical series were associated in the field, and were in fact in contact with each other. This specimen was first referenced in Wellnhofer (1991b) as the 'small' *Quetzalcoatlus* sp. and depicted as the anterior end of the skull. Kellner and Langston (1996) stated that it had been inadvertently referred to *Quetzalcoatlus* sp., and they described the skull (TMM 42489-2.1 and 42489-2.2) and associated cervical material (TMM 42489-2.3 to 42489-2.7) as belonging to a more short-faced animal with smaller cervical vertebrae. Only the skull material has been discussed in the literature since then, with the exception of Andres and Myers (2013). Kellner (2004a) hypothesized that the skull likely represented a tapejarid pterosaur and provided a skull reconstruction along those lines. Similarly, Martill and Naish (2006)

provided an outline of the rostrum and stated that it had an aspect ratio more similar to that of *Tupuxuara* than to that of *Quetzalcoatlus*; they referred to the specimen as the Javelina *Tupuxuara* in their Figure 5. Andres and Myers (2013) recovered TMM 42489-2 as a basal azhdarchid distinct from *Quetzalcoatlus*, whether the cervical material was coded or not.

LSID—urn:lsid:zoobank.org:act:0848DA26-B08C-43C8-AFE1-4F30E4EBBE21

DESCRIPTION

The holotype and only specimen of *Wellnhopterus brevirostris* (TMM 42489-2) is articulated in two regions: the occluded anterior end of the cranium and mandible and the dorsiflected cervicals IV through VIII (Fig. 50). Dimensions of the elements for this species and their measurements are listed in Table 19.

Skull

The skull of *W. brevirostris* (TMM 42489-2.1 and 42489-2.2) is greatly flattened laterally. This is due in part to its preservation—the anterior rami of the pterygoid are touching in an unnatural contact—but even so, the animal would have had quite a narrow skull in life. It is also comparatively large, both in relation to its cervical material (Kellner and Langston, 1996) and to that of *Q. lawsoni*. *Wellnhopterus brevirostris* is edentulous (Wellnhofer, 1991b). The specimen is quite fragile and so the cranium and mandible were left in contact, obscuring the occlusal/palatal surfaces.

Cranium—The cranium (skull without mandible) of TMM 42489-2.1 consists of the rostrum, the premaxillary and maxillojugal bars, and anterior palate defining most of the anterior and ventral edges of the nasoantorbital fenestra (i.e., premaxilla, maxilla, and jugal bones). The possible anterior process of the right jugal (TMM 42489-2.1), and a number of concretions presumably containing fragments of skull (TMM 42489-8 and 9) are also preserved. The cranium reaches its greatest height 493.54 mm from the tip of the mandible, giving the skull a low aspect ratio of 2.59, roughly equivalent to the rostral index of 2.39 found in this specimen. The dorsal and ventral margins of the cranium are nearly straight, and so these aspect ratios give angles of 21.85° and 23.63° in lateral view for the anterior end of skull and rostrum, respectively. The rostrum comprises less than 42% of the preserved skull length, but the incomplete skull precludes determining how much less.

Fenestrae—The anterior end of the dorsal and ventral margins of the nasoantorbital fenestra (confluent naris and antorbital fenestra) are preserved in TMM 42489-2.1, as well as possibly the posteroventral margin in the jugal fragment. The dorsal and ventral margins of this fenestra are straight. It reaches its greatest height 195 mm from its anterior termination, giving an aspect ratio of 1.38 (39.83°), which is significantly deeper than the skull. The anteroventral and possibly posteroventral margins of the nasoantorbital fenestra are rounded as opposed to being sharp angles.

It is possible to see the anterior end of the confluent choanae and postpalatine fenestrae in dorsal view. Although laterally compressed and partially obscured anteriorly by matrix, it can be discerned that the medial margins of the palatines and pterygoids delineate the lateral margins of the confluent choanae. This opening is a very elongate, narrow, and triangular fenestra that does not contact the maxillae, unlike the anurognathids (Andres, 2021). The complete length of the anterior rami of the pterygoids is not preserved, and therefore it is not possible to rule out that the pterygoids contacted to separate an interpterygoid vacuity from the choanae.

Only the anterior 45.17 mm of right postpalatine fenestra is preserved, including the medial and lateral margins. It tapers
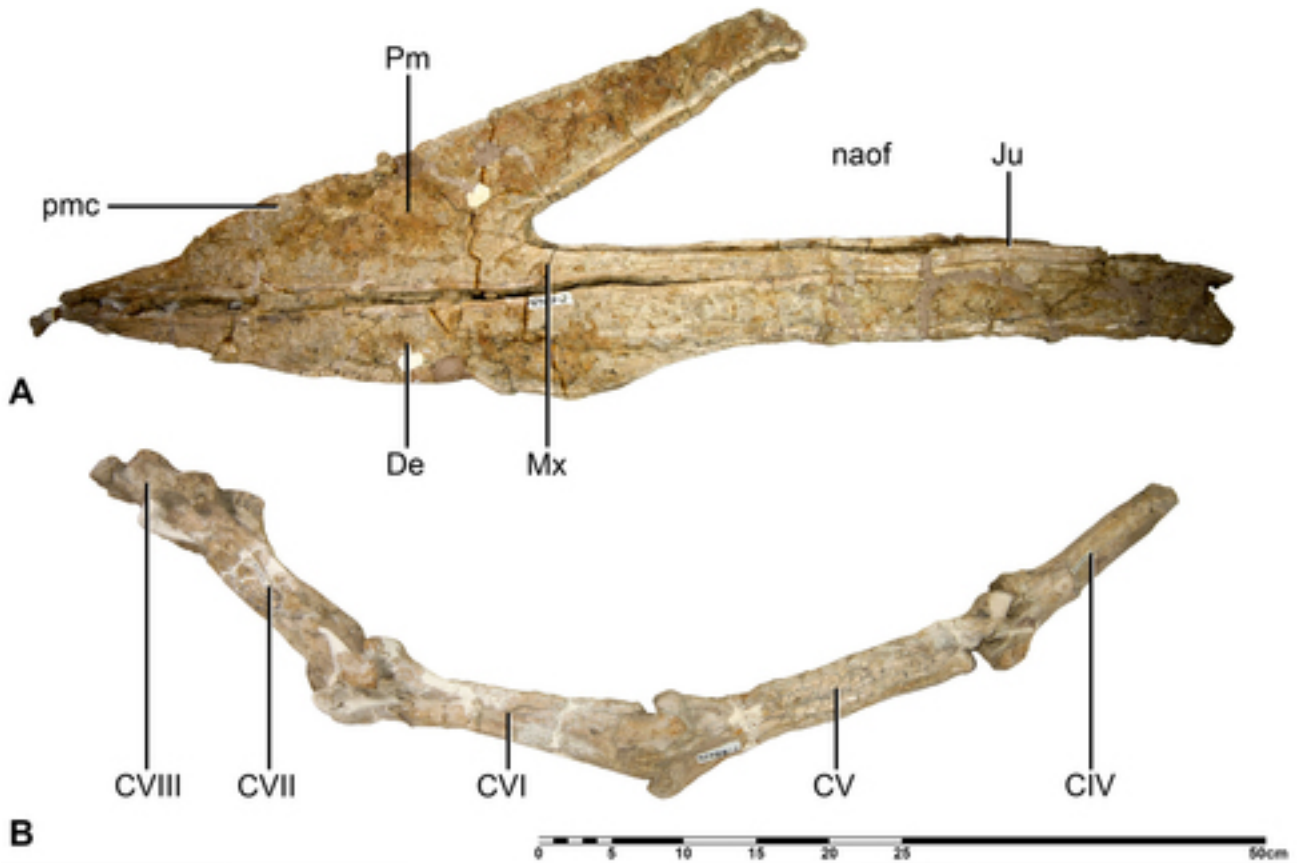
FIGURE 50. *Wellnhopterus brevirostris*, gen. et sp. nov.: **A**, cranium (TMM 42489-2.1) and mandible anterior end (TMM 42489-2.2) in left lateral view; and **B**, cervicals IV to VIII (TMM 42489-2.3 to 2.7) in right lateral views. **Abbreviations: CX**, cervical X; **De**, dentary; **Ju**, jugal; **Mx**, maxilla; **naof**, nasoantorbital fenestra; **Pm**, premaxilla; and **pmc**, premaxillary crest. Scale bar equals 50 cm.

anteriorly with straight margins to a sharp point giving the preserved portion of the fenestra a right triangle shape. The centimeter-long preserved lateral margin of this fenestra contacts the maxillary lower half of the right maxillojugal bar.

Premaxilla—The premaxilla appears to have the greatest surface area of the bones preserved in TMM 42489-2.1 (Fig. 50A). The premaxilla-maxilla contact is difficult to locate in pterosaurs in the best of conditions, and the preservation of this specimen prevents identifying it here. These bones appear fused as in most pterosaurs, but this cannot be categorically confirmed. The anterior tip of the rostrum is sharp, anteriorly oriented, and triangular in cross-section but without a sharp dorsal keel. The cranium is laterally attenuated toward the rostrum tip and lacks a lateral expansion, but it is not laterally flattened. The occlusal margins at the anterior end of the rostrum flare slightly laterally, making its lateral surfaces apparently concave, but this concavity flattens out by 15 cm from the tip. There is no lateral sulci, foramina, or fossa immediately anterior to the nasoantorbital fenestra on the jaws. The occlusal margins are sharp anteriorly but become rounded a few centimeters posterior to the anterior margin of the nasoantorbital fenestra. The anterior end of the occlusal surface of the rostrum is flat as opposed to concave or convex and lacks slit-like foramina, but the rest of the cranium ventral aspect is obscured. The rostrum increases in height posteriorly, but the dorsal margin does so at a lesser rate, giving the skull a convex dorsal margin. This curvature is identified as natural; otherwise, this would become the only pterosaur skull taller than long. The premaxillary bar (the contact with nasal is not known) is

as wide as in *Q. lawsoni*. The ventral surface of the premaxillary bar is concave ventrally with sharp lateral margins.

Kellner (2004a) identified and illustrated the presence of a premaxillary sagittal crest based on the photograph on page 144 of Wellnhofer (1991b). The structure Kellner (2004a) figures is a long, low, and laterally compressed plate that may be a crest. Baumel and Witmer (1993:86) stated that "'Crest' is descriptively apt for laterally compressed, plate-like processes." This plate ascends from the rostrum 87.40 mm from the anterior tip and descends 342.89 mm posteriorly. We consider these changes in elevation significant enough to constitute a process, and therefore identify this structure as a premaxillary sagittal crest here. This crest is long and low with a narrow dorsal margin resembling a table knife. Damage along the middle of its dorsal margin gives its outline in lateral view a slight anteriorly humped appearance. A humped outline is present in wukongopterid crests (Andres, 2021), but a photograph of the specimen *in situ* in the field supports a crest of constant height with a straight dorsal margin. Kellner (2004a) believed instead that the entire dorsal margin was damaged and that the crest continued posteriorly to the preserved portion of the cranium. This is a very thin crest with nearly parallel lateral surfaces. Enough of the texture of the crest is preserved to discern that it lacks striae or a branching network of grooves.

Maxilla—The maxilla contacts the premaxilla anteriorly, the jugal posteriorly, and the palatine medially with fused sutures (Fig. 50A). It is not possible to identify the margins of the ascending process of the maxilla on the premaxillary bar at the anterior end of the nasoantorbital fenestra. The maxilla posterior ramus has an elliptical cross-section that does not decrease in

TABLE 19. Measurements of *Wellnhopterus brevirostris*, gen. et sp. nov. (TMM 42489-2). Values in millimeters. Values in millimeters. >, preserved value; ~, approximate value; a-p, anteroposterior dimension; d-v, dorsoventral dimension; lat, lateral dimension; long, long axis dimension; med, medium axis dimension, orthogonal to long and short axis dimensions; and short, short axis perpendicular to long axis dimension. Holotype specimen in italics.

Dimension:	Skull length (a-p)	Skull height (d-v)	Skull width (lat)	Rostrum length (p-d)	Rostrum posterior height (d-v)	Premaxillary crest length (long)	Premaxillary crest height (short)
Specimen Number:							
TMM 42489-2.1	>845	>190.59	>36.07	326	136.44	343	14.39
	Nasoantorbital fenestra length (a-p)	Nasoantorbital fenestra height (d-v)	Confluent choanae length (a-p)	Confluent choanae width (lat)	Postpalatine fenestra length (a-p)	Postpalatine fenestra width (lat)	Subtemporal fenestra length (a-p)
TMM 42489-2.1	>479	>141.72	>301	~7.76	>45.17	>16.72	>7.62
	Mandible length (a-p)	Symphysis length (a-p)	Width at symphysis posterior margin (lat)	Depth at symphysis posterior margin (d-v)	Rami depth (d-v)	Rami breadth (lat)	
TMM 42489-2.2	>791	407	~21.50	63.72	48.11	10.57	
	Cervical IV total length (a-p)	Cervical IV mid-width (lat)	Cervical IV mid-depth (d-v)				
TMM 42489-2.3	>195.22	23.75	20.16				
TMM 42489-2.8	>45.43	23.71	20.89				
	Cervical V total length (a-p)	Cervical V mid-width (lat)	Cervical V mid-depth (d-v)				
TMM 42489-2.4	219	25.92	21.14				
	Cervical VI total length (a-p)	Cervical VI mid-width (lat)	Cervical VI mid-depth (d-v)				
TMM 42489-2.5	191.61	25.34	25.81				
	Cervical VII total length (a-p)	Cervical VII mid-width (lat)	Cervical VII mid-depth (d-v)				
TMM 42489-2.6	149.06	27.34	27.82				
	Cervical VIII total length (a-p)	Cervical VIII mid-width (lat)	Cervical VIII mid-depth (d-v)				
TMM 42489-2.7	49.45	34.08	>30.14				
	Length (long)	Mid-width (med)	Mid-depth (short)				
TMM 42489-2.9	>128	31.63	11.86				

(mediolateral) width over its length. After tapering in depth just posterior to the anterior end of the nasoantorbital fenestra, it keeps a depth of about 20 mm for the first 200 mm of the length of the maxillojugal bar. Where it contacts the jugal, it decreases in depth posteriorly as the jugal increases in depth so that the bar keeps a nearly constant depth over its length. The jugal overlies the maxilla dorsally along their contact. The posterior end of the maxilla is not preserved and so the posterior ramus of the maxilla must have been quite long.

Palatine—The palatine is a long plate of bone that is a scalene triangle in outline and extends along the medial surface of the maxilla in TMM 42489-2.1. Although the anterior end of the jugal reaches the level of the posterior end of the maxilla-palatine contact, the jugal and palatine do not touch. The palatine contact with the premaxilla is not visible.

Pterygoid—At the posterior end of the palatine is a posteromedially oriented process that defines the medial margin of the postpalatine fenestra. In other pterosaurs, this process is the anterior ramus of the pterygoid in part or in whole. There is no trace of a suture or contact with the palatine, and so it is not known how much of each bone comprises the anterior margin of the postpalatine fenestra.

Jugal—The maxillary ramus of the jugal reaches to a point about 21 cm from the anterior end of the nasoantorbital fenestra in TMM 42489-2.1 (Fig. 50A). A long process of bone originally cataloged with the concretions was identified as a jugal fragment. If correct, this would correspond to the posterior end of the maxillary ramus of the jugal. Its disarticulation from the rest of the skull precludes discerning its orientation. It has an oval cross-section anteriorly that mediolaterally flattens and dorsally expands to produce a narrow lacriform cross-section posteriorly. If the identification is correct, the dorsal flange would correspond to the base of the ascending (lacrimal) process of the jugal and define the ventroposterior edge of the nasoantorbital fenestra. The shape and inclination of the entire process cannot be discerned. This dorsal flange curves to the left of bone in anterior view, and the jugal ascending processes of *Q. lawsoni* (TMM 41961-1.1) curve medially, suggesting that this is a right jugal fragment. This flange gives the dorsal margin of the jugal, and presumably the posteroventral edge of the nasoantorbital fenestra, a concave outline in medial/lateral view. A thin ridge that expands posteriorly would then be on the medial surface and might indicate a contact with the pterygoid. A similar ridge is found in *Q. lawsoni* positioned more anteriorly, but does not contact the palatal bones. The element appears smaller than the rest of the preserved maxillojugal bar, but it is larger than any jugal component of that bar. A thin ridge on its ventral surface might indicate a ventral contact with the maxilla that would make this element more comparable in size to the rest of the maxillonasal bar if the maxilla was detached. However,

maxilla–jugal contact is fused in the rest of TMM 42489-1, and there is no other evidence of a ventral contact. The posterior end of this fragment becomes deeper posteriorly as well, indicating a concave ventral margin. This process is slightly smaller than the comparable region in *Q. lawsoni* (TMM 41961-1.1), similar to how the cervicals of *W. brevirostris* are smaller than the cervicals of *Q. lawsoni*, but the rest of the *W. brevirostris* skull appears larger than *Q. lawsoni*. The separate TMM 42489-2.1 process is a skull element, and a right jugal is the most defensible identification.

Mandible—TMM 42489-2.2 preserves the dentary, but it is not possible to ascertain if the postdentary bones are preserved due to the poor preservation (Fig. 50A). Based on the portions of the mandible present in this specimen, it is very unlikely that they are preserved. A piece of matrix plastered to the tip of the mandible appears to contain no bone and was likely left by a preparator out of abundance of caution, and is shown in Fig. 50A here for the same reason. The anterior end of the mandible mirrors the anterior end of the rostrum, a sharp anteriorly oriented tip that expands posteriorly with a triangular and laterally compressed cross-section. No lateral expansions or dorsal eminences are present. The anterior end is ventrally keeled, but it is not deep and does not terminate in a sharp ridge. The lateral surfaces are smooth and flat. The symphysis is fused and becomes deep posteriorly, reaching its greatest depth a few centimeters posterior to the anterior margin of the nasoantorbital fenestra. The symphysis constitutes half of the preserved mandible length. The divergent dorsal and ventral margins of the symphysis and a couple of centimeters of damaged bone in the middle of its ventral margin give the impression of a mandibular crest in lateral view. The jaw rami extend all the way to the greatest depth of the mandible, and the symphysis ventral margin is only slightly curved. No part of the ventral margin of the symphysis sticks out that could be a laterally compressed and plate-like process considered a mandibular crest. The occlusal surfaces are obscured, and so it is not possible to ascertain if they are concave or if there are ridges, sulci, depressions, or a symphyseal shelf. The lateral margins of the occlusal surfaces are visible and terminate in sharp ridges anteriorly, but they transition to rounded margins a few centimeters posterior to the symphysis. These lateral margins of the occlusal surfaces parallel the rest of the jaw margins. The mandibular rami are deep and very laterally compressed. The preserved portions of the rami appear to curve ventrally and diverge from each other at a shallow 5.4° angle. The dorsal margins of the rami are convex, but the dorsal margin of the left ramus also appears to curve medially, unlike the ventral margin and right ramus, and so this curvature is attributed to preservation. The medial aspects of the rami are obscured, and therefore it is not possible to discern if a Meckelian foramen is present. The ramus dorsal and ventral margins are slightly thicker than the rest of the width, but there are no other changes in width along the length of the rami.

Cervical vertebrae

The TMM 42489-2.3 to 2.7 (Fig. 50B) articulated series preserves the posterior half of cervical IV to cervical VIII. In the material assigned to TMM 42489-2.8 is the anterior end of cervical IV (Table 19). The cervical vertebrae of *W. brevirostris* are relatively much smaller with respect to the skull than in *Q. lawsoni*.

The middle-series cervicals are elongate and parallel-sided but show less variation in length than within some of the cervicals in *Q. lawsoni*. They differ by no more than 7 cm in length. The middle-series cervicals are nearly circular in cross-section, compared with the elliptical cross-sections of *Quetzalcoatlus*. Preexapophyses are not identified in *W. brevirostris* middle-series cervicals. Transverse ridges are also not visible on the lateral surfaces of the cervicals. The centra and neural arches are fused and

confluent without a trace of the contact except posteriorly, where the centrum appears to be constricted ventrally whereas the neural arch maintains the same width anterior to the postzygapophyses. The zygapophyseal articulations are oriented more vertically than in *Quetzalcoatlus*. The postexapophyses have laterally constricted bases. The anterior and posterior neural canals are obscured or poorly preserved, and so it is not possible to identify if there are pneumatic foramina adjacent to the neural canal.

Cervical IV—TMM 42489-2.8 is the isolated anterior end of the fourth cervical vertebra lacking the anterior cotyle, anterior vestibule, and prezygapophyses. TMM 42489-2.3 is the posterior end of the same vertebra but articulated with the rest of the preserved cervical series (Fig. 50B), and it preserves the posterior half of the cervical without the left postzygapophysis or most of the right postzygapophysis and posterior condyle. Combined, both pieces preserve about 195 mm of the original length (Table 19). No trace of the neural canal or pneumatic foramina can be seen in the cross-sectional breaks. This cross-section is subcircular but may have been circular before preservation. This vertebra has a bifid (divided) neural spine separated by a very thin neural ridge. The anterior and posterior spinous processes are mirror image low ridges that are triangular in cross-section. A middle constriction is absent. The postexapophyses are positioned ventrally near the midline, as in *Q. lawsoni*. They have much shorter laterally constricted bases than succeeding cervical vertebrae. The posterior end of the fourth cervical does not preserve the neural canal, condyle, or pneumatic foramina, if present.

Cervical V—Cervicals V–VIII are articulated and moderately crushed, obscuring much of their detail (Fig. 50B). Cervical V (TMM 42489-2.4) is the longest (219 mm) and most elongate (8.46 aspect ratio) vertebra in *W. brevirostris* (Table 19), as in other pterosaurs. The anterior end is severely damaged, and only the right prezygapophysis can be identified. There appears to be only an anterior spinous process of the neural spine, which extends posteriorly as a neural ridge until it reaches the end of the neural arch without a posterior rise or process. There is no visible constriction, save for that of the posterior centrum. The midsection of this bone is laterally crushed but was likely similar in cross-section to the fourth. The posterior end of the fifth cervical is mostly obscured by matrix and the articulation with the sixth cervical. The postzygapophyses are dorsoventrally expanded into a rounded outline in lateral view. The epipophyses are positioned dorsally, semicircular in outline, and curve medially. A long lateral excavation is ventral to the postzygapophyses and formed in part by a ridge extending along the lateral margin of the equally long postexapophyseal base. The postexapophyses are nearly circular in ventral view and situated farther from the midline than in cervical IV. A shallow fossa is present ventral to the posterior condyle and medial to the postexapophyses, but it does not have a distinct rim defining its boundaries as in *Q. lawsoni*.

Cervical VI—Cervical VI (TMM 42489-2.5) is in the middle of the articulated series and so has both ends obscured (Fig. 50B). It is slightly smaller (191.61 mm) and more elongate (7.56 aspect ratio) than the fifth, but otherwise resembles the fifth (Table 19). The sixth and seventh cervicals preserve hypapophyses on the ventral surface of their anterior ends. The hypapophysis on the sixth cervical is much larger and flanked by distinct fossae. A transverse foramen is visible on its left side, and so it appears a C-shaped cervical rib has fused to the vertebra. A significant notch in the interzygapophyseal ridge dorsal to the neural canal appears to be present. The prezygapophyses are anteriorly oriented and flare only slightly laterally. The prezygapophyseal articulations appear to be oriented anterodorsally at about a 45° angle. The neural spine is divided into anterior and posterior spinous processes by the thin neural ridge. Matrix adhering to this bone makes the ridge appear larger. The anterior spinous process is a high ridge, whereas the posterior neural

process forms a flange that extends dorsally over a posterior process that overhangs the neural canal. There is a slight constriction in the vertebra two-thirds down its length. Lateral crushing obscures the rest of the cross-sectional shape. There is a posterior vestibule of the neural arch, but its details are obscured. The postzygapophyseal articular surface contacts the lateral surface of the postzygapophysis to give it a straight posteroventral margin, but overall it has a semicircular lateral outline. The dorsal edges of the postzygapophyses are damaged, but they preserve robust, medially curving epipophyses. There is an excavation between the postzygapophyses and postexapophyses, but with lateral flanges restricted to the base of the postexapophysis. The postexapophyses project more ventrolaterally than in other vertebrae, with greater constrictions at their bases. A tubercle appears to delineate the lateral margin of the postexapophyseal articulation on the dorsal surface of the postexapophysis.

Cervical VII—Cervical VII (TMM 42489-2.6) is articulated with and has its articular ends obscured by cervicals VI and VIII (Fig. 50B). It has the typical pterosaur arrangement of being shorter (149.06 mm length) and less elongate (5.45 aspect ratio) than the fourth cervical (Table 19). The seventh cervical has a short and narrow hypapophysis but crushing prevents identifying whether fossae are lateral to the hypapophysis. It has a slight notch in the interzygapophyseal ridge dorsal to the neural canal. The left transverse foramen is present as a broken groove; the right has been filled in with plaster but appears to be complete. The prezygapophyses are more laterally separated than in the other cervicals of *W. brevirostris*, but not to the degree of the seventh cervicals in *Q. lawsoni*. The articular surface of the prezygapophysis is nearly vertical and appears to have a dorsal projection on the left prezygapophysis. The right prezygapophysis lacks this projection but a fragment of bone dorsal to it and attached to the medial surface of the cervical VI postzygapophysis appears to be the shorn-off dorsal projection. The neural spine is divided into low but flange-like anterior spinous process and a tall plate of a posterior spinous process, similar to the neural spine reported in *P. mauritanicus* (Pereda Suberbiola et al., 2003:82) and other azhdarchids. The posterior spinous process does not reach onto the posterior process overhanging the neural canal. There is apparently a small fossa on the dorsal surface of the posterior process. A thin neural ridge extends between the two spinous processes, but there is no trace of transverse ridges. The vertebra expands laterally from a constriction positioned one-third the total length from the posterior end, as in but not to the degree found in the *Q. lawsoni* seventh cervicals. The cross-sectional shape of this vertebra is obfuscated by lateral crushing, but it appears to be wider than tall anteriorly and taller than wide posteriorly. The postzygapophyses are damaged, but the right postzygapophysis appears to have a vertical flange on its dorsal surface that may be part of the epipophysis. The lateral edge of the postexapophysis is a flange, but it is shorter than in the other cervicals and does not form a lateral excavation between it and the postzygapophysis. The cervical VII has the smallest postexapophyses of the series. They expand to form their articular surfaces only at their posterior ends. The postzygapophyseal articulations are oriented vertically to articulate with the cervical VIII prezygapophyses.

Cervical VIII—Cervical VIII (TMM 42489-2.7) is poorly preserved and largely obscured (Fig. 50B). Its transverse processes have been abraded and both the neural spine and postzygapophyses are missing. It is the stoutest bone in the preserved cervical series: 49.45 mm long, 1.45 (length/width) aspect ratio (Table 19). The centrum is triangular in ventral view and appears to have a blunt hypapophysis. The left fossa lateral to the hypapophysis is visible. Lateral excavations are present at the contact between the centrum and the neural arch, but they are filled with matrix so that it is not possible to tell if pneumatic

foramina were present in this area. The combined prezygapophyses and transverse processes curve anterolaterally in the horizontal plane. The prezygapophyseal articular surfaces are obscured but appear to be oriented vertically. There is no midline emargination in the interzygapophyseal ridge dorsal to the neural canal. The preexapophyseal articulations and fused cervical rib appear to be present, but the transverse foramen is not visible. The posterior end of the neural canal is visible with a waisted-oval outline (figure-of-eight) and no lateral pneumatic foramina. The posterior condyle is a strong crescent shape. Postexapophyses are present and anterior to the posterior condyle. They are semicircular in posterior and ventral view.

AZHDARCHIDAE indeterminate

Material—TMM 41839-2.1, right wing metacarpal distal end; TMM 41839-2.2, right first wing phalanx proximal end; TMM 41839-3.1, left femur proximal end; TMM 41839-3.2, right femur shaft; TMM 41839-3.3, left tibiotarsus proximal and distal ends; TMM 41839-3.4, right first wing phalanx fragments; TMM 41839-3.5, limb shaft fragment; TMM 41839-3.6, left third wing phalanx shaft fragment; TMM 41839-3.7, left second wing phalanx shaft fragment; TMM 41839-7, right first wing phalanx; TMM 41839-8, left first wing phalanx shaft fragment; TMM 41839-10, left second metatarsal missing distal end; TMM 41839-11, left third metatarsal shaft and ventral end of proximal articulation; TMM 41839-12, left first metatarsal shaft fragment; and TMM 42538-1, anterior fragment of a mid-cervical vertebra midsection (Table 20).

Localities and Horizons—Specimens were collected from the overbank flood-plain deposits of localities TMM 41839 and TMM 42538 in the north and east regions of Big Bend National Park, Brewster County, Texas, U.S.A. These specimens are located in the Javelina Formation, Maastrichtian Age, latest Cretaceous Period (Lehman, 2021).

Remarks—In Big Bend National Park, the vast majority of the pterosaur specimens are found in the abandoned channel-lake deposits of Pterodactyl Ridge (including all the specimens of *Q. lawsoni* and *W. brevirostris*), whereas the majority of pterosaur localities have their specimens found in stream-channel deposits (including all specimens of *Q. northropi* and cf. *northropi*), with the remaining pterosaur specimens found in a couple of abandoned channel-lake deposits outside of Pterodactyl Ridge (localities TMM 45616 and 45888) and a couple of overbank flood-plain deposits (localities TMM 41839 and 42538). The flood-plain localities are found high (locality TMM 41839) and low (locality TMM 42538) in the Javelina Formation and contain the only material outside of the named species that can be referred to the Azhdarchidae. These also include the only 'small' pterosaurs in the Park (TMM 41839-2 to 41839-8 and 42538-1) as well as three giant pterosaur metatarsals (TMM 41839-10 to 41839-12). Whereas the abandoned channel-lake and stream-channel deposits preserve moderate-to-large and giant pterosaurs that likely lived in those paleoenvironments, respectively, the overbank flood-plain deposits preserve a few small and giant pterosaurs that were likely entrained by flooding events (Brown et al., 2021; Lehman, 2021).

Most of the TMM41839 material consists of one specimen preserving fragments of seven limb elements (TMM 41839-3.1 to 41839-3.7), making it one of the more complete pterosaurs in the Park. It includes the shaft of a third wing phalanx (TMM 41839-3.6) that has the τ-shaped cross-section diagnostic of the azhdarchids. Although it should be noted that this cross-section is present in all azhdarchid second or third wing phalanges and the Azhdarchidae has a node-based name, and it is possible that the sister group of the Azhdarchidae could have this cross-section as well. What unites the small TMM 41839 pterosaurs are their poor preservation, such that not a single bone is

TABLE 20. Measurements and identifications of other pterosaur material in Big Bend National Park. Values in millimeters. >, preserved length; a-p, anteroposterior dimension; d-v, dorsoventral dimension; lat, lateral dimension; and p-d, proximodistal dimension.

Dimension: Element: Specimen Number:	Total length (a-p)	Width (lat)	Height (d-v)
Mid-cervical vertebra			
TMM 42538-1	>34.58	20.83	18.20
TMM 45888-2.1	>68.39	>47.33	>28.17
Distal syncarpal	Length (p-d)	Width (a-p)	Height (d-v)
TMM 45888-2.2	37.82	66.91	55.30
Metacarpal IV	Length (p-d)	Width (d-v)	Breadth (a-p)
TMM 41839-2.1	>29.21	13.18	15.33
First wing phalanx	Length (p-d)	Width (a-p)	Breadth (d-v)
TMM 41839-2.2	>214	12.39	9.06
TMM 41839-3.4	>216	13.69	8.19
TMM 41839-7	>156.45	14.68	9.62
TMM 41839-8	>97.58	13.50	8.16
Second wing phalanx	Length (p-d)	Width (a-p)	Breadth (d-v)
TMM 41839-3.7	>144.87	9.38	8.22
Third wing phalanx	Length (p-d)	Width (a-p)	Breadth (d-v)
TMM 41839-3.6	>19.33	7.31	5.18
Femur	Length (p-d)	Mid-width (lat)	Height (a-p)
TMM 41839-3.1	>57.01	10.63	9.86
TMM 41839-3.2	>227	11.54	15.52
Tibiotarsus	Length (p-d)	Mid-width (lat)	Height (a-p)
TMM 41839-3.3	>104.35	11.86	10.56
Metatarsal I	Length (p-d)	Mid-width (lat)	Height (d-v)
TMM 41839-12	>58.56	6.04	9.09
Metatarsal II	Length (p-d)	Mid-width (lat)	Height (d-v)
TMM 41839-10	>120.19	6.16	10.33
Metatarsal III	Length (p-d)	Mid-width (lat)	Height (d-v)
TMM 41839-11	>98.26	5.71	8.94
Long bone fragments	Length	Mid-width	Height
TMM 41839-3.5	>23.67	8.17	6.48

complete as well as being characterized by displacive mineralization and expansive cracking, obscuring the features that would help determine their relationships. TMM 41839-2, 41839-7, and 41839-8 are the same size as TMM 41839-3, differing by no more than a couple of millimeters in the widths of their first wing phalanges, and share similar cross-sectional outlines. They can be confirmed to be pterosaurs and likely belong to the same species as TMM 41839-3 based on their similar size and first wing phalanx shapes, but their preservation prevents confirmation. TMM 41839-2, 41839-7, and 41839-8 are therefore considered ?Azhdarchidae, as has been put forward for other such dubious specimens (e.g., Bennett and Long, 1991:figs. 2–3; Wellnhofer and Buffetaut, 1999:136; Unwin et al., 2000:Table 1; Frey et al., 2003b:249; Obata et al., 2007; Martin-Silverstone et al., 2016:3).

TMM 42538-1 is the only pterosaur fossil found at its locality. It was originally identified as a limb bone shaft fragment. However, an ossified tube is visible in the broken cross-sections of this bone that is identified here as a neural canal, making this a vertebra. It appears to be from the shaft of a long bone because it comes from the midsection of one of the elongate mid-cervical vertebrae (cervicals IV-VI). It can be identified as an azhdarchid based on its suboval cross-section and extremely reduced neural spine (Andres, 2021). The fragment is only about 35 mm in length, and so it is not possible to determine its length or degree of elongation. However, the specimen has very little attenuation along its length such that even a conservative assessment of its elongation would put it well within the range of azhdarchid mid-cervical vertebrae.

The exact size of the small azhdarchid specimens is not known, but the elements have about half the diameter of comparable *Q. lawsoni* elements, and so a wingspan of about half of *Q. lawsoni* (i.e., just over a couple of meters) would be a rational estimate. This is a bit larger than the small ?azhdarchid RBCM. EH.2009.019.0001 estimated to have a wingspan circa 1.5 meters

(Martin-Silverstone et al., 2016:10) at the cusp of what Martin-Silverstone et al. (2016) considered to be a small pterosaur (i.e., two meter wingspan). It is an open question whether these specimens represent a new species of small azhdarchids or are juveniles of other pterosaur species found in the Park. The poor preservation of this material obscures features that normally would be used to assess ontogenetic age (e.g., fusion of the extensor tendon process to the first wing phalanx). However, the fibula is not fused in TMM 41839-3.3, suggesting that it might not be an osteological adult.

The metatarsals of a giant pterosaur (TMM 41839-10 to 12) were also found at this locality. Despite being incomplete, they are three-dimensionally preserved and in better condition than the *Q. lawsoni* material for their preserved portions. They are also quite similar in morphology to the *Q. lawsoni* metatarsals despite their differences in size, facilitating their identification as the left metatarsals I-III. However, three-dimensional metatarsals (or even well preserved metatarsals) are exceedingly rare in pterosaurs, and so the similarities they share may be inherited from a more distant common ancestor. Unfortunately, the giant pterosaur that is present in the Park, *Q. northropi*, does not have preserved metatarsal material. TMM 41839-10 to 12 can be confirmed to be pterosaurs and probably belong to the same individual. It should be noted that among giant pterosaur groups, only the azhdarchids have enlarged metatarsals, and so we consider these specimens to be ?Azhdarchidae subject to future discoveries.

DESCRIPTION

Cervical vertebra

TMM 42538-1 is a pterosaur long bone fragment. The ossified neural canal found in the cervical vertebrae of the Azhdarchidae

(Nesov, 1984:49) is visible in the cross-sections of the broken ends, allowing this to be identified as a cervical vertebra. Other traces of bone visible in the cross-sections are presumably trabeculae that suspended and supported the neural canal. One cross-section has the wide oval outline of non-giant azhdarchiform middle-series cervical vertebrae (Andres, 2021). Whereas the other cross-section has a more lemon-shaped outline, suggesting that this fragment comes from the anterior or posterior part of the midsection where the spinous processes begin to appear. The ventral margin of this outline is also elevated, implying that it may be part of a hypapophysis or raised band at the anterior end of the cervical. Much of the cortical bone is missing in this specimen, but the neural arch and centrum can be seen to be confluent, as in the middle-series cervicals of other neopterodactyloids (Andres, 2021). The neural spine is extremely reduced and split into anterior and posterior spinous processes (bifid), as in other azhdarchids. Damage to the cortical bone prevents determining if there was a neural ridge or transverse ridges between the anterior and posterior ends of the vertebrae. There is very little attenuation along this bone, even though it comes from the likely anterior end of the midsection based on the presence of a spinous process and ventral raised band. This indicates that it is one of the elongate mid-cervical vertebrae {cervicals IV–VI} and almost certainly would have had an aspect ratio greater than five, which would place it in the Azhdarchidae. TMM 42538-1 is the smallest mid-cervical vertebra in the Park, but it does approach the mid-width of the *W. brevirostris* cervical IV in size. However, the TMM 42538-1 fragment comes from a wider anterior part of the vertebra and in all other respects appears to be a smaller bone. It remains possible that TMM 42538-1 is a juvenile of *W. brevirostris* or one of the other pterosaur species in the Park.

Metacarpus

TMM 41839-2.1 is the poorly preserved distal end of a left wing metacarpal articulated with the first wing phalanx TMM 41839-2.2 (Table 20). However, expansive cracking at the articulation obscures the margins and contacts between these bones. It is only possible to identify the presence of the wing metacarpal and the approximate dimensions of the distal end.

Wing Phalanges

First Wing Phalanx—TMM 41839-2.2 is the wing phalanx attached to the TMM 41839-2.1 wing metacarpal (Table 20). It consists of four fragments: two from the proximal half, one from the shaft, and the distal end. The proximal bicotylar articulation has been obliterated by displacive mineralization, obscuring the extensor tendon process that would help determine the ontogenetic age of this specimen. The transition from being deeper anteriorly to deeper posteriorly along the shaft produces a slightly concave area extending down the shaft on the anterior half of the ventral surface. This appears as a slight emargination on the ventral edge of the oval cross-section. This cross-section is deep with a width only 1.37 times the depth. This concave surface disappears in the shaft fragment, which is more dorsoventrally depressed. This wing phalanx fragment has the same width as the proximal fragment and so must be from the same phalanx in this specimen. The distal end is still partially obscured by matrix. The posterior expansion lacks a posterior process. The distal articular surface is convex with a median apex and a subcircular cross-section.

TMM 41839-3.4 is a wing phalanx shaft and distal articulation in five pieces (Table 20). It is identified as a left first phalanx based on its subtriangular cross-section that transitions from being deeper posteriorly to deeper anteriorly at the proximal end, or at least deeper at the midline at the preserved proximal

break. The shaft is 1.67 times wider than deep. The many breaks and damaged surfaces obscure its orientation and curvature. The distal fragment consists only of the articular surface. This distal surface is circular in outline. However, the proximal end of the fragment reveals the broken posterior half of the medullary cavity, indicating that this fragment is the posterior expansion of the articular surface, which could be between oval and ovate in shape.

TMM 41839-7 preserves the first phalanx but from the right side (Table 20). The proximal expansion is preserved, but the cotyles, intercotylar sulcus, and extensor tendon process are missing, and so the proximal margin is not preserved. This preserved end is oval in cross-section with the greatest depth at the midline. Posteriorly, the shaft becomes subtriangular and then ovate where uncrushed, approximately one-and-a-half times wider than deep.

TMM 41839-8 is a very poorly preserved left first wing phalanx shaft with a posteriorly expanded subtriangular cross-section.

Second Wing Phalanx—TMM 41839-3.7 is an extremely fragmentary wing phalanx still preserved in matrix (Table 20). It is between the size of the preserved first and third phalanges and is therefore identified as a second wing phalanx in the TMM 41839-3 specimen.

Third Wing Phalanx—TMM 41839-3.6 is a fragment from the distal shaft of a left third wing phalanx (Table 20). This phalanx has the τ-shaped cross-section of other azhdarchid third phalanges, allowing it to be referred to the Azhdarchidae. By this point of the shaft, slight concavities represent the anteroventral and posteroventral sulci. The midline ventral ridge is ventroposteriorly oriented and well developed, producing a depth 71% of the width (1.41 aspect ratio). The shaft fragment tapers significantly over its short preserved length.

Hind limb

Femur—Two femora are preserved in this material (Table 20): TMM 41839-3.1 is a left femur proximal end missing the femoral head and greater trochanter, and TMM 41839-3.2 is a right femur shaft missing more of the proximal end and broken into a number of fragments due to displacive mineralization (Lehman, 2021). The fragmentary nature of this material obscures the shape of the entire femur, but it can be observed to bow anteriorly (concave posteriorly, convex anteriorly). The femoral head is broken off in both TMM 41839-3 specimens, but the base of the neck is preserved in TMM 41839-3.1, which is angled anteromedially at an angle of 155° to the shaft. This angle is significantly larger than the *Quetzalcoatlus* species and the only indication that this specimen may belong to a new species or *W. brevirostris*. An elliptical proximal pneumatic foramen, as found in the Ornithocheiroidea (Andres, 2021), and the base of an anteriorly curving greater trochanter, as found in the Neoazhdarchia (Andres, 2021), can be seen. The lesser trochanter is a distinct crescentic ridge ventral to the greater trochanter on the lateral margin of the anterior surface. A thin line continues from the ventral end of the lesser trochanter to curve around onto the posterior surface and then curve distally down the midline of the shaft. Another jagged ridge curves from the dorsal margin of the lesser trochanter to extend down the anterior surface of the shaft. A rugose ridge extends ventrally from the greater trochanter on the lateral half of the femur posterior surface. The internal trochanter is a rugose tubercle medial to the termination of this ridge and distal to the femoral neck on the femur posterior surface. A flat surface extends from the medial surface of the base of the neck to curve onto the posterior surface ventrally. A jagged ridge identified as the adductor ridge of Bennett (2001a) forms the anterior margin of this flat surface at the preserved end of this bone. This preserved end of the shaft has a circular cross-section with a flattened medial surface.

Tibiotarsus—TMM 41839-3.3 includes the proximal and distal ends of a left tibiotarsus (Table 20). No trace of the fibula can be found, which suggests that it was not fused to the tibia and that this individual was not osteologically mature. There are no distinct articular surfaces on the proximal surface. There are raised medial and lateral edges on this proximal surface with an anterior emargination between the two. The posterior margin of the proximal end is damaged. The cnemial crest is absent. The shaft appears to curve slightly medially and posteriorly. The cross-section at the broken end has a flat posterior surface so that the cross-section is an isosceles triangle. The distal end has been subject to displacive mineralization, but the distal cross-section appears to be subcircular. The distal condyles are greatly anteroposteriorly expanded and both mediolaterally and proximodistally compressed. They curve about 270° from the anterior surface to a further extent up the posterior surface. The proximal and distal ends of the condyles are directed medially. A distinct intercondylar sulcus separates the condyles for their entire length. The medial condyle appears to be expanded anteriorly and the lateral condyle expanded posteriorly. Both condyles narrow and converge posteriorly. The epicondyles are apparent as tubercles.

Metatarsus—TMM 41839-10 to 41839-12 are metatarsals I–III from a giant pterosaur (Table 20). Based on their ventral curvature and medial concavities of their proximal end, they can be identified as left metatarsals. This curvature is slight, and the shafts are laterally compressed.

TMM 41839 to 10 is the most complete of these specimens, missing only the distal articulation. Its proximal end is laterally compressed, indicating that it is either a metatarsal II or III. It lacks the figure-of-eight cross-section and expanded flexor tubercles of the metatarsal III in *Q. lawsoni*. TMM 41839-10 also shares a laterally curving flange on the proximal end of the dorsal margin and a laterally expanded ventral tubercle with the metatarsal II of *Q. lawsoni*, as well as the lack of a significant tarsal articulation surface, and so this element is identified as a second metatarsal.

TMM 41839-11 is a metatarsal III shaft and ventral end of the proximal articulation. It is identified as a second metatarsal because of its large, mediolaterally expanded, and proximoventrally oriented plantar flexor tubercle, as found in *Q. lawsoni*. The slightly curved and laterally compressed shaft also supports this identification.

TMM 41839-12 is a metatarsal shaft fragment. Its nearly straight orientation and equant cross-section at the distal preserved end indicate that this is a metatarsal I shaft.

PTEROSAURIA indeterminate

Material—TMM 45616-2, 66 long bone fragments; TMM 45616-3, 42 long bone fragments; TMM 45888-2.1, midcervical partial anterior end; TMM 45888-2.2, left distal syncarpal; TMM 45888-2.3, six fragments; TMM 45888-2.4, three fragments; and TMM 45888-2.5, 13 fragments (Table 20).

Localities and Horizons—Specimens were collected from probable abandoned channel-lake deposits (localities TMM 45616 and 45888) in the central and east regions of Big Bend National Park, Brewster County, Texas, U.S.A. These specimens are located in the upper part of the Javelina Formation, Maastrichtian Stage, latest Cretaceous Period (Lehman, 2021).

Remarks—Although the vast majority of the Big Bend pterosaur fauna is found in the abandoned channel-lake deposits of Pterodactyl Ridge, there are a couple of isolated localities that also preserve pterosaur specimens in smaller abandoned channel-lake deposits. These are extremely fragmentary and poorly preserved specimens encased in carbonate nodules. Diminishingly few elements can be identified in this material, although a number of shaft fragments have cross-sections similar to wing phalanges. These and the two identifiable elements are comparable in size to elements found in *Q. lawsoni*, considered to be a large pterosaur. The TMM 45616 locality preserves 108 shaft fragments from indeterminate pterosaurs (TMM 45616-2: 66 fragments, and TMM 45616-3: 42 fragments). The TMM 45888 locality specimen cannot be confirmed to come from abandoned channel-lake deposits because it was found as float, but its preservation is identical to that of the TMM 45616 specimens and matches the unit C subfacies of the abandoned channel-lake deposits (Brown et al., 2021). TMM 45888-2 weathered out some time ago and so the only surviving material is either encased in nodules (TMM 45888-2.3 to -2.5) and/or has lost its cortical bone (TMM 45888-2.1 and -2.2); surprisingly, the latter of which can be identified. TMM 45888-2.1 is the anterior cotyle and left prezygapophysis of a pterosaur mid-cervical vertebra, but its poor preservation prevents determining which vertebra or whether it is an azhdarchid. TMM 45888-2.2 is a distal syncarpal with a rectangular cross-section, indicating that it is a non-pteranodontoid pterosaur (Andres, 2021).

CONCLUSION

The Big Bend National Park pterosaur fauna consists of 356 skeletal elements from 229 specimens found at 31 locality numbers in the abandoned channel-lake, stream-channel, and overbank flood-plain deposits of the Javelina and Black Peaks formations that are referred here to three species and a small azhdarchid taxon. The vast majority of these specimens come from stratigraphic unit 15 of the abandoned channel-lake deposits at Pterodactyl Ridge, with most excavated from the main quarry level at the Amaral Site. These specimens form a diagnosable natural group of large pterosaurs (4.5 m wingspan) most closely related to but also taxonomically distinct from *Quetzalcoatlus northropi* that is erected here as *Quetzalcoatlus lawsoni*, gen, et sp. nov., which has previously been referred to as *Quetzalcoatlus* sp. in the literature. A specimen lower down in stratigraphic unit 10 of the abandoned channel-lake deposits at Pterodactyl Ridge is a moderate-sized azhdarchid pterosaur (3 meter wingspan) that is distinct from *Quetzalcoatlus* and other pterosaur species, and so it is erected here as *Wellnhopterus brevirostris*, gen. et sp. nov. Two smaller abandoned channel lake deposits in the Park preserve three large pterosaur specimens, but these are too poorly preserved to classify. Five localities preserve pterosaur specimens in stream-channel deposits, and all of this material belongs to giant individuals (greater than 7 meter wingspan) including the holotype of *Quetzalcoatlus northropi* (10 meter wingspan). One of the giant specimens shares autapomorphies with the holotype and can be referred to *Q. northropi*, with the remaining stream-channel giants referred here as *Quetzalcoatlus* cf. *northropi*. Pterosaur specimens are found in the overbank flood-plain deposits at two localities, consisting of five specimens from small azhdarchids (2 meter wingspan) and three metatarsals from a giant pterosaur. Big Bend National Park preserves a diverse pterosaur fauna from the end of the Mesozoic Era including both the largest and youngest pterosaurs.

The Big Bend pterosaur fauna is exceptional, but it is also representative of Maastrichtian Age pterosaur deposits. Wherever there is a good sample of Maastrichtian pterosaurs, there is a diverse assemblage of azhdarchid pterosaurs at multiple sizes including giant individuals. The most comparable example to Big Bend is the Transylvanian Basin of Romania that also includes three azhdarchid species: the giant *Hatzegopteryx thambema* and cf. *Hatzegopteryx* sp., the large *Albadraco tharmisensis*, and the moderate-sized *Eurazhdarcho langendorfensis*, as well as small Pterosauria indet. specimens (Vremir et al., 2013a; Solomon et al., 2020). The third possible ten-meter wingspan pterosaur species, the giant *Arambourgiania philadelphiae* and cf.

Arambourgiania philadelphiae, comes from Jordan that also has a couple of large azhdarchid specimens (Frey and Martill, 1996; Martill and Moser, 2017; Rosenbach et al., 2018). A giant ? *Arambourgiania* ulna has been reported in the marine sediments of Morocco with the large *Phosphatodraco mauritanicus* and another azhdarchid cervical, but there are also non-azhdarchid pterosaurs represented by a large pteranodontid as well as small, moderate-sized, and large nyctosaurid species (Longrich et al., 2018). Although lacking named species, small, moderate-sized, large, and giant azhdarchids are reported in southern France (Buffetaut, 2008), as well as large and giant azhdarchids at the La Solana locality in Spain (Company et al., 1999, 2001). This pattern is also not unique to the Maastrichtian considering that small, moderate-sized, large, and giant specimens are referred to the Campanian Age *Cryodrakon boreas* of Dinosaur National Park in Canada (Hone et al., 2019), and the giant UNCUYO-LD 350 humerus is associated with a smaller specimen in the upper Coniacian-lower Santonian ages of the Neuquén Basin in Argentina (David et al., 2018). The Gurilin Tsav locality of Mongolia seems to be the only place in which giant pterosaurs are found in isolation (Tsuihiji et al., 2017). The Big Bend pterosaur fauna represents a global pattern during the Late Cretaceous in which pterosaurs were experiencing a spike in diversity at a great range of sizes just before the end-Cretaceous extinctions (Watabe et al., 2009; Tsuihiji et al., 2017).

ACKNOWLEDGMENTS

ORCID

Brian Andres http://orcid.org/0000-0002-9958-0134

LITERATURE CITED

Aires, A. S. S., A. W. A. Kellner, R. T. Müller, L. R. Da Silva, C. P. Pacheco, and S. Dias-Da-Silva. 2014. New postcranial elements of the Thalassodrominae (Pterodactyloidea, Tapejaridae) from the Romualdo Formation (Aptian–Albian), Santana Group, Araripe Basin, Brazil. Palaeontology 57:343–355.

Andres, B. 2010. Systematics of the Pterosauria. Doctoral Dissertation thesis/dissertation, Department of Geology and Geophysics, Yale University, New Haven, 347 pp.

Andres, B. 2021. Phylogenetic systematics of *Quetzalcoatlus* Lawson 1975 (Pterodactyloidea: Azhdarchoidea); pp. 203–217 in K. Padian and M. A. Brown (eds.), The Late Cretaceous pterosaur *Quetzalcoatlus* Lawson 1975 (Pterodactyloidea: Azhdarchoidea). Society of Vertebrate Paleontology Memoir 19. Journal of Vertebrate Paleontology 41(2, Supplement):203–217.

Andres, B., and Q. Ji. 2006. A new species of *Istiodactylus* (Pterosauria, Pterodactyloidea) from the Lower Cretaceous of Liaoning, China. Journal of Vertebrate Paleontology 26:70–78.

Andres, B., and Q. Ji. 2008. A new pterosaur from the Liaoning Province of China, the phylogeny of the Pterodactyloidea, and convergence in their cervical vertebrae. Palaeontology 51:453–470.

Andres, B., and T. S. Myers. 2013. Lone star pterosaurs. Earth and Environmental Science Transactions of the Royal Society of Edinburgh 103:383–398.

Andres, B., and M. Norell. 2005. The first record of a pterosaur from the Early Cretaceous Strata of Öösh (Övörkhangai; Mongolia). American Museum Novitates 3472:6pp.

Andres, B., and K. Padian. 2020a. Pterosauria[†]; pp. 1201–1204 in K. de Queiroz, P. D. Cantino, and J. A. Gauthier (eds.), Phylonyms. A Companion to the PhyloCode. CRC Press, Boca Raton, FL.

Andres, B., and K. Padian. 2020b. Pterodactyloidea[†]; pp. 1205–1208 in K. de Queiroz, P. D. Cantino, and J. A. Gauthier (eds.), Phylonyms. A Companion to the PhyloCode. CRC Press, Boca Raton, FL.

Andres, B., J. M. Clark, and X. Xu. 2010. A new rhamphorhynchid pterosaur from the Upper Jurassic of Xinjiang, China, and the phylogenetic relationships of basal pterosaurs. Journal of Vertebrate Paleontology 30:163–187.

Andres, B., J. M. Clark, and X. Xu. 2014. The earliest pterodactyloid and the origin of the group. Current Biology 24:1011–1016.

Andres, B., K. Padian, T. B. Rowe, C. J. Bell, M. A. Brown, J. C. Sagebiel, T. M. Lehman, and J. R. Cunningham. 2017. Case 3728 — *Quetzalcoatlus northropi* (Reptilia, Pterosauria): proposed availability and attribution of authorship to Lawson, 1975. Bulletin of Zoological Nomenclature 74:34–37.

Anonymous. 1975. Front Matter. Science 187:873–1004.

Arambourg, C. 1959. *Titanopteryx philadelphiae* nov. gen., nov. sp., pterosaurien geant. Notes et Memoires sur le Moyen-Orient 7:229–234.

Arthaber, G. v. 1921. Studien über flugsaurier auf grund der Bearbeitung des Wiener exemplares von Dorygnathus banthensis Theod. sp. Denkschriften Akademie der Wissenschaften in Wien Mathematisch-naturwissenschaftliche Klasse 97:391–464.

Astibia, H., E. Buffetaut, A. D. Buscalioni, H. Cappetta, C. Corral, R. Estes, F. Garcia Garmilla, J. J. Jaeger, E. Jimenez-Fuentes, J. Le Loeuff, and J.-M. Mazin. 1990. The fossil vertebrates from Lano (Basque Country, Spain); new evidence on the composition and affinities of the Late Cretaceous continental faunas of Europe. Terra Nova 2:460–466.

Atanassov, M. N., and R. E. Strauss. 2002. How much did *Archaeopteryx* and *Quetzalcoatlus* weigh? Estimation of the mass of fossil organisms by multivariate analysis of bone dimensions. Journal of Vertebrate Paleontology 22 (3, Supplement):33A.

Averianov, A. O. 2004. New data on Cretaceous flying reptiles (Pterosauria) from Russia, Kazakhstan, and Kyrgyzstan. Paleontologicheskii Zhurnal 38:73–83.

Averianov, A. O. 2007. New records of azhdarchids (Pterosauria, Azhdarchidae) from the Late Cretaceous of Russia, Kazakhstan, and central asia. Paleontological Journal 41:189–197.

Averianov, A. O. 2010. The osteology of *Azhdarcho lancicollis* Nessov, 1984 (Pterosauria, Azhdarchidae) from the Late Cretaceous of Uzbekistan. Proceedings of the Zoological Institute Russian Academy of Sciences 314:264–317.

Averianov, A. O. 2013. Reconstruction of the neck of *Azhdarcho lancicollis* and lifestyle of azhdarchids (Pterosauria, Azhdarchidae). Paleontological Journal 47:203–209.

Averianov, A. O. 2014. Review of taxonomy, geographic distribution, and paleoenvironments of Azhdarchidae (Pterosauria). ZooKeys 432:1–107.

Averianov, A. O. 2020. Taxonomy of the Lonchodectidae (Pterosauria, Pterodactyloidea). Proceedings of the Zoological Institute RAS 324:41–55.

Averianov, A. O., and A. A. Yarkov. 2004. On the occurrence of a giant flying reptile (Pterosauria) in the terminal Late Cretaceous of the Lower Volga Region. Paleontologicheskii Zhurnal 38:669–671.

Averianov, A. O., M. S. Arkhangelsky, E. M. Pervushov, and A. V. Ivanov. 2005. A new record of an azhdarchid (Pterosauria: Azhdarchidae) from the Upper Cretaceous of the Volga Region. Paleontological Journal 39:91–97.

Averianov, A. O., G. Dyke, I. Danilov, and P. Skutschas. 2015. The paleoenvironments of azhdarchid pterosaur localities in the Late Cretaceous of Kazakhstan. ZooKeys 483:59–80.

Baird, D., and P. M. Galton. 1981. Pterosaur bones from the Upper Cretaceous of Delaware. Journal of Vertebrate Paleontology 1:67–71.

Bakhurina, N. N., and D. M. Unwin. 1995. A survey of pterosaurs from the Jurassic and Cretaceous of the Former Soviet Union and Mongolia. Historical Biology 10:197–245.

Baumel, J. J., and L. M. Witmer. 1993. Osteologia; pp. 45–132 in J. J. Baumel (ed.), Handbook of Avian Anatomy. Publications of the Nuttal Ornithological Club, Cambridge.

Bennett, S. C. 1990. A pterodactyloid pterosaur pelvis from the Santana Formation of Brazil: implications for terrestrial locomotion. Journal of Vertebrate Paleontology 10:80–85.

Bennett, S. C. 1991. Morphology of the Late Cretaceous pterosaur *Pteranodon* and the systematics of the Pterodactyloidea. Ph.D. dissertation thesis/dissertation, University of Kansas, Lawrence, 680 pp.

Bennett, S. C. 1992. Sexual dimorphism of *Pteranodon* and other pterosaurs, with comments on cranial crests. Journal of Vertebrate Paleontology 12:422–434.

Bennett, S. C. 1993. The ontogeny of *Pteranodon* and other pterosaurs. Paleobiology 19:92–106.

Bennett, S. C. 1994. The pterosaurs of the Niobrara Chalk. The Earth Scientist 11:22–25.

Bennett, S. C. 1995. A statistical study of *Rhamphorhynchus* from the Solnhofen Limestone of Germany: year-classes of a single large species. Journal of Paleontology 69:569–580.

Bennett, S. C. 1996. The phylogenetic position of the Pterosaurs within the Archosauromorpha. Zoological Journal of the Linnean Society:261–308.

Bennett, S. C. 2001a. The osteology and functional morphology of the Late Cretaceous pterosaur *Pteranodon*: Part I. General description of osteology. Palaeontographica Abteilung A 260:1–112.

Bennett, S. C. 2001b. The osteology and functional morphology of the Late Cretaceous pterosaur *Pteranodon*: Part II. Size and functional morphology. Palaeontographica Abteilung A 260:113–153.

Bennett, S. C. 2003. New crested specimens of the Late Cretaceous pterosaur *Nyctosaurus*. Paläontologische Zeitschrift 77:67–75.

Bennett, S. C. 2004. New information on the pterosaur *Scaphognathus crassirostris* and the pterosaurian cervical series. Journal of Vertebrate Paleontology 24 (Supplement to 3):38A.

Bennett, S. C. 2007a. A second specimen of the pterosaur *Anurognathus ammoni*. Paläontologische Zeitschrift 81:376–398.

Bennett, S. C. 2007b. Articulation and function of the pteroid bone of pterosaurs. Journal of Vertebrate Paleontology 27:881–891.

Bennett, S. C. 2008. Morphological evolution of the wing of pterosaurs: Myology and function. Zitteliana Reihe B: Abhandlungen der Bayerischen Staatssammlung fur Palaontologie und Geologie 28:127–141.

Bennett, S. C. 2013. The morphology and taxonomy of the pterosaur *Cycnorhamphus*. Neues Jahrbuch für Geologie und Paläontologie, Abhandlungen 267:23–41.

Bennett, S. C. 2014. A new specimen of the pterosaur *Scaphognathus crassirostris*, with comments on constraint of cervical vertebrae number in pterosaurs. Neues Jahrbuch für Geologie und Paläontologie, Abhandlungen 271:327–348.

Bennett, S. C. 2018a. Status and affinities of *Bennettazhia oregonensis*; pp. 15–16 in Flugsaurier 2018: The 6th International Symposium on Pterosaurs, M. Habib, D. W. E. Hone, B. Breithaupt, E. Martin-Silverstone, T. Rodrigues, J. Lü, and N. Carroll eds. University of Southern California, Los Angeles.

Bennett, S. C. 2018b. New smallest specimen of the pterosaur *Pteranodon* and ontogenetic niches in pterosaurs. Journal of Paleontology 92:254–271.

Bennett, S. C., and J. A. Long. 1991. A large pterodactyloid pterosaur from the Late Cretaceous (Late Maastrichtian) of Western Australia. Records of the Western Australian Museum 15:435–443.

Bestwick, J., D. M. Unwin, R. J. Butler, D. M. Henderson, and M. A. Purnell. 2018. Pterosaur dietary hypotheses: a review of ideas and approaches. Biological Reviews 93:2021–2048.

Bonaparte, J. F. 1970. *Pterodaustro guinazui* gen. et sp. nov. Pterosaurio de la Formación Lagarcito, Provincia de San Luis, Argentina y su significado en la geologia regional (Pterodactylidae). Acta Geologica Lilloana 10:207–226.

Bonde, N., and P. Christiansen. 2003. The detailed anatomy of *Rhamphorhynchus*: axial pneumaticity and its implications; pp. 217–232 in E. Buffetaut and J.-M. Mazin (eds.), Evolution and Palaeobiology of Pterosaurs. Geological Society, Special Publications, London.

Britt, B. B., F. M. Dalla Vecchia, D. J. Chure, G. F. Engelmann, M. F. Whiting, and R. D. Scheetz. 2018. *Caelestiventus hanseni* gen. et sp. nov. extends the desert-dwelling pterosaur record back 65 million years. Nature Ecology & Evolution 2:1386–1392.

Brower, J. C., and J. Veinus. 1981. Allometry in pterosaurs. The University of Kansas Paleontological Contributions 105:1–32.

Brown, M. A., J. C. Sagebiel, B. Andres. 2021. The discovery, local distribution, and curation of the giant azhdarchid pterosaurs from Big Bend National Park; pp. 2–20 in K. Padian and M.A. Brown (eds.), The Late Cretaceous pterosaur *Quetzalcoatlus* Lawson 1975 (Pterodactyloidea: Azhdarchoidea). Society of Vertebrate Paleontology Memoir 19. Journal of Vertebrate Paleontology 41 (2, Supplement).

Buckland, W. 1829. On the discovery of a new species of Pterodactyle in the Lias at Lyme Regis. Proceedings of the Geological Society of London, Series 2 3:217–222.

Buffetaut, E. 2001. An azhdarchid pterosaur from the Upper Cretaceous of Cruzy (Hérault, France). Comptes Rendus de l'Académie des Sciences - Series IIA - Earth and Planetary Science 333:357–361.

Buffetaut, E. 2008. Late Cretaceous pterosaurs from France: a review. Zitteliana Reihe B: Abhandlungen der Bayerischen Staatssammlung fur Palaontologie und Geologie 28:249–255.

Buffetaut, E. 2011. *Samrukia nessovi*, from the Late Cretaceous of Kazakhstan: a large pterosaur, not a giant bird. Annales de Paléontologie 97:133–138.

Buffetaut, E., J. B. Clarke, and J. Le Loeuff. 1996. A terminal Cretaceous pterosaur from the Corbiéres (southern France) and the problem of pterosaur extinction. Bulletin de la Société Géologique de France 167:753–759.

Buffetaut, E., D. Grigorescu, and Z. Csiki. 2002. A new giant pterosaur with a robust skull from the latest Cretaceous of Romania. Naturwissenschaften 89:180–184.

Buffetaut, E., D. Grigorescu, and Z. Csiki. 2003. Giant azhdarchid pterosaurs from the terminal Cretaceous of Transylvania (western

Romania); pp. 91–104 in E. Buffetaut and J.-M. Mazin (eds.), Evolution and Palaeobiology of Pterosaurs. Geological Society, Special Publications, London.

Buffetaut, E., P. Mechin, and A. Mechin-Salessy. 2006. An azhdarchid pterosaur from the Upper Cretaceous of Provence (southern France); pp. 95–100 in Z. n. Csiki (ed.), Mesozoic and Cenozoic vertebrates and paleoenvironments, tributes the career of Professor Dan Grigorescu. Editura Ars Docendi, Bucharest.

Buffetaut, E., A. Ősi, and E. Prondvai. 2011. The pterosaurian remains from the Grünbach Formation (Campanian, Gosau Group) of Austria: A reappraisal of 'Ornithocheirus buenzeli'. Geological Magazine 148:334–339.

Buffetaut, E., Y. Laurent, J. Le Loeuff, and M. Bilotte. 1997. A terminal Cretaceous giant pterosaur from the French Pyrenees. Geological Magazine 134:553–556.

Busbey, A. B., and T. M. Lehman. 1989. Vertebrate paleontology, biostratigraphy and depositional environments, latest Cretaceous and Tertiary, Big Bend area, Texas. Guidebook, Field Trip Numbers 1 A, B, C. 49th Annual Meeting of the Society of Vertebrate Paleontology, Austin, Texas, 90 pp.

Cai, Z., and F. Wei. 1994. *Zhejiangopterus linhaiensis* (Pterosauria) from the Upper Cretaceous of Linhai, Zhejiang, China. Vertebrata Palasiatica 32:181–194.

Cantino, P. D., and K. de Queiroz. 2020. International Code of Phylogenetic Nomenclature (PhyloCode). 1st Edition. CRC Press, Boca Raton, FL, 189 pp.

Carrier, D. R., and C. G. Farmer. 2000. The Evolution of Pelvic Aspiration in Archosaurs. Paleobiology 26:271–293.

Carroll, N. R. 2013. Functional morphology of the azhdarchid manus. Journal of Vertebrate Paleontology. 34(3, Supplement):102.

Carroll, N. R., A. W. Poust, and D. J. Varricchio. 2013. A third azhdarchid pterosaur from the Two Medicine Formation (Campanian) of Montana; pp. 40–42 in Short Communications / International Symposium on Pterosaurs, Rio Ptero 2013, Vol. 50, J. M. Sayão, F. R. Costa, R. A. M. Bantim, and A. W. A. Kellner eds. Universidade Federal do Rio de Janeiro, Museu Nacional, Rio De Janeiro.

Chatterjee, S. 1982. Phylogeny and classification of thecodontian reptiles. Nature 295:317–320.

Chatterjee, S., and R. J. Templin. 2004. Posture, locomotion, and paleoecology of pterosaurs. Geological Society of America Special Paper:64 pp.

Chen, H., S. Jiang, A. W. A. Kellner, X. Cheng, X. Zhang, R. Qiu, Y. Li, and X. Wang. 2020. New anatomical information on *Dsungaripterus weii* Young, 1964 with focus on the palatal region. PeerJ 8:e8741.

Claessens, L. P. A. M., and M. Vickaryous. 2008. A reevaluation of prepubic skeletal elements in archosaurs. Journal of Vertebrate Paleontology 28:64A.

Claessens, L. P. A. M., P. M. O'Connor, and D. M. Unwin. 2009. Respiratory evolution facilitated the origin of pterosaur flight and aerial gigantism PLoS ONE 4:e4497.

Clark, J. M., J. A. Hopson, R. Hernandez, D. E. Fastovsky, and M. Montellano. 1998. Foot posture in a primitive pterosaur. Nature 391:886–889.

Cohen, J. E., T. C. Hunt, J. A. Frederickson, J. L. Berry, and R. L. Cifelli. 2018. Azhdarchid pterosaur from the Upper Cretaceous (Turonian) of Utah, USA. Cretaceous Research 86:60–65.

Company, J., J. I. Ruiz-Omeñaca, and X. Pereda-Suberbiola. 1999. A long-necked pterosaur (Pterodactyloidea, Azhdarchidae) from the Upper Cretaceous of Valencia, Spain. Geologie en Mijnbouw 78:319–333.

Company, J., D. M. Unwin, X. Pereda-Suberbiola, and J. I. Ruiz-Omeñaca. 2001. A giant azhdarchid pterosaur from the latest Cretaceous of Valencia, Spain – the largest flying creature ever? Journal of Vertebrate Paleontology 21(3, Supplement):41A–42A.

Costa, F. R., O. Rocha-Barbosa, and A. W. A. Kellner. 2013. A biomechanical approach on the optimal stance of *Anhanguera piscator* (Pterodactyloidea) and its implications for pterosaur gait on land. Historical Biology: DOI: 10.1080/08912963.2013.807253.

Costa, F. R., O. Rocha-Barbosa, and A. W. A. Kellner. 2014. Myological reconstruction of the pelvic girdle of *Anhanguera piscator* (Pterosauria: Pterodactyloidea) using three-dimensional virtual animation. Revista Brasileira de Paleontologia 17:11–21.

Csiki-Sava, Z., M. M. Vremir, Ş. Vasile, S. L. Brusatte, G. Dyke, D. Naish, M. A. Norell, and R. Totoianu. 2016. The east side story — the Transylvanian latest Cretaceous continental vertebrate record and

its implications for understanding Cretaceous–Paleogene boundary events. Cretaceous Research 57:662–698.

Currie, P. J., and A. R. Jacobsen. 1995. An azhdarchid pterosaur eaten by a velociraptorine theropod. Canadian Journal of Earth Sciences 32:922–925.

Dalla Vecchia, F. M. 1995. A new pterosaur (Reptilia, Pterosauria) from the Norian (Late Triassic) of Friuli (Northeastern Italy). Preliminary note. Gortania - Atti del Museo Friulano di Storia Naturale 16:59–66.

Dalla Vecchia, F. M. 2003a. An *Eudimorphodon* (Diapsida, Pterosauria) specimen from the Norian (Late Triassic) of North-Eastern Italy. Gortania - Atti del Museo Friulano di Storia Naturale 25:47–72.

Dalla Vecchia, F. M. 2003b. New morphological observations on Triassic pterosaurs; pp. 23–44 in E. Buffetaut and J.-M. Mazin (eds.), Evolution and Palaeobiology of Pterosaurs. Geological Society, Special Publications, London.

Dalla Vecchia, F. M. 2009. Anatomy and systematics of the pterosaur *Carniadactylus* gen. n. *rosenfeldi* (Dalla Vecchia, 1995). Rivista Italiana di Paleontologia e Stratigrafia 115:159–188.

Dalla Vecchia, F. M. 2014. Gli Pterosauri Triassici, Memorie del Museo Friulano di Storia Naturale, Volume 54. Comune di Udine, Udine, Italy, 319 pp.

Dalla Vecchia, F. M. 2019. *Seazzadactylus venieri* gen. et sp. nov., a new pterosaur (Diapsida: Pterosauria) from the Upper Triassic (Norian) of northeastern Italy. PeerJ 7:e7363 DOI 10.7717/peerj.7363.

Dalla Vecchia, F. M., and A. Cau. 2015. Re-examination of the purported pterosaur wing metacarpals from the Upper Triassic of England. Historical Biology 27:684–696.

Dalla Vecchia, F. M., P. Arduini, and A. W. A. Kellner. 2001. The first pterosaur from the Cenomanian (Late Cretaceous) Lagerstätten of Lebanon. Cretaceous Research 22:219–225.

David, L. D. O., B. J. González Riga, and A. W. A. Kellner. 2018. Discovery of the largest pterosaur from South America. Cretaceous Research 83:40–46.

de Buisonje, P. H. 1981. *Santanadactylus brasilensis*: Skelet-reconstructie van een vliegend reptiel met zes meter vlucht. Gea: Driemaandelijks tijdschrift van de Stichting Geologische Aktivieiten voor belangstellenden in de geologie en mineralogie 14:37–48.

de Ricqlès, A. J., K. Padian, J. R. Horner, and H. Francillon-Vieillot. 2000. Palaeohistology of the bones of pterosaurs (Reptilia: Archosauria): Anatomy, ontogeny, and biomechanical implications. Zoological Journal of the Linnaean Society 129:349–385.

Döderlein, L. 1923. Anurognathus Ammoni, ein neuer Flugsaurier. Sitzungsberichte der Bayerischen Akademie der Wissenschaften, Mathematisch-naturwissenschaftliche Abteilung 1923:117–164.

Dong, Z., J.-W. Sun, and S.-Y. Wu. 2003. On a new pterosaur from the Lower Cretaceous of Chaoyang Basin, western Liaoning, China. Global Geology 22:1–7.

Eck, K., R. A. Elgin, and E. Frey. 2011. On the osteology of *Tapejara wellnhoferi* KELLNER 1989 and the first occurrence of a multiple specimen assemblage from the Santana Formation, Araripe Basin, NE-Brazil. Swiss Journal of Palaeontology 130:277–296.

Elgin, R. A. 2014. Palaeobiology, Morphology, and Flight Characteristics of Pterodactyloid Pterosaurs. Dissertation thesis/dissertation, Faculty of Chemistry and Geological Sciences, University of Heidelberg, Heidelberg, Germany, 273 pp.

Elgin, R. A., and E. Frey. 2011. A new azhdarchoid pterosaur from the Cenomanian (Late Cretaceous) of Lebanon. Swiss Journal of Geosciences 104:S21–S33.

Elżanowski, A. 2001. A new genus and species for the largest specimen of *Archaeopteryx*. Acta Palaeontologica Polonica 46:519–532.

Fastnacht, M. 2005. The first dsungaripterid pterosaur from the Kimmeridgian of Germany and the biomechanics of pterosaur long bones. Acta Palaeontologica Polonica 50:273–288.

Frey, E., and D. M. Martill. 1994. A new pterosaur from the Crato Formation (Lower Cretaceous, Aptian) of Brazil. Neues Jahrbuch für Geologie und Paläontologie, Abhandlungen 194:379–412.

Frey, E., and D. M. Martill. 1996. A reappraisal of *Arambourgiania* (Pterosauria, Pterodactyloidea): One of the world's largest flying animals. Neues Jahrbuch für Geologie und Paläontologie, Abhandlungen 199:221–247.

Frey, E., and D. M. Martill. 1998. Late ontogenetic fusion of the processus tendinis extensoris in Cretaceous pterosaurs from Brazil.

Neues Jahrbuch für Geologie und Paläontologie, Monatshefte 10:587–594.

Frey, E., and J. Riess. 1981. A new reconstruction of the pterosaur wing. Neues Jahrbuch für Geologie und Paläontologie, Abhandlungen 161:1–27.

Frey, E., D. M. Martill, and M.-C. Buchy 2003a. A new crested ornithocheirid from the Lower Cretaceous of northeastern Brazil and the unusual death of an unusual pterosaur; pp. 55–63 in E. Buffetaut, and J.-M. Mazin (eds.), Evolution and Palaeobiology of Pterosaurs. Geological Society. Special Publications, London.

Frey, E., H. Tischlinger, M.-C. Buchy, and D. M. Martill 2003b. New specimens of Pterosauria (Reptilia) with soft parts and implications for pterosaurian anatomy and locomotion; pp. 23–44 in E. Buffetaut, and J.-M. Mazin (eds.), Evolution and Palaeobiology of Pterosaurs. Geological Society. Special Publications, London.

Frey, E., C. A. Meyer, and H. Tischlinger. 2011. The oldest azhdarchoid pterosaur from the Late Jurassic Solnhofen Limestone (Early Tithonian) of Southern Germany. Swiss Journal of Geosciences 104:S35–S55.

Frey, E., M.-C. Buchy, W. Stinnesbeck, A. G. González, and A. di Stefano. 2006. *Muzquizopteryx coahuilensis* n. g., n. sp., a nyctosaurid pterosaur with soft tissue preservation from the Coniacian (Late Cretaceous) of northeast Mexico (Coahuila). Oryctos 6:19–39.

Frigot, R. A. 2017. Pelvic musculature of *Vectidraco daisymorrisae* and consequences for pterosaur locomotion; pp. 45–55 in D. W. E. Hone, M. P. Witton, and D. M. Martill (eds.), New Perspectives on Pterosaur Palaeobiology. Geological Society of London, London.

Funston, G. F., E. Martin-Silverstone, and P. J. Currie. 2017. The first pterosaur pelvic material from the Dinosaur Park Formation (Campanian) and implications for azhdarchid locomotion. FACETS 2:559–574.

Funston, G. F., E. Martin-Silverstone, and P. J. Currie. 2018. Correction: The first pterosaur pelvic material from the Dinosaur Park Formation (Campanian) and implications for azhdarchid locomotion. FACETS 3:192–194.

Galton, P. M. 1981. A rhamphorhynchoid pterosaur from the Upper Jurassic of North America. Journal of Paleontology 55:1117–1122.

Gasparini, Z. M., M. Fernandez, and M. de la Fuente. 2004. A new pterosaur from the Jurassic of Cuba. Palaeontology 47:919–927.

Geist, N. R., W. J. Hillenius, E. Frey, T. D. Jones, and R. A. Elgin. 2014. Breathing in a box: constraints on lung ventilation in giant pterosaurs. The Anatomical Record 297:2233–2253.

Gilmore, C. W. 1928. A new pterosaurian reptile from the marine Cretaceous of Oregon. Proceedings of the U. S. National Museum 73:1–5.

Godfrey, S. J., and P. J. Currie. 2005. Pterosaurs; pp. 292–311 in P. J. Currie and E. B. Koppelhus (eds.), Dinosaur Provincial Park: A Spectacular Ancient Ecosystem Revealed. Indiana University Press, Bloomington, Indianapolis.

Goldfuß, G. A. 1831. Beiträge zur Kenntnis verschiedener Reptilien der Vorwelt. Nova acta Academiae caesareae Leopoldino-Carolinae germanicae naturae curiosorum 15:61–128.

Goloboff, P. A., and S. A. Catalano. 2016. TNT version 1.5, including a full implementation of phylogenetic morphometrics. Cladistics 32:221–238.

Greenewalt, C. H. 1975. Could Pterosaurs Fly? Science 188:676.

Harksen, J. C. 1966. *Pteranodon sternbergi*, a new fossil pterodactyl from the Niobrara Cretaceous of Kansas. Proceedings of the South Dakota Academy of Sciences 45:74–77.

Harrell, T. L., M. A. Gibson, and W. Langston. 2017. A cervical vertebra of *Arambourgiania philadelphiae* (Pterosauria, Azhdarchidae) from the Late Campanian micaceous facies of the Coon Creek Formation in McNairy County, Tennessee, USA. Bulletin of the Alabama Museum of Natural History 33:96–105.

Henderson, D. M. 2010. Pterosaur body mass estimates from three-dimensional mathematical slicing. Journal of Vertebrate Paleontology 30:768–785.

Henderson, M. D., and J. E. Peterson. 2006. An azhdarchid pterosaur cervical vertebra from the Hell Creek Formation (Maastichtian) of Southeastern Montana. Journal of Vertebrate Paleontology 26:192–195.

Henderson, D. M., D. Krentz, and M. Habib. 2018. It's big . . . REALLY BIG – new mass estimates for *Quetzalcoatlus northropi* from a new restoration; pp. 44–46 in Flugsaurier 2018: The 6th International Symposium on Pterosaurs, M. Habib, D. W. E. Hone, B.

Breithaupt, E. Martin-Silverstone, T. Rodrigues, J. Lü, and N. Carroll eds. The University of Southern California, Los Angeles, USA.

Hone, D. W. E., M. B. Habib, and F. Therrien. 2019. *Cryodrakon boreas*, gen. et sp. nov., a Late Cretaceous Canadian azhdarchid pterosaur. Journal of Vertebrate Paleontology 39:e1649681.

Hooley, R. W. 1913. On the skeleton of *Ornithodesmus latidens*; an ornithosaur from the Wealden Shales of Atherfield (Isle of Wight). Quarterly Journal of the Geological Society 69:372–421.

Hooley, R. W. 1914. On the ornithosaurian *Ornithocheirus*, with a review of the specimens from the Cambridge Greensand in the Sedgwick Museum, Cambridge. Annals and Magazine of Natural History Series 8:529–557.

Howse, S. C. B. 1986. On the cervical vertebrae of the Pterodactyloidea (Reptilia: Archosauria). Zoological Journal of the Linnean Society 88:307–328.

Huene, F. v. 1914. Beiträge zur Geschichte der Archosaurier. Geologische und palaeontologische Abhanglungen, N. F. 13:1–53.

Hyder, E. S. 2012. The osteomorphology and functional anatomy of the pterosaurian pelvis with descriptions of new specimens (Pterodactyloidea) from the Santana Formation (Cretaceous) of Brazil. Masters thesis/dissertation, School of Earth and Environmental Sciences, University of Portsmouth, Portsmouth, UK, 135 pp.

Hyder, E. S., M. P. Witton, and D. M. Martill. 2014. Evolution of the pterosaur pelvis. Acta Palaeontologica Polonica 59:109–124.

Ibrahim, N., D. M. Unwin, D. M. Martill, L. Baidder, and S. Zouhri. 2010. A new pterosaur (Pterodactyloidea: Azhdarchidae) from the Upper Cretaceous of Morocco. PLoS ONE 5:e10875.

ICZN. 1999. International Code of Zoological Nomenclature. Fourth Edition. The International Trust for Zoological Nomenclature, London, UK, 306 pp.

ICZN. 2019. Opinion 2440 (Case 3728) – *Quetzalcoatlus northropi* Lawson, 1975 (Reptilia, Pterosauria): generic and specific names ruled available with the indicated authorship. The Bulletin of Zoological Nomenclature 76:155–156.

Ikegami, N., A. W. A. Kellner, and Y. Tomida. 2000. The presence of an azhdarchid pterosaur in the Cretaceous of Japan. Paleontological Research 4:165–170.

Kellner, A. W. A. 1989. A new edentate pterosaur of the Lower Cretaceous from the Araripe Basin, Northeast Brazil. Anais da Academia Brasileira de Ciencias 61:439–446.

Kellner, A. W. A. 1995: Description of a juvenile specimen of *Tapejara* (Pterodactyloidea, Tapejaridae) from Brazil. Journal of Vertebrate Paleontology, 15(3, Supplement):38A–39A.

Kellner, A. W. A. 1996. Description of new material of Tapejaridae and Anhangueridae (Pterosauria, Pterodactyloidea) and discussion of pterosaur phylogeny. Dissertation thesis/dissertation, Columbia University, New York, 347 pp.

Kellner, A. W. A. 2003. Pterosaur phylogeny and comments on the evolutionary history of the group; pp. 105–137 in E. Buffetaut and J.-M. Mazin (eds.), Evolution and Palaeobiology of Pterosaurs. Geological Society, Special Publications, London.

Kellner, A. W. A. 2004a. New information on the Tapejaridae (Pterosauria, Pterodactyloidea) and discussion of the relationships of this clade. Ameghiniana 41:521–534.

Kellner, A. W. A. 2004b. The ankle structure of two pterodactyloid pterosaurs from the Santana Formation (Lower Cretaceous), of Brazil. Bulletin of the American Museum of Natural History 285:25–35.

Kellner, A. W. A. 2010. Comments on the Pteranodontidae (Pterosauria, Pterodactyloidea) with the description of two new species. Anais da Academia Brasileira de Ciencias 82:1063–1084.

Kellner, A. W. A. 2013. A new unusual tapejarid (Pterosauria, Pterodactyloidea) from the Early Cretaceous Romualdo Formation, Araripe Basin, Brazil. Earth and Environmental Science Transactions of the Royal Society of Edinburgh 103:409–421.

Kellner, A. W. A. 2015. Comments on Triassic pterosaurs with discussion about ontogeny and description of new taxa. Anais da Academia Brasileira de Ciencias 87:669–689.

Kellner, A. W. A., and D. d. A. Campos. 1994. A new species of *Tupuxuara* (Pterosauria, Tapejaridae) from the Early Cretaceous of Brazil. Anais da Academia Brasileira de Ciencias 66:467–474.

Kellner, A. W. A., and D. A. Campos. 2002. The function of the cranial crest and jaws of a unique pterosaur from the Early Cretaceous of Brazil. Science 297:389–392.

Kellner, A. W. A., and W. Langston. 1996. Cranial remains of *Quetzalcoatlus* (Pterosauria, Azhdarchidae) from Late Cretaceous sediments of Big Bend National Park, Texas. Journal of Vertebrate Paleontology 16:222–231.

Kellner, A. W. A., and Y. Tomida. 2000. Description of a new species of Anhangueridae (Pterodactyloidea) with comment on the pterosaur fauna from the Santana Formation (Aptian-Albian), Northeastern Brazil, National Science Museum Monographs, Volume 17, Tokyo, 135 pp.

Kellner, A. W. A., M. B. Agguirre-Uretta, and V. A. Ramos. 2003. On the pterosaur remains from the Río Belgrano Formation (Barremian), Patagonian Andes of Argentina. Anais da Academia Brasileira de Ciencias 75:487–495.

Kellner, A. W. A., L. C. Weinschütz, B. Holgado, R. A. M. Bantim, and J. M. Sayão. 2019a. A new toothless pterosaur (Pterodactyloidea) from Southern Brazil with insights into the paleoecology of a Cretaceous desert. Anais da Academia Brasileira de Ciências 91: e20190768.

Kellner, A. W. A., M. W. Caldwell, B. Holgado, F. M. Dalla Vecchia, R. Nohra, J. M. Sayão, and P. J. Currie. 2019b. First complete pterosaur from the Afro-Arabian continent: insight into pterodactyloid diversity. Scientific Reports 9:1–9.

Langston, W. 1978. The great pterosaur. Discovery 2:20–23.

Langston, W. 1981. Pterosaurs. Scientific American 244:122–136.

Langston, W. 1986. Rebuilding the world's biggest flying creature: the second coming of *Quetzalcoatlus northropi*; pp. 125–128 in P. H. Pausé and R. G. Spears (eds.), Geology of the Big Bend Area and Solitario Dome. West Texas Geological Society 1986 Field Trip Guidebook.

Lawson, D. A. 1972. Paleoecology of the Tornillo Formation, Big Bend National Park, Brewster County, Texas. Master of Arts thesis/dissertation, Department of Geological Sciences, The University of Texas at Austin, Austin, Texas, 182 pp.

Lawson, D. A. 1975a. Pterosaur from the latest Cretaceous of West Texas. Discovery of the largest flying creature. Science 187:947–948.

Lawson, D. A. 1975b. Could pterosaurs fly? Science 188:676–678.

Lee, Y.-N. 1994. The Early Cretaceous pterodactyloid pterosaur *Coloborhynchus* from North America. Palaeontology 37:755–763.

Lehman, T. M. 2021. Habitat of the giant pterosaur *Quetzalcoatlus* Lawson 1975 (Pterodactyloidea: Azhdarchoidea): a paleoenvironmental reconstruction of the Javelina Formation (Upper Cretaceous), Big Bend National Park, Texas; pp. 21–45 in K. Padian and M.A. Brown (eds.), The Late Cretaceous pterosaur *Quetzalcoatlus* Lawson 1975 (Pterodactyloidea: Azhdarchoidea). Society of Vertebrate Paleontology Memoir 19. Journal of Vertebrate Paleontology 41(2, Supplement).

Lehman, T. M., and W. Langston. 1996. Habitat and behaviour of *Quetzalcoatlus*: paleoenvironmental reconstruction of the Javelina Formation (Upper Cretaceous), Big Bend National Park, Texas. Journal of Vertebrate Paleontology 16(3, Supplement):48A.

Leonardi, G., and G. Borgomanero. 1985. *Cearadactylus atrox* nov. gen., nov. sp. novo Pterosauria (Pterodactyloidea) da Chapada do Araripe, Ceará, Brasil. Resumos dos communicaçoes VIII Congresso brasileiro de Paleontologia e Stratigrafia 27:75–80.

Longrich, N. R., D. M. Martill, and B. Andres. 2018. Late Maastrichtian pterosaurs from North Africa and mass extinction of Pterosauria at the Cretaceous-Paleogene boundary. PLoS Biology 16:e2001663.

Lü, J. 2010. A new boreopterid pterodactyloid pterosaur from the Early Cretaceous Yixian Formation of Liaoning Province, northeastern China. Acta Geologica Sinica - English Edition 84:241–246.

Lü, J., and Q. Ji. 2005a. New azhdarchid pterosaur from the Early Cretaceous of Western Liaoning. Acta Geologica Sinica 79:301–307.

Lü, J., and Q. Ji. 2005b. A new ornithocheirid from the Early Cretaceous of Liaoning Province, China. Acta Geologica Sinica 79:157–163.

Lü, J., and C. Yuan. 2005. New tapejarid pterosaur from Western Liaoning, China. Acta Geologica Sinica 79:453–458.

Lü, J., and B.-K. Zhang. 2005. New pterodactyloid pterosaur from the Yixian Formation of western Liaoning. Geological Review 51:458–462.

Lü, J., X. Fucha, and J. Chen. 2010a. A new scaphognathine pterosaur from the Middle Jurassic of Western Liaoning, China. Acta Geoscientica Sinica 31:263–266.

Lü, J., D. M. Unwin, L. Xu, and X. Zhang. 2008. A new azhdarchoid pterosaur from the Lower Cretaceous of China and its implications for pterosaur phylogeny and evolution. Naturwissenschaften 95:891–897.

Lü, J., Y. Gao, L. Xing, Z. Li, and Q. Ji. 2007. A new species of *Huaxiapterus* (Pterosauria: Tapejaridae) from the Early Cretaceous of Western Liaoning, China. Acta Geologica Sinica 81:683–687.

Lü, J., D.M. Unwin, X. Jin, Y. Liu, and Q. Ji. 2010b. Evidence for modular evolution in a long-tailed pterosaur with a pterodactyloid skull. Proceedings of the Royal Society B: Biological Sciences 277:383–389.

Lü, J., D. M. Unwin, B. Zhao, C. Gao, and C. Shen. 2012. A new rhamphorhynchid (Pterosauria: Rhamphorhynchidae) from the Middle/Upper Jurassic of Qinglong, Hebei Province, China. Zootaxa 3158:1–19.

Lü, J., J. Liu, X. Wang, C. Gao, Q. Meng, and Q. Ji. 2006a. New material of Pterosaur *Sinopterus* (Reptilia: Pterosauria) from the Early Cretaceous Jiufotang Formation, Western Liaoning, China. Acta Geologica Sinica 80:783–789.

Lü, J., X. Jen, D. M. Unwin, L. Zhao, Y. Azuma, and Q. Ji. 2006b. A new species of *Huaxiapterus* (Pterosauria: Pterodactyloidea) from the Lower Cretaceous of Western Liaoning, China with comments on the systematics of tapejarid pterosaurs. Acta Geologica Sinica 80:315–326.

Lü, J., D. M. Unwin, D. C. Deeming, X. Jin, Y. Liu, and Q. Ji. 2011. An egg-adult association, gender, and reproduction in pterosaurs. Science 331:321–324.

Lü, J., F. Teng, D. Sun, C. Shen, G. Li, X. Gao, and H. Liu. 2016. The toothless pterosaurs from China. Acta Geologica Sinica 90:2513–2525.

MacCready, P. B. 1985. The great pterodactyl project. Engineering and Science 49:18–24.

Manzig, P. C., A. W. A. Kellner, L. C. Weinschütz, C. E. Fragoso, C. S. Vega, G. B. Guimaraães, L. C. Godoy, A. Liccardo, J. H. Z. Ricetti, and C. C. de Moura. 2014. Discovery of a rare pterosaur bone bed in a Cretaceous desert with insights on ontogeny and behavior of flying reptiles. PLoS ONE 9:e100005.

Marden, J. H. 1994. From damselflies to pterosaurs: how burst and sustainable flight performance scale with size. American Journal of Physiology 266:1077–1084.

Marsh, O. C. 1876. Notice of a new sub-order of Pterosauria. American Journal of Science Series 3:507–509.

Marsh, O. C. 1884. Principal characters of American Cretaceous pterodactyls. Part 1. The skull of *Pteranodon*. American Journal of Science, Series 3 27:423–426.

Martill, D. M., and M. Moser. 2017. Topotype specimens probably attributable to the giant azhdarchid pterosaur A*rambourgiania philadelphiae* (Arambourg 1959); pp. 159–169 in D. W. E. Hone, M. P. Witton, and D. M. Martill (eds.), New Perspectives on Pterosaur Palaeobiology. Geological Society, London.

Martill, D. M., and D. Naish. 2006. Cranial crest development in the azhdarchoid pterosaur *Tupuxuara*, with a review of the genus and tapejarid monophyly. Palaeontology 49:925–941.

Martill, D. M., M. O'Sullivan, and C. Newman. 2013. A possible azhdarchid pterosaur (Pterosauria, Azhdarchidae) in the Durlston Formation (Early Cretaceous, Berriasian) of southern England. Cretaceous Research 43:26–39.

Martill, D. M., E. Frey, R. M. Sadaqah, and H. N. Khoury. 1998. Discovery of the holotype of the giant pterosaur *Titanopteryx philadelphiae* Arambourg 1959, and the status of *Arambourgiania* and *Quetzalcoatlus*. Neues Jahrbuch für Geologie und Paläontologie, Abhandlungen 207:57–79.

Martin-Silverstone, E., M. P. Witton, V. M. Arbour, and P. J. Currie. 2016. A small azhdarchoid pterosaur from the latest Cretaceous, the age of flying giants. Royal Society Open Science 3:160333.

McGowan, C. 1991. Dinosaurs, Spitfires, and Sea Dragons. Harvard University Press, Cambridge, 365 pp.

McGowen, M. R., K. Padian, M. A. De Sosa, and R. J. Harmon. 2002. Description of *Montanazhdarcho minor*, an azhdarchid pterosaur form the Two Medicine Formation (Campanian) of Montana. PaleoBios 22:1–9.

McMasters, J. H. 1976. Aerodynamics of the long pterosaur wing. Science 191:899.

McPhee, J., N. Ibrahim, A. Kao, D. M. Unwin, R. Smith, and D. M. Martill. 2020. A new ?chaoyangopterid (Pterosauria:

Pterodactyloidea) from the Cretaceous Kem Kem beds of southern Morocco. Cretaceous Research 110:104410.

Molnar, R. E. 1987. A pterosaur pelvis from western Queensland, Australia. Alcheringa: An Australasian Journal of Palaeontology 11:87–94.

Molnar, R. E., and J. Wiffen. 1994. A Late Cretaceous polar dinosaur fauna from New Zealand. Cretaceous Research 15:689–706.

Murry, P. A., D. A. Winkler, and L. L. Jacobs. 1991. An azhdarchid pterosaur humerus from the Lower Cretaceous Glen Rose Formation of Texas. Journal of Paleontology 65:167–170.

Myers, T. S. 2010. A new ornithocheirid pterosaur from the Upper Cretaceous (Cenomanian–Turonian) Eagle Ford Group of Texas. Journal of Vertebrate Paleontology 30:280–287.

Naish, D., and M. P. Witton. 2017. Neck biomechanics indicate that giant Transylvanian azhdarchid pterosaurs were short-necked arch predators. PeerJ 5:e2908.

Naish, D., M. M. Vremir, and G. Dyke. 2013a. Pterosaur size-classes in the Transylvanian Late Cretaceous?; pp. 85–86 in Short Communications / International Symposium on Pterosaurs, Rio Ptero 2013, Vol. 50, J. M. Sayão, F. R. Costa, R. A. M. Bantim, and A. W. A. Kellner eds. Universidade Federal do Rio de Janeiro, Museu Nacional, Rio De Janeiro.

Naish, D., M. Simpson, and G. Dyke. 2013b. A new small-bodied azhdarchoid pterosaur from the Lower Cretaceous of England and its implications for pterosaur anatomy, diversity and phylogeny. PLoS ONE 8:e58451.

Naish, D., G. Dyke, A. Cau, F. Escuillié, and P. Godefroit. 2011. A gigantic bird from the Upper Cretaceous of Central Asia. Biology Letters 8:97–100.

Nesov, L. A. 1984. Upper Cretaceous pterosaurs and birds from central Asia. Paleontological Journal 18:38–49.

Nesov, L. A. 1991. Gigantskiye letayushchiye yashchery semeystva Azhdarchidae. II. Sreda obitaniya, sedimentologicheskaya obstanovka zakhoroneniya ostatkov. Vestnik Leningrad State University Series 7 3:16–24.

Newton, E. T. 1888. On the skull, brain and auditory organ of a new species of pterosaurian (*Scaphognathus purdoni*) from the Upper Lias near Whitby, Yorkshire. Philosophical Transactions of the Royal Society of London, B. Biological Sciences 179:503–537.

Nikolov, V., D. Dochev, P. Pavlishina, S. L. Brusatte, M. Yaneva, R. Konyovska, V. Vergilov, N. Simov, N. Spassov, and L. Hristova. 2020. Welcome to "Cretaceous Park": Three years of research at the Late Cretaceous tetrapod fossil site near the town of Tran, Western Srednogorie. Review of the Bulgarian Gelogical Society 81:141–143.

Novas, F. E., M. Kundrat, F. L. Agnolín, M. D. Ezcurra, P. E. Ahlberg, M. P. Isasi, A. Arriagada, and P. Chafrat. 2012. A new large pterosaur from the Late Cretaceous of Patagonia. Journal of Vertebrate Paleontology 32:1447–1452.

O'Sullivan, M., and D. M. Martill. 2017. The taxonomy and systematics of *Parapsicephalus purdoni* (Reptilia: Pterosauria) from the Lower Jurassic Whitby Mudstone Formation, Whitby, U.K. Historical Biology 29:1009–1018.

Obata, I., K. Shibata, M. Matsukawa, and D. M. Unwin. 2007. New record of a pterosaur from the Late Cretaceous Izumi Group, Awaji Island, Hyogo Prefecture, Japan. Annual Report of the Fukada Geological Institute 8:149–162.

Ősi, A., E. Buffetaut, and E. Prondvai. 2011. New pterosaurian remains from the Late Cretaceous (Santonian) of Hungary (Iharkút, Csehbánya Formation). Cretaceous Research 32:456–653.

Ősi, A., D. B. Weishampel, and C. M. Jianu. 2005. First evidence of azhdarchid pterosaurs from the Late Cretaceous of Hungary. Acta Palaeontologica Polonica 50:777–787.

Ősi, A., E. Prondvai, E. Frey, and B. Pohl. 2010. New interpretation of the palate of pterosaurs. The Anatomical Record 293:243–258.

Owen, R. 1842. Report on British Fossil Reptiles, Part II; pp. 60–204 in Report of the Eleventh Meeting of the British Association for the Advancement of Science, Vol. 1841 John Murray, Plymouth.

Owen, R. 1859. On the vertebral characters of the Order Pterosauria, as exemplified in the Genera *Pterodactylus* (Cuvier) and *Dimorphodon* (Owen). Philosophical Transactions of the Royal Society of London 149:161–169.

Owen, R. 1861. Monograph of the Fossil Reptilia of the Cretaceous and Purbeck Strata; Including Supplement No. III. Cretaceous Pterosauria and Sauropterygia. Supplement No. II. Iguanodon, and Purbeck Lacertilia. Monographs of the Palæontographical Society 12:1–30.

Owen, R. 1870. The Reptilia of the Liassic Formations, Part II. Pterosauria. Monographs of the Palæontographical Society 23:41–82.

Owen, R. 1874. The Fossil Reptilia of the Mesozoic Formations, Part I. Pterosauria (Pterodactylus). [Gault–Lias.]. Monographs of the Palæontographical Society 27:1–14.

Padian, K. 1983a. Osteology and functional morphology of *Dimorphodon macronyx* (Buckland) (Pterosauria: Rhamphorhynchoidea) based on new material in the Yale Peabody Museum. Postilla 189:1–44.

Padian, K. 1983b. A functional analysis of flying and walking in pterosaurs. Paleobiology 9:218–239.

Padian, K. 1984a. A large pterodactyloid pterosaur from the Two Medicine Formation (Campanian) of Montana. Journal of Vertebrate Paleontology 4:516–524.

Padian, K. 1984b. The origins of pterosaurs; pp. 163–168 in W.-E. Reif and F. Westphal (eds.), Third Symposium on Mesozoic Terrestrial Ecosystems. Attempto Verlag, Tübingen.

Padian, K. 1984c. Biological aerodynamics: flight of fancy planned for the largest pterosaur. Nature 311:511.

Padian, K. 1986. A taxonomic note on two pterodactyloid families. Journal of Vertebrate Paleontology 6:289–289.

Padian, K. 1988. The flight of pterosaurs: were the first flapping vertebrates batlike or birdlike-or were they something completely different? Natural History 12:58–65.

Padian, K. 1991. Pterosaurs: were they functional birds or functional bats?; pp. 145–160 in J. M. V. Rayner and R. J. Wootton (eds.), Biomechanics and Evolution. Cambridge University Press, Cambridge.

Padian, K. 2008a. The Toarcian (Early Jurassic) pterosaur *Campylognathoides* Strand 1928. Palaeontology 80:65–107.

Padian, K. 2008b. The Toarcian (Early Jurassic) pterosaur *Dorygnathus* Wagner 1860. Palaeontology 80:1–64.

Padian, K. 2017. Structure and evolution of the ankle bones in pterosaurs and other ornithodirans. Journal of Vertebrate Paleontology 37:e1364651.

Padian, K., and M. Smith. 1992. New light on Late Cretaceous pterosaur material from Montana. Journal of Vertebrate Paleontology 12:87–92.

Padian, K., and R. Wild. 1992. Studies of Liassic Pterosauria, I. The holotype and referred specimens of the Liassic Pterosaur *Dorygnathus banthensis* (Theodori) in the Petrefaktensammlung Banz, Northern Bavaria. Palaeontographica Abteilung A 225:59–77.

Padian, K., A. J. de Ricqlès, and J. R. Horner. 1995. Bone histology determines identification of a new fossil taxon of pterosaur (Reptilia: Archosauria). Comptes Rendus de l'Academie de Science, Serie II 320:77–84.

Padian, K., J. R. Cunningham, W. A. Langston, and J. Conway. 2021. Functional morphology of *Quetzalcoatlus* Lawson 1975 (Pterodactyloidea: Azhdarchoidea); pp. 218–251 in K. Padian and M. A. Brown. The Late Cretaceous pterosaur *Quetzalcoatlus* Lawson 1975 (Pterodactyloidea: Azhdarchoidea). Society of Vertebrate Paleontology Memoir 19. Journal of Vertebrate Paleontology 41(2, Supplement).

Palmer, C., and G. J. Dyke. 2010. Biomechanics of the unique pterosaur pteroid. Proceedings of the Royal Society B 277:1121–1127.

Park, E. 1981. New dinosaur hall brings back to life the Age of Reptiles. Smithsonian 12:109–114.

Parker, W., C. Bell, C. Brochu, R. Irmis, C. Jass, and M. Stocker eds. 2013. The Full Profession: A Celebration of the Life and Career of Wann Langston, Jr., Quintessential Vertebrate Palaeontologist. Vol. 103. Royal Society of Edinburgh, Edinburgh, 408 pp.

Parris, D. C., B. S. Grandstaff, and D. Clemets. 2004. Pterosaur femur from the Upper Cretaceous of North Carolina. Southeastern Geology 43:51–55.

Paul, G. S. 1987. Pterodactyl habits - real and radio controlled. Nature 328:481.

Paul, G. S. 1991. The many myths, some old, some new, of dinosaurology. Modern Geology 16:69–99.

Paul, G. S. 2002. Dinosaurs of the Air: The Evolution and Loss of Flight in Dinosaurs and Birds. John Hopkins Universtiy Press, Baltimore, 472 pp.

Pêgas, R. V., F. R. Costa, and A. W. A. Kellner. 2018. New information on the osteology and a taxonomic revision of the genus *Thalassodromeus* (Pterodactyloidea, Tapejaridae, Thalassodrominae). Journal of Vertebrate Paleontology:DOI: 10.1080/02724634.2018.1443273.

Pêgas, R. V., B. Holgado, M. E. C. Leal, and A. W. A. Kellner. 2017. On the flight metabolic balance of the largest known pterosaur, *Quetzalcoatlus northropi* (Pterodactyloidea; Azhdarchidae); pp. 70 in 15th Annual Meeting of the European Association of Vertebrate Palaeontologists Munich, Germany, Vol. 91, G. Rößner, G. Wörheide, and M. Reich eds. Zitteliana, Munich, Germany.

Pereda-Suberbiola, X., J. Company, and J. I. Ruiz-Omeñaca. 2007. Azhdarchid pterosaurs from the Late Cretaceous (Campanian-Maastrichtian) of the Iberian Peninsula: an update; pp. 27 in Flugsaurier Wellnhofer Pterosaur Meeting, Vol. 27, D. W. E. Hone ed Bavarian State Collection for Palaeontology, Munich, Germany.

Pereda-Suberbiola, X., N. Bardet, S. Jouve, M. Iarochène, B. Bouya, and M. Amaghzaz. 2003. A new azdarchid pterosaur from the Late Cretaceous phosphates of Morocco; pp. 79–90 in E. Buffetaut and J.-M. Mazin (eds.), Evolution and Palaeobiology of Pterosaurs. Geological Society, Special Publications, London.

Pinheiro, F. L., and C. L. Schultz. 2012. An unusual pterosaur specimen (Pterodactyloidea, ?Azhdarchoidea) from the Early Cretaceous Romualdo Formation of Brazil, and the evolution of the pterodactyloid palate. PLoS ONE 7:e50088.

Plieninger, F. 1894. *Campylognathus zitteli*. Ein neuer Flugsaurier aus dem Oberen Lias Schwabens. Palaeontographica 41:192–222.

Plieninger, F. 1901. Beiträge zur Kenntnis der Flugsaurier. Palaeontographica 48:65–90.

Prieto, I. R. 1998. Functional morphology and feeding habits of *Quetzalcoatlus* (Pterosauria). Coloquios de Paleontología 49:129–144.

Prondvai, E. 2008. New models for the wing extension in pterosaurs. Historical Biology 20:237–254.

Quenstedt, F. A. 1855. Über *Pterodactylus suevicus* im lithographischen Schiefer Württembergs. Dissertation thesis/dissertation, Tübingen University, Tübingen, 52 pp.

Quenstedt, F. A. 1858. Über *Pterodactylus liasicus*. Paläontographica 53:209–213.

Rigal, S., D. M. Martill, and S. C. Sweetman. 2017. A new pterosaur specimen from the Upper Tunbridge Wells Sand Formation (Cretaceous, Valanginian) of southern England and a review of *Lonchodectes sagittirostris* (Owen 1874); pp. 221–232 in D. W. E. Hone, M. P. Witton, and D. M. Martill (eds.), New Perspectives on Pterosaur Palaeobiology. Geological Society, London.

Rodrigues, T., A. W. A. Kellner, B. J. Mader, and D. A. Russell. 2011. New pterosaur specimens from the Kem Kem beds (Upper Cretaceous, Cenomanian) of Morocco. Rivista Italiana di Paleontologia e Stratigrafia 117:149–160.

Romer, A. S. 1956. Osteology of the Reptiles. University of Chicago Press, Chicago, 772 pp.

Romer, A. S., and T. S. Parsons. 1977. The Vertebrate Body. Holt-Saunders International, Philadelphia, 394 pp.

Sangster, S. 2003. The Anatomy, Functional Morphology and Systematics of *Dimorphodon macronyx* (Diapsida: Pterosauria). Dissertation thesis/dissertation, Gonville and Caius College, Cambridge University, Cambridge, UK, 239 pp.

Sato, K., K. Q. Sakamoto, Y. Watanuki, A. Takahashi, N. Katsumata, C.-A. Bost, and H. Weimerskirch. 2009. Scaling of soaring seabirds and implications for flight abilities of giant pterosaurs. PLoS ONE 4:1–6.

Sayão, J. M., and A. W. A. Kellner. 2006. Novo esqueleto parcial de pterossauro (Pterodactyloidea, Tapejaridae) do Membro Crato (Aptiano), Formacao Santana, Bacia do Araripe, Nordeste do Brasil 1. Estudos Geologicos 16.

Schaeffer, B. 1941. The morphological and functional evolution of the tarsus in amphibians and reptiles. Bulletin of the American Museum of Natural History 78:345–472.

Schindelin, J., I. Arganda-Carreras, E. Frise, V. Kaynig, M. Longair, T. Pietzsch, S. Preibisch, C. Rueden, S. Saalfeld, B. Schmid, J.-Y. Tinevez, D. J. White, V. Hartenstein, K. Eliceiri, P. Tomancak, and A. Cardona. 2012. Fiji: An open-source platform for biological-image analysis. Nature Methods 9:676–682.

Seeley, H. G. 1870. The Ornithosauria: an elementary study of the bones of pterodactyles, made from fossil remains found in the Cambridge Upper Greensand, and arranged in the Woodwardian Museum of the University of Cambridge. Deighton, Bell, and Co., Cambridge, 135 pp.

Seeley, H. G. 1891. The ornithosaurian pelvis. Journal of Natural History Series 6 7:237–255.

Seeley, H. G. 1901. Dragons of the Air: An account of extinct flying reptiles. D. Appleton & Co., New York, 239 pp.

Sereno, P. C. 1991. Basal archosaurs: phylogenetic relationships and functional implications. Society of Vertebrate Paleontology Memoir 2 supplement to Journal of Vertebrate Paleontology 11:1–53.

Shipman, P. 1998. Taking wing: *Archaeopteryx* and the Evolution of Bird Flight. Weidenfeld and Nicolson, London, 336 pp.

Smith, R. E., D. M. Martill, A. Kao, S. Zouhri, and N. R. Longrich. 2020. A long-billed, possible probe-feeding pterosaur (Pterodactyloidea: ?Azhdarchoidea) from the mid-Cretaceous of Morocco, North Africa. Cretaceous Research:https://doi.org/10.1016/j.cretres.2020.104643.

Solomon, A. A., V. A. Codrea, M. r. Venczel, and G. Grellet-Tinner. 2020. A new species of large-sized pterosaur from the Maastrichtian of Transylvania (Romania). Cretaceous Research:104316.

Sömmerring, S. T. v. 1812. Über einen *Ornithocephalus*. Denkschriften der Königlich Bayerischen Akademie der Wissenschaften. Mathematisch-Physikalische Klasse 3:89–158.

Sullivan, R. M., and D. W. Fowler. 2011. *Navajodactylus boerei*, n. gen., n. sp., (Pterosauria, ?Azhdarchidae) from the Upper Cretaceous Kirtland Formation (upper Campanian) of New Mexico; pp. 393–404 in R. M. Sullivan, S. G. Lucas, and J. A. Spielmann (eds.), Fossil Record 3. New Mexico Museum of Natural History and Science, Albuquerque.

Theodori, C. v. 1830. Knochen vom *Pterodactylus* aus der Liasformation der Gegen von Banz. Frorieps Notizen zur Natur- und Heilkund 19:101–103.

TMM catalog. Texas Vertebrate Paleontology Collections catalog;The University of Texas at Austin, Austin, Texas.

Tsuihiji, T., B. Andres, P. M. O'Connor, M. Watabe, K. Tsogtbaatar, and B. Mainbayar. 2017. Gigantic pterosaurian remains from the Upper Cretaceous of Mongolia. Journal of Vertebrate Paleontology 37:e1361431.

Unwin, D. M. 1987. Joggers or waddlers? Nature 327:13–14.

Unwin, D. M. 1988. New remains of the pterosaur *Dimorphodon* (Pterosauria: Rhamphorhynchoidea) and the terrestrial ability of early pterosaurs. Modern Geology 13:57–68.

Unwin, D. M. 1991. The morphology, systematics and evolutionary history of pterosaurs from the Cretaceous Cambridge Greensand of England. Unpublished Ph.D. Dissertation thesis/dissertation, Department of Pure and Applied Zoology, University of Reading, Reading, 527 pp.

Unwin, D. M. 1995. Preliminary results of a phylogenetic analysis of the Pterosauria (Diapsida: Archosauria); pp. 69–72 in A. Sun and Y. Wang (eds.), Sixth Symposium on Mesozoic Terrestrial Ecosystems and Biota, Short Papers. China Ocean Press, Beijing.

Unwin, D. M. 2002. On the systematic relationships of *Cearadactylus atrox*, an enigmatic Early Cretaceous pterosaur from the Santana Formation of Brazil. Mitteilungen aus dem Museum für Naturkunde, Berlin, Geowissenschaftlichen Reihe 5:239–263.

Unwin, D. M. 2003. On the phylogeny and evolutionary history of pterosaurs; pp. 139–190 in E. Buffetaut and J.-M. Mazin (eds.), Evolution and Palaeobiology of Pterosaurs. Geological Society, Special Publications, London.

Unwin, D. M. 2006. Pterosaurs from Deep Time. Pi Press, New York, 347 pp.

Unwin, D. M., and N. N. Bakhurina. 2000. Pterosaurs from Russia, middle Asia and Mongolia; pp. 420–433 in M. J. Benton, M. A. Shishkin, D. M. Unwin, and E. N. Kurochkin (eds.), The age of dinosaurs in Russia and Mongolia. Cambridge University Press, Cambridge.

Unwin, D. M., J. Lü, and N. N. Bakhurina. 2000. On the systematic and stratigraphic significance of pterosaurs from the Lower Cretaceous Yixian Formation (Jehol Group) of Liaoning, China. Mitteilungen aus dem Museum für Naturkunde in Berlin, Geowissenschaftliche Reihe 3:181–206.

Unwin, D. M., and J. Lü. 1997. *Zhejiangopterus* and the relationship of pterodactyloid pterosaurs. Historical Biology 12:199–210.

Unwin, D. M., E. Frey, D. M. Martill, J. B. Clarke, and J. Riess. 1996. On the nature of the pteroid in pterosaurs. Proceedings of the Royal Society of London B 263:45–52.

Veldmeijer, A. J. 2003. Description of *Coloborhynchus spielbergi* sp. nov. (Pterodactyloidea) from the Albian (Lower Cretaceous) of Brazil. Scripta Geologica 125:35–139.

Vremir, M. M. 2010. New faunal elements from the late Cretaceous (Maastrichtian) continental deposits of Sebeş area (Transylvania). Acta Musei Sabesiensis 2:635–684.

Vremir, M. M., G. J. Dyke, and Z. Csiki. 2011. Late Cretaceous pterosaurian diversity in the Transylvanian and Hateg basins (Romania): new results; pp. 131–132 in Eighth Romanian Symposium on Palaeontology, Abstract Volume, Z. n. Csiki ed, Bucharest.

Vremir, M. M., D. Naish, and G. Dyke. 2013a. Pterosaur size classes in the Transylvanian Late Cretaceous? Journal of Vertebrate Paleontology Program and Abstracts, 2013:233.

Vremir, M. M., A. W. A. Kellner, D. Naish, and G. J. Dyke. 2013b. A new azhdarchid pterosaur from the Late Cretaceous of the Transylvanian Basin, Romania: Implications for azhdarchid diversity and distribution. PLoS ONE 8:e54268.

Vremir, M. M., G. Dyke, Z. Csiki-Sava, D. Grigorescu, and E. Buffetaut. 2018. Partial mandible of a giant pterosaur from the uppermost Cretaceous (Maastrichtian) of the Haţeg Basin, Romania. Lethaia: https://doi.org/10.1111/let.12268.

Vremir, M. M., M. P. Witton, D. Naish, G. Dyke, S. L. Brusatte, M. Norell, and R. Totoianu. 2015. A medium-sized robust-necked azhdarchid pterosaur (Pterodactyloidea: Azhdarchidae) from the Maastrichtian of Pui (Haţeg Basin, Transylvania, Romania). American Museum Novitates 3827:1–16.

Vullo, R., G. Garcia, P. Godefroit, A. Cincotta, and X. Valentin. 2018. *Mistralazhdarcho maggii*, gen. et sp. nov., a new azhdarchid pterosaur from the Upper Cretaceous of southeastern France. Journal of Vertebrate Paleontology 38:1–16.

Vullo, R., J. Marugán-Lobón, A. W. A. Kellner, A. D. Buscalioni, B. Gomez, M. d. l. Fuente, and J. J. Moratalla. 2012. A new crested pterosaur from the Early Cretaceous of Spain: the first European tapejarid (Pterodactyloidea: Azhdarchoidea). PLoS ONE 7:e38900.

Wagner, J. A. 1861. Charakteristik einer neuen Flugeidechse, *Pterodactylus elegans*. Sitzungsberichte der Bayerischen Akademie der Wissenschaften Mathematisch-naturwissenschaftliche Abteilung 1:363–365.

Wang, X., and J. Lü. 2001. Discovery of a pterodactylid pterosaur from the Yixian Formation of western Liaoning, China. Chinese Science Bulletin 46:1112–1117.

Wang, X., A. W. A. Kellner, S. Jiang, and X. Cheng. 2012. New toothed flying reptile from Asia: close similarities between early Cretaceous pterosaur faunas from China and Brazil. Naturwissenschaften 99:249–257.

Wang, X., A. W. A. Kellner, S. Jiang, and X. Meng. 2009. An unusual long-tailed pterosaur with elongated neck from western Liaoning of China. Anais Academia Brasileira de Ciêncas 81:793–812.

Wang, X., A. W. A. Kellner, Z. Zhou, and D. d. A. Campos. 2005. Pterosaur diversity and faunal turnover in Cretaceous terrestrial ecosystems in China. Nature 437:875–879.

Wang, X., A. W. A. Kellner, Z. Zhou, and D. d. A. Campos. 2008. Discovery of a rare arboreal forest-dwelling flying reptile (Pterosauria, Pterodactyloidea) from China. Proceedings of the National Academy of Science 105:1983–1987.

Wang, X., S. Jiang, J. Zhang, X. Cheng, X. Yu, Y. Li, G. Wei, and X. Wang. 2017. New evidence from China for the nature of the pterosaur evolutionary transition. Scientific Reports 7:doi: 10.1038/srep42763.

Wang, X., A. W. A. Kellner, S. Jiang, Q. Wang, Y. Ma, Y. Paidoula, X. Cheng, T. Rodrigues, X. Meng, J. Zhang, N. Li, and Z. Zhou. 2014. Sexually dimorphic tridimensionally preserved pterosaurs and their eggs from China. Current Biology 24:1323–1330.

Watabe, M., T. Tsuihiji, S. Suzuki, and K. Tsogtbaatar. 2009. The first discovery of pterosaurs from the Upper Cretaceous of Mongolia. Acta Palaeontologica Polonica 54:231–242.

Wauer, R. H., and C. M. Fleming. 2002. Naturalist's Big Bend: an introduction to the trees and shrubs, wildflowers, cacti, mammals, birds, reptiles and amphibians, fish, and insects. Second edition Edition, Louise Lindsey Merrick Natural Environment Series, Volume 33. Texas A&M University Press, College Station, TX, 232 pp.

Wellnhofer, P. 1970. Die Pterodactyloidea (Pterosauria) der Oberjura-Plattenkalke Suddeutschlands. Bayerische Akademie der Wissenschaften, Mathematisch-Wissenschaftlichen Klasse, Abhandlungen 141:1–133.

Wellnhofer, P. 1974. *Campylognathoides liasicus* (Quenstedt), an Upper Liassic pterosaur from Holzmaden—The Pittsburgh specimen. Annals of Carnegie Museum 45:5–34.

Wellnhofer, P. 1975a. Die Rhamphorhynchoidea (Pterosauria) der Oberjura-Plattenkalke Suddeutschlands: Systematische Beischreibung. Palaeontographica A 148:132–186.

Wellnhofer, P. 1975b. Die Rhamphorhynchoidea (Pterosauria) der Oberjura-Plattenkalke Suddeutschlands: Allgemeine Skelettemorphologie. Palaeontographica A 148:1–33.

Wellnhofer, P. 1978. Pterosauria, Handbuch der Palaeoherpetologie, Volume 19. Gustav Fischer Verlag, Stuttgart, 82 pp.

Wellnhofer, P. 1980. Flugsaurierreste aus der Gosau-Kreide von Muthmannsdorf (Niederösterreich) – ein Beitrag zur Kiefermechanik der Pterosaurier. Mitteilungen der Bayerischen Staatsammlung für Paläontologie und Historische Geologie 20:95–112.

Wellnhofer, P. 1985. Neue Pterosaurier aus der Santana-Formation der Chapada do Araripe, Brasilien. Palaeontographica, A 187:105–182.

Wellnhofer, P. 1987. New crested pterosaurs from the Lower Cretaceous of Brazil. Mitteilung der Bayerischen Staatssammlung für Paläontologie und historische Geologie 27:175–186.

Wellnhofer, P. 1988. Terrestrial locomotion in pterosaurs. Historical Biology 1:3–16.

Wellnhofer, P. 1991a. Weitere Pterosaurierfunde aus der Santana-Formation (Apt) der Chapada do Araripe, Brasilien. Palaeontographica 215:43–101.

Wellnhofer, P. 1991b. The Illustrated Encyclopedia of Prehistoric Flying Reptiles. Salamander Books, Ltd., London, 192 pp.

Wellnhofer, P. 2003. A late Triassic pterosaur from the Northern Calcareous Alps (Tyrol, Austria); pp. 105–137 in E. Buffetaut and J.-M. Mazin (eds.), Evolution and Palaeobiology of Pterosaurs. Geological Society, Special Publications, London.

Wellnhofer, P., and E. Buffetaut. 1999. Pterosaur remains from the Cretaceous of Morocco. Paläontologische Zeitschrift 73:133–142.

Wellnhofer, P., and A. W. A. Kellner. 1991. The skull of *Tapejara wellnhoferi* Kellner (Reptilia: Pterosauria) from the Lower Cretaceous Santana Formation of the Araripe Basin, Northeastern Brazil. Mitteilung der Bayerischen Staatssammlung für Paläontologie und historische Geologie 31:89–106.

Wellnhofer, P., and B.-W. Vahldiek. 1986. Ein Flugsaurier-Rest aus dem Posidonienschiefer (Unter-Toarcium) von Schandelah bei Braunschweig. Paläontologische Zeitschrift 60:329–340.

Wiffen, J., and R. E. Molnar. 1988. First pterosaur from New Zealand. Alcheringa 12:53–59.

Wild, R. 1979. Die Flugsaurier (Reptilia, Pterosauria) aus der Oberen Trias von Cene bei Bergamo, Italien. Bollettino della Societa Paleontologica Italiana 17.

Wild, R. 1990. Pterosaur remains (Reptilia, Pterosauria) from the Lower Cretaceous (Hauterivian) of Hannover, Lower Saxony. Neues Jahrbuch für Geologie und Paläontologie, Abhandlungen 181:241–254.

Wild, R. 1994. A juvenile specimen of *Eudimorphodon ranzii* Zambelli (Reptilia, Pterosauria) from the Upper Triassic (Norian) of Bergamo. Rivista del Museo Civico di Scienze Naturali 16:91–115.

Wilkinson, M. T., D. M. Unwin, and C. P. Ellington. 2006. High lift function of the pteroid bone and forewing of pterosaurs Proceedings of the Royal Society B 273:119–126.

Williston, S. W. 1897. Restoration of *Ornithostoma* (*Pteranodon*). Kansas University Quarterly, Series A 6: :35–51.

Williston, S. W. 1902. On the skull of *Nyctodactylus*, an Upper Cretaceous pterodactyl. The Journal of Geology 10:520–531.

Williston, S. W. 1903. On the osteology of *Nyctosaurus* (*Nyctodactylus*), with notes on American pterosaurs. Field Columbian Museum Publications, Geological Series 2:125–163.

Williston, S. W. 1904. The fingers of pterodactyls. Geological Magazine 1:59–60.

Witton, M. P. 2007. Titans of the skies: azhdarchid pterosaurs. Geology Today 23:33–38.

Witton, M. P. 2008. A new approach to determining pterosaur body mass and its implications for pterosaur flight. Zitteliana Reihe B: Abhandlungen der Bayerischen Staatssammlung fur Palaontologie und Geologie 28:143–158.

Witton, M. P. 2012. New insights into the skull of *Istiodactylus latidens* (Ornithocheiroidea, Pterodactyloidea). PLoS ONE 7:e33170.

Witton, M. P. 2013. Pterosaurs: Natural History, Evolution, Anatomy. Princeton University Press, Princeton, 291 pp.

Witton, M. P., and M. B. Habib. 2010. On the size and flight diversity of giant pterosaurs, the use of birds as pterosaur analogues and comments on pterosaur flightlessness. PLoS ONE 5:1–18.

Witton, M. P., and D. Naish. 2008. A reappraisal of azhdarchid pterosaur functional morphology and paleoecology. PLoS ONE 3:1–16.

Witton, M. P., and D. Naish. 2015. Azhdarchid pterosaurs: water-trawling pelican mimics or "terrestrial stalkers"? Acta Palaeontologica Polonica 60:651–660.

Woodward, A. S. 1902. On two skulls of ornithosaurian *Rhamphorhynchus*. The Annals and Magazine of Natural History Series 7:1–5.

Wu, W.-H., C.-F. Zhou, and B. Andres. 2017. The toothless pterosaur *Jidapterus edentus* (Pterodactyloidea: Azhdarchoidea) from the Early Cretaceous Jehol Biota and its paleoecological implications. PLoS ONE 12:e0185486.

Young, C.-C. 1964. On a new pterosaurian from Sinkiang, China. Vertebrata Palasiatica 8:221–256.

Young, C.-C. 1973. Reports of Paleontological Expedition to Sinkiang (II). Pterosaurian Fauna from Wuerho, Sinkiang. Memoir of the Institute of Vertebrate Palaeontology and Paleoanthropology, Academica Sinica 11:18–35.

Zambelli, R. 1973. *Eudimorphodon ranzii* gen. nov., sp. nov., uno pterosauro Triassico (nota preliminare). Rendiconti Scienze di Instituto Lombardo, B 107:27–32.

Zhou, C.-F. 2010a. New material of *Chaoyangopterus* (Pterosauria: Pterodactyloidea) from the Early Cretaceous Jiufotang Formation of western Liaoning, China. Neues Jahrbuch für Geologie und Paläontologie, Abhandlungen 257:341–350.

Zhou, C.-F. 2010b. New material of *Elanodactylus prolatus* ANDRES & JI, 2008 (Pterosauria: Pterodactyloidea) from the Early Cretaceous Yixian Formation of western Liaoning, China. – Neues Jahrbuch für Geologie und Paläontologie, Abhandlungen 255:277–286.

Zhou, C.-F., K.-Q. Gao, H. Yi, J. Xue, Q. Li, and R. C. Fox. 2017. Earliest filter-feeding pterosaur from the Jurassic of China and ecological evolution of Pterodactyloidea. Royal Society Open Science 4:160672.